

Electrochemotherapy, Electrogenetherapy, and Transdermal Drug Delivery

*Electrically Mediated Delivery
of Molecules to Cells*

Edited by

Mark J. Jaroszeski

Richard Heller

Richard Gilbert



Humana Press

Principles of Membrane Electroporation and Transport of Macromolecules

Eberhard Neumann, Sergej Kakorin, and Katja Toensing

1. Introduction

The phenomenon of membrane electroporation (ME) methodologically comprises an electric technique to render lipid and lipid–protein membranes porous and permeable, transiently and reversibly, by electric voltage pulses. It is of great practical importance that the *primary* structural changes induced by ME, condition the electroporated membrane for a variety of *secondary* processes, such as, for instance, the permeation of otherwise impermeable substances.

Historically, the *structural* concept of ME was derived from *functional* changes, explicitly from the electrically induced permeability changes, which were indirectly judged from the partial release of intracellular components (**1**) or from the uptake of macromolecules such as DNA, as indicated by electrotransformation data (**2–4**). The electrically facilitated uptake of foreign genes is called the direct electroporative gene transfer or electrotransformation of cells. Similarly, electrofusion of single cells to large syncytia (**5**) and electroinsertion of foreign proteins (**6**) into electroporated membranes are also based on ME, that is, electrically induced structural changes in the membrane phase.

For the time being, the method of ME is widely used to manipulate all kinds of cells, organelles, and even intact tissue. ME is applied to enhance iontophoretic drug transport through skin—see, for example, Pliquett et al. (**7**)—or to introduce chemotherapeutics into cancer tissue—an approach pioneered by L. Mir (**8**).

Medically, ME may be qualified as a novel microsurgery tool using electric pulses as a microscalpel, transiently opening the cell membrane of tissue for the penetration of foreign substances (4,9,10). The combination of ME with drugs and genes also includes genes that code for effector substances such as interleukin-2 or the apoptosis proteins p53 and p73. Therefore, the understanding of the electroporative DNA transport is of crucial importance for gene therapy in general and antitumor therapy in particular.

Clearly, goal-directed applications of ME to cells and tissue require knowledge not only of the molecular membrane mechanisms, but potential cell biological consequences of transient ME on cell regeneration must be also elucidated, for instance, adverse effects of loss of intracellular compounds such as Ca^{2+} , ATP, and K^+ . Due to the enormous complexity of cellular membranes, many fundamental problems of ME have to be studied at first on model systems, such as lipid bilayer membranes or unilamellar lipid vesicles. When the primary processes are physicochemically understood, the specific electroporative properties of cell membranes and living tissue may also be quantitatively rationalized.

Electrooptical and conductometrical data of unilamellar liposomes showed that the electric field causes not only membrane pores but also shape deformation of liposomes. It appears that ME and shape deformation are strongly coupled, mutually affecting each other (4,11,12). The primary field effect of ME and cell deformation triggers a cascade of numerous secondary phenomena, such as pore enlargement and transport of small and large molecules across the electroporated membrane. Here we limit the discussion to the chemical-structural aspects of ME and cell deformation and the fundamentals of transport through electroporated membrane patches. The theoretical part is essentially confined to those physicochemical analytical approaches that have been quantitatively conceptualized in some molecular detail, yielding transport parameters, such as permeation coefficients, electroporation rate coefficients, and pore fractions.

2. Theory of Membrane Electroporation

The various electroporative transport phenomena of release of cytosolic components and uptake of foreign substances, such DNA or drugs are indeed ultimately caused by the external voltage pulses. It is stressed again that the transient permeability changes, however, result from field-induced structural changes in the membrane phase. Remarkably, these structural changes comprise transient, yet long-lived permeation sites, pathways, channels, or pores (3,13–17).

2.1. The Pore Concept

Field-induced penetrations of small ions and ionic druglike dyes are also observed in the afterfield time period, that is, in the absence of the electrodiffusive driving force (**Fig. 1**). Therefore, the electrically induced permeation sites must be polarized and specifically ordered, local structures which are potentially “open for diffusion” of permeants. As indicated by the longevity of the permeable membrane state, these local structures of lipids are long-lived (milliseconds to seconds) compared to the field pulse durations (typically, 10 μs to 10 ms). Thus, the local permeation structures may be safely called transient pores or electropores in model membranes as well as in the lipid part of cell membranes. The special structural order of a long-lived, potential permeation site may be modeled by the so-called inverted or hydrophilic (HI) pore (**Fig. 2**) (*17–19*). On the same line, the massive ion transport through planar membranes, as observed in the dramatic conductivity increase when a voltage ($\geq 100\text{--}500$ mV) is applied, can hardly be rationalized without field-induced open passages or pores (*17*).

The afterfield uptake of substances like dyes or drug molecules, added over a time period of minutes after the pulse application, suggests a kind of interactive diffusion, probably involving the transient complex formation between the permeant and the lipids of the pore wall to yield leaky, but transiently occluded, pores (*9*).

2.1.1. Pore Visualization

Up to now there is no visible evidence for small electropores such as electromicrographs. But also the movement of a permeant through an electroporated membrane patch has also not been visualized. The large porelike crater structures or volcano funnels of 50 nm to 0.1 μm diameter, observed in electroporated red blood cells, most probably result from specific osmotic enlargement of smaller primary pores, invisible in microscopy (*14*). Voltage-sensitive fluorescence microscopy at the membrane level has shown that the transmembrane potential in the pole caps of sea urchin eggs goes to a saturation level or even decreases, both as a function of pulse duration and external field strength, respectively. If the membrane conductivity would remain very low, the transmembrane potential linearly increases with the external field strength. Leveling off and decrease of the transmembrane potential at higher fields indicate that the ionic conductivity of the membrane has increased, providing evidence for ion-conductive electropores (*15*). On the same line, in direct current (DC) electric fields the fluorescence images of the contour of

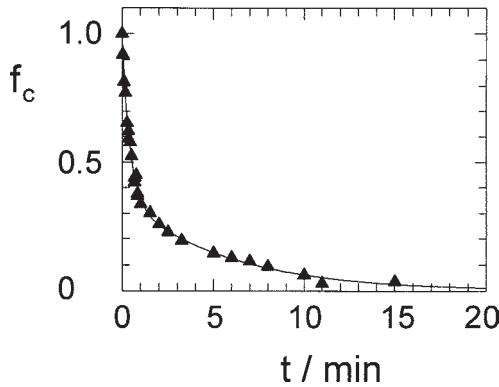


Fig. 1. Pore resealing kinetics indicated by dye uptake. The fraction f_c of colored cells as a function of the time $t = t_{\text{add}}$ of dye addition after the pulse. B-lymphoma cells (line IIA1.6) were exposed to one rectangular electric field pulse ($E=1.49 \text{ kV cm}^{-1}$; pulse duration $t_E=110 \mu\text{s}$) in the presence of the dye SERVA blue G ($M_r = 854$). (From ref. 9, with permission.)

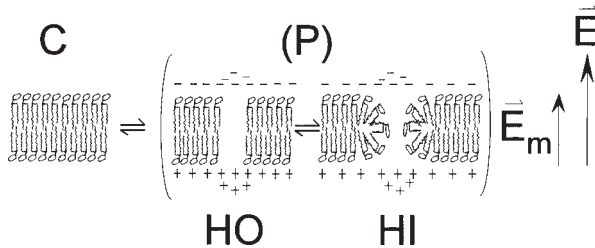


Fig. 2. Specific chemical state transition scheme for the molecular rearrangements of the lipids in the pore edges of the lipid vesicle membrane. C denotes the closed bilayer state. The external electric field causes ionic interfacial polarization of the membrane dielectrics analogous to condenser plates (+, -). $E_m = E_{\text{ind}}$ is the induced membrane field, leading to water entrance in the membrane to produce pores (P); cylindrical hydrophobic (HO) pores or inverted hydrophilic (HI) pores. In the pore edge of the HI pore state, the lipid molecules are turned to minimize the hydrophobic contact with water. In the open condenser the ion density adjacent to the aqueous pore (ϵ_w) is larger than in the remaining part (ϵ_L) because of $\epsilon_w \gg \epsilon_L$.

elongated and electroporated giant vesicle shows large openings in the pole caps opposite to the external electrodes (20). Apparently, these openings are appearing after coalescence of small primary pores invisible in microscopy. Theoretical analysis of the membrane curvature in the vesicle pole caps suggests that vesicle elongation under Maxwell stress must facilitate both pore formation and enlargement of existing pores.

2.1.2. Born Energy and Ion Transport

Membrane electropermeabilization for small ions and larger ionic molecules cannot be simply described by a permeation across the densely packed lipids of an electrically modified membrane (17). Theoretically, a small monovalent ion, such as $\text{Na}^+(\text{aq})$ of radius $r_i = 0.22$ nm and of charge $z_i e$, where e is the elementary charge and z_i the charge number of the ion i (with sign), passing through a lipid membrane encounters the Born energy barrier of

$$\Delta G_B = z_i^2 \cdot e^2 (1/\epsilon_m - 1/\epsilon_w)/(8 \cdot \pi \cdot \epsilon_0 \cdot r_i),$$

where ϵ_0 the vacuum permittivity, $\epsilon_m \approx 2$ and $\epsilon_w \approx 80$ are the dielectric constants of membrane and water, respectively. At $T = 298\text{K}$ (25°C), $\Delta G_B = 68 \cdot kT$, where k is the Boltzmann constant and T is the absolute temperature. To overcome this high barrier, the transmembrane voltage $|\Delta\phi| = \Delta G_B / |z_i \cdot e|$ has to be 1.75 V. An even larger voltage of 3.5 V is needed for divalent ions such as Ca^{2+} or Mg^{2+} ($z_+ = 2$, $r_i = 0.22$ nm). Nevertheless, the transmembrane potential required to cause conductivity changes of the cell membrane usually does not exceed 0.5 V (16,17). The reduction of the energy barrier can be readily achieved by a transient aqueous pore. Certainly, the stationary open electropores can only be small (about ≤ 1 nm diameter) to prevent discharging of the membrane interface by ion conduction (4,9,18).

2.2. Transmembrane Field

In line with the Maxwell definition of the electric field strength as the negative electric potential gradient, we define the membrane field strength by

$$E_m = -\Delta\phi_m / d, \quad (1)$$

where $\Delta\phi_m$ is the intrinsic cross membrane potential difference and $d \approx 5$ nm the dielectric membrane thickness. This inner-membrane potential difference may generally consist of several contributions.

2.2.1. Natural Membrane Potential and Surface Potential

All living cell membranes are associated with a natural, metabolically maintained, (diffusion) potential difference $\Delta\phi_{\text{nat}}$, defined by $\Delta\phi_{\text{nat}} = \phi^{(i)} - \phi^{(o)}$ as the difference between cell inside (i) and outside (o) (see Fig. 3). Typically, this resting potential amounts to $\Delta\phi_{\text{nat}} \approx -70$ mV, where $\phi^{(o)} = 0$ is taken as the reference potential (21).

Biomembranes usually have an excess of negatively charged groups at the interfaces between membrane surfaces and aqueous media. The contribution of these fixed charges and that of the screening small ions are covered by the surface potentials $\phi_s^{(o)}$ and $\phi_s^{(i)}$. If cells are exposed to low ionic strength, the inequality $|\phi_s^{(o)}| > |\phi_s^{(i)}|$ may apply. Therefore there will be a finite value for

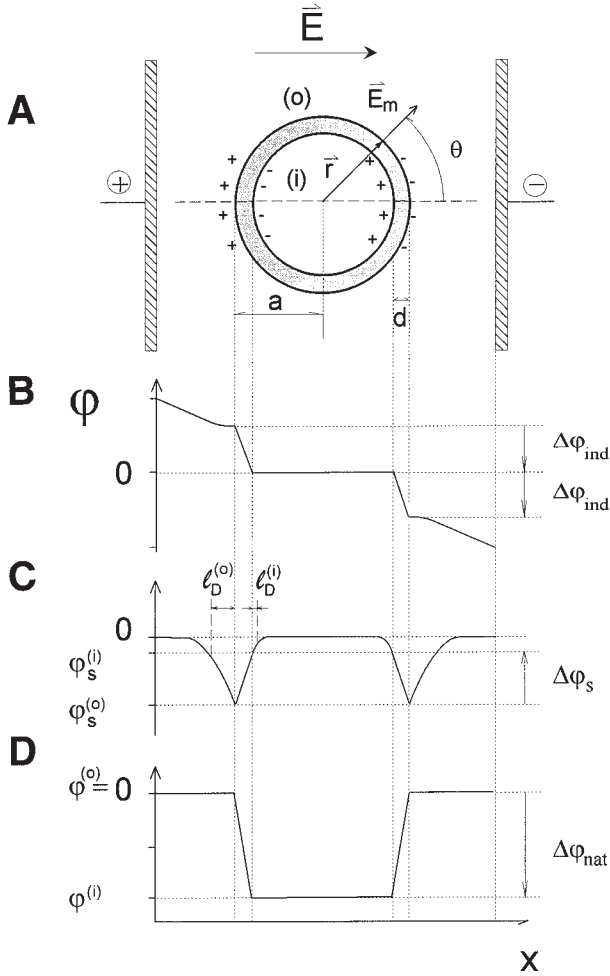


Fig. 3. Electric membrane polarization of a cell of radius a . **(A)** Cross section of a spherical membrane in the external field E . The profiles of **(B)** the electrical potential ϕ across the cell membranes of thickness d , where $\Delta\phi_{\text{ind}}$ is the drop in the induced membrane potential in the direction of E and **(C)** the surface potential ϕ_s at zero external field as a function of distance, respectively; **(D)** $\Delta\phi_{\text{nat}}$ is the natural (diffusive) potential difference at zero external field, also called resting potential.

the surface potential difference $\Delta\phi_s = \phi_s^{(o)} - \phi_s^{(i)}$ (defined analogous to $\Delta\phi_{\text{nat}}$), which in this case is positive and therefore *opposite* to the diffusion potential $\Delta\phi_{\text{nat}}$ (see **Fig. 3**). Provided that additivity holds the field-determining potential difference is $\Delta\phi_m = \Delta\phi_{\text{nat}} + \Delta\phi_s$. At larger values of $\Delta\phi_s$, the term $\Delta\phi_{\text{nat}}$ may be compensated by $\Delta\phi_s$ and therefore $\Delta\phi_m \approx 0$. If lipid vesicles containing a

surplus of anionic lipids are salt-filled and suspended in low ionic strength medium, the surface potential difference $\Delta\phi_s > 0$ is finite, but $\Delta\phi_{\text{nat}} = 0$. Generally, even in the absence of an external field, there can be a finite membrane field $E_m = |\Delta\phi_{\text{nat}} + \Delta\phi_s| / d$ (21). Here we may neglect the locally very limited, but high (150–600 mV) dipole potentials in the boundary between lipid head groups and hydrocarbon chains of the lipids (22,23).

2.2.2. Field Amplification by Interfacial Polarization

In static fields and low-frequency alternating fields dielectric objects such as cells, organelles, and lipid vesicles in electrolyte solution experience ionic interfacial polarization (**Fig. 3A**) leading to an induced cross-membrane potential difference $\Delta\phi_{\text{ind}}$, resulting in a size-dependent amplification of the membrane field. For spherical geometry with cell or vesicle radius a the induced field $E_{\text{ind}} = -\Delta\phi_{\text{ind}} / d$ at the angular position θ relative to the external electric field vector E (**Fig. 3B**) is given by

$$E_{\text{ind}} = \frac{3 \cdot a}{2 \cdot d} \cdot E \cdot f(\lambda_m) \cdot \text{lcos } \theta, \quad (2)$$

where the conductivity factor $f(\lambda_m)$ can be expressed in terms of a and d and the conductivities λ_m , λ_i , λ_0 of the membrane, the cell (vesicle) interior and the external solution, respectively (21). Commonly, $d \ll a$ and $\lambda_m \ll \lambda_0$, λ_i such that

$$f(\lambda_m) = [1 + \lambda_m(2 + \lambda_i / \lambda_0) / (2\lambda_i d/a)]^{-1}.$$

At $\lambda_m \approx 0$ or for negligibly small membrane conductivity we have $f(\lambda_m) = 1$.

The field amplification factor $(3 \cdot a / 2 \cdot d)$ is particularly large for large cells and vesicles; for typical values such as $a = 10 \mu\text{m}$ and $d = 5 \text{ nm}$, we have a field amplification of $(3 \cdot a / 2 \cdot d) = 3 \cdot 10^3$. For elongated cells like bacteria aligned by the field in the direction of E , the contribution of E_{ind} at the pole caps, where $\text{lcos } \theta = 1$, amounts to

$$E_{\text{ind}} = (L / 2 \cdot d) \cdot E,$$

where the amplification factor $(L / 2 \cdot d)$ is proportional to the bacterium length L (24).

2.2.3. Vesicles and Cells in Applied Fields

In the case of lipid vesicles there is no natural membrane potential, that is, $\Delta\phi_{\text{nat}} = 0$. However, for charged lipids and unequal electrolyte concentrations within and outside the vesicle, the surface potentials are different from zero, and therefore $\Delta\phi_m = \Delta\phi_{\text{ind}} + \Delta\phi_s$ (25). Hence at the angle θ we obtain (21,26):

$$E_m^\theta = E_{\text{ind}}^\theta + \Delta\phi_s \cdot \text{lcos } \theta / (d \cdot \cos \theta).$$

Note that $|\cos \theta| / \cos \theta = +1$ for the right hemisphere and -1 for the left one. Therefore, at the right hemisphere $\Delta\varphi_s/d$ adds to the applied field and at the left hemisphere $\Delta\varphi_s/d$ reduces the induced field.

For living cells, there is always a finite E_m field, because $\Delta\varphi_{\text{nat}} \neq 0$ (**Fig. 3D**). Generally, the stationary value of the transmembrane field at the angular position θ for cells with finite natural and surface potential membrane potentials relative to the direction of the external field, can be expressed as:

$$E_m = \left\{ \frac{3 \cdot a}{2 \cdot d} \cdot E \cdot f(\lambda_m) + \frac{\Delta\varphi_{\text{nat}} + \Delta\varphi_s}{d \cdot \cos \theta} \right\} \cdot \lvert \cos \theta \rvert. \quad (3)$$

Normally, $\Delta\varphi_{\text{nat}}$ and $\Delta\varphi_s$ are independent of θ . For the special case when $\Delta\varphi_{\text{nat}}$ and $\Delta\varphi_s$ have equal signs, there can be a major asymmetry. At the left pole cap the sum $\Delta\varphi_{\text{nat}} + \Delta\varphi_s$ is in the same direction as $\Delta\varphi_{\text{ind}}$, whereas at the right pole cap $\Delta\varphi_{\text{nat}} + \Delta\varphi_s$ is opposite to $\Delta\varphi_{\text{ind}}$. For example, if $\Delta\varphi_{\text{nat}} = -70$ mV and $\Delta\varphi_{\text{ind}} = -500$ mV, one has at the left pole cap $\Delta\varphi_m = -570$ mV and at the right one $\Delta\varphi_m = -430$ mV. Therefore membrane electroporation will start at the left hemisphere where the field $E_m = -(\Delta\varphi_{\text{ind}} + \Delta\varphi_{\text{nat}} + \Delta\varphi_s)/d$ is larger than $E_m = -(\Delta\varphi_{\text{ind}} - \Delta\varphi_{\text{nat}} - \Delta\varphi_s)/d$ at the right hemisphere. In the case of opposite signs of $\Delta\varphi_s$ and $\Delta\varphi_{\text{nat}}$ the natural potential $\Delta\varphi_{\text{nat}}$ may be compensated by $\Delta\varphi_s$, the asymmetry in the two hemispheres of cells gets smaller.

2.2.4. Condenser Analog

The redistribution of ions in the electrolyte solution adjacent to the membrane dielectrics results in charge separations which are equivalent to an electrical condenser with capacity

$$C_m = \varepsilon_m \cdot \varepsilon_0 \cdot S_m/d,$$

where S_m is the membrane surface area (**Fig. 2**). However, unlike conventional solid state dielectric condensers, the lipid membrane and adjacent ionic layers are highly dynamic phases of *mobile lipid molecules* in contact with *mobile water molecules* and ions. The lipid membrane is hydrophobically kept together by the aqueous environment. Such a membrane condenser with both mobile interior and mobile environment favors the entrance of water molecules to produce localized cross-membrane pores (P) with higher dielectric constant $\varepsilon_w \approx 80$ compared with $\varepsilon_L \approx 2$ of the replaced lipids (state C).

In the case of charged membranes there are two additional condensers due to the electrical double layers of fixed surface charges and mobile counterions on the two sides of the charged membrane, represented by the capacities

$$C_i = \varepsilon_w \cdot \varepsilon_0 \cdot S_m/l_D^{(i)} \text{ and } C_o = \varepsilon_w \cdot \varepsilon_0 \cdot S_m/l_D^{(o)},$$

where $l_D^{(i)}$ and $l_D^{(o)}$ are the Debye screening lengths inside and outside the cell (vesicle), respectively (**Fig. 3C**).

In the absence of an external field the total potential difference across the membrane is defined solely by the condenser charge $q = q_+ = |q_-|$ due to the natural diffusion potential and charged surface groups:

$$\Delta\varphi_m = \Delta\varphi_{\text{nat}} + \Delta\varphi_s,$$

with

$$\Delta\varphi_s = q / (1/C_i - 1/C_o).$$

Explicitly the contribution by the surface charge potential is given by:

$$\Delta\varphi_s = \frac{1}{F} \cdot \sqrt{\frac{RT}{2 \cdot \epsilon_0 \cdot \epsilon_w}} \cdot \left(\frac{\sigma_i}{\sqrt{J_i}} - \frac{\sigma_o}{\sqrt{J_o}} \right), \quad (4)$$

where F is the Faraday constant, R the gas constant, $\sigma_i = q_i/S_m$ and $\sigma_o = q_o/S_m$ are the charge densities on the inner and outer membrane surfaces, respectively, and J_i and J_o are the molar ionic strengths of the inside and the outside bulk electrolyte, respectively. Note that

$$J_{i(o)} = \left(\sum_j z_j^2 \cdot c_j \right)_{i(o)} / 2,$$

where j refers to all mobile ions and fixed ionic groups; frequently J is determined by the salt ions of the buffer solution. When the salt concentrations inside and outside are largely different, $\Delta\varphi_s$ may appreciably contribute to E_m .

2.3. Electroporation–Resealing Cycle

2.3.1. Chemical Scheme for Pore Formation

The field-induced pore formation and resealing after the electric field is viewed as a state transition from the intact closed lipid state (C) to the porous state (P) according to the reaction scheme (21):



The state transition involves a cooperative cluster (L_n) of n lipids L forming an electropore (19). The degree of membrane electroporation f_p is defined by the concentration ratio

$$f_p = \frac{[P]}{[P] + [C]} = \frac{K}{1 + K}, \quad (6)$$

where $K = [P] / [C] = k_1/k_{-1}$ is the equilibrium distribution constant, k_1 the rate coefficient for the step $C \rightarrow P$ and k_{-1} the rate coefficient for the resealing step ($C \leftarrow P$). In an external electric field, the distribution between C and P states is shifted in the direction of increasing $[P]$. Note, the frequently encountered observation of very small pore densities means that $K \ll 1$. For this case $f_p \approx K$. Hence the thermodynamic, field-dependent quantity K is directly obtained from the experimental degree of poration.

2.3.2. Reaction Rate Equation

Kinetically, the reaction rate equation for the time course of the electroporation-resealing cycle describes the differential increase $d[P]$ in pore concentration at the expense of lipids outside the pore wall, $d[C]$, in the form of the conventional differential equation (4):

$$\frac{d[P]}{dt} = -\frac{d[C]}{dt} = k_1[C] - k_{-1}[P]. \quad (7)$$

Mass conservation dictates that the total concentration is $[C_0] = [P] + [C]$. Substitution into **Eq. 7** and **Eq. 6**, integration yields the time course of the degree of pore formation:

$$f_p^{C \rightarrow P} = \frac{K}{1+K} \cdot (1 - e^{-t/\tau}), \quad (8)$$

where the practical assumption that $f_p(0) = 0$ at $E = 0$ and $t = 0$ was applied. The relaxation time is given by:

$$\tau = (k_1 + k_{-1})^{-1} = [k_{-1}(1+K)]^{-1}. \quad (9)$$

For the after-field time range $t > t_E$ where $k_{-1} \gg k_1$ and

$$f_p(t_E) = K/(1+K) \cdot (1 - e^{-t_E/\tau}),$$

integration of **Eq. 7** yields:

$$f_p^{P \rightarrow C} = f_p(t_E) \cdot e^{-k_{-1}(t-t_E)}. \quad (10)$$

It is readily seen that the experimentally accessible quantities τ and K yield both rate coefficients k_1 and k_{-1} . The symbol P may include several different pore states. If, for instance, we have to describe the pore formation by the sequence $C \rightleftharpoons HO \rightleftharpoons HI$, then (P) represents the equilibrium $HO \rightleftharpoons HI$ between hydrophobic (HO) and hydrophilic (HI) pore states (**Fig. 2**). In this case normal mode analysis is required and k_{-1} in the expressions for f_p must be replaced by $k_{-1}/(1+K_2)$, where $K_2 = [HI]/[HO]$ is the equilibrium constant of the second step $HO \rightleftharpoons HI$ (**19**).

2.3.3. θ Averages

For the curved membranes of cells and organelles, the dependence of the induced potential difference $\Delta\phi_{\text{ind}}$ and thus the transmembrane field $E_{\text{ind}} = -\Delta\phi_{\text{ind}}/d$ on the positional θ angle leads to the shape-dependent θ distribution of the values of K and k_1 ; k_{-1} is assumed to be independent of E and thus independent of θ . Therefore, all conventionally measured quantities (f_p and τ) are θ averages. The stationary value of the actually measured θ -average fraction \bar{f}_p of porated area is given by the integral:

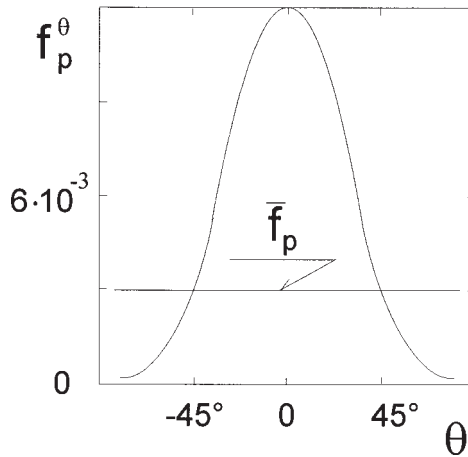


Fig. 4. The fraction, f_p^θ , of membrane surface area covered by electropores as a function of the positional angle θ . The θ average \bar{f}_p of membrane electroporation is by a factor of 4 smaller than f_p^θ in the cell pole caps opposite to the electrodes ($\theta = 0^\circ$, $\theta = 180^\circ$, respectively).

$$\bar{f}_p = \frac{1}{2} \int_0^\pi \frac{k_1(\theta)}{k_{-1} + k_1(\theta)} \sin \theta \, d\theta. \quad (11)$$

The actual pore density f_p^θ in the cell pole caps, where $\theta \approx 0^\circ$ and 180° , respectively, can be a factor of 4 larger than the θ average fraction \bar{f}_p (Fig. 4). It is found that \bar{f}_p is usually very small (11,12), for example, $\bar{f}_p \leq 0.003$, that is, 0.3%. Even the pole cap values $f_p^\theta(0^\circ, 180^\circ) = 4 \cdot \bar{f}_p = 0.012$ certainly correspond to a small pore density.

3. Thermodynamics of Membrane Electroporation

As already mentioned, the lipid membrane in an external electric field is an open system with respect to H_2O molecules and surplus ions, charging the membrane condenser. Therefore, to ensure the minimization of the adequate Gibbs energy with respect to the field E_m , we have to transform the normal Gibbs energy G with dG proportional to $E_m \cdot dM$, where M is the global electric dipole moment, to yield the transformed Gibbs energy $\hat{G} = G - E_m M$ with $d\hat{G}$ proportional to $-M dE_m$ (27). Now, E_m in dE_m is the explicit variable and membrane electroporation can be adequately described in terms of E_m and the induced electric dipole moment M of the pore region.

The global equilibrium constant K of the poration–resealing process is directly related to the standard value of the transformed reaction Gibbs energy $\Delta_r \hat{G}^\ominus$ by (28):

$$K = e^{-\Delta_r \hat{G}^\ominus / RT}. \quad (12)$$

The molar work potential difference

$$\Delta_r \hat{G}^\ominus = \hat{G}^\ominus(P) - \hat{G}^\ominus(C),$$

between the two states C and P in the presence of an electric field generally comprises chemical and physical terms (18):

$$\Delta_r \hat{G}^\ominus = \sum_\alpha \sum_j (v_j \cdot \mu_j^\ominus)^\alpha + \int_0^L \Delta_r \gamma dL + \int_0^S \Delta_r \Gamma dS + \int_0^H \Delta_r \beta dH - \int_0^{E_m} \Delta_r M dE_m. \quad (13)$$

Note that $\Delta_r = d/d\xi$, where $d\xi = dn_j/v_j$ is the differential molar advancement of a state transition, n_j is the amount of substance and v_j is the stoichiometric coefficient of component j , respectively. The single terms of the right-hand side of **Eq. 13** are now separately considered.

3.1. Chemical Contribution, Pore Edge Energy, and Surface Tension

The first term is the so-called chemical contribution. The pure concentration changes of the lipid ($j = L$) and water ($j = W$) molecules involved in the formation of an aqueous pore with edges are described by v_j^α and the conventional standard chemical potential $\mu_j^{\ominus\alpha}$ of the participating molecule j , constituting the phase α , either state C or state P (27); here,

$$\Delta_r \hat{G}^\ominus = \sum_\alpha \sum_j (v_j \cdot \mu_j^\ominus)^\alpha = (v_w \cdot \mu_w^\ominus + v_L \cdot \mu_L^\ominus)^P - (v_w \cdot \mu_w^\ominus + v_L \cdot \mu_L^\ominus)^C.$$

In **Eq. 13**, γ is the line tension or pore edge energy density and L is the edge length, Γ is the surface energy density and S is the pore surface in the surface plane of the membrane. Explicitly, for cylindrical pores (HO-pore, **Fig. 2**) of mean pore radius \bar{r}_p the molar pore edge energy term reads:

$$\int_0^L \Delta_r \gamma dL = N_A \int_0^L (\gamma_P - \gamma_C) dL = 2 \cdot \pi \cdot N_A \cdot \gamma \cdot \bar{r}_p, \quad (14)$$

where $\gamma_P = \gamma$ (because $\gamma_C = 0$, no edge) and $L = 2\pi \cdot \bar{r}_p$ is the circumference line; $N_A = R/k$ is the Avogadro constant.

The surface pressure term for spherical bilayers in water:

$$\int_0^S \Delta_r \Gamma dS = N_A \int_0^S (\Gamma_P - \Gamma_C) dS \quad (15)$$

is usually negligibly small because the difference in Γ between the states P and C is in the order of $\leq 1.2 \text{ mN m}^{-1}$ for phosphatidylcholine in the fluid bilayer state (29).

3.2. Curvature Energy Term

The explicit expression for the curvature energy term of vesicles of radius a and membrane thickness d is given by (18,30):

$$\begin{aligned} \int \Delta_r \beta dH &= N_A \int (\beta_P - \beta_C) dH \\ &\approx - \frac{64 \cdot N_A \cdot \pi^2 \alpha \cdot \kappa \cdot \bar{r}_P^2 \cdot \zeta}{d} \cdot \left(\frac{1}{a} + \frac{H_0^{\text{el}}}{2\pi \cdot \alpha} \right), \end{aligned} \quad (16)$$

where differently to reference (30) here the total surface area difference refers to the middle of the two monolayers (31). Note that the aqueous pore part has no curvature, hence the curvature term is reduced to $\beta_P - \beta_C = -\beta_C$. $H = H_0 + 1/a$ is the membrane curvature inclusively the spontaneous curvature $H_0 = H_0^{\text{chem}} + H_0^{\text{el}}$, where H_0^{chem} is the mean spontaneous curvature due to different chemical compositions of the two membrane leaflets and H_0^{el} is the electrical part of the spontaneous curvature, for example, at different electrolyte surroundings at the two membrane sides. If $H_0 = 0$, then, in the case of spherical vesicles, we have $H = 1/a$. Further on, κ is the elastic module, α (≈ 1) is a material constant (31), ζ is a geometric factor characterizing the pore conicity (18). It appears that the larger the curvature and the larger the H_0^{el} term, the larger is the energetically favorable release of the (transformed) Gibbs energy during the pore formation. The curvature term $\int \Delta_r \beta dH$ can be as large as a few kT per one pore (30). For small vesicles or small organelles and cells the curvature term is particularly important for the energetics of ME.

The effect of membrane curvature on ME has been studied with dye-doped vesicles of different size, that is, for different curvatures. At constant transmembrane potential drop (e.g., $\Delta\phi_m = -0.3$ V), an increased curvature greatly increases the amplitude and rate of the absorbance dichroism, characterizing the extent of pore formation (Figs. 5A,B) (19,30). This observation was quantified in terms of the area difference elasticity (ADE) energy resulting from the different packing density of the lipid molecules in the two membrane leaflets of curved membranes (Fig. 5C) (31,32). Strongly curved membranes appear to be electroporated easier than planar membrane parts (4).

Different electrolyte contents on the internal and external sides of membranes with charged lipids cause different charge screening. This has become apparent when salt-filled vesicles were investigated by electrooptical and conductometrical methods. The larger the electrolyte concentration gradient across the membrane, the larger the turbidity dichroisms, characterizing the extent of pore formation and vesicle deformation (19). The effect of different charge screening on ME is theoretically described in terms of the surface

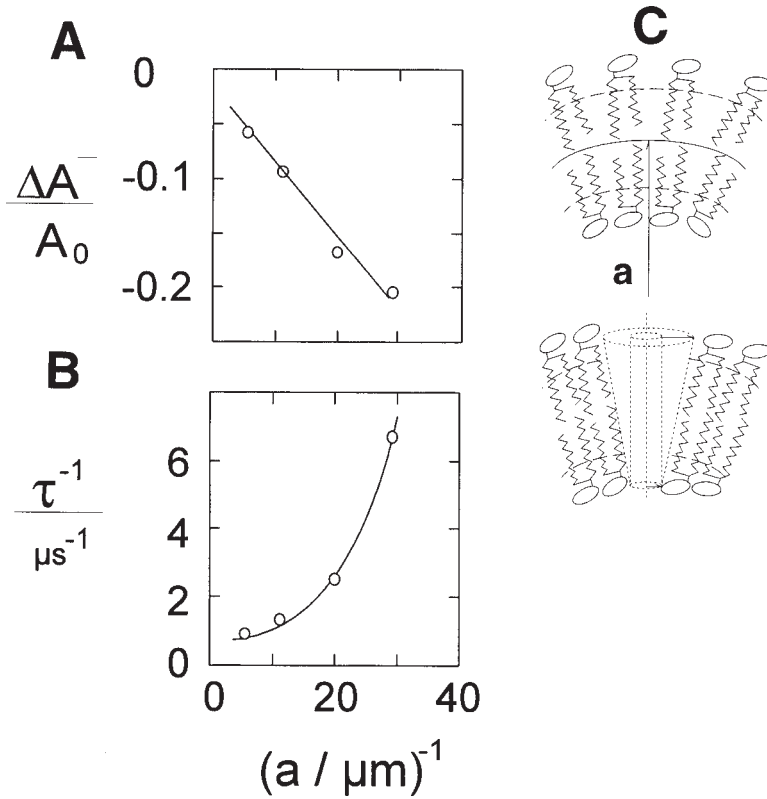


Fig. 5. The effect of vesicle size on the extent and rate of electroporation. The amplitudes of the absorbance dichroism $\Delta A^-/A_0$ (A) and (B) the relaxation rate τ^{-1} as functions of the vesicle curvature $H=1/a$ at constant total lipid concentration $[L_T] = 1.0 \text{ mM}$ and the same nominal transmembrane voltage drop $\Delta\phi_m^N = -1.5 \cdot a \cdot E = -0.3 \text{ V}$. The unilamellar vesicles are composed of L- α -phosphatidyl-L-serine (PS) and 1-palmitoyl-2-oleoyl-*sn*-glycero-3-phosphocholine (POPC) in the molar ratio PS : POPC of 1:2 doped with 2-(3-(diphenylhexatrienyl)propanoyl)-1-hexadecanoyl-*sn*-glycero-3-phosphocholine (β -DPH pPC, $M_r = 782$); total lipid concentration $[L_T] = 1.0 \text{ mM}$; $[\beta\text{-DPH pPC}_T] = 5 \mu\text{M}$; 0.66 mM HEPES ($\text{pH} = 7.4$), $130 \mu\text{M CaCl}_2$; vesicle density $\rho_V = 2.1 \cdot 10^{15} \text{ L}^{-1}$. Application of one rectangular electric pulse of the field strength E and pulse duration $t_E = 10 \mu\text{s}$ at $T = 293 \text{ K}$ (20°C). (C) The membrane curvature is associated with a lipid packing difference between the two membrane leaflets and a lateral pressure gradient across the membrane. Membrane electroporation, causing conical hydrophobic (HO) pores, reduces the lipid packing density difference between the two monolayers and, consequently, the gradient of lateral pressure across the membrane.

potential drop $\Delta\phi_s$, see **Eq. 4**, and the electrical part of membrane spontaneous curvature H_0^{el} .

Extending previous approaches (**33,34**), we obtain for a thin membrane ($d \ll a$), 1 : 1 electrolyte and for small values of the dimensionless parameter

$$s_{i(o)} = e \cdot \sigma_{i(o)} \cdot \lambda_D^{i(o)} / (\epsilon_0 \cdot \epsilon_{i(o)} \cdot kT) \ll 1,$$

that H_0^{el} is given by:

$$H_0^{\text{el}} = (2/3) \cdot (s_i^2 - s_o^2) / (s_i^2 \cdot \lambda_D^i + s_o^2 \cdot \lambda_D^o),$$

where in the SI notation

$$\lambda_D^{i(o)} = [\epsilon_0 \cdot \epsilon_{i(o)} \cdot kT / (2 \cdot e^2 \cdot J_{i(o)} \cdot N_A)]^{1/2}$$

is the explicit expression for the Debye screening length, $\epsilon_{i(o)}$ the dielectric constant of the inner (i) and outer (o) medium, respectively. It has been found that large salt concentration gradients across strongly curved charged membranes permit electroporative efflux of electrolyte ions at surprisingly low transmembrane potential differences, for instance $|\Delta\phi_m| = 37.5$ mV at a vesicle radius of $a = 50$ nm and pulse durations of $t_E = 100$ ms compared with $|\Delta\phi_m| \approx 500$ mV for planar noncurved membranes (**11,35**).

3.3. Electric Polarization Term

In the electric polarization term $\int \Delta_r M dE_m$, the electric reaction moment $\Delta_r M = M_m(P) - M_m(C)$ refers to the difference in the molar dipole moments M_m of state C and P, respectively. The field-induced reaction moment in the electrochemical model is given by (**21**):

$$\Delta_r M = N_A \cdot V_p \cdot \Delta_r P \quad (17)$$

where $V_p = \pi \cdot \bar{r}_p^2 \cdot d$ is the average (induced) pore volume of the assumed cylindrical pore.

Inspired by the physical analysis of Abidor et al. (**35**), we define the chemical reaction polarization as (**19**):

$$\Delta_r P = \epsilon_0 (\epsilon_W - \epsilon_L) E_m, \quad (18)$$

The difference $\epsilon_W - \epsilon_L$ in the dielectric constants of water and of lipids, respectively, refers to the replacement of lipids by water. Note that the possible difference in the values of $E_m(C)$ and $E_m(P)$ is not too essential for the calculation of $\Delta_r P$, because usually $\epsilon_W \gg \epsilon_L$ and $E_m(C) \approx E_m(P)$, thus we may approximate $\epsilon_0 (\epsilon_W(P) - \epsilon_L E_m(C)) \approx \epsilon_0 (\epsilon_W - \epsilon_L) E_m(P)$. In general, this approximation is valid only for small pores of radius < 1 nm, which are not yet too conductive. Since $\epsilon_W \gg \epsilon_L$, the formation of aqueous pores is strongly favored

in the presence of a cross-membrane potential difference $\Delta\phi_m = \Delta\phi_{\text{ind}} + \Delta\phi_s + \Delta\phi_{\text{nat}}$, in particular when the contribution $\Delta\phi_{\text{ind}}$ is large; see **Eq. 3**.

The final expression of the electrical energy term is obtained by sequential insertions and integration; explicitly at the angle θ , we obtain (**18,19**):

$$\int_0^{E_m} \Delta_r M dE_m = \frac{9\pi\epsilon_0 \cdot a^2 \cdot (\epsilon_W - \epsilon_L) \cdot \bar{r}_p^2 \cdot N_A}{8 \cdot d} f^2(\lambda_m) \cdot \cos^2 \theta \cdot E^2, \quad (19)$$

where we see that the polarization energy depends on the square of the field strength.

If the relation between K and E can be formulated as $K = K_0 \exp[\int \Delta_r M dE_m / RT]$, where K_0 refers to $E = 0$, **Eq. 19** can be used to calculate the mean pore radius \bar{r}_p from the field dependence of K or of f_p (the degree of poration). Typically, at $\Delta\phi_{\text{ind}} = -0.42$ V and pulse duration $t_E = 10$ μs , we obtain $\bar{r}_p = 0.35$ nm (**19**).

4. Membrane Electroporation and Cell Deformation

Besides direct visualization of porous patches and elongations of vesicles and cells in the direction of the external field, there are many electrooptical and conductometrical data on lipid vesicles filled with electrolyte which convincingly show that the external electric field causes membrane electroporation and electromechanical vesicle elongation (**18**). In the case of these vesicles the overall shape deformation under the field-induced Maxwell stress is associated with at least two kinetically distinct phases (**11,12**).

4.1. Electroporative Shape Deformation at Constant Volume

The initial very rapid phase (microsecond time range) is the electroporative elongation from the spherical shape to an ellipsoid in the direction of the field vector E . In this phase, previously called phase 0 (**Fig. 6A**) (**4**), there is no measurable release of salt ions. Hence the internal volume of the vesicle remains constant. Elongation is therefore only possible if, in the absence of membrane undulations in small vesicles, the membrane surface can be increased by ME. The formation of aqueous pores means entrance of water and thus increase in the overall membrane volume and surface. Thus, vesicle elongation is rapidly coupled to ME according to the scheme: $C \rightleftharpoons P < = >$ (elongation).

It is important, that the characteristic time constant τ_{def} of vesicle deformation is usually smaller than the θ average time constant of ME ($\bar{\tau} \approx 0.5$ to 1 μs). Actually, for vesicles of radius $a = 50$ nm, a typical membrane bending rigidity of $\kappa = 2.5 \cdot 10^{-20}$ J and the viscosity of water $\eta = 10.05 \cdot 10^{-4}$ kg m⁻¹ s⁻¹ at 20°C, the upper limit of the shape deformation time constant at zero field is (**36**):

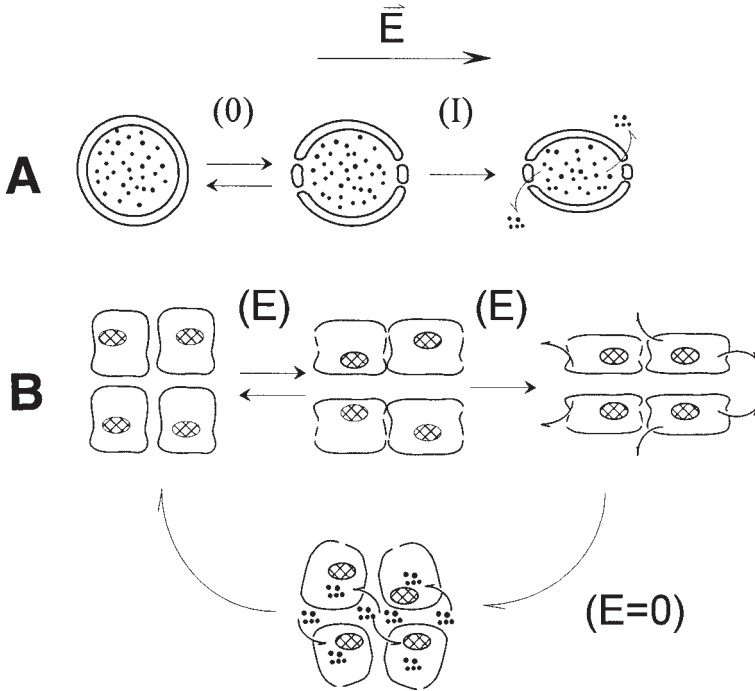


Fig. 6. Electroporative deformation of unilamellar lipid vesicles (or biological cells). **(A)** Phase 0: fast (μs) membrane electroporation rapidly coupled to Maxwell deformation at constant internal volume and slight (0.01–0.3%) increase in membrane surface area. Phase I: slow (milliseconds to minutes) electromechanical deformation at constant membrane surface area and decreasing volume due to efflux of the internal solution through the electropores. Maxwell stress and electrolyte flow change the pore dimension from initially $\bar{r}_p = 0.35 \pm 0.05$ nm to $\bar{r}_p = 0.9 \pm 0.1$ nm. **(B)** Membrane electroporation and shape deformation in cell tissue subjected to an externally applied electric field. The electrical Maxwell stress “squeezes” the cells, permitting drug and gene delivery to electroporated cells through the interstitial pathways between the cells into electroporated cells distant from the site of application of drug or genes. At $E = 0$, resealing and return to original shape occurs slowly.

$$\tau_{\text{def}}(0) = 0.38 \cdot \eta \cdot a^3 / \kappa = 0.9 \mu\text{s}.$$

It can be shown that in electric fields of typically $1 \leq E/\text{MVm}^{-1} \leq 8$, the shape relaxation time constant $\tau_{\text{def}}(E)$ is 100-fold smaller than $\tau_{\text{def}}(0)$, say 10 ns (*Kakorin et al., unpublished*). Therefore, because $\bar{\tau} \gg \tau_{\text{def}}(E)$, it is the structural change of pore formation, inherent in ME, that controls not only the extent, but also the rate of the vesicle deformation in the phase 0. Vesicle and cell deforma-

tions, and thus ME, can be easily measured by electrooptic dichroism, either turbidity dichroism or absorbance dichroism. Proper analysis of the respective electrooptic data provides the electroporative deformation parameter $p = cb$, where c and b are the major and minor ellipsoid axis, respectively, of the vesicle or cell. Specifically, from p we obtain the θ average degree \bar{f}_p of ME (4).

4.2. Shape Deformation at Constant Surface

In the second, slower phase (millisecond time range), previously called phase I (**Fig. 6A**) (4), there is an efflux of salt ions under Maxwell stress through the electropores created in phase 0, leading to a decrease in the vesicle volume under practically constant membrane surface (including the surfaces of the aqueous pores). The increase in the suspension conductivity, $\Delta\lambda^I/\lambda_0$, in the phase I reflects the efflux of salt ions under the electrical Maxwell stress through the electropores. The kinetic analysis in terms of the volume decrease yields the membrane bending rigidity $\kappa = 3.0 \pm 0.3 \times 10^{-20}$ J. At the field strength $E = 1.0$ MV m⁻¹ and in the range of pulse durations of $5 \leq t_E/\text{ms} \leq 60$, the number of water-permeable electropores is found to be $N_p = 35 \pm 5$ per vesicle of radius $a = 50$ nm, with mean pore radius $\bar{r}_p = 0.9 \pm 0.1$ nm (11). This pore size refers to the presence of Maxwell stress causing pore enlargement from an originally small value ($\bar{r}_p = 0.35 \pm 0.05$ nm) under the flow of electrolyte through the pores.

4.3. Electroporative Deformation of Cells in Tissue

The kinetic analysis developed for vesicles may be readily applied to tissue cells. The external electric field in tissue produces membrane pores as in isolated single cells and the electric Maxwell stress squeezes the cells (**Fig. 6B**) (12). The electromechanical cell squeezing can enlarge preexisting, or create new, pathways in the intercellular interstitial spaces, facilitating the migration of drugs and genes from the periphery to the more internal tissue cells. The results of single vesicles or vesicle aggregates finally aim at physicochemical guidelines to optimize the membrane electroporation techniques for the direct transfer of drugs and genes into tissue cells.

5. Electroporative Transport of Macromolecules

It is emphasized again that the ion efflux from the salt-filled vesicles in an electric field is caused by membrane electroporation and by the hydrostatic pressure under Maxwell stress and that the electrooptic signals reflect electroporative vesicle deformations coupled to ME. The analysis of electrooptic dichroisms yields characteristic parameters of ME such as electri-

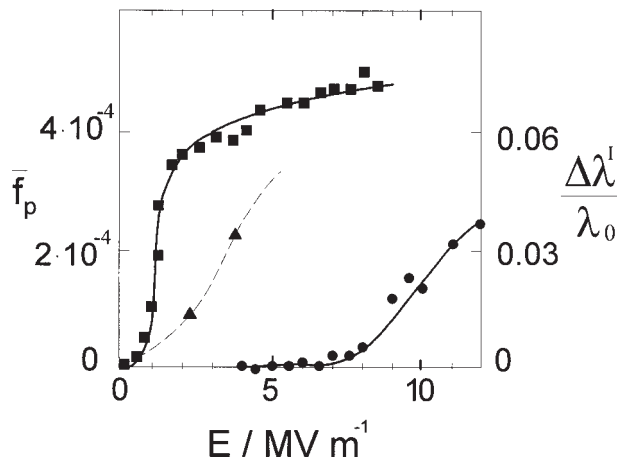


Fig. 7. The average fraction \bar{f}_p of the electroperated membrane area, (■) at a large NaCl concentration difference (in the vesicle interior $[\text{NaCl}]_{\text{in}} = 0.2 \text{ M}$, in the medium $[\text{NaCl}]_{\text{out}} = 0.2 \text{ mM}$, osmotically balanced with 0.284 M sucrose), (▲) at equal concentrations ($[\text{NaCl}]_{\text{in}} = [\text{NaCl}]_{\text{out}} = 0.2 \text{ mM}$, smoothly increases with the field strength E , whereas the massive conductivity increase $\Delta\lambda^1 / \lambda_0$, (●) of the suspension of the salt filled vesicles of radius $a = 160 \pm 30 \text{ nm}$ ($\lambda_0 = 7.5 \mu\text{S cm}^{-1}$, $T = 293 \text{ K}$ (20°C)) (18) indicates an apparent threshold value $E_{\text{thr}} = 7 \text{ MV m}^{-1}$. The ratio $\bar{f}_p = S(t_E) / S_m$ was calculated from the electrooptic relaxations, yielding characteristic rate parameters of the electroperation–resealing cycle in its coupling to ion transport.

cal pore densities for ion transport across the electroperated membrane patches. The fraction \bar{f}_p of the electroperated membrane surface (derived from electrooptics) smoothly increases with the field strength (Fig. 7). In terms of the chemical model there is no threshold of the field strength (4,18). Experimentally there is always a trivial threshold when the actual data points emerge out of the margin of measuring error. The conductivity increase ($\Delta\lambda^1 / \lambda_0$) in the suspension of the salt filled vesicles however appears to have a “threshold value” of the field strength (Fig. 7). The large pore dimensions refer to the pores maintained by medium efflow under Maxwell stress or reflect fragmentation of a small ($<1\%$) fraction of vesicles (*U. Brinkmann et al., unpublished data*).

5.1. Electroporative Transport of Ionic Macromolecules

The transport kinetics of larger macromolecules such as drugs and DNA indicates that there are several kinetically distinct stages. Transport is greatly facilitated if there is at first adsorption of the macromolecules to the membrane surface (10,24). For charged macromolecules, adsorption is followed by elec-

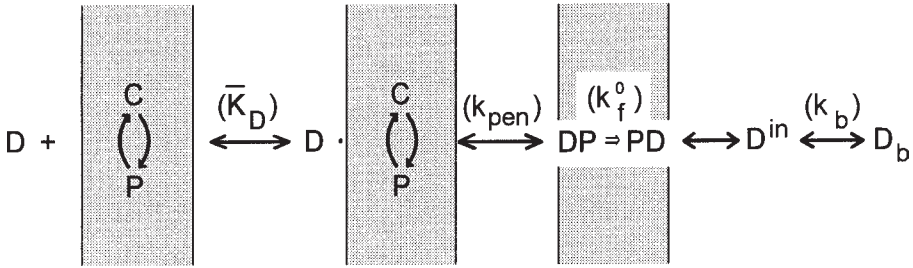


Fig. 8. Scheme for the coupling of the binding of a macromolecule (D), either a dyelike drug or DNA (described by the equilibrium constant \bar{K}_D of overall binding), electrodiffusive penetration (rate coefficient k_{pen}) into the outer surface of the membrane and translocation across the membrane, in terms of the transport coefficient k_f^0 ; and the binding of the internalized DNA or dye molecule (D^{in}) to a cell component b (rate coefficient k_b) to yield the interaction complex D_b as the starting point for the actual genetic cell transformation or cell coloring, respectively.

trophoretic penetration into the surface of electroporated membrane patches. Further steps are the afterfield diffusion, dissociation from the internal membrane surface and, finally, binding with cell components in the cell interior (Fig. 8) (9,10).

5.1.1. Surface Adsorption

The transient adsorption of potential permeants on the membrane surface may change both the local surface structure and the local membrane composition (phase separation) in the outer membrane leaflet. The alterations of the molecular structure and redistributions of membrane components can lead to local changes in the membrane's spontaneous curvature, bending rigidity and surface tension, respectively (31,32). Increased spontaneous curvature can either hinder or facilitate ME (30). For instance, the Ca^{2+} mediated adsorption of the protein annexinV to anionic lipids increases the lipid packing density by insertion of the tryptophan side chain into the membrane surface. This in turn, reduces the electroporability of the remaining membrane parts (30). Alternatively, the adsorption of plasmid DNA on the membrane surface, mediated by calcium or sphingosine, obviously facilitates ME and thus the transport of small ions (leak) and DNA itself across the membrane (10,37,38).

The degree of transformation f_T of yeast cells by plasmid DNA as a function of pulse duration is characterized by a long "delay phase" (Fig. 9A) (10). The delay phase gets shorter with increasing field strength. The degree f_C of cell coloring of B cells by dye SERVA blue G exhibits a similar functional dependence as f_T of yeast cells (Fig. 9B) (9).

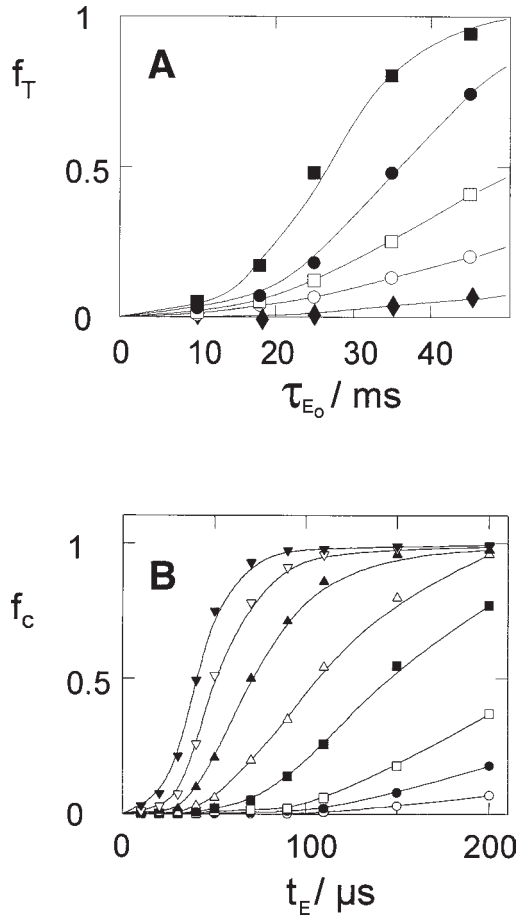


Fig. 9. Kinetics of the electroporative uptake of DNA and dye. (A) Degree of transformation f_T of yeast cells by plasmid DNA ($M_r = 3.5 \cdot 10^6$) and (B) degree of coloring f_C of mouse B cells by druglike dye SERVA blue G ($M_r = 854$) as a function of pulse duration at different field strengths: $E_0 / \text{kVcm}^{-1} = 2.5$ (\blacklozenge); 3.0 (\circ); 3.25 (\square); 3.5 (\bullet); 4.0 (\blacksquare), for cell transformation, and $E / \text{kV cm}^{-1}$: (\circ) 0.64; (\bullet) 0.85; (\square) 1.06; (\blacksquare) 1.28; (\triangle) 1.49; (\blacktriangle) 1.7; (∇) 1.91; (\blacktriangledown) 2.13, for cell coloring, respectively. E_0 is the amplitude and τ_{E_0} is the characteristic time constant of an exponential pulse used for the transformation of yeast cells by plasmid DNA ($M_r = 3.5 \cdot 10^6$). E is the amplitude and t_E is the duration of the rectangular pulse used for the coloring of mouse B cells by the (druglike) dye SERVA blue G ($M_r = 854$).

5.1.2. Flow Equation for Drug and DNA Uptake

The similarities of cell transformation and cell coloring suggest that the mechanism for the electroporative transport of both genes and drugs into

the cell interior has essential features in common. Therefore a general formalism was developed for the electroporative uptake of drug and genes.

In line with Fick's first law, the radial inflow (vector) of macromolecules is given by:

$$\frac{dn_c^{\text{in}}}{dt} = -D_m \cdot S_m \cdot \frac{dc_m}{dx}, \quad (20)$$

where n_c^{in} is the molar amount of the transported molecule in the compartment volume V_c , c_m and D_m are the concentration and the diffusion coefficient of the permeant in the membrane phase, respectively, S_m is the membrane surface through which the diffusional translocation occurs. The concentration gradient within the membrane is usually approximated by:

$$dc_m/dx = (c_m^{\text{out}} - c_m^{\text{in}})/d, \quad (21)$$

where c_m^{out} and c_m^{in} are the concentrations of the permeant in the outer and inner membrane/ medium interfaces, respectively (**Fig. 10**). The partition of the permeant between the bulk solution and the membrane surfaces may be quantified by a single distribution constant according to: $\gamma = c_m^{\text{out}}/c^{\text{out}} = c_m^{\text{in}}/c^{\text{in}}$, where c^{out} and $c^{\text{in}} = n_c^{\text{in}}/V_c$ are the bulk concentrations inside and outside the cell (or vesicle), respectively. We now define a flow coefficient k_f for the cross-membrane transport:

$$k_f = \frac{\gamma \cdot D_m}{d} \cdot \frac{S_m}{V_c} = \frac{P_m \cdot S_m}{V_c}, \quad (22)$$

where the permeability coefficient P_m for the porated membrane patches is given by:

$$P_m = \frac{\gamma \cdot D_m}{d} = k_f \cdot \frac{V_c}{S_m}. \quad (23)$$

P_m can be calculated from the experimental value of k_f , provided S_m is known. Substitution of **Eqs. 21** and **23** into **Eq. 20** yields the linear inflow equation:

$$dc^{\text{in}}/dt = -k_f \cdot (c^{\text{out}} - c^{\text{in}}).$$

Frequently, the external volume V_0 is much larger than the intracellular or intravesicular volume, that is, $N_c \cdot V_c \ll V_0$, where N_c is the number of cells or vesicles in suspension. Mass conservation dictates that the amount n^{out} of permeant in the outside volume is given by $n^{\text{out}} = n_0 - n_c^{\text{in}} \cdot N_c$. Hence the inequality $N_c \cdot V_c \ll V_0$ yields: $c^{\text{out}} = n^{\text{out}}/V_0 = c_0 - c^{\text{in}} \cdot N_c \cdot V_c/V_0 \approx c_0$, where n_0 and $c_0 = n_0/V_0$ are the initial amount and the initial total concentration of

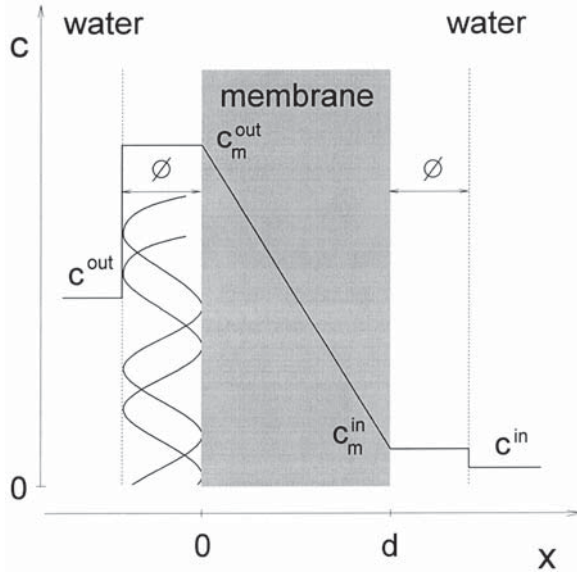


Fig. 10. Profile of concentration of a lipid-soluble or surface adsorbed permeant across the lipid plasma membrane of the thickness d , between the outer (out) and inner (in) cell compartments, respectively, in the direction x . Because of adsorption of permeant on the cell surface, the bulk concentrations c^{out} and c^{in} of the permeant are smaller than c_m^{out} and c_m^{in} , respectively; c_m refers to the very small volume of a shell with thickness δ , where δ is given by the diameter of the flatly adsorbed DNA, sketched as double-helical backbones. For the data in **Fig. 9A**, the distribution constant is $\gamma = c_m^{\text{out}}/c^{\text{out}} = 1.3 \cdot 10^3$.

the permeant in the outside volume, respectively. Substitution of the approximation $c^{\text{out}} = c_0$ into the flow equation yields the simple transport equation:

$$\frac{dc^{\text{in}}}{dt} = -k_f \cdot (c_0 - c^{\text{in}}) \quad (24)$$

If the effective diffusion area S_m changes with time, for instance, due to electroporation-resealing processes, the flow coefficient $k_f(t)$ is time-dependent. In this case we may specify $S_m(t)$ with the degree of electroporation f_p according to $S_m(t) = f_p(t) \cdot S_c$, where $S_c = 4\pi \cdot a^2$ is the total area of the outer membrane surface. The explicit form of the pore fraction $f_p(t)$ is dependent on the model applied. The time dependent flow coefficient can now be expressed as: $k_f(t) = k_f^0 \cdot f_p(t)$, where the characteristic flow coefficient for the radial inflow is defined by

$$k_f^0 = \frac{P_m \cdot S_c}{V_c} = \frac{3 \cdot P_m}{a}. \quad (25)$$

Note that k_f^0 and thus P_m are independent of the electrical pulse parameters E and t_E . Hence these transport quantities are suited to compare vesicles and cells of different size and different lipid composition. Substitution of $k_f(t) = k_f^0 \cdot f_p(t)$ into **Eq. 24** and integration yields the practical equation for the increase in the internal permeant concentration with time:

$$c^{\text{in}} = c_0 \cdot \left\{ 1 - \exp \left[-k_f^0 \cdot \left(\int_{t_0}^{t_E} f_p^{C \rightarrow P}(t) dt + \int_{t_E}^{t_{\text{obs}}} f_p^{P \rightarrow C}(t) dt \right) \right] \right\}. \quad (26)$$

If the transported molecules are added before the pulse, we have $t_0 = 0$. For the postfield addition the first integral for $f_p^{C \rightarrow P}$ in **Eq. 26** cancels and we set $t_E = t_0 = t_{\text{add}}$, where t_{add} is the time point of adding the molecules after pulse termination (t_E). Usually, the appearance of the transported molecules becomes noticeable at observation times t_{obs} which are much larger (min) than the characteristic time of pore resealing $(k_{-1})^{-1}$ which is in the milliseconds to seconds time range. For these cases the approximation $t_{\text{obs}} \rightarrow \infty$ holds (**9,10**). Note that the integrals in **Eq. 26** contain implicitly the pulse duration t_E and the field strength E in the degree of poration $f_p(t, t_E, E)$.

In the case of charged macromolecules like DNA or the dye SBG, the presence of an electric field across the membrane causes electrodiffusion. The enhancement of the transport of a macroion only refers to that side of the cell or vesicle where the electric potential drop $\Delta\phi_m$ is in the favorable direction. The electrodiffusive efflux of the macromolecules from the cell cytoplasm is usually negligibly small compared with the influx and may be neglected. Formally, for the boundaries t_0 and t_E , D_m in **Eq. 26** must be replaced by the electrodiffusional coefficient (**10**):

$$D_m(E) = D_m \cdot \left(\frac{1 + |z_{\text{eff}}| \cdot e_0 \cdot \Delta\phi_m}{kT} \right), \quad (27)$$

where $\Delta\bar{\phi}_m = -(3/8) a E \cdot f(\bar{\lambda}_m)$ is the θ average transmembrane potential drop, $\bar{\lambda}_m$ the angular average of the membrane conductivity and z_{eff} the effective charge number (with sign) of the transported macromolecule.

On the same line, the permeability coefficient with respect to electrodiffusion is given by:

$$P_m(E) = \frac{\gamma \cdot D_m(E)}{d}. \quad (28)$$

It is instructive to compare the present analysis of (electro) diffusion through porous membrane patches characterized by the quantities k_f^0 , P_m , and f_p with the conventional approach with the permeability coefficient P in the context of

formally $f_p = 1$. The conventional coefficient P is related to P_m of the present analysis by: $P = f_p(t_E) \cdot P_m$.

The analysis of the kinetic data of cell transformation and cell coloring by dyes (**Fig. 9**) suggests that the rate-limiting step is the binding of the permeants to intracellular components. The simplest binding scheme is given by (*see Fig. 8*):



where D^{in} symbolizes the macromolecules in the cell interior (c^{in}), b the yet unoccupied binding sites in the cell and k_b is the overall rate coefficient of binding. The degree of binding of molecule D is defined by:

$$f_b = [D_b] / [b_0], \quad (30)$$

where $[D_b]$ is the concentration of bound macromolecules and $[b_0]$ is the total concentration of binding sites in the cell interior.

The integration of the binding rate equation $d[D_b] / dt = k_b \cdot c^{\text{in}} \cdot [b]$ for the **Eq. 29**, and substitution of **Eq. 26** yields (**10**):

$$f_b(t_E, t_{\text{obs}}) = \frac{c^{\text{in}} \cdot \{1 - \exp A\}}{[b_0] - c^{\text{in}} \cdot \exp A}, \quad (31)$$

where the dependence on t_E and t_{obs} is explicitly in $c^{\text{in}}(t_E, t_{\text{obs}})$ and

$$A(t_E, t_{\text{obs}}) = k_b \cdot t_{\text{obs}} \cdot (c^{\text{in}}(t_{\text{obs}}, t_E) - [b_0]).$$

For the cell transformation the time of observation is $t_{\text{obs}} \approx 2$ hours. Note that $c^{\text{in}}(t_E, t_{\text{obs}})$ refers to the total amount of the transported molecule which enters the cell interior in the time interval $t_0 \leq t \leq t_{\text{obs}}$ when a pulse of duration t_E was applied. In a previous study the equation for f_b contains a misprint (**10**).

As previously suggested (**24**), the degree of transformation $f_T = T / T_{\text{max}}$, where T_{max} is the maximum number of transformants, may be equated with the degree of bound molecules f_b . Hence the data analysis uses $f_{T/C} = f_b$ and **Eq. 31**. Obviously, at least one binding site b has to be occupied with DNA to permit transformation. In the following we present the reevaluation of previous data in terms of the transport parameters k_f^0 , P_m , and f_p .

5.2.1. Uptake of DNA by Yeast Cells

For an efficient uptake, DNA should be present, preferably adsorbed already before pulse application. Both the adsorption of DNA, directly measured with ^{32}P -dC DNA, and the number of transformants are collinearly enhanced with increasing total concentrations $[D_t]$ and $[Ca_t]$ of DNA and of Ca^{2+} , respectively. At the total bulk concentration $[D_t] = 2.7$ nM, the molar concentration of DNA bound to the membrane surface amounts to $[D_b^s] = 2$ nM

(10). At the cell density $\rho_c = 10^9 \text{ cm}^{-3}$, there are $N_{\text{DNA}} = N_A \cdot [D_b^s] / \rho_c = 1.2 \cdot 10^3$ DNA molecules per cell of radius $a = 2.7 \text{ }\mu\text{m}$. Presumably all adsorbed DNA is located in the head group region of the outer leaflet of membrane bilayer. The actual concentration of DNA in the membrane surface refers to a thin layer of thickness $\theta = 2.37 \text{ nm}$, where θ is the diameter of the β helix of DNA. We obtain $c_m^{\text{out}} = [D_b^s] / (\rho_c \cdot S_c \cdot \theta) = 9.2 \text{ }\mu\text{M}$ (Fig. 10). Since the bulk concentration of DNA is $c^{\text{out}} = [D_t] - [D_b^s] = 0.7 \text{ nM}$, the partition coefficient amounts to $\gamma = c_m^{\text{out}} / c^{\text{out}} = 1.3 \cdot 10^3$; that is, the concentration of the adsorbed DNA is about 10^3 -fold larger than the bulk concentration. This feature was not considered so far and requires a partial reevaluation of previous data (10), Fig. 9A, where it was found that the direct electroporative transfer of plasmid DNA (YEpl 351, 5.6 kbp, supercoiled, $M_r \approx 3.5 \cdot 10^6$) in yeast cells (*Saccharomyces cerevisiae*, strain AH 215) is basically due to (electro) diffusive processes. At the field strength $E_0 = 4.0 \text{ kV cm}^{-1}$, the diffusion coefficient ratio is $D_m(E) / D_m \approx 10.3$. Hence electrodiffusion of DNA is about 10 times more effective than simple diffusion. Addition of DNA after the field pulse only occasionally leads to transformants. The most decisive stage in the cell transformation is the electrodiffusive surface penetration of DNA followed either by further electrodiffusive, or by passive (after field) diffusive, translocation of the inserted DNA into the cell interior (Fig. 8).

Actually, the rather long sigmoid phase of $f_T(t_E)$, Fig. 9A, requires a description in terms of an at least two-step process: $C \xrightarrow{k_p} P_1 \xrightarrow{k_p} P_2$, where the state P_1 denotes pore structures of negligible permeability for DNA; P_2 is the porous membrane state of finite permeability for DNA. The electroporation rate coefficient k_p is assumed to be the same for both steps, associated with the same reaction volume $\Delta_r V_p$. This assumption is theoretically justified by the corresponding minima in the hydrophobic force profiles as a function of pore radius (39). Pore resealing, that is, the reverse reaction steps ($P_2 \rightarrow P_1 \rightarrow C$), may be neglected for the time range $0 \leq t \leq t_E$ in the presence of the external field. We recall that k_p explicitly occurs in the integral:

$$\int_0^{t_E} f_p^{C \rightarrow P}(t) dt = f_p^0 \cdot \{t_E + k_p^{-1}[(2 + k_p \cdot t_E) \cdot e^{-k_p t_E} - 2]\},$$

where $f_p^{C \rightarrow P} = f_p^0 \cdot \{1 - (1 + k_p \cdot t) \cdot e^{-k_p t}\}$ for the reaction $P_2 \rightarrow P_1 \rightarrow C$ and f_p^0 is the amplitude value of $f_p^{C \rightarrow P}(t)$. Applying Eq. 31 for the exponential pulse of the initial field strength $E_0 = 4.0 \text{ kV cm}^{-1}$ and the decay time constant $\tau_E = 45 \text{ ms}$, we find with $t_E = \tau_E$ that $k_p = 7.2 \text{ s}^{-1}$.

The mean minimum radius of DNA-permeable pores has been calculated from the field dependence of $k_p(E_0)$: $\bar{r}_p(P_2) = 0.39 \pm 0.05 \text{ nm}$ (10). If we assume that deviations of the data points from the relationship

$$\ln(k_p/k_p(E=0)) = b * \cdot \cos^2 \theta \cdot E^2,$$

where

$$b^* = (9/8) \cdot \pi \cdot \epsilon_0 \cdot a^2 \cdot (\epsilon_W - \epsilon_L) \cdot \bar{r}_p^2 \cdot N_A \cdot f^2(\bar{\lambda}_m) \cdot E^2 / (d \cdot kT)$$

at higher field strengths is due to the increase in the average transmembrane conductivity by $\Delta\bar{\lambda}_m = 2.5 \cdot 10^{-7} \text{ S cm}^{-1}$ from $\bar{\lambda}_m(E_0 = 0)$ to $\bar{\lambda}_m(E_0 = 4 \text{ kV cm}^{-1}) = \bar{\lambda}_m(E_0 = 0) + \Delta\bar{\lambda}_m$. This conductivity increase corresponds to a replacement of 0.0025% of the membrane area by pores filled with the intracellular medium of conductivity $\lambda_i = 1.0 \cdot 10^{-2} \text{ S cm}^{-1}$ under Maxwell stress. The fractional increase in the transport area for small ions (Na^+ , Cl^-) is given by $f_p^i = \Delta\bar{\lambda}_m / \lambda_i = 2.5 \cdot 10^{-5}$ (15). For these conditions the mean number of conductive pores per cell is $\bar{N}_p = S_c \cdot f_p / \pi \cdot \bar{r}_p^2 = 4.8 \cdot 10^3$, corresponding to an average minimum distance between the pore centers $\bar{l}_p = (S_c / N_p)^{1/2} = 138 \text{ nm}$. In order to estimate the permeability coefficient P_m of DNA, one may identify the fraction f_p of DNA permeable membrane area (pore state P_2) with that of small ions: $f_p = f_p^i$. If the DNA permeable membrane area is smaller than the area of ion permeable pores: $f_p < f_p^i$, we obtain only an upper limit of P_m for DNA.

Apparently, the mean radius $\bar{r}_p(P_2) = 0.39 \text{ nm}$ of the pores in DNA-permeable pore patches is too small for free diffusion of large plasmid DNA. Such a small pore radius is not even sufficient for the entrance of a free end of a linear DNA molecule, because the diameter of the type B-DNA is $\varnothing \approx 2.37 \text{ nm}$. Nevertheless, small parts of the adsorbed DNA may interact with many small pores, and the DNA-polymer may penetrate part by part into the membrane. The total length of a 6.5 kbp DNA is about $l_{\text{DNA}} = 6.5 \cdot 10^3 \cdot 0.34 \text{ nm} = 2.2 \cdot 10^3 \text{ nm}$ and the corresponding surface area on the membrane is $S_{\text{DNA}} = l_{\text{DNA}} \cdot \varnothing = 5.2 \cdot 10^3 \text{ nm}^2$. On average, one totally adsorbed DNA may cover only $4 \cdot N_p \cdot S_{\text{DNA}} / S_c \approx 1$ membrane electropore in the cell pole caps (see **Fig. 4**). Since the DNA is probably only partially inserted into porous patches, the regions can be considered as closed, but leaky. If the occlusions locally decrease the membrane conductivity, the transmembrane field gets larger such that the membrane somewhere in the vicinity of the inserted DNA part is electroporated. As a consequence, a neighboring part of DNA can penetrate into the newly porated membrane patch. In any case the interaction of the adsorbed DNA with the lipid membrane appears to largely facilitate ME, yielding larger transiently occluded pores. Leaky porelike channel structures are indicated by ionic current events if DNA interacts with lipid bilayers. Furtheron, if DNA is present in the medium, there is a sharp increase in the membrane permeability of Cos-1 cells to fluorescent dextrin molecules in the electric field (40).

The reevaluation of the data (**Fig. 9**) for $E_0 = 4.0 \text{ kV cm}^{-1}$ and $t_E = \tau_E = 45 \text{ ms}$ yields $k_f = 2 \cdot 10^2 \text{ s}^{-1}$. With $f_p(t_E) \approx f_p^i = 2.5 \cdot 10^{-5}$ the characteristic flow coefficient is $k_f^0 = \gamma \cdot D_m(E) \cdot S_c / d \cdot V_c = 8.0 \cdot 10^6 \text{ s}^{-1}$ at $T = 293 \text{ K}$. From **Eq. 23** we obtain the corresponding permeability coefficient $P_m = k_f^0 \cdot a / 3 = 7.2 \cdot 10^2 \text{ cm s}^{-1}$. Because $D_m(E) = D_m \cdot 10.3$, we see that at $E = 0$ formally $P_m^0 = P_m / 10.3 = 70 \text{ cm s}^{-1}$. Note that the conventional membrane permeability coefficient P^0 refers to the total membrane surface area by $P^0 = P_m^0 \cdot f_p(t_E) = 1.8 \cdot 10^{-3} \text{ cm s}^{-1}$. With $\gamma = 1.3 \cdot 10^3$ and $d = 5 \text{ nm}$, the electrodiffusion coefficient $D_m(E)$ of DNA in the electroporated membrane patches at $E = 4 \text{ kV cm}^{-1}$ is $D_m(E) = P_m d / \gamma = 2.8 \cdot 10^{-7} \text{ cm}^2 \text{ s}^{-1}$, and at $E = 0$ we have $D_m = D_m(E) / 10.3 = 2.7 \cdot 10^{-8} \text{ cm}^2 \text{ s}^{-1}$. If the diffusion of DNA is formally related to the total membrane surface (electroporated patches and the larger nonelectroporated part), $D = D_m \cdot f_p(t_E) = 6.7 \cdot 10^{-13} \text{ cm}^2 \text{ s}^{-1}$. Compared with the diffusion coefficient of free DNA in solution $D^{\text{free}} \approx 5 \cdot 10^{-8} \text{ cm}^2 \text{ s}^{-1}$ (**41**), the bulk diffusion is about $7 \cdot 10^4$ -fold faster than the interactive diffusion of DNA through the electroporated membrane, reflecting the occluding interaction of DNA with perhaps many small membrane electropores.

For practical purposes of optimum transformation efficiency, 1 mM Ca^{2+} is necessary for sufficient DNA binding and the relatively long pulse duration of 20–40 ms is required to achieve efficient electrodiffusive transport across the cell wall and into the outer surface of electroporated cell membrane patches.

5.2.2. Uptake of Druglike Dyes by Mouse B Cells

The color change of electroporated intact Fc γ R⁻ mouse B cells (line IIA1.6, cell diameter 25 μm) after direct electroporative transfer of the drug-like dye Serva Blue G (SBG) ($M_r = 854$) into the cell interior is shown to be prevalingly due to diffusion of the dye *after* the electric field pulse (**9**). The net influx of the dyes ceases, even if the pores stay open, when the concentration equality $c^{\text{in}} \approx c_0$ is attained. For this limiting case, the fraction $f_c = c^{\text{in}} / c_0$ of the colored cells equals unity. The data in (**Fig. 9**) suggest that at least three different pore states (P) in the reaction cascade $C \rightleftharpoons P_1 \rightleftharpoons P_2 \rightleftharpoons P_3$ are required to model the sigmoid kinetics of pore formation as well as the biphasic pore resealing. The rate coefficient for pore formation k_p was taken equal for all the three steps: $C \rightleftharpoons P_1$, $P_1 \rightleftharpoons P_2$ and $P_2 \rightleftharpoons P_3$. At $E = 2.1 \text{ kV cm}^{-1}$ and $T = 293 \text{ K}$, we find from the respective integral $\int f_p^{C \rightarrow P}(t) dt$ that $k_p = 2.4 \pm 0.2 \times 10^3 \text{ s}^{-1}$. The resealing rate coefficients are $k_{-2} = 4.0 \pm 0.5 \times 10^{-2} \text{ s}^{-1}$ and $k_{-3} = 4.5 \pm 0.5 \times 10^{-3} \text{ s}^{-1}$, independent of E as expected for $E = 0$. Analysis of the field dependence of $k_p(E)$ yields the mean radius of the dye permeable pore state $\bar{r}(P_3) = 1.2 \pm 0.1 \text{ nm}$ (**9**).

The maximum value of the fractional surface area of the dye-conductive pores is approximated by the fraction of conductive pores: $f_p = \Delta \bar{\lambda}_m / \lambda_i =$

$1.0 \cdot 10^{-3}$, where $\overline{\Delta\lambda_m} = 1.3 \cdot 10^{-5} \text{ S cm}^{-1}$ is the increase in the transmembrane conductivity at $E = 2.1 \text{ kV cm}^{-1}$ and $\lambda_i = 1.3 \cdot 10^{-2} \text{ S cm}^{-1}$. Hence the maximum number of dye permeable pores is $N_p = S_c \cdot f_p / \pi \cdot \bar{r}_p^2(P_3) = 4.4 \cdot 10^5$ per average cell, where $S_c = 4 \cdot \pi \cdot a^2 = 2.0 \cdot 10^{-5} \text{ cm}^2$. Data reevaluation yields $k_f = 1 \cdot 10^{-2} \text{ s}^{-1}$. From $k_f(t) = k_f^0 \cdot f_p(t)$ we obtain the characteristic flow coefficient $k_f^0 = (1.0 \pm 0.1) \cdot 10^1 \text{ s}^{-1}$. Since there is no evidence for adsorption of SBG on the membrane surface, the partition coefficient was assumed to be $\gamma \approx 1$. The corresponding permeability coefficient of dye in the pores is: $P_m = k_f^0 \cdot a/3 = 4.2 \cdot 10^{-3} \text{ cm s}^{-1}$. If the permeability coefficient is related to the total membrane surface area, we obtain $P = P_m \cdot f_p = 4.2 \cdot 10^{-6} \text{ cm s}^{-1}$. The diffusion coefficient of SBG is $D_m = P_m \cdot d = 2.1 \cdot 10^{-9} \text{ cm}^2 \text{ s}^{-1}$ and $D = D_m \cdot f_p = 2.1 \cdot 10^{-12} \text{ cm}^2 \text{ s}^{-1}$, respectively. It is seen that D_m is by the factor $D^{\text{free}} / D_m = 2.4 \cdot 10^{-5}$ smaller than $D^{\text{free}} = 5 \cdot 10^{-6} \text{ cm}^2 \text{ s}^{-1}$ estimated for free dye diffusion. This large difference apparently indicates transient interaction of the dye with the pore lipids during translocation and partial occlusion of the pores.

5.3. Field–Time Relationship for the Electroporative Transport

Obviously the two pulse parameters E and t_E are of primary importance to control extent and rate of the transmembrane transport. Within certain ranges of E and t_E a relationship of the type $E^2 \cdot t_E = c$ holds (**Fig. 11**), where c is a constant (**9,10,26**). However, very large field strengths or very long pulse durations may lead to secondary effects like bleb formation (**9**) or fragmentation of the vesicles and cells under Maxwell stress. Therefore in the range of massive cell deformation and fragmentation the constant c has a different value than in the range of short pulse durations. In any case, the empirical correlation $E^2 \cdot t_E = \text{constant}$ is theoretically rationalized in terms of the interfacial polarization mechanism of ME (**24,26**).

6. Summary and Conclusions

Since the electroporative transport of permeants is caused by ME, the transport quantities $f_T(t)$ and $f_C(t)$ are closely connected to the degree $f_p(t)$ of ME, permitting to investigate the mechanism of formation and development of membrane pores by the electric field. The results of our theoretical approach, based on electrooptical data of vesicles, as well as on the kinetics of cell electrotransformation and cell coloring, can be used to specify conditions for the practical purposes of gene transfer and drug delivery into the cells. In electrochemotherapy, for instance, the optimization of the electroporative channeling of the cytotoxic drugs into the tissue cells may be refined by using the electroporative transport theory (**4,42–44**). Future work may include optical probes like DPH in cell plasma membranes to elucidate the sequence of events of the electroporative DNA and protein transfers as well as to investigate

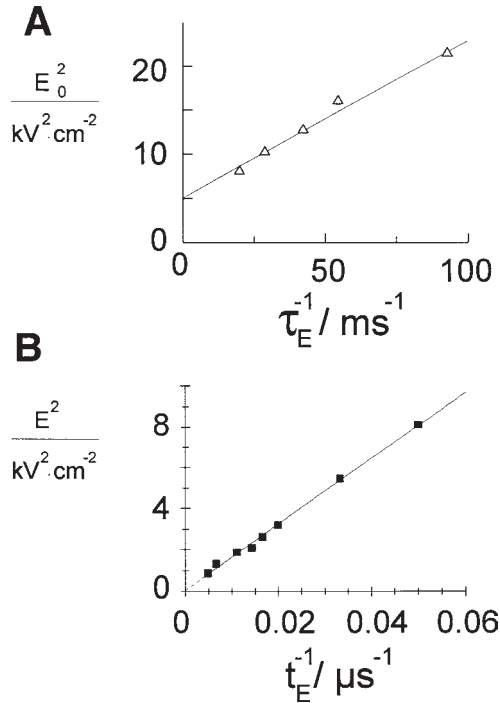


Fig. 11. Field strength/pulse duration relationship. The data refer to the selected fraction f of (A) transformed ($f_T = 0.5$) and (B) colored cells ($f_C = 0.5$). Experimental parameters as in Fig. 9. The linear dependencies are consistent with the interfacial electric polarization mechanism ($E^2 \cdot t_E = c$) preceding cell membrane electroporation.

molecular details of other electroporation phenomena such as electrofusion and electroinsertion.

In conclusion, the theory of ME has been developed to such a degree that analytical expressions are available for the optimization of the ME techniques in biotechnology and medicine, in particular in the new fields of electroporative drug delivery and gene therapy. The electroporative gene vaccination is certainly a great challenge for modern medicine.

Acknowledgments

We thank the Deutsche Forschungsgemeinschaft for grant Ne 227/9-2 to E. Neumann.

Glossary

SBG	Serva Blue G
[Ca _t]	total concentration of Ca

$[D_t] = c^0$	total concentration of DNA
$[D_b]$	concentration of bound DNA
$[P_2]$	concentration of DNA-permeable pores
$[P_3]$	concentration of SBG-permeable pores
a	cell/vesicle radius
$c_m^{\text{out}}, c_m^{\text{in}}$	molar concentrations of the permeant in the outer and inner membrane/medium interfaces, respectively
$c^{\text{out}}, c^{\text{in}}$	bulk concentrations of the permeant inside and outside the cell (or vesicle), respectively
c_0	initial total concentration of permeant in the outside medium
D_m	diffusion coefficient in electroporated membrane patches
$D_m(E)$	electrodiffusion coefficient in electroporated membrane patches
D	diffusion coefficient related to the total membrane surface area
$[D_b]$	concentration of bound macromolecules to the intracellular sites
$[D_b^s]$	concentration of bound macromolecules to the membrane surface
E	electric field strength
E_m	transmembrane field strength
e	elementary charge
ϵ_0	vacuum permittivity
ϵ_w	dielectric constant of water
ϵ_L	dielectric constant of the lipid phase
f_T	degree of cell transformation
f_C	degree of cell coloring
f_b	degree of binding of permeants to intracellular sites
f_p	fraction of porated membrane area
$f(\lambda_m)$	conductivity factor
γ	partition coefficient of permeant between membrane and solution
$\Delta\phi_m$	electrical potential difference across the electroporated membrane patches
k_1	rate coefficient for the step $C \rightarrow P$
k_{-1}	rate coefficient for the step $P \rightarrow C$
k	Boltzmann constant
k_b	rate coefficient for intracellular permeant binding ($M^{-1} s^{-1}$)
k_p	electroporation rate coefficient (s^{-1})
k_f	flow coefficient for cross-membrane transport (s^{-1})
k_f^0	characteristic flow coefficient (s^{-1}), independent of E and t_E
λ_m	transmembrane conductivity ($S m^{-1}$)
λ_0	conductivity of bulk solution
λ_i	conductivity of cell interior
N_p	number of electropores per cell
n_c^{in}	molar amount of DNA or SBG in one cell

n^{out}	molar amount of DNA or SBG in the bulk solution
P_m	permeability coefficient for the electroporated membrane patches
P	conventional permeability coefficient (related to the total membrane)
\bar{r}_p	mean pore radius
ρ_c	cell density
S_c	cell surface area
S_m	electroporated area of cell surface
S_p	surface area of the average pore
t_E	electrical pulse duration
τ_E	decay time constant of an exponentially decaying field pulse
V_c	volume of an average cell
V_0	external volume
z_i	charge number (with sign) of ion i
z_{eff}	effective charge number of the DNA-phosphate group

References

1. Neumann, E. and Rosenheck K. (1972) Permeability changes induced by electric impulses in vesicular membranes. *J. Membr. Biol.* **10**, 279–290.
2. Wong, T. K. and Neumann, E. (1982) Electric field mediated gene transfer. *Biophys. Biochem. Res. Commun.* **107**, 584–587.
3. Neumann, E., Schaefer-Ridder, M., Wang, Y., and Hofschneider, P. H. (1982) Gene transfer into mouse lyoma cells by electroporation in high electric fields. *EMBO J.* **1**, 841–845.
4. Neumann, E. and Kakorin, S. (1998) Digression on membrane electroporation and electroporative delivery of drugs and genes. *Radiol. Oncol.* **32**, 7–17.
5. Neumann, E., Gerisch, G., and Opatz, K. (1980) Cell fusion induced by electric impulses applied to dictyostelium. *Naturwissenschaften* **67**, 414–415.
6. Mouneimne, Y., Tosi, P. F., Gazitt, Y., and Nicolau, C. (1989) Electro-insertion of xenoglycophorin into the red blood cell membrane. *Biochem. Biophys. Res. Commun.* **159**, 34–40.
7. Pliquett, U., Zewert, T. E., Chen, T., Langer, R., and Weaver, J. C. (1996) Imaging of fluorescent molecule and small ion-transport through human stratum-corneum during high-voltage pulsing-localized transport regions are involved. *Biophys. Chem.* **58**, 185–204.
8. Mir, L. M., Orłowski, S., Belehradek, J. Jr., Teissié, J., Rols, M. P., Serša, G., Miklavčič, D., Gilbert, R., and Heller, R. (1995) Biomedical applications of electric pulses with special emphasis on antitumor electrochemotherapy. *Bioelectrochem. Bioenerg.* **38**, 203–207.
9. Neumann, E., Toensing, K., Kakorin, S., Budde, P., and Frey, J. (1998) Mechanism of electroporative dye uptake by mouse B cells. *Biophys. J.* **74**, 98–108.
10. Neumann, E., Kakorin, S., Tsoneva, I., Nikolova, B., and Tomov, T. (1996) Calcium-mediated DNA adsorption to yeast cells and kinetics of cell transformation. *Biophys. J.* **71**, 868–877.

11. Kakorin, S., Redeker, E., and Neumann, E. (1998) Electroporative deformation of salt filled lipid vesicles. *Eur. Biophys. J.* **27**, 43–53.
12. Kakorin, S. and Neumann, E. (1998) Kinetics of electroporation deformation of lipid vesicles and biological cells in an electric field. *Ber. Bunsenges. Phys. Chem.* **102**, 670–675.
13. Winterhalter, M., Klotz, K.-H., Benz, R., and Arnold, W. M. (1996) On the dynamics of the electric field induced breakdown in lipid membranes. *IEEE Trans. Ind. Appl.* **32**, 125–128.
14. Chang, C. (1992) Structure and dynamics of electric field-induced membrane pores as revealed by rapid-freezing electron microscopy. *Guide to Electroporation and Electrofusion* (Chang, C., Chassy, M., Saunders, J., and Sowers, A., eds.), Academic Press, San Diego, CA, pp. 9–28.
15. Hibino, M., Itoh, H., and Kinosita, K. (1993) Time courses of cell electroporation as revealed by submicrosecond imaging of transmembrane potential. *Biophys. J.* **64**, 1789–1800.
16. Weaver, J. C. (1994) Molecular-basis for cell-membrane electroporation. *Ann. N.Y. Acad. Sci.* **720**, 141–152.
17. Weaver, J. and Chizmadzhev, Yu. (1996) Theory of electroporation: A review. *Bioelectrochem. Bioenerg.* **41**, 135–160.
18. Neumann, E. and Kakorin, S. (1996) Electrooptics of membrane electroporation and vesicle shape deformation. *Curr. Opin. Colloid Interface Sci.* **1**, 790–799.
19. Kakorin, S., Stoylov, S. P., and Neumann, E. (1996) Electro-optics of membrane electroporation in diphenylhexatriene-doped lipid bilayer vesicles. *Biophys. Chem.* **58**, 109–116.
20. Kinosita, Jr., Hibino, M., Itoh, H., Shigemori, M., Hirano, H., Kirino, Y., and Hayakawa, T. (1992) Events of membrane electroporation visualized on time scale from microsecond to second. *Guide to Electroporation and Electrofusion* (Chang, C., Chassy, M., Saunders, J., and Sowers, A., eds.), Academic Press, San Diego, CA, pp. 29–47.
21. Neumann, E. (1989) The relaxation hysteresis of membrane electroporation. *Electroporation and Electrofusion in Cell Biology* (Neumann, E., Sowers, A. E., and Jordan, C., eds.), Plenum, New York, pp. 61–82.
22. Smaby, J. and Brockman, H. (1990) Surface dipole moments of lipids at the argon–water interface. *Biophys. J.* **58**, 195–204.
23. Cevc, G. and Seddon, J. (1993) Physical characterization. *Phospholipid Handbook* (Cevc G., ed.), Marcel Dekker, New York, pp. 351–402.
24. Neumann, E. (1992) Membrane electroporation and direct gene transfer. *Biochem. Bioenerg.* **28**, 247–267.
25. Cevc, G. (1990) Membrane electrostatics. *Biochim. Biophys. Acta* **1031**, 311–382.
26. Neumann, E. and Boldt, E. (1989) Membrane electroporation: Biophysical and biotechnical aspects. *Charge and Field Effects in Biosystems*, Vol. 2 (Allen, M., Cleary, S., and Hawkrige, F., eds.), Plenum, New York, pp. 373–382.
27. Neumann, E. (1986) Elementary analysis of chemical electric field effects in

- biological macromolecules I and II. *Modern Bioelectrochemistry* (Gutmann, F. and Keyzer, H., eds.), Plenum, New York, pp. 97–132 and 133–175.
28. Neumann, E. (1986) Chemical electric field effects in biological macromolecules. *Prog. Biophys. Mol. Biol.* **47**, 197–231.
 29. Steiner, U. and Adam, G. (1984) Interfacial properties of hydrophilic surfaces of phospholipid films as determined by method of contact angles. *Cell Biophys.* **6**, 279–299.
 30. Tönsing, K., Kakorin, S., Neumann, E., Liemann, S., and Huber, R. (1997) Annexin V and vesicle membrane electroporation. *Eur. Biophys. J.* **26**, 307–318.
 31. Seifert, U. and Lipowsky, R. (1995) Morphology of vesicles. *Structure and Dynamics of Membranes*, Vol. 1A (Lipowsky, R. and Sackmann, E., eds.), Elsevier, Amsterdam, pp. 403–463.
 32. Lipowsky, R. (1998) Vesicles and Biomembranes. *Encycl. Appl. Phys.* **23**, 199–222.
 33. Winterhalter, M. and Helfrich, W. (1988) Effect of surface charge on the curvature elasticity of membranes. *J. Phys. Chem.* **92**, 6865–6867.
 34. Fogden, A., Mitchell, D. J., and Ninham B. W. (1990) Undulations of charged membranes. *Langmuir* **6**, 159–162.
 35. Abidor, I. G., Arakelyan, V. B., Chernomordik, L. V., Chizmadzhev, Y. A., Pastuchenko, V. P., and Tarasevich, M. R. (1979) Electric breakdown of bilayer lipid membrane. I. The main experimental facts and their theoretical discussion. *Bioelectrochem. Bioenerg.* **6**, 37–52.
 36. Klösgen, B. and Helfrich, W. (1993) Special features of phosphatidylcholine vesicles as seen in cryo-transmission electron-microscopy. *Eur. Biophys. J.* **22**, 329–340.
 37. Spassova, M., Tsoneva, I., Petrov, A. G., Petkova, J. I., and Neumann, E. (1994) Dip patch clamp currents suggest electrodiffusive transport of the polyelectrolyte DNA through lipid bilayers. *Biophys. Chem.* **52**, 267–274.
 38. Hristova, N. I., Tsoneva, I., and Neumann, E. (1997) Sphingosine-mediated electroporative DNA transfer through lipid bilayers. *FEBS Lett.* **415**, 81–86.
 39. Israelachvili, J. N. and Pashley, R. M. (1984) Measurement of the hydrophobic interaction between two hydrophobic surfaces in aqueous electrolyte solutions, *J. Colloid Interface Sci.* **98**, 500–514.
 40. Sukharev, S. I., Klenchin, V. A., Serov, S. M., Chernomordik, L. V., and Chizmadzhev, Y. A. (1992) Electroporation and electrophoretic DNA transfer into cells: The effect of DNA interaction with electropores. *Biophys. J.* **63**, 1320–1327.
 41. Chirico, G., Beretta, S., and Baldini, G. (1992) Light scattering of DNA plasmids containing repeated curved insertions: Anomalous compaction. *Biophys. Chem.* **45**, 101–108.
 42. Mir, L., Tounekti, O., and Orlowski, S. (1996) Bleomycin: Revival of an old drug. [Review] *Gen. Pharmacol.* **27**, 745–748.
 43. Gehl, J., Skovsgaard, T., and Mir, L. (1998) Enhancement of cytotoxicity by electroporation: An improved method for screening drugs. *Anticancer Drugs* **9**, 319–325.

44. Heller, R., Jaroszeski, M., Glass, L., Messina, J., Rapaport, D., DeConti, R., Fenske, N., Gilbert, R., Mir, L., and Reintgen, D. (1996) Phase I/II trial for the treatment of cutaneous and subcutaneous tumors using electrochemotherapy. *Cancer* **77**, 964–971.

Instrumentation and Electrodes for In Vivo Electroporation

Gunter A. Hofmann

1. Introduction

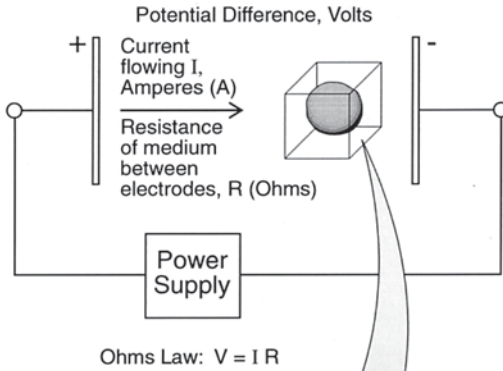
Electroporation (EP) of drugs and genes into cells in vitro became a standard procedure in molecular biology laboratories in the last decade. Numerous protocols aid the researcher in selecting appropriate procedures; commercial instrumentation is readily available and discussed (*1*). The more recent transition to applying EP to living tissue poses a new set of requirements and few practical guidelines are available.

In general, the requirements for successful in vivo electroporation for delivery of drugs or genes are twofold: the molecules need to be present at the site to be treated, and an appropriate electrical field needs to be applied to this site within a time window. For the choice of electrical parameters, the type of tissue appears to be of less importance than the molecule to be delivered: drug versus genes.

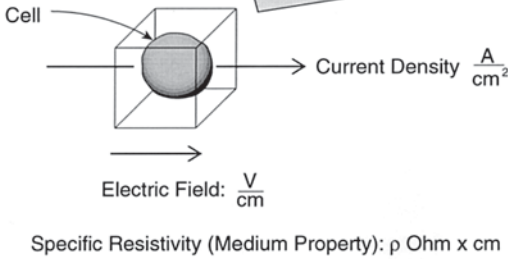
In vivo EP requires techniques for the delivery of the drug/gene to the tissue site, and techniques for the delivery of the field. The delivery of the field is done by a voltage pulse generator and applicators that transform the voltage into an efficacious electric field in the tissue. **Figure 1** shows the relationship between the macroscopic parameters of voltage, current, and resistance and the microscopic, effective, parameter, the electric field strength as well as the current density, which is a function of the medium specific resistivity.

The generator provides a voltage output to the electrodes. This voltage, or potential difference, between electrodes results in the generation of an electric field in the volume between the electrodes and extending somewhat beyond. The voltage needs to be selected so that in the volume between the electrodes

1. Macroscopic Parameters



2. Microscopic (Local) Effects



Microscopic Ohms Law: $E = i \rho$

Macroscopic	Microscopic
I	i
V	E
R	ρ

E is the efficacious parameter for electroporation

Fig. 1. Important electrical parameters for electroporation.

the efficacious field strength is achieved or exceeded. It is desirable to provide a field amplitude that has a safety margin above the marginally efficacious field strength. These issues are the subject of the following sections.

The process of developing a new *in vivo* therapeutic application of EP generally proceeds in the following steps: Uptake of the drug or gene is demonstrated *in vitro*, then efficacy shown *in vivo* in an appropriate animal model,

then, if possible, *in situ* in an animal model, and, finally, in human clinical trials. We will discuss only *in vivo* and comment briefly on hardware issues relating to the steps from animal experimental trials to human clinical trials. A large variety of drugs or genes can be electroporated into widely differing tissues *in vivo*. In the following, we will focus on a few representative examples.

2. Delivery of Drug/Gene to the Tissue

In vivo EP is a process of delivering drugs and genes from the interstitial tissue space into cells by temporary permeabilization of cell membranes. As a first step, the molecule of interest is typically brought into the tissue before EP. Several techniques are being used: systemic delivery by intravenous injection (IV) or intratumoral injection (IT). Tumors differ from normal tissue by elevated interstitial pressure which is typically between 10 and 40 mmHg, whereas normal skin has 0.4 mmHg pressure (2). This high pressure and gradient towards normal tissue makes systemic delivery less effective than IT. When IT is used, a technique of fanning the syringe throughout the tumor aids in the distribution of the drug. IT delivery of bleomycin into tumors and subsequent EP gave superior results over the IV route (3). Iontophoresis might be employed as a transport mechanism of charged molecules across tissue to the site of EP.

The transport of molecules through the skin is made difficult by the presence of the *stratum corneum* (SC), the outermost layer of the skin made up of dead cells. Iontophoresis can be used to transport charged molecules through existing pathways such as sweat glands and hair follicles through the skin; brief electrical pulses across the SC can create additional pathways by breakdown and formation of aqueous pores. Ultrasound can enhance the transport of molecules across skin (4,5).

3. Electric Field Configurations

The voltage delivered from the EP pulse generator needs to be transmitted to the tissue so an efficacious electric field can be generated at the desired tissue site. A variety of possible basic electrode configurations are shown in **Fig. 2**.

If the tissue is easily accessible, not too large in volume and raised, outside electrodes (**Fig. 2-1**) in form of parallel plates can be utilized. Early gene EP experiments (6) and tumor treatments by EP (7,8) used parallel plate type electrodes. If it is desirable to confine the electric field to a shallow layer of tissue, as in transdermal drug delivery, then closely spaced surface electrodes as shown in **Fig. 2-2** are useful. Deeper-seated tissue can be reached with insertion electrodes or needles (**Fig. 2-3**). The resulting electric field distribution can be improved by arranging needles in arrays of different geometries (**Fig. 2-4**).

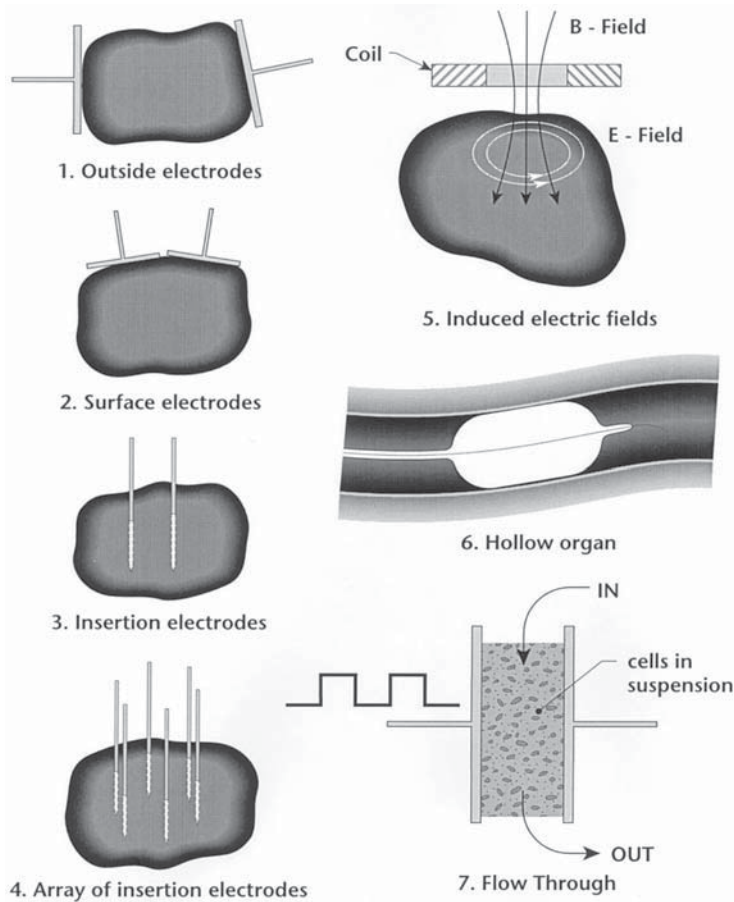


Fig. 2. Basic field applicator configurations.

In principle, an electric field can be generated by induction according to Faraday's law from a coil with a fast varying electrical current. Though this approach allows for an electrodeless creation of the electric field in tissue, it is not very practical. Very high currents at high frequency are needed in order to create induced fields of an amplitude sufficient to induce EP. A tumor response effect was demonstrated with this technique even without addition of a drug (9).

Hollow organs and cardiovascular applications of EP require catheter-type configurations (Fig. 2–6). Some cardiovascular implementations are described in (10–12). A flow-through EP system (Fig. 2–7) can be used either for ex vivo EP therapy or, in a shunt mode, to electroporate bodily fluids extracorporeally. Practical implementations of some of these electrode configura-

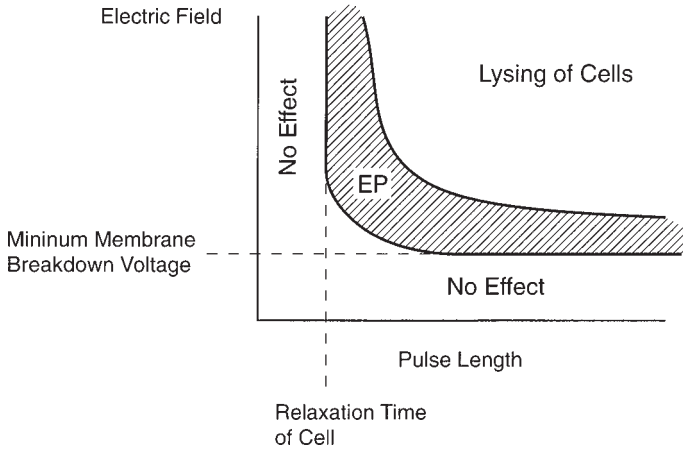


Fig. 3. General electroporation relationships.

tions will be discussed in **Subheading 6**. The determination of the minimum efficacious field strength for EP will be discussed in **Subheading 4**.

4. Minimum Efficacious Field Strength

The parameters which determine the efficacy of the delivery of molecules into cells are field strength, pulse length, wave shape of the pulse and number of pulses. The combination of all of these is too large to address their specific importance, especially when one considers that the molecule to be delivered may change the optimal parameter combination. However, some general statements can be made which will help in trade-off considerations of the most important parameters which are field strength and pulse length. **Figure 3** shows the area of EP efficacy. If the field strength is too low, the transmembrane potential required to permeabilize the cell membrane (typically 0.7 V) can not be reached. Similarly, if the pulse length is too short (microseconds), the membrane capacitance does not charge up high enough to reach the required transmembrane potential. If the delivery of genes is intended, the parameters need to be selected within the EP effective area. However, if the goal is the destruction of tumors by delivery of chemotherapeutic agents with EP, lysing of cells, which results from excessive field strength or pulse length, is not detrimental to the ultimate goal of tumor destruction.

There appears to be a difference in effective parameters between drug and gene for delivery by EP. High field strength, short pulse length gives good results at least with some of the drugs investigated (i.e., bleomycin), whereas gene EP benefits more from a combination of low electric field and long pulse length. The majority of presently ongoing drug EP is applied to the treatment

of tumors, and the drug of choice is mostly bleomycin. We will therefore discuss the determination of the minimum efficacious field strength for this application.

Belehradek and colleagues (*13*) injected bleomycin into nude mice bearing subcutaneously T-DC-3F clone 4 tumors (Chinese hamster lung transformed fibroblast cell line). Tumors were removed and sliced. Slices were electroporated in the presence of bleomycin with 100 μ sec pulses between parallel electrodes, which provided a reasonable homogeneous field. The lower limit of effective field was between 400 V/cm and 600 V/cm. In a study comparing the efficacy of different needle arrays and voltages in a human prostate cancer model in mice (*14*), a good tumor response was found in the center of a needle array at a field strength of 780 V/cm, which was the lowest field strength investigated.

Does this critical minimum field vary much with the tumor cell type? The critical parameter for the electroporation of mammalian cells is the achievement of a transmembrane potential of about 0.7–1 V. For a given field strength, the induced voltage V is inversely proportional to the cell diameter: $V = 1.5Er \cos \theta$, where E is the field strength, r is the cell radius, and θ is the angle between the direction of the field and the cell surface vector. If the cells are of similar size, similar minimum efficacious field strength can be expected.

5. Effect of Electroporation on Normal Tissue

The following issues are of importance when considering inserting electrodes into a tumor and transversing healthy tissue: What is the safe level of the electric field and what is the effect of EP of a drug into healthy tissue?

5.1. Electric Field Effects

Reilly (*15*) offers some comments on the effect of electric fields in tissue. Only the field strength is given but, unfortunately, no pulse length. The effects listed may not occur at the very short pulse length (100 μ s) used in most EP drug delivery experiments. The minimum field to stimulate nerves is 6 V/m = 0.06 V/cm. No significant alterations in the evoked response in the peripheral nerves of hogs occur up to 33 V/cm. To generate lesions in tissue requires field strengths above 100 V/cm. Similar levels are probably necessary for neural damage as well. In vitro muscle cells rupture between 50 and 300 V/cm. Fibroblasts rupture above 1 kV/cm.

5.2. Electroporation of Healthy Tissue

Recently Hasegawa and coworkers (*16*) have published an interesting paper that discusses results of electrochemotherapy (ECT) of squamous cell carci-

noma and hepatocellular carcinoma transplanted into the tongues of rats. They used bleomycin as the agent and electrical parameters typical for those used for parallel plates, 1200 V/cm and $8 \times 100 \mu\text{s}$ pulse length at 1 Hz. The authors made detailed observation of (i) not only the tumor but also the surrounding normal tissue, (ii) the epithelium in or not in contact with the electrodes, (iii) the nuclei of the endothelial cells and also changes in the muscle on day 1, and (iv) the nature of the healing process throughout day 14 after the treatment.

The readers are referred to the actual paper for details, but the following features are notable and summarized. On day 1, they observed massive destruction of the tumor and edema which by now are well established phenomena following ECT. The epithelium in contact with the electrodes peeled off but the tissue surrounding the tumor, not in contact, was found to be normal. Nuclei of the endothelial cells were enlarged and some skeletal muscle lost the striation pattern. As days progressed, several important features became evident; the epithelium close to the necrotic tissue was regenerated and the granulation tissue proliferated. Eventually, the necrosis fell off, the wound healing was nearly complete and the tongue was covered with stratified epithelium.

We point out that because of the presence of the mucosal component in the tongue, some of the features seen by the authors are not necessarily the same as are seen in the xenografted subcutaneous tumors. The bleomycin dose the authors use for subcutaneous injection is very high, ~ 7 – 10 times of what is normally used intratumorally (0.5 U [0.5 mg] for a tumor close to 8 mm in the maximum dimension) (17–19). The authors conclude, “The healing process following ECT progressed smoothly, including that of normal tissue within the electrical field that was seriously damaged.”

6. Applicators

The role of the applicators is to act as a conduit to transform the voltage pulse from a pulse generator into local electric fields in tissue.

6.1. Plate Electrodes

The simplest configuration and the one best suited to generate a more or less uniform electric field are parallel plate electrodes in the form of calipers (Fig. 4). The use of parallel plates is facilitated if a scale is attached so that the distance between the electrodes can be measured. These plates are often mounted on a Vernier caliper as shown in the figure. The voltage can then be determined from the desired field strength and the distance ($V = E \times \text{distance}$). Parallel plate electrodes produced good results in human clinical trials (7,8) with tumors close to the surface. However, superficial skin burning was observed as a consequence of the breakdown of the SC. Though the breakdown

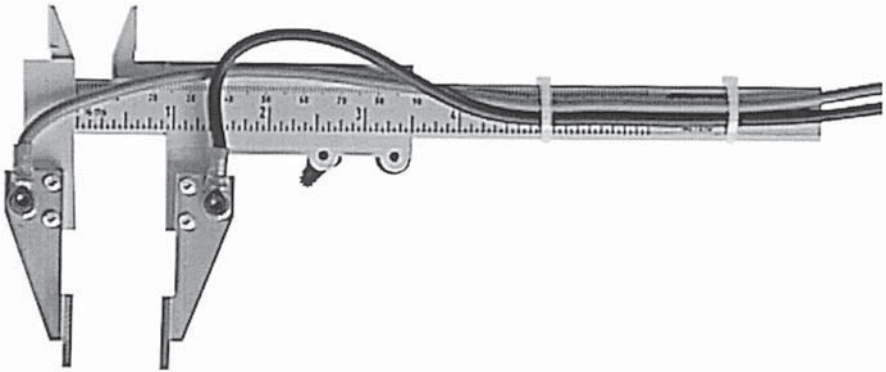


Fig. 4. Caliper electrodes for the treatment of subcutaneous tumors. The scale on the caliper allows measurement of the electrode distance so that the generator voltage can be set according to the desired field strength: $E = V/\text{distance}$.

occurs at low voltages of about 60 V, the high-current density after the breakdown is detrimental to the structure of the skin. Plate electrodes are less efficacious for deeper-seated tumors (20); needles in the form of arrays are better suited. Improved efficacy with parallel plate electrodes can be obtained by rotating the field (position of electrodes) 90° between pulses (21).

6.2. Needle Electrodes

6.2.1. Computer Simulation of Electric Field Distribution

The electric field between needles has been calculated with a three-dimensional computer program (E3 Electrostatic Field Solutions in Three Dimensions, produced by Field Precision of Albuquerque, New Mexico). For needle arrays, the field was calculated in a first step between one pair of needles with the appropriate geometry. The contour lines of constant electric field (absolute amplitude) were plotted and then plots were superposed after rotating by 60° (for the six-needle array) or 90° for the square needle array. Ultimately, lines were drawn around areas where the electric field amplitude was equal to 600 V/cm and 100 V/cm. Inside the shaded area, the electric field is everywhere above 600 V/cm.

6.2.2. Needle Pair

Early experiments in animals were performed with single pairs of needles (22–25). **Figure 5** shows a typical experiment with needle pairs. The field is highly divergent, with a high field strength at the needle surface. **Figure 6** shows the 600 V/cm iso field contour line in a cross section of two parallel needles 0.65 cm apart and with an applied voltage of 942 V. The nominal field

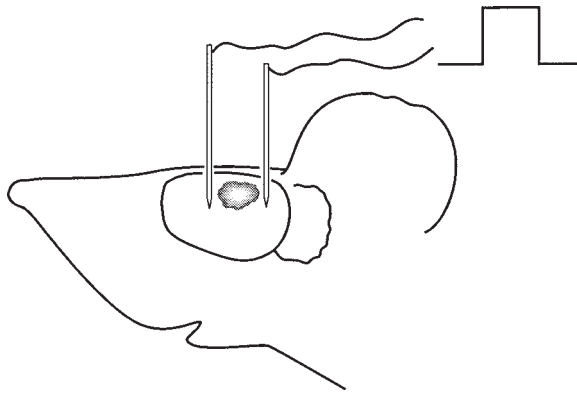


Fig. 5. Electroporation of tissue (tumors) with two needles.

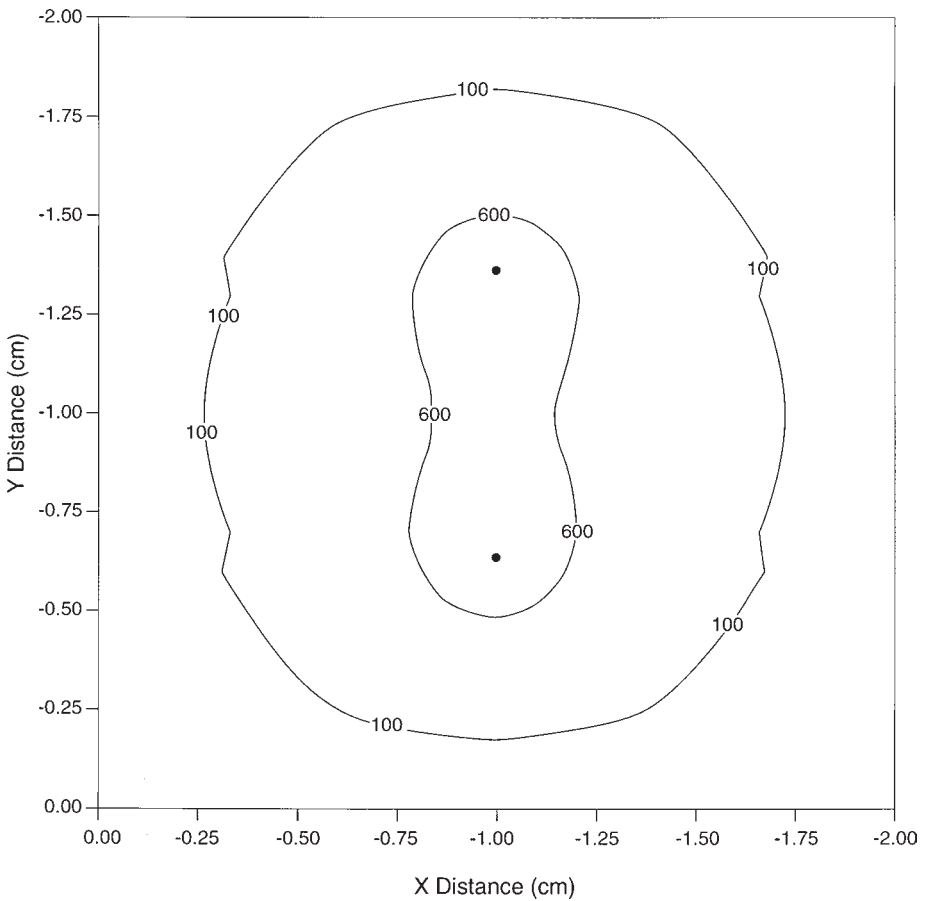


Fig. 6. Isoelectric field lines around a two-needle array. Field strength: V/cm; potential applied: 942 V; distance between needles: 0.65 cm.

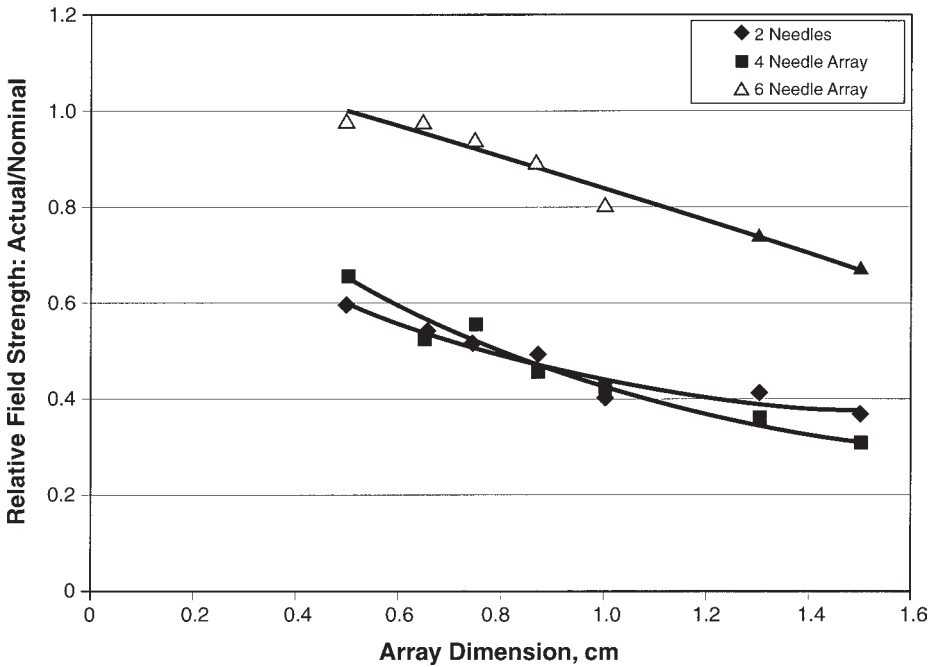


Fig. 7. Ratio of actual versus nominal field strength.

strength in the center between needles is often given as the voltage on the needles divided by the needle distance. However, the actual center field strength is quite different (lower) as shown in **Fig. 7**. A better field configuration results from multiple needles or needle arrays. Gilbert and colleagues (26) investigated several needle configurations; the needle pair showed the lowest efficacy, parallel plates were better. The highest efficacy resulted from the use of a six-needle array.

6.2.3. Six-Needle Arrays

In a six-needle array configuration, six needles are placed equidistant in a circle. Six pulses are applied to consecutive pairs of needles around the circle. **Figure 8** shows the six-needle array concept and the switching scheme. By switching the field between different pairs of needles, a good coverage of the area within the needle array is achieved (**Fig. 10**). As shown in **Fig. 7**, the actual field strength in the center is closer to the nominal field strength (voltage divided by the array diameter) than with two needles. Six-needle arrays were used (27,28) in clinical trials with good efficacy. A variety of needle array diameters, angles of the tip, and needle lengths is needed to reach tumors

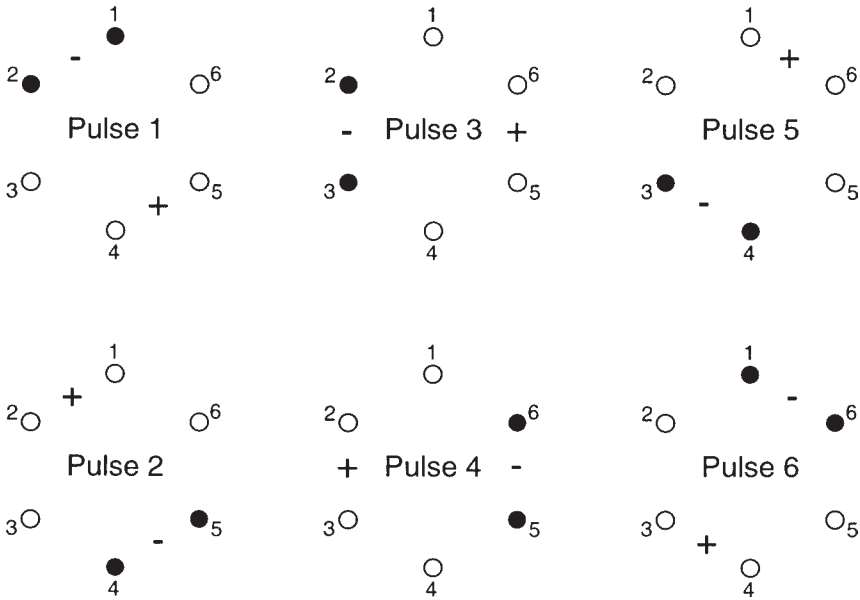


Fig. 8. Sequence used to energize individual needles for a six-needle array around the treatment site.

at different locations in the body (**Fig. 11**). Though the six-needle arrays showed good efficacy, the disadvantage of this configuration is the requirement to increase the array voltage with the array diameter. Some tumors can be quite large; though it is possible to use an overlapping multiple entry treatment strategy, the accuracy of the array placement is not assured. Furthermore, the voltage between needles can not be increased indefinitely. Above about 1500 V, arcing occurs at the needle tips because of the high field enhancement factor. It is therefore desirable to restrict the voltage to lower values. A very good solution to this problem is the subdivision of an array into treatment zones, with square needle arrays as the most practical approach (29).

6.2.4. Square Needle Arrays

An arrangement of 4 needles in a square (a treatment zone) and pulsing between opposing pairs, provides a good area of efficacious field (**Figs. 9 and 12**). Uptake of agents is increased by delivering 4 pulses in a sequence between opposing pairs, changing the orientation by 90° between pulses. The total treatment area can be increased by adding treatment zones. **Figure 13** shows the field distribution in a 9-needle array. This configuration allows the electrically paralleling of zones so that the number of switching steps is vastly reduced.

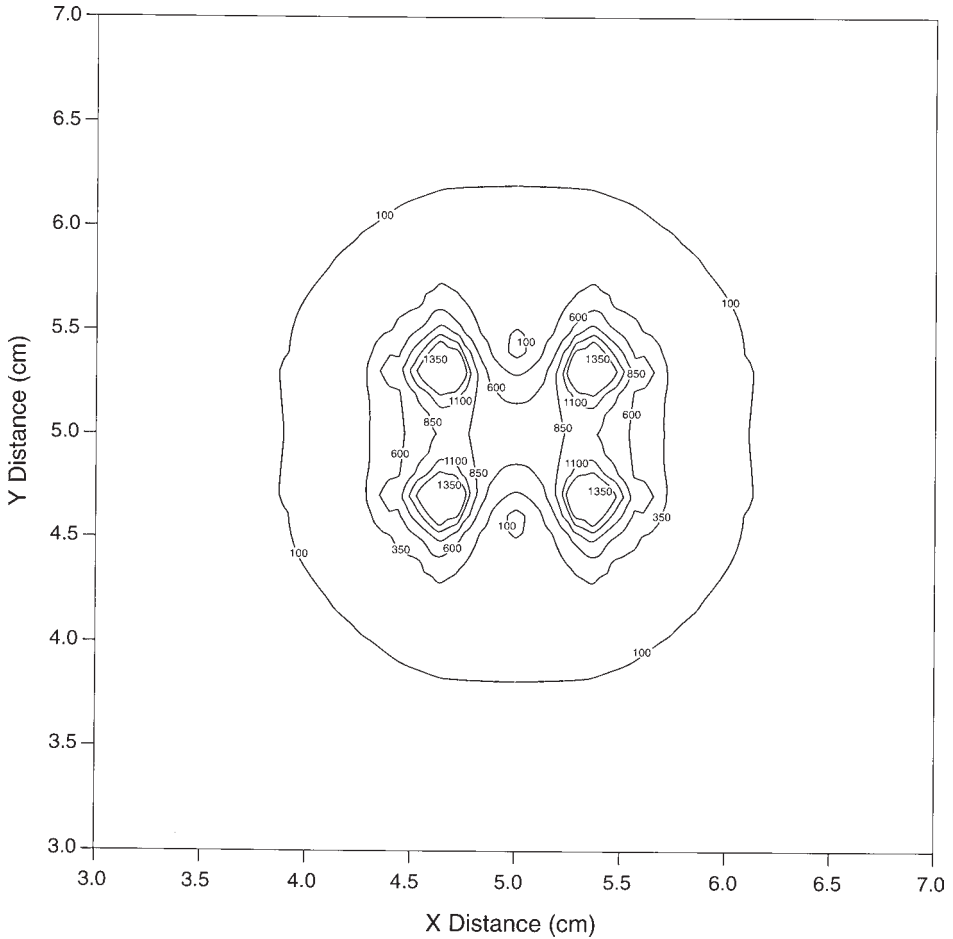


Fig. 9. Isoelectric field lines around a four-needle array; 0.65 cm base length. Cross section is taken in the middle plane of the array. Field strength: V/cm; electrode spacing: 0.65 cm; needle diameter: 0.04 cm; potential applied: 845 V.

The required voltage remains the same as for one square; the current and power requirements increase with the addition of treatment zones. **Figure 14** shows the electrical arrangement of a 25-needle array covering an area of 2.6×2.6 cm with a 0.65 cm zone base length. All needles with the same number are connected electrically in parallel. The required voltage is only 940 V; the minimum field in the treatment zones is 780 V/cm, which reflects a margin of efficacy of 30% over the assumed minimum efficacious field of 600 V/cm. Only 4 pulses are required which can be delivered by the MedPulser™ (28)

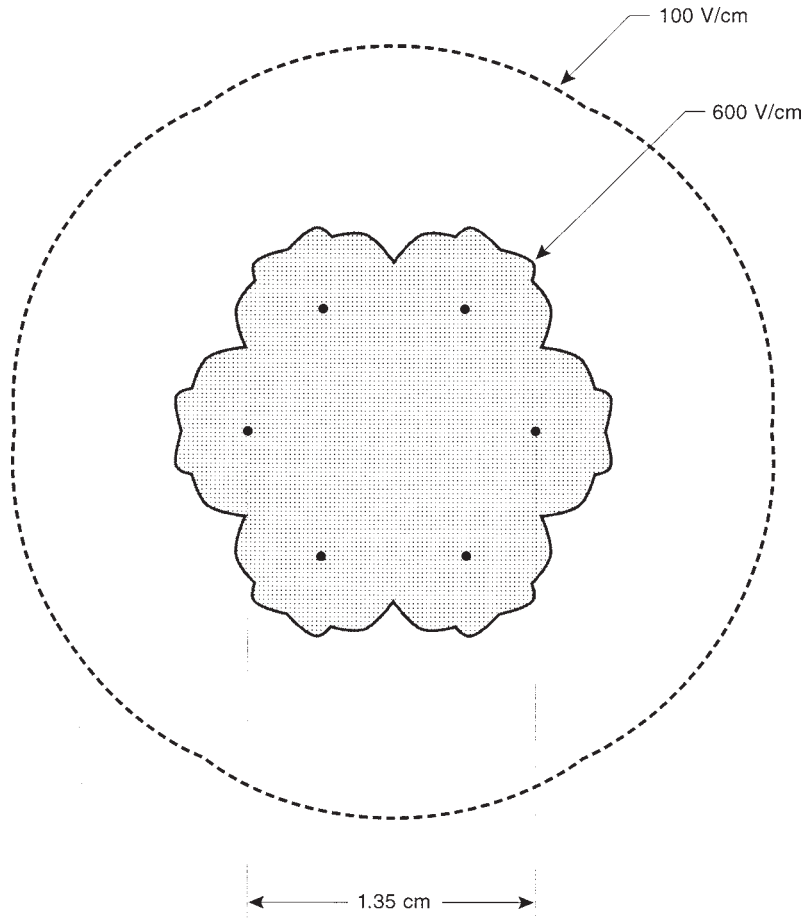


Fig. 10. Isoelectric field lines generated by a six-needle array (four are active), after switching 60° ; 1.35 cm diameter; 1500 V between needle pairs.

generator in one second: first pulse: Needles 1–2 pulsed against 3–4; second pulse: reversed polarity; third pulse: 1–3 pulsed against 2–4; fourth pulse: reversed polarity.

6.3. Surface (Meander) Electrodes for the Electroporation of Skin

The biophysical phenomenon of electroporation is pronounced when a thin, highly resistive membrane surrounds or shields a conductive medium. A very strong field enhancement will take place in the membrane which can lead to permeabilization or electroporation. The field enhancement is in first order proportional to the ratio of the thickness of the conductive medium to the

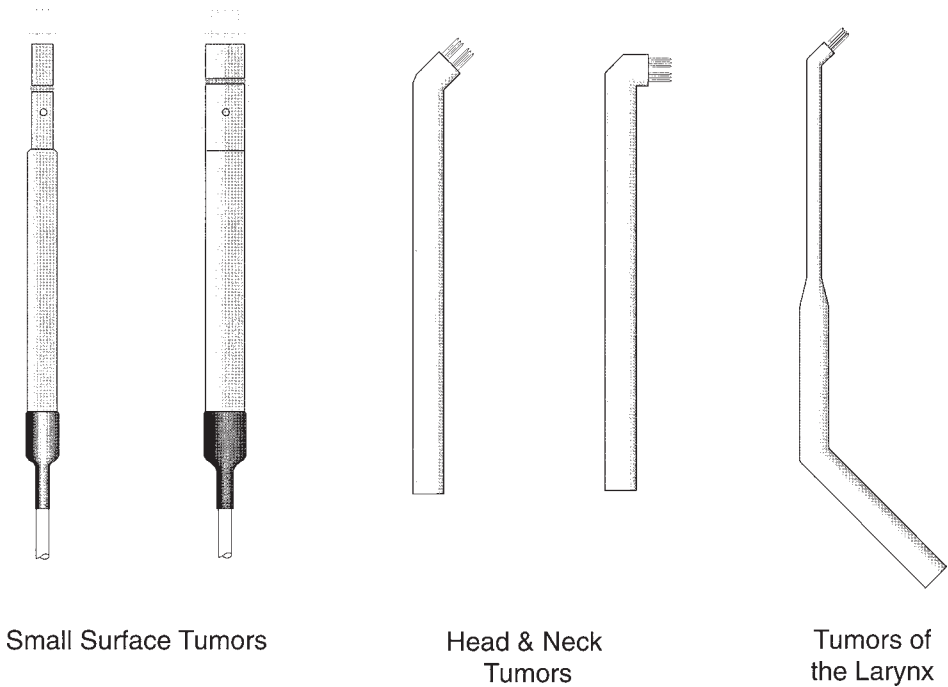


Fig. 11. Various six-needle array applicators.

membrane thickness. In the classical case of cells, the cell membrane and the cytoplasm play this role.

The skin presents a similar biophysical model. A very thin (typically 15 μm), highly resistive layer, the SC is surrounding the highly conductive epidermis and dermis (30). A very low potential difference applied to the skin, for example, 60 V across two layers of SC (representative for adjacent surface electrodes), results in very high fields in the SC of about 20 kV/cm. Such a high field appears to suffice for the breakdown and formation of aqueous pores in the SC. The SC is normally a very effective barrier against penetration of outside agents; electroporation of the SC allows the transport of agents across this barrier by several methods (31,32).

In tissue electroporation, the goal is an even distribution of efficacious field. In the electroporation of skin for transdermal delivery of agents, it is desirable to contain the electric field to a shallow skin surface layer so that underlying nerves and muscles are not subjected to a strong electrical stimulus. This objective can be realized by meander electrodes, which consist of closely spaced opposing finger electrodes (Fig. 15). Figure 16 shows the field and potential distribution around a meander electrode. As can be seen, the potential

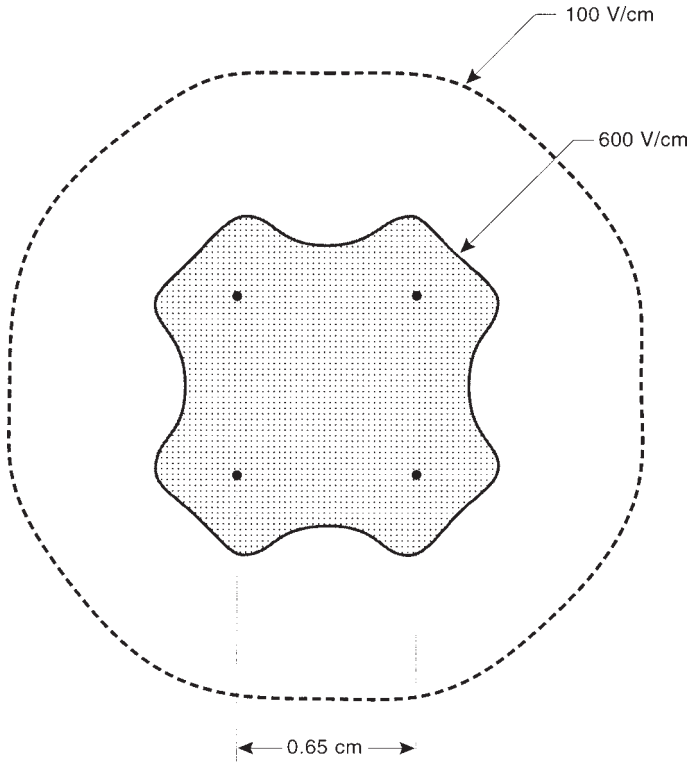


Fig. 12. Isoelectric field lines generated by a four-needle square array after switching 90°; 0.65 cm base length.

drop between the electrodes is mainly confined to the SC. After breakdown, the range in depth of the electric field is related to the electrode spacing; a narrow spacing will confine the field to a shallow surface region.

6.4. Electroporation in Vessels: Catheters

In vivo electroporation of agents into the walls of vessels requires first positioning of the agents proximal to the vessel wall without being washed away. A double-balloon catheter as shown in **Fig. 17** blocks the blood flow after inflation of the two balloons. Infusion of the agent occurs into the volume between the balloons. The electrical pulse is applied between an electrode located between the balloons and the catheter guide wire as the current return path. **Figure 18** shows the field distribution around the double-balloon catheter. A strong electric field exists between the center electrode and the adjacent tissue. Double balloons were successfully employed for the intravascular delivery of heparin (**12**) and DNA-binding propidium iodide (**10**).

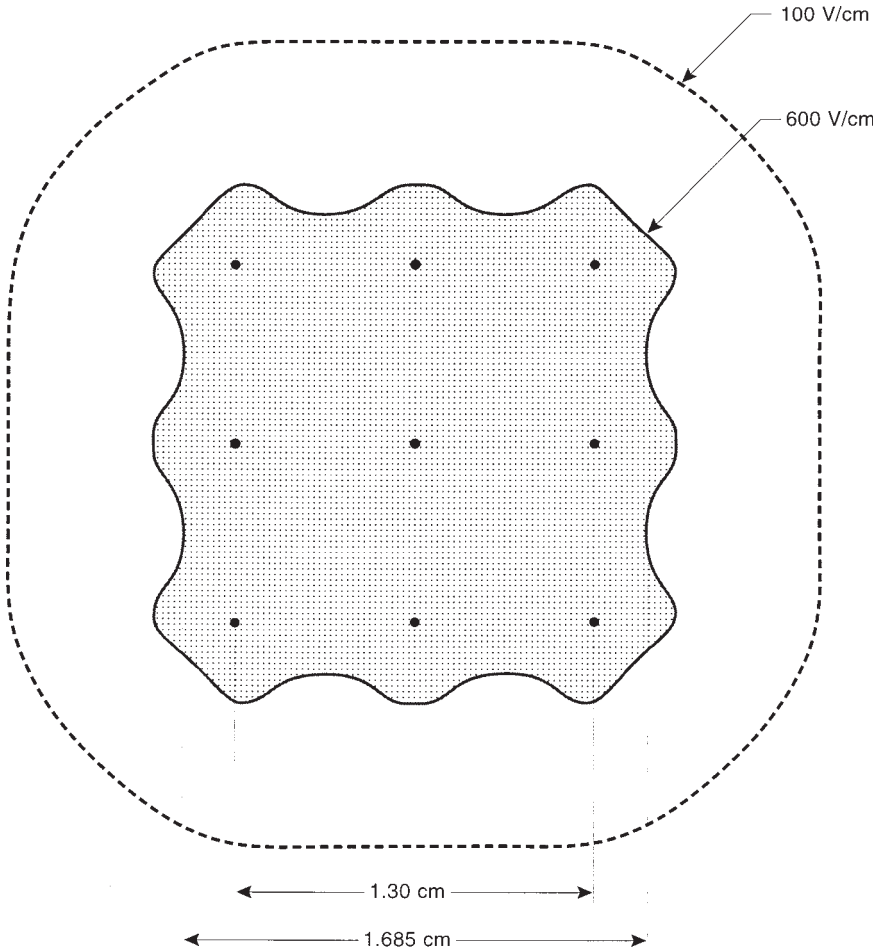


Fig. 13. Isoelectric field lines generated by array of four-needle squares after switching 90°; 0.65 cm base length; 940 V between needle pairs.

6.5. Other Electrode Configurations

An interesting application of EP *in vivo* is the delivery of bleomycin into the eye for the treatment of high intraocular pressure (33). A special cup shaped applicator was developed to fit around the eye of rabbits. Earlier *in vivo* work described the fusing of cells to the cornea of rabbits (34) by means of pulsed electric fields with a cup-shaped applicator.

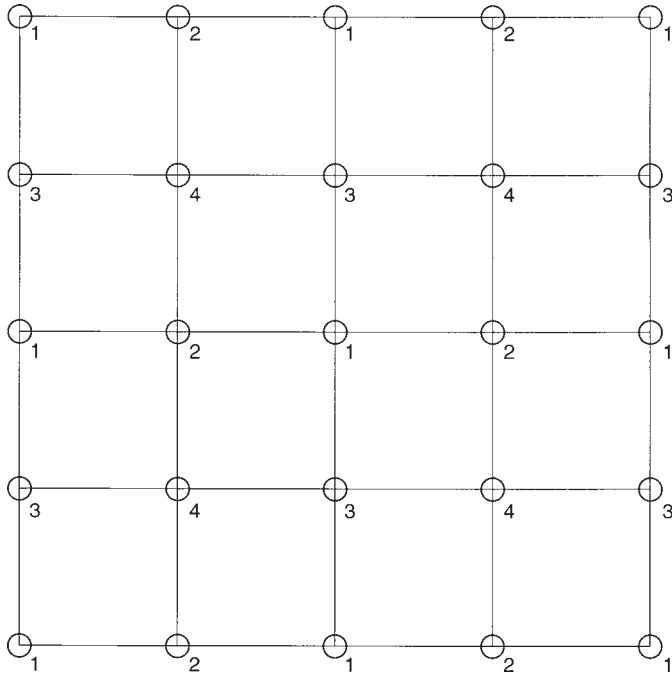


Fig. 14. Square needle array (2.6 cm \times 2.6 cm) with paralleling all switching zones.

7. Pulse Generators

The pulse generators for *in vivo* drug and gene delivery need to deliver on command a voltage wave form which the electrodes transform into an efficacious electric field in the tissue. The important parameters are voltage amplitude, length of the pulse, shape of the pulse, and the number of repeat applications.

In vitro, a variety of different wave shapes are used with varying effectiveness: square pulses, exponentially decaying pulses or bursts of radiofrequency waveforms. In the overwhelming majority of *in vivo* applications, square waves are being used. They have the advantage of allowing the user to preset an exact amplitude and pulse length, provided that the generator was designed to supply the tissue with the required current. The design requirements for a square pulse generator are described in detail by Hofmann and associates (29). **Table 1** compares the specifications of the generators which were used in the majority of animal work, preclinical and clinical human trials.

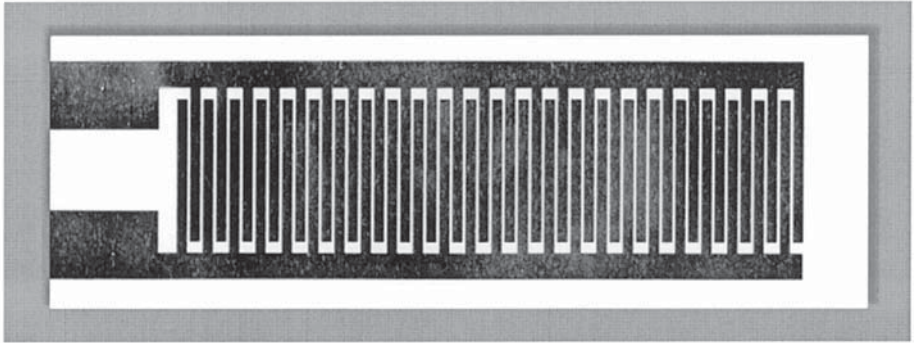


Fig. 15. Meander electrodes: electrode gap, 0.2 mm; electrode width, 0.2 mm.

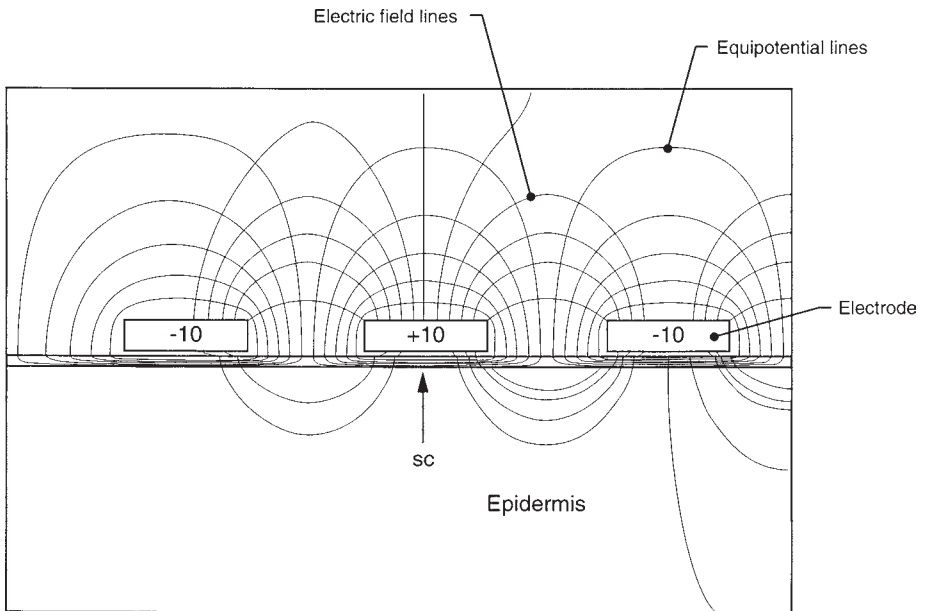


Fig. 16. Plot of equipotential and electrostatic field lines of meander electrodes on top of the SC with a distance of 10 μm . Specific resistivities: medium surrounding the meander electrodes, $1000 \Omega \times \text{cm}$; SC, $6 \times 10^8 \Omega \times \text{cm}$; viable epidermis, $10^5 \Omega \times \text{cm}$. Potential difference between meander electrodes: $\pm 10 \text{ V}$.

High electric fields and short pulse length are generally used for the delivery of chemotherapeutic drugs into tumors, typically 1000 V/cm and 100 μs . Genes, however, were shown to be delivered at high efficiency (35,36) with low field strength (100 V/cm) and long pulse lengths (10–50 msec).

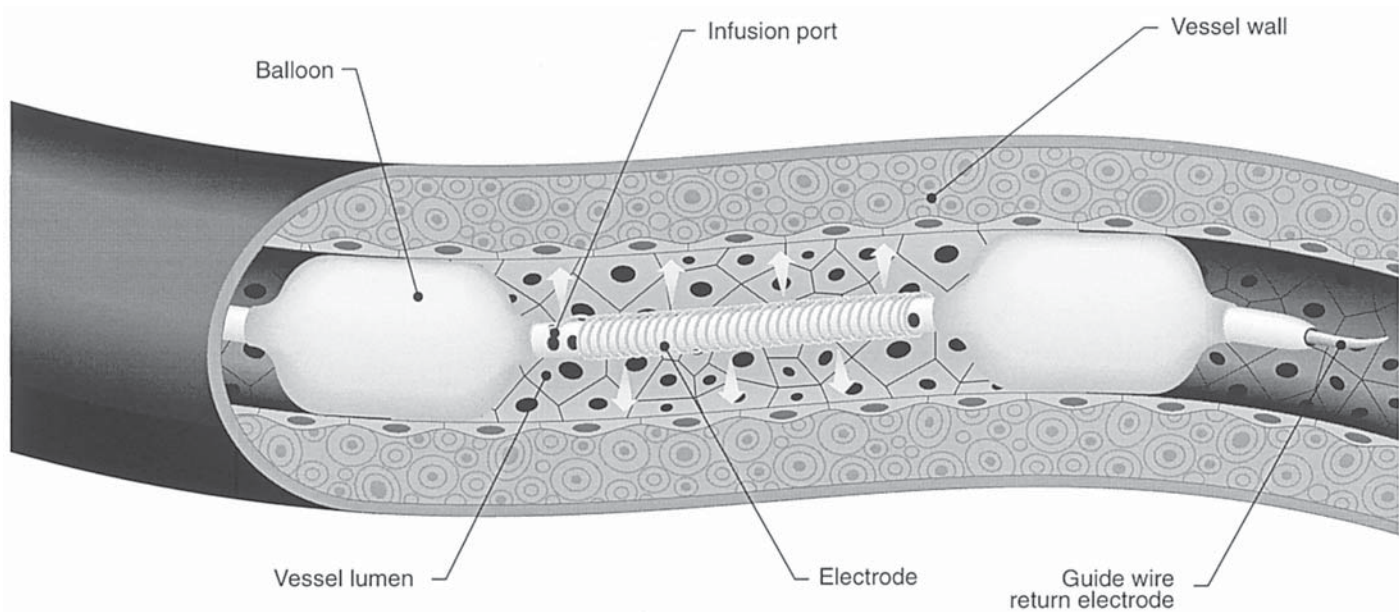


Fig. 17. Double-balloon electroporation catheter.

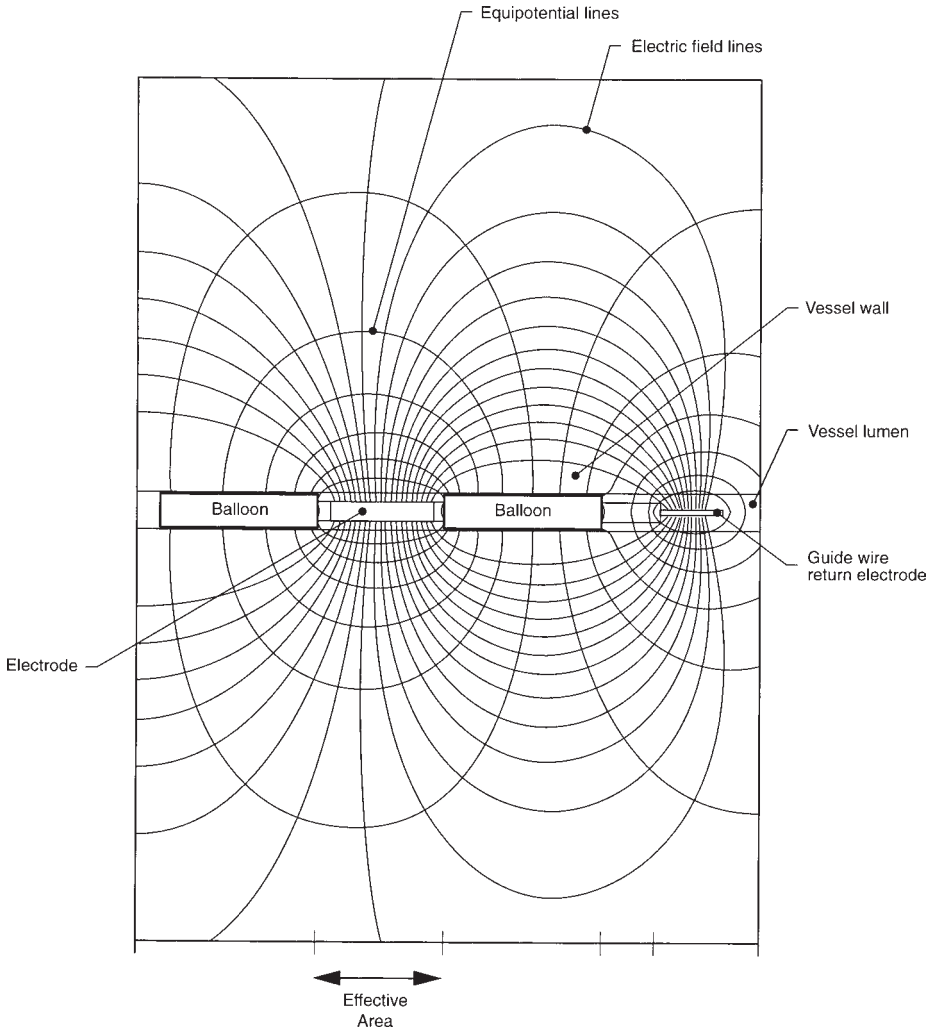


Fig. 18. Electric field and equipotential lines around a double-balloon catheter.

Though a researcher in most cases is not involved in bringing a therapeutic EP system to the market, the step from *in vivo* experiments in animals to initial preclinical trials should be understood. For animal electroporation experiments and preclinical human trials, commercially available generators, which are available for *in vitro* electroporation, were generally used. The following section discusses the additional steps in generator design which will make it perform to regulatory requirements. These requirements must be met in order to be able to perform large-scale multi-center clinical trials.

Table 1
Square Wave Generators for In Vivo Drug/Gene Delivery

Manufacturer	Ref.	Voltage Range	Pulse Length	Electrodes
Jouan, France Electropulsator PS 15 Commercially available	7	0–1500 V Variable	5 μ s–24 msec Variable	Parallel plates
BTX, a division of Genetronics, Inc. San Diego, CA ElectroSquare Porator T 820 Commercially available	29	0–500 V 20–3000 V Variable	0.3 ms–99 msec 5 μ s–99 μ sec Variable	Parallel plates; needle electrodes with auxiliary switch
Genetronics, Inc. San Diego, CA MedPulser In use for multicenter clinical trials	14, 28	1500 Vmax; preset for each needle array applicator type	100 μ s fixed	Needle electrodes only

8. Regulatory Requirements for Clinical Applications

To encourage the discovery and development of useful medical devices, the Food and Drug Administration (FDA) provides exemptions for investigational devices from the premarket approval process. An Investigational Device Exemption (IDE) permits a device to be shipped in interstate commerce for clinical investigation to determine its medical safety and effectiveness. Although the IDE regulation exempts the device from certain requirements, it requires safeguards for humans who are subjects of investigations: maintenance of sound ethical standards, and procedures to ensure development of reliable scientific data.

Certain device investigations are exempt from the requirements of the IDE regulation. This determination is based upon the risk presented to the patient either directly from device use or indirectly from medical decisions made with data from the device. Depending on the device, an IDE may be approved either by an Institutional Review Board (IRB) or by both an IRB and FDA; informed consent for all patients, adequate monitoring and necessary records and reports are required in either case.

If the device has patient contact, it should be constructed with safe, biocompatible materials and their evaluation should be consistent with the International Organization for Standardization (ISO)–10993 guidelines, “Bio-

logical Evaluation of Medical Devices.” Potential risks should be addressed in a formal risk analysis and measures should be taken to limit patient risk whenever possible and feasible.

The products used for investigations should be designed with the clinical researcher in mind. The following design objectives should be considered in the clinical product design:

1. The design should preclude the opportunity for operator mistakes.
2. If that is not feasible, then reduce the likelihood of mistakes (e.g. interlocks).
3. If reduction cannot be achieved, then mitigate or limit the adverse consequences when a mistake is made.

Relying on the user to adjust and compensate for problems presented by a poorly designed user interface is the least desirable alternative. The goal is to design devices that are easy to use (user-friendly) and minimize the chance for users to make mistakes. In addition, since it is not possible to predict and prevent all errors, the design must also be error tolerant.

The most common cause of human factors problems is the failure of the device designers and developers to anticipate and deal with the characteristics of the people who interact with the device and the nature of these interactions. Common problems include:

1. Unusual or unexpected device operation.
2. Lack of protection against incorrect use.
3. Confusing or complex controls, labeling or operation.
4. Defeatable or ignorable safety features.

Although Investigative Devices are exempt from most FDA Quality System Requirements (QSR), they are not exempt from the Design Control regulations. At a minimum, the clinical product should be designed based on a product development plan, formal design input and output specifications, risk analysis, and verification tests that demonstrate that the product performs as designed and intended. The product should be manufactured under a controlled condition with a stable and repeatable process. The design and manufacturing revision and history records must be documented and maintained. Acceptance test and inspection procedures must be developed.

9. Summary and Conclusions

In vivo delivery of drugs and genes to cells in tissue is becoming a powerful tool, which compares favorably to other delivery modalities (37). Efficacy depends mainly on two requirements: to have the drug or gene at the tissue site and to apply the appropriate field pulse to the site. For the treatment of tumors, it is desirable to investigate a lower drug dosage of bleomycin than currently

used, while maintaining tumor response, in order to minimize the effect of ECT on healthy tissue. Some future developments include the selection of the optimum drug or gene; determination of the most efficacious electrical parameters: amplitude, pulse length, waveform (it is desirable to minimize muscle reactions and pain caused by the EP treatment); and development of the most appropriate applicator: catheter type applicators for hollow organs, minimally invasive laparoscopic applicators, and possibly implantable EP applicators.

As the medical field moves from treatment of diseases with drugs to treatment with genes, the EP delivery systems being developed now will be able to make this transition with ease.

Acknowledgment

The editorial assistance of Nancy Martorana, as well as help from many colleagues in reading the manuscript and providing material for this review, is greatly appreciated.

References

1. Hofmann, G. A. (1995) Instrumentation. *Methods Mol. Biol.* **48**, 41–59.
2. Jain, R. K. (1994) Barriers to drug delivery in solid tumors. *Sci. Am.* **271**, 58–65.
3. Heller, R., Jaroszeski, M. J., Reintgen, D. S., Puleo, C. A., DeConti, R. C., Gilbert, R. A., and Glass, L. F. (1998) Treatment of cutaneous and subcutaneous tumors with electrochemotherapy using intralesional bleomycin. *Cancer* **83**, 148–157.
4. Prausnitz, M. R. (1997) Reversible skin permeabilization for transdermal delivery of macromolecules. *Crit. Rev. Ther. Drug Carrier Sys.* **14**, 455–483.
5. Banga, A. K. (1998) Electrically assisted transdermal and topical drug delivery. Taylor & Francis Ltd., London.
6. Titomirov, A. V., Sukharev, S. I., and Kistanova, E. (1991) In vivo electroporation and stable transformation of skin cells of newborn mice by plasmid DNA. *Biochim. Biophys. Acta* **1088**, 131–134.
7. Mir, L. M., Belehradek, M., Domenge, C., Orłowski, S., Poddevin, B., Belehradek, J. J., Schwaab, G., Luboinski, B., and Paoletti, C. (1991) Electrochemotherapy, a novel antitumor treatment: first clinical trial. *C.R. Acad. Sci. III* **313**, 613–618.
8. Heller, R., Jaroszeski, M. J., Glass, L. F., Messina, J. L., Rapaport, D. P., DeConti, R. C., Fenske, N. A., Gilbert, R. A., Mir, L. M., and Reintgen, D. S. (1996) Phase I/II trial for the treatment of cutaneous and subcutaneous tumors using electrochemotherapy. *Cancer* **77**, 964–971.
9. Malignancy Treatment (1997) U.S. Patent 4,665,898.
10. Cui, J., Robinson, K. A., Brown, J. E., Chronos, N. A. F., Cipolla, G. D., Dev, S. B., Hofmann, G. A., Crawford, N., and King III, S. B. (1997) Local drug delivery to pig carotid arteries by direct vessel wall electroporation using a novel catheter. [Abstract]. *Proc. Am. Coll. Cardiol.* **29**, 201A.

11. Dev, N. B., Preminger, T. J., Hofmann, G. A., and Dev, S. B. (1998) Sustained local delivery of heparin to the rabbit arterial wall with an electroporation catheter. *Cathet. Cardiovasc. Diagn.* **45**, 337–345.
12. Dev, S. B., Hofmann, G. A., Preminger, T. J., and Dev, N. B. (1997) In vivo delivery of heparin into arterial wall with electroporation catheters. *Proc. World Congr. Electr. Magn. Biol. Med.* Bologna, Italy, **C4**, 95–96.
13. Belehradek, J. J., Orłowski, S., Ramirez, L. H., Pron, G., Poddevin, B., and Mir, L. M. (1994) Electroporabilization of cells in tissues assessed by the qualitative and quantitative electroloading of bleomycin. *Biochim. Biophys. Acta* **1190**, 155–163.
14. Nanda, G. S., Merlock, R. A., Hofmann, G. A., and Dev, S. B. (1998) A novel and effective therapy for prostate cancer. [Abstract]. *Proc. Am. Assoc. Cancer Res.* **39**, 2911.
15. Reilly, J. P., (1992) *Electrical Stimulation and Electropathology*. Cambridge University Press, Victoria, Australia, pp.120, 388, 417.
16. Hasegawa, H., Kano, M., Hoshi, N., Watanabe, K., Satoh, E., Nakayama, B., and Suzuki, T. (1998) An electrochemotherapy model for rat tongue carcinoma. *J. Oral Pathol. Med.* **27**, 249–254.
17. Dev, S. B., Nanda, G. S., An, Z., Wang, X., Hoffman, R. M., and Hofmann, G. A. (1997) Effective electroporation therapy of human pancreatic tumors implanted in nude mice. *Drug Deliv.* **4**, 293–299.
18. Nanda, G. S., Sun, F. X., Hofmann, G. A., Hoffman, R. M., and Dev, S. B. (1998) Electroporation therapy of human larynx tumors Hep-2 implanted in nude mice. *Anticancer Res.* **18**, 999–1004.
19. Nanda, G. S., Sun, F. X., Hofmann, G. A., Hoffman, R. M., and Dev, S. B. (1998) Electroporation enhances therapeutic efficacy of anticancer drugs: Treatment of human pancreatic tumor in animal model. *Anticancer Res.* **18**, 1361–1366.
20. Domenge, C., Orłowski, S., Luboinski, B., DeBaere, T., Schwaab, G., Belehradek, J., and Mir, L. M. (1996) Antitumor electrochemotherapy: New advances in the clinical protocol. *Cancer* **77**, 956–963.
21. Serša, G., Čemažar, M., Šemrov, D., and Miklavčič, D. (1996) Changing electrode orientation improves the efficacy of electrochemotherapy of solid tumors in mice. *Bioelectrochem. Bioenerg.* **39**, 61–66.
22. Okino, M. and Mohri, H. (1987) Effects of a high-voltage electrical impulse and an anticancer drug on in vivo growing tumors. *Jpn. J. Cancer Res.* **78**, 1319–1321.
23. Okino, M. and Esato, K. (1990) The effects of a single high voltage electrical stimulation with anticancer drug on in vivo growing malignant tumors. *Jpn. J. Surg.* **20**, 197–204.
24. Salford, L. G., Persson, B. R. R., Brun, A., Ceberg, C. P., Kongstad, P., and Mir, L. M. (1993) A new brain tumor therapy combining bleomycin with in vivo electroporabilization. *Biochem. Biophys. Res. Commun.* **194**, 938–943.
25. Nishi, T., Yoshizato, K., Yamashiro, S., Takeshima, H., Sato, K., Hamada, K., Kitamura, I., Yoshimura, T., Saya, H., Kuratsu, J., and Ushio, Y. (1996) High

- efficiency in vivo gene transfer using intra arterial plasmid DNA injection following in vivo electroporation. *Cancer Res.* **56**, 1050–1055.
26. Gilbert, R. A., Jaroszeski, M. J., and Heller, R. (1997) Novel electrode designs for electrochemotherapy. *Biochim. Biophys. Acta* **1334**, 9–14.
 27. Glass, L. F., Pepine, M. L., Fenske, N. A., Jaroszeski, M. J., Reintgen, D. S., and Heller, R. (1996) Bleomycin-mediated electrochemotherapy of metastatic melanoma. *Arch. Dermatol.* **132**, 1353–1357.
 28. Panje, W. R. (1998) Electroporation therapy of head and neck cancer. *Ann. Otol. Rhinol. Laryngol.* **107**, 779–785.
 29. Hofmann, G. A., Dev, S. B., and Nanda, G. S. (1996) Electrochemotherapy: Transition from laboratory to the clinic. *IEEE Eng. Med. Biol.* **15**, 124–132.
 30. Chien, Y. W. (1993) *Dermal and Transdermal Drug Delivery: New Insights and Perspectives*. (Gurny, R. and Teubner, A., eds.), Wissenschaftliche Verlagsges., Stuttgart, p. 136.
 31. Hofmann, G. A., Rustrum, W. V., and Suder, K. S. (1995) Electro-incorporation of microcarriers as a method for the transdermal delivery of large molecules. *Bioelectrochem. Bioenerg.* **38**, 209–222.
 32. Prausnitz, M. R. (1996) The effects of electric current applied to skin: A review for transdermal drug delivery. *Adv. Drug Deliv. Rev.* **18**, 395–425.
 33. Sakamoto, T., Oshima, Y., Sakamoto, M., Kawano, Y. I., Ishibashi, T., Inomata, H., and Ohnishi, Y. (1997) Electroporation and bleomycin in glaucoma-filtering surgery. *Invest. Ophthalmol. Vis. Sci.* **38**, 2864–2868.
 34. Grasso, R. J., Heller, R., Cooley, J. C., and Haller, E. M. (1989) Electrofusion of individual animal cells directly to intact corneal epithelial tissue. *Biochim. Biophys. Acta* **980**, 9–14.
 35. Muramatsu, T., Shibata, O., Ryoki, S., Ohmori, Y., and Okumura, J. (1997) Foreign gene expression in the mouse testis by localized in vivo gene transfer. *Biochem. Biophys. Res. Commun.* **233**, 45–49.
 36. Nishi, T., Goto, T., Yoshizato, K., Takeshima, H., Kuratsu, J., Ushio, Y., Hofmann, G. A., and Dev, S. B. (1997) High efficiency gene transfer in solid tumors by in vivo electroporation. [Abstract]. *Proc. Sixth Intl. Conf. Gene Ther. Cancer* **4**, P-56, S27.
 37. Muramatsu, T., Nakamura, A., and Park, H. M. (1998) In vivo electroporation: A powerful and convenient means of nonviral gene transfer to tissues of living animals. *Int. J. Mol. Med.* **1**, 55–62.

Numerical Modeling for In Vivo Electroporation

Dejan Šemrov and Damijan Miklavčič

1. Introduction

Electropermeabilization of cell plasma membrane is a threshold phenomenon. When a cell is exposed to electric field a spatially dependent transmembrane potential is induced (**1**). Above a certain threshold value of transmembrane potential permeability of plasma membrane drastically increases. Thus, in order to obtain plasma membrane permeabilization an above threshold transmembrane potential needs to be obtained. This is achieved by an above threshold electric field intensity. Electropermeabilization is therefore characterized by electric field intensity, but also by the duration and number of applied pulses, as well as their shape (**2**). Electric field intensity of the pulses of selected duration must reach a threshold, typical for a particular type of cell (**3**). This threshold is also different for the cells in tissue compared to the threshold for electropermeabilization of the membrane of isolated cells (**4**). Selected electric field intensity, appropriate for electroporation, should at the same time not exceed the value which will cause irreversible permeabilization or even death of the cell (**5**). This is particularly important for electro-gene transfection.

For the in vitro electroporation of cultured cells in suspension (**6**) it can be considered, that the cells are exposed to a homogenous electric field, meaning that its direction is uniform and the magnitude of electric field intensity is unique throughout all of the conducting volume. Namely, the distances between the cells in the suspension are very large compared to the diameter of each particular cell (**7**). Also, the dimensions of the typical chamber, used for the in vitro experiments, and the dimensions of electrodes by which the electric pulses are delivered to the suspension are much larger compared to diameters of the cells and their mutual distance. The electric field intensity can then be

calculated using a simple formula $E = U/l$, which is the electric field intensity inside ideal capacitor, constructed of two charged parallel plates of infinite surface, where l is the distance and U is the voltage between the plates. For the ex vivo electroporation of tissues or in vivo electroporation in the living organisms, the electric field resulting from the pulse delivery with electrodes usually used (8) can no longer be considered homogenous.

In the case of ex vivo electroporation there is usually only one type of tissue involved, but the pulses are delivered using either plate electrodes of various shapes, placed on the surface of the tissue, or needle electrodes, inserted into the tissue. Both types of electrodes will result in an inhomogeneous field. Furthermore, the biological tissue can not be considered a homogenous conductor. It is composed of cells, which have plasma membranes with very low electric conductivities compared to the conductivity of cytoplasm and extracellular medium. The shape of the cells and their organizations in the tissue are different for each particular type of the tissue (9) thus resulting in different distributions of electric field inside the tissue. In the case of electroporation, the electric conductivity of plasma membrane is increased, which substantially changes the electric phenomena inside the tissue and makes electric field distribution even more complex.

In the case of in vivo electroporation, there are usually many different tissues/organs with different electrical properties involved. Together with the diversity of their geometry, dimensions, and structure this results in even higher degree of inhomogeneity of the electric field resulting from the pulse delivery. The variety of the electrodes' shapes, dimensions and positions used for the in vivo electroporation and the difference in the resulting biological responses (10,11) further point to the difference in electric field distribution resulting from specific electroporation regime.

Mathematical modeling is a new approach in evaluation of the electrical phenomena during electroporation in vivo. Calculation of electric field distribution is a relatively simple, yet efficient tool for the analysis and explanation of experimental results. The influence of electric parameters (shape, dimensions and position of the electrodes), as well as tissue/organ characteristics on the distribution of electric field can easily be evaluated. Different electroporation regimes and experimental conditions can be analyzed and new experiments planned at lower costs. However, all mathematical models must be rigorously validated with adequate measurements of electrical parameters in vivo. Furthermore, mathematical modeling can not replace experimental work, it is merely a source for additional information in the explanation of the phenomena and experimental planning. Anyway, it can contribute to the knowledge and the understanding of the processes involved in electroporation.

Mathematical modeling has a rather long history in the field of biomedical

engineering and bioelectromagnetism. First reports were published in the sixties (12) and were related to electrocardiology. Electromagnetic field calculation has preserved its importance in the cardiology until now (13,14). The majority of reports dealing with the use of different analytical and numerical calculations were from this field of medicine. In the so called forward or direct problem, the aim of the research was to determine body surface potentials from the known active sources in the heart. The objective of the so called inverse problem was to estimate the source current density in the heart which results in electromagnetic signals measured outside or on the surface of the body i.e. electrocardiograms (ECGs) and magnetocardiograms (MCGs). Calculations of electric fields were also used in the studies of external cardiac pacing (15) and defibrillation (16), where they proved to be an efficient tool for the optimization of electrode systems. Similar approach can be found in the studies of the electromagnetic fields in the human brain (17,18), where forward and inverse problems are defined in a similar way relating cerebral electromagnetic sources with the electromagnetic signals outside or on the scalp, that is, magnetoencephalograms (MEGs) and electroencephalograms (EEGs), respectively. Magnetic and electric neurostimulation of the brain were also analyzed using mathematical modeling (19,20). In oncology, mathematical modeling was widely used in the analysis of the hyperthermia where both the electromagnetic and thermal phenomena were analyzed (21). Electrode configuration (position, sizes and driving voltages) for radio frequency (RF) hyperthermia was also optimized by means of mathematical modeling (22). In the last decade with the increased awareness of the possible health risk effects of electromagnetic fields (cellular phones, power transmission lines, radars, magnetic resonance imaging systems, home appliances, etc.) a lot of research groups were calculating energy absorbed in human body. Many different numerical methods were applied in those studies (23,24) due to diversity of problems in this area of research.

2. Definitions and Basic Theory

2.1. Volume Conductor Theory

The electric field in the biological tissue, resulting from an application of constant direct electric current, can be considered quasi-stationary, i.e. its time variations can be neglected (25). Its distribution is described by equations for the steady electric currents in the volume conductor. The relation of electric current to voltage and resistance is described by Ohm's law. For the biological tissue, where both positive and negative charge carriers are present with different characteristics, the electric current density \mathbf{J} (units: A/m²) is defined by the point form of Ohm's law:

$$\mathbf{J} = \gamma \cdot \mathbf{E}, \quad (1)$$

where \mathbf{E} (units: V/m) is electric field intensity and is defined as the negative gradient of the scalar electric potential u (units: V):

$$\mathbf{E} = -\nabla u. \quad (2)$$

γ is the electric conductivity of the material (units: S/m) and is in the most generalized case of the anisotropic volume conductor described as a tensor:

$$\gamma = \begin{bmatrix} \gamma_{xx} & \gamma_{xy} & \gamma_{xz} \\ \gamma_{yx} & \gamma_{yy} & \gamma_{yz} \\ \gamma_{zx} & \gamma_{zy} & \gamma_{zz} \end{bmatrix}. \quad (3)$$

When the conductivity of the material can be described in an orthogonal coordinate system (x - y - z) and referred to the principal axes, and both the electric field and the current density are related to the same coordinate system, then all nondiagonal elements are equal to zero and the above matrix becomes diagonal:

$$\gamma = \begin{bmatrix} \gamma_{xx} & 0 & 0 \\ 0 & \gamma_{yy} & 0 \\ 0 & 0 & \gamma_{zz} \end{bmatrix}. \quad (4)$$

There are two different conductivities in the anisotropic biological tissue (skeletal and cardiac muscles), the parallel or longitudinal, and the perpendicular or transversal. The directions are referred to the orientation of the muscle fibers. If the muscle tissue is oriented along one of the principal axes in the coordinate system, two of the elements in the above matrix, describing conductivities in the perpendicular direction, are equal. Computation of the electric field is simplified if the model can be described in cylindrical co-ordinate system.

Boundary conditions across interface of two volume conductors with different conductivities are:

$$J_{n1} = J_{n2}, \quad (5)$$

where J_{n1} and J_{n2} are the normal components of \mathbf{J} at the boundary surface in the volume conductors 1 and 2, and:

$$E_{t1} = E_{t2}, \quad (6)$$

where E_{t1} and E_{t2} are the tangential components of \mathbf{E} at the interface.

The equation of the continuity for current states that free charge cannot remain within a conductor and is the field equivalent of Kirchoff's current law, which states that the net current leaving a junction of several conductors is zero. The continuity equation in the differential form is:

$$\nabla \cdot \mathbf{J} = 0. \quad (7)$$

Considering the point form of Ohm's law **Eq. 1** we obtain:

$$\nabla \cdot (\gamma \cdot \mathbf{E}) = 0. \quad (8)$$

Using the definition of the electric field intensity **Eq. 2** yields:

$$\nabla \cdot [\gamma \cdot (-\nabla u)] = 0 \quad (9)$$

If the volume conductor is homogeneous and isotropic (γ is scalar), then the above equation becomes Laplace's equation:

$$\nabla^2 u = 0. \quad (10)$$

Equation 10 is a partial differential equation of elliptic type, which together with two types of boundary conditions describes electric field inside the volume conductor. The two types of boundary conditions are: the Dirichlet boundary condition defined as a fixed scalar electric potential, that is, applied voltage on the surface of the model:

$$u = \bar{u}, \quad (11)$$

and the Neumann boundary condition defined as a first derivative of the scalar electric potential in the direction normal to the boundary surface of the model, that is, current density flowing in/out of the model in the direction normal to the surface, divided by the conductivity of the tissue:

$$q = \frac{\partial u}{\partial n} = - \frac{\vec{\mathbf{J}}_n}{\gamma}. \quad (12)$$

Laplace's equation can be solved analytically or using one of the numerical methods. The analytic method is suitable when the geometry, inhomogeneities and anisotropies of the volume conductor are describable in the same coordinate system, i.e. Cartesian, spherical or cylindrical. Models in which this condition is not fulfilled result in complicated systems of equations, which are difficult to solve. A majority of numerical methods, on the other hand, allow approximation of any geometry, material properties, and boundary conditions. Most methods also allow definition of various material inhomogeneities and in some methods anisotropies can be defined. Complex geometry, inhomogeneities and anisotropies of the tissue are characteristic properties of most of the biological systems. The use of numerical techniques is therefore more appropriate in such studies.

2.2. Finite Element Method

The finite element method has proven to be very effective in numerous computations of the electric field inside biological systems (26,27). The discretization of the domain is the first step in majority of the numerical

methods. In the so-called domain methods, for example, finite element or finite difference, the whole volume of a three dimensional model has to be discretized. In the so-called boundary methods, e.g. boundary element method, only boundary surfaces bounding regions of the model with the same material properties, for example, specific biological tissue (skin, muscle, etc.), have to be discretized. The discretization of the domain in finite element method involves the decision about the type, number, size, and shape of the finite elements to model the real biological system, for example, tissue, organ, whole or part of the body. There are no theoretical guidelines on how to perform this step. It is merely an art, which depends on the use of engineering judgment, but can produce inaccurate results if not done properly.

The next step of the finite element method approach is the selection of the electric quantity which will be calculated and from which all other electrical quantities will be derived. The scalar electric potential u is a good choice in the volume conductor calculation since it results in less complex calculations. The continuous function of electric potential u is then approximated by a discrete model composed of a set of piecewise continuous functions, usually polynomials, defined over each particular finite element. Appropriate material properties, i.e. electric conductivities, have to be assigned to each particular element. Anisotropic conductivities can as well be applied and result in a specific type of finite element i.e. different function. This is a very important step since it has a strong influence on the results. Several reports about electrical properties of living tissues can be found in the literature (28,29). Then the boundary conditions are applied. As described in the previous subsection, two types of boundary conditions apply in the volume conductor modeling: fixed scalar electric potential and/or first derivative of the scalar electric potential in the direction normal to the boundary surface of the model, that is, current density flowing in/out of the model in the direction normal to the surface, divided by the conductivity of the tissue. In the modeling of in vivo electroporation, different positions and electrode shapes in models can be represented by applying appropriate boundary conditions, for example, correspondent values of electric scalar potential.

After this a set of simple equations describing the discretized scalar electric potential throughout the whole volume of the model is obtained. After rearranging, this system of equations is solved using one of the appropriate numerical methods. At the end, all other desired electrical quantities are calculated from the resulting discrete values of scalar electric potential. The finite element method is described in greater detail in numerous references (30,31).

3. Analysis of Electric Field Distribution in Electrochemotherapy

As it was mentioned in the introduction, various electrode geometries were used in the *in vivo* studies involving plasma membrane electropermeabilization. In electrochemotherapy, membrane permeabilization is used to enhance delivery of chemotherapeutic drugs into the tumor cells and increase antitumor effectiveness. Namely, some chemotherapeutic drugs used in cancer therapy have poor access into the tumor cells. Furthermore, lower systemic doses of chemotherapeutic drugs are required for successful therapy and thus adverse side effects are reduced. Numerical modeling can be used as a tool for the explanation of the observed effects.

In one of the several studies of the efficacy of electrochemotherapy of solid tumors, performed in Ljubljana (10), it was demonstrated that changing electrode orientation improves the efficacy of electrochemotherapy of solid tumors in mice (*see* also Chapter 14 by Čemažar). Ehrlich ascites tumor in CBA mice was used as a tumor model. When the tumors reached approximately 40 mm³ in volume, they were treated with the combination of intravenously injected Bleomycin (Mack, Germany) and trains of square-wave high voltage DC pulses (amplitude 1040 V, pulse width 100 μs, repetition frequency 1 Hz). Electric pulses were delivered by two parallel stainless steel plate electrodes 8 mm apart (two stainless steel strips, 7 mm in width with rounded tips). Good contact between the electrodes and the skin was ensured by means of conductive gel. Tumors were treated either with 4, 8, or 4+4 pulses in train. In the last group the second train of 4 pulses was delivered with electrodes oriented perpendicularly with respect to the first one with a time interval of 1 s between the two trains of pulses, that is, 4+4 pulses. This changing of the electrode orientation resulted in improved anti-tumor efficacy of the electrochemotherapy: prolonged tumor growth delay and higher percentage of short and long term complete responses of the tumors.

3.1. Finite Element Model of a Mouse With Subcutaneous Solid Tumor

In order to explain improved antitumor effectiveness in changing electrode orientation experiments and to gain more detailed insight into electrical phenomena inside tumour and in the surrounding tissue during different electrochemotherapy regimes, a three-dimensional (3D) anatomically based finite element model of the mouse with injected subcutaneous solid tumor was built (32). The geometry of the model was based on the 14 cross section scans of a typical animal with a subcutaneous tumor obtained by magnetic resonance

Table 1
Electric Conductivities of the Tissues Used in the Model
of the Mouse With Subcutaneous Tumor

Tissue	Conductivity γ (S/m)
Skin	0.04
Fat	0.046
Muscle	$\gamma_{xx} = 0.225$ $\gamma_{yy} = 0.225$ $\gamma_{zz} = 0.9$
Bone	0.025
Connective tissue	0.025
Intestine	0.55
Kidneys	1.01
Liver	0.333
Lungs	0.07
Heart	$\gamma_{xx} = 0.2$ $\gamma_{yy} = 0.2$ $\gamma_{zz} = 0.9$
Tumor	0.125

imaging (MRI). The distance between the two neighboring cross sections in the longitudinal direction was 2.7 mm. There were eleven MRI scans in the abdominal and three in the thoracic part of the body of the mouse. Resulting three-dimensional geometric structure was built of eleven different tissues (organs), that is, skin, fat, skeletal and heart muscles, bone, connective tissue, intestine, kidney, liver, lung and tumor. Each of these tissues (organs) formed a closed region and a mesh of 3D finite elements was generated inside with appropriate material properties assigned to the elements in each region. Anisotropic characteristics were considered for skeletal and heart muscles, while all other tissues (organs) were modeled as isotropic. The values of the electric conductivities of tissues (organs) used in the model were collected from literature and used in one of previous studies where similar model was verified with the measurements of electric potential in the 5 points in the tumor and surrounding tissue (27). All tissue conductivities are listed in **Table 1**. Resulting 3D model was made of 7089 3D finite elements which were defined by 7578 grid points. The cross section through the tumor in which the results were observed is shown in **Fig. 1**.

Different electrode orientations were obtained by applying appropriate boundary conditions in the grid points on the outer surface of the model corresponding to each of the two electrodes. Increased area with the same electric

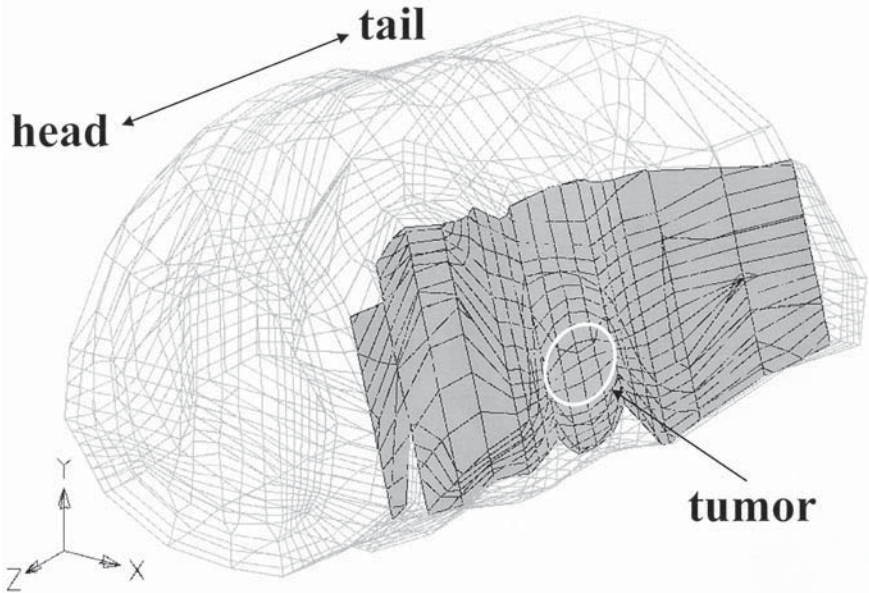


Fig. 1. Three-dimensional anatomically based finite element model of a mouse with subcutaneous solid tumor. Shaded plane represents cross section through the middle of the tumor in which the results were shown.

potential under each electrode resulting from the use of conductive gel was also considered. Fixed values of scalar electric potential, that is, Dirichlet boundary conditions, were assigned to grid points in the regions where electrodes were placed. Two electrode configurations were modeled according to the position of the electrodes with respect to the tumor, e.g. cranial/caudal and dorsal/ventral. Potentials of 0 V and 1040 V were assigned to groups of appropriate grid points of the finite element mesh corresponding to each of the electrodes thus modeling the conditions in the experimental study. The width of both electrodes was 7 mm and their thickness was 0.9 mm. In the cranial/caudal electrode configuration the positive electrode was placed on the left side of the tumor in the direction towards the head of the mouse. The distance between the electrode and the edge of the tumor was 0.9 mm. The negative electrode was placed on the other (right) side of the tumor in the direction towards the tail of the mouse and the distance between the electrode and the edge of the tumor was again 0.9 mm. In the dorsal/ventral electrode configuration the positive electrode was placed above the tumor in the direction towards the back of the mouse. The distance between the electrode and the edge of the tumor was 0.9 mm. The negative electrode was placed on the other side below the tumor

and the distance between the electrode and the edge of the tumor was again 0.9 mm. On the remaining outer surfaces of the model, the Neumann boundary condition was applied. This boundary was considered as the interface between a conducting medium and air (assumed as an ideal dielectric). Since the conductor (skin layer) was linear and isotropic, the usual Neumann condition was applied i.e. the normal derivative of the electric potential on the interface between the model and surrounding air was zero.

3.2. Validation of the Model

The process of the mathematical model validation is of utmost importance. A very basic method of validating *in vivo* models is simply to compare measured and calculated values of total currents flowing in/out of the model and correspondent potentials/voltages for each particular experimental regime. If there is high correlation between calculated and measured values, the model can be considered a good approximation of the actual electrical phenomena inside biological tissue.

In order to validate previously described model in greater detail current density distributions in tumor were qualitatively evaluated for different specific electrode sets by means of magnetic resonance current density imaging (33). Electric current density imaging (CDI) is a magnetic resonance imaging (MRI) technique that images current density by acquiring data from phase shifts in proton precession. Phase shifts are caused by short pulses of direct electric current, which are passing through the sample during imaging time (34,35). In this study, four point copper electrodes with diameter of 0.6 mm were used, two by two placed on each cross-plane of the tumor. The point electrodes were connected to the voltage amplifier as shown in **Fig. 2**. Two configurations of electrodes were thus used: the 2+2 electrode set, where all four electrodes were connected to the voltage amplifier (**Fig. 2c**); and the 2+1 electrode set, where just three electrodes were connected to the voltage amplifier as depicted in **Fig. 2b**. These two electrode configurations were chosen in order to produce notably different current density and thus electric field distribution in the observed plane (dashed line in **Fig. 2**) of the tumor as well as in the whole tumor. This difference allowed us to validate the model by means of current density imaging (CDI) and electrochemotherapy effectiveness. CDI was used to map spatial distribution of electric currents through mice tumors. Mice were placed into a stereotactic frame and four point electrodes in pairs two by two with a small amount of conductive gel were affixed to the tumor. The electrodes were connected to a DC voltage amplifier and the voltage applied to the tumor was 50 V with total duration of current pulses 10 ms. Throughout the imaging time electric current was controlled with an oscilloscope and a voltmeter. To construct a map of electric current density spatial distribution (j_z in

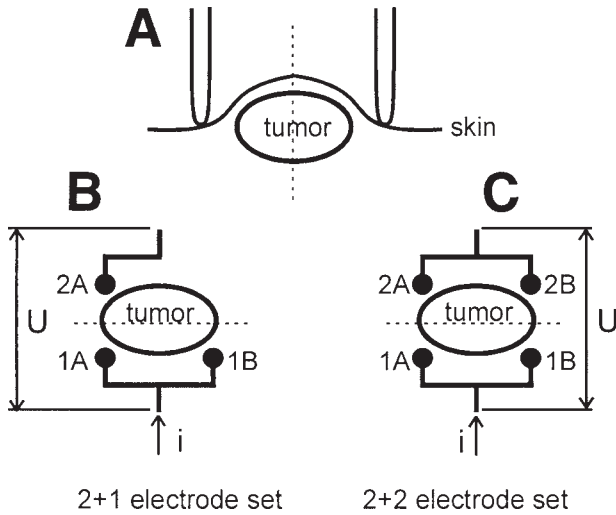


Fig. 2. Schematic presentation of 2+1 and 2+2 electrode set positioning with respect to the tumor and point electrodes electrical connections. The plane of current density images and presentation of numerical results is depicted with dashed line.

xy-plane), mice were imaged at two orientations 90° apart about z-axis, as required by theory.

CDI images qualitatively show the effect of the two different electrode sets on the current density spatial distribution through the tumor. **Figures 3A** and **3C** are conventional MR images, where anatomical structures of the mouse can be seen, with current density maps superimposed in the tumor area. In the 2+1 electrode set, a small region of higher signal intensity was observed in the CDI image (Figure 3a), which corresponds to higher current density and thus to higher electric field intensity. CDI signal was decreasing towards the opposite side of the imaged plane, where the unconnected electrode was placed. When all four electrodes were connected to the voltage amplifier (2+2 electrode set) current density throughout the imaging plane can be observed with two regions of higher current density (**Fig. 3C**) and thus higher electric field intensity. Qualitatively similar results in spatial distribution of current density were obtained by calculating current density in the observed plane of the finite element model at 50 V for 2+1 electrode set (**Fig. 3B**) and 2+2 electrode set (Fig. 3d). The results clearly show that spatial distribution of current density obtained by means of CDI is qualitatively similar to the calculated spatial distribution of current density in the observed plane using 3D FE model of a mouse with subcutaneous solid tumor.

In addition, the current measured during CDI was 4.7 ± 0.3 mA and

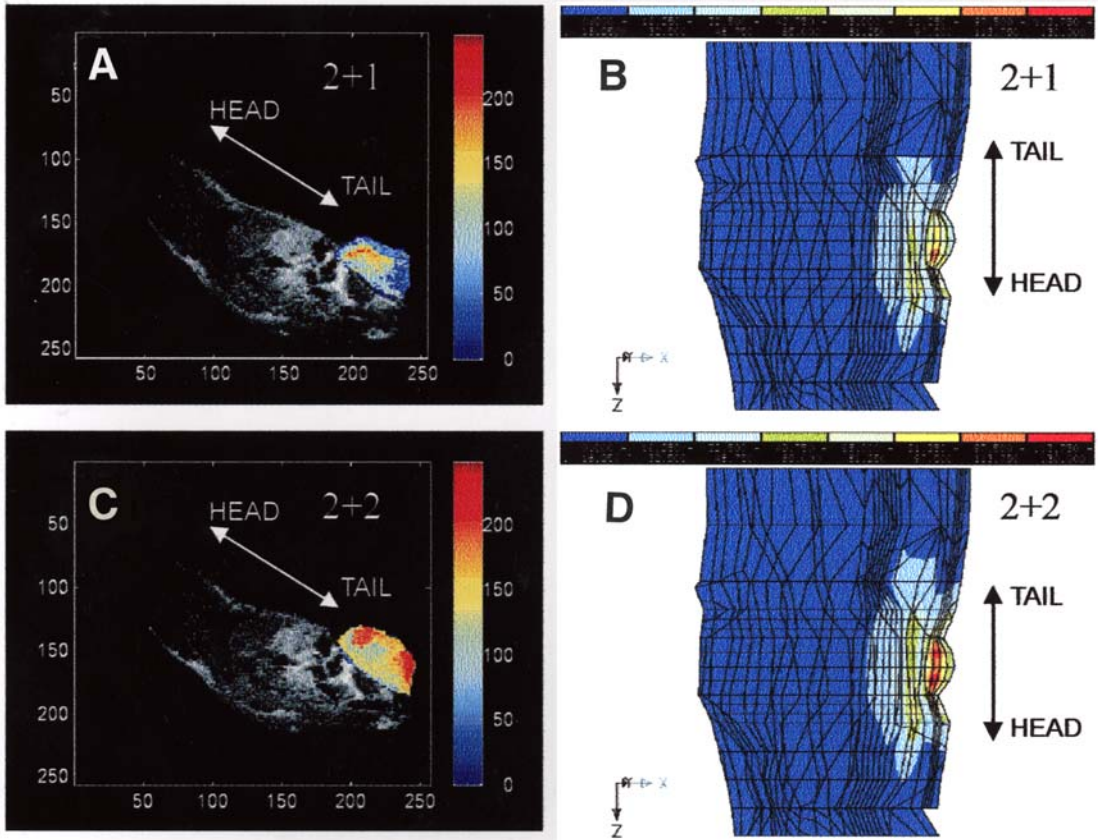


Fig. 3. Two-dimensional current density spatial distribution: (A) current density imaging (CDI) map using 2+1 electrode set (C) using 2+2 electrode set, both superimposed on a conventional MR images of a mouse with solid subcutaneous tumor; (B) calculated current densities from the finite element 3D model for 2+1 and (D) 2+2 electrode set. For CDI images current density is given in arbitrary units, i.e. pixel intensity (a and c). Calculated current density is given in A/m (b and d).

6.3 ± 0.6 mA (mean \pm standard deviation) in 2+1 and 2+2 electrode set, respectively at voltage being kept constant at 50 V. The total current in the model for 50 V was 4.5 mA and 6.1 mA for 2+1 and 2+2 electrode set, respectively.

The above validation attempts demonstrate that numerical model is reliable and can be very useful in further search for electrodes which would make electrochemotherapy and in vivo electroporation in general even more efficient.

Table 2
Mean Values of the Magnitude of Electric Field Intensity Compared to the Antitumor Effectiveness of Electrochemotherapy with 2+1 and 2+2 Point Electrode Set

Electrochemotherapy	E_{mean} Inside Tumor (V/cm)	Growth Delay (days)
2+1 electrode set	202	7.7 ± 1.3
2+2 electrode set	251	14.0 ± 2.0

3.3. Effect of Electric Field Distribution on Electroporation: Comparison of Numerical and Experimental Results

In order to further validate our numerical model we performed electrochemotherapy with 2+1 and 2+2 point electrodes on solid subcutaneous fibrosarcoma SA-1 tumors in A/J mice. Eight square pulses of 1300V, 100 μ s, repetition frequency 1Hz were delivered 3 minutes after intravenous injection of 5mg/kg bleomycin. Control experimental groups comprised bleomycin alone, electric pulses alone and not treated tumors. As expected from numerical results and current density images, electrochemotherapy with 2+2 electrode set was more efficient than 2+1 electrode set (**Table 2**).

Distribution of scalar electric potential was also calculated for cranial/caudal and dorsal/ventral plate electrodes configuration. Distribution of electric field intensity was then calculated from the values of the scalar electric potential in the grid points of the model. For the electrode configuration 4+4, where for the last 4 pulses the electrodes were oriented perpendicularly with respect to the position of the electrodes for the first 4 pulses, electric field distribution was determined as a combination of the results for the cranial/caudal and dorsal/ventral electrode configurations. Since electroporation is a threshold phenomenon, it can be assumed that in the 4+4 electrode configuration the effective magnitude of electric field intensity in each finite element of the model is the highest of the magnitudes for cranial/caudal and dorsal/ventral electrode configurations in that particular element. Based on this assumption we determined the values of the electric field intensity for all 7089 finite elements of the model.

The results were observed in the cross section plane through the middle of the tumor alongside it (*see Fig. 1*), since we were most interested in the electrical phenomena inside tumor tissue. In **Fig. 4** the results for the all three electrode configurations are shown. In both cranial/caudal and dorsal/ventral electrode configurations, the maximum magnitude of electric field intensity

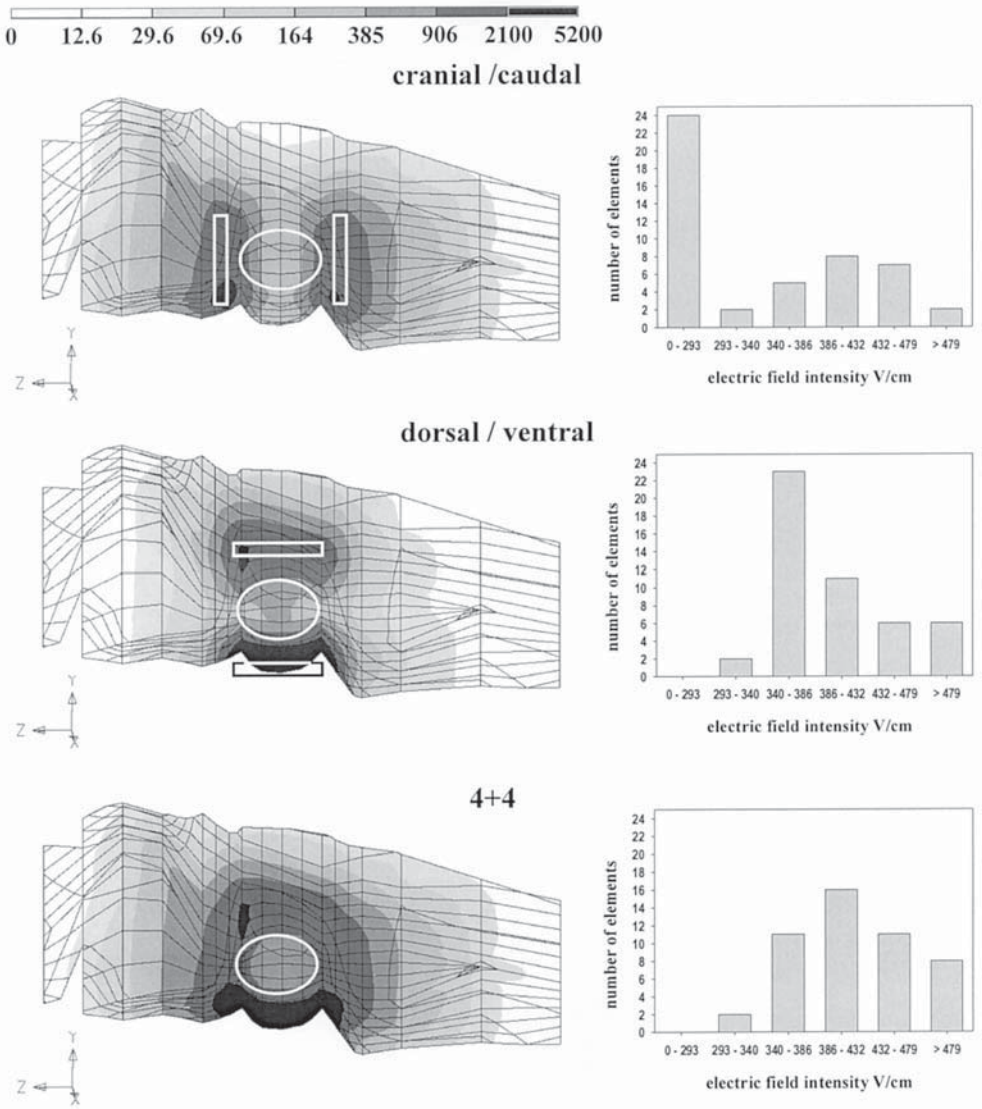


Fig. 4. Electric field distribution (from the top) for the cranial/caudal, dorsal/ventral and 4+4 electrode configurations in the observed cross section (left) and histograms of electric field intensity in total 48 elements representing the tumor in 3D finite element model (right). Projection of the electrodes to the observed cross section and tumor location is marked in cranial/caudal and dorsal/ventral electrode configurations.

Table 3
Mean Values of the Magnitude of Electric Field Intensity Compared to the Antitumor Effectiveness of Electrochemotherapy With Electrodes in Different Orientations and Changing of the Electrodes, i.e., 4+4 electrode configuration

Electrochemotherapy	E_{mean} Inside Tumor (V/cm)	Growth Delay (days)
Cranial/caudal	327	17.10 ± 1.60
Dorsal/ventral	406	21.35 ± 1.94
4+4	425	26.17 ± 2.32

inside the tumor is obtained on the opposite sides in proximity of the electrodes. It is much lower in the middle of the tumor and it falls even more towards edges of the tumor in the direction away from the line connecting electrodes. This pattern is in good agreement with the experimental results. Namely, in the group where electrode orientation was not changed many of the tumors regrew after successful treatment in the margins where there was no contact with the electrodes (**10**) (see Chapter 14 in **ref. 3**).

The distribution of the electric field was more precisely studied for 48 elements representing subcutaneous tumor since we were most interested in the electrical phenomena inside tumor tissue. The values of electric field intensity are presented in **Fig. 4** in the form of histograms for each of the electrode orientations. The summary of the data together with experimental results, i.e. growth delays are listed in **Table 3**. Good agreement between the level of anti-tumor effectiveness and the mean value of electric field intensity for each particular electrochemotherapy treatment regime can be noted.

4. Summary and Conclusions

Mathematical modeling for in vivo electroporation has proven to be simple and efficient tool for the analysis of electrical phenomena inside biological tissue. It is very useful for the explanation of experimental results and analysis of different electroporation regimes. It was also demonstrated, that better coverage of tumors with sufficiently high electric field is necessary for improved effectiveness of electrochemotherapy and so this approach can be very useful in further search for electrodes which would make electrochemotherapy and in vivo electroporation in general more efficient. The objective of such studies would be to optimize electrode configuration in order to obtain electric fields over threshold value in the whole selected tissue, for example, tumor, and minimize it in the surrounding and deeper tissues.

Validated mathematical models make possible analysis and optimization of the shape, position and dimensions of the electrodes used in electrochemo-

therapy for its better antitumor effectiveness and reduction of the required quantity of chemotherapeutic drug for the successful therapy that will reduce its undesired side effects on the healthy tissue. Furthermore they can help to minimize other possible side effects (pain, contraction of the surrounding muscles, influence of the induced currents on the deeper lying tissues and organs). Mathematical modeling can also provide information about electric currents in deeper lying organs, e.g. heart, and will be very useful in studies of safety measures that need to be taken in clinical use. In addition, the results obtained are also relevant for *in vivo* gene transfection by means of electroporation.

Mathematical modeling can be very useful in the transfer of the knowledge gained in experimental work into clinical practice. With its contribution to the development of electrochemotherapy and electro gene transfection it can bring benefits to individual patients as well as to the society. Electrochemotherapy is an attractive approach to the treatment of cancer not only because it seems to be effective in local tumor control, but also because it is an approach that can help to circumvent the side effects of chemotherapy. This would reduce the costs of cancer treatment induced by the care of the side effects, which are frequently responsible for prolonged stays in the hospitals and large consumption of drugs other than the cytotoxic drugs. With its possibilities in the optimization of the electrochemotherapeutic regimes and local *in vivo* gene transfection, mathematical modeling can substantially contribute to this aims. The long term perspective of mathematical modeling is to contribute to understanding and wider clinical applicability of electrochemotherapy in treatment of cancer and of electro gene transfection as a future treatment for various diseases.

Acknowledgments

This work was performed in close collaboration with Gregor Serša and Maja Čemažar from Institute of Oncology, Ljubljana, Franci Demšar, Katarina Beravs, and Igor Serša from Institute Jožef Stefan, Ljubljana. The authors would also like to thank to Alenka Maček-Lebar, Tadej Kotnik, Vojko Valenčič, Tomaž Jarm, Jani Pušenjak, Rudi Kragelj, and Lojze Vodovnik which contributed their skills and expertise in various phases of this work. The research work has been supported under various grants from The Ministry of Science and Technology of The Republic of Slovenia and PROTEUS programme of scientific, technological and cultural cooperation between the Republic of France and the Republic of Slovenia.

References

1. Kotnik, T., Bobanović, F., and Miklavčič, D. (1997) Sensitivity of transmembrane voltage induced by applied electric fields: A theoretical analysis. *Bioelectrochem. Bioenerg.* **43**, 285–291.
2. Orłowski, S. and Mir, L. M. (1993) Cell electroporation: A new tool for biochemical and pharmacological studies. *Biochim. Biophys. Acta* **1154**, 51–63.
3. Čemažar, M., Jarm, T., Miklavčič, D., Maček-Lebar, A., Ihan, A., Kopitar, N. A., and Serša, G. (1998) Effect of electric field intensity on electroporabilization and electrosensitivity of various tumor-cell lines in vitro. *Electr. Magnetobiol.* **17**, 261–270.
4. Belehradek, J., Orłowski, S., Ramirez, L. H., Pron, G., Poddevin, B., and Mir, L. M. (1994) Electroporation of cells in tissues assessed by the qualitative and quantitative electroloading of bleomycin. *Biochim. Biophys. Acta* **1190**, 155–163.
5. Weaver, J. C. (1993) Electroporation: A general phenomenon for manipulating cells and tissues. *J. Cell. Biochem.* **51**, 426–435.
6. Orłowski, S., Belehradek, J. Jr., Paoletti, C., and Mir, L. M. (1988) Transient electroporation of cells in culture. *Biochem. Pharmacol.* **37**, 4727–4733.
7. Susil, R., Šemrov, D., and Miklavčič, D. (1998) Electric field induced transmembrane potential depends on cell density and organization. *Electr. Magnetobiol.* **17**, 391–399.
8. Puc, M., Reberšek, S., and Miklavčič, D. (1997) Requirements for a clinical electrochemotherapy device: Electroporator. *Radiol. Oncol.* **31**, 368–373.
9. Van De Graaff, K. M. and Rhees, R. W. (1987) *Schaum's Outline of Theory and Problems of Human Anatomy and Physiology*. McGraw-Hill, New York, pp. 39–53.
10. Serša, G., Čemažar, M., Šemrov, D., and Miklavčič, D. (1996) Changing electrode orientation improves the efficacy of electrochemotherapy of solid tumors in mice. *Bioelectrochem. Bioenerg.* **39**, 61–66.
11. Gilbert, R. A., Jaroszeski, M. J., and Heller, R. (1997) Novel electrode designs for electrochemotherapy. *Biochim. Biophys. Acta* **1334**, 9–14.
12. Barr, R. C., Pilkington, T. C., Boineau, J. P., and Spach, M. S. (1966) Determining surface potentials from current dipoles, with application to electrocardiography. *IEEE Trans. Biomed. Eng.* **13**, 88–92.
13. Neonen, J. T. (1994) Solving the inverse problem in magnetocardiography. *IEEE Eng. Med. Biol.* **13**, 487–496.
14. MacLeod, R. S. and Brooks, D. H. (1998) Recent progress in inverse problems in electrocardiology. *IEEE Eng. Med. Biol.* **17**, 73–83.
15. Panescu, D., Webster, J. G., Tompkins, W. J., and Stratbucker, R. A. (1995) Optimisation of transcutaneous cardiac pacing by three-dimensional finite element modeling of the human thorax. *Med. Biol. Eng. Comp.* **33**, 769–775.
16. Hutchinson, S. A., Kwong, T. Ng., Shadid, J. N., and Nadeem, A. (1997) Electri-

- cal defibrillation optimization: An automated, iterative parallel finite-element approach. *IEEE Trans. Biomed. Eng.* **44**, 278–289.
17. Haueisen, J., Ramon, C., Eiselt, M., Brauer, H., and Nowak, H. (1997) Influence of tissue resistivities on neuromagnetic fields and electric potentials studied with a finite element model of the head. *IEEE Trans. Biomed. Eng.* **44**, 727–735.
 18. Awada, K. A., Jackson, D. R., Williams, J. T., Wilton, D. R., Baumann, S. B., and Papanicolau, A. C. (1997) Computational aspects of finite element modeling in EEG source localization. *IEEE Trans. Biomed. Eng.* **44**, 736–752.
 19. Eaton, H. (1992) Electric field induced in a spherical volume conductor from arbitrary coils: application to magnetic stimulation and MEG. *Med. Biol. Eng. Comp.* **30**, 433–440.
 20. Ferdjallah, M., Bostock, F. X., and Barr, R. E. (1996) Potential and current density distributions of cranial electrotherapy stimulation (CES) in a four-concentric-spheres model. *IEEE Trans. Biomed. Eng.* **43**, 939–943.
 21. Gentili, G. B., Leoncini, M., Trembly, B. S., and Schweizer, S. E. (1997) FDTD electromagnetic and thermal analysis of interstitial hyperthermic applicators. *IEEE Trans. Biomed. Eng.* **42**, 973–980.
 22. Tsuda, N., Kuroda, K., and Suzuki, Y. (1996) An inverse method to optimize heating conditions in RF-capacitive hyperthermia. *IEEE Trans. Biomed. Eng.* **43**, 1029–1037.
 23. Gandhi, O. P. and Deford, J. F. (1988) Calculation of EM power deposition for operator exposure to RF induction heaters. *IEEE Trans. Biomed. Eng.* **30**, 63–68.
 24. Kuster, N (1993) Multiple multipole method for simulating EM problems involving biological bodies. *IEEE Trans. Biomed. Eng.* **40**, 611–620.
 25. Plonsey, R. and Heppner, D. (1967) Considerations of quasi-stationarity in electrophysiological systems. *Bull. Math. Biophys.* **29**, 657–664.
 26. Šemrov, D., Karba, R., and Valenčič, V. (1997) DC electrical stimulation for chronic wound healing enhancement. Part 2. Parameter determination by numerical modeling. *Bioelectrochem. Bioenerg.* **43**, 271–277.
 27. Miklavčič, D., Šemrov, D., Valenčič, V., Serša, G., and Vodovnik, L. (1997) Tumor treatment by direct electric current: Computation of electric current and power density distribution. *Electr. Magnetobiol.* **16**, 119–128.
 28. Geddes, L. A. and Baker, L. E. (1967) The specific resistance of biological material: A compendium of data for the biomedical engineer and physiologist. *Med. Biol. Eng.* **5**, 271–293.
 29. Foster, K. R. (1995) Dielectric properties of tissues. *The Biomedical Engineering Handbook* (Bronzino, J. D., ed.). CRC Press and IEEE Press, Boca Raton, FL and New York, pp. 1385–1394.
 30. Brauer, J. R. (1988) *What Every Engineer Should Know About Finite Element Analysis*. Marcel Dekker, New York.
 31. Zienkiewicz, O. C. (1977) *The Finite Element Method*. McGraw-Hill, New York.
 32. Šemrov, D. and Miklavčič, D. (1998) Calculation of the electrical parameters in electrochemotherapy of solid tumors in mice. *Comp. Biol. Med.* **28**, 439–448.

33. Miklavčič, D., Beravs, K., Šemrov, D., Čemažar, M., Demšar, F., and Serša, G. (1998) The importance of electric field distribution for effective in vivo electroporation. *Biophys. J.* **74**, 2152–2158.
34. Joy, M., Scott, G., and Henkelman, M. (1989) In vivo detection of applied electric currents by magnetic resonance imaging. *Magn. Reson. Imaging* **7**, 89–94.
35. Serša, I., Jarh, O., and Demšar, F. (1994) Magnetic resonance microscopy of electric currents. *J. Magn. Reson. Ser. A* **111**, 93–99.

In Vitro Delivery of Drugs and Other Molecules to Cells

Marie-Pierre Rols, Muriel Golzio,
Christine Delteil, and Justin Teissié

1. Introduction

The permeability of a cell membrane can be transiently increased locally when an external electric field pulse with an overcritical intensity is applied. A position dependent modulation of the membrane potential difference is induced during the pulse. A local membrane alteration is created, which may reseal. Its molecular definition remains unknown. This phenomenon is now commonly known as *electroporation* or *electropermeabilization*. The former term implies that physical pores are created in the lipid matrix. However their existence has never been clearly demonstrated. The term electroporation is therefore rather misleading.

The term electropermeabilization specifies a change in permeability without any mechanistic description. A free exchange of hydrophilic molecules indeed takes place across the membrane. This means that a leakage of cytosolic metabolites is present. Loading of polar drugs into the cytoplasm can be obtained. Under suitable conditions depending mainly on the pulse parameters (field strength, pulse duration, number of pulses), the viability of the cell can be preserved. Electropulsation is therefore an elegant way to gain access to the cytoplasm and to introduce well-defined foreign molecules (1–3). This approach is routinely used in cell and molecular biology, in biotechnology, and more recently in medicine. It is now proposed as a very efficient way for drug, oligonucleotide, antibody and plasmid delivery in vitro and in vivo for clinical applications (4–7). Moreover, by affecting the stratum corneum, it could enhance transdermal delivery mediated by iontophoresis (8,9).

There is a general agreement that very little is known about what is really occurring in the cell and its membranes at the molecular levels. The focus of this chapter is to review the current facts dealing with in vitro mammalian cell permeabilization to small molecules such as drugs and to large molecules such as proteins.

2. In Vitro Delivery of Small Molecules

2.1. Effect of Electric Field Parameters

Cells in an electric field are submitted to different effects. The most important is the modulation of their native transmembrane potential difference $\Delta\Psi_0$. This is due to the electrical discontinuity built by the membrane which is considered as a dielectric with leaks. The electrically induced potential difference $\Delta\Psi_E$ at a point M on the cell surface can be written as:

$$\Delta\Psi_E = Fg(\lambda)rE \cos \theta (M) \quad (1)$$

where F is related to the shape of the cell (often assimilated to a sphere for cells in suspension), g depends on the conductivity λ of the membrane, which is not a pure dielectric and where conducting leaks are present, r is the radius of the cell, E the field strength and $\theta (M)$ the angle between the normal to the membrane at the position M and the direction of the field (**10**). The field induced potential difference is added to the resting one (**11**). Being dependent on an angular parameter (θ), the field effect is position dependent on the cell surface. Therefore, one side of the cell is going to be hyperpolarized while the other side is depolarized (**Fig. 1**).

2.1.1. Effect of Electric Field Strength

Permeabilization is triggered as soon as the resulting potential difference reaches a critical threshold. Permeabilization is then controlled by the field strength E . It occurs only on the part of the cell surface where the membrane potential difference has been brought to its critical rupturing value (**12,13**). The field strength controls two effects: (i) it is the trigger of permeabilization. For a given cell, it must be larger than a critical value E_p for the membrane unbalance to appear; (ii) when larger than E_p , it controls the geometry of the part of the cell surface which is affected. E_p is linked to the reciprocal of r from **Eq. 1**. Larger cells are therefore permeabilized at electric field values lower than the ones required to permeabilize smallest cells (**5**). For a given cell population, with inhomogeneous sizes, increasing E induces an increase in the percentage of cells that are permeabilized (**Fig. 2**). But the structural alteration, which occurs in this altered cap, is not controlled by the field strength (**14,15**).

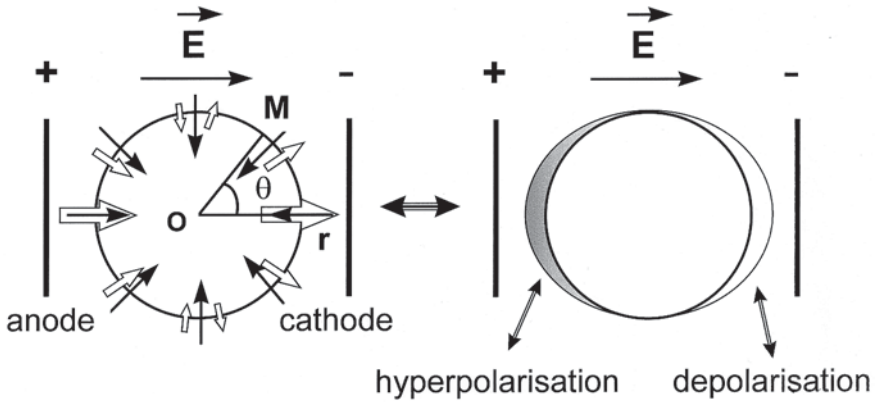


Fig. 1. Effect of electric field on the modulation of the transmembrane electric potential difference of a cell. The electric field leads to the induction of a transmembrane potential difference $\Delta\Psi_E$ which surrimposes to the native one $\Delta\Psi_o$. The arrows are representative of the electrical potential gradient direction: closed arrows, resting potential, open arrows, electric field induced potential. Their length is indicative of the magnitude of the potential difference. Cell is then hyperpolarized at the anode facing side, and depolarized at the cathode facing side.

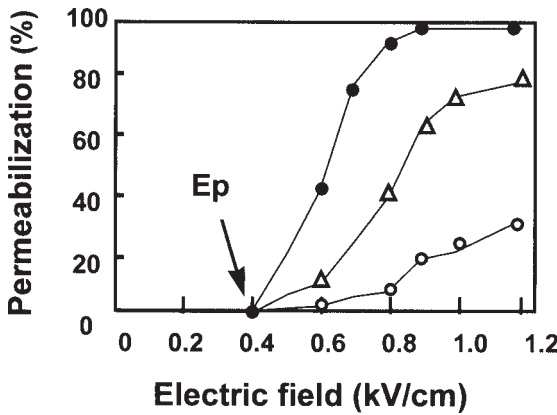


Fig. 2. Effect of the electric field parameters on the electroporation of cells. CHO cells are pulsed at a 1-Hz frequency in the pulsation buffer in the presence of propidium iodide. The percentage of fluorescent cells is plotted as a function of the electric field intensity for different number of pulses and duration values: 10 pulses at 0.1 ms duration (○), 10 pulses at 5 ms (△), 20 pulses at 5 ms (●).

2.1.2. Effect of Pulse Duration

At a given electric field strength E , higher than E_p , increasing T induces an increase in permeabilization efficiency (**Fig. 2**). The fraction of the cell surface which is affected by the electric pulse is not dependent on the pulse duration T , it is controlled by E . But the extent of permeabilization, that is, the density of alterations is strongly controlled by T , not by E .

2.1.3. Effect of the Number of Pulses

The fraction of the cell surface where permeabilization takes place does not depend on the number of pulses N . But, as for pulse duration, the density of alterations, meaning the efficiency of permeabilization, is controlled by N (**Fig. 2**).

2.2. Electropemeabilization

2.2.1. A Fast and Localized Process

Using video observation of single cells under a fluorescence microscope gives more direct observations. Membrane conductance changes can be observed (**16**). Uptake can be visualized by videomicroscopy. Specific labeling with hydrophilic markers is obtained during and after the pulse (**17,18**). Propidium iodide passive diffusion in cells is a very slow process, with half-time of 2.5 hours. In electropemeabilized cells, half-time values of uptake in the cytoplasm and the nuclei decreased to 1.3 and 1.6 minutes (**18**), that is, by two orders of magnitude.

Micrographs of uptake of propidium iodide into CHO cells submitted to electric pulses are shown in **Fig. 3**. Propidium iodide uptake in the cytoplasm is a fast process that can be detected in the seconds following pulsation. Less than one minute later, it appears at the nuclei level. Moreover, and in agreement with other works, exchange across the pulsed cell membrane is not homogeneous. It occurs at the positions of the cells facing the electrodes on an asymmetrical way mainly at the anode facing side of the cells (**19–22**).

The critical potential difference value $\Delta\Psi_{\text{perm}}$ leading to cell permeabilization is the sum between $\Delta\Psi_o$ and $\Delta\Psi_E$; it has been recently reevaluated to be of the order of 200 mV (**17,23**). From **Eq. 1**, it is clear that this is obtained for low critical field intensities, only for θ close to 0 or π . It is only the parts of the cell surface facing the electrodes, which are affected. E_p is such that:

$$\Delta\Psi_E = Fg(\lambda)rE_p \quad (2)$$

This electropemeabilized state of the membrane is observed to be only local on the cell surface as predicted. The extent of the permeabilized part of the cell surface, A_{perm} , is given by:

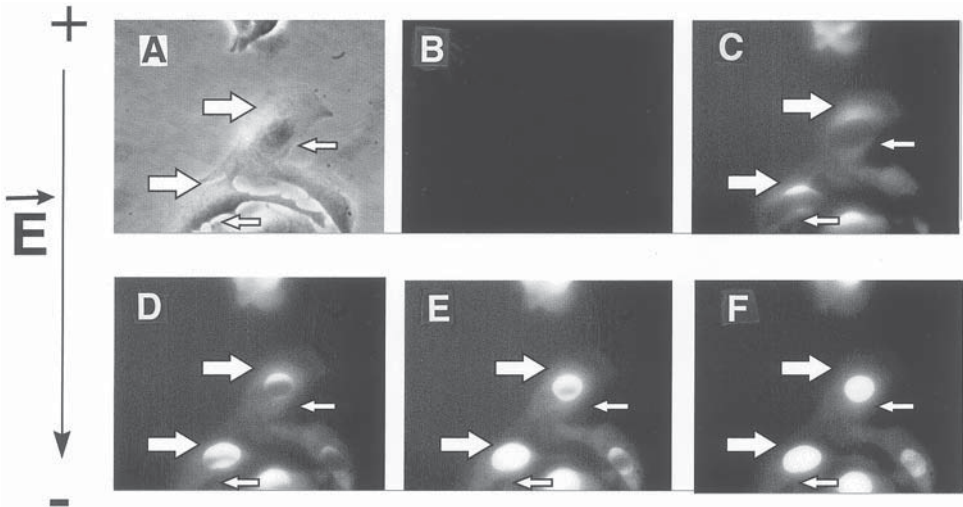


Fig. 3. Visualization of propidium iodide penetration into electropermeabilized cells. Plated B16 cells have been permeabilized on culture dish under the microscope by application of 10 pulses, 5 ms, 1 Hz frequency at 0.8 kV/cm intensity in the presence of the dye propidium iodide. The set of events is reported with time. Large arrows indicate the side of cells facing the anode, while thin arrows are relative to the side of cells facing the cathode. (A) Cells under phase contrast. (B) before pulsation. (C) 1 second after the last pulse. (D) 5 seconds after the last pulse. (E) 30 seconds after the last pulse. (F) 60 seconds after the last pulse.

$$A_{perm} = A_{tot} (1 - E_p/E)/2 \tag{3}$$

where A_{tot} is the cell surface, assumed to be a sphere, and E is the applied field intensity (when a square wave pulse is applied). The factor 2 is relevant of the asymmetry of the field effect (Fig. 1).

2.2.2. A Reversible Process

A key feature of cell electroporation is that it is long-lived. It must nevertheless vanish to preserve cell viability. This reversibility in the membrane alteration is strongly controlled by the postpulse temperature (24). Kinetic studies of electroporation lead to a description in four steps:

1. The field induces the membrane potential difference increase which gives local defects (may be due to kinks in the lipid chains) when it reaches a critical value (about 200 mV) (“Induction step”). This occurs only if the field strength is larger than a threshold value (E_p).
2. These defects expand in size as long as the field is present and with a strength larger than a critical value (“Expansion step”).

3. As soon as the field intensity is lower than this threshold value, a stabilization occurs which brings the membrane to the permeabilized state for small molecules (“Stabilization step”).
4. A slow resealing then occurs (24–26). It is a first-order process.

The pulse duration and the number of pulses control the second step. A key observation is that when the delay between the pulses is short enough (second time range) to make the contribution of **step 4** negligible between pulses, an additive effect of successive pulses is present. **Step 3** has a dramatic consequence when a capacitor discharge electropulser is used. The effective pulse duration is position dependent on the cell surface. An heterogeneous permeabilization is present in the cap which is affected by the field (27).

2.2.3. Molecule Exchange Controlled by Chemical Nature

Electropermeabilization allows the free diffusion of small molecules and ions whatever their chemical nature. Polar compounds easily cross the membrane. Free diffusion is observed even with dextrans and oligonucleotides with molecular weights up to 4 kDa. In intact cells, the intrinsic cytotoxicity of a drug can be hindered by a limited diffusion across the plasma membrane and/or by its accumulation and degradation in lysosomes.

Electropermeabilization of cells allows cytotoxic drugs to have a direct access to the cytosol (28). For the last 20 years, different attempts have been described to use electropulsation for clinical purposes. In clinical applications, targeted drug delivery faces several problems. As most pharmacological compounds are hydrophilic, they cannot freely cross the membrane. They must use transporters. The efficiency of the transfer is always very low. It is then clear that as electropermeabilization gives a free access to the cytoplasm, hydrophilic drugs will show their potency when added to electropermeabilized cells. This is used in electrochemotherapy (4). For drugs chosen on the basis of their physico-chemical properties, their intrinsic cytotoxicity can be increased (28). The cytotoxic effect of *cis*-dichlorodiammineplatinum(II) on electropermeabilized cells is 2 to 3 times higher compared with intact cells (29). This effect is enhanced by the hydrophilic properties of the drugs as shown for anthracycline derivatives (30). Indeed, amphiphilic or small hydrophilic molecules (actinomycin D, melphalan) displayed a moderate, 2- to 5-fold, increase in cytotoxicity, while hydrophilic molecules such as bleomycin displayed a gain of 700-fold.

2.3. Associated Transmembrane Exchange Quantification

Free diffusion of low weight molecules across the electropulsed cell membrane (after the pulse) can be described by using the Fick equation on its

electropermeabilized part (**14**). This gives the following expression for a given molecule S and a cell with a radius r :

$$\Phi(S) = 2\pi r^2 P_s \Delta S X(N,T) (1 - E_p/E) \exp(-k(N,T)t) \quad (4)$$

where $\Phi(S)$ is the flow at time t after N pulses of duration, T (the delay between the pulses being short compared to t), P_s is the permeability coefficient of S across the permeabilized membrane and ΔS is the concentration gradient of S across the membrane. E_p depends on r . The resealing time (the reciprocal of k) is not dependent on the field intensity for a given cell. It is controlled by the cumulated pulse duration (NT). Note that **Eq. 4** is valid only under the assumption that no resting potential difference is present, and that S is uncharged. Efflux of a charged molecule such as calcein has been indeed reported to be controlled by the surface charges (**31**). Charge repulsion would then alter the concentration gradient across the membrane. By taking into account the Gouy-Chapman theory, the following relationship is obtained:

$$S_{\text{interface}} = S_{\text{bulk}} \exp(-ze \Psi_o / kT) \quad (5)$$

where z is the number of charges, e is the charge of an electron, k is the Boltzman constant, T is the temperature, Ψ_o is the membrane surface potential. The membrane surface potential and as such ΔS is not the bulk-to-bulk gradient, but the interfacial one which is under the control of Ψ_o . The membrane surface potential and as such ΔS are directly affected by the surface charge (**31**). Moreover, and always in the case of charged molecules, the diffusion across the permeabilized membrane is modulated by the transmembrane potential difference $\Delta\Psi$. An electrodiffusive component Φ_E is present, it is given by the Nernst-Plank relationship by:

$$\Phi_E(S) = - (P_s S \Delta\Psi z F) / RT \quad (6)$$

where F is the Faraday constant and R is the gas constant. So, in the case of charged molecules, the flow Φ of diffusion of the molecule is given by :

$$\Phi(S) = 2\pi r^2 P_s S_{\text{bulk}} [\exp(-ze \Psi_o / kT) - (\Delta\Psi z F) / RT] X(N,T) (1 - E_p / E) \exp(-k(N,T)t) \quad (7)$$

2.4. Electropermeabilization-Associated Physiological Effects

Cell electropermeabilization can lead to cell lysis. This has to be taken into account in experiments where cell viability must be preserved. Optimization of different electric field parameters (E, N, T) and of the pulsing conditions (buffer composition, temperature) has to be performed for each cell line in order to preserved cell viability. Electropulsation of cells can induce the generation of reactive oxygen species in the part of the membrane surface where

permeabilization is induced (32). But, under controlled parameters, cells can be permeabilized without affecting their functionality. This is the case for phagocytic cells electroloaded with a drug which maintain oxydizing activities for several hours after pulsation (33), and also for electropemabilized C6 glioma cells which keep their affinity for isoproterenol and the density of the beta-adrenergic receptor (34).

3. In Vitro Delivery of Large Molecules

Clear differences of processes by which molecules of different sizes translocate across the electropemabilized membrane have therefore been proposed. While small molecules could rather freely cross the permeabilized membrane for a time much longer than the duration of the electric pulse application, macromolecules transfer could involve more complex steps of interaction with the membrane and no free diffusion after pulse application (35).

3.1. Effect of Electric Field Parameters

3.1.1. Effect of Electric Field Strength

Only few experimental studies have provided determinations of permeabilization versus the different electric field parameters (13–36). The respective effects of the electric field pulse parameters on the transfer of macromolecules by electric fields remain therefore not clearly defined. A strong increase in the electric field intensity is not needed to incorporate macromolecules into cells as previously shown in the case of bacteria (37). But, the transfer of macromolecules occurs in the area of membrane where permeabilization to small size molecules occurs (38,39).

3.1.2. Effect of Pulse Duration

Optimum conditions for macromolecules transfer are obtained at high pulse duration T values but moderate values of the electric field intensity E to preserve the viability. A quantitative study of molecular transport of bovine serum albumin in erythrocyte ghosts has been described, a cell model where viability however cannot be evaluated (40). In that study, BSA uptake was correlated with the total time integral of field strength ($E_0 \tau$). In another study, transfer of DNA has been reported to be proportional to the power of the pulse ($E^2 \tau_{1/2}$) according to a polarization mechanism (41,42). These results are in line with previous works showing the importance of optimizing E and T in gene transfer experiments (37–43). It was suggested that excessive field strength could lead to permeation of a wider area, or forming larger pores that may exceed the resealing limit (43). The same conclusion was also reported by Rosemberg and Korenstein (44); E controlling the total area of membrane that undergoes

permeabilization, and T the diameter of “electropores.” Longer pulses corresponding to low field strength were reported to be more advantageous than the short ones in terms of gene transfer (45) and protein transfer (46).

3.1.3. Effect of the Number of Pulses

It has been shown that increasing N led to an increase in permeabilization in mammalian cells (47). This was already observed in the case of low molecular weight molecules. But, as far as macromolecule transport is concerned, pulse durations in the ms time range are required as previously reported (48,49), suggesting a contribution of electrophoretic forces (50). Nevertheless, accumulation of a high number of pulses with shorter duration at a constant cumulated value, that is, with a given electrophoretic contribution, allowing efficient permeabilization to small size molecules, is associated with a decrease in macromolecule transfer (39). One single pulse with the same cumulated duration, that is, with the electrophoretic contribution, brings the transfer of macromolecules (39). However, one should note that short pulses have been reported to efficiently deliver plasmid DNA to cells *in vivo* (50,51).

3.2. Direct Transfer Only Occurs When Macromolecules Are Present During the Pulses

Several models assumed that transfer of molecules across the membrane occurred across pores, which have never been observed. Different calculations of the “electropores” diameter have been proposed from 0.39 to 5.8 nm that correspond to 0.01% to 2% of the membrane area (41,44,53,54). If these values look reasonable for the transfer of small size molecules (MW < 4 kDa), they cannot support the penetration of macromolecules such as plasmid DNA and proteins.

According to the pore percolation model of Sugar et al. (55), it was proposed that the macromolecule induces coalescence and fusion of permeated structures when increasing their number with the number of pulses. The transfer could then result (42). Furthermore, the major difference between electroporation of cells to small and to large molecules is the lifetime of the competent state for transfer. In the case of macromolecules, the molecule must be present during the pulse for direct transfer. In the case of FITC-dextran and β -galactosidase, addition of these macromolecules in the minutes following pulsation was associated with a vesicular distribution due to a macropinocytosis induced phenomenon (56–58). These results agree with other studies showing that recovery of membrane integrity after the pulse treatment assayed from membrane conductance revealed the existence of at least two recovery processes. Conductance decreased strongly in about one millisecond

after the pulse, a fast process that alone did not lead to complete recovery, which occurred more slowly (53). The existence of two kinds of permeated structures for small and for large molecules can therefore be suggested in agreement with previous reports. Hui (43) suggested the implication of two populations of pores, in which the macromolecules can penetrate only at high field strength or long pulse duration via a population of larger size pores.

3.3. Transfer of Macromolecules by Electrofusion

Another way to load cells with macromolecules is to fuse cells with erythrocyte ghosts loaded with the molecule of interest (59). This approach can be used in the case of fragile cells where long pulses cause their lysis. Cells and ghosts are electropermeabilized separately under their optimum conditions and with short pulse duration. Their fusion is then induced by the creation of contact between them by gentle centrifugation. Penetration of FITC-dextran (70 kDa) and intact tetrameric β -galactosidase into 90–95% of CHO cells has been obtained by this method.

4. Summary and Conclusions

The electric field strength parameter is the trigger of permeabilization. It defines the area of membrane where permeabilization is created. But, the number of pulses and their duration control its extent. These parameters have to be adjusted to each cell line and to each drug to be electroloaded into the cells. The associated unpairing of the membrane permeability is a stress for the cells. The physiology of the cell has to be taken into account in the process of electropermeabilization of cells, in particular in studies where viability has to be preserved.

Clinical applications of the modifications of cells associated to their electropulsation are just at the very beginning. The most advanced procedure is Electrochemotherapy, which clinical applications are now developing rapidly only 6 years after the first reports by Okino reported in 1987 (60). Technical difficulties are due to the definition of the local values of the applied field (61). One of the limiting problems for other applications is that very few experimental facts have been gathered to explain the physicochemical mechanisms supporting the reorganization of the membrane in cells. Studies are therefore needed to understand the cascade of events triggered at the cell (and tissue) level by electropulsation. They are required to open new methods for clinical applications.

Electropermeabilization of cell membranes appears not as punching holes in a lipid layer (the so called electroporation hypothesis) but as a complex process where mostly the membrane/solution interface is altered. The recovery

(resealing) is dependent on the cell metabolism. This biological aspect must be taken into account in its use in in vivo drug delivery.

Acknowledgments

We thank the Region Midi-Pyrénées and the Association Française contre les Myopathies for their financial support.

References

1. Neumann, E., Sowers, A. E., and Jordan, C. A. (1989) *Electroporation and Electrofusion in cell biology*. Plenum, New York.
2. Allen, M. J., Cleary, S. F., Sowers, A. E., and Shillady, D. D. (1992) *Charge and Field Effects in Biosystems*, Vol. 3. Birkhäuser, Boston.
3. Chang, D. C., Chassy, B. M., Saunders, J. A., and Sowers, A. E. (1992) *Guide to Electroporation and Electrofusion*. Academic Press, San Diego, CA.
4. Belehradek, M., Domenge, C., Luboinski, B., Orlowski, S., Belehradek, J., and Mir, L. M. (1993) Electrochemotherapy, a new antitumor treatment: First clinical phase I-II trial. *Cancer* **72**, 3694–3700.
5. Sixou, S. and Teissié, J. (1990) Specific electroporation of leucocytes in a blood sample and application to large volumes of cells. *Biochim. Biophys. Acta* **1028**, 154–160.
6. Titomarov, A. V., Sukharev, S., and Kistanova, E. (1991) In vivo electroporation and stable transformation of skin cells of newborn mice by plasmid DNA. *Biochim. Biophys. Acta* **1088**, 131–134.
7. Zeira, M., Tozi, P. F., Moumeine, Y., Lazarte, J., Sneed, L., Volsky, D. J., and Nicolau, C. (1991) Full length CD4 electroinserted in the red blood cell membrane as a long-lived inhibitor of HIV infection. *Proc. Natl. Acad. Sci. USA* **88**, 4409–4413.
8. Prausnitz, M. R. (1996) The effects of electric current applied to the skin: a review for transdermal drug delivery. *Adv. Drug Deliv. Rev.* **18**, 395–425.
9. Vanbever, R., Lecouturier, N., and Preat, V. (1994) Transdermal delivery of metoprolol by electroporation. *Pharmacol. Res.* **11**, 1657–1662.
10. Bernhard, J. and Pauly, H. (1973) On the generation of potential difference across the membranes of ellipsoidal cells in an alternating electric field. *Biophysik* **10**, 89–98.
11. Tekle, E., Astumian, R. D., and Chock, P. B. (1990) Electroporation of cell membranes: effect of the resting membrane potential. *Biochem. Biophys. Res. Commun.* **172**, 282–287.
12. Hibino, M., Shigemori, M., Itoh, H., Nagayama, K., and Kinoshita, K. (1991) Membrane conductance of an electroporated cell analyzed by submicrosecond imaging of transmembrane potential. *Biophys. J.* **59**, 209–220.
13. Schwister, K. and Deuticke, B. (1985) Formation and properties of aqueous leaks induced in human erythrocytes by electrical breakdown. *Biochim. Biophys. Acta* **816**, 332–348.

14. Rols, M. P. and Teissié, J. (1990) Electroporation of mammalian cells. *Biophys. J.* **58**, 1089–1098.
15. Gabriel, B. and Teissié, J. (1997) Direct observation in the millisecond time range of fluorescent molecule asymmetrical interaction with the electroporated cell membrane. *Biophys. J.* **73**, 2630–2637.
16. Kinoshita, K. and Tsong, T. Y. (1977) Formation and resealing of pores of controlled sizes in human erythrocytes membrane. *Nature*, **268**, 438–443.
17. Gabriel, B. and Teissié, J. (1998) Fluorescence imaging in the millisecond time range of membrane electroporation of single cells, using a rapid ultra low light intensifying detection system. *Eur. Biophys. J.* **27**, 291–298.
18. Sixou, S. and Teissié, J. (1993) Exogenous uptake and release by electroloaded cells: a digitized videomicroscopy study. *Bioelectrochem. Bioenerg.* **31**, 237–257.
19. Mehrle, W., Zimmermann, U., and Hampp, R. (1985) Evidence for asymmetrical uptake of fluorescent dyes through electroporated membranes of *avena mesophyll* protoplasts. *FEBS Lett.* **185**, 89–94.
20. Rossignol, D. P., Decker, G. L., Lennarz, W. J., Tsong, T. Y., and Teissié, J. (1983) Induction of calcium dependent localized cortical granule breakdown in sea urchin eggs by voltage pulsation. *Biochim. Biophys. Acta* **763**, 346–355.
21. Dimitrov, D. S. and Sowers, A. E. (1990) Membrane electroporation—fast molecular exchange by electroosmosis. *Biochim. Biophys. Acta* **1022**, 381–392.
22. Teruel, M. N. and Meyer, T. (1997) Electroporation induced formation of individual calcium entry sites in the cell body and processes of adherent cells. *Biophys. J.* **73**, 1785–1796.
23. Teissié, J. and Rols, M. P. (1993) An experimental evaluation of the critical potential difference inducing cell membrane electroporation. *Biophys. J.* **65**, 409–413.
24. Teissié, J. and Rols, M. P. (1994) Manipulation of cell cytoskeleton affects the lifetime of cell membrane electroporation. *Ann. N.Y. Acad. Sci.* **720**, 98–110.
25. Rols, M. P. and Teissié, J. (1990) Modulation of electrically induced permeabilization and fusion of chinese hamster ovary cells by osmotic pressure. *Biochemistry* **29**, 4561–4567.
26. Rols, M. P., Dahhou, F., Mishra, K. P., and Teissié, J. (1990) Control of electric field induced cell membrane permeabilization by membrane order. *Biochemistry* **29**, 2960–2966.
27. Teissié, J. and Ramos, C. (1998) Correlation between electric field pulses induced long lived permeability and fusogenicity in cell membranes. *Biophys. J.* **74**, 1889–1898.
28. Orłowski, S. and Mir, L. M. (1993) Cell electroporation: a new tool for biochemical and pharmacological studies. *Biochim. Biophys. Acta* **1154**, 51–63.
29. Melvik, J. E., Pettersen, E. O., Gordon, P. B., and Seglen, P. O. (1986) Increase of *cis*-Dichlorodiamineplatinum(II) cytotoxicity upon reversible electroporation of the plasma membrane in culture human NHIK3025 cells. *Eur. J. Cancer Clin. Oncol.* **22**, 1523–1530.

30. Müllig, P., Forster, W., Jacob, H. E., Berg, H., Roglin, G., and Wohlrabe, K. (1984) Cell membrane permeabilization of the anthracyclines violamycin BI and BII induced by an electric field pulse. *Stud. Biophys.* **104**, 207–213.
31. Raffy, S. and Teissié, J. (1997) Surface charge control of electroporation and glycophorin electroinsertion with 1,2-diacyl-*sn*-glycero-3-phosphocholine (lecithin) liposomes. *Eur. J. Biochem.* **250**, 315–319.
32. Gabriel, B. and Teissié, J. (1994) Generation of reactive-oxygen species induced by electroporation of chinese hamster ovary cells and their consequence on cell viability. *Eur. J. Biochem.* **223**, 25–33.
33. Sixou, S. and Teissié, J. (1995) Electroporation of peripheral blood phagocytes induces a long lived cell membrane alteration which does not affect their viability. *Bioelectrochem. Bioenerg.* **38**, 129–136.
34. Volker, T., Pianet, I., Labouesse, J., and Teissié, J. (1989) Signal transduction by membrane receptors in viable electroporated cells: Isoproterenol-stimulated cyclic AMP synthesis in C6 glioma cells. *Biochim. Biophys. Acta* **984**, 243–251.
35. Morgan, W. F. and Day, J. P. (1995) The introduction of proteins in mammalian cells by electroporation. *Methods Mol. Biol.* **48**, 63–71.
36. Liang, H., Purucker, W. J., Stenger, D. A., Kubiniec, R. T., and Hui, S. W. (1988) Uptake of fluorescence-labeled dextrans by 10 T_{1/2} fibroblasts following permeation by rectangular and exponential-decay electric field pulse. *Biotechniques* **6**, 550–555.
37. Xie, T. D. and Tsong, T. Y. (1992) Study of mechanisms of electric field-induced DNA transfection III. Electric parameters and other conditions for effective transfection. *Biophys. J.* **63**, 28–34.
38. Wolf, H., Rols, M. P., Neumann, E., and Teissié, J. (1994) Control by pulse parameters of electric field mediated gene transfer in mammalian cells. *Biophys. J.* **66**, 524–531.
39. Rols, M. P. and Teissié, J. (1998) Control by pulse duration of electroporation of mammalian cells to macromolecules. *Biophys. J.* **75**, 1415–1423.
40. Prautnitz, M., Milano, C., Gimm, A., and Langer, R. (1994) Quantitative study of molecular transport due to electroporation: Uptake of bovine serum albumin by erythrocytes ghosts. *Biophys. J.* **66**, 1522–1530.
41. Kubiniec, R.T., Liang, H., and Hui, S. W. (1990) Effect of pulse length and pulse strength on transfection by electroporation. *Biotechniques*, **8**, 16–21.
42. Neumann E., Kakorin, S., Tsoneva, I., Nikolova, B., and Tomov, T. (1996) Calcium-mediated DNA adsorption to yeast cells and kinetics of cell transformation by electroporation. *Biophys. J.* **71**, 868–877.
43. Hui, S. W. (1996) Effects of pulse length and strength on electroporation efficiency. *Methods Mol. Biol.* **55**, 29–40.
44. Rosemberg, Y. and Korenstein, R (1990) Electroporation of the photosynthetic membrane. *Biophys. J.* **58**, 823–832.
45. Kubiniec, R. T., Liang, H., and Hui, S. W. (1988) Use of fluorescence-labeled dextrans by 10 T_{1/2} fibroblasts following permeation by rectangular and exponential decay electric field pulses. *Biotechniques* **8**, 16–20.

46. Rols, M. P., Delteil, C., Golzio, M., Dumont, P., Cros, S., and Teissié, J. (1998) In vivo electrically mediated protein and gene transfer in murine melanoma. *Nature Biotech.* **16**, 168–171.
47. Kwee, S., Nielsen, H. V., Celis, J. E., Celis, A., and Madsen, P. S. (1989) Permeabilization of mammalian cells in monolayer culture by electroporation at low electric field strength. *Stud. Biophys.* **130**, 173–176.
48. Chu, G. H., Hayakawa, H., and Berg, P. (1987) Electroporation for the efficient expression of mammalian cells with DNA. *Nucl. Acids Res.* **15**, 1311–1326.
49. Potter, H. (1989) Molecular genetic applications of electroporation. *Electroporation and Electrofusion in Cell Biology*. (Neumann, E., Sowers, A., and Jordan, C., eds.). Plenum, New York pp. 331–342.
50. Sukharev, S. I., Klenchin, V. A., Serov, S. M., Chernomordik, L. V., and Chizmadzhev, Y. 1992. Electroporation and electrophoretic DNA transfer into cells: The effect of DNA interaction with electropores. *Biophys. J.* **63**, 1320–1327.
51. Heller, R., Jaroszeski, M., Atkin, A., Moradpour, D., Gilbet, R., Wands, J., and Nicolau, C. (1996) In vivo gene electroinjection and expression in rat liver. *FEBS Lett.* **389**, 225–228.
52. Nishi, T., Yoshizato, K., Yamashiro, S., Takeshima, H., Sato, K., Hamada, K., Kitamura, I., Yoshimura, T., Saya, H., Kuratsu, J. I., and Ushio, Y. (1996) High-efficiency in vivo gene transfer using intraarterial plasmid DNA injection following in vivo electroporation. *Cancer Res.* **56**, 1050–1055.
53. Kinoshita, K. Jr., Ashikawa, I., Nobuyuki, S., Yoshimura, H., Hiroyasu, I., Nagayama, K., and Ikegami, A. (1988) Electroporation of cell membrane visualized under a pulsed-laser fluorescence microscope. *Biophys. J.* **53**, 1015–1019.
54. Hibino, M., Hiroyasu, I., and Kinoshita, K. Jr. (1993) Time courses of cell electroporation as revealed by submicrosecond imaging of transmembrane potential. *Biophys. J.* **64**, 1789–1800.
55. Sugar, I. P., Forster, W., and Neumann, E. (1987) Model of cell electrofusion: Membrane electroporation, pore coalescence and percolation. *Biophys. Chem.* **26**, 321–335.
56. Rols, M. P., Femenia, P., and Teissié, J. (1995) Long lived macropinocytosis takes place in electropermeabilized mammalian cells. *Biochem. Biophys. Res. Commun.* **208**, 26–38.
57. Lambert, H., Pankow, R., Gauthier, J., and Hancock, R. (1990) Electroporation-mediated uptake of proteins into mammalian cells. *Biochem. Cell Biol.* **68**, 729–734.
58. Glogauer, M., Lee, W., and McCulloch, A. G. (1993) Introduction of large molecules into viable fibroblasts by electroporation: Optimization of loading and identification of labelled cellular compartments. *Exp. Cell. Res.* **208**, 232–240.
59. Rols, M. P., Dahhou, F., and Teissié, J. (1994) Pulse-first heterofusion of cells by electric field pulses and associated loading of macromolecules into mammalian cells. *Biotechniques* **17**, 762–769.

60. Okino, M. and Mohri, H. (1987) Effects of a high-voltage electrical impulse and an anticancer drug on in vivo growing tumors. *Jpn. J. Cancer Res.* **78**, 1319–1321.
61. Miklavčič, D., Beravs, K., Šemrov, D., Čemažar, M., Demšar, F., and Serša, G. (1998) The importance of electric field distribution for effective in vivo electroporation of tissues. *Biophys. J.* **74**, 2152–2158.

The Basis of Electrochemotherapy

Lluís M. Mir and Stéphane Orlowski

1. Introduction: Electroporation as a New Drug Delivery Approach

Antitumor electrochemotherapy is a treatment of solid tumors which combines a cytotoxic nonpermeant drug, like bleomycin, with locally delivered permeabilizing electric pulses (1–3). More generally, a new form of vectorization is achieved by the combination of nonpermeant molecules with intracellular targets and of a physical perturbation that locally permeabilizes the cells. This vectorization does not require chemical, biochemical or biological modifications of the targeted compound, since the modification is performed on the target cells. A very convenient way to transiently permeabilize the cells is the use of appropriate electric pulses (short and intense square-wave electric pulses) that are not cytotoxic by themselves (1). These electric pulses reversibly permeabilize the electropulsed cells. Consequently, they allow increased drug delivery inside cells, particularly in the case of drugs for which the plasma membrane is a barrier that limits their access inside the cell [termed nonpermeant drugs] (4). As illustrated in the various protocols reported in this volume, electrochemotherapy using bleomycin is efficient to eradicate subcutaneously transplanted and spontaneous small tumors in mice and rats as well as experimental internal tumors transplanted in rat brain or in rabbit or rat liver. All the clinical trials (3,5–10) confirm the efficacy of this new therapeutic approach based on an original way to deliver nonpermeant cytotoxic drugs inside the tumor cells.

The basis of antitumor electrochemotherapy that allows the understanding of the potentialities of this new treatment of solid tumors and to determine what type of electric pulses and what type of drugs may be used to obtain an efficient treatment is described. A good understanding of the basis of

electrochemotherapy will allow to adapt the general protocols presented in the second section of this volume to the more specific situations that researchers and clinicians can find in their practice.

2. In Vitro and In Vivo Cell Electroporation

2.1. Electroporation of Cells in Suspension

It has been previously well established that, in vitro, appropriate brief and intense electric pulses transiently and reversibly permeabilize cells in suspension (11–13). It has been shown that the biophysical change induced by the external electric field imposed during the pulse duration is a position- and external voltage-dependent modification (ΔV) of the plasma membrane potential (11,14–16). At the point M on the cell surface, the value of ΔV can be determined according to the formula :

$$\Delta V_M = f \times E_{\text{ext}} \times r \times \cos \Theta$$

where r is the radius of the cell, Θ is the angle made by the direction of the external electric field E_{ext} and by the normal to the cell surface at the point M, and f is a geometrical factor ($f = 1.5$ for spherical cells in suspension). The biochemical and structural consequences of this transmembrane potential change, that result in cell permeabilization, are not yet fully described at the molecular level. However, it is known that they locally occur when ΔV_M reaches a value above a threshold value. The existence of this threshold value results in the occurrence of a “permeabilization threshold” in the applied external electric field (11,14–16).

In vitro, it is easy to experimentally determine the threshold value of the external electric field resulting in cell electroporation (also termed cell electropermeabilization). It is also easy to determine the external electric field value above which irreversible membrane changes are induced and therefore loss of cell viability is observed. This is essentially due to the fact that in vitro experimental systems have simple geometries in which homogeneous electric fields can be generated. Thus in vitro, it is easy to determine optimal conditions simultaneously allowing the achievement of cell permeabilization and the preservation of cell viability.

2.2. Electroporation of Cells in Tissues

Electrochemotherapy is a drug delivery method based on in vivo cell electroporation. The achievement of efficient drug delivery inside cells is restricted to the volume of tissue submitted to electric pulses of an electric field intensity sufficient to obtain cell permeabilization. Consequently, electrochemotherapy is a local treatment. For cancer treatment, this approach

is adequate for the treatment of localized nodules but obviously not convenient, as a single treatment, for the efficient attack of disseminated diseases.

Cell electroporation in animal tissues exposed *in vivo* to appropriate electric pulses was first characterized in 1994 (17) and is now well established. *In vivo*, due to geometrical constraints among other experimental difficulties, it is not easy to determine the optimal electrical conditions resulting in cell permeabilization and cell viability.

It is important to note that in electrochemotherapy the electric pulses are just a means for delivering drug inside living cells. On the one hand, this implies that drug has to be already present in the vicinity of the cells at the time of the electric pulses application, and on the other hand, this imposes that the electric pulses must not be detrimental to the cells. Indeed, if the intensity of the electric pulses is too far above the permeabilization threshold value, the permeabilized state is irreversible and results in the death of the cells. In that case, the skin and the normal tissues surrounding the tumors would also be destroyed (18), precluding any clinical use of this approach.

The aim of the new method is to deliver supportable electric pulses, using electric field intensities necessary to transiently permeabilize the cells. As a matter of fact, all the controls performed in antitumor electrochemotherapy preclinical trials using square-wave pulses of 100 μ s showed that these electric pulses never perturbed tumor growth in the absence of bleomycin. Transient small burns or marks in the areas just in contact with the electrodes can be observed *in vivo* in the presence of bleomycin, but the same preclinical experiments as well as the clinical trials (3,5–10) showed that these consequences of the procedure are benign and reversible and that the treatment is safe and tolerable.

Electroporation of cells in tissues is still much less characterized than that of cells in suspension. The existence of an electric field intensity threshold for bleomycin uptake demonstrated the occurrence of cell permeabilization in tissues (17). It is noteworthy that the threshold in the tumor tissue was inferior to the threshold found with the same tumor cells in suspension exposed to the same type of electric pulses. The reasons for that difference in sensitivity to the external electric fields have not yet been elucidated. Similarly, it is not yet known if different intensities of the electric pulses are necessary to obtain cell permeabilization in different types of tissues or tumors. However, what is definitively established is that cell electroporation is a general phenomenon, resulting from the interaction of the plasma membrane with the external electric field, and that in consequence it can be obtained for all tumor types. Therefore, as demonstrated by the initial clinical trials (3,5–10), electrochemotherapy is applicable to all histological types of solid tumors.

2.3. Methods of Study

In vitro, several rapid tests have been proposed to find the appropriate conditions for the simultaneous achievement of cell permeabilization and cell survival. All of them use molecules that cannot diffuse through the plasma membrane of intact cells, like the fluorescent marker Lucifer Yellow (4), propidium iodide (19) or trypan blue (20). Lucifer Yellow is very interesting because it does not bind to intracellular macromolecules. Therefore, it can leak from permeabilized cells that have permanent cell membrane damage and that should die. Thus, after cell washing, the cells that contain Lucifer Yellow in their cytosol are only the cells reversibly permeabilized that, very likely, will survive their transient permeabilization (4).

In vivo, the tests for the determination of cell permeabilization are much less easy to perform, and quantitative studies are scarce. Belehradec and colleagues (17) showed a four times increased retention of radioactive bleomycin in tumors exposed to permeabilizing electric pulses as compared to unexposed tumors. This factor was equivalent to the one observed in vitro (21) using cells in suspension exposed to external concentrations of radioactive bleomycin similar to those measured in mice blood at the time of tumor exposure to the electric pulses. This factor is low compared to the huge increase in cytotoxicity due to cell electropermeabilization (*see Subheading 3.2.1.*).

Cell electropermeabilization in vivo was also demonstrated using the huge increase in bleomycin cytotoxicity when the electric field intensity is above the threshold necessary to achieve cell permeabilization (17). Indeed, using an appropriate drug concentration, all the unpermeabilized cells remain alive in spite of the external presence of bleomycin, while all the permeabilized cells are killed by the internalized bleomycin. In practice, electric pulses of various field intensities were applied to pieces of tumors removed from mice three minutes after bleomycin injection and the cell killing due to the permeabilization-facilitated uptake of bleomycin was carefully determined using in vitro cell viability tests.

It is also possible to use the small radioactive nonpermeant molecule ⁵¹Chromium-EDTA (22,23). The interest of this marker is its large renal clearance that rapidly reduces its plasma concentration. Therefore the accumulation of this marker in any reversibly electropermeabilized tissue becomes detectable after very short times (e.g., one hour), which reduces the experimental constraints linked to the injection of radioactive isotopes in living animals.

2.4. Role of the Different Electric Pulse Parameters

Since the theory as well as the practice show that the control of the electrical parameters is critical to find conditions simultaneously allowing the achieve-

ment of cell permeabilization and the preservation of cell survival, it is necessary to analyze the reasons guiding the choice of appropriate electric pulses for cell electropermeabilization in tissues.

2.4.1. Electric Pulse Shape

In vitro, various types of electric pulses have been employed to obtain cell permeabilization (20,24,25) but only two types of direct current short and intense electric pulses are commonly used: exponentially decaying pulses (24) and square-wave pulses (25).

Exponentially decaying pulses can be obtained using simple devices that rapidly became very popular. However, the control of permeabilization is limited, even in the case where these devices possess several capacitances. In contrast, using square-wave electric pulses, the achievement of reversible permeabilization in almost all the electropulsed cells can be obtained (26) because generators allow the independent setting of the voltage delivered and of the length of every electric pulse. This is very important since, on the one hand, once the external electric field is established, it has to stand for several microseconds for the generation of the membrane-permeabilizing structural rearrangements. With the exponentially decaying pulses, the maintenance of the electric field intensity above the threshold for this minimal period of time requires initial electric field intensities much higher than the threshold, thus deleterious for the cells. On the other hand, the achievement of permeabilization depends on the intensity of the external electric field to which cells are exposed. The square-wave pulses allow to set the voltage at a constant predetermined value, not too much higher than the threshold, whatever the pulse length. Moreover, the use of square-wave pulse generators allows to maintain the chosen electrical parameters in spite of experimental variations of the volume or of the conductivity of the samples exposed to the electric pulses.

Therefore, with square-wave pulse generators, contrary to the exponentially decaying pulses, it is not necessary to expose the cells to detrimental, too intense, electric field intensities in order to fulfil the need to expose the cells for a sufficient time to the permeabilizing electric fields. Actually, it seems now well established, both theoretically and experimentally, that square-wave pulses allow to define in vitro experimental conditions resulting in levels of electropermeabilized cell survival that cannot be reached using the exponentially decaying pulses (26,27).

Since in vivo, the actual purpose of the method is to achieve an efficient way to deliver drugs into the cells, it is necessary to avoid direct cell killing by the electric pulses. In fact, very intense exponentially decaying pulses that lead to marked burns in the skin around the electrodes were only used in the first

articles of Okino's group (18). Since the initial experiments of Mir and colleagues (1,2), square-wave electric pulses have been used in vivo in all pre-clinical as well as in all clinical trials.

2.4.2. Electric Pulse Intensity

In vitro, the choice of the appropriate electric field intensity is a crucial point to be successful in the reversible permeabilization of the entire population of living cells submitted to the electric pulses. Indeed, the electric field intensity delivered has to be above the intensity that results in transmembrane potential changes above the permeabilization threshold. However, the electric field intensity has to remain below intensities leading to permanent nonreversible changes in cell membrane structure. It often occurs that in vitro the range of intensities comprised between these two limits is very narrow. Therefore, this range should be determined for each cell type manipulated in preliminary experiments.

In vivo, the permeabilization threshold can be masked and the effects of the electric pulses seem to increase continuously with electric field increasing intensities. This is due to geometrical constraints in the electrode setting and positioning that result in inhomogeneous electric fields inside the tissues (17). For the same type of reasons, the intensities of transcutaneous electric pulses efficient in tumor treatment have been experimentally found to be higher than the intensities of electric pulses directly applied to tumors (17).

2.4.3. Electric Pulse Duration and Frequency

With the exception of the first articles of Okino's group (18), all the other electrochemotherapeutic treatments, including those performed later by this group (28), have been performed using 4, 6, or 8 square-wave pulses of 100 μ s of duration at a frequency of 1 Hz, that is using parameters notably lower (1,2). The reason for the choice of this duration (100 μ s) is due to the experimental work on cells in culture performed prior to the preclinical trials on mice (4,21,29). In agreement with Rols and Teissié (30), it was also found that in vitro, pulses of 100 μ s were the best compromise to be sure that pulse duration was (i) longer than the time required to obtain membrane modifications and (ii) not too long as to create irreversible membrane modifications due in particular to an excessive heating of the medium containing the cells.

In fact, the preliminary experiments necessary to develop the electrochemotherapy concept were performed in vitro (4,21,29). In all these experiments, the electroporeabilization of cells in culture was achieved in conductive media (the usual cell culture medium or variations introduced to

avoid the presence of free calcium). Therefore, the optimal conditions found in vitro were applied in the initial in vivo trials since interstitial fluid in tissues is also highly conductive. In consequence, already in the first in vivo experiment, these conditions gave excellent results. Therefore, this pulse duration has been widely accepted but has not been the subject of a systematic investigation.

The considerations concerning the electric pulse duration apply similarly to the choice of the frequency of 1 Hz to deliver the 4, 6, or 8 consecutive pulses of the treatment.

2.4.4. Electric Pulse Number and Electrode Orientation

The number of pulses, 4, 6, or 8, is not a crucial parameter provided that bleomycin is in excess in the treated tissue. If bleomycin is injected at limiting doses, better antitumor effects are obtained with 8 pulses (*1*). Moreover, Serša and colleagues showed that changing the electrode orientation during the delivery of the 8 transcutaneous pulses improved the efficacy of electrochemotherapy of solid subcutaneous tumors in mice. In other words, they compared the delivery of either 4 pulses in a row, or 8 pulses in a row, or “4+4” pulses, that is two rows of 4 pulses with the orientation of the external electrodes during the second run of 4 pulses being perpendicular to the orientation during the first run. This last setting gave the best results. This can be explained by a better coverage of the tumor volume actually exposed to the permeabilizing electric fields (*31*).

3. Nonpermeant Drugs Possessing a High Intrinsic Cytotoxicity

Uptake of cell hydrophilic metabolites is a process mediated by channels or transporters located at the plasma membrane whereas lipophilic and amphiphilic molecules can diffuse across the plasma membrane because of their partial solubility in the lipid bilayer. A nonpermeant drug is a molecule that cannot cross the plasma membrane because it is hydrophilic and devoid of transporters or channels at the plasma membrane level that would be able to introduce it directly into the cell cytosol (*4*). Therefore cell electropermeabilization allows the internalization of nonpermeant molecules, impossible in the absence of drug vectorization or plasma membrane alteration. Obviously, cell electropermeabilization is without interest for the nonpermeant drugs with a cell surface target, for which internalization is not necessary to exert their biological activity. In anticancer pharmacology, almost all cytotoxic drugs have their targets located inside the cells. However, most of them are lipophilic or actively transported across the plasma membrane (*29*). This is not the case of bleomycin (*32*).

3.1. Biological Characteristics of Bleomycin

3.1.1. Bleomycin Is a Nonpermeant Drug

Bleomycin is an excellent example of a nonpermeant cytotoxic drug (21,29,32). It was demonstrated in vitro that bleomycin cannot diffuse through the plasma membrane of intact cells (21). In unpermeabilized cells, large amounts of bleomycin are entrapped in the endocytosis vesicles, but they cannot diffuse through the membrane of the vesicles to reach the true cell inside, the cytosol and the cell nucleus (21,33). The amounts of bleomycin entering the cell by this mechanism of fluid phase endocytosis (pinocytosis) are proportional to the external bleomycin concentration, but they are unrelated to the cytotoxic effects of this drug that are not proportional to the external concentration (21,29,32). Therefore, the bleomycin molecules entering the cell by pinocytosis are not responsible for the cytotoxic effects of this drug. The cytotoxicity of bleomycin on intact unpermeabilized cells is due to the fact that this drug interacts with specific membrane proteins at the cell surface. These proteins bind the bleomycin molecules (34) and play a role in the complex mechanism of bleomycin internalization in intact living cells that follows the cell endocytosis pathway (33). Thus the bleomycin internalization mechanism possesses the characteristics of a receptor-mediated endocytosis (35,36). It is important to understand that only the bleomycin molecules following this pathway are able to enter the cell cytosol and thus the nucleosol, and to interact with cell DNA, the target of the drug. Because this internalization pathway is slow and has a very limited transport capacity, bleomycin is actually a nonpermeant drug, taking into account that the large amounts of bleomycin entrapped in the fluid phase of the endocytic vesicles cannot reach the cell cytosol and do not exert cytotoxic effects.

3.1.2. Bleomycin Molecules Possess a High Intrinsic Cytotoxicity

In spite of the reduced transport capacities of the mechanism of internalization reported above, bleomycin displays some cytotoxicity on unpermeabilized cells. This bleomycin activity implies that bleomycin molecules possess a very high intrinsic cytotoxicity, that is a very high toxicity when the plasma membrane is not a barrier that limits drug internalization and bleomycin accessibility to the DNA. In fact, using cell electroporabilization as an in vitro investigative tool, we showed that the rapid internalization of 200 molecules in an electroporabilized cell is sufficient to kill the cell and that an average of 2000 internalized molecules results in the death of all the treated cells (21). Therefore, the intrinsic cytotoxicity of bleomycin is extremely high. This property of the bleomycin molecule is linked to its mechanism of action on DNA (see **Subheading 3.2.2.**).

The high intrinsic cytotoxicity of bleomycin molecules is also the reason for which bleomycin is an anticancer drug currently used in various conventional chemotherapy protocols (i.e., in the absence of the electric pulses) in spite of its nonpermeant character.

3.2. Electrochemotherapy With Bleomycin

3.2.1. Basic Mechanism

Bleomycin is a nonpermeant cytotoxic drug possessing high intrinsic cytotoxicity. These two properties explain why it is possible to obtain a huge potentiation of bleomycin cytotoxicity after cell electropermeabilization. Indeed, nonpermeant molecules reach either the vesicle inside in the case of unpermeabilized cells or the cell cytosol in the case of electropermeabilized cells (4,37). This change in the cell compartment that bleomycin can directly reach is the main reason of the *in vitro* increase in bleomycin cytotoxicity resulting from cell electropermeabilization. It allows to understand why a small increment [from 2 to 15 times] (21) of the total amount of bleomycin in the cell (vesicles plus cytosol) can result in large increases in cell cytotoxicity [from hundreds to thousands of hundreds times] (21,29). *In vivo*, provided that bleomycin is already present in the tumor interstitial fluid, the transient electropermeabilization *in situ* of the tumor cells similarly allows bleomycin delivery into the cytosol and nucleosol of tissue cells and thus increases bleomycin antitumor effects by several orders of magnitude (1,17).

One interesting consequence of the nonpermeant character of bleomycin is the fact that the doses of bleomycin injected in the electrochemotherapy trials did not reduce tumor growth in the absence of permeabilizing electric pulses, whatever the experimental or clinical model tested. This means that these doses of bleomycin result in an extremely reduced toxicity on the remaining parts of the body not exposed to electric fields. Therefore, the locally applied permeabilizing electric pulses are a drug delivery system that introduces a high specificity in the effects of the cytotoxic agent.

Electrochemotherapy can be performed on all histological types of tumors. Indeed, once inside the cell, the reaction between bleomycin and DNA is merely a chemical reaction that will occur in all cells since DNA has the same structure and composition in all cells (whether tumoral or not). Once the problem of bleomycin internalization is circumvented by the use of electropermeabilization as a drug delivery system, bleomycin acts as a mini-endonuclease, active on all cell types. The preclinical and clinical data collected until now confirm that electrochemotherapy is effective in all types of tumors tested.

3.2.2. Additional Interests of Bleomycin Use

Other important reasons for performing electrochemotherapy with bleomycin are (i) the way in which bleomycin kills the cells, (ii) the fact that it is known that bleomycin is not an immunodepressant agent, and (iii) the possibility to administer the bleomycin by various safe ways.

Indeed, *in vitro*, bleomycin kills cells by two different mechanisms, either mitotic cell death or pseudoapoptosis, depending on the amount of bleomycin internalized in the cells (32,38,39). These cell death mechanisms are linked to the ability of bleomycin to make single- and double-strand DNA breaks and are actually based on the double-strand DNA break generation. *In vivo*, bleomycin, at the therapeutical doses, kills the cells by a process of slow cell death that recalls the mitotic cell death observed *in vitro* (H. Mekid et al., unpublished results). Interestingly, only dividing cells can be killed by this mechanism of mitotic cell death, which introduces some bleomycin specificity on the tumor cells with respect to the normal cells inside or around the tumor. Moreover, bleomycin does not induce apoptosis. Consequently, there is no cell shrinking and disappearance of the tumor cells never occurs without an inflammatory response. As a matter of fact, a peritumoral edema is always observed after electrochemotherapy. Therefore, the bleomycin-induced cell death is a slow process that could help the host in raising an immunological response against the treated tumor (*see Subheading 4.2.*).

It is also important to highlight that bleomycin is not an immunosuppressant agent (40). Moreover, it has been shown that bleomycin, under specific regimens of administration, results in the stimulation of various compartments of the immune response: increase of the tumoricidal activity of macrophages (41), elimination of tumor specific T-suppressor activity (42,43), and induction of interleukin-2 secretion (44).

Moreover, contrary to other anticancer drugs that are extremely aggressive at the injection site, bleomycin can be safely administered either intramuscularly, intravenously, intra-arterially or, intratumorally. In the initial preclinical and clinical trials, bleomycin was administered systemically [intramuscularly (1,2,18) or intravenously (3,6,7)], with high response rates. This means that, after bleomycin dilution in the whole body, even if the small concentration of bleomycin is inactive in the absence of concomitant permeabilizing electric pulses, this low concentration is still very active where the local electric pulses are applied. Therefore, not only is the treatment almost devoid of side effects, but moreover, the systemic injection of the bleomycin allows treatment of several nodules or very large tumors masses in a patient with a unique dose of bleomycin (5). However, in the case of the treatment of very few, small nod-

ules, it is very attractive to use still lower amounts of bleomycin injected intratumorally. This possibility was explored in mice and rats by Heller and colleagues (45,46). They demonstrated the feasibility of this approach, that has been successfully applied later in the treatment of basal cell carcinomas and melanomas in humans (9,10,47). The intra-arterial administration route was also applied in two patients. Results showed that a dose of bleomycin given intra-arterially resulted in more intense antitumor effects than given intravenously (5).

Finally, BLM cytotoxicity is not restricted by multidrug resistance mechanisms. Therefore, due to all these various biological characteristics, bleomycin seems a very appropriate drug for electrochemotherapy.

3.3. Electrochemotherapy With Other Anticancer Drugs

Among the drugs currently used in cancer chemotherapy, only bleomycin possesses a marked nonpermeant character (29,32). All the other anticancer drugs are permeant molecules for which the plasma membrane is not a barrier to enter cells (26,29). Some drugs like melphalan and methotrexate are actively transported inside cells, while most of the other anticancer drugs have an amphiphilic character that allows their diffusion through the lipid bilayer of the plasma membrane. Only cisplatin complexes seem to be low permeant drugs. The mechanism of cisplatin internalization has not yet been fully described: a fraction of the cisplatin molecules entering the cells are supposed to cross the plasma membrane by diffusion, whereas another fraction should enter the cells through a facilitated transport (48). In vitro, experimental results show that cell electropermeabilization increases cisplatin toxicity by a factor of 3 (49), 2.3 (24) or up to 8 (50) depending on the experimental conditions. Cisplatin cytotoxicity is proportional to cisplatin uptake (48,49), and therefore, the observed increase in antitumor effects after electrochemotherapy is similar to the increase in cisplatin uptake resulting from cell electropermeabilization (49,51,52).

Besides bleomycin, as a consequence of these in vitro observations, only cisplatin has been used in vivo in combination with cell permeabilizing electric pulses, in preclinical as well as in clinical trials (as reported in Chapter 6 of this volume). Even if the increase in cisplatin effectiveness resulting from cell electropermeabilization is much less than the increase obtained with bleomycin, cisplatin is another candidate for use in electrochemotherapy. Moreover, since cisplatin alone is already an efficient anticancer treatment, electrochemotherapy with cisplatin could be used as local adjuvant treatment in patients who are already treated by a cisplatin-based conventional chemotherapy.

4. Other Mechanisms

4.1. Vascular Effects of Permeabilizing Electric Pulses

Electric pulses delivered in vivo, besides their main predictable effect, that is, cell electropermeabilization achievement, also induce transient vascular effects in the tissue volume exposed to the electric pulses (53–55) (*J. Gehl et al., unpublished results*). For a few minutes after the electric pulses application, the treated volume of tissue is not accessible to molecules arriving through the blood flow such as the diffusion marker Patent Blue (*G. Serša, personal communication*). Such an inaccessibility has also been demonstrated using fluorescent tracers, like fluorescein (53), or radioactive molecules, like $^{51}\text{Cr-EDTA}$ (*J. Gehl et al., unpublished results*), injected intravenously within the minutes following the electric pulses application. Some differences have already been evidenced between normal and tumor tissues. Recovery times in normal tissues, that is, in tissues with a regular microvasculature, are shorter than those in tumors. Normal tissue in both mice and rabbits, blood flow is re-established within a few minutes after the electric pulse application (53) (*J. Gehl et al., unpublished results*). By contrast, in tumors, Serša and colleagues, using the $^{86}\text{RbCl}$ extraction technique, recently showed that the transient reduction in blood flow was maintained for one hour (55). The pretreatment level progressively recovered 18 to 24 hours after the electric pulses application (55). In the presence of bleomycin, these transient vascular effects seem to be reinforced and prolonged because the endothelial cells could also be killed by the treatment. In fact, infarction areas have been detected after the treatment of transplanted carcinomas in the liver of rabbits (27). It has also been shown that the inaccessibility of the Patent Blue to tumors treated by electrochemotherapy with bleomycin lasts for more than 24 hours (*G. Serša, personal communication*).

Bleomycin has always been injected before the electric pulses delivery, whatever the mode of administration of the drug, because, based on in vitro determinations, the transient permeation structures generated by the electric pulses in the tumor cell membrane should disappear rapidly at 37°C. In the case of the intravenous or of the intra-arterial way of administration, the existence of these unexpected vascular effects reinforces the obligation of administering the bleomycin prior to electric pulses application. Indeed, bleomycin injected after the electric pulses application should have a restricted access to the electropermeabilized areas and therefore could not be potentiated. Moreover, if the drug is already present in the tissue submitted to the electric pulses, it is likely that the vascular effects should help in the delivering of the drug to the cells in the pulsed volume (besides the permeabilizing effects of the electric pulses, of course). Indeed, these vascular effects should keep high the con-

centration of bleomycin (or of any other nonpermeant drug) locally in the treated volume by transiently stopping the wash-out of the drug from this part of the body. Even in the case of the bleomycin intratumoral injection, this should apply, and in fact, experiments in mice showed that the optimal schedule was to inject the drug 10 minutes before the electric pulses application (45). Therefore, the vascular effects of the permeabilizing electric pulses could have important consequences on the efficacy of electrochemotherapy.

4.2. Role of the Host Immune System

Since the first preclinical trials, the role of host immune response in the efficacy of electrochemotherapy was evident (1). Indeed, using an immunogenic murine fibrosarcoma, Mir and colleagues (1) observed peritumoral edema occurrence and they obtained cures among the syngeneic tumor-bearing immunocompetent C57Bl/6 mice treated by electrochemotherapy with bleomycin. However, the same treatment of the same tumor type but in immunodeficient (nude) mice resulted in the arrest of tumor growth but never in the achievement of cures (1). A parallel situation has been described in the case of electrochemotherapy with cisplatin (56). To demonstrate the role of the host immune system in the eradication of residual tumor cells surviving the direct effects of bleomycin electrochemotherapy, the immunocompetent C57Bl/6 mice bearing the same immunogenic tumor were transiently immunodepressed: the percentage of cures fell down, from 60% of mice cured after a single electrochemotherapy treatment to only 10% of cured animals (57). The host immune response is thus an additional mechanism playing an important role in electrochemotherapy efficacy.

It is possible to take advantage of the participation of host immune response to improve electrochemotherapy antitumor effects using an adequate immunostimulation. Until today, only two groups have explored the possibilities offered by the combination of electrochemotherapy with biological response modifiers like tumor necrosis factor- α (58) or interleukin-2 (57,59,60). In both cases, a significant increase in the number of cures was achieved.

Moreover, using the same immunogenic murine fibrosarcoma, systemic antitumor effects were obtained by the combination of electrochemotherapy with injections of cells engineered in vitro to continuously secrete high amounts of interleukin-2 (59,61). The interest of this combination is the wide applicability of this approach: on the one hand, electrochemotherapy is applicable whatever the tumor type to be treated, and, on the other hand, the immunotherapeutic arm of this combination used xenogeneic interleukin-2-secreting cells (61) that can be administered to all the patients, irrespectively of the individual polymorphism of the major histocompatibility phenotype. Even in the

case of a poorly immunogenic murine tumor model prone to rapidly generate lung metastases (the Lewis lung carcinoma), improvement of the systemic antitumor effects has been achieved by its combination with this immunotherapy (62). Therefore it appears that the association of electrochemotherapy with an appropriate immunotherapy is a convenient way to potentiate the local efficacy of the treatment as well as to obtain distant systemic antitumor effects. This combination increases the interest of electrochemotherapy and broadens the number of carcinologic situations to which this new treatment could be applied.

5. Summary and Conclusions

Antitumor electrochemotherapy is a new treatment based on the local potentiation of the cytotoxic activity of nonpermeant anticancer drugs by cell permeabilizing electric pulses delivered at the level of the tumor nodules. On the one hand, electrochemotherapy consists in the local application of short and intense electric pulses that transiently permeabilize the cells in culture as well as in tissues. The choice of the electric pulse parameters is crucial to obtain this permeabilization without provoking a direct cell killing. On the other hand, the nonpermeant drugs that can be associated to the electric pulses have to possess intracellular targets and a high intrinsic cytotoxicity. The most convenient drug is bleomycin, a currently used anticancer drug, but cisplatin cytotoxicity is also increased *in vivo* by means of this original drug delivery approach. The existence of vascular effects of the permeabilizing electric pulses and the complementary role of the host's immune system also contribute to antitumor electrochemotherapy efficacy and they can be considered as part of the basic mechanisms of this new treatment method.

Electrochemotherapy is thus the first medical application of *in vivo* cell electropermeabilization, that can be considered as a new promising drug delivery system. Antitumor electrochemotherapy using bleomycin has been tested in a variety of animal tumor models and has already been entered in clinical trials. The basis of the efficacy of this combination are established. However, it must be possible to find other adequate nonpermeant drugs, undetected until now because the screening procedures were never performed on electropermeabilized cells. The use of new drugs that could still have less side effects than bleomycin, or oligonucleotides, or even DNA, as well as the combination of electrochemotherapy with appropriate immunotherapies, offer many possibilities for the future development of this new treatment.

Acknowledgments

This work was essentially supported by the Centre National de la Recherche Scientifique and the Institut Gustave-Roussy (IGR), by grants from the Institut

Electricité Santé, the Association pour la Recherche contre le Cancer and the Ligue contre le Cancer (Comités du Val d'Oise, Essonne et Val de Marne). We thank the staff of the Service Commun d'Expérimentation Animale of the IGR for animal maintenance and all the colleagues who participated in the experiments reported and in fruitful discussions.

References

1. Mir, L. M., Orlowski, S., Belehradek, J. Jr., and Paoletti, C. (1991) Electrochemotherapy: potentiation of antitumour effect of bleomycin by local electric pulses. *Eur. J. Cancer* **27**, 68–72.
2. Belehradek, J. Jr., Orlowski, S., Poddevin, B., Paoletti, C., and Mir, L. M. (1991) Electrochemotherapy of spontaneous mammary tumours in mice. *Eur. J. Cancer* **27**, 73–76.
3. Belehradek, M., Domenge, C., Luboinski, B., Orlowski, S., Belehradek, J. Jr., and Mir L. M. (1993) Electrochemotherapy, a new antitumour treatment: First clinical phase I-II trial. *Cancer* **72**, 3694–3700.
4. Mir, L. M., Banoun, H., and Paoletti, C. (1988) Introduction of definite amounts of nonpermeant molecules into living cells after electroporation: Direct access to the cytosol. *Exp. Cell Res.* **175**, 15–25.
5. Domenge, C., Orlowski, S., Luboinski, B., De Baere, T., Schwaab, G., Belehradek, J. Jr., and Mir, L. M. (1996) Antitumor electrochemotherapy: New advances in the clinical protocols. *Cancer* **77**, 956–963.
6. Heller, R., Jaroszeski, M., Perrott, R., Glass, L. F., Puleo, C., Messina, J. L., Rapaport, D. P., DeConti, R. C., Fenske, N. A., Gilbert, R., Mir, L. M., and Reintgen, D. S. (1996) Phase I/II for the treatment of cutaneous and subcutaneous tumors using electrochemotherapy. *Cancer* **77**, 964–972.
7. Rudolf, Z., Štabuc, B., Čemažar, M., Miklavčič, D., Vodovnik, L., and Serša, G. (1996) Electrochemotherapy with bleomycin: The first clinical experience in malignant melanoma patients. *Radiol. Oncol.* **27**, 229–235.
8. Glass, L. F., Fenske, N. A., Jaroszeski, M. J., Perrott, R., Harvey, D. T., Reintgen, D. S., and Heller, R. (1996) Bleomycin-mediated electrochemotherapy of basal cell carcinoma. *J. Am. Acad. Dermatol.* **34**, 82–86.
9. Glass, L. F., Jaroszeski, M., Gilbert, R., Reintgen, D. S., and Heller, R. (1997) Intralesional bleomycin-mediated electrochemotherapy in 20 patients with basal cell carcinoma. *J. Am. Acad. Dermatol.* **37**, 596–599.
10. Mir, L. M., Glass, F. L., Serša, G., Teissié, J., Domenge, C., Miklavčič, D., Jaroszeski, M. J., Orlowski, S., Reintgen, D. S., Rudolf, Z., Belehradek, M., Gilbert, R., Rols, M. P., Belehradek, J. Jr, Bachaud, J. M., DeConti, R., Štabuc, B., Čemažar, M., Coninx, P., and Heller, R. (1998) Effective treatment of cutaneous and subcutaneous malignant tumours by electrochemotherapy. *Br. J. Cancer* **77**, 2336–2342.
11. Zimmermann, U., Pilwat, G., and Riemann, F. (1974) Dielectric breakdown of cell membranes. *Biophys. J.* **14**, 881–899.

12. Zimmermann, U. (1982) Electric field-mediated fusion and related electrical phenomena. *Biochim. Biophys. Acta* **694**, 227–277.
13. Neumann, E. (1992) Membrane electroporation and direct gene transfer. *Bioelectrochem. Bioenerg.* **28**, 247–267.
14. Neumann, E. and Rosenheck, K. (1972) Permeability changes induced by electric impulses in vesicular membranes. *J. Membr. Biol.* **10**, 279–290.
15. Kinosita, K. Jr. and Tsong, T. Y. (1977) Formation and resealing of pores of controlled sizes in human erythrocyte membrane. *Nature* **268**, 438–441.
16. Gross, D., Loew, L. M., and Webb, W. W. (1986) Optical imaging of cell membrane potential changes induced by applied electric fields. *Biophys. J.* **50**, 339–348.
17. Belehradek, J. Jr., Orlowski, S., Ramirez, L. H., Pron, G., Poddevin, B., and Mir, L. M. (1994) Electroporabilization of cells in tissues assessed by the qualitative and quantitative electroloading of bleomycin. *Biochim. Biophys. Acta* **1190**, 155–163.
18. Okino, M. and Mohri, H. (1987) Effects of a high voltage electrical impulse and an anticancer drug on in vivo growing tumors. *Jpn. J. Cancer Res. (Gann)* **78**, 1319–1321.
19. Djuzenova, C. S., Zimmermann, U., Frank, H., Sukhorukov, V. L., Richter, E., and Fuhr, G. (1996) Effect of medium conductivity and composition on the uptake of propidium iodide into electroporabilized myeloma cells. *Biochim. Biophys. Acta* **1284**, 143–152.
20. Rols, M-P. and Teissié, J. (1990) Electroporabilization of mammalian cells. Quantitative analysis of the phenomenon. *Biophys. J.* **58**, 1089–1098.
21. Poddevin, B., Orlowski, S., Belehradek, J. Jr., and Mir, L. M. (1991) Very high cytotoxicity of bleomycin introduced into the cytosol of cells in culture. *Biochem. Pharmacol.* **42 (Suppl.)**, 67–75.
22. Gehl, J., Sørensen, T. H., Nielsen, K., Raskmark, P., Nielsen, S. L., Skovsgaard, T. and Mir, L. M. (1999) In vivo electroporation of skeletal muscle: threshold, efficacy and relation to electric field distribution. *Biochim. Biophys. Acta* **1428**, 233–240.
23. Gehl, J. and Mir, L. M. (1999) Determination of optimal parameters for in vivo gene transfer by electroporation, using a rapid in vivo test for cell permeabilization. *Biochem. Biophys. Res. Comm.* **261**, 377–380.
24. Neumann, E., Schaefer-Ridder, M., Wang, Y., and Hofschneider, P. H. (1982) Gene transfer into mouse lymphoma cells by electroporation in high electric fields. *EMBO J.* **1**, 841–845.
25. Chang, D. C., Gao, P.-Q., and Maxwell, B. L. (1991) High efficiency gene transfection by electroporation using a radio-frequency electric field. *Biochim. Biophys. Acta* **1092**, 153–160.
26. Gehl J., Skovsgaard T., and Mir, L. M. (1998) Enhancement of cytotoxicity by electroporabilization: An improved method for screening drugs. *Anti-Cancer Drugs* **9**, 319–325.
27. Takahashi, M., Furukawa, T., Saitoh, H., Aoki, A., Koike, T., Moriyama, Y., and Shibata, A. (1991) Gene transfer into human leukemia cell lines by electro-

- poration: Experience with exponentially decaying and square-wave pulses. *Leuk. Res.* **15**, 507–513.
28. Okino, M., Tomie, H., Kanesada, H., Marumoto, M., Esato, K., and Suzuki, H. (1992) Optimal electric conditions in electrical impulse chemotherapy. *Jpn. J. Cancer Res. (Gann)* **83**, 1095–1101.
 29. Orłowski, S., Belehradek, J. Jr., Paoletti, C., and Mir, L. M. (1988) Transient electropermeabilization of cells in culture: Increase of the cytotoxicity of anticancer drugs. *Biochem. Pharmacol.* **37**, 4727–4733.
 30. Rols, M-P. and Teissié, J. (1989) Ionic-strength modulation of electrically-induced permeabilization and associated fusion of mammalian cells. *Eur. J. Biochem.* **179**, 109–115.
 31. Serša, G., Čemažar, M., Šemrov, D., and Miklavčič, D. (1996) Changing the electrode orientation improves the efficacy of electrochemotherapy of solid tumors in mice. *Bioelectrochem. Bioenerg.* **39**, 61–66.
 32. Mir, L. M., Tounekti, O., and Orłowski, S. (1996) Bleomycin: Revival of an old drug. *Gen. Pharmacol.* **27**, 745–748.
 33. Pron, G., Belehradek, J. Jr., Orłowski, S., and Mir, L. M. (1994) Involvement of the membrane bleomycin-binding sites in the bleomycin cytotoxicity. *Biochem. Pharmacol.* **48**, 301–310.
 34. Pron, G., Belehradek, J. Jr., and Mir, L. M. (1993) Identification of a plasma membrane protein that specifically binds bleomycin. *Biochem. Biophys. Res. Commun.* **194**, 333–337.
 35. Lazo, J. S., Schisselbauer, J. C., Herring, G. M., and Kennedy, K. A. (1990) Involvement of the cellular vacuolar system with the cytotoxicity of bleomycin-like agents. *Cancer Commun.* **2**, 81–86.
 36. Pron, G., Mahrouf, N., Orłowski, S., Tounekti, O., Poddevin, B., Belehradek, J. Jr., and Mir, L. M. (1999) Internalisation of the bleomycin molecules responsible for bleomycin toxicity: A receptor-mediated endocytosis mechanism. *Biochem. Pharmacol.* **57**, 45–56.
 37. Orłowski, S. and Mir, L. M. (1993) Cell electropermeabilization: A new tool for biochemical and pharmacological studies. *Biochim. Biophys. Acta* **1154**, 51–63.
 38. Tounekti, O., Pron, G., Belehradek, J. Jr., and Mir, L. M. (1993) Bleomycin, an apoptosis-mimetic drug that induces two types of cell death depending on the number of molecules internalized. *Cancer Res.* **53**, 5462–5469.
 39. Tounekti, O., Belehradek J. Jr., and Mir, L. M. (1995) Relationships between DNA fragmentation, chromatin condensation and changes in flow cytometry profiles detected during apoptosis. *Exp. Cell Res.* **217**, 506–516.
 40. Mitchell, M. S. (1988) Combining chemotherapy with biological response modifiers in treatment of cancer. *J. Natl. Cancer Inst.* **80**, 1445–1450.
 41. Morikawa, K., Hosokawa, M., Hamada, J., Xu, Z., and Kobayashi, H. (1986) Possible participation of tumoricidal macrophages in the therapeutic effect of bleomycin on a transplantable rat fibrosarcoma. *Cancer Res.* **46**, 684–688.
 42. Morikawa, K., Hosokawa, M., Hamada, J., Sugawara, M., and Kobayashi, H.

- (1985) Host-mediated therapeutic effects produced by appropriately timed administration of bleomycin on a rat fibrosarcoma. *Cancer Res.* **45**, 1502–1506.
43. Xu, Z., Hosokawa, M., Morikawa, K., Hatakeyama, M., and Kobayashi, H. (1988) Overcoming suppression of antitumor immune reactivity in tumor-bearing rats by treatment with bleomycin. *Cancer Res.* **48**, 6658–6663.
44. Abdul Hamied, T. A. and Turk, J. L. (1987) Enhancement of interleukin-2 release in rats by treatment with bleomycin and adriamycin in vivo. *Cancer Immunol. Immunother.* **25**, 245–249.
45. Heller, R., Jaroszeski, M. J., Perrott, R., Messina, J., and Gilbert, R. (1997) Effective treatment of B16 melanoma by direct delivery of bleomycin using electrochemotherapy. *Melanoma Res.* **7**, 10–18.
46. Jaroszeski, M. J., Gilbert, R., and Heller, R. (1997) In vivo antitumor effects of electrochemotherapy in a hepatoma model. *Biochim. Biophys. Acta* **1334**, 15–18.
47. Heller, R., Jaroszeski, M. J., Reintgen, D. S., Puleo, C. A., DeConti, R. C., Gilbert, R. A., and Glass, L. F. (1998) Treatment of cutaneous and subcutaneous tumors with electrochemotherapy using intralesional bleomycin. *Cancer* **83**, 148–157.
48. Gately, D. F. and Howell, S. B. (1993) Cellular accumulation of the anticancer agent cisplatin: A review. *Br. J. Cancer* **67**, 1171–1176.
49. Melvik, J. E., Pettersen, E. O., Gordon, P. B., and Seglen, P. O. (1986) Increase in cis-dichlorodiammineplatinum(II) cytotoxicity upon reversible electropermeabilization of the plasma membrane in cultured human NHIK 3025 cells. *Eur. J. Cancer Clin. Oncol.* **22**, 1523–1530.
50. Serša, G., Čemažar, M., and Miklavčič, D. (1995) Antitumor effectiveness of electrochemotherapy with cis-diamminedichloroplatinum(II) in mice. *Cancer Res.* **55**, 3450–3455.
51. Čemažar, M., Milačič, R., Miklavčič, D., Dolžan, V., and Serša, G. (1998) Intratumoral cisplatin administration in electrochemotherapy: antitumor effectiveness, sequence dependence and platinum content. *Anti-Cancer Drugs* **9**, 525–530.
52. Čemažar, M., Miklavčič, D., Ščančar, J., Dolžan, V., Golouh, R., and Serša, G. (1999) Increased platinum accumulation in SA-1 tumour cells after in vivo electrochemotherapy with cisplatin. *Br. J. Cancer* **79**, 1386–1391.
53. Ramirez, L. H., Orlowski, S., An, D. J., Bindoula, G., Dzodic, R., Ardouin, P., Bognel, C., Belehradek, J. Jr., Munck, J.-N., and Mir, L. M. (1998) Electrochemotherapy on liver tumors in rabbits. *Br. J. Cancer* **77**, 2104–2111.
54. Serša, G., Beravs, K., Čemažar, M., Miklavčič, D., and Demšar, F. (1998) Contrast enhanced MRI assesment of tumor blood volume after application of electric pulses. *Electr. Magnetobiol.* **17**, 297–304.
55. Serša, G., Čemažar, M., Parkins, C. S., and Chaplin, D. J. (1999) Tumour blood flow changes induced by application of electric pulses. *Eur. J. Cancer* **35**, 672–677.
56. Serša, G., Miklavčič, D., Čemažar, M., Belehradek, J. Jr., Jarm, T., and Mir, L. M. (1997) Electrochemotherapy with CDDP on LPB sarcomas: Comparison of the anti-tumor effectiveness in immunocompetent and immunodeficient mice. *Bioelectrochem. Bioenerg.* **43**, 279–283.

57. Mir, L. M., Orlowski, S., Poddevin, B., and Belehradek, J. Jr. (1992) Electrochemotherapy tumor treatment is improved by interleukin-2 stimulation of host's defenses. *Eur. Cytokine Netw.* **3**, 331–334.
58. Serša, G., Čemažar, M., Menart, V., Gaberc-Porekar, V., and Miklavčič, D. (1997) Anti-tumor effectiveness of electrochemotherapy with bleomycin is increased by TNF- α on SA-1 tumors in mice. *Cancer Lett.* **116**, 85–92.
59. Mir, L. M., Roth, C., Orlowski, S., Quintin-Colonna, F., Fradelizi, D., Belehradek, J. Jr., and Kourilsky, P. (1995) Systemic antitumor effects of electrochemotherapy combined with histoincompatible cells secreting interleukin-2. *J. Immunother.* **17**, 30–38.
60. Mir, L. M., Roth, C., Orlowski, S., Belehradek, J. Jr, Fradelizi, D., Paoletti, C., and Kourilsky, P. (1992) Potentiation of the antitumoral effect of electrochemotherapy by an immunotherapy with allogeneic cells producing interleukin-2. *C. R. Acad. Sci. III* **314**, 539–544.
61. Roth, C., Mir, L. M., Cressent, M., Quintin-Colonna, F., Ley, V., Fradelizi, D., and Kourilsky, P. (1992) Inhibition of tumor growth by histoincompatible cells expressing interleukin-2. *Int. Immunol.* **4**, 1429–1436.
62. Orlowski, S., An, D., Belehradek, J. Jr., and Mir, L. M. (1998) Antimetastatic effects of electrochemotherapy and of histoincompatible interleukin-2-secreting cells in the murine Lewis lung tumor. *Anticancer Drugs* **9**, 551–556.

Electrochemotherapy

Animal Model Work Review

Gregor Serša

1. Introduction

The major disadvantage of clinically established chemotherapeutic agents is their lack of selectivity for tumor cells. Therefore, for a pronounced antitumor effect, high doses of the chemotherapeutic drugs are needed, which often cause systemic toxicity and severe side effects. Some chemotherapeutic drugs do not exert their antitumor effects because they have hampered transport through the plasma membrane, but once inside the cell, they can be very potent. To overcome membrane restriction, much effort has been put into the development of drug delivery systems. These systems are aimed at facilitating the delivery of a chemotherapeutic drug into tumor cells at concentrations that are sufficient for effective cell killing and, at the same time, to minimize the drug concentration in normal tissue.

In view of this, several approaches to selective drug delivery have been made, including local application of the drugs (*1,2*), targeting by binding of the drugs to tumor specific antibodies (*3*), magnetic drug targeting (*4*), incorporation of the drugs into liposomes or other vehicles (*5–7*), or by selectively increasing permeability of plasma membrane on tumor cells by chemical methods (*8*). Many of these methods are based on a systemic approach, however, another approach to better drug delivery is to potentiate the effect locally, at the tumor site, by exposure of tumors to electric pulses (*9*).

Exposure of cells to electric pulses induces a position-dependent transmembrane potential that, above the threshold level, results in a marked perturbation of membrane structure, that is, in the formation of still undefined transient

permeabilization structures, also termed electropores (10,11). Under suitable conditions, these membrane changes are reversible and cell viability is thus maintained (12). Consequently, the plasma membrane becomes permeable to a variety of hydrophilic molecules that are otherwise unable to diffuse through the plasma membrane. This electrically induced permeabilization has been used successfully in the insertion of drugs, dyes, genes, oligonucleotides and monoclonal antibodies into living cells (13,14).

In vitro data have demonstrated that electroporation of cells can potentiate cytotoxicity of some chemotherapeutic drugs, predominantly those that have hampered access into the cytosol through the plasma membrane. One of the molecules, which demonstrated a 700-fold increased cytotoxicity after electroporation of cells is bleomycin (15,16). This drug was demonstrated by L. M. Mir and colleagues to be one of the best candidates for drug delivery with electroporation (13). However, there are also other drugs like Adriamycin, netropsin, methotrexate, melphalan, mitramycin, mitomycin C, actinomycin D, cyclophosphamide, and cisplatin, which are much more cytotoxic when cells are electroporated (13,17–19). Among these chemotherapeutic drugs cisplatin proved to be a good choice, its cytotoxicity can be potentiated up to 70-fold by electroporation of cells (18). Although there may be even more candidates, only bleomycin and cisplatin have been extensively studied in vivo on animal tumor models and also in Phases I and II clinical trials (Fig. 1). The aim of this review is to present the results of the combined use of chemotherapeutic drugs and application of electric pulses in vivo on animal tumor models.

2. Electrochemotherapy With Bleomycin

Although electroporation has been known for quite some time to be an effective method for introduction of molecules into cells in vitro, only in the last 10 years has it been used in vivo. The first report on combining chemotherapeutic drug and application of electric pulses to treat subcutaneous hepatocellular tumors in rats was given by Okino and Mohri (20). Shortly after that, L. M. Mir and colleagues performed a detailed study on application of electric pulses as a drug delivery system for bleomycin on transplanted and spontaneous tumors in mice and termed it *electrochemotherapy* (21,22). Since then, a number of studies have been conducted with great success, bleomycin being the most often used chemotherapeutic drug. The pioneering work of Okino and Mir has been followed by several groups demonstrating that in vivo application of electric pulses dramatically increases antitumor effectiveness of bleomycin (23–26). Potentiation of antitumor effectiveness of bleomycin in vivo was demonstrated to be about 10,000-fold (21).

Since electrochemotherapy combines local application of electric pulses after systemic injection of bleomycin, the toxicity of this combined treatment

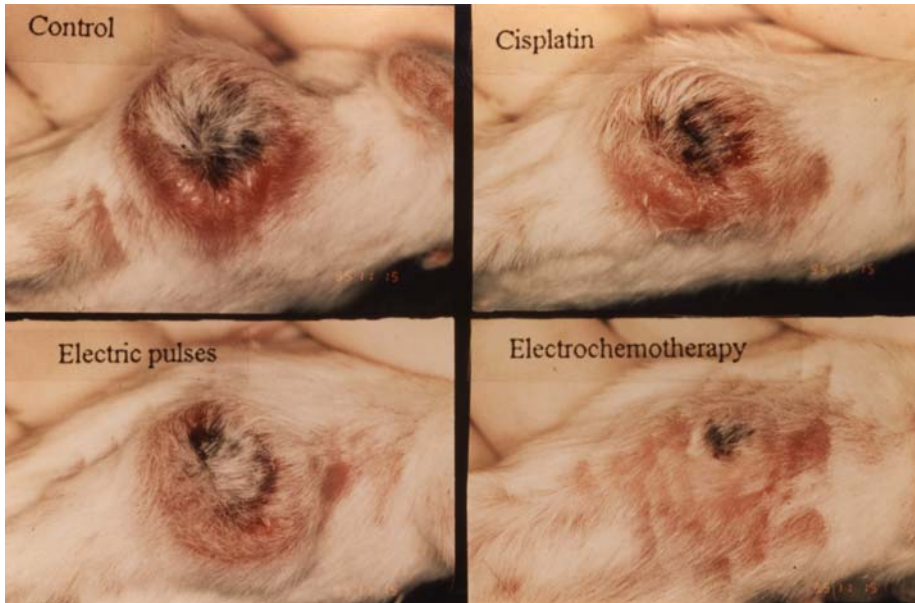


Fig. 1. Macroscopic changes on tumors observed after electrochemotherapy. Significant reduction in tumor volume is observed in tumors treated by electrochemotherapy with cisplatin (4 mg/kg) 2 weeks after the beginning of treatment, compared to tumors that were without treatment, treated with cisplatin or electric pulses only.

is predominantly dependent on the toxicity of bleomycin. This treatment has minimal side effects because, even with low doses of bleomycin good antitumor effect of electrochemotherapy can be obtained (21,25,26). In addition, electric pulses are delivered locally and confined to the tumor area. Therefore, the potentiated effect is localized and restricted to the area where the electric pulses are applied. However, application of electric pulses may induce muscle contraction which subside after their application. Sometimes local burns on the skin are observed when plate electrodes are used (21,25,26). The electric pulses are the means for delivering the drug into the tumor cells and are not intended to reduce cell viability. However, the combination of both treatments can result in tumor cure, as demonstrated by several groups that have performed experiments with electrochemotherapy on different animal tumors (9,21,25,26).

Similarities exist in the way in which the experiments on electrochemotherapy were performed. Most groups administered bleomycin intravenously, except L. M. Mir in his first study where he injected the drug intramuscularly (21), but later, also applied intravenous injection of the drug. Shortly after the

drug reaches the tumor, electric pulses are applied. In the initial studies, exponential electric pulses were used (27). However, in most studies square wave electric pulses were used with an amplitude to electrode distance ratio 1300 V cm^{-1} or 1500 V cm^{-1} , repetition frequency of 1 Hz, and pulse duration $100 \mu\text{s}$ (21,25,26). Since antitumor effectiveness is dependent on drug concentration in the tumor during application of electric pulses, interval between the drug and pulse treatments is very important. A 3-minute interval between the treatments was found to be optimal (21,25,26). The amplitude of electric pulses is even more important; amplitudes of 1200 V cm^{-1} or higher are needed to obtain a good antitumor effect. With higher amplitudes of electric pulses, more cells in the tumor are permeabilized. Permeabilization of the tumor cells is dependent also on the number of electric pulses applied. It has been found that at least four pulses are needed; however, most of the studies have been performed with eight electric pulses (21,28).

A finding common to all the studies is that after electrochemotherapy with bleomycin, at least a considerable growth delay of solid tumors in mice and rats is obtained. The tumors studied were sarcomas, malignant melanoma, hepatocellular, mammary, and bladder carcinomas, Ehrlich ascites carcinoma, and others (21,24,30). Many studies reported that with bleomycin doses far below toxicity, antitumor effectiveness of electrochemotherapy induced complete responses of the tumors and often also tumor cures, even above 80% in the most responsive tumors (Fig. 2).

Electrochemotherapy with bleomycin was performed also on tumors in internal organs. The first study on internal organs was performed on glioblastoma transplanted into the brain of rats (23). Later, when new electrode design was introduced in electrochemotherapy, several studies reported good results in the treatment of tumors transplanted into other internal organs. The results of these studies demonstrated that electrochemotherapy can be used also in the treatment of different tumors seeded in the liver of rats, cats, and rabbits (31–34). The results of the studies demonstrated that the antitumor effectiveness of electrochemotherapy with bleomycin is as effective on tumors growing in the liver as on solid subcutaneous tumors, indicating that shortly we can expect the first reports on electrochemotherapy on internal organs in cancer patients.

In spite of very good results, differences in responsiveness of tumors to electrochemotherapy were observed. Comparison between the responsiveness of tumors and the sensitivity of cells *in vitro* to bleomycin demonstrated that intrinsic sensitivity to bleomycin predetermines responsiveness of the tumors to electrochemotherapy with bleomycin. It has been found that some tumors are more sensitive to one drug than to another used in electrochemotherapy (34). In another study, it was demonstrated that the difference in sensitivity to electrochemotherapy *in vitro* was the same as the difference in sensitivity to

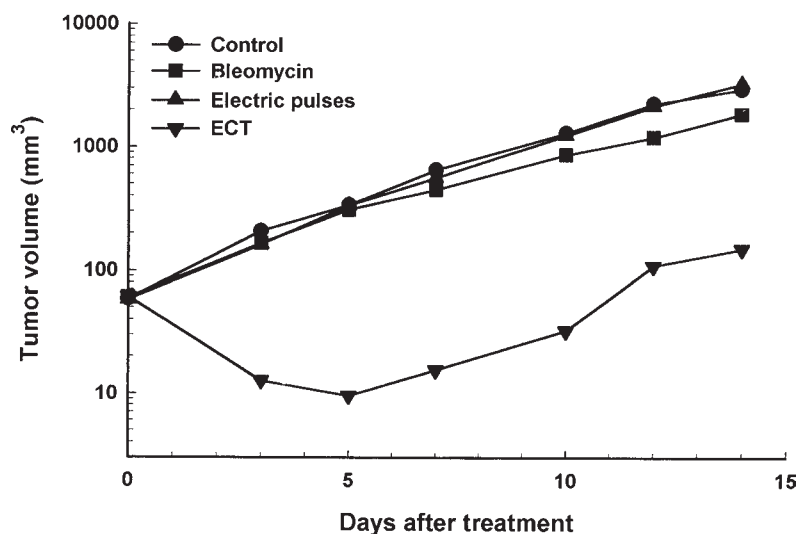


Fig. 2. Growth curves of tumors treated by electrochemotherapy (ECT) with bleomycin. B16 malignant melanoma tumors were treated with bleomycin injected intravenously and 3 minutes thereafter exposed to eight electric pulses. (Adapted from ref. 26, with permission.)

chronic exposure to bleomycin, and was reflected in difference in responsiveness to electrochemotherapy *in vivo* (16). Therefore, all these data indicate that not all tumors have equal level of sensitivity to electrochemotherapy with bleomycin, but all tumor types have shown a response to electrochemotherapy. In the cases when tumors cannot be optimally treated by electrochemotherapy with bleomycin, some other drug can be used.

3. Electrochemotherapy With Cisplatin

Although Melvik et al. (17) demonstrated in the early eighties that cytotoxicity of cisplatin *in vitro* can be potentiated by exposure of cells to exponentially decaying electric pulses, cisplatin was applied in electrochemotherapy protocol using square wave electric pulses no sooner than in the nineties. At that time, we demonstrated that with square wave electric pulses even better cytotoxicity of cisplatin can be obtained; on B16 melanoma cells, up to 70-fold potentiation was demonstrated (18). Although this potentiation is not as outstanding as with bleomycin, cisplatin has high potential in clinical practice because it is already effectively used in many chemotherapeutic protocols.

The first extensive study using cisplatin in electrochemotherapy was elaborated on parameters that established its optimal use in the treatment of cutaneous tumors (18). Electric pulses used in the study for electroporation of tumors

were the same as used in electrochemotherapy with bleomycin in order to be able to compare antitumor effectiveness of both treatments. Similarly as with bleomycin, it was found that optimal timing for cisplatin administration, when injected intravenously, was three minutes before the application of electric pulses. The antitumor effectiveness of cisplatin was potentiated severalfold and was dependent on the amplitude of electric pulses as well as cisplatin dose. Again, electric pulses of at least 1200 V cm^{-1} were needed to obtain good antitumor effect. The optimal dose for cisplatin used in electrochemotherapy was demonstrated to be 4 mg kg^{-1} , which corresponds to the suboptimal clinically effective dose.

The antitumor effectiveness was demonstrated on four subcutaneous tumor models in mice, fibrosarcomas SA-1 and LPB as well as on B-16 malignant melanoma and Ehrlich-Lette ascites carcinoma (18,35). With doses of 8 mg kg^{-1} specific tumor growth delay of at least 20 days was obtained, and up to 80% tumor cures, as demonstrated on LPB sarcoma in C57Bl/6 mice (35). These results are comparable with the results obtained with bleomycin. Confirmation that electrochemotherapy is also effective in the treatment of tumors implanted into the liver came in the latest study of Heller's group. They demonstrated that electrochemotherapy with cisplatin could be as effective as electrochemotherapy with bleomycin in the treatment of hepatomas implanted into the liver (34). Furthermore, evidence exists that electroporation of tumors increases access of cisplatin into tumor cells in vivo. Approximately a twofold increase in platinum bound to DNA and accumulated in tumors was obtained in tumors exposed to electric pulses than in those that were not (36).

Clear evidence that different tumors respond to electrochemotherapy with one drug better than with another is found when comparison is made between results on the same tumor models with the same protocol (18,25). It is evident that sarcomas are more responsive to electrochemotherapy with bleomycin than to cisplatin, and that melanoma is more responsive to electrochemotherapy with cisplatin. However, further studies are needed to demonstrate which tumors are more susceptible to treatment with specific drug in electrochemotherapy.

Resistance that develops to the drug during the chemotherapy protocols is one of the issues that has to be considered. Cisplatin is one of the drugs that induces resistance mechanisms in cells, often early in the course of the treatment. Some studies have already addressed this issue, and demonstrated that electroporation can overcome resistance of cells to cisplatin, at least to some degree (37). Resistance of cells to cisplatin can be related to several mechanisms, but until now studies have not indicated which mechanism is overcome by electroporation. Presumably membrane restricted mechanisms are overcome by electric pulses, however, to confirm this, further studies are needed.

4. Other Drugs in Electrochemotherapy

It is not surprising that only bleomycin and cisplatin have found successful application in electrochemotherapy. Since bleomycin has proved already in the first experimental studies to be so effective, there was no need to test other drugs. Nevertheless, we initiated the first studies with cisplatin, with the thought that clinicians are more receptive to new protocols if performed with drugs that are already widely used in routine chemotherapeutic schemes. Because electrochemotherapy is more effective than the use of drugs alone, that have hampered access to the cytosol, the search for drugs that are hydrophilic, nonpermeant, and very cytotoxic when reaching intracellular targets has to be conducted.

Some attempts to determine whether other drugs would be effective in electrochemotherapy protocol *in vivo* were made. In the study of Kanesada (38) it was shown that some potentiation of antitumor effectiveness can be obtained with the use of peplomycin, cyclophosphamide, and mitomycin C. Also Heller's group (34) performed a study on the drugs doxorubicin, 5-fluorouracil, and taxol used in combination with electric pulses. The treatment was tested on hepatoma and sarcoma tumors implanted into the rat liver. All drugs proved to be ineffective in electrochemotherapy protocol used on hepatomas, and only doxorubicin was moderately effective in the electrochemotherapy treatment of sarcoma.

The search for new drugs to be used in electrochemotherapy will most probably not continue, because of the disappointing results of these studies. Drugs already used in chemotherapeutic protocols do not seem to be good candidates because of their lipophilicity. Good candidates may come only when new drugs will be synthesized and their cytotoxicity will be hampered by poor plasma membrane permeability.

5. Attempts to Increase Effectiveness of Electrochemotherapy

Although electrochemotherapy has proven to be very effective in cancer treatment, many researchers have undertaken steps to improve its effectiveness. The aim of their work was to improve electrochemotherapy in order to increase local tumor control. Three different approaches were made. The first was to improve electric current distribution within the tumor for better electroporation of cells in the tumors; the second was by local delivery, that is, intratumoral injection of the chemotherapeutic drug to increase drug concentration in the tumors and consequently effectiveness of electrochemotherapy; the third means of improving effectiveness was by repetitive treatment of the tumors to have better control over tumors that tend to regrow after the first treatment.

The first electrochemotherapy studies were performed using eight electric pulses to electroporate the tumors after administration of the chemotherapeutic drug. In those studies, plate electrodes were used which encompassed the tumors when being electroporated. If the tumors were small enough and adequately encompassed by the electrodes, good antitumor effect was observed. However, when the tumors were bigger, deeper parts of the tumor and its margins were suboptimally electroporated. Although many tumors can be successfully treated after substantial period of partial or complete response, some tumors regrow at their margins where there was no contact with the electrodes. In those areas some clonogenic tumor cells must have remained, we presume that they were suboptimally permeabilized, survived and eventually regrew into a tumor. Based on this observation, a study was undertaken to model and verify a hypothesis that by changing the electric field orientation during electroporation better antitumor effects can be obtained (28,39). This protocol, described in a separate chapter of this volume, indicates that the optimization of electric field distribution in tumors is a prerequisite step for effective electrochemotherapy. The explanation for the underlying mechanism is that electric field intensity in the midplane of the tumor falls substantially, and is further dropping toward the edges of the tumor. On the cellular level the explanation could be that, due to different shapes of the cells, there is higher probability of optimally electroporating each cell by changing the orientation of the applied electric pulses (28).

Research has been initiated to develop a device to electroporate even bigger tumor areas, using optimal electric field parameters. The idea was to construct needle electrodes that could be inserted into the tumors and electroporate also deeper parts of the tumors (40). Besides, by applying electric pulses between the needle electrodes and rotating the sequences of the pulses, the idea of optimally electroporating the entire tumor area can be realized. The approach was developed by two groups, R. Heller's group in cooperation with Genetronics Inc. and L. M. Mir's group. The first group constructed an array of needles on a holder and rotated the application of electric pulses. To electroporate different sizes of tumors they have constructed different sizes of applicators (41,42). In the comparative study, they demonstrated that needle array electrodes showed a 50% increase in tumor doubling time and in complete response rate compared to standard parallel plate electrodes (42). L. M. Mir's group approached the problem by constructing a honeycomb structured array of electrodes (32,33). This kind of electrode array has an advantage that, in sequences, it can electroporate varying sizes of tumor masses. This is only a brief description of this very important field, that has to be developed to bring electrochemotherapy into broader clinical practice. More data about construction and modeling of different electrodes for electrochemotherapy are avail-

able in other chapters of this volume. Both groups provided the evidence that needle array electrodes were very effective in treatment of subcutaneous as well as tumors in internal organs. Their response rate of the tumors was even better than those obtained with plate electrodes and was above 80%.

The second approach to increase effectiveness of electrochemotherapy is to deliver chemotherapeutic drug for electrochemotherapy locally, into the tumor. Injection of the drug directly into the tumor exposes cells to a higher concentration of the drug during application of electric pulses, without prior distribution of the drug in the vascular system. For effective electrochemotherapy, sufficient amount of the drug in the tumor is needed, but often because of the physiological problems after intravenous administration of the drug, suboptimal drug concentration in the tumor is achieved. Both bleomycin and cisplatin have been tested in preclinical trials for their effectiveness in electrochemotherapy. Heller's group demonstrated that electrochemotherapy with bleomycin was an effective treatment when the drug was injected intratumorally (43,44). The effect was dependent on the drug dosage as well as on intensity of the electric pulses used for electroporation. Objective responses on melanoma B16 tumors were more than 80%. It was also established that the time span for intratumoral drug injection was optimal up to 30 minutes before application of electric pulses (43). Another study that we conducted demonstrated basically the same. Electrochemotherapy with cisplatin proved to be also very effective when the drug was injected intratumorally, and was dependent on the drug dosage as well as the timing (39,45). The best antitumor effect was observed when cisplatin was injected 5 minutes before or simultaneously with application of electric pulses, inducing up to 65% tumor cures. Confirmation that electroporation increases intracellular accumulation of cisplatin was obtained by measuring the platinum content in the tumors and platinum bound to DNA. It was found that approximately two times more platinum was retained in the tumors and bound to DNA (45). This treatment can be very effective, inducing high degree of tumor cures, as compared to the same drug dosage used at electrochemotherapy with intravenously injected cisplatin (Fig. 3). In summary, electrochemotherapy with intratumoral drug administration is as effective as intravenous, it can be performed using longer time interval, the treatment of multiple tumor sites is less constrained and the drug dosage can be based on the tumor volume instead of total body surface area. Based on these conclusions, some clinical trials were conducted that used intratumoral injection of the drug in electrochemotherapy. The results of these clinical studies are encouraging and are summarized in another chapter of this volume.

The third approach to increasing the effectiveness of electrochemotherapy is to perform repetitive treatment. When tumors are suboptimally permeabilized or drug concentration in tumors is suboptimal, tumors often

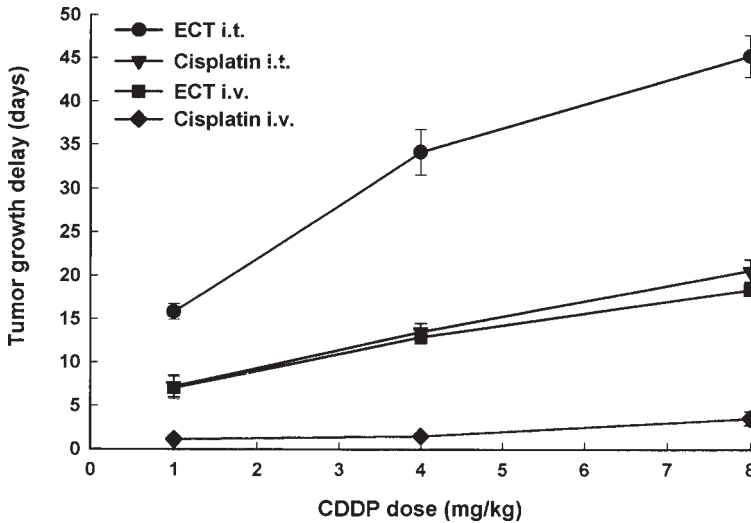


Fig. 3. Electrochemotherapy (ECT) with cisplatin. Comparison of antitumor effectiveness when cisplatin is injected intravenously or intratumorally into SA-1 tumor-bearing mice.

regrow. In such cases, treatment can be successfully repeated on the remaining viable part of the tumor. So far, only two studies have been performed on electrochemotherapy with bleomycin, both demonstrating that antitumor effectiveness of multiple treatments is superior to single treatment. In the first study, Mir et al. (21) demonstrated that three repetitive treatments in a weekly interval yielded superior results to single treatment on LPB sarcoma by increasing the curability of tumors from 30% to 50%. The results of the second study on B16 melanoma tumors demonstrated a twofold increase in tumor doubling time and greater percentages of complete responses as a result of multiple treatments (44). Both studies also demonstrated that, by repetitive treatment, approximately a 15-fold decrease in drug dose could be used, and still yielded results that were equivalent to a single treatment. Although there are no data demonstrating that similar effects can be obtained by electrochemotherapy with cisplatin, experiences from clinical trials support this notion (46).

All these attempts have been made to increase antitumor effectiveness of electrochemotherapy, by increasing its effectiveness at local tumor control. As electrochemotherapy is a localized treatment, this is self explanatory. But many researchers that are involved in electrochemotherapy are focused at adding a systemic component to this treatment.

6. Immune System and Electrochemotherapy

Most electrochemotherapy studies were performed on immunocompetent mice. The importance of the immune system was demonstrated in the study that compared the same electrochemotherapy protocol with bleomycin on tumors with different immunogenicity (25). Immunogenicity of tumors could be correlated with the antitumor effectiveness of electrochemotherapy with bleomycin, since electrochemotherapy resulted in a higher curability rate (62%) for immunogenic tumors, and in a low curability rate (5%) for moderately immunogenic tumors.

Studies comparing antitumor effectiveness of electrochemotherapy with bleomycin on immunocompetent and immunodeficient mice supported the presumption that the immune system of the organism contributes to antitumor effectiveness (21). Much higher percentage of tumor cures was obtained in immunocompetent than in immunodeficient mice. Similar results were obtained in the study comparing the effectiveness of electrochemotherapy with cisplatin on the same tumor model in immunocompetent and immunodeficient mice (35). Tumor growth delay was approximately twice longer in immunocompetent than in immunodeficient mice. Furthermore, high percentage of cures was obtained in immunocompetent mice (82%), but none in immunodeficient mice.

All these studies demonstrated that the immune system plays a central role in the long-term control of tumor growth and that both, monocytes and lymphocytes are affected by electrochemotherapy (47). T lymphocytes were found to be important, since their depletion by monoclonal antibodies reduced curability of the tumors from 60% to 20% (48). However, stimulation of the immune response by adjuvant immunotherapy with biological response modifiers can increase effectiveness of electrochemotherapy. Both T lymphocytes and monocytes-stimulating agents were used as adjuvant immunotherapy. Following this idea, preclinical studies combining electrochemotherapy with bleomycin, and interleukin-2 (IL-2) or IL-2 secreting cells have already been performed (48–50). Stimulation of T cells by systemic injection of IL-2 or IL-2 secreting cells resulted in an increased, almost 100% cure rate of the mice (48,49). Furthermore, systemic antitumor immunity mediated by CD4+ and CD8+ T cells was observed after adjuvant therapy with IL-2 secreting cells (50). In addition to localized tumor control, a systemic response was observed as well, leading to tumor regression in almost 50% of the tumors at distant sites where no electrochemotherapy was performed (Fig. 4) (50).

When a monocyte stimulating agent, tumor necrosis factor- α (TNF- α) was used, similar results were obtained. In the study, a suboptimal dose of bleomycin was used, electrochemotherapy induced moderate (5.6 days) tumor

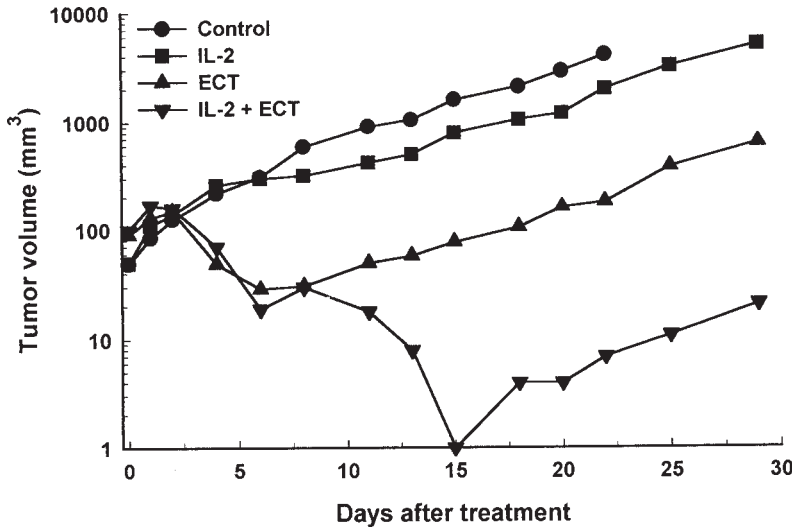


Fig. 4. Effect of electrochemotherapy (ECT) with bleomycin combined with injection of allogenic P815 (interleukin-2; IL-2) cells. IL-2-secreting cells were injected on the flank on days 1, 2, and 5 after electrochemotherapy. (Adapted from **ref. 50**, with permission.)

growth delay, however, when adjuvant immunotherapy with TNF- α , given intratumorally was added, the combined use induced 15.1 day tumor growth delay and even cured 33% of the mice (51). The increased antitumor effectiveness was neither the result of potentiated antitumor effectiveness of TNF- α due to exposure to electric pulses, nor due to interaction with bleomycin.

Based on the data of these studies, immunotherapy has great potential as an adjuvant therapy in electrochemotherapy. It does not only augment antitumor activity of electrochemotherapy, but possibly adds a systemic component to the localized electrochemotherapy treatment.

7. Effect of Electrochemotherapy on Metastatic Potential of the Tumors

Metastatic capacity of malignant tumors represents one of the major problems in cancer treatment. Since electrochemotherapy is a locoregional treatment, the issue of its impact on metastatic capacity of tumors has to be addressed; however, very few studies have done that (20,38,52). Most of them have scored distant metastases after treatment of the primary tumor. Results of these studies, although lacking in extensiveness and scientific rigor, have demonstrated that electrochemotherapy does not induce increased metastatic potential of the tumors. The data that they have provided do not support

their conclusion that electrochemotherapy reduces the formation of metastases. However, the study examining electrochemotherapy with bleomycin in rabbits and adjuvant immunotherapy with IL-2 demonstrated a decreased number of metastases (32), as well as the study on murine Lewis lung carcinoma (52). But, this effect was predominantly due to adjuvant immunotherapy, and could not be ascribed to electrochemotherapy alone. Also, clinical studies support the presumption that electrochemotherapy does not stimulate the metastatic spread of the tumors. The studies were predominantly done on tumors that have low metastatic capability (basal cell carcinoma, squamous cell carcinoma). Only clinical studies on malignant melanoma could be instrumental, however, those patients had terminal disease and it was impossible to demonstrate prolonged survival in those patients after electrochemotherapy. As already mentioned, the issue of metastases has to be addressed in well controlled preclinical and clinical studies to demonstrate what is the impact of electrochemotherapy on the formation of metastases.

8. Summary and Conclusions

It is evident from the preclinical and clinical studies that electrochemotherapy is very effective locoregional treatment. The administration of the drug either intravenously or intratumorally combined with local application of electric pulses is an effective treatment, but the drug dosage needed for the pronounced antitumor effect is too low for systemic side effects. Furthermore, the application of electric pulses is strictly local, confined to the tumor area. Since the applied electric pulses are the means to introduce the cytotoxic drug into the cells, their potentiating effect is confined to the area of their application. Another advantage of electrochemotherapy is that normal tissue damage is restricted to the area which was subjected to application of electric pulses in the presence of the drug. Although cancer is a systemic disease, many other treatments in cancer are also locoregional, such as surgery and radiotherapy. It was often postulated that good local control in the treatment of cancer is very important for the outcome of the disease. Therefore, although electrochemotherapy is locoregional, it holds promise as such and will find its place in the treatment of cancer.

Based on the current preclinical studies, electrochemotherapy is being tested in treatment of tumors seeded in internal organs. This is an important step forward which will broaden the application of electrochemotherapy from treatment of accessible tumor lesions in the skin to intraoperative treatment of tumor lesions in gastrointestinal and gynecological organs as well as to tumors in the lung. When electrodes are designed that will be minimally invasive (laparoscopy), almost any internal organ will be accessible with minimally invasive technique.

Many of the chemotherapeutic drugs are also radiosensitizers. Therefore, electrochemotherapy with such drugs will find its application in radiotherapy of tumors. Preclinical and clinical studies are already in progress and based on these results we can predict that combined electrochemotherapy and irradiation of tumors will be effective in treatment of patients.

Electric pulses also have a blood-modifying effect. An area that is exposed to electric pulses has a temporary shutdown of blood flow (53,54). This is another advantage of electrochemotherapy since the drug that is used in the protocol is trapped in the area, and has a prolonged period of its cytotoxic action. On the other hand, when needle array electrodes are used, this vascular occlusion prevents bleeding of the electroporated area (33).

Blood modifying effect of electric pulses can be exploited also in another direction. Use of bioreductive drugs that are effective in hypoxic environment could be potentiated by application of electric pulses. This is especially of interest since the desired physiological condition can be induced only in the confined area where the pulses are applied.

These are the most evident future directions of electrochemotherapy. In addition, there are many other applications that are already in progress, such as electrogene therapy, or others that have not yet been foreseen.

References

1. Begg, A. C., Deurloo, M. J., Kop, W., and Bartelink, H. (1991) Improvement of combined modality treatment with cisplatin and radiation using intratumoral drug administration in murine tumors. *Radiother. Oncol.* **31**, 129–133.
2. Landrito, J. E., Yoshiga, K., Sakurai, K., and Takada, K. (1994) Effects of intralesional injection of cisplatin on squamous cell carcinoma and normal tissue of mice. *Anticancer Res.* **14**, 113–118.
3. De Vita, V. T. Jr., Hellman, S., and Rosenberg, S. A. (1991) *Biologic Therapy of Cancer*. Lippincott, Philadelphia.
4. Lübke, A. S., Bergemann, C., Riess, H., Schriever, F., Reicsardt, P., Possinger, K., Matthias, M., Dürken, B., Herrmann, F., Gürtler, R., Hohenberger, P., Haas, N., Sohr, R., Sander, B., Lemke, A-J., Ohlendorf, D., Huhnht, W., and Huhn, D. (1996) Clinical experience with magnetic drug targeting: A phase I study with 4'-epidoxorubicin in 14 patients with advanced solid tumors. *Cancer Res.* **56**, 4686–4693.
5. Deurloo, M. J., Kop, W., van Tellingen, O., Bartelink, H., and Begg, A. C. (1991) Intratumoral administration of cisplatin in slow-release devices. II. Pharmacokinetics and intratumoral distribution. *Cancer Chemother. Pharmacol.* **27**, 347–353.
6. Kuang, L., Yang, D. J., Inoue, T., Liu, W. C., Wallace, S., and Wright, K. C. (1996) Percutaneous intratumoral injection of cisplatin microspheres in tumor-bearing rats to diminish acute nephrotoxicity. *Anti-Cancer Drugs* **7**, 220–227.
7. Steerenberg, P. A., Storm, G., De Groot, G., Claessen, A., Bergers, J. J.,

- Franken, M. A. M., van Hoesel Q. G. C. M., Wubs, K. L., and de Jong, W. H. (1988) Liposomes as drug carrier system for cis-diamminedichloroplatinum(II). II: Antitumor activity in vivo, induction of drug resistance, nephrotoxicity and Pt distribution. *Cancer Chemother. Pharmacol.* **21**, 299–307.
8. Jekunen, A. P., Shalinsky, D. R., Hom, D. K., Albright, K. D., Heath, D., and Howell, S. B. (1993) Modulation of cisplatin cytotoxicity by permeabilization of the plasma membrane by digitinin in vitro. *Biochem. Pharmacol.* **45**, 2079–2085.
 9. Mir, L. M., Orłowski, S., Belehradek, J. Jr., Tessie, J., Rols, M. P., Serša, G., Miklavčič, D., Gilbert, R., and Heller, R. (1995) Biomedical application of electric pulses with special emphasis on antitumor electrochemotherapy. *Bioelectrochem. Bioenerg.* **38**, 203–207.
 10. Neumann, E., Sowers, A. E., and Jordan, C. A., (1989) *Electroporation and Electrofusion in Cell Biology*. Plenum, New York.
 11. Neumann, E. and Kakorin, S. (1998) Digression of membrane electroporation and electroporative delivery of drugs and genes. *Radiol. Oncol.* **32**, 7–17.
 12. Čemažar, M., Jarm, T., Miklavčič, D., Maček-Lebar, A., Ihan, A., Andreja-Kopirat, N., and Serša, G. (1998) Effect of electric-field intensity and electropermeabilization and electrosensitivity of various tumor-cell lines in vitro. *Electr. Magnetobiol.* **17**, 263–272.
 13. Orłowski, S. and Mir, L. M. (1993) Cell electropermeabilization: A new tool for biochemical and pharmacological studies. *Biochim. Biophys. Acta* **1154**, 51–63.
 14. Jaroszeski, M. J., Gilbert, R., and Heller, R. (1997) Electrochemotherapy: An emerging drug delivery method for the treatment of cancer. *Adv. Drug Deliv. Rev.* **26**, 185–197.
 15. Poddevin, B., Orłowski, S., Belehradek, J. Jr., and Mir, L. M. (1991) Very high cytotoxicity of bleomycin introduced into the cytosol of cells in culture. *Biochem. Pharmacol.* **42 (Suppl.)**, S67–S75.
 16. Čemažar, M., Miklavčič, D., and Serša, G. (1998) Intrinsic sensitivity of tumor cells to bleomycin as an indicator of tumor response to electrochemotherapy. *Jpn. J. Cancer Res.* **89**, 328–333.
 17. Melvik, J. E., Pettersen, E. O., Gordon, P. B., and Selgen, P. O. (1986) Increase in cis-diamminedichloroplatinum (II) cytotoxicity upon reversible electropermeabilization of the plasma membrane in cultured human HNK 3025 cells. *Eur. J. Cancer Clin. Oncol.* **22**, 1523–1530.
 18. Serša, G., Čemažar, M., and Miklavčič, D. (1995) Antitumor effectiveness of electrochemotherapy with cis-diamminedichloroplatinum(II) in mice. *Cancer Res.* **55**, 3450–3455.
 19. Yabushita, H., Yoshikawa, K., Hirata, M., Furuya, H., Joghoy, T., Fukatsu, H., Noguchi, M., and Nakanishi, M. (1997) Effects of electrochemotherapy on CaSki cells derived from a cervical squamous cell carcinoma. *Gynecol. Oncol.* **65**, 297–303.
 20. Okino, M. and Mohri, H. (1987) Effects of high voltage electrical impulse and an anticancer drug on in vivo growing tumors. *Jpn. J. Cancer Res.* **78**, 1319–1321.
 21. Mir, L. M., Orłowski, S., Belehradek, J. Jr., and Paoletti, C. (1991) Electroche-

- motherapy potentiation of antitumour effect of bleomycin by local electric pulses. *Eur. J. Cancer* **27**, 68–72.
22. Belehradec, J. Jr., Orlowski, S., Poddevin, B., Paoletti, C., and Mir, L. M. (1991) Electrochemotherapy of spontaneous tumors in mice. *Eur. J. Cancer* **27**, 73–76.
 23. Salford, L. G., Persson, B. R. R., Brun, A., Ceberg, C. P., Kongstad, P. Ch., and Mir, L. M. (1993) A new brain tumour therapy combining bleomycin with in vivo electropermeabilization. *Biochim. Biophys. Acta* **194**, 938–943.
 24. Yamaguchi, O., Irisawa, C., Baba, K., Ogihara, M., Yokota, T., and Shiraiwa, Y. (1994) Potentiation of antitumor effect of bleomycin by local electric pulses in mouse bladder tumor. *Tokohu J. Exp. Med.* **172**, 291–293.
 25. Serša, G., Čemažar, M., Miklavčič, D., and Mir, L. M. (1994) Electrochemotherapy: variable anti-tumor effect on different tumor models. *Bioelectrochem. Bioenerg.* **35**, 23–27.
 26. Heller, R., Jaroszeski, M., Leo-Messina, J., Perrot, R., Van Voorhis, N., Reintgen, D., and Gilbert, R. (1995) Treatment of B16 mouse melanoma with the combination of electropermeabilization and chemotherapy. *Bioelectrochem. Bioenerg.* **36**, 83–87.
 27. Okino, M., Tomie, H., Kanesada, H., Marumoto, M., Esato, K., and Suzuki, H. (1992) Optimal electric conditions in electrical impulse chemotherapy. *Jpn. J. Cancer Res.* **83**, 1095–1101.
 28. Serša, G., Čemažar, M., Šemrov, D., and Miklavčič, D. (1996) Changing electrode orientation improves the efficacy of electrochemotherapy of solid tumors in mice. *Bioelectrochem. Bioenerg.* **39**, 61–66.
 29. Okino, M. and Esato, K. (1990) The effect of single high voltage electrical stimulation with an anticancer drug on in vivo growing malignant tumors. *Jpn. J. Surg.* **20**, 197–204.
 30. Yabushita, H., Yoshikawa, K., Hirata, M., Furuya, H., Hojyoh, T., Fukatsu, H., Noguchi, M., and Nakanishi, M. (1997) Effects of electrochemotherapy on CaSki cells derived from a cervical squamous cell carcinoma. *Gynecol. Oncol.* **65**, 297–303.
 31. Jaroszeski, M. J., Gilbert, R. A., and Heller, R. (1997) In vivo antitumor effect of electrochemotherapy in a hepatoma model. *Biochim. Biophys. Acta* **1334**, 15–18.
 32. Ramirez, L. H., Orlowski, S., An, D., Bindoula, G., Dzodic, R., Ardouin, P., Bognel, C., Belehradec, J. Jr., Munck, J. N., and Mir, L. M. (1998) Electrochemotherapy on liver tumors in rabbits. *Br. J. Cancer* **77**, 2104–2111.
 33. Mir, L. M., Devauchelle, P., Quintin-Colonna, F., Delisie, F., Doliger, S., Fradelizi, D., Belehradec, J. Jr., and Orlowski, S. (1997) First clinical trial of cat soft-tissue sarcomas treatment by electrochemotherapy. *Br. J. Cancer* **76**, 1617–1622.
 34. Pendas, S., Jaroszeski, M. J., Gilbert, R., Hyacinthe, M., Dang, V., Hickey, J., Pottinger, C., Illingworth, P., and Heller, R. (1998) Direct delivery of chemotherapeutic agents for the treatment of hepatomas and sarcomas in rat models. *Radiol. Oncol.* **32**, 53–64.

35. Serša, G., Miklavčič, D., Čemažar, M., Belehradek, J. Jr., Jarm, T., and Mir, L. M. (1997) Electrochemotherapy with CDDP on LPB sarcoma: Comparison of the anti-tumor effectiveness in immunocompetent and immunodeficient mice. *Bioelectrochem. Bioenerg.* **43**, 279–283.
36. Čemažar, M., Miklavčič, D., Ščančar, J., Dolža, V., Golouh, R., and Serša, G. (1999) Increased platinum accumulation in SA-1 tumor cells after in vivo electrochemotherapy with cisplatin. *Br. J. Cancer* **79**, 1386–1391.
37. Čemažar, M., Serša, G., and Miklavčič, D. (1998) Electrochemotherapy with cisplatin in treatment of tumor cells resistant to cisplatin. *Anticancer Res.* **18**, 4463–4466.
38. Kanesada, H. (1990) Anticancer effect of high voltage pulses combined with concentration dependent anticancer drugs on Lewis lung carcinoma in vivo. *J. Jpn. Soc. Cancer Ther.* **25**, 2640–2648.
39. Čemažar, M., Miklavčič, D., Vodovnik, L., Jarm, T., Rudolf, Z., Štabuc, B., Čufer, T., and Serša, G. (1995) Improved therapeutic effect of electrochemotherapy with cisplatin by intratumoral drug administration and changing of electrode orientation for electropermeabilization of EAT tumor model in mice. *Radiol. Oncol.* **29**, 121–127.
40. Puc, M., Reberšek, S., and Miklavčič, D. (1997) Requirement for a clinical electrochemotherapy device—electroporator. *Radiol. Oncol.* **31**, 368–373.
41. Hofmann, G. A., Dev, S. B., and Nanda, G. S. (1996) Electrochemotherapy: Transition from laboratory to the clinic. *IEEE Eng. Med. Biol.* **Nov/Dec**, 124–132.
42. Gilbert, R. A., Jaroszeski, M. J., and Heller, R. (1997) Novel electrode designs for electrochemotherapy. *Biochim. Biophys. Acta* **1334**, 9–14.
43. Heller, R., Jaroszeski, M., Perrott, R., Messina, J., and Gilbert, R. (1997) Effective treatment of B16 melanoma by direct delivery of bleomycin using electrochemotherapy. *Melanoma Res.* **7**, 10–18.
44. Jaroszeski, M. J., Gilbert, R., Perrot, R., and Heller, R. (1996) Enhanced effects of multiple treatment electrochemotherapy. *Melanoma Res.* **6**, 427–433.
45. Čemažar, M., Milačič, R., Miklavčič, D., Dolžan, V., and Serša, G. (1998) Intratumoral cisplatin administration in electrochemotherapy: antitumor effectiveness, sequence dependence and platinum content. *Anticancer Drugs* **9**, 525–530.
46. Serša, G., Štabuc, B., Čemažar, M., Jančar, B., Miklavčič, D., and Rudolf, Z. (1998) Electrochemotherapy with cisplatin: Potentiation of local cisplatin antitumor effectiveness by application of electric pulses in cancer patients. *Eur. J. Cancer* **34**, 1213–1218.
47. Serša, G., Kotnik, V., Čemažar, M., Miklavčič, D., and Kotnik, A. (1996) Electrochemotherapy with bleomycin in SA-1 tumor-bearing mice—natural resistance and immune responsiveness. *Anticancer Drugs* **7**, 785–791.
48. Mir, L. M., Orłowski, S., Poddevin, B., and Belehradek, J. Jr. (1992) Electrochemotherapy tumor treatment is improved by interleukin-2 stimulation of the host's defenses. *Eur. Cytokine Netw.* **3**, 331–334.

49. Mir, L. M., Roth, C., Orlowski, S., Belehradek, J. Jr., Fradelizi, D., Paoletti, C., and Kourilsky, P. (1992) Potentiation of antitumoral effect of electrochemotherapy with allogeneic cells producing interleukin-2. *C. R. Acad. Sci. Paris* **314**, 539–544.
50. Mir, L. M., Roth, C., Orlowski, S., Quintin-Colonna, F., Fradelizi, D., Belehradek, J. Jr., and Kourilsky, P. (1995) Systemic antitumor effect of electrochemotherapy combined with histoincompatible cells secreting interleukin-2. *J. Immunother.* **17**, 30–38.
51. Serša, G., Čemažar, M., Menart, V., Gaberc-Porekar, V., and Miklavčič, D. (1997) Anti-tumor effectiveness of electrochemotherapy with bleomycin is increased by TNF- α on SA-1 tumors in mice. *Cancer Lett.* **116**, 85–92.
52. Orlowski, S., An, D., Belehradek, J. Jr., and Mir, L. M. (1998) Antimetastatic effect of electrochemotherapy and histoincompatible interleukin-2-secreting cells in the murine Lewis lung tumor. *Anticancer Drugs* **9**, 551–556.
53. Serša, G., Beravs, K., Čemažar, M., Miklavčič, D., and Demšar, F. (1998) Contrast enhanced MRI assessment of tumor blood volume after application of electric pulses. *Electr. Magnetobiol.* **17**, 299–306.
54. Serša, G., Čemažar, M., Parkins, C. S., and Chaplin, D. J. (1999) Tumour blood flow changes induced by application of electric pulses. *Eur. J. Cancer* **35**, 672–677.

Clinical Trials for Solid Tumors Using Electrochemotherapy

Richard Heller, Richard Gilbert, and Mark J. Jaroszeski

1. Introduction

Chemotherapy is a standard treatment for a wide variety of cancers. However, response rates are usually low. In melanoma, for example, partial response rates range from 20–45 % with complete responses of less than 5% (1–4). The cell membrane can be a significant barrier for agents with an intracellular site of action. The inability to cross the cell membrane and enter the cell could lead to a low response rate. The effectiveness of these agents could be enhanced if combined with a procedure that increases the permeability of the cell membrane.

A new approach is being explored as a potential means of enhancing drug delivery to tumor cells. This approach involves the use of electric pulses to increase the permeability of cell membranes and is currently being explored for the treatment of several types of malignancies. The application of electric pulses alters membrane permeability to facilitate the transport of the drug into cells. This transient increased permeability is due to a reversible breakdown of membranes that is induced by exposing cells to direct current pulses at a sufficient electric field strength. This electrically induced permeabilization, also called electroporation, has also become the preferred method for the transformation of cells. The exposure of cells to electric fields has been used for electroporation as well as the related process of electrofusion. Potential uses for both of these techniques have recently been demonstrated (5–8).

The process of electroporation is a physical phenomenon. The physical nature of electroporation makes it applicable to all cell types. In addition, a variety of applications are enhanced by utilizing this procedure to gain tempo-

rary access to the cytosol. These include production of monoclonal antibodies (9,10), cell–cell fusion (10–12), cell-tissue fusion (13,14), insertion of membrane proteins (13,15,16), and genetic transformation (17–19). The most clinically significant application of pulsed electric fields currently under investigation is the delivery of drugs into cells. The use of electric pulses to deliver chemotherapy drugs has been termed electrochemotherapy (ECT) (20,21).

Preclinical ECT studies have focused on delivering drugs for the treatment of solid tumors. These studies have mainly used bleomycin as the chemotherapeutic agent, however, cisplatin has also been used in combination with electroporation. Studies performed in both mice and rats have shown that when bleomycin or cisplatin is administered in combination with electroporation their effectiveness as an antitumor agent is greatly enhanced. These studies have been performed with a variety of tumor types including, melanoma, hepatocellular carcinoma, lung carcinoma, breast carcinoma, fibrosarcoma, and glioma (22) (see Chapter 6 in this volume for a review). These studies obtained objective response rates as high as 90% and complete response rates as high as 85%.

Promising results from early animal studies motivated the translation of ECT from the laboratory to the clinic. Mir et al. (23,24) performed the first ECT clinical trial in 1991. Since then, clinical ECT research has been conducted in the United States, France, and Slovenia. Trials for the treatment of head and neck squamous cell carcinoma, basal cell carcinoma, and melanoma have been conducted. All trial results have shown ECT to be a very effective treatment. This chapter summarizes the results from clinical ECT studies to provide an updated status of drug delivery by electroporation for the treatment of cancer.

2. Clinical Results Using Intravenous Bleomycin

Mir and collaborators performed the first clinical trial using ECT at the Institut Gustave-Roussy, Villejuif, France (23,24). Patients with recurrent or progressive permeation nodules (cutaneous metastases) of head and neck squamous cell carcinoma located in the anterior cervical region or in the upper part of the thorax were enrolled in this trial. The ECT procedure utilized bleomycin administered intravenously in combination with electric pulses administered at a nominal field strength of 1300 V/cm. Following the success of the Villejuif trial, several other centers around the world initiated trials using either the exact Villejuif protocol or a slightly modified one. Tumor types treated in these other studies including melanoma, basal cell carcinoma, adenocarcinoma, and squamous cell carcinoma.

Success of the therapy was evaluated by determining the response of each treated nodule. Response rates were based on the tumor volume by measuring

the longest diameter (a) and the next longest diameter (b) perpendicular to a . The tumor volume was calculated by the formula: $V = ab^2\pi/6$, where V represents the tumor volume. The number of objective responses (OR) was determined by adding the number of complete responses (CR; no palpable or measurable tumor detected for at least 30 days following treatment) and partial responses (PR; greater than 50% decrease in tumor volume for at least 30 days following treatment). Stable disease (SD) was defined as no growth but less than 50% reduction of tumor volume; and progressive disease (PD) was defined as continued growth.

There were a total of 199 nodules (34 patients) treated in all the studies using intravenous bleomycin. An objective response rate of 80% (160 nodules responded) was obtained. In addition, complete responses were seen in 88 treated lesions (44%); 10 lesions (5%) had progressive disease. The results with respect to tumor type are described in detail in the remainder of this subheading.

The treatment resulted in little or no adverse side effects (23–29). In general, the patients were reported as tolerating the treatment well. Slight muscle contractions were observed during each pulse. An unpleasant sensation was associated with these contractions, which varied in intensity from patient to patient, and was dependent on the location of the site treated. However, in every case this unpleasant feeling subsided immediately after each electric pulse. No residual sensations were noted. Reactions at the site of treatment included slight oedema and erythema beginning 1–2 h after treatment. These conditions disappeared within 24 h. No significant modification of cardiologic or hemodynamic parameters was noted during or after ECT treatment.

2.1. Head and Neck Squamous Cell Carcinoma

Patients with squamous cell carcinoma of the head and neck were enrolled at three centers in France: Villejuif, Toulouse, and Reims. All patients enrolled in the studies had been previously treated with radiation therapy, surgery, and/or chemotherapy. The three centers enrolled a total of 17 patients and a total of 87 nodules were treated at these three centers. Before treatment, patients with a small number of treatment sites received only sedatives (Lorazepan or Levomepromazine) and those with large tumors or with numerous sites were treated under neuroleptanalgesia using Midazolam and Alfentanyl or under general anesthesia. Following ECT treatment, 77 of the 87 nodules treated were able to be evaluated. The other 10 could not be evaluated for various reasons, the most common being a short follow-up period. Of the 77 lesions that were evaluated, objective responses were seen in 48 (62%) with 33 (43%) showing a complete response.

The protocol utilized by these trials was similar to the preclinical methods for administering ECT. The chemotherapeutic agent used was bleomycin. The

dose administered was 18 U/m^2 , and it was injected as a bolus. Pulses were administered to the first tumor beginning 3.5 min after injection. Subsequent tumors were treated in series with a 1-min interval between electrical treatment. Two parallel stainless steel strips with a fixed distance of 6 mm were used as the electrodes (23,24). Eight $99 \mu\text{s}$ electric pulses were generated using a PS 15 electropulsator (Jouan, Nantes, France). Clinical responses were determined by periodic measurement of the tumors that were treated with ECT.

Eight patients were enrolled in the initial Villejuif study (first of two studies performed in Villejuif), and a total of 42 nodules were treated (Table 1). Objective responses were seen in 29 (69%) of the nodules, and 23 (55%) of the 42 tumors responded completely (23,24). No responses were seen in nodules that did not receive electric pulses even though they were subjected to the same bleomycin dose as the electrically treated tumors. The 70% response rate was extremely encouraging when taking into account that this was the first ECT trial ever performed in humans, the treatment was administered only once, and the enrolled patients had recurred or failed other therapies before to ECT treatment.

The trials conducted in Reims and Toulouse were performed using the same ECT protocol used in Villejuif except the Reims trial used a 27 U/m^2 bleomycin dose (Table 1). Three patients were enrolled in the Reims trial and a total of 10 nodules were treated. Objective responses were seen in 4 (40%) of the lesions with 1 (10%) complete response (30). One patient with 6 nodules was treated in Toulouse. Objective responses were seen in 6 (100%) with 5 (83%) complete responses (30).

The potential of ECT as an effective cancer therapy was examined further in a second trial performed in Villejuif. Five patients were enrolled in this study that included the treatment of larger and deeper head and neck squamous cell carcinomas (25). The dimensions of these tumors were up to 20 cm in diameter which was considerably larger than previously treated nodules. In addition, these tumors had a greater depth. As in the previous trials bleomycin was administered intravenously, however, intraarterial injection was used for two patients as a means of allowing the drug to reach the treated area more easily. Both injection procedures used a dose of 27 U/m^2 .

ECT treatment of these large nodules resulted in large antitumor effects at the superficial regions of the nodules while the deeper portions continued to grow. This difference in response may have been due to an uneven administration of the electric field. The parallel plate electrodes were positioned on the tumor/skin during pulse delivery which probably limited the electrical treatment of the deeper portions of the nodule. This would have resulted in the tumor cells in these deeper regions from being subjected to fields of sufficient intensity to cause electropermeabilization. Even with the difficulty of properly

Table 1
Intravenous Bleomycin ECT Clinical Trial Results^a

Trial Location	Cancer Type ^b	No. of Patients	No. of Tumors Treated	Bleomycin Administration Route	Clinical Tumor Responses (%) ^c			
					NE	PR	CR	OR
Villejuif	HNSCC	8	42	Intravenous bolus	31	14	55	69
Reims	HNSCC	3	10	Intravenous bolus	50	30	10	40
Toulouse	HNSCC	1	6	Intravenous bolus	0	17	83	100
Villejuif	HNSCC	5	19 ^b	Intravenous bolus	53	26	21	47
Tampa	Melanoma	3	10	Intravenous infusion	50	20	30	50
Ljubljana	Melanoma	7	30	Intravenous bolus	10	10	80	90
Toulouse	Melanoma	4	54	Intravenous bolus	4	87	9	96
Tampa	BCC	2	6	Intravenous infusion	0	83	17	100
Villejuif	Adeno	2	20 ^c	Intravenous bolus	0	0	100	100
Tampa	Adeno	1	2	Intravenous infusion	0	0	100	100

HNSCC, head and neck squamous cell carcinoma; BCC, basal cell carcinoma; Adeno, adenocarcinoma; NE, no effect; PR, partial response; CR, complete response; OR, objective response.

^aAll treatments performed with parallel plate electrodes.

^bA total of 29 tumors were treated but a response could not be evaluated on 10.

^cA total of 28 tumors were treated but a response could not be evaluated on 8.

administering the electric fields, complete (21%) and partial responses (26%) were obtained. However, treatment effectiveness was lower than the previously treated small nodules.

Although the response rates were lower in this study several important observations were made. Maximum antitumor effects were obtained when pulses were administered between 8 and 28 minutes after injection of a bolus bleomycin dose. This indicated the time when bleomycin concentrations were highest in the interstitial fluid surrounding the tumor cells. In addition, intra-arterial bleomycin injection was observed to result in increased effectiveness in two patients.

2.2. Melanoma

Melanoma was treated using electrochemotherapy at three centers around the world: Tampa, United States; Ljubljana, Slovenia; and Toulouse, France. Patients enrolled in these centers had been previously treated with either surgery, chemotherapy and/or radiation therapy. The three centers enrolled 14 patients and a total of 94 metastatic malignant melanoma nodules were treated. Objective responses were seen in 84 (89%) nodules and there were 32 (34%) nodules that had a complete response. Those lesions that had a CR rapidly disappeared within 1 to 2 weeks after electrochemotherapy. No regrowth of these nodules have been reported.

Three patients were enrolled in the Tampa trial and a total of 10 nodules were treated (26–28,30). Bleomycin was administered at a dose of 10 U/m² at a rate of 1–1.5 U/minute. The electric pulses were administered between 5 and 15 minutes following administration of 1% lidocaine, containing 1:100,000 epinephrine, around the treatment sites and after bleomycin infusion. A total of eight 99 μ s direct current pulses were delivered to tumors. The electrodes consisted of two flat stainless steel squares that were 20 mm on each side and were mounted on a vernier caliper (26). The calipers allowed the distance between the electrodes to be adjusted depending on the size of the tumor. The electric pulses were generated using a BTX T820 (Genetronics, Inc., San Diego, California). Objective responses were seen in 5 (50%) of the nodules with 3 (30%) complete responses (Table 1). All eight lesions that were exposed to only bleomycin did not respond and continued to grow.

Bleomycin was administered as a bolus injection at a dose of 18 U/m² as part of both the Ljubljana trial (29,30) and the Toulouse trial (30). Patients treated at the Slovenian center received lidocaine spray over the treated surface. Patients at the Toulouse center were treated after receiving either only sedatives (Lorazepam or Levomepromazine), under neuroleptanalgesia using Midazolam and Alfentanil or under general anesthesia. Eight 100 μ s electric pulses were administered using the flat stainless steel electrodes with a fixed

gap. The electrode used in Ljubljana had a gap of 7 mm, while the electrode used in Toulouse had a 6-mm gap. The Ljubljana trial enrolled seven patients and a total of 30 nodules were treated. Objective responses were obtained in 27 (90%) of the lesions with 24 (80%) having a complete response (**Table 1**). An additional three nodules were only exposed to the bleomycin and did not receive electric pulses. These 3 nodules did not respond and continued to grow. Four patients were enrolled in the Toulouse trial and a total 54 nodules were treated. Objective responses were seen in 52 (96%) with complete responses found in 5 (9%) of the treated nodules (**Table 1**).

2.3. Basal Cell Carcinoma

Electrochemotherapy was used to treat basal cell carcinomas at the Tampa center. Two patients were enrolled and 6 tumors were treated under the same drug and electrical conditions as were used to treat melanomas in Tampa (**26,27,30**). Eight 99 μ s electric pulses were applied using the caliper electrodes and a BTX T820. Both patients had surgery several times previously. Objective responses were seen in 6 (100%) tumors with 1 (17%) complete response (**Table 1**). No response was seen in the six lesions exposed to bleomycin only and not to electric pulses.

2.4. Adenocarcinoma

The use of electrochemotherapy for the treatment of adenocarcinoma was tested at two sites. Three patients were enrolled in trials being conducted in Villejuif (2 patients) and Tampa (1 patient). ECT was used to treat a total of 30 nodules (28 in Villejuif and 2 in Tampa). Follow-up allowed evaluation of 22 of these metastatic nodules. All 22 (100%) responded to electrochemotherapy (**Table 1**) and all were CR (**26,30**). Eight additional metastatic nodules were treated but could not be evaluated because of a follow-up period that was too brief. An additional 2 nodules (Tampa) received bleomycin alone and had progressive disease.

3. Clinical Results Using Intratumor Bleomycin

Intratumor injections of bleomycin was in combination with electric pulses was first used in a clinical trial performed at the H. Lee Moffitt Cancer Center and Research Institute in Tampa, Florida. Patients with melanoma, basal cell carcinoma, squamous cell carcinoma, and Kaposi's sarcoma were included in the study (**30–32**). A response to the treatment was seen in all 34 patients that were enrolled in the study. ECT was performed on a total of 143 tumors of various sizes. Objective responses were found in 142 (99%) of which 130 (91%) were complete responses (**Table 2**). A complete description of the results with respect to tumor type is given below.

Table 2
Intratumor Bleomycin ECT Clinical Trial Results

Trial Location	No. of Patients	Cancer Type	No. of Tumors Treated	Electrode Type	Clinical tumor responses (%)			
					NE	PR	CR	OR
Tampa	2	Melanoma	8	Parallel plate	0	0	100	100
Tampa	10	Melanoma	76	Needle array	1.3	10.5	88.2	98.7
Tampa	5	BCC	13	Parallel plate	0	7.7	92.3	100
Tampa	15	BCC	41	Needle array	0	5	95	100
Tampa	1	KS	4	Parallel plate	0	0	0	100
Tampa	1	SCC	1	Needle array	0	100	0	100
Chicago	8	HNSCC	8	Needle array	25	25	50	75
Chicago	1	Adeno	1	Needle array	0	100	0	100
Chicago	1	ACC	1	Needle array	0	0	100	100

BCC, basal cell carcinoma; KS, Kaposi's sarcoma; SCC, squamous cell carcinoma; HNSCC, head and neck squamous cell carcinoma; Adeno, adenocarcinoma; ACC, adenoid cystic carcinoma; NE, no effect; PR, partial response; CR, complete response; OR, objective response.

A second clinical trial utilizing intratumor bleomycin was initiated at Rush Presbyterian-St. Luke's Medical Center in Chicago, IL. Patients with biopsy-proven head and neck cancer were enrolled in this study (33). Ten patients were treated at this center and eight showed a response to treatment. ECT was performed on a total of 10 tumors and objective responses were found in 8 (80%) of which 5 (50%) were complete responses (Table 2).

The treatments performed at both centers were tolerated well by all patients. Bleomycin was administered intratumorally, approximately at a dose of 1.0 U/cm³ of treated tumor, in less than 30 seconds at least 10 minutes before electric pulse delivery (31,32). Prior to the application of electric pulses, patients at the Tampa, FL center received a peritumoral injection of 1–3 ml of 1% lidocaine containing 1:100,000 ephinephrine per lesion. Patients at the Chicago center received general anesthesia which typically lasted less than 1 hour. In addition, the tumor site was injected around its perimeter with 1% lidocaine containing 1:100,000 ephinephrine (33). The electrodes used for the first 8 patients in the Tampa trial consisted of two flat stainless steel squares that were 20 mm on each side and were mounted on a vernier caliper (same as used in the Tampa IV trial). The remaining Tampa patients and all the Chicago patients were treated using an electrode that consisted of a circular array of six needles (34,35). This needle array electrode was fixed at various sizes including 5, 7.5, 10, and 15 mm diameter. BTX T820 generator (calipers or needles) or a Medpulsor (needles) instrument (Genetronics, Inc., San Diego, CA) were used to deliver electric pulses administered at a nominal field strength of 1300 V/cm. Muscle contractions occurred during each pulse, but subsided at the end of each pulse. The majority of patients reported feeling discomfort at the treatment site during each pulse that disappeared immediately at the end of each pulse. It was also observed that the needle array electrodes caused less discomfort than the caliper electrodes. None of the patients reported any residual pain or discomfort following treatment and no significant modification of cardiologic parameters were observed.

3.1. Melanoma

Twelve patients with metastatic melanoma patients were enrolled in the study being conducted in Tampa. These patients had been previously treated with either surgery, chemotherapy and/or radiation therapy. Electrochemotherapy was used to treat a total of 84 melanoma nodules. Standard ECT protocol was used which included an intratumor injection of bleomycin followed 10 minutes later by electric pulses. Partial treatment (bleomycin alone or electric pulses alone) was performed on an additional 12 nodules. Objective responses were seen in 83 (99%) of the 84 metastatic malignant melanoma nodules receiving the full ECT treatment (Table 2); 75 (89%) of these tumors com-

pletely disappeared within 2–3 wk after electrochemotherapy and were called CR (27,32). No regrowth of these nodules was reported in the 20-mo mean follow-up period (7–27 mo). There was no observed effect on the twelve nodules that received only partial treatment as these tumors continued to get larger. Although ECT was successful in removing the treated lesions it did not prevent the appearance of new metastatic lesions.

3.2. Basal Cell Carcinoma

A total of 20 patients with basal cell carcinoma were enrolled in the Tampa trial. These patients had 65 BCC primary tumors (20 patients) that were treated as part of this trial. Electrochemotherapy was performed on 54 tumors, while the other 11 tumors received partial treatment (drug only or electric pulses only). All BCCs treated as part of this protocol were diagnosed as a nodular subtype. No superficial, aggressive growth or morpheaform BCC subtypes were included in this trial (31). A 100% objective response rate was obtained in the 54 BCC primary tumors receiving the complete ECT treatment (Table 2). Of these, 51 (94.4%) disappeared within 1 month and were designated CR. During a mean follow-up period of 20 months (14–28 months) no recurrences were observed. Among the 11 BCCs that were treated with either bleomycin or electric pulses alone, only one nodule (drug only) had a partial response; the remaining 10 BCC tumors progressed.

In this BCC study, objective responses were obtained with all tumors and CRs were obtained in all but 3 (PR). Two of these PR tumors were retreated and complete responses were obtained. Therefore, examining BCCs that received an intratumor dose of bleomycin and one or two treatments, CR were obtained in 53 of 54 (98.1%) treated tumors. An excisional biopsy was performed on the remaining PR tumor; therefore, it could not be retreated.

3.3. Kaposi's Sarcoma and Squamous Cell Carcinoma

Electrochemotherapy was performed on one patient with Kaposi's sarcoma (KS) and one patient with squamous cell carcinoma (SCC; 1 nodule) (Table 2). The KS patient had four sites treated by ECT and an additional 3 sites that received an intratumor injection of bleomycin only. All four ECT sites completely responded (32). By contrast, the partially treated sites were observed to have progressive disease. The single SCC tumor that was treated with ECT responded partially (32).

3.4. Head and Neck Squamous Cell Carcinoma

Eight patients with squamous cell carcinoma were enrolled (Table 2). Seven of the eight patients enrolled in the study had been previously treated with either surgery, radiation therapy and/or chemotherapy, the remaining patient

refused surgery and radiation therapy. All eight patients had a single tumor treated. The tumors were located either floor of mouth (2), nasal septum (1), retromolar trigone (1), oropharynx (1), maxillary sinus (1), base of tongue (1) or supraglottic larynx (1). Seven of the eight patients were treated while under general anesthesia, the other patient was treated using local anesthetic. A transitory masticator and tongue muscle spasm was observed in all patients. Objective responses were seen in 6 of the 8 (75%) patients and 4 (50%) showed a complete response (33).

3.5. Adenocarcinoma and Adenoid Cystic Carcinoma of the Head and Neck

Two additional patients were enrolled in the Rush Presbyterian trial (Table 2). One patient had an adenocarcinoma of the ethmoid sinus. Patient had previously undergone radiation therapy. ECT therapy of this tumor resulted in a partial response. The other patient had an adenoid cystic carcinoma of the parotid. Patient had previously received radiotherapy and chemotherapy. Treatment with ECT resulted in a complete response (33).

4. Clinical Results Using Intratumor Cisplatin

Clinical evaluation of ECT using a drug other than bleomycin was first performed at the Institute of Oncology in Ljubljana, Slovenia. This trial utilized intratumor injections of cisplatin followed by administration of electric pulses. The trial included patients with melanoma, basal cell carcinoma, and squamous cell carcinoma (36). Four patients were enrolled in the study and all patients showed a response to the treatment. ECT was performed on a total of 19 tumors of various sizes and of various histological types. Complete responses were found in all 19 (100%) of the tumors treated (Table 3).

Cisplatin was administered intratumorally at doses ranging from 0.25 to 2 mg dependent on the tumor size. Electric pulses were delivered 1–2 min following the cisplatin injection. A total of eight 100- μ s pulses at a nominal field strength of 1300 V/cm were delivered using two parallel stainless steel electrodes with a fixed distance of 7 mm between them. The electric pulses were generated using a Jouan GHT 1287 (Jouan, France). The eight pulses were delivered in two sequences of 4 pulses, with 1 s intervals and in two perpendicular directions (37–38). The treatment was well tolerated with minimal scarring and a slight depigmentation of the skin. A complete description of the results with respect to tumor type is given below.

4.1. Melanoma

Two melanoma patients were enrolled in the study. Patients had been previously treated with either surgery, chemotherapy, and/or immunotherapy. A

Table 3
Intratumor Cisplatin ECT Clinical Trial Results^a

Trial Location	No. of Patients	Cancer Type	No. of Tumors Treated	Clinical Tumor Responses (%)			
				NE	PR	CR	OR
Ljubljana	2	Melanoma	13	0	0	100	100
Ljubljana	1	BCC	4	0	0	100	100
Ljubljana	1	HNSCC	2	0	0	100	100

BCC, basal cell carcinoma; HNSCC, head and neck squamous cell carcinoma; NE, no effect; PR, partial response; CR, complete response; OR, objective response.

^aAll treatments performed with parallel plate electrodes.

total of 13 melanoma nodules received ECT treatment which included an intratumor injection of cisplatin followed one to two minutes later by electric pulses. An additional 6 nodules received no or partial treatment. Complete responses were seen in 13 (100%) of the 13 metastatic malignant melanoma nodules treated with a combination of cisplatin and electric pulses (**Table 3**). No regrowth of these nodules has been observed during the 7- 11-mo follow-up period (patients still being followed). Two nodules were not treated and one nodule was treated with electric pulses only; these nodules continued to grow. Three lesions were treated with intratumor cisplatin only; two had a complete response and one remained the same (**36**).

4.2. Basal Cell Carcinoma

One patient with basal cell nevus syndrome was enrolled in this study. The patient had previously undergone multiple surgeries as well as treatment with interferon- α and vitamin A. Four lesions were treated with the electrochemotherapy protocol using intralesional cisplatin. An additional five lesions received either no treatment or partial treatment. The four lesions receiving the full ECT treatment completely responded (**36**). No regrowth of these tumors has been observed during the 9- to 11-month follow-up period (patients still being followed). Three tumors were not treated and there was no change in the size of the lesions. Two other tumors received only an injection of cisplatin. Both of these lesions partially responded.

4.3. Squamous Cell Carcinoma

One patient with squamous cell carcinoma of the head and neck was enrolled in this study. The patient had previously undergone multiple surgeries as well as treatment with interferon- α and vitamin A. Two lesions were treated with the electrochemotherapy protocol using intralesional cisplatin. Both lesions completely responded to the treatment (**36**). No regrowth of these nodules has been observed during the 9- to 11-mo follow-up period (patients still being followed).

5. Summary and Conclusions

Electric pulses can be a powerful tool to increase the effectiveness of chemotherapeutic agents. The combination of chemotherapy and electric pulses has been termed electrochemotherapy and has already been demonstrated to be a potent antitumor treatment in both animal (**20,21,37-51**) and human studies (**23-33,36**). The vast majority of these studies have utilized bleomycin; however, cisplatin has also been shown to be enhanced when used with ECT (**38**). Although conventional chemotherapy studies have demonstrated that bleomycin is not generally effective as a single agent for the treatment of solid

tumors (52,53), when used in combination with electric pulses, bleomycin becomes effective against a variety of tumors (20,21,37–51).

Bleomycin works by gaining access to the cell's nucleus and then binding to the DNA and therefore must be internalized by a cell to be effective. The inability bleomycin to efficiently cross the cell membrane is the reason it has been a failure as a single agent. However, this is also the reason why it is an excellent candidate for ECT. Bleomycin is a nonpermeant drug, and its entrance into the cell is restricted by the cell membrane (54,55). The application of electric pulses to the cell membrane causes a temporary destabilization of the membrane, which facilitates the internalization of the drug and allows the drug to reach its target, thus the combination becomes a potent antitumor treatment.

Cisplatin has a similar mode of action as bleomycin and also must reach the nucleus to be effective. In contrast to bleomycin, cisplatin is a permeant drug and can cross the cell membrane. This is probably the reason why in the cisplatin trial some tumors treated with only intratumor cisplatin responded. However, there was still an increased response when combining cisplatin with electric pulses. ECT with cisplatin is still advantageous because the permeabilization of the cell membranes allows for increased uptake of the drug which could lead to increased effectiveness. In addition, this increased efficiency would allow a lower dose of the drug to be used.

This chapter reviewed several ECT clinical studies. All of the studies demonstrated the potent antitumor effect of electrochemotherapy (23–33,36). Bleomycin was used in all but one of the trials which used cisplatin (36). Bleomycin was administered either via an intravenous or intratumor injection, while cisplatin was administered via intratumor injection. Several different applicators were used to deliver the electric pulses. In addition, many different histologic tumor types were treated with this therapy. Even with these variations of the treatment protocol, ECT has consistently shown high response rates.

It should not be surprising that ECT can elicit a high response rate regardless of histologic type. The basic underlying principle of ECT is the electropermeabilization of cell membranes using electroporation. All types of mammalian cells are susceptible to the physical phenomenon of electroporation. The phenomenon results from the interaction of electric fields with a low conductive membrane composed of lipids and proteins (56,57). The permeabilization of the cell membrane allows free and unrestricted access of the drug to the inside of the cell. Once inside the cell, interaction of the drug (bleomycin or cisplatin) with DNA eventually results in cell death (53,56–57). Thus, all histological types of tumors should be sensitive to electrochemotherapy.

Successful treatment with ECT requires that both drug and electric pulses must be used in combination and within a critical time frame. Partial treatment with either bleomycin alone or electric pulses alone has been shown to be ineffective and treatment with cisplatin alone has been shown to be less effective. Therefore, it is important to administer the electric pulses at a time when the drug concentration in the tumor is sufficient to allow for maximum uptake while the cells are in a permeabilized state. This time interval was established by Mir and collaborators to be from 8 to 28 minutes after intravenous bolus injection of bleomycin. The time interval for intratumor injections of bleomycin were determined by Heller and collaborators to be 10 minutes (42) and for intratumor injections of cisplatin to be 1–2 minutes (36,38).

Electrochemotherapy was performed at several centers by administering bleomycin either by intravenous or via intratumor injection. Both routes of administration proved to be effective when combined with electric pulses. One advantage of using the intratumor route of injection was the ability to treat every tumor independently which allowed the whole electrochemotherapy session to be split in as many partial sessions as required. It also allowed the administration of a tumor dose as opposed to a systemic dose of the drug, allowing for a reduction of the overall dose as well as concentrating the dose at the treatment site. It was also interesting to note that although both injection routes gave high objective responses, the complete response rate resulting from ECT treatment with intratumor bleomycin represented a dramatic improvement when compared to the CRs obtained with intravenous administration (88% vs 44%). This difference was even more dramatic when comparing the treatment of basal cell carcinoma (94% vs 17%). Although both modes have proven to be effective, utilizing intratumor administration may be an important consideration when treating patients with circulation problems or tumors that are not highly vascularized. Overall, the results indicate that electrochemotherapy is a very effective treatment irrespective of the drug administration route and the treatment can be administered in a variety of ways depending on the clinical situation.

Electrochemotherapy can be an effective means for the local control of a variety of cancer types. ECT has been demonstrated to be an excellent alternative therapy for use as a local treatment. The use of drug delivery with electric fields is practical for the treatment of solitary tumors as well as local and regional disease. An ideal application for ECT would be the treatment of nonmetastatic cancers, such as basal cell carcinoma. There are several major advantages of ECT over surgery such as reduction in scarring, tissue sparing and maintenance of tissue functionality. ECT may be an excellent choice for patients with lesions on sun damaged skin particularly the ears, lips, and nose. The use of ECT, in its current form, for extensive metastatic disease is cur-

rently not practical. In the future, ECT may be combined with other therapies that could add a systemic component that could produce a potent systemic therapy. Preclinical studies have examined the possibility of combining ECT with interleukin-2 to treat distant disease (60–62). However, even in its present form, ECT may be used for patients with extensive disease as a palliative treatment or for the treatment of recurrent or metastatic tumors that can not be surgically removed or have previously failed other therapies. It is quite apparent from the results of these early studies that combining electric pulses with chemotherapeutic agents may become a powerful weapon in the treatment of solid tumors.

References

1. Coates, A. S. (1992) Systemic chemotherapy for malignant melanoma. *World J. Surg.* **16**, 277–281.
2. Nathanson, L. and Jilani, S. (1993) Chemotherapy of malignant melanoma. *Cancer Treat. Rev.* **19**, 17–28.
3. Yeung, R. S. (1994) Management of recurrent cutaneous melanoma. *Curr. Probl. Cancer* **18**, 143–186.
4. Buzaid, A. C. and Murren, J. (1992) Chemotherapy for advanced malignant melanoma. *Int. J. Clin. Lab. Res.* **21**, 205–209.
5. Chang, D. C., Chassy, B. M., Saunders, J. A., and Sowers, A. E. (1992) *Guide to Electroporation and Electrofusion*. Academic Press, San Diego, CA.
6. Potter, H. (1988) Electroporation in biology: Methods, applications and instrumentation. *Anal. Biochem.* **174**, 361–373.
7. Weaver, J. C. (1993) Electroporation: a general phenomenon for manipulating cells and tissues. *J. Cell. Biochem.* **51**, 426–435.
8. Heller, R. and Gilbert, R. (1992) Biological applications of cell-tissue electrofusion. *Guide to Electroporation and Electrofusion* (Chang, D. C., Chassy, B. M., Saunders, J. A., and Sowers, A. E., eds.). Academic Press, San Diego, CA, pp. 393–410.
9. Foug, S. K. H. and Perkins, S. (1989) Electric field-induced cell fusion and human monoclonal antibodies. *J. Immunol. Methods* **116**, 117–122.
10. Lo, M. M. S., Tsong, T. Y., Conrad, M. K., Strittmatter, S. M., Hester, L. D., and Snyder, S. H. (1984) Monoclonal antibody production by receptor-mediated electrically induced cell fusion. *Nature* **310**, 792–794.
11. Teissié, J., Knutson, V. P., Tsong, T. Y., and Lane, M. D. (1982) Electric pulse-induced fusion of 3T3 cells in monolayer culture. *Science* **216**, 537–538.
12. Jaroszeski, M. J., Gilbert, R., Fallon, P. G., and Heller, R. (1994) Mechanically facilitated cell-cell electrofusion. *Biophys. J.* **67**, 1574–1581.
13. Heller, R. and Grasso, R. J. (1990) Transfer of human membrane surface components by incorporating human cells into intact animal tissue by cell-tissue electrofusion in vivo. *Biochem. Biophys. Acta* **1024**, 185–188.
14. Grasso, R. J., Heller, R., Cooley, J. C., and Haller, E. M. (1989) Electrofusion of

- individual animal cells directly to intact corneal epithelial tissue. *Biochem. Biophys. Acta* **980**, 9–14.
15. Mouneimne, Y., Pierre-Francois, T. Barhoumi, R., and Nicolau, C. (1991) Electroinsertion of xeno proteins in red blood cell membranes yields a long lived protein carrier in circulation. *Biochim. Biophys. Acta* **1066**, 83–89.
 16. Mouneimne, Y., Pierre-Francois, T. Barhoumi, R., and Nicolau, C. (1990) Electroinsertion of full length recombinant CD4 into red blood cell membrane. *Biochim. Biophys. Acta* **1027**, 53–58.
 17. Chernomordik, L. V., Sokolov, A. V., and Budker, V. G. (1990) Electrostimulated uptake of DNA by liposomes. *Biochem. Biophys. Acta* **1024**, 179–183.
 18. Zheng, Q. and Chang, D. C. (1991) High-efficiency gene transfection by in situ electroporation of cultured cells. *Biochem. Biophys. Acta* **1088**, 104–110.
 19. Heller, R., Jaroszeski, M. J., Atkin, A., Moradpour, D., Gilbert, R., Wands, J., and Nicolau, C. (1996) In vivo gene electroinjection and expression in rat liver. *FEBS Lett.* **389**, 225–228.
 20. Mir, L. M., Orłowski, S., Belehradek J. Jr., and Paoletti, C. (1991) Electrochemotherapy: Potentiation of antitumor effect of bleomycin by local electric pulses. *Eur. J. Cancer* **27**, 68–72.
 21. Belehradek, J. Jr., Orłowski, S., Poddevin, B., Paoletti, C., and Mir, L. M. (1991) Electrochemotherapy of spontaneous mammary tumors in mice. *Eur. J. Cancer* **27**, 73–76.
 22. Jaroszeski, M. J., Gilbert, R., and Heller, R. (1997) Electrochemotherapy: an emerging drug delivery method for the treatment of cancer. *Adv. Drug Deliv. Rev.* **26**, 185–197.
 23. Mir, L. M., Belehradek, M., Domenge, C., Orłowski, S., Poddevin B., Belehradek J. Jr., Schwab, G., Luboinnski, B., and Paoletti, C. (1991) Electrochemotherapy, a novel antitumor treatment: First clinical trial. *C. R. Acad. Sci. Paris* **313**, 613–618.
 24. Belehradek, M., Domenge, C., Luboinnski, B., Orłowski, S., Belehradek, J., and Mir, L. M. (1993) Electrochemotherapy, a new antitumor treatment: First clinical phase I-II trial. *Cancer* **72**, 3694–3700.
 25. Domenge, C., Orłowski, S., Luboinnski, B., De Baere, T., Schwaab, G., Belehradek J. Jr., and Mir, L. M. (1996) Antitumor electrochemotherapy: New advances in the clinical protocol. *Cancer* **77**, 956–963.
 26. Heller, R., Jaroszeski, M. J., Glass, L. F., Messina, J. L., Rapaport, D. P., DeConti, R. C., Fenske, N. A., Gilbert, R., Mir, L. M., and Reintgen, D. S. (1996) Phase I/II trial for the treatment of cutaneous and subcutaneous tumors using electrochemotherapy. *Cancer* **77**, 964–971.
 27. Reintgen, D. S., Jaroszeski, M. J., and Heller, R. (1996) Electrochemotherapy: A novel approach to cancer. *J. Skin Cancer Foundation* **14**, 17–19, 83.
 28. Glass, L. F., Pepine, M. L., Fenske, N. A., Jaroszeski, M. J., Reintgen, D. S., and Heller, R. (1996) Bleomycin-mediated electrochemotherapy of metastatic melanoma. *Arch. Dermatol.* **132**, 1353–1357.
 29. Rudolf, Z., Štabuc, B., Čemažar, M., Miklavčič, D., Vodovnik, L., and Serša, G.

- (1995) Electrochemotherapy with bleomycin: The first clinical experience in malignant melanoma patients. *Radiol. Oncol.* **29**, 229–235.
30. Mir, L. M., Glass, L. F., Serša, G., Teissié, J., Domenge, C., Miklavčič, D., Jaroszeski, M. J., Orlowski, S., Reintgen, D. S., Rudolf, Z., Belehradec, M., Gilbert, R., Rols, M-P, Belehradec, J. Jr., Bachaud, J. M., DeConti, R. C., Štabuc, B., Čemažar, M., Coninx, P., and Heller, R. (1998) Effective treatment of cutaneous and subcutaneous malignant tumours by electrochemotherapy. *Br. J. Cancer* **77**, 2336–2342.
 31. Glass, L. F., Jaroszeski, M. J., Gilbert, R., Reintgen, D. S., and Heller, R. (1997) Intralesional bleomycin-mediated electrochemotherapy in 20 patients with basal cell carcinoma. *J. Am. Acad. Dermatol.* **37**, 596–599.
 32. Heller, R., Jaroszeski, M. J., Reintgen, D., Puleo, C., DeConti, R., Gilbert, R., and Glass, L. F. (1998) Treatment of cutaneous and subcutaneous tumors with electrochemotherapy using intralesional bleomycin. *Cancer* **83**, 148–157.
 33. Panje, W. R., Hier, M. P., Garman, G. R., Harrell, E., Goldman, A., and Bloch, I. (1998) Electroporation therapy of head and neck cancer. *Ann. Otol. Rhinol. Laryngol.* **107**, 779–785.
 34. Hofmann, G. A., Dev, S. B., and Nanda, G. S. (1996) Electrochemotherapy: transition from laboratory to the clinic. *IEEE Eng. Med. Biol.* **15**, 124–132.
 35. Gilbert, R., Jaroszeski, M. J., and Heller, R. (1997) Novel electrode designs for electrochemotherapy. *Biochem. Biophys. Acta* **1334**, 9–14.
 36. Serša, G., Štabuc, B., Čemažar, M., Jančar, B., Miklavčič, D., and Rudolf, Z. (1998) Electrochemotherapy with cisplatin: Potentiation of local cisplatin antitumor effectiveness by application of electric pulses in cancer patients. *Eur. J. Cancer* **34**, 1213–1218.
 37. Serša, G., Čemažar, M., Šemrov, D., and Miklavčič, D. (1996) Changing electrode orientation improves the efficacy of electrochemotherapy of solid tumors in mice. *Bioelectrochem. Bioenerg.* **39**, 61–66.
 38. Čemažar, M., Miklavčič, D., Vodovnik, L., Jarm, T., Zvonimir, R., Štabuc, B., Čufer, T., and Serša, G. (1995) Improved therapeutic effect of electrochemotherapy with cisplatin by intratumoral drug administration and changing of electrode orientation for electroporation on EAT tumor model in mice. *Radiol. Oncol.* **29**, 121–127.
 39. Okino, M., Tomie, H., Kanesada, H., Marumoto, M., Esato, K., and Suzuki, H. (1992) Optimal electric conditions in electrical impulse chemotherapy. *Jpn. J. Cancer Res.* **83**, 1095–1101.
 40. Heller, R., Jaroszeski, M., Messina, J. L., Perrott, R., Van Voorhis, N., Reintgen, D. D., and Gilbert, R. (1995) Treatment of B16 melanoma with the combination of electroporation and chemotherapy. *Bioelectrochem. Bioenerg.* **36**, 83–87.
 41. Sersa, G., Cemazar, M., Miklavcic, D., and Mir, L. M. (1994) Electrochemotherapy: variable anti-tumor effect on different tumor models. *Bioelectrochem. Bioenerg.* **35**, 23–27.
 42. Heller, R., Jaroszeski, M. J., Perrott, R., Messina, J., and Gilbert, R. (1997) Effec-

- tive treatment of B16 melanoma by direct delivery of bleomycin using electrochemotherapy. *Melanoma Res.* **7**, 10–18.
43. Okino, M., Marumoto, M., Kanesada, H., Kuga, K., and Mohri, H. (1987) Electrical impulse chemotherapy for rat solid tumors. *Proc. Jpn. Cancer Congr.* **46**, 420.
 44. Okino, M. and Esato, K. (1990) The effects of a single high voltage electrical stimulation with anticancer drug on in vivo growing malignant tumors. *Jpn. J. Surg.* **20**, 197–204.
 45. Okino, M., Tomie, H., Kanesada, H., Marumoto, M., Morita, N., Esato, K., and Suzuki, H. (1991) Induction of tumor specific selective toxicity in electrical impulse chemotherapy-analysis of dose response curve. *Oncologia* **24**, 71–79.
 46. Kanesada, H. (1990) Anticancer effect of high voltage pulses combined with concentration dependent anticancer drugs on Lewis lung carcinoma. *J. Jpn. Soc. Cancer Ther.* **25**, 2640–2648.
 47. Salford, L. G., Persson, B. R. R., Brun, A., Ceberg, C. P., Kongstad, P. Ch., and Mir, L. M. (1993) A new brain tumor therapy combining bleomycin with in vivo electropermeabilization. *Biochem. Biophys. Res. Commun.* **194**, 938–943.
 48. Yamaguchi, O., Irisawa, C., Baba, K., Ogihara, M., Yokota, T., and Shiraiwa, Y. (1994) Potentiation of antitumor effect of bleomycin by local electric pulses in mouse bladder tumor. *Tohoku J. Exp. Med.* **172**, 291–293.
 49. Jaroszeski, M. J., Gilbert, R., and Heller, R. (1997) Successful treatment of hepatomas with electrochemotherapy in a rat model. *Biochem. Biophys. Acta* **1334**, 15–18.
 50. Jaroszeski, M. J., Gilbert, R., Perrott, R., and Heller, R. (1996) Enhanced effects of multiple treatment electrochemotherapy. *Melanoma Res.* **6**, 427–433.
 51. Mir, L. M., Devauchelle, P., Quintin-Colonna, F., Delisle, F., Fradelizi, D., Belehradek, J. Jr., and Orłowski, S. (1997) First clinical trial of cat soft-tissue sarcomas treatment by electrochemotherapy. *Br. J. Cancer* **76**, 1617–1622.
 52. Balch, C. M., Houghton, A. N., and Peters, L. J. (1993) *Cancer Principles and Practice of Oncology*. (DeVita Jr., V. T., Hellman, S., and Rosenberg, S. A., eds.) Lippincott, Philadelphia, p. 1637 and Table 46-7.
 53. Retsas, S. (1995) Strategies for improving survival in malignant melanoma; focus on vindesine. *J. Drug Dev. Clin. Prac.* **7**, 159–171.
 54. Pron, G., Belehradek, J. Jr. and Mir, L. M. (1993) Identification of a plasma membrane protein that specifically binds bleomycin. *Biochem. Biophys. Res. Commun.* **194**, 333–337.
 55. Poddevin, B., Orłowski, S., Belehradek, J. Jr., and Mir, L. M. (1991) Very high cytotoxicity of bleomycin introduced into the cytosol of cells in culture. *Biochem. Pharmacol.* **42 (Suppl.)**, 67–75.
 56. Neumann, E., Sowers, A. E., and Jordan, C. A. (1989) *Electroporation and Electrofusion in Cell Biology*. Plenum, New York.
 57. Orłowski, S. and Mir, L. M. (1993) Cell electropermeabilization: A new tool for biochemical and pharmacological studies. *Biochim. Biophys. Acta* **1154**, 51–63.
 58. Tounekti, O., Pron, G., Belehradek, J. Jr., and Mir, L. M. (1993) Bleomycin, an

- apoptosis-mimetic drug that induces two types of cell death depending on the number of molecules internalized. *Cancer Res.* **53**, 5462–5469.
59. Reed, E. (1993) Platinum analogs. In: *Cancer Principles and Practice of Oncology*. (DeVita, V. T. Jr, Hellman, S., and Rosenberg, S. A., eds.). Lippincott, Philadelphia, pp. 390–400.
 60. Mir, L. M., Orlowski, S., Poddevin, B., and Belehradec, J. Jr. (1992) Electrochemotherapy tumor treatment is improved by interleukin-2 stimulation of the host's defenses. *Eur. Cytokine Netw.* **3**, 331–334.
 61. Mir, L. M., Roth, C., Orlowski, S., Belehradec, J. Jr., Fradelizi, F., Paoletti, C., and Kourilsky, P. (1992) Potentiation of the antitumoral effect of electrochemotherapy by an immunotherapy with allogeneic cells producing interleukin-2. *C. R. Acad. Sci. Paris* **314**, 539–544.
 62. Mir, L. M., Roth, C., Orlowski, S., Quintin-Colonna, F., Fradelizi, F., Belehradec, J. Jr., and Kourilsky, P. (1995) Systemic antitumor effects of electrochemotherapy combined with histocompatible cells secreting interleukin-2. *J. Immunol.* **17**, 30–38.

In Vitro and Ex Vivo Gene Delivery to Cells by Electroporation

Sek Wen Hui and Lin Hong Li

1. Introduction

Electroporation generally refers to the technique of permeabilizing cell membranes by applying a short and intense electric pulse across a cell, such that the barrier function of the membrane is instantaneously compromised. During such time, genetic materials may travel across the membrane. For a successful gene transfer process, the barrier function of the cell membrane is rapidly restored, and the cell survives. The electrotransfection process thus comprises two steps. The first step is electroporation, which is governed by the electrical properties of the cell and the suspension medium. The controlling parameters are mainly electrical. The second step is recovery, which must take into account the biological characteristics of the cells. We consider these two steps in this chapter.

The phenomenon of reversible electric breakdown of cell membranes was first observed in the 1970s (1–3). It was later realized that the method might be used to entrap molecules in cells (4,5). Successful transport of DNA across cell membranes was reported by Auer et al. (6), and later by Wong and Neumann (7) as well as Xie et al. (8). Today, this technique has become a standard procedure for transfection and cell loading. A number of commercial electroporation equipment manufacturers currently have products for sale. In addition, a large collection of published and manufacturer-supplied protocols are available.

As the method becomes widely acceptable and popular, many variations have been proposed for various cells and plasmid DNA. Many of these protocols are results of trial and error. Because experimental conditions vary case by case, new and modified protocols are constantly needed to optimize trans-

fection yields. Developing new protocols for new cases by trial and error is wasteful in terms of time and energy. Increasing number of users tend to follow empirical protocols rather than following basic principles. To comprehend the vast literature and to derive the maximum benefit from the electroporation methodology, it is critical to understand basic principles involved as well as what obstacles remain for its broader applicability. This chapter is intended to present a guide based on known theories of electroporation. It should be helpful to all users as an aid for modifying existing protocols and developing new protocols.

2. Factors Governing Electroporation

2.1. Energetics of Electropore Formation

Although the detailed molecular mechanism of electroporation still needs to be clarified, recent fundamental studies give us a general picture of the events happening during the electroporation process. We know that membrane permeabilization is due to the electric breakdown of the lipid bilayer when the transmembrane potential exceeds the breakdown potential of the bilayer. Pores or permeabilization sites are formed and maintained by the electric pulse field. In contrast to lipid bilayers that reseal immediately after the breakdown, the permeabilized state of cell membranes may last tens of minutes after the termination of the pulse field. During and shortly after the pulse, molecules may enter the cell in a number of ways, including electrophoresis (of charged molecules such as DNA), electroosmotic and colloid-osmotic flow, as well as diffusion.

In terms of energy, a membrane pore is created when the energy stored in the membrane capacitor exceeds the energy of keeping the membrane intact against pore expansion. The energy of forming a pore of a given radius r in a membrane is determined by the balance between the line tension γ of the pore edge and the surface tension χ of the membrane.

$$E_p = 2\pi r\gamma - \pi r^2\chi. \quad (1)$$

This pore energy reaches a maximum at a critical value of pore radius $r_c = \gamma/\chi$ (9,10). The line tension of the pore edge depends on the molecular packing of the membrane. Pores with radii smaller r_c tend to reseal, while those with radii greater than r_c tend to expand if the membrane is under tension.

When subjected to an imposed electric field E , which charges the membrane capacitor, the energy stored in the membrane capacitor over an equivalent area of the pore precursor is:

$$E_e = \pi r^2 \epsilon_0 (\epsilon_w - \epsilon_m) V^2 / 2d, \quad (2)$$

where ϵ denotes the dielectric constant and the subscripts 0, w, and m refer to free space, water, and membrane, respectively. V is the transmembrane voltage

(membrane potential) imposed by the pulse field across the membrane of thickness d . For a given membrane, an electropore of radius r will form if the electric energy E_e given in **Eq. 2** is greater than the energy E_p required (in **Eq. 1**) to form a pore of such size. This energy defines the breakdown voltage V_b , over which the membrane will breakdown and pores of diameter r will form. If $r < r_c$, the electric breakdown is reversible. Otherwise the pore will expand once it is formed. A macroscopic relationship has been described by Zelev and Needham (**10**).

2.2. Kinetics of Electroporation

Consider the simpler case of a spherical cell. The imposed membrane potential, or transmembrane voltage V experienced by the cell is (**11**)

$$V = 1.5aE \cos \phi [1 - \exp(-t/\tau)], \quad (3)$$

where E is the imposed pulse electric field, a is the radius of the cell, and ϕ is the angle between the field direction and the radial vector of the surface point where membrane potential is considered. The highest V is, of course, at the poles along or against the field direction where ϕ is 0 and π , respectively. Since the breakdown voltage (V_b) of most biomembranes is around 1 V, a 0.7 kV/cm pulse of sufficient length is enough to produce a breakdown potential at the poles for a cell that is 10 μm in diameter. A threshold electric field strength needed for cell permeabilization has been documented (**12**).

The time required to develop this potential across the membrane is governed by τ . The charging or relaxation time τ of the membrane is determined by the internal and external conductivities of the cell (**13**).

$$\tau = aC_m (1/\sigma_i + 0.5/\sigma_e). \quad (4)$$

C_m is the membrane capacitance, and σ_i and σ_e are the internal and external conductivities. For a cell of 5 μm in radius, with a $\sigma_i = 58 \mu\text{S/cm}$ and $\sigma_e = 9 \mu\text{S/cm}$, τ is 25 μs . Thus the minimum pulse length required for the electropore to form is expected to be about 25 μs . Larger cells require longer time to reach the membrane breakdown potential. The minimum pulse length requirement may be shorter with higher internal and external conductivities.

The electric pressure, Π , from the charge buildup across the membrane at the pole is

$$\Pi = 0.5\epsilon_0\epsilon_e \{1.5aE [1 - \exp(-t/\tau)] / d\}^2 \quad (5)$$

where d is the membrane thickness. The pressure is generated against the mechanical resilience of the membrane. Therefore, the time for the membrane to break down depends not only on the time for the electric pressure to build up but also on the lateral viscosity of the membrane materials to retract in order

for the membrane to thin and eventually break. A discussion of the mechanical breakdown process is given by Needham and Hochmuth (14). The combined electric relaxation time of the cell in suspension and the mechanical relaxation time of the membrane determine the temporal process of electroporation.

The imposed membrane potential is felt simultaneously at all points at the cell surface, according to Eq. 3, because the mechanical relaxation time is usually longer than the electric relaxation time for most cells. The higher the imposed field strength E , the farther from the poles extend the area where membrane breakdown potential is experienced, that is, the wider the breakdown area (12). It can take the form of multiple pores or other forms of membrane defects over the breakdown areas. The detailed geometry of the permeabilized area is still controversial.

2.3. Transport of DNA Across Membranes

Apart from the extent of membrane permeabilization, there are several other factors that control the intake of exogenous DNA by the cell. It is believed that most exogenous DNA transport into electroporated cells is through electrophoresis (15,16). Even if cells remain permeabilized long after the pulse, as determined by dye penetration, adding DNA immediately after the pulse usually results in a much lower transfection efficiency compared to adding DNA before the pulse. Shielding the charge of DNA by cations also reduces the transfection efficiency. It has been reported that more DNA enters the cells during a second pulse of lower field strength, once the cell is permeabilized by the first pulse (17,18). Uptake of DNA adsorbed on cell surfaces has also been suggested (8). For a given pore-forming pulse voltage, the transfection efficiency depends more on the total length of pulses than on the time span when cells remain permeable, thus the diffusion of DNA into cells through electropores is not an important contribution in transfection efficiency. Other physical factors such as the geometry and concentration of DNA are also important (19), because the physical forms of DNA affects their electrophoretic mobility.

If most of the DNA entering the cell does so during the pulse, the transfection efficiency should be proportional to the integral of the extent of membrane permeabilization with respect to the pulse time. For simple rectangular pulses or exponentially decaying pulses, the time integral is the pulse length (or decay time constant) T , which is usually much greater than the membrane relaxation time. If the permeabilized area of the cell is limited to the polar regions as is normally the case (20), the extent of membrane permeabilization, in terms of the number, density and size of electropores, is approximately proportional to $E - E_b$, where E_b is the pulse field strength needed to produce the membrane

breakdown voltage V_b . Thus we expect the transfection efficiency to be roughly proportional to

$$(E - E_b)T. \quad (6)$$

If multiple rectangular pulses are used, T represents the sum of all pulse periods. If an exponentially decaying pulse from a capacitor-type pulse generator is used, T represents the decay time constants of the pulse. The relationship should hold as long as E is not too much greater than E_b , such that the electropores so created are reversible.

The dependence of macromolecule transport on $(E - E_b)T$ has been verified by using fluorescence molecules as tracers (21–23). Macromolecule intake during electroporation was indeed proportional to the quantity $(E - E_b)T$. **Figure 1** shows the uptake of fluorescein isothiocyanate labeled dextran by C3H/10T_{1/2} cells as a function of T when E is fixed. Because cells take up dextran spontaneously without electroporation, the best fit line does not intercept the origin. The linear relationship holds for a wide range of E and T combinations, regardless of voltage and time ranges, as long as the reversible breakdown limit is not exceeded (22). However, if viable cells only are counted, the intake drops off once the viability limit is reached. Measurements of bovine serum albumin uptake by erythrocyte ghosts shows the same trend (23).

If the transfection efficiency is proportional to the percentage of permeabilized cells that take in DNA, then transfection efficiency would also be a linear function of $(E - E_b)T$. A linear relation was reported for the transfection efficiency of HeLa cells by pRSVgpt plasmids (24), when the number of transfected clones was plotted as a function of ET . The x -axis intercept of the least square fit line gives $E_b T = 0.5$ kV ms/cm. This value implies that, for a 0.75-ms pulse, the threshold applied field strength to cause reversible breakdown in some cells is 0.7 kV/cm. A linear relationship was found when the logarithm of transfection efficiency was plot against $\log [E]$ or $\log [T]$ for the transfection of *E. coli* JM105 with pBR³²² (25). The effect of pulse strength and duration on the transfection of CHO cells was investigated by Wolf et al. (16). The transfection efficiency of CHO cells in suspension, with pSV2CAT or pBR322- β gal plasmids, was also found to be a linear function of either E or T while the other parameter was held constant. **Figure 2** shows the linear relationship between ET and transfection efficiency for JTL B-lymphoid cells. The decline at high ET value apparently is caused by cell death (as discussed later). The minimum field strength E_b for detectable permeability as well as transfection was found to be 0.6 kV/cm. These values approximately equal that given by **Eq. 3**, and agrees with most threshold field strength values for electroporation (16,26). Interestingly, the transfection efficiency decreases with

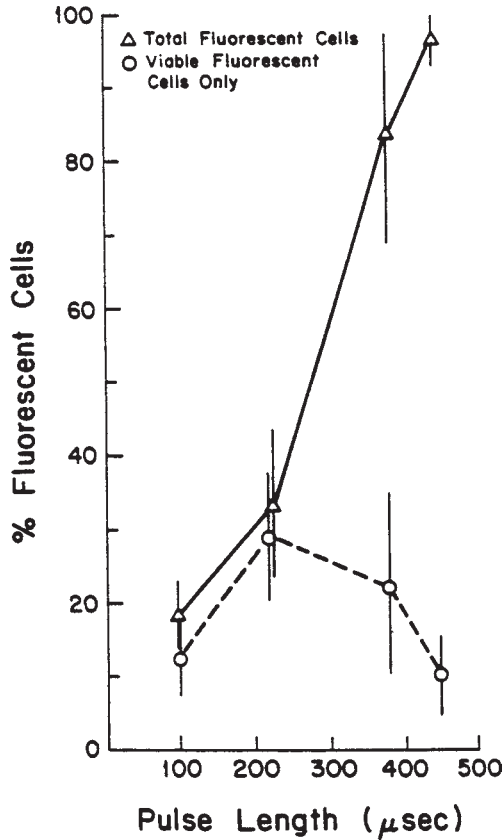


Fig. 1. The percentage of fluorescent C3H/10T_{1/2} cells after electroporation in FITC-Dextran (72 kD), using a 4.2 kV/cm exponential pulse of various decay times (pulse length). The total percentages of fluorescent cells and viable fluorescent cells (by trypan blue exclusion test) are represented by (Δ) and (\circ), respectively. (From **ref. 22**, with permission.)

increasing delay between repeating pulses, indicating that DNA is collected on the cell surface and driven through the electropores by electrophoretic force, in agreement with previous experiments using two consecutive pulses to increase transfection yield (18).

The above analysis applies only to reversible breakdown of cell membranes by the electric pulses, such that membranes reseal in time, and cells recover from the traumatic event of electroporation. In cases that the applied field is high enough to trigger irreversible membrane breakdown, that is, $E \gg E_b$ such that $r > r_c$, electropores do not reseal, and the cell viability is low. As a con-

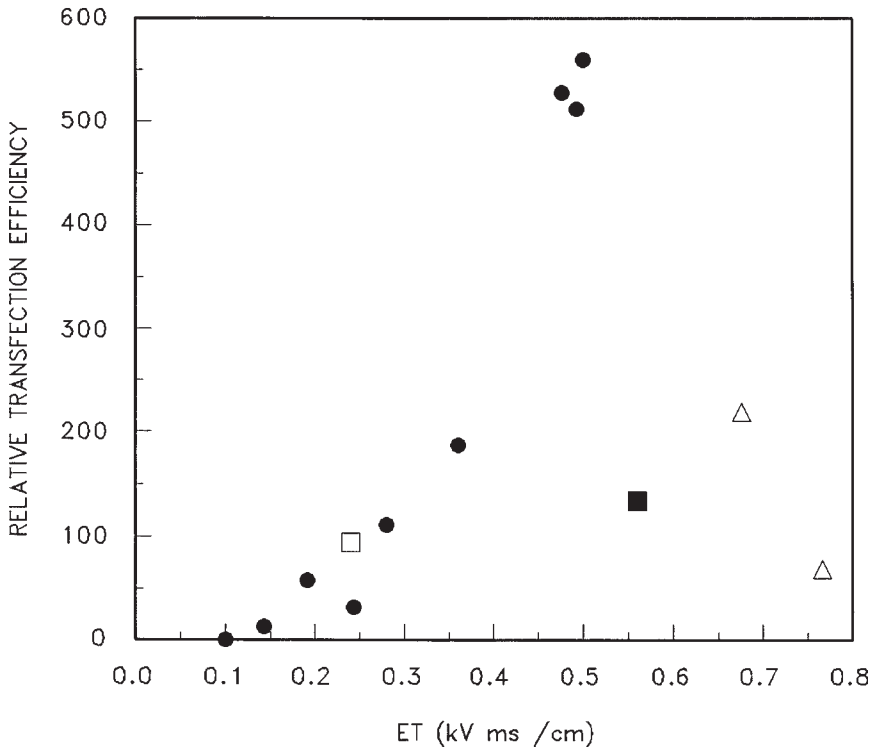


Fig. 2. The relative transfection efficiency of human JTL lymphoid cells transfected with pCEP4-FUC. The activity of α -fucosidase is plotted as a function of the product of the pulse field strength E and the equivalent integral pulse time T . The samples were subjected to three exponentially decaying pulses of given decay half-times: (□) 0.2 msec, (●) 0.24–0.28 ms, (△) 0.34–0.35 ms, at $E = 0.5$ –2 kV/cm, and (■) 0.14 ms at $E = 4$ kV/cm.

sequence, cell viability imposes an upper limit on the transfection efficiency (Fig. 2).

Many electroporation protocols give electric parameters in terms of voltage and capacitor value (in microfarads, for instance). These quantities are meaningful only if the sample resistance and interelectrode distance are given as well. For a uniform sample in a cuvette, the pulse field strength E is the applied voltage divided by the interelectrode distance. The pulse decay time $T = RC$ is the capacitance C used in the pulse generator and the capacitance of the sample, times the total resistance R of the sample plus any circuit elements. The formulae relating voltage and capacitance to the relevant electric parameters E and T

are sample- and instrument-dependent; therefore voltage and capacitance should not be cited as independent electric parameters.

3. Recovery After Electroporation

3.1. Colloidal Osmotic Swelling

Cells maintain osmotic balance with the external environment via a system of membrane transport mechanisms. Although the total osmotic pressure inside and outside the cell is kept equal, the composition of individual ionic species are usually different. For instance, the equilibrium between excess intracellular potassium and excess extracellular sodium is maintained by Na-K-ATPase at the plasma membrane. The concentration of intracellular calcium is kept two orders of magnitude lower than that of extracellular fluid by the calcium pump system of the membrane. Electropores created at the plasma membrane can abolish these carefully maintained ionic gradients and lead to cell death. Cells may recover if the electropores are rapidly resealed and the ion pump system remain largely intact after the electroporation pulse to counter the ion mixing through electropores. The resealing times of electropores at cell membranes are typically seconds to minutes. Cell death due to ionic imbalance can be reduced by using a reverse Na/K buffer with reduced calcium during electroporation (27).

A different, and usually more damaging type of osmotic effects is the colloidal-osmotic effect. The origin of this effect is the selective permeability of the membrane after electroporation. Cells contain molecules that are larger than ions, such as proteins, nucleic acids, and various macromolecules that make up the organelles and the cytosol. Because of a high concentration of these large molecules within the cells, ionic concentrations inside cells are necessarily lower than that of the external environment in order to maintain a general osmotic equilibrium. Small electropores allow ions to pass through to attain ionic equilibrium while large molecules are kept within the cell. An osmotic imbalance is thus set up by the ion flux. Water is then transported through the membrane to counter the osmotic imbalance, and the cells swell indefinitely. This is known as colloidal-osmotic swelling. If electropores are not resealed rapidly, continuous swelling may lead to cell bursting and death. The increased tension of the membrane due to swelling further hinders the resealing process and hastens cell lysis. An example is electroporation-induced hemolysis even if erythrocytes are pulsed in isoosmotic media. Cell lysis can be reduced if dextran or PEG is added to the external medium to balance out the colloidal osmotic effect (28).

3.2. Inhibiting Cell Swelling Improves Transfection

Most cell death after electroporation is a result of colloidal osmotic swelling rather than a result of “electrocution” (damage of cellular structure and function directly by the electric field). In conventional electroporation protocols, the optimal transfection efficiency is usually achieved when half of the cell population is killed. If cell swelling can be controlled, the electric pulses can be stronger (i.e., higher pulse field strength and longer pulses), and the success rate of transfection would improve. Placing large polymer molecules, such as PEG or dextran, in the electroporation solution, as described above, may reduce and even prevent colloidal osmotic swelling of electroporated cells. The colloidal osmotic balance has to be carefully adjusted so that cells do not swell or shrink beyond its limit before the membrane reseal.

One method to control swelling is to pulse cells in a centrifugation pellet (28,29). Intercellular spacing is limited when cells are in a pellet form, and the transport of ions and macromolecules into and from the pellet to the supernatant is slow. Permeabilized cells in the pellet have insufficient room to swell even if the colloidal osmotic pressure favors swelling. Limited swelling causes the electric resistance of the pellet to rise after each pulse due to the closure of the intercellular spacing. The rise time of resistance, typically several minutes, indicates the swelling time of the cells (28). There is enough time to form the pellet after pulsing the cells in suspension. This is the postpulse pelleting method. This method improves the chance for cell survival, which affords opportunity for DNA in solution to enter permeabilized cells. Transfection efficiency of a number of cell types, including NK-L, K562 (Fig. 3), L1210 and MC2 cells, has been shown to improve by applying this method (29). These first three cell lines are extremely difficult to transfect by methods other than electroporation.

Another method of reducing the colloidal osmotic swelling is to confine the target cells and DNA in droplets of a phase-separated two-phase polymer mixture. By adjusting the partition coefficients of cells and DNA for a particular phase, and by also matching the osmolarities of the two phases, it is possible to select and to compact the cells and DNA into the condensing phase (30). Shaking the polymer mixture breaks the condensing phase into droplets. Electric pulses are then applied to the suspension. DNA uptake increases because the cells and DNA are sequestered together within confining droplets. Swelling also is limited. Post-pulse survival and transfection rate both improve as a result (Fig. 4). This method has been applied to a number of cell lines, including CHO, COS-7, Melan C, and JTL human B-lymphoid cells. The last cell

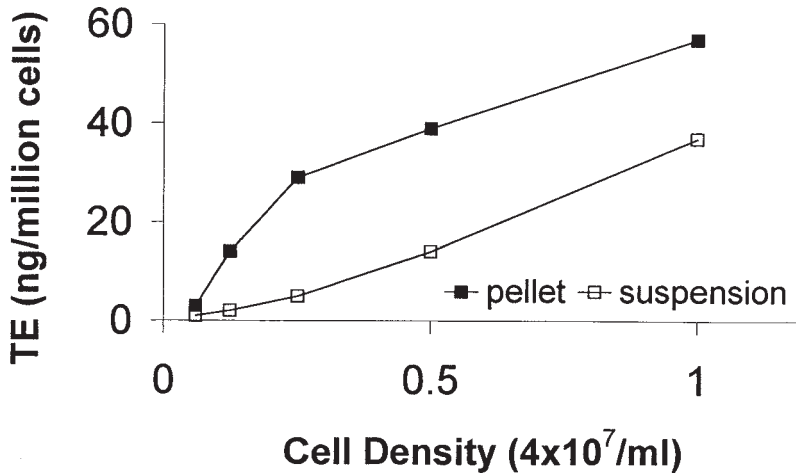


Fig. 3. The dependence of electrotransfection efficiency (TE) of K-562 erythroleukemic cells on cell density. Cells were transfected with the pEGFP-N1 plasmid using four 400- μ s pulses at a field strength of 2.3 kV/cm. Solid and open squares represent the transfection efficiency of cells incubated in pellet and suspension, respectively. (From *ref. 22*, with permission.)

type has not been successfully transfected by any other methods including conventional electroporation.

3.3. Electroporation-Induced Apoptosis

Pulse-induced apoptosis is a major obstacle to postpulse recovery for certain cells. Those cells were often found to die at 6 or more hours after pulsing rather than instantaneously. Closer examination revealed that the majority of cell death was the result of pulse-induced apoptosis. What lead to apoptosis was not the damage caused by the pulsed electric field but the importation of foreign DNA into the cells. It is known that pulsing cells in the presence of DNA or other charged macromolecules causes additional damage to the cell membrane due to the threading of these molecules through electropores (18). It was only recently found that this type of damage leads to apoptosis in certain cells (31). By treating cells with an inhibitor (Boc-ASP-FMK) of caspase, an enzyme responsible for initiating apoptosis, the transfection efficiency of subclone 3.3 of L1210 lymphoma cells was significantly improved (Fig. 5).

For any transfection operation, only a portion of cells are transfected, even if all of the above precautions are taken. Within a given sample, cells vary in size and shape as well as in the dielectric and conductive properties of cellular components. These variations dictate that the critical field and membrane relaxation time differ from cell to cell. In addition to this physical variation are

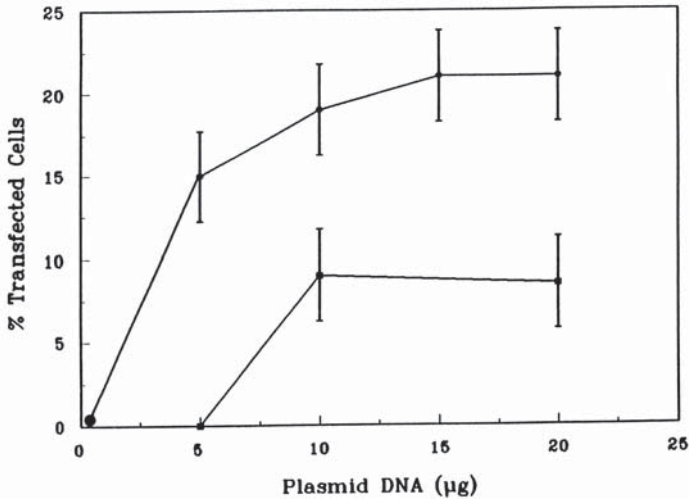


Fig. 4. The transfection efficiency of CHO cells with the plasmid pSV- β -gal. Cells were transfected by electroporation in a two-phase polymer system (PEG8000 10%; dextran75000 20%) using three 320 μ sec pulses at 2.2 kV/cm. The percentage of transfected cells was measured as a function of plasmid concentration. The lower curve represents results of electroporating cells suspended in Baker and Knight medium (27). (From ref. 30, with permission.)

the more important biological differences of cell cycle, age, and gene expression controls. Therefore, the analysis presented here should be treated only as a guide. The actual response depends on the homogeneity of the cell population.

4. Summary and Conclusion

The existing theory for reversible electric breakdown of cell membranes and the transport of DNA across plasma membranes through electropores adequately describes a linear relation between transfection efficiency and $(E - E_b)T$. E_b is determined by the electric energy derived from the applied pulses and the energy cost to form an electropore in the membrane of cells of a given size. Although the viability limit varies from cell line to cell line, within this limit, the linear relationship between transfection efficiency and ET seems to hold over a wide range of E and T combinations, and is applicable to most cells. It serves as a guideline for selection of electric parameters in various applications.

Since the transfection efficiency is proportional to ET , there is a choice of optimizing either E or T . Excessive field strength leads to permeabilization of a wider area, or forming larger pores that may exceed the reseal limit $r_c = \gamma/\chi$. As long as pores remain reversible, the necessary T value may be satisfied by

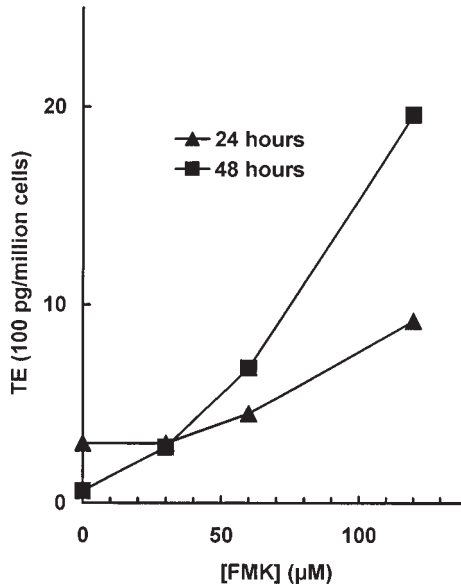


Fig. 5. The dependence of electrotransfection efficiency (TE) of subclone 3.3 of L1210 lymphomas on the caspase inhibitor FMK concentration. Transfection was carried out using 400- μs pulses at a field strength of 1.7 kV/cm and with the pEGFP-N1 plasmid. The curves with triangles and squares represent the TE assayed 24 and 48 hours after pulse, respectively. (From **ref. 31**, with permission.)

applying longer and multiple pulses. Cell membranes do not reseal as rapidly as lipid bilayers, so that multiple pulses may not form additional pores in the membranes. There are advantages of multiple pulses over single pulse, and offset AC bursts over rectangular pulses (8,32). A bipolar oscillating field is reported to have more advantages than unipolar oscillating field, since both poles of the cells are permeabilized (33). Clearly there is a merit in using lower applied field strength and increasing the duration and number of pulses to attained the required *ET* value.

Postpulse recovery is as important a factor as electroporation in determining transfection efficiency. The major culprit of postpulse cell death is colloidal osmotic swelling. Limiting the swelling by confining cells in pellets or in two-phase polymer droplets improves cell viability and transfection efficiency significantly. Controlling post-pulse apoptosis can also improve transfection efficiency for some cells. The transfection efficiency is sufficiently high such that the technique can be applied to *ex vivo* gene delivery to a limited number of target cells.

Protocols for electroporation continue to develop as cases demand. The present knowledge of the electroporation mechanism is capable to guide the rational design of new protocols. It is hoped that the above analysis will take some guesswork out of applying electrotransfection in new situations.

Acknowledgments

The results from this laboratory cited in this chapter are the work of Drs. R. T. Kubiniec, D. A. Stenger, H. Liang, N. G. Stoicheva, Y. L. Zhao, and the late Prof. I. G. Abidor. The work was supported by grant GM 30969 from the National Institutes of Health.

References

1. Neumann, E. and Rosenheck, K. (1972) Permeability changes induced by electric impulses in vesicular membranes, *J. Membr. Biol.* **10**, 279–290.
2. Zimmermann, U., Pilwat, G., and Riemann, F. (1974) Dielectric breakdown of cell membranes. *Biophys. J.* **14**, 881–899.
3. Kinosita, K. and Tsong, T. Y. (1975) Formation and reeling of pores of controlled sizes in human erythrocyte membranes. *Nature* **268**, 438–441.
4. Zimmermann, U., Riemann, F., and Pilwat, G. (1976) Enzyme loading of electrically homogeneous human red blood cell ghosts prepared by dielectric breakdown. *Biochim. Biophys. Acta* **436**, 460–474.
5. Vienken, J., Jeltsch, E., and Zimmermann, U. (1978) Penetration and entrapment of large particles in erythrocytes by electrical breakdown techniques. *Cytobiologie* **17**, 182–196.
6. Auer, D., Brandner, G., and Bodemer, W. (1976) Dielectric breakdown of the red blood cell membrane and uptake of SV40 DNA and mammalian RNA. *Naturwissenschaften* **63**, 391–393.
7. Wong, T. K. and Neumann, E. (1982) Electric field mediated gene transfer. *Biochem. Biophys. Res. Commun.* **107**, 584–587.
8. Xie, T. D., Sun, L., and Tsong, T. Y. (1990) Study of mechanisms of electric field-induced DNA transfection. I. DNA entry by surface binding and diffusion through membrane pores. *Biophys. J.* **58**, 13–19.
9. Abidor, I. G., Arakelyan, V. B., Chernomordik, L. V., and Chizmadzhev, Yu., A. (1979) Electric breakdown of bilayer membranes. I. The main experimental facts and their qualitative discussion. *Bioelectrochem. Bioenerg.* **6**, 37–52.
10. Zelev, D. V. and Needham, D. (1993) Tension-stabilized pores in giant vesicles: Determination of pore size and pore line tension. *Biochim. Biophys. Acta* **1147**, 89–104.
11. Holzapfel, C. J., Vienkan, J., and Zimmermann, U. (1982) Rotation of cells in an alternating electric field: Theory and experimental proof. *J. Membr. Biol.* **67**, 13–26.
12. Rols, M. P. and Teissié, J. (1990) Electroporabilization of mammalian cells: Quantitative analysis of the phenomenon. *Biophys. J.* **58**, 1089–1098.

13. Stenger, D. A., Kaler, K. V. I. S., and Hui, S. W. (1991) Dipole interactions in electrofusion: contributions of membrane potential and effective dipole to interaction pressure. *Biophys. J.* **59**, 1074–1084.
14. Needham, D. and Hochmuth, R. M. (1989) Electro-mechanical permeabilization of lipid vesicles: Role of membrane tension and compressibility. *Biophys. J.* **55**, 1001–1009.
15. Klenchin, V. A., Sukharev, S. I., Serov, S. M., Chernomodok, L. V., and Chizmadzhev, Yu. A. (1991) Electrically induced DNA uptake by cells is a fast process involving DNA electrophoresis. *Biophys. J.* **60**, 804–811.
16. Wolf, H., Rols, M. P., Boldt, E. Neumann, E., and Teissié, J. (1994) Control by pulse parameters of electric field-mediated gene transfer in mammalian cells. *Biophys. J.* **66**, 524–531.
17. Andreason, G. L. and Evans, G. A. (1989) Optimization of electroporation for transfection of mammalian cells. *Anal. Biochem.* **180**, 269–275.
18. Sukharev, S. I., Klenchin, V. A., Serov, S. M., Chernomodok, L. V., and Chizmadzhev, Yu. A. (1992) Electroporation and electrophoretic DNA transfer into cells: The effect of DNA interaction with electropores. *Biophys. J.* **63**, 1320–1327.
19. Nickoloff, J. A. and Reynolds, R. J. (1992) Electroporation-mediated gene transfer efficiency is reduced by linear plasmid carrier DNAs. *Anal. Biochem.* **205**, 237–243.
20. Hibino, M., Shigemori, M., Itoh, H., Nagayama, K., and Kinosita, K. Jr. (1991) Membrane conductance of an electroporated cell analyzed by submicrosecond imaging of transmembrane conductance. *Biophys. J.* **59**, 209–220.
21. Schwister, K. and Deuticke, B. (1985) Formation and properties of aqueous leaks induced in human erythrocytes by electrical breakdown. *Biochim. Biophys. Acta* **816**, 332–348.
22. Liang, H., Purucker, W. J., Stenger, D. A., Kubiniec, R. T., and Hui, S. W. (1988) Uptake of fluorescence-labeled dextrans by 10T-1/2 fibroblasts following permeation by rectangular and exponential-decay electric field pulse. *Biotechniques* **6**, 550–558.
23. Prausnitz, M. R., Milano, C. D., Gimm, J. A., Langer, R., and Weaver, J. C. (1994) Quantitative study of molecular transport due to electroporation: Uptake of bovine serum albumin by erythrocyte ghosts. *Biophys. J.* **66**, 1522–530.
24. Kubiniec, R. T., Liang, H., and Hui, S. W. (1990) Effects of pulse length and pulse strength on transfection by electroporation. *Biotechniques* **8**, 1–3.
25. Xie, T. D. and Tsong, T. Y. (1992) Study of mechanisms of electric field-induced DNA transfection, III. Electric parameters and other conditions for effective transfection. *Biophys. J.* **63**, 28–34.
26. Chang, D. C., Chassy, B. M., Saunders, J. A., and Sowers, A. E. (1992) *Guide to Electroporation and Electrofusion*. Academic Press, San Diego, CA.
27. Baker, P. F. and Knight, D. E. (1983). High voltage techniques for gaining access to the interior of cells: Application to the study of exocytosis and membrane turnover. *Methods Enzymol.* **98**, 23–37.

28. Abidor, I. G., Li, L. H., and Hui, S. W. (1994) Studies of cell pellets. II. Osmotic properties, electroporation and related phenomena. Membrane interactions. *Biophys. J.* **67**, 427–435.
29. Li, L. H., Ross, P., and Hui, S. W. (1999) Improving electrotransfection efficiency by post-pulse centrifugation. *Gene Ther.* **6**, 364–372.
30. Hui, S. W., Stoicheva, N., and Zhao, Y-L. (1996) High efficiency loading, transfection and fusion of cells by electroporation in two-phase polymer systems. *Biophys. J.* **71**, 1123–1130.
31. Li, L. H., Sen, A., Murphy, S. P., Jahreis, G. P., and Hui, S. W. (1999) DNA-update induces apoptosis and limits transfection efficiency. *Exp. Cell Res.* (in press).
32. Chang, D. C., Gao, P. Q., and Maxwell, B. L. (1991) High efficiency gene transfection by electroporation using a radio-frequency electric field. *Biochim. Biophys. Acta* **1992**, 153–160.
33. Tekle, E., Austumian, R. D., and Chock, P. B. (1991) Electroporation by using bipolar oscillating electric field: an improved method for DNA transfection of NIH/3T3 cells. *Proc. Natl. Acad. Sci. USA* **88**, 4230–4234.

Delivery of Genes In Vivo Using Pulsed Electric Fields

Mark J. Jaroszeski, Richard Gilbert,
Claude Nicolau, and Richard Heller

1. Introduction

The first research that focused on the effects of pulsed electric fields on living cells described the phenomena of reversible and irreversible membrane breakdown in an in vitro environment in the 1960s and 1970s (1–6). This early research led to the current understanding that exposing cells to intense electric fields induces a transmembrane potential that is superposed on the resting potential. Induced potentials of sufficient magnitude cause a dielectric breakdown of the membrane. This physical phenomenon was termed electroporation, or electropermeabilization, because it was observed that molecules that do not normally pass through the membrane gain intracellular access after the cells were treated with electric fields.

All of the molecular events that take place at the membrane level during electropermeabilization have not yet been elucidated; however, there is agreement in the literature (7–9) that the applied field induces structural defects or changes in the membrane, which serve as pathways from the extracellular space to the cell interior. The porated state was noted to be temporary. Electrically treated cells could recover from their porated state to again have intact membranes as long as the applied field was within certain limits. Specifically, an induced transmembrane voltage of 0.5 to 1 V is generally accepted as the minimum potential required to induce membrane breakdown in most mammalian cell types (10). The induced potential can be increased above conditions required to achieve this threshold potential typically by increasing the applied field. However, induced potentials above this threshold can cause irreversible

membrane damage which results in cell death. The minimum threshold and sensitivity to increased fields are cell type-dependent. It is, however, common for the fraction of damaged cell to be proportional to the severity of electrical treatment. Cells that are treated with fields that are sufficient to cause membrane breakdown but minimum irreversible damage remain in a destabilized state for a time that is on the order of minutes (11).

The effects of pulsed electric fields on biological membranes are physical in nature. This characteristic makes the use of electric fields universally applicable. Although the characteristics of the applied field that are necessary to induce membrane breakdown may vary from one cell type to another, electroporation can be effectively utilized with negligible effects on cell viability. A variety of in vitro procedures that capitalize on the effects of electroporation have been developed. These include monoclonal antibody production (12,13), cell-cell fusion (13-15), cell-tissue fusion (16,17), membrane protein insertion (16,18,19), and drug delivery into cells (20). Pulsed electric fields have also become a very popular means of loading genetic material into cells in vitro (21-23).

The use of electric fields in vivo to deliver molecules is a more recent application of this technology than the above-mentioned in vitro applications. One clinically important application of pulsed electric fields is the delivery of chemotherapeutic agents to tumor cells. This type of treatment has been termed electrochemotherapy (ECT). The first published studies used pulsed fields to facilitate the uptake of bleomycin (a chemotherapeutic agent) by tumor cells in animal models (24-27). This technology has rapidly advanced to the clinic. Several trials for the treatment of cutaneous and subcutaneous tumors have been performed with objective response rates ranging from 72% to 100% (28-34).

The prospect of using pulsed electric fields to facilitate gene delivery to cells in vivo is evident based on the success of delivering genes in vitro and effective delivery of drugs in ECT studies. In addition, the molecular nature of many recent medical advances has provided an enormous quantity of information about genes that translate to molecules that have a tremendous potential for therapeutic benefit (35-37). Based on these recent advances, gene therapy has been an extremely popular research topic within many scientific disciplines as well as with the popular press. Therapy with genes coding for corrective, cytotoxic, chemopreventive, antisense, and immunostimulatory molecules (36) has been of research interest using standard gene delivery methods. The success of using pulsed fields to deliver molecules coupled with the potential of therapeutic genes to alter many different disease processes in humans makes the use of electric fields to deliver genes worthy of intense investigation.

For gene therapy to be successful, the gene of interest must be transferred efficiently to target cells. Standard transfer methods employ retroviruses and adenoviruses (35). Several different physical methods have also been investigated for transferring genes. Three of these methods include the use of plasmid liposome complexes, cationic lipids, and direct injection (38). Another interesting physical method involves bombarding the cells with particles that have been coated with DNA (38).

An ideal gene transfer method would allow the introduction of DNA into the desired cells/tissue in an efficient manner with minimal side effects. None of the currently used methods is ideal (38). For example, the use of viruses has a safety concern relative to introducing exogenous DNA into the host genome, low efficiency, potential immunological effects (35). In spite of these drawbacks, viral methods remain the most common method for gene transfer in the literature and with researchers. This is probably due to the lack of other suitable methods. However, the number of published papers that utilize physical methods for gene delivery is increasing which indicates the need for alternative delivery mechanisms.

The use of electric fields to deliver genes *in vivo* has recently become an area of greater research interest. The universal applicability of electric fields coupled with the successful delivery of many types of chemotherapeutic agents *in vivo* suggests that electroporation may be an attractive alternative for site specific gene delivery. Although this type of gene transfer is a very young technology, some very encouraging results have been obtained. These studies have demonstrated the utility of electric fields for delivering genes to cells which may make a significant impact on gene therapy by providing an efficient delivery method that can be adapted to any tissue. This review chapter focuses on these studies.

2. Gene Delivery by Electroporation

In vivo electrically mediated gene transfer has been successfully performed in a variety of animal models. As this is a new gene delivery technology, the majority of the experimental work has utilized reporter genes (contained in plasmids) to investigate and develop delivery protocols. These types of studies are logical precursors to preclinical efficacy studies. However, several studies have utilized genes that code for functional molecules. The methods, animal models, electrodes, electrical impulses used for delivery, and results differ for each published study. Consideration of these aspects of electric field-mediated gene delivery are essential to understanding this developing technology.

2.1. Gene Delivery to Normal Tissues

2.1.1. Liver

The groups of Heller and Nicolau have successfully delivered β -galactosidase and luciferase to healthy liver tissue of Sprague Dawley Rats (39). The method used to deliver the two reporter genes for this study involved surgically exposing the right half of the median liver lobe. An injection of plasmid DNA containing the reporter sequence was administered directly into the treatment site. Pulsed electric fields were applied to the injection site 1.5 minutes after injection of the plasmid. The time delay between injection and pulsing was scheduled in order to allow time for the plasmid to disseminate within the tissue. The electrode used to administer electric fields to the tissue was a circular array of six needles that were equispaced around a 1-cm diameter circle (Genetronics, Inc., San Diego, CA). The electrode was inserted into liver so that the needles encircled the injection site. A total of six 100- μ s electric pulses were delivered to the tissue using the electrode and a BTX T820 (Genetronics, Inc.) rectangular pulse generator. These pulses were applied in a manner that rotated the field around the treatment site. Analysis was conducted on the treated volume of liver tissue.

Expression was evaluated based on luminescence for luciferase and flow cytometric method for β -galactosidase. The study results indicated that maximum luciferase expression occurred 48 hours after treatment when DNA transfer was conducted using voltage to electrode spacing ratios of 1000 to 1500V/cm. Expression using these fields was approximately 10 times greater than control samples that received an injection of plasmid without pulses. These results indicated that electroporation was successfully used to transfer the plasmid DNA into the tissue.

This research also focused on optimizing the luciferase dose for their particular system. Plasmid doses ranging from 0 to 500 μ g per treatment were utilized. Interestingly, a 25 μ g dose resulted in the highest expression in the tissue. Quantities of plasmid above 25 μ g resulted in diminished expression, which perhaps indicates some cytotoxicity due to locally high plasmid doses.

The luciferase assay used for this study did not provide information about how many cells were transfected. Consequently, the researchers utilized the β -galactosidase reporter gene and flow cytometry to determine that approximately 30% to 35% of the cells within the treated tissue expressed the gene. This value is significantly higher than any other *in vivo* transfection efficiency reported to date. Histologic examination of tissue treated with β -galactosidase followed by nominal fields of 1000 to 1500 V/cm did not result in tissue necrosis. The electrotransfected cells were reported to be randomly distributed throughout the treated tissue.

Another study that used electroporation to facilitate gene uptake in normal liver has been published by Suzuki et al. (40). The study utilized male Wistar rats and a plasmid coding for the green fluorescent protein (GFP) reporter gene. Delivery was conducted intraoperatively by holding a section of the liver between two parallel disk electrodes that were mounted on forceps. The disks were 1 cm in diameter. Plasmid was then injected centrally into the tissue between the electrodes. One to eight rectangular direct current pulses were then applied using a BTX T820 (Genetronics, Inc.) generator at one second intervals. Pulses with either 25-, 50-, or 99-ms durations were applied. Voltages of 25, 50, or 100 V were used. The distance between the two-disk electrodes was approximately 2 mm. Thus, the voltage to electrode spacings used for this study were 125, 250, and 500 V/cm.

Analysis for GFP expression was conducted on specimens that were collected 48 hours after treatment using fluorescent image analysis and laser confocal microscopy. The methods and apparatus used in the study successfully delivered GFP plasmid to the normal liver based on image analysis data. The optimal electrical conditions for delivery were eight 50-V pulses with a duration of 50 ms per pulse. The authors clearly showed increases in expression as the number of pulses was increased from 1 to 8 under these conditions. Also, a dose response with respect to the injected plasmid quantity resulted in increased GFP expression over the 1 to 80 μ g range tested.

Normal liver sections were histologically examined for necrosis in the study of Suzuki et al. (40). It was noted that all samples treated with 100 V pulses (500 V/cm) resulted in extreme cell damage within the tissue between the electrodes. The area of necrosis enlarged as the duration of the 100-V pulses was increased. The necrotized area for samples treated with 100 V conditions was about fivefold greater than the necrotic area in samples treated with 50 V conditions. Results from this study indicated that most of the GFP expressing cells were located within the surviving region of cells near necrotic areas. The authors of the successful study concluded that modifying electrodes, and presumably electrical parameters, to minimize tissue damage and retain efficient gene expression is a desirable future direction of the work.

2.1.2. Muscle

The injection of plasmid DNA directly into skeletal muscle is perhaps the most simple method for gene transfer that has been successful (41,42). It has also been shown that significantly higher levels of protein are produced in muscle that has been treated with cardiotoxin or bupivacaine to induce regeneration before plasmid injection (43,44). Although this method has been successful, relatively low expression levels have limited its application.

A recent study conducted by Aihara and Miyazaki (45) focused on using pulsed electric fields to facilitate the uptake of plasmid DNA by regenerating muscle tissue. The study used the tibialis anterior muscle of mice as a target tissue. Three days before gene delivery, bupivacaine was injected bilaterally into the muscles. β -Galactosidase and interleukin 5 (IL-5) were injected (50- μ g doses) into the muscles. Pulses were applied using a BTX T820 (Genetronics, Inc.) generator and two stainless steel needles that were 5 mm long and 0.4 mm in diameter. Six pulses of 50 ms in duration were administered at 1-second intervals. The first three had the same polarity, and the polarity of the needles was reversed for the second set of three pulses.

Delivery of plasmid coding for IL-5 showed a clear dose dependence with respect to the applied voltage over a 30 to 200 V/cm range. Serum levels of IL-5 increased over this range as the applied field was increased; this dependence was evident on days 5 and 21 posttreatment. Delivery using fields of 300 and 400 V/cm resulted in reduced IL-5 levels at both time points. Maximum IL-5 expression was obtained using 200 V/cm fields; peak expression occurred at 5–7 days following delivery. Serum IL-5 concentrations resulting from these optimal delivery conditions were approximately 120 times that of control samples that received plasmid injection alone 5 days after treatment. The authors noted that expression decreases that resulted when higher fields were used were probably due to muscle damage induced by the fields.

Expression of IL-5 was detected for up to 6 wk after delivery in some samples which indicates the potential for long-term benefit. Also, IL-5 expression was the same when a field of 200 V/cm was applied in either the longitudinal or transverse direction relative to the muscle fibers. The authors also indicated that the use of bupivacaine pretreatment did not enhance expression of the plasmid using a suboptimal field for delivery. Expression of the *lacZ* reporter gene was used to confirm that electric pulses enhanced the number of expressing muscle fibers as well as the density of staining when compared to samples that received plasmid injection alone.

2.1.3. Skin

The earliest published work that utilized pulsed electric fields *in vivo* to deliver genes was conducted by Titomirov et al. (46). The study utilized two functional plasmids. One coded for the neomycin resistance gene and SV40 large T antigen. The other coded for the E1A region of adenovirus 2 which immortalizes rodent cells when expressed. The aim of the study was to demonstrate *in vivo* electrically mediated gene delivery of both plasmids that code for functional molecules. Newborn CBA mice (1–3 days of age) were treated with a combined dose of the plasmids. Neomycin resistance plasmid doses ranged

from 2 to 12.5 μg per treatment; E1A plasmid doses ranged from 10 to 12.5 μg . Injections were made subcutaneously. Then, the skin was pleated at the site of injection and a rectangular (2 cm^2) electrode was placed on either side of the skinfold. Pulses were administered 10 to 60 minutes after plasmid injection. Two exponentially decaying pulses of opposite polarity were administered for each treatment. The length of each pulse ranged from 100 to 300 μs . The applied field ranged from 400 to 600 V/cm .

The strategy for proving expression of both plasmids involved harvesting the treated tissue and placing the skin cells into selective cell culture conditions. Selection consisted of placing the antibiotic G418 into the media. This antibiotic ensures that only cells that express the neomycin resistance gene survive. Selection was started between 24 and 168 hours after the treated skin cells were placed into culture. Transformation efficiencies were computed by dividing the number of neomycin resistant colonies by the total number of attached cells 16 hours after seeding. Efficiencies ranging from 0.2×10^{-4} to 7.0×10^{-4} were obtained.

Zhang et al. (47) focused their study on the delivery of the *lacZ* gene into the skin of hairless mice. The study methods included a 40- μg dose of the plasmid applied topically to both sides of a skin fold. This skin fold was then clamped between two rectangular parallel plates (1 cm^2 each) that were mounted on a Vernier caliper. Three exponentially decaying pulses with a 120 V amplitude were applied to the skin fold using a electroporation generator (ECM 600; Genetronics, Inc.). The length of the applied pulses was either 10 ms or 20 ms, and the distance between the electrodes was approximately 1 mm. Pressure from the calipers was maintained for either 1- or 10-minute intervals after pulsing as a driving force for gene penetration into the skin. Biopsies and standard histologic techniques were utilized to examine the maximum depth at which expression was observed and the number of cells expressing the reporter gene within the skin.

The study indicated that longer pulse durations and maintaining pressure for a longer time led to increased success. This increased success was realized both in the depth of expression and the number of expressing cells. Application of 20 ms pulses and pressure for 10 minutes after pulsation resulted in a greater than twofold increase in the depth of expression below the epidermis. A maximum expression depth of 370 μm was achieved. Control samples that were subjected to topical gene application and pressure only had a maximum expression depth of 160 μm . Microscopic analysis for the number of expressing cells revealed that 20-ms pulses and pressure for 10 minutes resulted in 457 expressing cells per square millimeter. The control samples, gene and pressure only, had only 27 cells per square millimeter expressing the reporter gene.

2.1.4. Testes

Gene transfer into germ cells was accomplished by Muramatsu et al. (48). The study investigated the use of fields to deliver genes to the testes of ICR mice. The primary goal of the study was to develop a method for gene transfer into spermatogenic cells with an ultimate goal of producing transgenic animals. Reporter genes that coded for chloramphenicol acetyltransferase (CAT) and *lacZ* were utilized. A 10- μg dose of the plasmid coding for CAT was injected directly into the surgically exposed testis of the mice. Similarly, a 150- μg dose of *lacZ* plasmid was administered. Two electrodes fixed to a tweezer-type device (personal communication) were positioned on either side of the testes; the spacing of these electrodes was between 6 and 8 mm. Eight rectangular direct current pulses were applied for each treatment using a BTX T820 generator (Genetronics, Inc.). Voltages ranging from 0 to 100 V and pulse durations ranging from 0 to 50 ms were utilized.

The study results indicated that CAT activity was achieved 48 hours after transfection. Maximum activity was reported from 100 V pulses with a duration of 10 ms. Since the CAT assay did not reveal expression in individual cells, the expression of *lacZ* plasmid was detected with standard histologic methods to identify cells that were successfully transfected. Spermatogeniclike cells in the seminiferous tubules were shown to express the *lacZ* reporter.

2.2. Gene Delivery to Malignant Tissues

2.2.1. Brain Tumors

Nishi et al. (49) published a study in which the *lacZ* gene was transferred to the brain tumors and tissue in Wistar Rats. Tumors were induced by injecting cultured C6 rat glioma cells 10 days before treatment. Treatment consisted of inserting a pair of gold plated needle electrodes (0.5 mm in diameter and 5 mm in length) into the brain; one needle was placed on either side of the established tumors. The animals were electrically treated with eight rectangular 95 to 99 μs pulses administered by a BTX T820 (Genetronics, Inc.). The applied voltage was set, based on resistivity measurements, so that a current of 0.5 mA would result. The average applied voltage was 300 V per 0.5 cm of electrode spacing which translates to a 600 V/cm voltage to electrode spacing ratio. In contrast to most delivery methods that use electroporation, Nishi injected the *lacZ* plasmid dose immediately after electrical treatment was complete. Plasmid DNA was injected through the cannulated right carotid artery.

Histologic studies of samples harvested 3 days after gene transfer showed *lacZ* expression within the tumor tissue. More specifically, very high expression resulted in the border regions of the tumor and vascular walls. Expression

was more intense in tumor cells that were near vessel walls and less intense in the bulk of the tumor. No expression was detected in the brain tissue adjacent to the electroporated region. Expression was not noted in samples that received partial treatment in the form of electric pulses only. Plasmid injection alone resulted in expression in several cells within vascular structures. Tail vein injections of plasmid followed by pulses resulted in expression in only a few tumor cells in the brain.

The study of Nishi et al. (49) also utilized intraarterial plasmid injection immediately after pulse delivery to established C6 rat gliomas in order to deliver plasmid coding for human monocyte chemoattractant protein-1 (MCP-1). The plasmid used for this phase of the study included an origin of replication which allowed replication of the plasmid within the transfected cell. Immunohistochemistry was employed to determine the presence of the MCP-1 protein in rat brain sections. This analysis was conducted three weeks after treatment. This assay revealed MCP-1 protein only in animals that received both pulses and intraarterial MCP-1 plasmid. Animals that did not receive plasmid and pulses did not express the protein. In addition to expression, the chemoattractant protein appeared to be functional. A significantly large numbers of macrophages and lymphocytes were observed at the tumor periphery and within the tumor tissue.

2.2.2. Melanoma

A study conducted by Rols et al. (50) focused on delivering plasmid coding for β -galactosidase under control of the SV40 promoter into tumors in a murine model. Tumors were induced by transplanting fragments of B16 B1/6 murine melanoma tumors subcutaneously into B₆D₂F₁ female mice. Tumor treatment was conducted by first injecting a 12- μ g dose of plasmid into the center of the tumor and then placing two stainless steel electrodes in contact with the skin adjacent to the tumors. The electrodes were 20 mm long and 0.6 mm wide. One electrode was placed on either side of the tumors; electrocardiography paste was used to assure electrically conductive contact between the electrodes and skin. The distance between the electrodes was 4.2 mm. Electrical treatment consisted of ten 5-ms DC pulses administered at one second intervals by a rectangular wave generator (Jouan; St. Herblain, France).

Tumors were harvested 3 days after treatment and the cells were dissociated using a mechanical tissue disrupter and placed directly into culture. Three days later, direct observation was used to quantitate the number of cells expressing β -galactosidase. Voltages of 294, 336, and 378 V applied across the 4.2-mm electrode spacing (700–900 V/cm) resulted in detectable expression. The maximum percentage of β -galactosidase positive cells was 4% and was obtained by

applying 336 V across the electrodes. Higher and lower voltages resulted in 1–2% of the cells expressing the reporter gene. These data were confirmed using optical density measurements.

3. Summary and Conclusions

The studies reviewed above successfully delivered genes coding for luciferase, CAT, IL-5, β -galactosidase, GFP, MCP-1, SV40 large T antigen, and the E1A region of the adenovirus 2 to normal and malignant tissues in animal models. The fact that all of the studies focused on developing delivery protocols clearly indicates that this technology is in its infancy. But, success in a variety of different tissues is highly encouraging for potentially developing gene based therapies for the treatment of many different human diseases.

The use of electric fields to mediate gene delivery *in vivo* has several clear advantages. First, expression was noted only in cells that were electrically treated in the presence of plasmid DNA. This has been accomplished by pulsing a volume of tissue after perfusion with plasmid or by administering the DNA shortly after electropulsation. Thus, the nature of applying electric fields to the target tissue is a means of site specific gene delivery that assures expression to the cells/tissue of interest. Second, the use of plasmid DNA simplifies gene preparation, relative to using viruses, and also places few restrictions on the size of the gene for delivery. This, in turn, makes it much easier to test existing as well as new genes. An additional degree of specificity can be achieved by using tissue specific promoters on the delivered plasmid. Finally, the physical nature of electroporation makes this type of delivery applicable to all tissue types. This is demonstrated by the successful delivery of DNA to liver, testes, muscle, brain tumors, cutaneous tumors, and skin.

One interesting aspect of electric field mediated gene delivery is the difference in protocols that were used. Three studies used needle electrodes and the remainder utilized parallel plate electrodes. Pulse durations ranging from 100 μ s to 50 ms have been used successfully. Both rectangular and exponentially decaying pulses have produced excellent results at field strengths ranging from about 70 to 1500 V/cm. Optimal parameters exist for every particular delivery situation and cell type. Identifying these parameters was one goal of each presented study. However, a range of parameters did lead to successful delivery of genes in all of the studies detailed above. The ranges of parameters used to deliver genes indicates that a single highly specific protocol is not necessary to obtain positive results.

The future of this technology is quite promising. The studies reviewed in this paper clearly demonstrate that electric fields can be used to deliver genes efficiently. They also provide a foundation that can be used for further devel-

opment. Preclinical efficacy studies are a logical future direction of this technology. These types of studies are needed to determine if the expression levels that can be achieved will result in therapeutic benefit. These studies will also begin the maturation process from the laboratory to the clinic.

References

1. Coster, H. G. L. (1965) A quantitative analysis of the voltage-current relationships of fixed charge membranes and the associated property of "punch-through." *Biophys. J.* **5**, 669–686.
2. Sale, A. J. H. and Hamilton, W. A. (1967) Effects of high electric fields on microorganisms. I. Killing of bacteria and yeasts. *Biochem. Biophys. Acta* **148**, 781–788.
3. Sale, A. J. H. and Hamilton, W. A. (1968) Effects of high electric fields on microorganisms II. lysis of erythrocytes and protoplasts. *Biochem. Biophys. Acta* **163**, 37–43.
4. Pohl, H. A. and Crane, J. S. (1971) Dielectrophoresis of cells. *Biophys. J.* **11**, 711–727.
5. Crowley, J. M. (1973) Electrical breakdown of bimolecular lipid membranes as an electromechanical instability. *Biophys. J.* **13**, 711–724.
6. Zimmermann, U., Pilwat, G., and Friemann, F. (1974) Dielectric breakdown of cell membranes. *Biophys. J.* **14**, 881–899.
7. Prausnitz, M. R., Lau, B. S., Milano, C. D., Conner, S., Langer, R., and Weaver, J. C. (1993) A quantitative study of electroporation showing a plateau in net molecular transport. *Biophys. J.* **65**, 414–422.
8. Hibino, M., Shigemori, M., Itoh, M., Hagayama, K., and Kinoshita, K. (1991) Membrane conductance of an electroporated cell analyzed by submicrosecond imaging of transmembrane potential. *Biophys. J.* **59**, 209–220.
9. Chang, D. C. and Reese, T. S. (1990) Changes in membrane structure induced by electroporation as revealed by rapid-freezing electron microscopy. *Biophys. J.* **58**, 1–12.
10. Neumann, E., Sowers, A. E., and Jordan, D. A. (1989) *Electroporation and Electrofusion in Cell Biology*. Plenum, New York.
11. Teissié, J. and Rols, M. P. (1992) Time course of electroporation. In: *Charge and Field Effects in Biosystems*, Vol. 3 (Allen, M. J., Cleary, S. F., Sowers, A. E., and Shillady, D., eds.) Birkhauser, Boston, pp. 285–301.
12. Fong, S. K. H. and Perkins, S. (1989) Electric field-induced cell fusion and human monoclonal antibodies. *J. Immunol. Methods* **116**, 117–122.
13. Lo, M. M. S., Tsong, T. Y., Conrad, M. K., Strittmatter, S. M., Hester, L. D., and Snyder, S. H. (1984) Monoclonal antibody production by receptor-mediated electrically induced cell fusion. *Nature* **310**, 792–794.
14. Teissié, J., Knutson, V. P., Tsong, T. Y., and Lane, M. D. (1982) Electric pulse-induced fusion of 3T3 cells in monolayer culture. *Science* **216**, 537–538.
15. Jaroszeski, M. J., Gilbert, R., Fallon, P. G., and Heller, R. (1994) Mechanically facilitated cell-cell electrofusion. *Biophys. J.* **67**, 1574–1581.

16. Heller, R. and Grasso, R. J. (1990) Transfer of human membrane surface components by incorporating human cells into intact animal tissue by cell-tissue electrofusion in vivo. *Biochem. Biophys. Acta* **1024**, 185–188.
17. Grasso, R. J., Heller, R., Cooley, J. R., and Haller, E. M. (1989) Electrofusion of individual animal cells directly to intact corneal epithelial tissue. *Biochem. Biophys. Acta* **980**, 9–14.
18. Mouneimne, Y., Pierre-Francois, T., Barhoumi, R., and Nicolau, C. (1991) Electroinsertion of xeno proteins in red blood cell membranes yields a long lived protein carrier in circulation. *Biochim. Biophys. Acta* **1066**, 83–89.
19. Mouneimne, Y., Pierre-Francois, T., Barhoumi, R., and Nicolau, C. (1990) Electroinsertion of full length recombinant CD4 into red blood cell membrane. *Biochim. Biophys. Acta* **1027**, 53–58.
20. Orłowski, S., Belehradec, J. Jr., Paoletti, C., and Mir, L. M. (1988) Transient electroporeabilization of cells in culture. *Biochem. Pharmacol.* **37**, 4727–4733.
21. Zheng, Q. and Chang, D. C. (1991) High-efficiency gene transfection by in situ electroporation of cultured cells. *Biochem. Biophys. Acta* **1088**, 104–110.
22. Sukharev, S. I., Klenchin, V. A., Serov, S. M., Chernomordik, L. V., and Chizmadzhev, Y. A. (1992) Electroporation and electrophoretic DNA transfer into cells. *Biophys. J.* **63**, 1320–1327.
23. Klenchin, V. A., Sukharev, S. I., Serov, S. M., Chernomordik, L. V., and Chizmadzhev, Y. A. (1991) Electrically induced DNA uptake by cells is a fast process involving DNA electrophoresis. *Biophys. J.* **60**, 804–811.
24. Okino, M. and Mohri, H. (1987) Effects of a high-voltage electrical impulse and an anticancer drug on in vivo growing tumors. *Jpn. J. Cancer Res.* **78**, 1319–1321.
25. Mir, L. M., Orłowski, O., Belehradec, J. Jr., and Paoletti, C. (1991) Electrochemotherapy potentiation of antitumor effect of bleomycin by local electric pulses. *Eur. J. Cancer* **27**, 68–72.
26. Serša, G., Novakovic, S., and Miklavčič, D. (1993) Potentiation of bleomycin antitumor effectiveness by electrotherapy. *Cancer Lett.* **69**, 81–84.
27. Heller, R., Jaroszeski, M., Leo-Messina, J., Perrott, R., Van Voorhis, N., Reintgen, D., and Gilbert, R. (1995) Treatment of B16 melanoma with the combination of electroporation and chemotherapy. *Bioelectrochem. Bioenerg.* **36**, 83–87.
28. Jaroszeski, M. J., Gilbert, R., and Heller, R. (1997) Electrochemotherapy: an emerging drug delivery method for the treatment of cancer. *Adv. Drug Deliv. Rev.* **26**, 185–197.
29. Mir, L. M., Belehradec, M., Domenge, C., Orłowski, S., Poddevin, J. Jr., Schwab, G., Luboinnski, B., and Paoletti, C. (1991) Electrochemotherapy, a novel antitumor treatment: first clinical trial. *C. R. Acad. Sci. Paris* **313**, 613–618.
30. Belehradec, M., Domenge, C., Luboinnski, B., Orłowski, S., Belehradec, J., and Mir, L. M. (1993) Electrochemotherapy, a new antitumor treatment. *Cancer* **72**, 3694–3700.
31. Domenge, C., Orłowski, S., Luboinnski, B., DeBaere, T., Schwaab, G., Belehradec, J. Jr., and Mir, L. M. (1996) Antitumor electrochemotherapy. *Cancer* **77**, 956–963.

32. Heller, R., Jaroszeski, M. J., Glass, L. F., Messina, J. L., Rapaport, D. P., DeConti, R. C., Fenske, N. A., Gilbert, R. A., Mir, L. M., and Reintgen, D. S. (1996) Phase I/II trial for the treatment of cutaneous and subcutaneous tumors using electrochemotherapy. *Cancer* **77**, 964–971.
33. Heller, R., Jaroszeski, M. J., Reintgen, D. S., Puleo, C. A., DeConti, R. C., Gilbert, R. A., and Glass, L. F. (1998) Treatment of cutaneous and subcutaneous tumors with electrochemotherapy using intralesional bleomycin. *Cancer* **83**, 148–157.
34. Rudolf, Z., Štabuc, B., Čemažar, M., Miklavčič, D., Vodovnik, L., and Serša, G. (1995) Electrochemotherapy with bleomycin: The first clinical experience in malignant melanoma patients. *Radiol. Oncol.* **29**, 229–235.
35. Feuerbach, F. J. and Crystal, R. G. (1996) Progress in human gene therapy. *Kidney Int.* **49**, 1791–1794.
36. Vile, R. C. (1996) Gene therapy for cancer: In the dock, blown off course or full speed ahead? *Cancer and Metastasis Rev.* **15**, 283–286
37. Dranoff, G. (1997) Gene therapy 1996. *Biochem. Biophys. Acta* **1332**, R21–R24.
38. Fouillard, L. (1996) Physical methods for gene transfer: An alternative to viruses. *Hematol. Cell Ther.* **38**, 214–216.
39. Heller, R., Jaroszeski, M., Atkin, A., Moradpour, D., Gilbert, R., Wands, J., and Nicolau, C. (1996) In vivo gene electroinjection and expression in rat liver. *FEBS Lett.* **389**, 225–228.
40. Suzuki, T., Shin, B., Fujikura, K., Matsuzaki, T., and Takata, K., (1998) Direct gene transfer into rat liver cells by in vivo electroporation. *FEBS Lett.* **425**, 436–440.
41. Wolff, J. A., Malone, R. W., Williams, P., Chong, W., Ascadi, G., Jani, A., and Felgner, P. L. (1990) Direct gene transfer into mouse muscle in vivo. *Science* **247**, 1465–1468.
42. Wolff, J. A., Ludtke, J. J., Ascadi, G., Williams, P., and Jani, A. (1992) Long-term persistence of plasmid DNA and foreign gene expression in mouse muscle. *Hum. Mol. Genet.* **1**, 363–369.
43. Vitadello, M., Schiaffino, M.V., Picard, A., Scarpa, M., and Schiaffino, S. (1994) Gene transfer in regenerating muscle. *Hum. Gene Ther.* **5**, 11–18.
44. Wells, D. J. (1993) Improved gene transfer by direct plasmid injection associated with regenerations in mouse skeletal muscle. *FEBS Lett.* **332**, 179–182.
45. Aihara, H. and Miyazaki, J., (1998) Gene transfer into muscle by electroporation in vivo. *Nat. Biotechnol.* **16**, 867–870.
46. Titomirov, A. V., Sukharev, S., and Kistanova, E. (1991) In vivo electroporation and stable transformation of skin cells of newborn mice by plasmid DNA. *Biochem. Biophys. Acta* **1088**, 131–134.
47. Zhang, L., Lingna, L., Hofmann, G. A., and Hoffman, R. M. (1996) Depth-targeted efficient gene delivery and expression in the skin by pulsed electric fields: an approach to gene therapy of skin aging and other diseases. *Biochem. Biophys. Res. Commun.* **220**, 633–636.

48. Muramatsu, T., Shibata, O., Ryoki, S., Ohmori, Y., and Okumura, J. (1997) Foreign gene expression in the mouse testis by localized in vivo gene transfer. *Biochem. Biophys. Res. Commun.* **233**, 45–49.
49. Nishi, T., Kimio, Y., Yanashiro, S., Takeshima, H., Sato, K., Hamada, K., Kitamural, I., Yoshimura, T., Saya, H., Kuratsu, J., and Ushio, Y. (1996) High-efficiency in vivo gene transfer using intraarterial plasmid DNA injection following in vivo electroporation. *Cancer Res.* **56**, 1050–1055.
50. Rols, M. P., Delteil, C., Golzio, M., Dumond, P., Cros, S., and Teissié, J. (1998) In vivo electrically mediated protein and gene transfer in murine melanoma. *Nat. Biotechnol.* **16**, 168–171.

Mechanism of Transdermal Drug Delivery by Electroporation

Timothy E. Vaughan and James C. Weaver

1. Introduction

Human skin is a complex system, providing a formidable obstacle to drug delivery (**Fig. 1**) (1–3). In particular, the stratum corneum (SC) is the primary barrier to transdermal drug delivery. The stratum corneum is made up of corneocytes, which are flattened remnants of cells, surrounded by lipid bilayer membranes (2,3). Because lipid-based structures tend to exclude charged species, the multilamellar arrangement acts as a “brick wall” (4) to prevent ionic and molecular transport.

Controlled molecular transport through or around this barrier is widely viewed as a main objective of transdermal drug delivery (1,5–8). Electroporation, the creation of aqueous pathways across lipid-based systems by elevating the membrane potential, has been used to temporarily break down the skin’s barrier function. The electric field used to porate the skin also provides a driving force for transdermal transport of small ions and water soluble molecules. Evidence for electroporation exists for many biological systems. Membrane electroporation is widely used in cells (9–12). Viable frog skin undergoes electroporation (13), and several investigators have used electroporation *in vivo* to treat solid cancer tumors (14–19), or to introduce DNA into tissues (20–25). There is now considerable evidence that moderate voltage (MV) and high voltage (HV) pulses rapidly cause large increases in ionic and molecular transport across human skin (26–45), although in some cases transport into (but not through) the SC is reported (46,47).

The original “brick wall model” (**Fig. 1**) was introduced to describe passive permeation of lipophilic molecules across the SC (4), in which transported

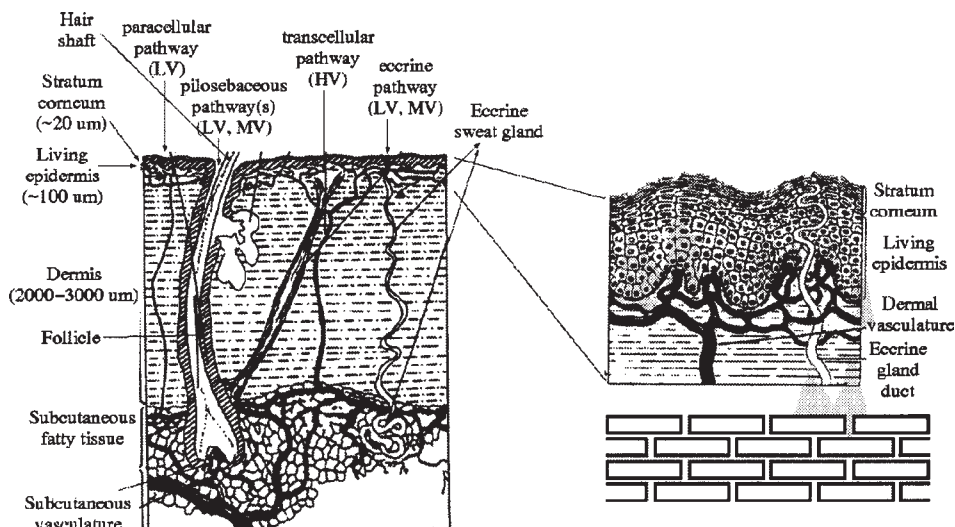


Fig. 1. Key features of skin, skin barriers (104) and hypothetical aqueous pathways. The stratum corneum (SC) is the dead outermost layer ($\approx 20 \mu\text{m}$ hydrated thickness) that is the main barrier to transport, particularly for charged molecules (1–3,5). Appendages (sweat ducts and hair follicles) penetrate the SC, but are lined with a double cell layer with tight junctions (105), which prevents significant transport. Hypothetical transport sites are labeled: LV (low voltage): Iontophoresis involves transport through preexisting aqueous pathways associated with appendages or around corneocytes within the SC (7,8,53,55,106). MV (moderate voltage) pulses: A relatively fast ($>10 \text{ ms}$) process of “macropore activation” is followed by cell lining electroporation, which is hypothesized to create new aqueous pathways at appendages (“appendageal electroporation”) (40,107). HV (high voltage) pulses: A very fast ($<10 \mu\text{s}$) process is hypothesized to involve a primary event of aqueous pathway creation based on electroporation of multilamellar lipid bilayers separating corneocytes (27,61,63,91,108), and secondary processes such as localized heating, or pathway-enlarging chemical introduction. Lower right: The original “brick wall model” of the SC (the largest area skin feature) intended to treat permeation of lipophilic molecules through the continuous “mortar” (4).

species mainly follow tortuous lipid-based pathways. In contrast, to consider the skin electroporation hypothesis it is essential to describe the development of voltages across lipids as MV or HV pulses are applied. Moreover, once the spontaneous localization of molecular transport by HV pulses was discovered (48), it became important to think about how spatially localized electroporation could occur within the SC. A modified brick wall model was introduced (49), featuring a more anatomically accurate but still idealized geometry (50,51) for the lipid bilayer membranes (the “mortar”) and the corneocytes (the “bricks”).

Two types of experimental information are relevant: (1) electrical behavior, due to the movement of small ions such as Na^+ and Cl^- , and (2) molecular transport, particularly fluorescent molecules, which can be measured in real time with a temporal resolution somewhat less than 1 min, and a spatial resolution prescribed by ordinary and confocal fluorescence microscopy. Both types of information have been obtained, but because of the well known variability within and between biological samples, experiments that obtain both types of information from the same preparation are particularly valuable.

When skin is pulsed electrically, only a fraction of a voltage applied across application electrodes appears across the biological system of interest. This division of an applied voltage across different resistances is a “voltage divider effect” (6), well established in electrical engineering. Electrochemical systems have the additional complication that resistances of electrode/electrolyte interfaces have complicated behavior, with resistance dependent on many factors, including current density. Thus, the divider effect is usually variable because at least one of the resistances is dependent on the current density, and will therefore change its resistance during pulsing. This basic experimental issue has been recognized and treated for in vitro cell electroporation protocols (52), but is often neglected for in vivo cell electroporation experiments. A similar but more complex problem arises for voltage stimulation of skin. A variable voltage divider arises in which the electrode voltage is split among three regions:

1. The electrode/electrolyte interface, particularly for HV pulses, which involve large current densities during the pulse
2. The electrolyte, which separates the electrodes and the skin
3. The skin itself, wherein most of the transdermal voltage within microseconds appears almost entirely across the SC.

Some skin electroporation experiments have quantitatively corrected for the variable voltage divider effect, by making measurements that allow the transdermal voltage, U_{skin} , to be determined through measurement and calculation (33,34,41,42,48). Determination of U_{skin} can be accomplished by using separate, nearby measurement electrodes in addition to the pulsing electrodes, and also making a correction for the voltage drop across the electrolyte between the measurement electrodes and the skin. In experiments that determine U_{skin} , typically about $100 \pm 50\text{V}$ appears across the SC.

1.1. Response of Skin to Low, Medium, and High Voltages

When describing the response of skin to voltage stimulation, it is useful to categorize the stimulation as low-, medium-, or high-voltage (6). Although these designations are approximate, it is still a useful distinction.

Low-voltage (LV) stimulation of the skin ($U_{\text{skin}} \leq 5$ V) results in iontophoresis (7,8,53). Such voltages are usually applied continuously, to provide ionic and molecular transport that is believed to take place mainly through preexisting pathways (7,8,53–55). Localized iontophoresis involving appendages (“macropores”) has been reported (56,57). These observations are consistent with staining of skin appendages by charged fluorescent molecules after prolonged exposure to low voltages (48), and the absence of significant transport of the same molecules (calcein and sulforhodamine) across snake skin, which has no appendages (41). There are also, however, reports of relatively nonlocalized transport (58). Overall, experimental evidence appears to support the view that spatially localized iontophoresis at LV occurs at appendages, whereas HV transport of charged molecules is concentrated at local transport regions (LTRs), which form away from appendages.

Note that the variable voltage divider effect mentioned above is potentially important in iontophoresis experiments. For example, if a current clamp protocol is used, a skin specimen with a high resistance may be exposed to a maximum output voltage of tens of volts. If so, inadvertent electroporation might occur within the first few tens of microseconds of reaching full voltage output, and the experiment then carried out on inadvertently altered skin. This problem can be avoided by slowly increasing the voltage available for current regulation.

Medium-voltage (MV) stimulation of the skin ($5 \leq U_{\text{skin}} \leq 50$ V) has been explored recently in a combined theoretical and experimental study (40). Electrical behavior for moderate pulses was treated theoretically by considering two parallel transport pathways: one (straight-through) crosses the multilamellar lipid bilayers and corneocytes within the SC, and the other involves the appendages (Fig. 1). The appendageal ducts were represented by tubes with distributed electrical parameters. Nonlinear equations take into account the electroporation of lipid lamella, or electroporation of cell layers which line the appendageal ducts. Numerical solutions to these equations were compared with both literature results and the companion experiments, with remarkable agreement. This theoretical analysis showed that the observed drop in R_{skin} is consistent with electroporation within appendages or the SC. For $U_{\text{skin}} < 30$ V, a decrease in R_{skin} of up to three orders of magnitude is attributed to electroporation of the duct lining. For larger voltage pulses there is an additional decrease in R_{skin} due to the formation of straight-through pathways within the SC (see below). Recent studies of the transport of fluorescent molecules are generally consistent with a transition from appendageal electroporation at moderate voltages, and a predominant contribution of SC electroporation at high voltages (41,42,59).

Most skin electroporation studies to date have used high-voltage (HV) stimulation of the skin ($U_{\text{skin}} \geq 50$ V), so this chapter will primarily focus on the mechanisms relevant to this voltage range. Experiments in this range are characterized by relatively large transdermal transport of ions and molecules, and very rapid decrease in R_{skin} , typically occurring within a few microseconds. Onset of molecular transport typically requires several tens of seconds (28,44), which is much faster than onset times for iontophoresis (which in turn is much more rapid than passive permeation).

An interesting feature of the skin's response to HV pulses is highly localized molecular transport, revealed by real time video imaging for fluorescent molecules (48). Other studies that characterized skin fluorescence after pulsing in the presence of fluorescent molecules also found sites of localized molecular transport (31,41,46,59,60). For "short" pulses, typical minimum LTR size is about 100 μm in diameter; "long" pulses lead to much larger LTR sizes (45,59,60). A study of snake skin, which has no appendages, revealed LTRs for HV pulsing in the presence of fluorescent molecules, but had insignificant molecular transport for LV iontophoresis conditions (41).

2. Aqueous Pathway Creation by HV Pulsing

As stated above, the electroporation hypothesis has been successful at describing phenomena involving molecular transport across a variety of lipid bilayer systems. The essential part of the hypothesis is that an elevated transmembrane voltage favors entry of water into a deformable membrane, and the aqueous pathways created greatly decrease the barrier for ion entry into the membrane. Furthermore, the electric field within the pathway drives transport. This hypothesis has been much more successful at explaining experimental results than a competing idea of continuum compression of a lipid bilayer membrane (62,63).

2.1. Description of Electropores

Basic aspects of a transient aqueous pore model have been recently reviewed (63), so only major features of lipid bilayer membrane theory are presented here. A fluid lipid bilayer membrane has conformational changes that can be occasionally reached by random thermal fluctuations. The first suggestions that transient aqueous pores could be created in lipid bilayer membranes were based on thermal fluctuations alone (64,65). Both spontaneous membrane rupture and "flip-flop" translocations of bilayer molecules were suggested, but the possible role of the transmembrane voltage was not considered.

The first theory of electroporation was presented within a series of seven consecutive papers that combined experiments and theory to explain the

essential features of irreversible membrane breakdown (“rupture”) in artificial planar bilayer membranes (62,66–71). An aqueous pore can be modeled as a cylinder (radius r_p) of membrane that is removed from a lipid membrane. (This is known as the “cookie cutter” model.) This involves an energy change in the membrane, with two contributions: (i) There is an “edge energy” from the formation of a deformed, stressed pore edge of length $2\pi r_p$. If the energy cost per length is γ , then cost to create the deformed edge is $2\pi r_p \gamma$; (ii) If a membrane area πr_p^2 is removed, and the membrane interfacial energy per area is Γ , then the membrane energy is changed by $-\pi r_p^2 \Gamma$, which is a decrease. The total free energy change is

$$\Delta W_p(r_p) = 2\pi\gamma r_p - \pi\Gamma r_p^2 \text{ at } U_m = 0, \quad (1)$$

where U_m is the membrane voltage. **Equation 1** describes a barrier for pore expansion. As pores are first created, and then expanded by additional thermal fluctuations, one or more pores may reach the barrier peak, and then expand indefinitely. This is tantamount to membrane rupture. Without a large U_m , thermal fluctuations were hypothesized to create pores, but the probability of surmounting the barrier is very small.

The effect of elevating U_m on a pore is described by considering the free energy change that accompanies the change of its specific capacitance, $C_{1 \rightarrow w}$ (62). It is energetically costly for ions to enter small pores ($r_p \approx 1$ nm), because the charge of the ion is brought close to the low dielectric constant lipids. Because small ions are the electrical current carriers their exclusion means that a pore’s electrical resistance, $R_p = \rho_e d_m / \pi r_p^2$, is large. With this in mind a small pore was initially modeled as a water-filled, rather than electrolyte-filled, capacitor. However, for small hydrophilic pores, even if bulk electrolyte exists within the pores, the permittivity would be $\epsilon \approx 70\epsilon_0$, about ten percent smaller than the permittivity of pure water. Thus, small pores transport ions relatively poorly.

A small pore’s high resistance is also large relative to the spreading resistance, and microscopic, localized variable voltage divider effect. The local voltage across a pore, $U_{p,local}$, is close to U_m , so that nearly all of U_m appears across the pore, and the free energy of pore formation is (62)

$$\Delta W_p(r_p, U_m) = 2\pi\gamma r_p - \pi\Gamma r_p^2 - 0.5\pi C_{1w} U_m^2 \pi r_p^2, \quad (2)$$

where C_{1w} is the capacitance change per area for a pore. In subsequent transient aqueous pore models $U_{p,local}$ was used (72–74), which explicitly recognizes that some ion conduction occurs, and that conduction is larger for larger pores.

The specific capacitance change due to water replacing lipid as a pore forms is

$$C_{1w} = C_0 \left[\frac{\epsilon_w}{\epsilon_m} - 1 \right]. \quad (3)$$

Here $C_0 = \epsilon_m/d_m$ is the capacitance per area of a pore-free lipid bilayer of thickness d_m , and $\epsilon_w = K_w \epsilon_0$ and $\epsilon_m = K_l \epsilon_0$ are the permittivities of water and lipid, respectively. Using usual values of $K_l \approx 2$ and $K_w \approx 80$, the barrier $\Delta W_p(r_p, U)$ is found to become smaller as the voltage increases.

2.2. Dynamics of the Pore Population

No detailed molecular-level theory for pore creation yet exists. In spite of this, progress has been made using a phenomenological estimate of the creation rate. The theoretical description of pore creation contains a Boltzmann factor and its prefactor, $v_0 V_m$, which is the attempt rate for overcoming the pore creation barrier (75). v_0 is an estimate of the attempt rate density, based on a collision frequency density. The order of magnitude of v_0 was obtained by estimating the volume density of collisions per time in the fluid membrane. V_m is the volume of the membrane. It is plausibly assumed that pores are created independently of each other, except through indirect coupling via $U_m(t)$, which interacts through the membrane conductance due to all of the pores. In lieu of its solution, it is assumed that a voltage-dependent energy barrier must be overcome (74). How pores disappear from a membrane is not well understood in any detail. A plausible assumption is that individual pore disappearance occurs independently of other pores, because pores are widely spaced even when a large number of pores exist, and the total (aqueous) area of the membrane is at a maximum (74). The rate of pore destruction can be written as proportional to the number of pores present, to a Boltzmann factor, and to an attempt rate. This approximate treatment has contributed to reasonable theoretical descriptions of some experimental behavior.

In the absence of thermal fluctuations, all pores would quickly shrink to the radius corresponding to the energy minimum of **Eq. 2** and remain at the size. Instead, thermal fluctuations lead to a distribution of pore sizes. This broadening is counteracted by the increase in energy required for larger pores. A dynamic pore population is expected, with some pores appearing and expanding, with others shrinking and disappearing. A mathematical description of these dynamics is based on a one-dimensional probability flux, J_p , in pore radius space, and involves a partial differential equation that describes the pore population (76). This theory involves D_p , a diffusion constant for pore size in pore radius space, and a description of pore population evolution which arises from fundamental equations that are believed to describe the essential features of transient aqueous pores. Additional interactions in cell membranes is expected to yield a more complicated situation.

Pores are prevented from growing in size by an energy barrier. The barrier height is

$$\Delta W_{p, \max} = \frac{\pi\gamma^2}{\Gamma + 0.5C_{lw}U_m^2}, \quad (4)$$

and occurs at a “critical radius” of (62),

$$r_{p,c} = \frac{\gamma}{\Gamma + 0.5C_{lw}^2}. \quad (5)$$

Pores that reach the critical radius will grow without bound. At $U_m = 0$ the barrier is high, and the chance of a pore becoming “supracritical” is tiny. As U_m becomes larger, however, the barrier height decreases, and the critical radius becomes smaller. So the probability of the membrane acquiring one or more pores with $r_p > r_{p,c}$ (due to stochastic fluctuations) increases. But creation of even one supracritical pore is sufficient to rupture the membrane, through expansion until it reaches the macroscopic aperture that defines the planar membrane, all of the membrane material collects at the aperture, and the membrane is no longer present. Rupture depends nonlinearly on U_m ; even a moderate increase in U_m can destabilize a planar membrane. It should be noted that in skin electroporation, it is presumably possible that the bilayer lipid membranes could rupture, but the keratin matrix within the corneocytes should remain intact.

The average membrane lifetime has been described in detail (66), and by a simpler theory (75). In the latter an absolute rate equation was used to estimate the rate of critical pore appearance.

A Boltzmann factor, $\Delta W_p/\kappa T$, and an order of magnitude estimate for its prefactor was used, yielding

$$\bar{\tau} \approx \frac{1}{\nu_0 V_m} \exp [+ \Delta W_{p,c}/\kappa T]. \quad (6)$$

If a plausible mean lifetime, $\bar{\tau}_m \approx 1$ s is used, the magnitude of $\Delta W_{p,c}$ can be estimated, and from that, $U_{m,c}$, the approximate critical voltage for rupture. It should be emphasized that $U_{m,c}$ is not a true critical parameter, because instead it is relevant to a stochastic event: irreversible breakdown. $U_{m,c}$ is interpreted as the critical voltage for rupture. Because of the strong nonlinear behavior of **Eq. 6**, an order of magnitude difference in the choice of mean lifetime, for example, 0.1 or 10 seconds, results in only small differences in the estimate of $U_{m,c}$. Essentially the same critical pore mechanism for rupture was proposed independently by Sugar at about the same time (77).

2.3. Electrical Interaction of Membrane and Pulsar

Pores within the membrane interact with the transmembrane voltage, which itself is coupled through pulse application electrodes and the intervening

electrolyte to the pulse generator (“pulsar”). One theoretical approach uses an electrical circuit to represent these three interacting subsystems (78): (i) the pulse generator, (ii) the conducting pathway connecting the generator to the membrane (represented by a simple resistance), and (iii) the bilayer membrane, which is represented as the membrane capacitance, C_m , connected in parallel with the membrane resistance, $R_m(t)$. As pores are created, the membrane conductance $G_m(t) = 1/R_m(t)$ increases. However, the membrane does not experience the applied voltage pulse immediately. Instead, the membrane capacitance must charge through the external resistance of the solution which baths the membrane, the electrode/interface resistance, and the output resistance of the pulse generator. These three resistance are represented by a single resistor. Although an approximate treatment, this approach yields theoretical predictions which can be compared with experimental results.

Numerical solutions to the resulting circuit equations provide a quantitative description of planar membrane electroporation electrical behavior based on the transient aqueous pore model, which presently does not contain metastable pores and does not explicitly describe transport of large macromolecules. Nevertheless, this version of the theory provides a reasonable (but not perfect) explanation of the behavior of $U_m(t)$. This includes the sigmoidal decay of U_m associated with rupture; however the decay phase is longer than theoretically predicted. Four distinguishable types of electrical behavior are exhibited by the theoretical model, in general agreement with experiments (78–80). A striking feature is the very rapid electrical discharge associated with reversible electrical breakdown (REB), and a progressively smaller membrane resistance values found as the pulse magnitude is increased.

Replacement of some of the low dielectric constant lipid membrane interior by aqueous pores not only changes R_m , but also the membrane electrical capacitance, which should increase. This can be understood qualitatively by examining the simple expression for the capacitance, $C_{m,planar}$, of a “parallel plane capacitor” (an insulating dielectric sheet separating two conductors, here the two bathing solutions). A pore free planar membrane has

$$C_{m,planar} = \frac{K_m \epsilon_0 A_m}{d_m} . \quad (7)$$

Equation 7 shows that capacitance is proportional to the membrane dielectric constant, K_m . Thus, if a fraction of the membrane area is replaced by water (the total area of all the pores present), the average dielectric constant will be increased, and the membrane capacitance should be larger. But, as shown below, the fractional aqueous area of the membrane does not exceed 0.1%, and for this reason the slight increase in capacitance can usually be neglected. This

means that the circuit model for a planar membrane and its environment can use a constant value for C_m , an approximation that is consistent with the experimental observation (81).

An approximately constant membrane capacitance during electroporation is also consistent with the transient aqueous pore model (74). As discussed below, computer simulations based on the model correctly predict key behavior of $U_m(t)$. The largest fractional aqueous area found in these planar membrane simulations is $F_{w, \max} \approx 5 \times 10^{-4}$ (slightly less than 0.1%). This should be relevant to electroporation of single lipid bilayer membranes generally. For example, electroporation of large vesicles found $F_w \approx 10^{-3}$ (82).

One unexpected theoretical prediction is the emergence of an almost constant transmembrane voltage during an exponential pulse that is large enough to cause REB (74). This can be qualitatively understood in the following way. Initially, for small U_m the membrane charges passively, governed by the external resistance and the membrane capacitance. Once pores begin to be created at a significant rate, G_m rises nonlinearly, and the membrane begins to discharge through the pores even as it attempts to charge further. In theoretical simulations this leads rapidly to a peak voltage, with a rapid decrease as the pore population drops the membrane resistance faster than the membrane can charge. After an initial rapid rise time, the applied exponential pulse monotonically decays. The agile pore population responds by shrinking and removing pores in response to this decreases external stimulus, such that the variable voltage divider involving the membrane and the external environment leads to an almost constant voltage. Eventually, however, when U_m has reached a small value, the resistance associated with the pore population cannot increase quickly (pore destruction rates are limiting), and U_m now decreases much more rapidly.

Most ion and charged molecule transport should occur by electrophoresis and electroosmosis, not diffusion, for the case that pore lifetimes are short. Thus, if the voltage across the barrier is naturally limited by the pore population response, this means that the dominant local transport driving force is also limited. This therefore predicts that for a particular species of ion or molecule, the cumulative (net) transport should exhibit a plateau as a function of E_e , the electric field within the electrolyte. For cells, this leads to the qualitative prediction of a plateau in molecular uptake that is less than the equilibrium value achieved by passive permeation over a long time. Initial experiments determining the number of molecules taken up by electroporated cells found a subequilibrium value (83). Further experimental findings of subequilibrium

cellular uptake plateaus for both small (84,85) and large (86,87) charged molecules are consistent with this theoretical prediction.

2.4. Further Characteristics of the Pore Population

The portion of a lipid-based barrier that behaves as bulk electrolyte for ion and molecular transport is of interest, because it can be experimentally determined, and can also be sought theoretically. In the case of a planar bilayer membrane, numerical simulations obtained from a transient aqueous pore theory are consistent with the idea that a relatively small number of pores lead to large changes in ionic and molecular transport. In this sense, pores are catalytic in their effect on ionic and molecular transport, at least for water soluble molecules up to about 1000g mol^{-1} , as these are accommodated by even the minimum-size pores $r_{p,\text{min}} \approx 1\text{ nm}$.

Specifically, only a small fraction of the membrane area need be perforated by pores to cause a tremendous increase in transport, and for molecules less than 1000g mol^{-1} the molecule/pore interaction may be minimal, resulting in pore lifetimes much longer than the transport time for an individual ion or molecule. Each pore can transport many ions and molecules, although the actual number clearly depends on the ionic and molecular concentration as well as whatever driving forces are present.

Electrical behavior is more easily measured than molecular transport. It is of interest, therefore, that the electrical conduction of even small pores is sufficient to dominate the membrane conductance that is associated with REB. Even in this case there are so few pores present that the fractional aqueous area remains less than about 0.1%. That is, for small ions such as Na^+ and Cl^- if Born energy effects and steric hindrance are both neglected, the effective participating fractional area of the membrane is $F_{w,\text{ions}} \leq 10^{-3}$.

Pores are therefore predicted by theory to be widely spaced. The mean separation should decrease only to about $L_{\text{pore,pore}} \approx 60\text{ nm}$ during REB when G_m is maximal. Most of the time the spacing is significantly larger. That is, only a small fraction of the membrane need become electrically conducting to provide the protective effect of limiting $U_m(t)$ through a variable voltage divider effect that also involves the membrane's electrical environment. This is viewed as a consequence of the stochastic nature of the transient aqueous pore theory. If, however, some lipid-membrane barriers contain preexisting sites ("defects") that favor electroporation, these conclusions do not apply.

Macromolecules should interact more strongly with transient aqueous pores than molecules less than 1000g mol^{-1} . Such interaction may result in pore

deformation or prolonged pore lifetime (88). Fleeting passage of a long, highly charged DNA molecule may transiently enlarge a cell membrane pore, allowing smaller cotransported molecules to be moved at higher rates (89). A tethered macromolecule electrically or otherwise inserted into a transient aqueous pore should prevent its full shrinkage, thereby increasing pore lifetime by a “foot-in-the-door” effect (90). The idea that a large, usually charged molecule or particle can interact with a deformable membrane to alter a pore seems general. The “focusing electrical fields” outside the entrance to a conducting pore is expected as a consequence of the spreading or access resistance, so that charged molecules and even charged microparticles should be preferentially brought to sites of conducting pores. Once near the membrane, a highly charged macromolecule or microparticle can interact with the imposed field to further deform the membrane, including enlargement of a transient aqueous pore created initially by thermal fluctuations and an increased U_m . Although qualitatively plausible, a comprehensive quantitative theoretical treatment has not yet been achieved.

2.5. Electroporation of Stratum Corneum Lipid Bilayer Membranes

The SC is the primary skin barrier to charged molecules (1–3,5). This thin ($\approx 20 \mu\text{m}$ if hydrated) dead layer excludes ions and charged molecules through electrostatic interactions. As with single lipid bilayer membranes, changes in the Born energy prohibit entry of charged molecules into the multilamellar lipid bilayers of the SC. Some preexisting aqueous pathways exist, clearly demonstrated functionally by iontophoresis, which is believed to involve electrophoretic and electroosmotic transport through fixed pathways that can change their behavior as new electrolyte enters into them (54). Iontophoretic pathways appear to be mainly associated with the skin’s appendages (hair follicles and sweat ducts), consistent with our observations that at low voltages fluorescent molecules stain the appendages. MV pulses both activate (open) appendageal ducts (macropores) and cause electroporation of cells joined by tight junctions around these ducts within the viable epidermis (40). However, HV pulses produce local transport regions (LTRs) that form spontaneously away from appendages (31,41,46,48). Thus, as transdermal voltages are progressively increased from LV to MV to HV, a variety of transport behavior is observed. According to the skin electroporation hypothesis, both MV and HV pulses cause electroporation within skin lipid barriers. Some insights can be borrowed from single lipid bilayer membrane electroporation theory, but the greater complexity of skin suggests that extensions of the basic theory are required.

The simplest approach to theoretical predictions recognizes that approximately 100 lipid bilayer membranes must be traversed in crossing the SC. Thus,

an initial estimate is that if short pulses are required to create a transmembrane voltage of 0.5 to 1 V for single bilayer membranes, then the multilamellar bilayers of the SC may electroporate at about 50 to 100 V for short pulses, and perhaps as low as about 20 V for long pulses (27,90). This simple idea was greatly extended by applying transient aqueous pore electroporation theory to a system of multilamellar bilayer membranes (91), and provided support for the idea that transcellular (through-corneocyte) routes are involved for some MV pulses and for all HV pulses.

Electroporation theory developed for artificial planar bilayer membranes and for cell membranes presumes significant membrane conformational changes, such that the combination of thermal fluctuations and electrostatic free energy changes greatly favor aqueous pathway formation at large barrier voltages. Although there is considerable evidence that most of the SC lipids are in the crystalline state, and therefore relatively difficult to mechanically deform, there is reason to believe that SC lipids experience spontaneous microaggregation into fluid and crystalline domains (92–96). The size and spatial distribution of fluid microregions is unknown. It is likely, however, 0.1% or more of the lipid volume is in the fluid state, and in principle capable of experiencing electroporation. This hypothesis may therefore reconcile basic features of lipid bilayer membrane electroporation and known physiochemical properties of SC lipids.

The corneocyte surface parallel to the SC has an area of order $A_{\text{ccyte}} \approx \pi(50 \mu\text{m})^2 \approx 8 \times 10^{-9} \text{ m}^2$ ($\approx 8 \times 10^{-5} \text{ cm}^2$). One tenth of one percent of this area is $8 \times 10^{-12} \text{ m}^2$. A single primary aqueous pathway (“pore”) of radius $r_{\text{p,min}} \approx 1 \text{ nm}$ has an aqueous area of about $A_{\text{p,w}} \approx \pi r_{\text{p,min}}^2 \approx (3 \times 10^{-18} \text{ m}^2)$, but each such pore must involve structural rearrangements outside this aqueous core, such that an additional annular region of radial width $\Delta r \approx 0.5d_{\text{m}}$ (the length of one molecule comprising half a bilayer) is perturbed. The area to accommodate one such primary aqueous pathways is therefore

$$A_{\text{p,m,min}} \approx \pi [0.5d_{\text{m}} + r_{\text{p,min}}]^2. \quad (8)$$

For $r_{\text{p,min}} \approx 1 \text{ nm}$, **Eq. 8** gives $A_{\text{p,m,min}} \approx 5 \times 10^{-17} \text{ m}^2$. Approximately 2×10^5 primary aqueous pathways could therefore be accommodated in the 0.1% of a corneocyte face area. This agrees fortuitously well with a recent estimate based on skin resistance after pulsing (38). Nevertheless, the possible involvement of fluid microaggregates should be regarded as a hypothesis.

The structure and composition of the SC and the observations of LTRs suggest that the idealized model of **Fig. 2** is relevant. Two features of corneocytes are relevant to the skin electroporation hypothesis: (1) the 5–6 lipid bilayer membranes separating adjacent corneocytes, and (2) the keratin matrix within corneocyte interiors. The multilamellar bilayer membranes are the main site of



Fig. 2. Theoretical model of stochastic formation of LTRs, using a highly idealized SC model with rectangular “bricks” separated by lipid bilayer membrane “mortar.” This was used to test the hypothesis that stochastic spatial variations in membrane electroporation might account for spontaneous LTRs. A corresponding theoretical simulation accounts for the voltage redistribution that must occur after electroporation of the mortar (vertical or lateral) between bricks. **Left:** SC before electroporation; **Right:** SC during electroporation; Summary: Spontaneous appearance of LTRs is broadly consistent with some sort of stochastic aspect (e.g., number of bilayers, local electroporation probability) of aqueous pathway creation between adjacent corneocytes. The ability to partially predict random locations of LTRs is encouraging, but further theoretical work is needed.

electrical resistance, where most of the transdermal voltage appears within microseconds upon pulsing. The primary event is believed to be the creation of aqueous pathways across the lipid bilayers. For “short” pulses (≤ 1 ms) at not too large a voltage, these pathways appear to predominate. These “pores” are adequate to greatly increase the transport of small ions and molecules ranging up to about 1000g mol^{-1} . For significantly larger molecules, however, sieving of transport by the keratin matrix within corneocytes appears to take place. For example, linear oligonucleotides up to about 7000g mol^{-1} were transported across the skin, but only at some sites, and at other sites these molecules penetrated into (but not across) the skin, apparently becoming trapped within corneocytes (31).

Once primary aqueous pathways are created, however, secondary events may become important. For example, for long pulses (≥ 10 ms), heating within newly created and highly conducting aqueous pathways may become important, involving pathway enlargement. As another example, the introduction of long, charged macromolecules such as heparin can interact with the pathways, altering the transport of other molecules, and also greatly prolonging pathway life time (38,39). As still another example, introduction of keratin-disrupting molecules through the primary pathways can interrupt keratin matrix sieving, allowing much larger molecules such as antibody molecules to be transported across human skin (97,98). Thus, for macromolecules both the lipid bilayer membranes and the keratin matrix are transport barriers that can be greatly decreased by a protocol based on HV pulsing.

2.6. Localized Transport Regions

In vitro experiments using side-by-side permeation chambers have demonstrated that skin subjected to HV spontaneously develops sites with highly localized transport that are located away from appendages (31,41,46,48). Transport localization could possibly be due to either (1) random fluctuations, or (2) preexisting differences in structure or properties within the SC.

The first possibility has been initially studied using numerical simulations by considering a symmetric corneocyte model with rectangular cross-section corneocytes. The lipid membranes between corneocytes are assumed to be identical except for a random distribution of their number, between 2 and 6 bilayers between each pair of corneocytes. This leads to a resistor network model of the stratum corneum, with different resistance values depending on the number of bilayers. We then simulate the application of a voltage pulse to the network. If the voltage on a resistor (bilayer) reaches a critical value, then it “electroporates,” and its resistance value is correspondingly reduced. Some of the results from a simulation are shown in **Fig. 2**. According to this model, as the pulse voltage is increased, a first site with electroporation appears, followed by others as larger transmembrane voltages are achieved by larger pulses. Although this particular model involved a random spatial distribution of barrier magnitude, it may be equivalent to assuming a random spatial distribution for the probability of experiencing electroporation.

The second possibility has also been explored theoretically (49). As shown in **Fig. 3**, a preexisting preferred electroporation site is considered, in this case based on a slightly thinner SC, with a smaller number of lipid bilayer membranes. Preferred sites might also involve regions with many curved fluid bilayer membranes (99). Consistent with experimental observations, the minimum preferred site is taken to be a single corneocyte column, here for simplicity taken to be aligned (50), rather than offset (51). To account for measured skin resistance changes a large number of aqueous pathways must be created, of order 10^4 to 10^5 per minimum size LTR. This leads to the prediction that connectedness across the SC can be prolonged, due to the multiple pathway segments across the lipid bilayer membranes between corneocytes. Clearly, however, understanding of LTRs created by HV pulses is at an early stage.

2.7. Localized Heating Within Localized Dissipation Regions (LDRs)

The intense but brief electrical dissipation within aqueous pathways during HV pulsing leads naturally to the issue of localized heating. In vivo studies



Fig. 3. Modified “brick wall model” for a mostly deterministic LTR theory with straight-through aqueous pathways (38). This idealized drawing of a preferred site for LTR creation shows only about a third of the 15–16 corneocyte layers of the SC in region with ordered stacks (columns) of corneocytes (50), and does not apply directly to skin with disordered (off set) columns (51). However, slight offsets of corneocytes introduce only a slight tortuosity, and most of these primary (HV-created) aqueous pathways are therefore essentially straight through. **Left:** Site prior to aqueous pathway creation. **Right:** Site after several pulses, depicting a high area density of pathways within the LTR central regions, with some closed (recovered) and others open.

show that skin irritation can be small (27,100), even if long pulses are used (30,43). This suggests that major thermal perturbations do not occur, and motivated experimental and theoretical investigation of localized heating (101,102). Theoretical analysis of localized heating is based on assumption of an idealized, cylindrical LTR geometry, and spatially averaged heating within an LTR (102). The characteristic time constant for heat conduction is $\tau_{Q,SC} \approx 1$ ms, which provides a quantitative basis for the distinction of “short” and “long” pulses. Two cases are treated, one involving only heat conduction and the other involving both heat conduction and convection (flow), with the latter assumed to be due to electroosmosis. The predicted temperature rise is relatively small, and consistent with insignificant skin irritation in vivo (27,30,43,100). The coexistence of significant SC heating and essentially no damage to viable tissue is a remarkable situation, which supports the view that skin electroporation may have insignificant side effects.

Experiments show that as pulse duration or pulse magnitude are increased there is a progression to less recovery of R_{skin} , and a persistent elevated skin permeability. The mechanism underlying irreversibility in the SC has not been established. Candidate mechanisms include local heating, rupture of lipid bilayers, and entry of pathway-prolonging substances. In cases where little recovery takes place, however, it is a reasonable approximation to treat pathways as fixed.

Transport occurring through such pathways can then be considered as taking place in kind of porous medium. The associated theories do not actually describe electroporation itself, but instead focus on aspects of transport, such as the possibility of net transport due to pulses which alternate in polarity (36,103). In principle such pulses transport zero net charge across a barrier.

Nevertheless, net transport of an ion or molecule present on one side of the barrier is possible, essentially due to diffusional spreading between pulses, such that not all of what enters on a forward polarity pulse is returned upon subsequent application of a reverse polarity pulse.

3. Summary and Conclusions

Experiments have demonstrated that a variety of HV pulses cause both profound electrical resistance and molecular transport changes, and other, more limited, experiments are relevant to MV pulses. Clearly some type of aqueous pathway creation and/or enhancement is involved. Much of the experimental evidence is consistent with the skin electroporation hypothesis, in which new aqueous pathways are electrically created across skin barriers. However, a complete description is absent, and some conceptual difficulties remain. As noted above, much of the SC lipids are believed to be in the crystalline state, which presents basic problems for the transient aqueous pore nucleation theory of electroporation. Qualitatively, as also noted above, if a small fraction of SC lipids are in the fluid state, this conceptual problem may be overcome. Another challenge lies in understanding how LTRs form for short pulses, which appear not to involve significant local heating, what limits the spatial extent of LTRs, and what localized structural changes occur. The experimental observations for “short” and “long” pulses show that phenomena secondary to the primary event of electroporation may be important. Further, secondary phenomena associated with introduction of interacting molecules with aqueous pathways appears to occur, but is not yet quantitatively described by any theory. Thus, although some significant theoretical progress has been made, a theory for the mechanistic basis of the skin’s response to MV and HV pulses is far from complete.

Notation and Abbreviations

A_m	Area of membrane
c_s	Concentration of ion or molecule of species “s”
$C_{l \rightarrow w}$	Change in specific capacitance as water replaces lipid
e	1.6×10^{-19} C (magnitude of charge on monovalent ion)
E_e	Electric field within electrolyte
E_n	Nominal electric field based on applied electrode voltage
f_{molec}	Fraction of segments transporting larger molecules
F_w	Fractional aqueous area
$F_{w,\text{max}}$	Maximum fractional aqueous area
G_m	Membrane conductance
G_{skin}	Conductance of a skin sample
G_{SC}	Conductance of the stratum corneum

$G_{\text{LTR},s}$	Conductance of LTR to species “s”
$G_{\text{skin},s}$	Conductance of skin to species “s”
$G_{\text{SC},s}$	Conductance of stratum corneum to species “s”
$G_{\text{seg},s}$	Conductance of one aqueous pathway segment to species “s”
$G(t)$	LTR conductance at time t (after pulsing)
g^{Born}	Partition coefficient
$H(r_p, r_s)$	Steric hindrance factor
h_{SC}	Thickness of hydrated stratum corneum ($\sim 20 \mu\text{m}$)
h_{seg}	Length of a pathway segment ($\sim 40 \text{ nm}$)
I_s	Current carried by species “s”
$I_{\text{LTR},s}$	Current carried in one LTR by species “s”
$J_{\text{LTR},s}$	Molecular flux associated with current $I_{\text{LTR},s}$
K_m	Membrane dielectric constant
N_{cc}	Number of corneocytes in idealized corneocyte stack
N_p	Initial number of segments between corneocytes
$n(t)$	Number of segments between corneocytes that are available for transport of “s”
n_p	Initial number of segments available to species “s” ($f_{\text{molec}}N_p$)
q_s	Charge of species “s”
r_p	Minimum segment (electropore) radius ($\sim 1 \text{ nm}$)
R_m	Membrane resistance
R_{skin}	Resistance of skin ($1/G_{\text{skin}}$)
t	Time after pulsing
$U(t)$	Transmembrane (single bilayer) voltage as function of time
U_m	Transmembrane voltage
$U_{\text{m,force}}$	Transmembrane voltage needed to force ion across membrane without a pore
$U_{\text{p,local}}$	Local voltage across a pore interior
U_{SC}	Trans-SC voltage
U_{skin}	Transdermal voltage
V_m	Membrane volume
ϵ_e	Electrical permittivity of electrolyte ($\sim 7 \times 10^{-10} \text{ F m}^{-1}$)
ϵ_0	Electrical permittivity of free space ($\sim 8.85 \times 10^{-11} \text{ F m}^{-1}$)
σ_e	Electrical conductivity of electrolyte ($\sim 1 \text{ S m}^{-1}$)
μ_s	Electrophoretic mobility of species “s”
ν_0	Attempt rate density
$\tau_{\text{m,CHG}}$	Membrane charging time constant
$\tau_{\text{Q,SC}}$	Thermal time constant for SC
τ_{seg}	Average segment lifetime
dt	Short time interval
ξ	t/τ_{seg} , normalized time

Acknowledgments

This work was supported by NIH grant RO1-ARH4921 and Whitaker Foundation grant RR10963.

References

1. Schaefer, H. and Redelmeier, T. E. (1996) *Skin Barrier: Principles of Percutaneous Absorption*. Karger, Basel.
2. Goldsmith, L. A. (1991) *Physiology, Biochemistry, and Molecular Biology of the Skin*, 2nd ed. Oxford University Press, New York.
3. Elias, P. M. and Menon, G. K. (1991) Structural and lipid biochemical correlates of the epidermal permeability. *Adv. Lipid Res.* **24**, 1–26.
4. Michaels, A. S., Chandrasekaran, S. K., and Shaw, J. E. (1975) Drug permeation through human skin: Theory and in vitro experimental measurements. *AICHE. J.* **21**, 985–996.
5. Smith, E. W. and Maibach, H. I. (1995) *Percutaneous Penetration Enhancers*. CRC Press, Boca Raton, FL.
6. Weaver, J. C., Vaughan, T. E., and Chizmadzhev, Y. (1999) Theory of electrical creation of aqueous pathways across skin transport barriers. *Adv. Drug Deliv. Rev.* **35**, 21–39.
7. Green, P. G. (1996) Iontophoretic delivery of peptide drugs. *J. Controlled Release* **41**, 33–48.
8. Merino, V. Kalia, Y. N., and Guy, R. H. (1997) Transdermal therapy and diagnosis by iontophoresis. *Trends Biotechnol.* **15**, 288–290.
9. Neumann, E. (1992) Membrane electroporation and direct gene transfer. *Bioelectrochem. Bioenerg.* **28**, 247–267.
10. Nickoloff, J. A. (Ed.) (1995) *Electroporation Protocols for Microorganisms*, vol. 47, *Methods in Molecular Biology*, Humana Press, Totowa, NJ.
11. Nickoloff, J. A. (Ed.) (1995) *Animal Cell Electroporation and Electrofusion Protocols*, vol. 48, *Methods in Molecular Biology*, Humana Press, Totowa, NJ.
12. Nickoloff, J. A. (Ed.) (1995) *Plant Cell Electroporation and Electrofusion Protocols*, vol. 55, *Methods in Molecular Biology*, Humana Press, Totowa, NJ.
13. Powell, K. T., Morgenthaler, A. W., and Weaver, J. C. (1989) Tissue electroporation: Observation of reversible electrical breakdown in viable frog skin. *Biophys. J.* **56**, 1163–1171.
14. Okino, M. and Mohri, H. (1987) Effects of a high-voltage electrical impulse and an anticancer drug on in vivo growing tumors. *Jpn. J. Cancer Res.* **78**, 1319–1321.
15. Mir, L. M., Orlowski, Jr., S., Belehradek, J., and Paoletti, C. (1991) In vivo potentiation of the bleomycin cytotoxicity by local electric pulses. *Eur. J. Cancer* **27**, 68–72.
16. Heller, R., Jaroszeski, M., Leo-Messina, J., Perrot, R., Van Voorhis, N., Reintgen, D., and Gilbert, R. (1995) Treatment of b16 mouse melanoma with the combination of electropermeabilization and chemotherapy. *Bioelectrochem. Bioenerg.* **36**, 83–87.

17. Mir, L. M., Orlowski, S., Belehradec, J., Teissié, J., Rols, M. P., Serša, G., Miklavčič, D., Gilbert, R., and Heller, R. (1995) Biomedical applications of electric pulses with special emphasis on antitumor electrochemotherapy. *Bioelectrochem. Bioenerg.* **38**, 203–207.
18. Heller, R., Jaroszeski, M., Glass, L. F., Messina, J. L., Rapport, D. P., DeConti, R. C., Fenske, N. A., Gilbert, R. A., Mir, L. M., and Reintgen, D. S. (1996) Phase I/II trial for the treatment of cutaneous and subcutaneous tumors using electrochemotherapy. *Cancer* **77**, 964–971.
19. Nishi, T., Dev, S. B., Yoshizato, K., Kuratsu, J., and Ushio, Y. (1997) Treatment of cancer using pulsed electric field in combination with chemotherapeutic agents or genes. *Hum. Cell* **1**, 81–86.
20. Titomirov, A. V., Sukharev, S., and Kistoanova, E. (1991) In vivo electroporation and stable transformation of skin cells of newborn mice by plasmid DNA. *Biochim. Biophys. Acta* **1088**, 131–134.
21. Sukharev, S. I., Titomirov, A. V., and Klenchin, V. A. (1994) Electrically-induced DNA transfer into cells: Electrotransfection. *In Vivo Gene Therapeutics*. Birkhauser, Boston, pp. 210–232.
22. Heller, R., Jaroszeski, M., Atkin, A., Moradpour, D., Gilbert, R., Wands, J., and Nicolau, C. (1996) In vivo gene electroinjection and expression in rat liver. *FEBS Lett.* **389**, 225–228.
23. Nishi, T., Yoshizato, K., Yamashiro, S., Takeshima, H., Sato, K., Hamada, K., Kitamura, K., Yoshimura, T., Saya, H., Kuratsu, J., and Ushio, Y. (1996) High-efficiency in vivo gene transfer using intraarterial plasmid DNA injection following in vivo electroporation. *Cancer Res.* **56**, 1050–1055.
24. Rols, M. P., Delteil, C., Golzio, M., Dumond, P., Cors, S., and Teissié, J. (1998) In vivo electrically mediated protein and gene transfer in murine melanoma. *Nat. Biotechnol.* **16**, 168–171.
25. Aihara, H. and Miyazaki, J. (1998) Highly efficient gene transfer into muscle by electroporation in vivo. *Nat. Biotechnol.* **16**, 867–870.
26. Prausnitz, M. R., Bose, V. G., Langer, R. S., and Weaver, J. C. (1992) Transdermal drug delivery by electroporation. *Proc. Int. Symp. Controlled Release Bioact. Mater.* **19**, pp. 232,233.
27. Prausnitz, M. R., Bose, V. G., Langer, R., and Weaver, J. C. (1993) Electroporation of mammalian skin: A mechanism to enhance transdermal drug delivery. *Proc. Natl. Acad. Sci. USA* **90**, 10,504–10,508.
28. Prausnitz, M. R., Pliquett, U., Langer, R., and Weaver, J. C. (1994) Rapid temporal control of transdermal drug delivery by electroporation. *Pharmacol. Res.* **11**, 1834–1837.
29. Vanbever, R., Lecouturier, N., and Preat, V. (1994) Transdermal delivery of metoprolol by electroporation. *Pharmacol. Res.* **11**, 1657–1662.
30. Riviere, J. E., Monteiro-Riviere, N. A., Rogers, R. A., Bommannan, D., Tamada, J. A., and Potts, R. O. (1995) Pulsatile transdermal delivery of LHRH using electroporation: Drug delivery and skin toxicology. *J. Controlled Release* **36**, 229–233.

31. Zewert, T. E., Pliquett, U. F., Langer, R., and Weaver, J. C. (1995) Transport of DNA antisense oligonucleotides across human skin by electroporation. *Biochim. Biophys. Res. Commun.* **212**, 286–292.
32. Prausnitz, M. R., Edelman, E. R., Gimm, J. A., Langer, R., and Weaver, J. C. (1995) Transdermal delivery of heparin by skin electroporation. *Biotechnology* **13**, 1205–1208.
33. Pliquett, U., Langer, R., and Weaver, J. C. (1995) Changes in the passive electrical properties of human stratum corneum due to electroporation. *Biochim. Biophys. Acta* **1239**, 111–121.
34. Pliquett, U. and Weaver, J. C. (1996) Electroporation of human skin: Simultaneous measurement of changes in the transport of two fluorescent molecules and in the passive electrical properties. *Bioelectrochem. Bioenerg.* **39**, 1–12.
35. Pliquett, U. and Weaver, J. C. (1996) Transport of a charged molecule across the human epidermis due to electroporation. *J. Controlled Release* **38**, 1–10.
36. Prausnitz, M. R., Lee, C. S., Liu, C. H., Pang, J. C., Singh, T.-P., Langer, R., and Weaver, J. C. (1996) Transdermal transport efficiency during skin electroporation and iontophoresis. *J. Controlled Release* **38**, 205–217.
37. Gallo, S. A., Oseroff, A. R., Johnson, P. G., and Hui, S. W. (1997) Characterization of electric-pulse-induced permeabilization of porcine skin using surface electrodes. *Biophys. J.* **72**, 2805–2811.
38. Weaver, J. C., Vanbever, R., Vaughan, T. E., and Prausnitz, M. R. (1997) Heparin alters transdermal transport associated with electroporation. *Biochim. Biophys. Res. Commun.* **234**, 637–640.
39. Vanbever, R., Prausnitz, M. R., and Preat, V. (1997) Macromolecules as novel transdermal transport enhancers for skin electroporation. *Pharmacol. Res.* **14**, 638–644.
40. Chizmadzhev, Y., Indenbom, A. V., Kuzmin, P. I., Galinchenko, S. V., Weaver, J. C., and Potts, R. (1998) Electrical properties of skin at moderate voltages: Contribution of appendageal macropores. *Biophys. J.* **74**, 843–856.
41. Chen, T., Langer, R., and Weaver, J. C. (1998) Skin electroporation causes molecular transport across the stratum corneum through local transport regions. *J. Invest. Dermatol. Symp. Proc.* **3**, 159–165.
42. Chen, T., Segall, E. M., Langer, R., and Weaver, J. C. (1998) Skin electroporation: Rapid measurements of the transdermal voltage and flux of four fluorescent molecules show a transition to large fluxes near 50 V for 1 ms pulses. *J. Pharm. Sci.* **87**, 1368–1374.
43. Vanbever, R., Fouchard, D., Jadoul, A., De Morre, N., Preat, V., and Marty, J.-P. (1998) In vivo non invasive evaluation of hairless rat skin after high-voltage pulse exposure. *Skin Pharmacol. Appl. Skin Physiol.* **11**, 23–34.
44. Vanbever, R., Langers, G., Montmayeur, S., and Preat, V. (1998) Transdermal delivery of fentanyl: Rapid onset of analgesia using skin electroporation. *J. Controlled Release* **50**, 225–235.
45. Vanbever, R., Pliquett, U., Preat, V., and Weaver, J. C. (1999) Transport of charged molecules across human skin in vitro due to short and long “high-voltage” pulses. *J. Controlled Release*, in press.

46. Prausnitz, M. R., Gimm, J. A., Guy, R. H., Langer, R., Weaver, J. C., and Cullander, C. (1996) Imaging regions of transport across human stratum corneum during high voltage and low voltage exposures. *J. Pharm. Sci.* **85**, 1363–1370.
47. Wang, S., Kara, M., and Krishnan, T. R. (1998) Transdermal delivery of cyclosporin-A using electroporation. *J. Controlled Release* **50**, 61–70.
48. Pliquett, U. F., Zewert, T. E., Chen, T., Langer, R., and Weaver, J. C. (1996) Imaging of fluorescent molecule and small ion transport through human stratum corneum during high-voltage pulsing: Localized transport regions are involved. *J. Biophys. Chem.* **58**, 185–204.
49. Weaver, J. C., Vaughan, T. E., and Chizmadzhev, Y. (1998) Theory of skin electroporation: Implications of straight-through aqueous pathway segments that connect adjacent corneocytes. *J. Invest. Dermatol. Symp. Proc.* **3**, 143–147.
50. Menton, D. N. (1976) A minimum-surface mechanism to account for the organization of cells into columns in the mammalian epidermis. *Am. J. Anat.* **145**, 1–22.
51. Bergstresser, P. R. and Chapman, S. L. (1980) Maturation of normal human epidermis without an ordered structure. *Br. J. Dermatol.* **102**, 641–648.
52. Pliquett, U., Gift, E. A., and Weaver, J. C. (1996) Determination of the electric field and anomalous heating caused by exponential pulses in electroporation experiments. *Bioelectrochem. Bioenerg.* **39**, 39–53.
53. Cullander, C. (1992) What are the pathways of iontophoretic current flow through mammalian skin? *Adv. Drug Deliv. Rev.* **9**, 119–135.
54. Dinh, S. M., Luo, C-W., and Berner, B. (1993) Upper and lower limits of human skin electrical resistance in iontophoresis. *AIChE J.* **39**, 2011–2018.
55. Sage, B. H. (1995) Iontophoresis. *Percutaneous Penetration Enhancers*. CRC Press, Boca Raton, FL, pp. 351–368.
56. Cullander C. and Guy, R. H. (1992) Visualization of iontophoretic pathways with confocal microscopy and the vibrating probe electrode. *Solid State Ionics* **53–56**, 197–206.
57. Scott, E. R., White, H. S., and Phipps, J. B. (1992) Direct imaging of ionic pathways in stratum corneum using scanning electrochemical microscopy. *Solid State Ionics* **53–56**, 176–183.
58. Monteiro-Riviere, N. A., Inman, A. O., and Riviere, J. E. (1994) Identification of the pathway of iontophoretic drug delivery: Light and ultrastructure studies using mercuric chloride in pigs. *Pharmacol. Res.* **11**, 251–256.
59. Pliquett, U. F., Vanbever, R., Martin, G. T., Preat, V., and Weaver, J. C. (1999) Molecular transport across stratum corneum due to electric pulses: Behavior of local transport regions (LTRs). *Electricity and Magnetism in Biology and Medicine*. Plenum, New York, pp. 255–257.
60. Pliquett, U., Vanbever, R., Preat, V., and Weaver, J. C. (1999) Local transport regions (LTRs) in human stratum corneum due to long and short “high voltage” pulses. *Bioelectrochem. Bioenerg.* **47**, 151–161

61. Weaver, J. C. and Chizmadzhev, Y. A. (1996) Electroporation. *CRC Handbook of Biological Effects of Electromagnetic Fields*, 2nd ed. CRC Press, Boca Raton, FL, pp. 247–274.
62. Abidor, I. G., Arakelyan, V. B., Chernomordik, L. V., Chizmadzhev, Yu. A., Pastushenko, V. F., and Tarasevich, M. R. (1979) Electric breakdown of bilayer membranes: I. The main experimental facts and their qualitative discussion. *Bioelectrochem. Bioenerg.* **6**, 37–52.
63. Weaver, J. C. and Chizmadzhev, Y. A. (1996) Theory of electroporation: A review. *Bioelectrochem. Bioenerg.* **41**, 135–160.
64. Litster, J. D. (1975) Stability of lipid bilayers and red blood cell membranes. *Phys. Lett.* **53A**, 193,194.
65. Taupin, C., Dvolaitzky, M., and Sauterey, C. (1975) Osmotic pressure induced pores in phospholipid vesicles. *Biochemistry* **14**, 4771–4775.
66. Pastushenko, V. F., Chizmadzhev, Yu. A., and Arakelyan, V. B. (1979) Electric breakdown of bilayer membranes: II. Calculation of the membrane lifetime in the steady-state diffusion approximation. *Bioelectrochem. Bioenerg.* **6**, 53–62.
67. Chizmadzhev, Y. A., Arakelyan, V. B., and Pastushenko, V. F. (1979) Electric breakdown of bilayer membranes: III. Analysis of possible mechanisms of defect origin. *Bioelectrochem. Bioenerg.* **6**, 63–70.
68. Pastushenko, V. F., Chizmadzhev, Y. A., and Arakelyan, V. B. (1979) Electric breakdown of bilayer membranes: IV. Consideration of the kinetic stage in the case of the single-defect membrane. *Bioelectrochem. Bioenerg.* **6**, 71–79.
69. Arakelyan, V. B., Chizmadzhev, Y. A., and Pastushenko, V. F. (1979) Electric breakdown of bilayer membranes: V. Consideration of the kinetic stage in the case of the membrane containing an arbitrary number of defects. *Bioelectrochem. Bioenerg.* **6**, 81–87.
70. Pastushenko, V. F., Arakelyan, V. B., and Chizmadzhev, Y. A. (1979) Electric breakdown of bilayer membranes: VI. A stochastic theory taking into account the processes of defect formation and death: Membrane lifetime distribution function. *Bioelectrochem. Bioenerg.* **6**, 89–95.
71. Pastushenko, V. F., Arakelyan, V. B., and Chizmadzhev, Yu. A. (1979) Electric breakdown of bilayer membranes: VII. A stochastic theory taking into account the processes of defect formation and death: Statistical properties. *Bioelectrochem. Bioenerg.* **6**, 97–104.
72. Pastushenko, V. F. and Chizmadzhev, Y. A. (1982) Stabilization of conducting pores in BLM by electric current. *Gen. Physiol. Biophys.* **1**, 43–52.
73. Powell, K. T. and Weaver, J. C. (1986) Transient aqueous pores in bilayer membranes: A statistical theory. *Bioelectrochem. Bioenerg.* **15**, 211–227.
74. Freeman, S. A., Wang, M. A., and Weaver, J. C., (1994) Theory of electroporation for a planar bilayer membrane: Predictions of the fractional aqueous area, change in capacitance and pore-pore separation. *Biophysical J.* **67**, 42–56.
75. Weaver, J. C. and Mintzer, R. A. (1981) Decreased bilayer stability due to transmembrane potentials. *Phys. Lett.* **86A**, 57–59.

76. Deryagin, B. V. and Gutop, Y. V. (1962) Theory of the breakdown (rupture) of free films. *Kolloidn. Zh.* **24**, 370–374.
77. Sugar, I. P. (1981) The effects of external fields on the structure of lipid bilayers. *J. Physiol. Paris* **77**, 1035–1042.
78. Barnett A. and Weaver, J. C. (1991) Electroporation: A unified, quantitative theory of reversible electrical breakdown and rupture. *Bioelectrochem. Bioenerg.* **25**, 163–182.
79. Benz, R., Beckers, F., and Zimmermann, U. (1979) Reversible electrical breakdown of lipid bilayer membranes: A charge-pulse relaxation study. *J. Memb. Biol.* **48**, 181–204.
80. Weaver, J. C. and Barnett, A. (1992) Progress towards a theoretical model of electroporation mechanism: Membrane electrical behavior and molecular transport. *Guide to Electroporation and Electrofusion*. Academic Press, New York, pp. 91–117.
81. Chernomordik, L. V., Sukharev, S. I., Abidor, I. G., and Chizmadzhev, Y. A. (1982) The study of the BLM reversible electrical breakdown mechanism in the presence of UO_2^{2+} . *Bioelectrochem. Bioenerg.* **9**, 149–155.
82. Hibino, M., Shigemori, M. Itoh, H., Nagayama, K., and Kinosita, K. (1991) Membrane conductance of an electroporated cell analyzed by submicrosecond imaging of transmembrane potential. *Biophys. J.* **59**, 209–220.
83. Bartoletti, D. C., Harrison, G. I., and Weaver, J. C. (1989) The number of molecules taken up by electroporated cells: Quantitative determination. *FEBS Lett.* **256**, 4–10.
84. Prausnitz, M. R., Lau, B. S., Milano, C. D., Conner, S., Langer, R., and Weaver, J. C. (1993) A quantitative study of electroporation showing a plateau in net molecular transport. *Biophys. J.* **65**, 414–422.
85. Gift, E. A. and Weaver, J. C. (1995) Observatifon of extremely heterogeneous electroporative uptake which changes with electric field pulse amplitude in *saccharomyces cerevisiae*. *Biochim. Biophys. Acta* **1234**, 52–62.
86. Prausnitz, M. R., Milano, C. D., Gimm, J. A., Langer, R., and Weaver, J. C. (1994) Quantitative study of molecular transport due to electroporation: Uptake of bovine serum albumin by human red blood cell ghosts. *Biophys. J.* **66**, 1522–1530.
87. Gift, E. A., Hui, L., and Weaver, J. C. (1999) Molecular uptake in yeast by electroporation: Evidence for a plateau. *Electricity and Magnetism in Biology and Medicine*. Plenum, New York, pp. 923–926.
88. Pastushenko, V. P. and Chizmadzhev, Y. A. (1992) Energetic estimations of the deformation of translocated DNA and cell membrane in the course of electrotransformation. *Biol. Mem.* **6**, 287–300.
89. Klenchin, V. A., Sukharev, S. I., Serov, S. M., Chernomordik, L. V., and Chizmadzhev, Y. A. (1991) Electrically induced DNA uptake by cells is a fast process involving DNA electrophoresis. *Biophys. J.* **60**, 804–811.
90. Weaver, J. C. (1993) Electroporation: A general phenomenon for manipulating cells and tissue. *J. Cell. Biochem.* **51**, 426–435.
91. Chizmadzhev, Yu, A., Zarnytsin, V., Weaver, J. C., and Potts, R. O. (1995) Mechanism of electroinduced ionic species transport through a multilamellar lipid system. *Biophys. J.* **68**, 749–765.

92. Ongpipattanakul, B., Burnette, R. R., Potts, R. O., and Francoeur, M. L. (1991) Evidence that oleic acid exists in a separate phase within stratum corneum lipids. *Pharmacol. Res.* **8**, 350–354.
93. Potts, R. O., Francoeur, M. L., and Guy, R. H. (1992) Routes of ionic permeability through mammalian skin. *Solid State Ionics* **53–56**, 165–169.
94. Kitson, N., Thewalt, J., Lafleur, M., and Bloom, M. (1994) A model membrane approach to the epidermal permeability barrier. *Biochemistry* **33**, 6707–6715.
95. Ongpipattanakul, B., Francoeur, M. L., and Potts, R. O. (1994) Polymorphism in stratum corneum lipids. *Biochim. Biophys. Acta* **1190**, 115–122.
96. Bouwstra, J. A., Thewalt, J., Gooris, G. S., and Kitson, N. (1997) A model membrane approach to the epidermal permeability barrier: An x-ray diffraction study. *Biochemistry* **36**, 7717–7725.
97. Zewert, T. E., Pliquett, U., Vanbever, R., Chen, T., Langer, R., and Weaver, J. C. Creation of transdermal pathways for macromolecule transport by skin electroporation and a low-toxicity pathway-enlarging molecule. *Bioelectrochem. Bioenerg.* (in press).
98. Weaver, J. C., Pliquett, U. F., Zewert, T. E., Vanbever, R., Herndon, T. O., Gowrishankar, T. R., Chen, T., Prausnitz, M. R., Vaughan, T. E., Chizmadzhev, Y., Preat, V., and Langer, R. (1999) Recent Advances in Skin Electroporation: Mechanism and Efficacy. *Electricity and Magnetism in Biology and Medicine*. Plenum, New York, pp. 149–152.
99. Isambert, H. (1998) Understanding the electroporation of cells and artificial bilayer membranes. *Phys. Rev. Lett.* **80**, 3404–3407.
100. Prausnitz, M. R., Seddick, D. S., Kon, A. A., Bose, V. G., Frankenburg, S., Klaus, S. N., Langer, R., and Weaver, J. C. (1993) Methods for in vivo tissue electroporation using surface electrodes. *Drug Deliv.* **1**, 125–131.
101. Pliquett, U., Martin, G. T., and Weaver, J. C. (1999) Experimental measurement of localized heating in human skin subjected to “high-voltage” pulses. Submitted.
102. Martin, G., Pliquett, U., and Weaver, J. C. (1999) Theoretical analysis of localized heating in human skin subjected to high voltage pulses. Submitted.
103. Edwards, D. A., Prausnitz, M. R., Langer, R., and Weaver, J. C. (1995) Analysis of enhanced transdermal transport by skin electroporation. *J. Controlled Release* **34**, 211–221.
104. Flynn, G. (1979) *Modern Pharmaceutics*. Marcel Dekker, New York, p. 263.
105. Berridge, M. J. and Oschman, J. L. (1972) *Transporting Epithelia*. Academic Press, New York.
106. Pikal, M. J. (1992) The role of electroosmotic flow in transdermal iontophoresis. *Adv. Drug Deliv. Rev.* **9**, 201–237.
107. Chizmadzhev, Y., Kuzmin, P. I., Weaver, J. C., and Potts, R. (1998) Skin appendageal macropores as possible pathway for electrical current. *J. Invest. Dermatol. Symp. Proc.* **3**, 148–152.
108. Weaver, J. C. (1995) Electroporation in cells and tissues: A biophysical phenomenon due to electromagnetic fields. *Radio Sci.* **30**, 205–221.

Mechanistic Studies of Skin Electroporation Using Biophysical Methods

Mark R. Prausnitz, Uwe Pliquet, and Rita Vanbever

1. Introduction

The mechanism by which high-voltage pulses transiently disrupt lipid bilayers in cell membranes has been the subject of controversy since electroporation was first observed almost three decades ago. Determining the mechanism by which such pulses permeabilize the complex, multilamellar bilayer structures in skin poses an even greater challenge. To address this issue, a range of methods have been employed to perform biophysical characterization for skin electroporation studies. In this chapter, we provide an overview of these methods and highlight representative findings which biophysical characterization has yielded.

In single-bilayer systems, such as cell membranes and synthetic lipid membranes, a transmembrane voltage of hundreds of millivolts applied typically for at least microseconds causes the membrane to lose its barrier properties, shown primarily by dramatically increased electrical conductivity and molecular permeability (1–5). Under appropriate conditions, the membrane's barrier properties are restored within a timescale typically of seconds to minutes, although changes can persist for as long as hours before reversing. The mechanism by which these changes in membrane properties occur is generally believed to involve transient disruption of membrane structure, which results in the creation of aqueous pathways, or pores, across the membrane. Hence the name electroporation has been widely adopted. However, the exact structure of a pore and the role of other direct and indirect effects of the electric field remain the subject of active study.

In skin, transient disruption of barrier properties has also been induced by the application of short, high-voltage pulses. Skin's barrier properties are primarily due to a collection of multilamellar lipid bilayers stacked in the intercellular spaces of stratum corneum, the outermost 10–20 μm of human skin (6–8). Since on the order of 100 bilayers appear in a stratum corneum cross-section, one might expect electroporation to occur at a transdermal voltage of tens of volts (9–11). Indeed, with an apparent threshold between 30–60 V, skin conductivity and permeability have been observed to increase by orders of magnitude and show complete or partial reversibility, depending on experimental conditions (12–14).

Studies measuring the average flux of molecules across the skin make up the bulk of literature on high-voltage pulsing of skin and provide significant insight into what is proposed to be skin electroporation (15–19). They show as much as 10,000-fold flux increases which can be fully reversible, suggesting compelling applications in transdermal drug delivery. Mechanistically, flux studies indicate that high-voltage pulses induce physical changes in skin microstructure, since many experimental observations cannot be explained by electric field-induced electrophoresis or electroosmosis alone (15).

Although molecular transport studies have supported the hypothesis of electroporation-induced changes in skin structure, further biophysical characterization has provided a more complete picture. Those biophysical methods and their representative findings are summarized below. More detailed treatment of some of these methods as applied to skin outside the context of electroporation can be found in a recent book (8).

2. Characterization of Skin Microstructure

Skin's microstructure can be characterized by its interaction with different forms of electromagnetic radiation. Basic electrical resistance measurements provide a relatively straightforward assessment of skin barrier properties to ions with at least subsecond time resolution. Probing skin's full electrical impedance spectrum yields much more information about the physical environment within skin, but requires more sophisticated equipment, more complex analysis, and generally poorer time resolution. Measuring the scattering of x-rays has given insight into long-lived changes in supramolecular organization within skin (e.g., bilayers). Imaging with freeze fracture electron microscopy has provided pictures of altered skin microstructural morphology. Finally, other methods, including Fourier transform infrared spectroscopy, differential thermal analysis and measurement of skin ion content, have also been applied to study skin electroporation.

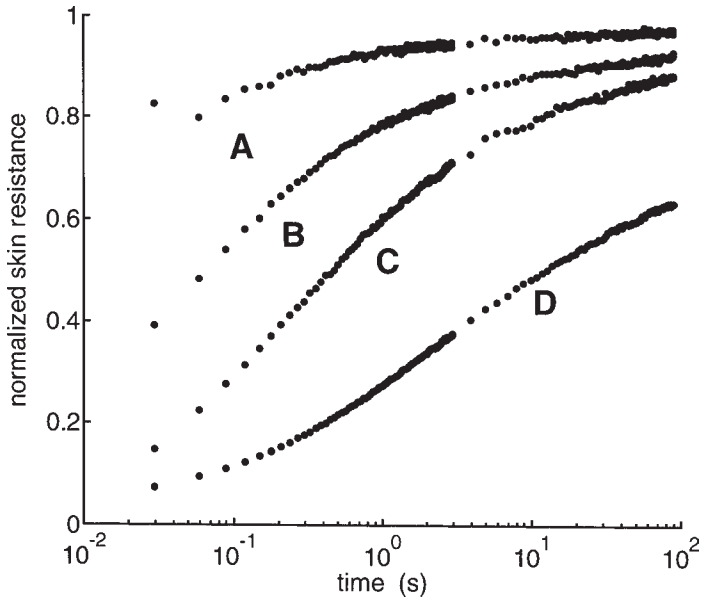


Fig. 1. Normalized skin resistance as a function of time after exposure to a high voltage pulse. Skin resistance dropped dramatically during the pulse and showed rapid recovery either partially or fully back to prepulse values. Resistance values were determined by calculating the DC resistance from impedance spectra collected after the pulse and have been normalized relative to prepulse values. The exponential-decay pulse time constant was 1.1 ms and the transdermal voltage was (A) 71 V, (B) 88 V, (C) 105 V, or (D) 123 V. Experiments were performed using human epidermis *in vitro*. (Adapted from **ref. 13**, with permission.)

2.1. Basic Resistance Measurements

Measuring skin resistance is especially useful because it provides information about the skin barrier with excellent time resolution using a relatively simple technique (13,14,20). Measurements of skin resistance can be arbitrarily fast and have been reported in the context of skin electroporation studies on the microsecond timescale. By contrast, the best reported time resolution of transdermal molecular flux measurements is on the order of 10 seconds using an optimized continuous flow-through system (see Chapter 31). **Figure 1** shows skin resistance as a function of time immediately following application of high-voltage pulses to cause skin electroporation. The rapid and dramatic drop in skin resistance followed by slow recovery is evident.

Skin resistance can be measured using direct current (DC) methods, but low-frequency alternating current (AC) methods are better. The simplest, but not preferred, way to measure skin resistance is to attach the leads of an ohmmeter to electrodes in electrical contact with the skin. This might be done in a standard diffusion chamber where both sides of the skin are bathed in saline. Silver–silver chloride electrodes are usually preferred, since their electrochemical interface with saline does not distort the measurement. However, measurement using a standard ohmmeter can alter the skin. Most ohmmeters operate by applying a known voltage and determine resistance by measuring the resulting current. Because skin resistance can be quite high, ohmmeters often apply large voltages (e.g., >1 V) to get a more accurate measurement and this voltage cannot be selected by the user. Such large voltages are known to change skin resistance (21). Thus, measurements using standard ohmmeters should be avoided.

To prevent the skin from being exposed to large measurement voltages, one can determine skin resistance without an ohmmeter, but use the same principle of measurement that the ohmmeter does. Using a constant voltage source, apply a known voltage ($\ll 1$ V) and measure the resulting current. The current can be measured by determining the voltage across a known resistance in series with the skin (good method) or by measuring it directly with a current transformer (better method). Alternatively, a constant current can be applied (such that the resulting transdermal voltage is $\ll 1$ V) and the transdermal voltage measured directly with a voltmeter or oscilloscope. Once the current and voltage are known, skin resistance can be calculated using Ohm's law (i.e., $R = V/I$) (22). In this way, the user can select the voltage applied to the skin and thereby prevent damaging it. Because this approach involves using lower voltages and currents for measurement, the sensitivity of the measurement is reduced compared to using an ohmmeter. However, this is preferable to using a larger voltage which alters the skin.

The best method to measure skin resistance is to apply an alternating current and determine the low-frequency skin impedance. An alternating current is preferable, because unlike direct current, it does not develop a polarization voltage which can distort measurements. At sufficiently low frequency (e.g., < 10 Hz), skin impedance has approximately the same value as DC (e.g., 0 Hz) resistance. Low frequency impedance can be determined using the same approach described in the preceding paragraph, except an AC power source is needed (23).

In each of these approaches where a transdermal voltage is measured during application of a constant current (AC or DC), it is better to measure the transdermal voltage using different electrodes from the ones through which the current is applied. This is because there can be a voltage drop across the current-application electrodes and their electrochemical interfaces, which

introduces artifacts into the measurement. The recommended four-electrode setup involves an outer electrode on each side of the skin, through which the current is applied, and an inner electrode between each outer electrode and the skin, which is used to measure voltage. The voltage measured will be the voltage across the skin plus the voltage across the saline between the electrodes and skin. The resistance of this saline can be significant; although before electroporation, skin resistance should be high (e.g., $100,000 \Omega \text{ cm}^2$) and therefore much greater than the resistance of saline, during and after electroporation, skin resistance can be as low as $100 \Omega \text{ cm}^2$ (13,24). For this reason, the resistance of the apparatus without skin should be measured and then subtracted from subsequent measurements made with skin.

2.2. Impedance Spectroscopy

Although a great deal can be learned from basic resistance measurements, probing the full impedance spectrum provides still more information (13,23,25–28). Generally, impedance spectroscopy yields not only skin resistance, but also provides values for skin capacitance (Fig. 2). Making impedance measurements, however, is usually slower, uses sophisticated hardware and requires more difficult analysis. Detailed advice on using impedance spectroscopy in skin electroporation studies is provided in Chapter 30.

Briefly, one should go to the effort to make impedance measurements if the capacitive, or possibly inductive, properties of the skin are important. Skin capacitance is primarily associated with stratum corneum lipids. Thus, the transient increases in skin capacitance shown in Fig. 2B support the hypothesis that high-voltage pulses alter stratum corneum lipids. The drawbacks of impedance measurements is that if one measures in the frequency domain, scans of measurements must be performed over a range of frequencies and this takes time. If one measures in the time domain, faster time resolution can be achieved, especially if an equivalent electrical circuit for the skin is assumed. However, selection of an appropriate equivalent circuit is critical, since the analysis can be distorted if an incorrect circuit is used or if the same circuit does not apply at all conditions.

2.3. X-Ray Scattering Techniques

The organization of lipid bilayers and other structures in the skin can be identified using X-ray scattering (29). Using small-angle X-ray scattering (SAXS), scattering features with dimensions of nanometers can be measured. Figure 3A shows the effects of electroporation on SAXS. The peaks seen at 4.7 and 6.3 nm in control samples represent scattering due to intercellular lipid lamellae of the stratum corneum. The great reduction in those peaks following

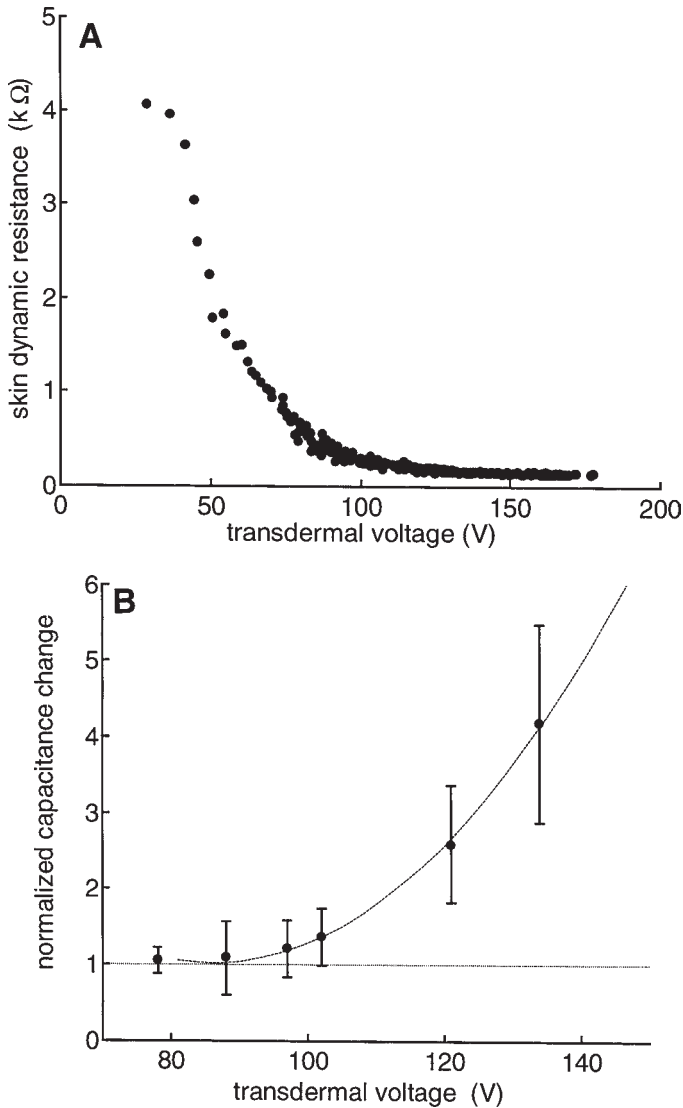


Fig 2. Skin dynamic resistance and normalized capacitance as functions of transdermal voltage. Dynamic resistance dropped precipitously at transdermal voltages greater than approximately 50 V, while capacitance increased at voltages above about 90 V. Exponential-decay pulses were used with a time constant of 1.1 ms. Experiments were performed using human epidermis *in vitro*. **(A)** Dynamic resistance was determined 20 μ s after the onset of the pulse (i.e., during the pulse). **(B)** Capacitance values were determined from impedance spectra collected 330 ms after the end of the pulse and have been normalized relative to prepulse values. (From **ref. 13**, with permission.)

high-voltage pulsing indicates a disorganization of the lipid bilayer structures, consistent with an electroporation mechanism. Weaker effects were seen for short or low-voltage pulses.

Wide-angle X-ray scattering (WAXS) is used to measure scattering features with Angstrom dimensions. **Figure 3B** shows the effects of electroporation on WAXS. The peaks seen at 3.8 Å and 4.1 Å are characteristic of orthorhombic lateral packing and/or lateral hexagonal packing of lipids in normal skin. The disappearance of those peaks after high-voltage pulsing indicates a change in lipid packing order, also consistent with electroporation. Greater effects were seen when more pulses were applied.

X-ray scattering techniques provide powerful insight into skin microstructure, but require expensive equipment and an experienced operator (30,31). Moreover, measurements must be made on isolated stratum corneum to eliminate noise from viable epidermis and dermis. Measurements also can only be made after (not during) exposure to electric pulses and take tens of minutes to acquire. This means that only long-lived changes can be detected; rapidly transient effects will have reversed before a measurement can be made. While only limited x-ray analysis has been done on electroporated skin, a number of studies have examined skin microstructure in other contexts using both SAXS and WAXS (32–35), including a recent review (36).

2.4. Freeze-Fracture Electron Microscopy

Freeze-fracture electron microscopy (FFEM) has been used to obtain direct images of changes in skin microstructure (37). **Figure 4A** shows a smooth surface with well-delineated stepwise interruptions (which correspond to the multilamellar lipid structures) characteristic of untreated stratum corneum. Desmosomes are apparent too. By contrast, the electroporated stratum corneum shown in **Fig. 4B** appears rough and lacks well-defined interruptions, displays spherical deformations and a network-like structure in the lamellar regions, and has few desmosomes. Such electron micrographs give a qualitative view of the microstructural changes caused by electroporation.

In general, electron microscopy requires not only costly equipment and a knowledgeable operator, but significant expertise to correctly interpret images. It is evident from **Fig. 4** that an inexperienced viewer might not be able to correctly analyze an electron micrograph of skin. Moreover, the outcome is extremely sensitive to sample freezing and preparation, a process which can require many days. Although FFEM specifically of electroporated skin has received only limited attention, general methods to study skin using FFEM, as well as transmission and scanning electron microscopy, have been more extensively developed (38–42).

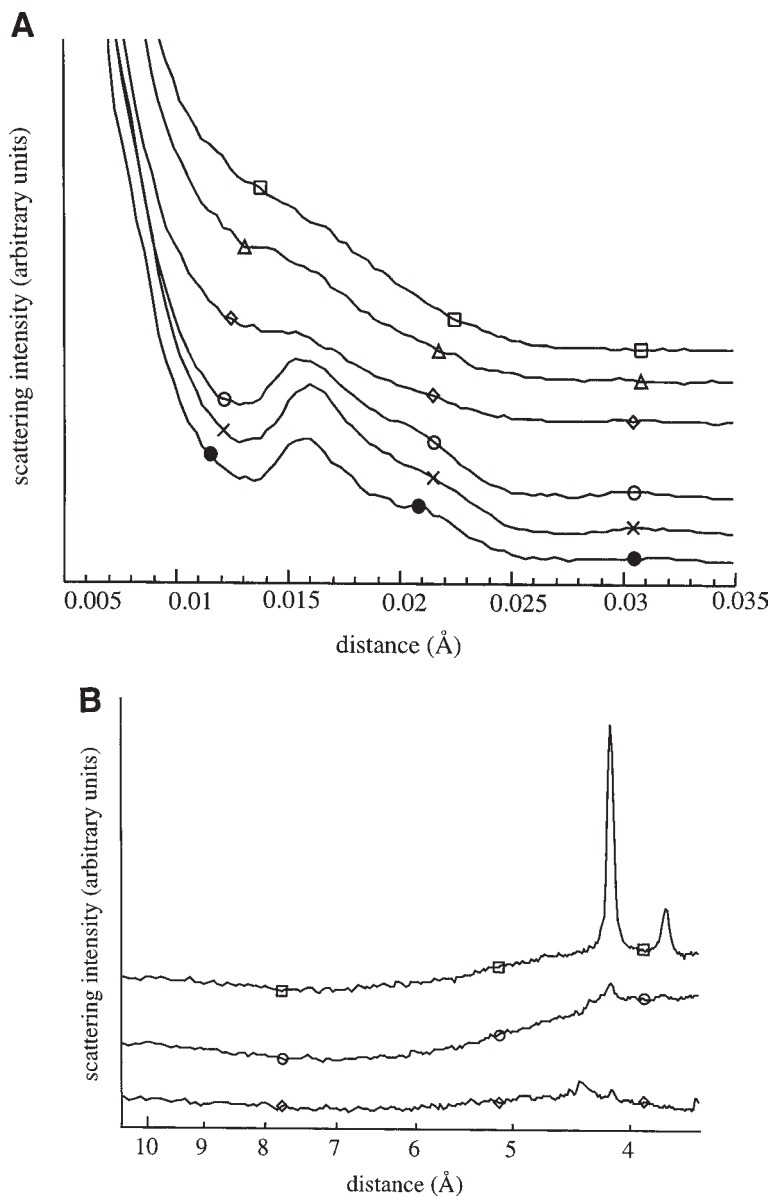


Fig. 3. X-ray analysis of electroporated human stratum corneum in vitro. Application of high-voltage pulses causes a loss of lipid structure within the skin (see text). **(A)** Small-angle X-ray scattering (SAXS): 20 pulses of 200 V and 160 ms (□), 20 × (200 V, 80 ms) (Δ), 5 × (200 V, 160 ms) (◇), 20 × (100 V, 160 ms) (○), 60 × (500 V, 1 ms) (×), no pulses (●). **(B)** Wide-angle X-ray scattering (WAXS): no pulses (□), 5 × (200 V, 160 ms) (○), 20 × (200 V, 160 ms) (◇). All listed voltages are applied (i.e., not transdermal) values. (From **ref. 29**, with permission.)

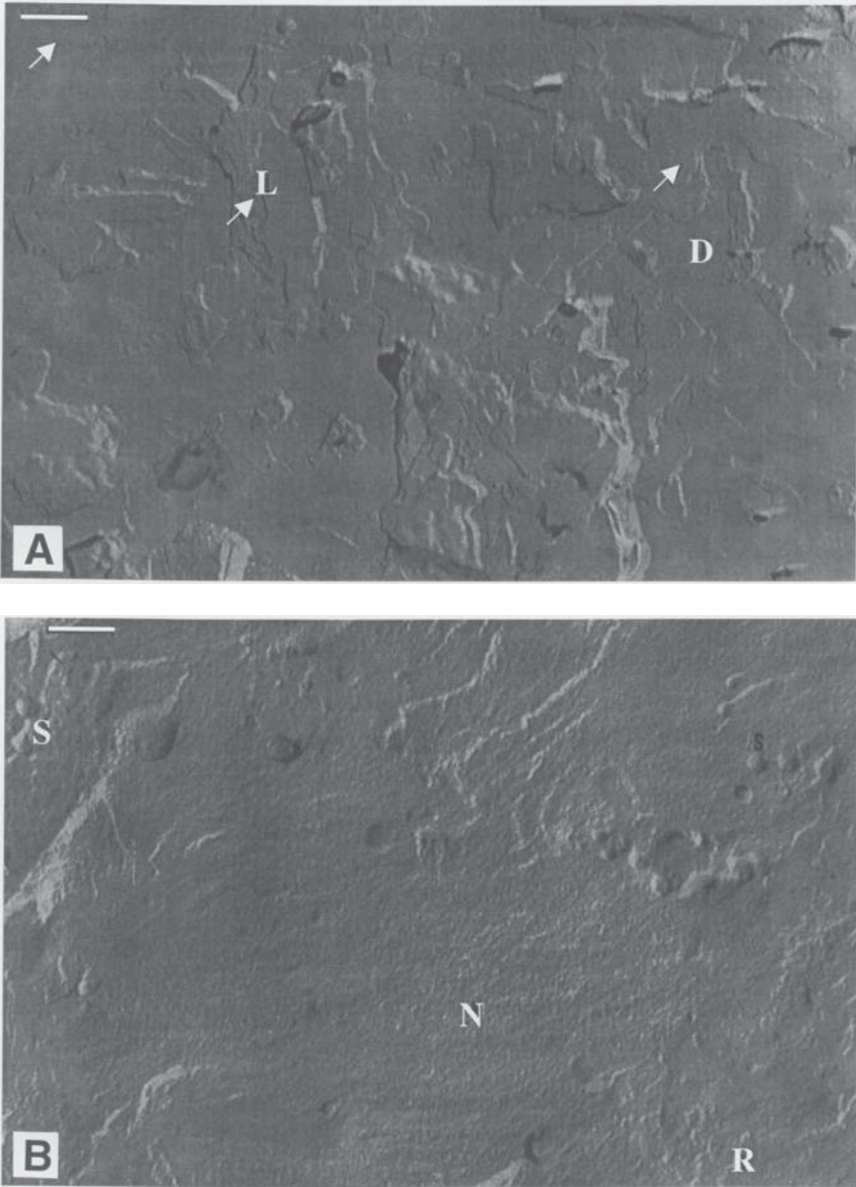


Fig. 4. Parallel fractures of human stratum corneum in vitro imaged using transmission electron microscopy. **(A)** Hydrated, untreated control skin shows lipid lamellar domains (L), well-delineated stepwise interruptions of the planes (arrow), and some desmosomes (D). Scale bar is 612 nm. **(B)** Electroporated skin shows few normal lipid bilayers, rough surfaces (R), a networklike structure (N), and spherical deformation (S). Electroporation was carried out using 20 pulses each of 300 V (applied) and 120 ms. Scale bar is 453 nm. (From [ref. 37](#), with permission.)

2.5. Other Methods

There are a number of other biophysical tools available to study the effects of electroporation on skin, including Fourier-transform infrared (FTIR) spectroscopy, differential scanning calorimetry (DSC) / differential thermal analysis (DTA), and measurement of ion content in skin.

FTIR spectroscopy measures the infrared absorbance characteristics of a material, which gives insight into its internal chemical make-up and environment (43,44). Because conventional FTIR is usually performed in transmittance mode, an attenuated total reflectance (ATR) crystal can be used to make measurements on the surface of a material (45). By selecting an appropriate ATR set-up, IR spectra from only the stratum corneum can be collected without significant contribution from deeper tissue. Approaches both with and without ATR have been used in a number of studies of skin (46–48), including *in vivo* investigations (49). FT-Raman spectroscopy has also been explored (50). Applied to electroporated skin, FTIR spectroscopic analysis showed increased stratum corneum hydration (determined by measuring changes in the ratio of two amide-associated peaks), but no detectable changes in spectral characteristics associated with stratum corneum lipids or proteins (51). In general, ATR-FTIR spectroscopy measurements are relatively straightforward to obtain, but their analysis requires some expertise.

Differential scanning calorimetry (DSC) and differential thermal analysis (DTA) (52,53) have also been used to study skin properties (46,48,54). Using these methods, the relationship between stratum corneum temperature and the energy required to heat stratum corneum to that temperature are measured. In the absence of phase changes, this measurement is related to the tissue heat capacity. Discontinuities in the relationship (i.e., an exceptionally large amount of heat required for a given temperature change) indicates a phase change and the amount of heat is related to the enthalpy of that phase change. In both untreated and electroporated stratum corneum, DTA transition temperatures were observed at approximately 70°C and 86°C, which is characteristic of normal stratum corneum (37). However, the enthalpy change associated with those transitions was less for electroporated samples. DSC and DTA measurement techniques and analysis can be learned relatively quickly from an experienced user.

A final biophysical test applied to the study of skin electroporation involves identifying changes in skin's ion composition and water content. After digesting the skin with either strong acid or strong base, sodium and potassium ions were detected by flame spectrophotometry, calcium by atomic absorption, and chloride using a silver electrochemical cell (55). In a test using full-thickness rat skin, sodium and calcium ion concentration were increased by electro-

poration, potassium levels were decreased, and chloride was unchanged. Increases in water content were evaluated by comparing the difference in weight between hydrated and thermally dehydrated stratum corneum (37).

3. Imaging of Transport Pathways

The previous section summarized ways to characterize changes in skin microstructure. This section addresses how to image the effects of those changes on skin permeability by identifying the pathways by which ions and molecules traverse the skin. This is important because one of the questions typically asked in transdermal studies concerns the role of transport through hair follicles and sweat ducts (i.e., appendages) versus transport through the bulk of the skin. If transport is through the bulk, then one often wants to know if transport occurs uniformly across the whole skin surface or if there are localized regions of transport. Moreover, it is of interest to determine if transport through the bulk involves pathways across the keratinocyte cells or if it winds around the cells through the intercellular lipids.

Imaging pathways both for electric current carried by ions (e.g., sodium, chloride) and for larger molecules has shown that there are distinct differences between the pathways followed during skin electroporation as opposed to passive diffusion or iontophoresis (i.e., low-voltage electrophoresis). Unlike passive diffusion which occurs via tortuous pathways between cells and may include routes through appendages and iontophoresis which concentrates transport through appendages, electroporation appears to create new pathways in the bulk of stratum corneum, resulting in local transport regions which do not correspond to appendages and appear to have non-tortuous pathways directly across the skin (56,57).

3.1. Imaging Electric Current Pathways

3.1.1. Plate Electrode Methods

The sites of chloride ion transport across the skin can be identified by imaging the conversion of silver to silver chloride on a flat plate electrode in contact with the skin (56). In this approach, a silver electrode is placed in direct contact with the underside of isolated stratum corneum and attached to the positive lead of the power supply. The counter electrode is placed in electrical contact with the other side of the stratum corneum to serve as the negative electrode. Passage of current across the skin in the presence of sodium chloride will cause chloride ions to cross the skin and electrochemically react at the silver surface to form silver chloride. The sites of this reaction can be interpreted to correspond to the sites of transdermal current flow.

Figure 5 shows the result of such an experiment, where current is observed

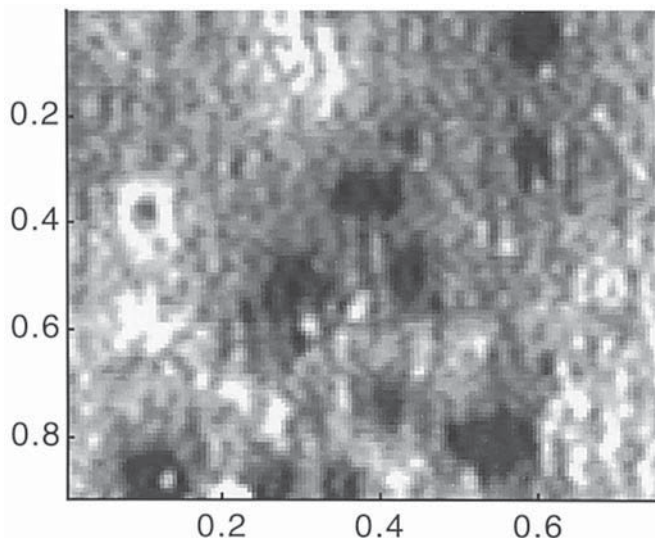


Fig. 5. Sites of electrochemical deposition of silver chloride (dark areas) on a silver plate electrode used during electroporation of human epidermis *in vitro*. The dark areas are interpreted as sites of transdermal current pathways, which correspond to locations in the bulk of the stratum corneum and do not correspond to hair follicles or sweat ducts. Skin was electroporated with 10 pulses each of 1000 V (applied) and 1 ms at a rate of 6 pulses per minute. (From **ref. 56**, with permission.)

in localized regions which do not correspond to sites of hair follicles or sweat ducts in the electroporated skin. While skin exposed to iontophoresis also shows localized regions of current flow, they are at a lower density and predominantly correspond to sites of hair follicles or sweat ducts (data not shown).

Two kinds of silver plate electrodes have been employed. One approach to image the sites of chloride ion transport uses a very thin silver electrode deposited onto a transparent polystyrene plate using Tollen's reagent as the source of silver (**56**). When silver chloride is electrochemically formed during an experiment, it dissociates from the electrode surface and leaves a clear spot on the polystyrene plate. In this way, the sites of current transport, which correspond to the sites of silver removal, can be monitored in real time using a bright-field microscope viewing the underside of the electrode.

An alternative approach involves the use of a polished silver plate and a thin (e.g., 5 mm) layer of agarose gel sandwiched between the silver plate and the skin (**56**). In this case, when silver chloride is electrochemically formed, its precipitates are trapped in the gel and remain at the sites of ion transport. The unreacted, polished silver appears shiny and bright, while the sites of silver

chloride production appear dull and black. This can be seen using a microscope either through the skin in real time or, for a better view, with the skin removed afterward.

3.1.2. Microelectrode Methods

A set of complementary approaches to identifying current pathways has been used for iontophoresis experiments, and could be used for skin electroporation studies as well. One method involves the use of a small vibrating probe electrode which is oscillated within micrometers of the skin surface to measure local voltage gradients and thereby determine local current densities (58,59). This probe can follow the current in a single location over time or can be rastered over a larger area to create a two-dimensional current density map, but with limited time resolution.

Another method, termed electrochemical microscopy (60,61), also uses a microelectrode positioned near the skin, but selectively measures the current carried by a specific ion, rather than the total current measured by the vibrating probe. This can be achieved by placing a $K_4Fe(CN)_6$ solution on one side of the skin and NaCl solution on the other side. The microelectrode, which is positioned on the NaCl side of the skin, can specifically measure the rate of appearance of $Fe(CN)_6^{4-}$ ions which have crossed the skin. As above, the measurement can be made in one location with good time resolution or as a series of measurements across a surface with limited time resolution.

As a final alternative, a microelectrode can be used to identify sites of ion transport by the electrochemical formation of a dye (61). A solution containing Fe^{3+} is placed on one side of the skin and a solution with $Fe(CN)_6^{4-}$ is placed on the opposite side. As current is passed and the two ions meet, they react to form $Fe_4[Fe(CN)_6]_3$, which is a dye called Prussian blue. Thus, the sites of current flow are marked by insoluble Prussian blue precipitates.

3.2. Imaging Molecular Transport Pathways

3.2.1. Post-Electroporation Imaging

The sites of molecular transport of dyes can be visualized by microscopy (62). While colorimetric dyes can be used, fluorescent dyes (63) are much more sensitive and can also be used for confocal microscopy. Microscopic imaging has shown that transport across electroporated stratum corneum occurs in localized regions (Fig. 6) (56,57). Because these regions were shown not to correspond to hair follicles or sweat ducts, transport due to electroporation is believed to occur through the bulk of the stratum corneum. Closer examination of the regions of transport show distinct ringlike staining (Fig. 7), which could be interpreted to indicate a central region with long-lasting permeability from

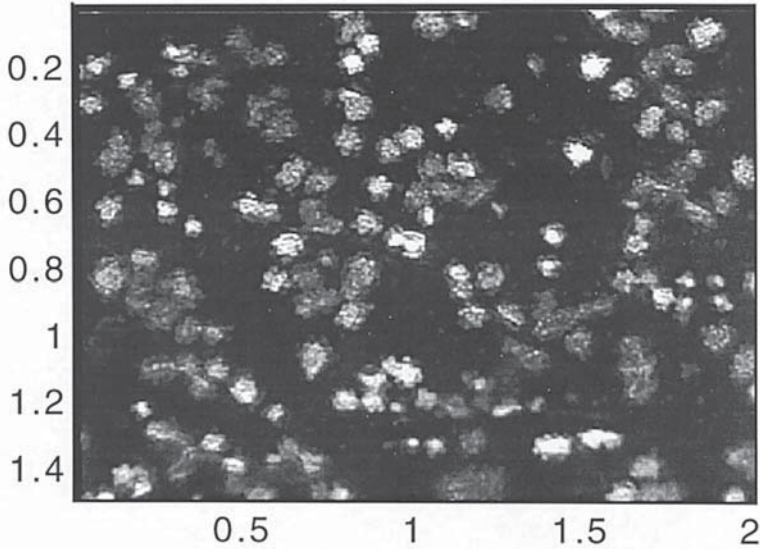


Fig. 6. Sites of transdermal calcein transport across human epidermis *in vitro* identified using a fluorescence microscope. The light areas are interpreted as sites of transdermal transport pathways, which correspond to locations in the bulk of the stratum corneum and do not correspond to hair follicles or sweat ducts. Skin was electroporated with 10 pulses of 157 V (transdermal) and 1 msec at a rate of 2 pulses per minute. (From **ref. 56**, with permission.)

which the dye was washed away and a peripheral region in which the increased permeability reversed and thereby trapped the dye (56,57). Moreover, these regions of molecular transport were shown to correspond to the regions of ion transport identified using the plate electrode technique described above (56).

To image transdermal transport pathways after an electroporation exposure, one skin surface is bathed in a dye solution and the skin is then treated with electric pulses in a standard diffusion chamber. After the skin is removed from the chamber, excess dye is washed away from the skin surface so that only dye that penetrated inside remains. Some investigators have just rinsed the skin well with saline, while others have soaked it for hours (56,57). The skin can then either be observed immediately or flash frozen and stored at -80°C until examination later. Microscopic imaging can be performed using either a conventional fluorescence microscope or, for improved spatial resolution, a scanning confocal fluorescence microscope (64,65). Additional information can be obtained from light microscopy (66–68), autoradiography (69,70), and confocal microscopy (59,71,72) methods developed for studies of transdermal transport pathways outside the context of electroporation.

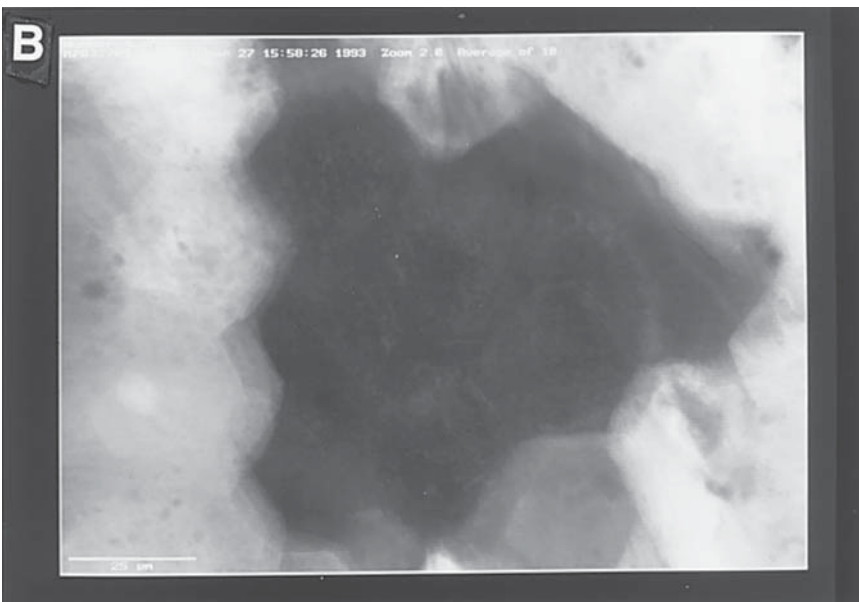
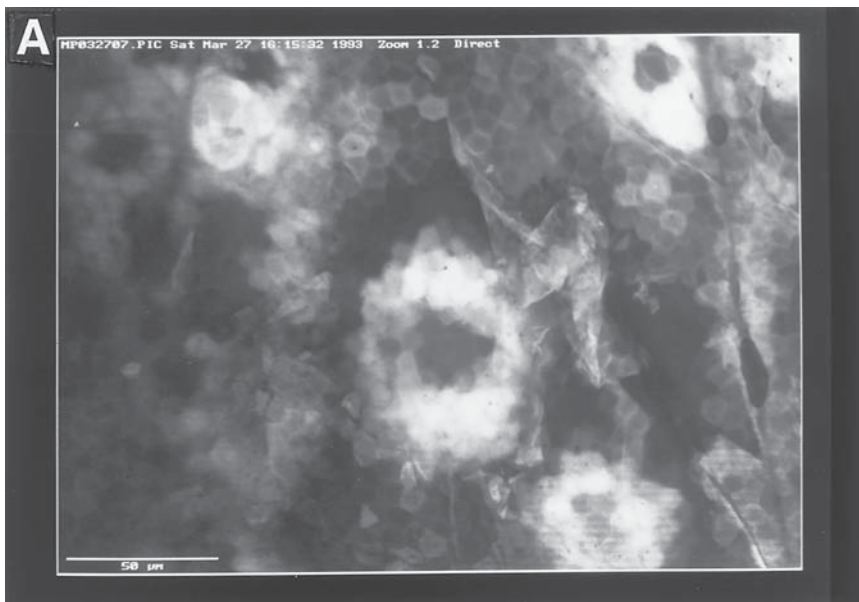


Fig. 7. Sites of transdermal calcein transport across human epidermis *in vitro* identified using a laser-scanning confocal microscope. Transport appears to occur in localized regions which have a ringlike appearance: bright along the rim and dark in the center. Skin was exposed to high-voltage pulsing at 300 V (transdermal) and 1 msec for 1 hour at a rate of 12 pulses per minute. (A) Low-magnification view of skin. (B) High-magnification optical section of same site at a depth of 10 μm below the surface. (From ref. 57, with permission.)

Dyes used to image transport pathways have generally been hydrophilic ones (e.g., calcein), which reduces binding to the skin (56,57). This is important because one wants to image the sites of transport and not view sites preferentially stained due to binding. As a separate procedure, dyes (of a different color than the dye used during pulsing) can be added after electroporation and just before microscopic imaging to selectively stain the skin and thereby facilitate histological or other interpretation. For example, viewing **Fig. 7** alone, it is not clear if the central region of the transport pathways contain intact tissue or if they each represent a single large hole. Staining of the skin with nonspecific lipophilic dyes (i.e., DiI and Nile Red) indicated that the central region was filled with lipophilic material and thus likely contained intact, but probably porous, tissue (data not shown) (57).

Electron microscopy techniques have also been used to image transdermal transport pathways by identifying the location of electron-dense tracers in skin, but these methods have not yet been applied to skin electroporation. Transmission (73,74), scanning (75) and freeze fracture (76,77) electron microscopy have similarly been employed to identify routes of transport. Electron microscopy has also been used in conjugation with in situ precipitation to image non-electron-dense permeants (68,78,79), as well as in combination with x-ray microanalysis for elemental analysis (79,80).

3.2.2. *In Situ Imaging During Electroporation*

Transport pathways can also be imaged by fluorescence microscopy in situ during an electroporation exposure (56). The advantage of this approach is that real-time information can be obtained and concerns about postexposure handling of the skin are removed. For example, using this approach, the number of local transport regions present during skin electroporation were shown to increase with both voltage and number of pulses applied (56). Despite its utility, difficulties with the in-situ imaging apparatus arise due to (i) bright fluorescence from the donor solution which overwhelms fluorescence from dye within the skin, (ii) electrodes blocking the view of skin from the microscope objective, and (iii) electrochemical formation of gas bubbles which interfere with transport and viewing.

An apparatus for an upright microscope which addresses these difficulties is composed of, sequentially from the bottom up, an electrode, donor solution in the form of a gel, stratum corneum, receiver solution which is surrounded by a porous cylinder (e.g., made of a ceramic material), cover slip, and microscope objective (56). The electrode on the receiver side is not in line with the rest of the apparatus, but is placed to the side of the receiver compartment and in electrical contact through the porous cylinder. The reason for this design is described in the following paragraphs.

To reduce fluorescence from the donor solution reaching the microscope objective, the donor solution should be placed on the opposite side of the skin (i.e., for an upright microscope, the donor solution should be below the skin). In addition, a thin layer of black ink should be added between the donor solution gel and the stratum corneum to reduce light penetration across the skin.

To prevent the electrode between the microscope objective and the skin from blocking the view, a ring-shaped electrode can be used, which provides a clear optical pathway. This electrode is therefore positioned around, but not inside, the receiver compartment, and must be in electrical contact.

To address the problem of bubbles, the lower electrode should not be a continuous plate, but should be made of a mesh or other porous design. In this way, bubbles produced at the lower electrode, which cannot rise through the donor solution because it is a gel, therefore escape through the open spaces in the lower electrode. Similarly, bubbles produced at the upper electrode cannot enter the receiver compartment because the porous cylinder blocks them. The bubbles therefore escape to the open surface above the upper electrode.

3.2.3. Molecular Trapping in Gel

To address the concern that sites containing dye may represent sites of binding rather than sites of transport, experiments which image those places where dye is found within skin (described above) can be coupled with experiments which identify the places where dye appears after it has crossed the skin (56). This approach is similar to that used with the silver plate to identify current pathways. To perform this study, a very thin layer of agarose gel (e.g., $\ll 1$ mm) is sandwiched between skin and a silver plate electrode. To maintain the gel thickness and to reduce lateral diffusion within the gel, a nylon mesh (e.g., 50 μm spacing) is also placed inside the gel. The skin is then electroporated in the presence of dye on the skin surface opposite the gel. The skin and gel are then quickly examined under the microscope (**Fig. 8**). In this way, dye which has crossed the skin is trapped in the gel. If the sites of skin staining correspond to the sites of gel staining, then one can conclude that the sites of skin staining are indeed transdermal transport pathways. Using this approach, sites of skin staining were shown to correspond to sites of transdermal transport for the conditions studied (56).

4. In Vivo Methods

As a companion to in vitro studies, which primarily address changes in stratum corneum, in vivo methods provide information about the response of viable skin to electroporation in a more physiologically relevant environment, which is especially important to assess safety. Noninvasive investigation of

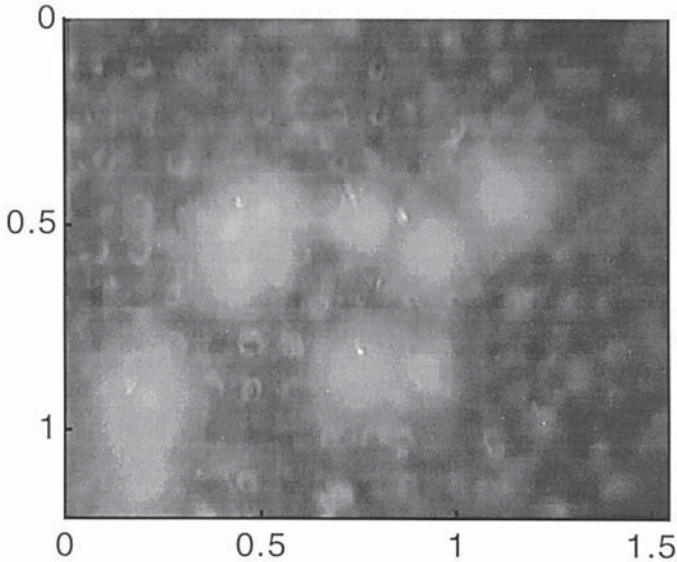


Fig. 8. Sites of sulforhodamine entrapped in agarose gel on the underside of human epidermis *in vitro*. Rather than identifying sites of staining within skin (e.g., **Figs. 6** and **7**), which only indirectly identify sites of transdermal transport, imaging sites of staining below the skin directly establishes sites of transdermal transport. Transport sites identified by both methods were in agreement, indicating that sites of skin staining in fact corresponded to sites of transdermal transport. Skin was electroporated with 10 pulses each of 1000 V (applied) and 1 ms at a rate of 6 pulses per minute. (From **ref. 56**, with permission.)

skin can be carried out *in vivo* with a number of different biophysical measurements using commercially available devices (**81–84**).

There are five principle biophysical parameters commonly measured to assess changes in skin integrity: skin color, blood flow, barrier properties, hydration, and thickness (**81,83**). Measurement of skin color, typically by colorimetry, allows quantification of erythema. Laser Doppler flowmetry (LDF) measures cutaneous blood flow and therefore detects vasodilation in case of inflammation. Evaporimetry measures transepidermal water loss (TEWL), which gives insight into the level of hydration and the skin's permeability barrier. Hydration of skin can also be assessed by measuring epidermal capacitance. Finally, high-frequency ultrasound measurement of skin thickness can be used to quantify edema. To properly characterize skin integrity, multi-parametric assessment using a number of techniques is generally required.

These bioengineering methods have been employed widely for noninvasive evaluation of skin, including electroporated skin. In studies of hairless rat skin

exposed to high-voltage pulses *in vivo*, changes in a number of skin properties were measured (85). These alterations were found to be short-lived and were similar to those observed following conventional iontophoresis, which suggests that electroporation of skin would be safe and well-tolerated by patients (86). In these studies, electrical protocols were applied using parallel-plate electrodes attached to calipers across a skin fold. Although this electrode configuration can effectively electroporate the stratum corneum, it also exposes underlying tissues (e.g., viable epidermis and dermis) to the high-voltage electric field. This means that alterations in skin functions observed in the study represent the combined effect of stratum corneum electroporation and any side effects caused in underlying tissues. The rest of this section provides more information on five methods used to assess changes in skin function and presents in greater detail the results of their use in skin electroporation studies.

4.1. Colorimetry

Skin color can be precisely measured using a colorimeter (e.g., Minolta CR 200, Osaka, Japan); this method is often used to quantify erythema, of interest for safety studies, and tanning, of interest for cosmetics (81,87). Colorimeter measurement is effected by illuminating the skin, usually with a xenon flash light, and measuring the reflected light. The color measurement is quantified using the three standard parameters a^* , b^* , and L^* , as established by the CIE (Commission Internationale de l'Eclairage) (87). The values for a^* and b^* represent the two color coordinates: a^* is a measure of the color range from green (–) to red (+) and generally correlates with the clinical perception of erythema, and b^* is a measure of the color range from blue (–) to yellow (+) and is usually associated with the perception of tanning. Luminance (L^*) is a measure of brightness (integrated reflection of light from the surface) which ranges from black (zero) to white (100) and correlates with both erythema and tanning.

Measurement of skin color after exposure to high-voltage pulses has been performed in hairless rats using a colorimeter (85). Parameter a^* was slightly and briefly increased after electroporation (Fig. 9), indicating transient erythema. In some cases, a small, short-lived decrease in lightness (L^*) was also observed. These alterations in color were similar in intensity to those induced by conventional iontophoresis (Fig. 9).

Colorimetry is a straightforward, reproducible, convenient, and inexpensive method to determine skin irritation as measured by erythema. Only minor expertise is required. However, it is not as sensitive to small changes in skin integrity as other techniques (e.g., TEWL measurement) (81). Since skin redness is influenced by temperature and emotional or physical stress, climate-controlled facilities are preferable and a period of rest is needed before measurement. Other techniques for measuring skin color include visual scoring,

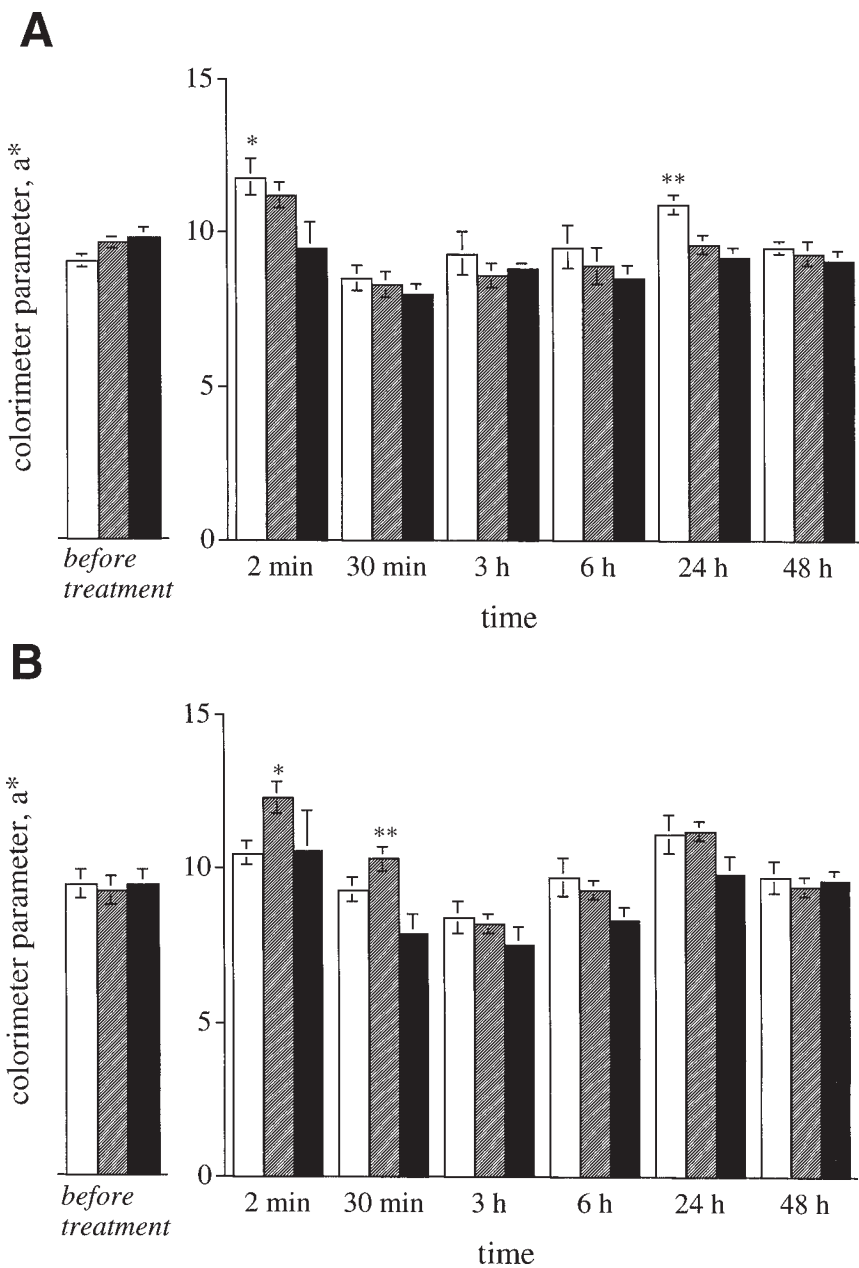


Fig. 9. Colorimetry measurement of the red-green parameter, a^* , for skin exposed to (A) electroporation or (B) iontophoresis. Measurements were made before and at different times after electrical treatment. Only small and transient changes in color (i.e., erythema) were observed using measurements at the cathode (white bars), anode (striped bars) and control (black bars). Electroporation was carried out using 15 pulses each of 100 V (applied) and 500 ms applied at a rate of 1 per minute in hairless rat

reflectance spectrophotometry, and measurement of erythema index (89,90). Visual scoring of color changes using the human eye provides excellent sensitivity, but measurements are often not reproducible (88). Colorimetry provides more reproducible and quantitative measurements and is therefore recommended. Reflectance spectrophotometry uses costly and cumbersome equipment to collect the spectrum of light reflected from skin, which can be interpreted to give information about erythema. Finally, measurement of the erythema index uses a portable and user-friendly instrument to collect a portion of the reflected spectrum which correlates with the amount of hemoglobin and therefore provides a direct measure.

4.2. Laser Doppler Flowmetry

Laser Doppler flowmetry (LDF) is a noninvasive optical technique that uses the Doppler effect to measure blood flow in many tissues including skin (91–94). Monochromatic laser light shines to a depth of about 1 mm into the tissue from an optical fiber placed on the skin surface. This light is reflected with Doppler-shifted frequencies from moving blood cells in the tissue (i.e., the dermis, since the epidermis is avascular) and with unshifted frequencies from stationary tissues. A LDF measurement is reported in arbitrary units and is proportional to red cell velocity (i.e., blood flow rate) and density (i.e., blood volume). LDF has been shown to correlate with erythema, as determined by clinical scoring and colorimetry. LDF and colorimetry differ, however, because colorimetry is sensitive to blood accumulation in capillaries, while LDF measures total blood flow determined mainly by arterial tone.

LDF has been used to assess alterations in cutaneous blood flow after exposure of skin to high-voltage pulses; a brief increase in LDF values was observed in hairless rats (Fig. 10) (85). The changes in LDF values observed after electroporation were similar to those induced by iontophoresis.

Although LDF requires sophisticated instrumentation, measurements are relatively straightforward to make. Skin blood flow can be measured continuously on virtually any site on the body. Moreover, LDF can detect changes in blood flow at levels below which the naked eye can detect erythema (91,93). Interpretation of LDF results is complicated because the cutaneous microcirculation is a dynamic system which depends on many variables, for example, anatomical site, physical and mental activities, ambient and local temperature. Best results are obtained when using a resting period before measurement and

Fig. 9. (continued) skin in vivo. Iontophoresis involved a 1-hour exposure to 0.5 mA/cm² direct current. Statistical significance: * $p < .05$ vs. control, ** $p < .01$ vs. control. (From ref. 85, with permission.)

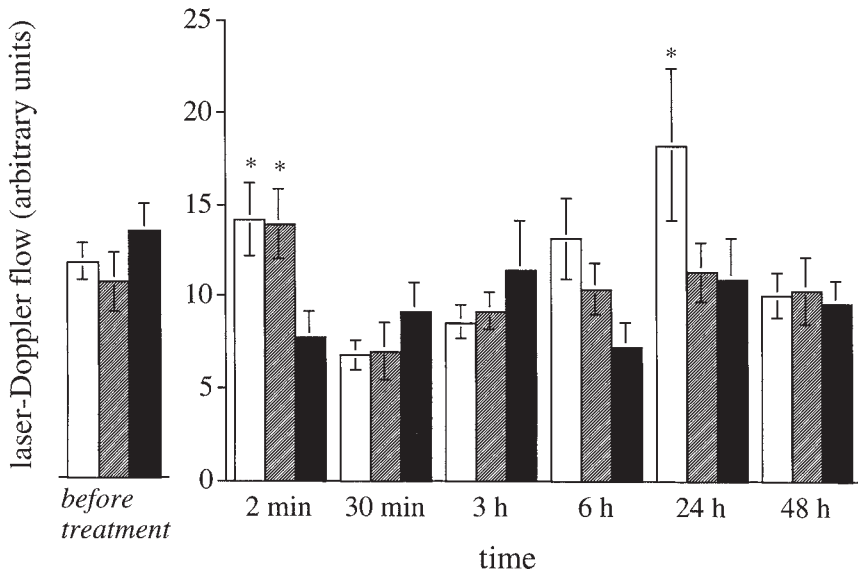
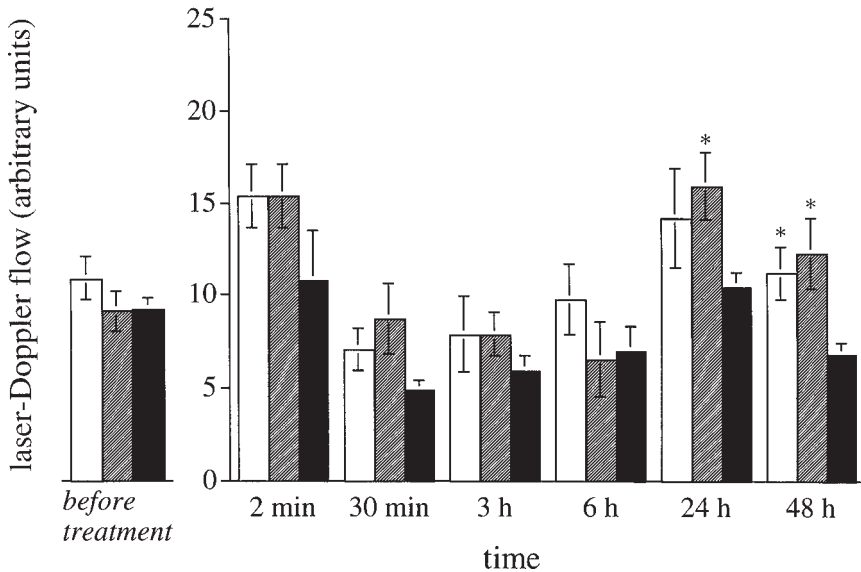
A**B**

Fig. 10. Laser-Doppler flowmetry measurement of skin blood flow following (A) electroporation or (B) iontophoresis. Only small and transient increases in blood flow (i.e., erythema) were observed. See Fig. 9 for experimental information. (From ref. 85, with permission.)

a climate-controlled facility. Identical anatomical sites should be used for comparison and multiple replicate recordings should be collected (92,94).

4.3. Transepidermal Water Loss

Transepidermal water loss (TEWL) commonly refers to the total amount of water lost across the skin by both eccrine sweating and transepidermal diffusion. This method provides an extremely sensitive measure of skin barrier integrity (95). Water transported across the skin evaporates and forms a boundary layer at the skin surface across which a water vapor gradient is created. TEWL is measured by placing a probe (containing sensors for relative humidity and temperature) within this boundary layer of estimated 1 cm thickness. The Evaporimeter EP1 (ServoMed, Stockholm, Sweden) is an open chamber in common use (81,95,96).

Measurement of TEWL after skin electroporation has been performed as a way to characterize decreases and recovery of stratum corneum barrier function (85). TEWL showed a twofold increase immediately after high-voltage pulse exposure (relative to hydrated controls) and later returned to control values (Fig. 11). Once again, these transient effects were similar to those induced by iontophoresis.

TEWL measurements are straightforward to carry out, although care must be taken to rigorously follow the measurement protocol (94,96). Accurate and reproducible measurements require attention to possible variation in the environment (e.g., ambient temperature and humidity, drafts), instrument (e.g., aging of the sensors) and individual (e.g., anatomical site and interindividual variation) (96). Variation can be partially addressed by using controlled-climate facilities and imposing a period of rest before measurements are made. Typically, room temperature is maintained at 20–22°C and relative humidity at 40%. Measurement of skin temperature is recommended to verify that it remains constant (96). TEWL has been found to be the most sensitive measure of early signs of skin irritancy when compared to colorimetry, LDF, and ultrasonic measurement of skin thickness (95).

4.4. Epidermal Capacitance

Epidermal capacitance correlates with the hydration level of skin's superficial layers (81,97). The most commonly used instrument, the Corneometer (Courage-Khazaka Electronic, Köln, Germany), uses a probe with an interdigitated grid of gold-covered electrodes. When applied to the skin surface, it establishes an electric field of variable frequency (40–75 kHz) in the upper ~ 100 µm of the skin. The measurement depends on the geometry of the electrodes, the capacitance of the dielectric material covering the electrodes (constant capacitance) and the capacitance of the skin (variable capacitance).

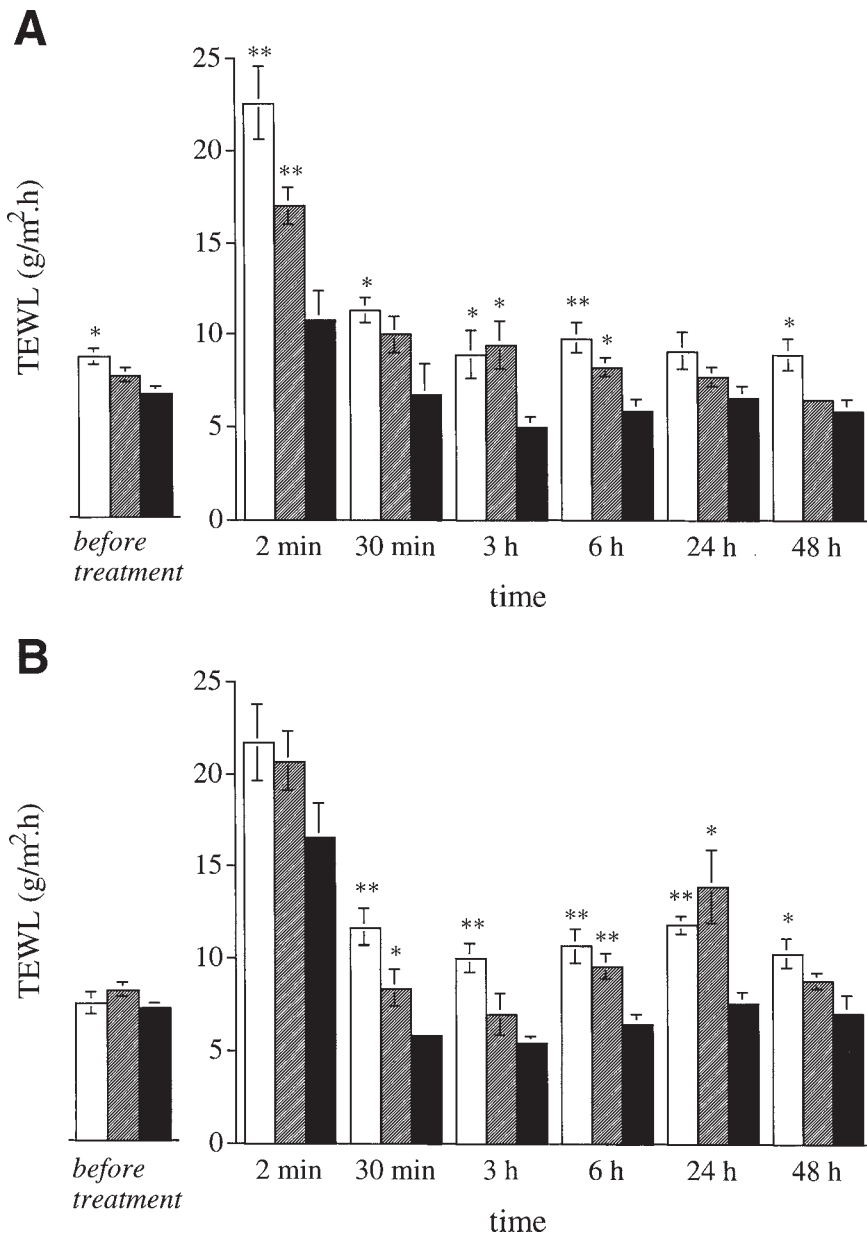


Fig. 11. Transepidermal water loss (TEWL) following (A) electroporation or (B) iontophoresis. TEWL, which is a measure of skin barrier integrity, increased temporarily after both electrical protocols, but rapidly returned to values close to controls. See Fig. 9 for experimental information. (From ref. 85, with permission.)

Hydration of the stratum corneum causes a significant change in its capacitance, which can be detected by the Corneometer.

Using this method, the effects of skin electroporation and iontophoresis on epidermal capacitance were shown overall not to be significant (**Fig. 12**) (85). However, a slight increase followed by a slow decrease to capacitances below prepulse values was observed. By contrast, using impedance spectroscopy with much better time resolution, rapidly reversible changes in skin capacitance were shown to occur (13), as described above.

The capacitance-measurement apparatus is a simple-to-use, convenient, low-cost instrument. The method is accurate, reproducible and sensitive, especially for measurement at low levels of hydration. The method is particularly suitable for quantitative evaluation of topical skin moisturizers. Because ambient temperature and relative humidity affect skin hydration, capacitance measurements must be performed at constant temperature and humidity. For valid comparison, identical and/or contralateral anatomical sites should be used (97). As an alternative, skin impedance is also sometimes measured at higher frequency (3.5 MHz) to assess the hydration state of the outermost portion of the stratum corneum (Skin Surface Hygrometer, Skicon, I.B.S. Co., Hamamatsu, Japan). It is reported that the Corneometer is more sensitive at low levels of skin hydration and the Skicon performs better at high levels of hydration (81,98).

4.5. Ultrasound Measurement of Skin Thickness

High-frequency ultrasound is used to measure skin thickness (one-dimensional A-mode scan) or to image skin structures (two-dimensional B-scan and three-dimensional C-scan) (99). Skin thickness measurements are useful for objectively assessing edema which, along with vasodilation, are the essential features of inflammation (81). Ultrasonic imaging measures the distance between an ultrasound probe and a surface within the skin (e.g., the interface between the dermis and subcutaneous fat) by measuring the time it takes for an echo to bounce off the internal surface and return to the ultrasound probe. Although ultrasound measurement of skin thickness has not yet been used in the context of skin electroporation, it represents an important noninvasive *in vivo* technique often used to investigate skin (81).

Ultrasound A-scan measurement of skin thickness is a simple and reproducible technique which provides a measure of skin irritancy almost as sensitive as TEWL. Some skill is needed to correctly interpret the graphical output which describes the spacing of the acoustically reflective interfaces within the skin. Compared to other bioengineering methods, ultrasound measurement of skin thickness has the advantage that modest changes in ambient conditions will not

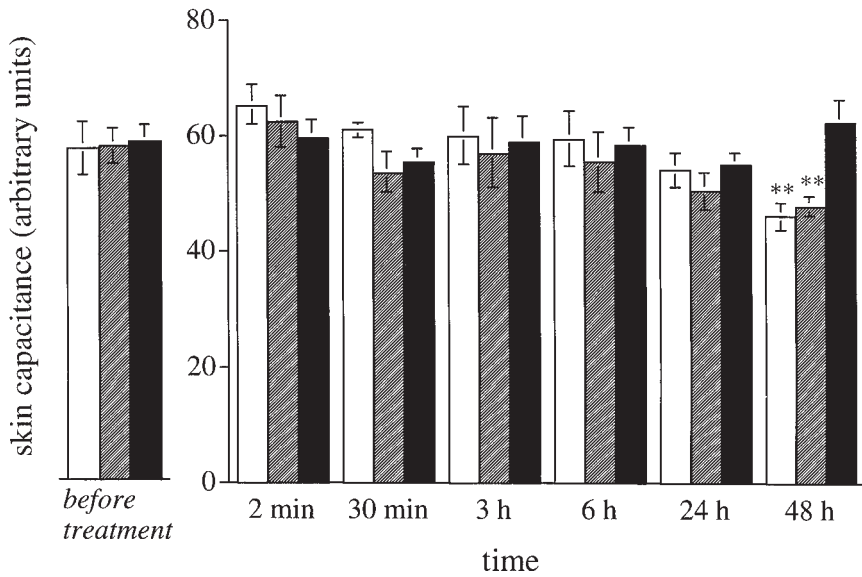
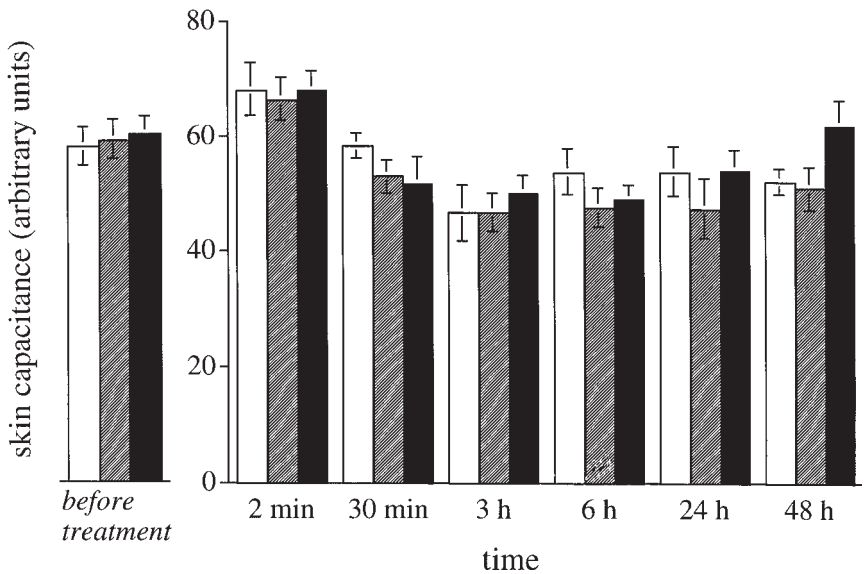
A**B**

Fig. 12. Skin capacitance following (A) electroporation or (B) iontophoresis. No significant increases in skin capacitance were observed, but a small decrease is apparent. See Fig. 9 for experimental information. (From ref. 85, with permission.)

influence the measurement and that no preconditioning of the subject's skin is needed (100).

5. Summary and Conclusions

The very large increases in rates of transdermal transport induced by high-voltage pulses make skin electroporation a compelling approach to transdermal drug delivery. To better understand the mechanisms by which skin is permeabilized, changes in skin's microstructure have been probed using electrical, X-ray, electron microscopy, and other techniques. Together, they suggest that significant changes occur and reverse at least partially over timescales ranging from microseconds to hours. Methods to image transport pathways have addressed sites of current flow using plate and microelectrode techniques as well as locations of molecular transport using microscopic analysis during or after electroporation. These studies identified the sites of both ionic and molecular transport to be localized in domains within the bulk of stratum corneum and not associated with appendages. In vivo studies have been carried out to assess electroporation effects on viable skin using colorimetry, laser-Doppler flowmetry, transepidermal water loss, and skin capacitance. Together they suggest that transient changes occur, but are generally no greater than those caused by iontophoresis protocols which are generally believed to be safe.

References

1. Neumann, E., Sowers, A. E., and Jordan, C. A. (1989) *Electroporation and Electrofusion in Cell Biology*. Plenum, New York.
2. Tsong, T. Y. (1991) Electroporation of cell membranes. *Biophys. J.* **60**, 297–306.
3. Chang, D. C., Chassy, B. M., Saunders, J. A., and Sowers, A. E. (1992) *Guide to Electroporation and Electrofusion*. Academic Press, New York.
4. Orłowski, S. and Mir, L. M. (1993) Cell electropermeabilization: A new tool for biochemical and pharmacological studies. *Biochim. Biophys. Acta* **1154**, 51–63.
5. Weaver, J. C. (1993) Electroporation: A general phenomenon for manipulating cells and tissues. *J. Cell. Biochem.* **51**, 426–435.
6. Bronaugh, R. L. and Maibach, H. I. (1999) *Percutaneous Absorption, Drugs—Cosmetics—Mechanisms—Methodology*. Marcel Dekker, New York.
7. Hadgraft, J. and Guy, R. H. (1989) *Transdermal Drug Delivery: Developmental Issues and Research Initiatives*. Marcel Dekker, New York.
8. Potts, R. O. and Guy, R. H. (1997) *Mechanisms of Transdermal Drug Delivery*. Marcel Dekker, New York.
9. Chizmadzhev, Y. A., Zarnytsin, V. G., Weaver, J. C., and Potts, R. O. (1995) Mechanism of electroinduced ionic species transport through a multilamellar lipid system. *Biophys. J.* **68**, 749–765.

10. Edwards, D. A., Prausnitz, M. R., Langer, R., and Weaver, J. C. (1995) Analysis of enhanced transdermal transport by skin electroporation. *J. Controlled Release* **34**, 211–221.
11. Weaver, J. C., Vaughan, T. E., and Chizmadzhev, Y. (1999) Theory of electrical creation of aqueous pathways across skin transport barriers. *Adv. Drug Deliv. Rev.* **35**, 21–39.
12. Prausnitz, M. R., Bose, V. G., Langer, R., and Weaver, J. C. (1993) Electroporation of mammalian skin: A mechanism to enhance transdermal drug delivery. *Proc. Natl. Acad. Sci. USA* **90**, 10,504–10,508.
13. Pliquett, U., Langer, R., and Weaver, J. C. (1995) Changes in the passive electrical properties of human stratum corneum due to electroporation. *Biochim. Biophys. Acta* **1239**, 111–121.
14. Chizmadzhev, Y. A., Indenbom, A. V., Kuzmin, P. I., Galichenko, S. V., Weaver, J. C., and Potts, R. O. (1998) Electrical properties of skin at moderate voltages: Contribution of appendageal macropores. *Biophys. J.* **74**, 843–856.
15. Prausnitz, M. R. (1996) Do high-voltage pulses cause changes in skin structure? *J. Controlled Release* **40**, 321–326.
16. Prausnitz, M. R. (1998) Electroporation, in *Electronically Controlled Drug Delivery* (Berner, B. and Dinh, S. M., eds.), CRC Press, Boca Raton, FL, pp. 185–214.
17. Pliquett, U. (1999) Mechanistic studies of molecular transdermal transport due to skin electroporation. *Adv. Drug Deliv. Rev.* **35**, 41–60.
18. Prausnitz, M. R. (1999) A practical assessment of transdermal drug delivery by skin electroporation. *Adv. Drug Deliv. Rev.* **35**, 61–76.
19. Vanbever, R. and Preat, V. (1999) In vivo efficacy and safety of skin electroporation. *Adv. Drug Deliv. Rev.* **35**, 78–88.
20. Gallo, S. A., Oseroff, A. R., Johnson, P. G., and Hui, S. W. (1997) Characterization of electric-pulse-induced permeabilization of porcine skin using surface electrodes. *Biophys. J.* **72**, 2805–2811.
21. Prausnitz, M. R. (1996) The effects of electric current applied to the skin: A review for transdermal drug delivery. *Adv. Drug Deliv. Rev.* **18**, 395–425.
22. Stubbins, W. F. (1986) *Essential Electronics*. Wiley, New York.
23. Macdonald, J. R. (1992) Impedance spectroscopy. *Ann. Biomed. Eng.* **20**, 289–305.
24. Prausnitz, M. R., Lee, C. S., Liu, C. H., Pang, J. C., Singh, T.-P., Langer, R., and Weaver, J. C. (1996) Transdermal transport efficiency during skin electroporation and iontophoresis. *J. Controlled Release* **38**, 205–217.
25. Yamamoto, T. and Yamamoto, Y. (1977) Analysis for the change of skin impedance. *Med. Biol. Eng. Comput.* **15**, 219–227.
26. Leveque, J. L. and Rigal, J. D. (1983) Impedance methods for studying skin moisturization. *J. Soc. Cosmet. Chem.* **34**, 419–428.
27. Ackmann, J. J. and Seitz, M. A. (1984) Methods of complex impedance measurements in biologic tissue. *Crit. Rev. Biomed. Eng.* **2**, 281–311.
28. Burnette, R. R. and DeNuzzio, J. D. (1997) Impedance spectroscopy: Applications to human skin, in *Mechanisms of Transdermal Drug Delivery* (Potts, P. O. and Guy, R. H., eds.), Marcel Dekker, New York, pp. 215–230.

29. Jadoul, A., Regnier, V., Doucet, J., Durand, D., and Pr eat, V. (1997) X-ray scattering analysis of the stratum corneum treated by high voltage pulses. *Pharmacol Res.* **14**, 1275–1277.
30. Woolfson, M. M. (1970) *X-Ray Crystallography*. Cambridge University Press, Cambridge, UK.
31. Rhodes, G. (1993) *Crystallography Made Crystal Clear*. Academic Press, San Diego, CA.
32. White, S. H., Mirejovsky, D., and King, G. I. (1988) Structure of lamellar lipid domains and corneocyte envelopes of murine stratum corneum. An x-ray diffraction study. *Biochemistry* **27**, 3725–3732.
33. Bouwstra, J. A., Gooris, G. S., de Vries, M. A., van der Spek, J. A., and Bras, W. (1991) Structural investigations of human stratum corneum by small-angle X-ray scattering. *J. Invest. Dermatol.* **97**, 1005–1012.
34. Garson, J., Doucet, J., Deveque, J. L., and Tsoucaris, G. (1991) Oriented structure in human stratum corneum revealed by X-ray diffraction. *J. Invest. Dermatol.* **96**, 43–49.
35. Bouwstra, J. A., Gooris, G. S., Salmones-de Vries, M. A., van der Spek, J. A., and Bras, W. (1992) Structure of human stratum corneum as a function of temperature and hydration: A wide-angle X-ray diffraction study. *Int. J. Pharm.* **84**, 205–216.
36. Bouwstra, J. A., Gooris, G. S., and White, S. H. (1997) X-ray analysis of the stratum corneum and its lipids, in *Mechanisms of Transdermal Drug Delivery* (Potts, R. O. and Guy, R. H., eds.), Marcel Dekker, New York, pp. 41–85.
37. Jadoul, A., Tanajo, H., Pr eat, V., Spies, F., and Bodd e, H. (1998) Electroperturbation of human stratum corneum fine structure by high voltage pulses: A freeze fracture electron microscopy and differential thermal analysis study. *J. Invest. Dermatol. Symp. Proc.* **3**, 153–158.
38. Madison, K., Schwartzendruber, D., Wertz, P., and Downing, D. (1987) Presence of intact intercellular lipid lamellae in the upper layers of the stratum corneum. *J. Invest. Dermatol.* **88**, 714–718.
39. Bodd e, H. E., Holman, B., Spies, F., Weerheim, A., Kempenaar, J., Mommaas, M., and Ponc, M. (1990) Freeze-fracture electron microscopy of in vitro reconstructed human epidermis. *J. Invest. Dermatol.* **95**, 108–116.
40. Holman, B. P., Spies, F., and Bodd e, H. E. (1990) An optimized freeze-fracture replication procedure for human skin. *J. Invest. Dermatol.* **94**, 332–335.
41. Elias, P. M. (1991) Epidermal barrier function: Intercellular lamellar lipid structures, origin, composition and metabolism. *J. Controlled Release* **15**, 199–208.
42. Tanojo, H., Bouwstra, J. A., Junginger, H. E. and Bodd e, H. E. (1994) Subzero thermal analysis of human stratum corneum. *Pharmacol. Res.* **11**, 1610–1616.
43. Casal, H. L. and Mantsch, H. H. (1984) Polymorphic phase behavior of phospholipid membranes studied by infrared spectroscopy. *Biochim. Biophys. Acta* **779**, 381–401.
44. Amey, R. L. and Chapman, D. (1989) Infrared spectroscopic studies of model and natural biomembranes, in *Biomembrane Structure and Function* (Chapman, D., ed.), Verlag Chemie, Weinheim, Germany.

45. Mirabella, F. M. (1993) *Internal Reflection Spectroscopy: Theory and Practice*. Marcel Dekker, New York.
46. Potts, R. O., Mak, V. H. W., Guy, R. H., and Francoeur, M. L. (1991) Strategies to enhance permeability via stratum coreum lipid pathways. *Adv. Lipid Res.* **24**, 173–210.
47. Potts, R. O. and Francoeur, M. L. (1993) Infrared spectroscopy of stratum corneum lipids, in *Pharmaceutical Skin Penetration Enhancement* (Walters, K. A. and Hadgraft, J., eds.), Marcel Dekker, New York.
48. Naik, A. and Guy, R. H. (1997) Infrared spectroscopic and differential scanning calorimetric investigations of the stratum corneum barrier function, in *Mechanisms of Transdermal Drug Delivery* (Potts, R. O. and Guy, R. H., eds.), Marcel Dekker, New York, pp. 87–162.
49. Bommannan, D., Potts, R. O., and Guy, R. H. (1990) Examination of stratum corneum barrier function in vivo by infrared spectroscopy. *J. Invest. Dermatol.* **95**, 403–408.
50. Williams, A. C., Barry, B. W., Edwards, H. G., and Farwell, D. W. (1993) A critical comparison of some Raman spectroscopic techniques for studies of human stratum corneum. *Pharmacol. Res.* **10**, 1642–1647.
51. Jadoul, A. (1997) *Skin Perturbations Induced by Iontophoresis and Electroporation: Enhancement in Drug Transport and Integrity of the Stratum Corneum*. Ph.D. Thesis. Université catholique de Louvain, Brussels, Belgium.
52. Donovan, J. W. (1984) Scanning calorimetry of complex biological structures. *Trends in Biol. Sci.* **9**, 340–344.
53. Lewis, R. N. A. H. and McElhaney, R. N. (1992) The mesomorphic phase behavior of lipid bilayers, in *The Structure of Biological Membranes* (Yeagle, P., ed.), CRC Press, Boca Raton, FL.
54. Golden, G. M., Guzek, D. B., Harris, R. R., McKie, J. E., and Potts, R. O. (1986) Lipid thermotropic transitions in human stratum corneum. *J. Invest. Dermatol.* **86**, 255–259.
55. Vanbever, R. (1997) *Skin Electroporation for Transdermal Drug Delivery*. Ph.D. Thesis. Université catholique de Louvain, Brussels, Belgium.
56. Pliquett, U., Zewert, T. E., Chen, T., Langer, R., and Weaver, J. C. (1996) Imaging of fluorescent molecule and small ion transport through human stratum corneum during high voltage pulsing: Localized transport regions are involved. *Biophys. Chem.* **58**, 185–204.
57. Prausnitz, M. R., Gimm, J. A., Guy, R. H., Langer, R., Weaver, J. C., and Cullander, C. (1996) Imaging of transport pathways across human stratum corneum during high-voltage and low-voltage electrical exposures. *J. Pharm. Sci.* **85**, 1363–1370.
58. Cullander, C. and Guy, R. H. (1991) Sites of iontophoretic current flow into the skin: Identification and characterization with the vibrating probe electrode. *J. Invest. Dermatol.* **97**, 55–64.

59. Cullander, C. and Guy, R. H. (1992) Visualization of iontophoretic pathways with confocal microscopy and the vibrating probe electrode. *Solid State Ionics* **53–56**, 197–206.
60. Scott, E. R., White, H. S., and Phipps, J. B. (1992) Direct imaging of ionic pathways in stratum corneum using scanning electrochemical microscopy. *Solid State Ionics* **53–56**, 176–183.
61. Scott, E. R., Laplaza, A. I., White, H. S., and Phipps, J. B. (1993) Transport of ionic species in skin: contribution of pores to the overall skin conductance. *Pharmacol. Res.* **10**, 1699–1709.
62. Turner, N. G. and Nonato, L. B. (1997) Visualization of stratum corneum and transdermal permeation pathways, in *Mechanisms of Transdermal Drug Delivery* (Potts, R. O. and Guy, R. H., eds.), Marcel Dekker, New York, pp. 1–40.
63. Haugland, R. P. (1997) *Handbook of Fluorescent Probes and Research Chemicals*. Molecular Probes, Eugene, OR.
64. Pawley, J. B. (1990) *Handbook of Biological Confocal Microscopy*. Plenum, New York.
65. Wilson, T. (1990) *Confocal Microscopy*. Academic Press, New York.
66. Grimnes, S. (1984) Pathways of ionic flow through human skin in vivo. *Acta Derm. Venereol.* **64**, 93–98.
67. Burnette, R. R. and Ongpipattanakul, B. (1988) Characterization of the pore transport properties and tissue alteration of excised human skin during iontophoresis. *J. Pharm. Sci.* **77**, 132–137.
68. Monteiro-Riviere, N. A., Inman, A. O., and Riviere, J. E. (1994) Identification of the pathway of iontophoretic drug delivery: Light and ultrastructural studies using mercuric chloride in pigs. *Pharmacol. Res.* **11**, 251–256.
69. Rutherford, T. and Black, J. G. (1969) The use of autoradiography to study the localization of germicides in skin. *Br. J. Dermatol.* **81 (Suppl. 4)**, 75–87.
70. Bidman, H. J., Pitts, J. D., Solomon, H. F., Bondi, J. V., and Stumpf, W. E. (1990) Estradiol distribution and penetration in rat skin after topical application, studies by high resolution autoradiography. *Histochem. J.* **95**, 43–54.
71. Simonetti, O., Hoogstraate, A. J., Bialik, W., Kempenaar, J. A., Schrijvers, A. H., Bodde, H. E., and Ponec, M. (1995) Visualization of diffusion pathways across the stratum corneum of native and in-vitro-reconstructed epidermis by confocal laser scanning microscopy. *Arch. Dermatol. Res.* **287**, 465–473.
72. Turner, N. G. and Guy, R. H. (1997) Iontophoretic transport pathways: Dependence on penetrant physicochemical properties. *J. Pharm. Sci.* **86**, 1385–1389.
73. Squier, C. and Hopps, R. (1976) A study of the permeability barrier in epidermis and oral epithelium using horseradish peroxidase as a tracer in vitro. *Br. J. Dermatol.* **95**, 123–129.
74. Menon, G. K., Bommannan, D. B., and Elias, P. M. (1994) High-frequency sonophoresis: permeation pathways and structural basis for enhanced permeability. *Skin Pharmacol.* **7**, 130–139.

75. Ogiso, T., Iwaki, M., Bechako, K., and Tsutsum, Y. (1992) Enhancement of percutaneous absorption by laurocapram. *J. Pharm. Sci.* **81**, 762–767.
76. Elias, P. M. and Friend, D. S. (1975) The permeability barrier in mammalian epidermis. *J. Cell Biol.* **65**, 180–191.
77. Hofland, H. E., Bouwstra, J. A., Boddé, H. E., Spies, F., and Junginger, H. E. (1995) Interactions between liposomes and human stratum corneum in vitro: Freeze fracture electron microscopical visualization and small angle x-ray scattering studies. *Br. J. Dermatol.* **132**, 853–866.
78. Nemanic, M. K. and Elias, P. M. (1980) In situ precipitation: A novel cytochemical technique for visualization of permeability pathways in mammalian stratum corneum. *J. Histochem. Cytochem.* **28**, 573–578.
79. Boddé, H. E., van den Brink, I., Koerten, H. K. and de Haan, F. H. N. (1991) Visualization of in vitro percutaneous penetration of mercuric chloride: Transport through intercellular space versus cellular uptake through desmosomes. *J. Controlled Release* **15**, 227–236.
80. King, C., Moore, N., Marks, R. and Nicholls, S. (1978) Preliminary studies into percorneal penetration and elemental content of the stratum corneum using x-ray microanalysis. *Arch. Dermatol. Res.* **263**, 257–265.
81. Agner, T. (1992) Noninvasive measuring methods for the investigation of irritant patch test reactions: A study of patients with hand eczema, atopic dermatitis and controls. *Acta Derm. Venereol. (Stockh.) Suppl.* **173**, 1–26.
82. Serup, J. and Jemec, G. B. E. (1995) *Handbook of Non-Invasive Methods and the Skin*. CRC Press, Boca Raton, FL.
83. Berardesca, E. and Maibach, H. I. (1988) Bioengineering and the patch test. *Contact Dermatitis* **18**, 3–9.
84. Elsner, P., Wilhelm, D., and Maibach, H. I. (1990) Multiple parameter assesment of vulvar irritant contact dermatitis. *Contact Dermatitis* **23**, 20–26.
85. Vanbever, R., Fouchard, D., Jadoul, A., De Morre, N., Preat, V., and Marty, J.-P. (1998) In vivo non-invasive evaluation of hairless rat skin after high-voltage pulse exposure. *Skin Pharmacol. Appl. Skin Physiol.* **11**, 23–24.
86. Ledger, P. W. (1992) Skin biological issues in electrically enhanced transdermal delivery. *Adv. Drug Deliv. Rev.* **9**, 289–307.
87. Westerhof, W. (1995) CIE Colorimetry, in *Handbook of Non-Invasive Methods and the Skin* (Serup, J. and Jemec, G. B. E., eds.), CRC Press, Boca Raton, FL, pp. 385–397.
88. Serup, J. and Agner, T. (1990) Colorimetric quantification of erythema: A comparison of two colorimeters (Lange Micro Color and Minolta Chroma Meter CR-200) with a clinical scoring scheme and laser-Doppler flowmetry. *Clin. Exp. Dermatol.* **15**, 267–272.
89. Bjerring, P. (1995) Spectrophotometric characterization of skin pigments and skin color, in *Handbook of Non-Invasive Methods and the Skin* (Serup, J. and Jemec, G. B. E., eds.), CRC Press, Boca Raton, FL, pp. 373–376.

90. Takiwaki, H. and Serup, J. (1995) Measurement of erythema and melanin indices, in *Handbook of Non-Invasive Methods and the Skin* (Serup, J. and Jemec, G. B. E., eds.), CRC Press, Boca Raton, FL, pp. 377–384.
91. Eun, H. C. (1995) Evaluation of skin blood flow by laser doppler flowmetry. *Clin. Dermatol.* **13**, 337–347.
92. Bircher, A., De Boer, E. M., Agner, T., Wahlberg, J. E., and Serup, J. (1994) Guidelines for measurement of cutaneous blood flow by laser Doppler flowmetry. *Contact Dermatitis* **30**, 65–72.
93. Belcaro, G. and Nicolaides, A. N. (1995) Laser-Doppler flowmetry: Principles of technology and clinical applications, in *Handbook of Non-Invasive Methods and the Skin* (Serup, J. and Jemec, G. B. E., eds.), CRC Press, Boca Raton, FL, pp. 405–410.
94. Bircher, A. J. (1995) Laser Doppler measurement of skin blood flux: Variation and validation, in *Handbook of Non-Invasive Methods and the Skin* (Serup, J. and Jemec, G. B. E., eds.), CRC Press, Boca Raton, FL, pp. 399–403.
95. Pinnagoda, J. and Tupker, R. A. (1995) Measurement of the transepidermal water loss, in *Handbook of Non-Invasive Methods and the Skin* (Serup, J. and Jemec, G. B. E., eds.), CRC Press, Boca Raton, FL, pp. 173–178.
96. Pinnagoda, J., Tupker, R. A., Agner, T., and Serup, J. (1990) Guidelines for transepidermal water loss (TEWL) measurement. *Contact Dermatitis* **22**, 164–178.
97. Barel, A. O. and Clarys, P. (1995) Measurement of epidermal capacitance, in *Handbook of Non-Invasive Methods and the Skin* (Serup, J. and Jemec, G. B. E., eds.), CRC Press, Boca Raton, FL, pp. 165–170.
98. Tagami, H. (1995) Measurement of electrical conductance and impedance, in *Handbook of Non-Invasive Methods and the Skin* (Serup, J. and Jemec, G. B. E., eds.), CRC Press, Boca Raton, FL, pp. 159–164.
99. Serup, J., Keiding, J., Fullerton, A., Gniadecka, M., and Gniadecki, R. (1995) High-frequency ultrasound examination of skin: Introduction and guide, in *Handbook of Non-Invasive Methods and the Skin* (Serup, J. and Jemec, G. B. E., eds.), CRC Press, Boca Raton, FL, pp. 239–256.
100. Agner, T. (1995) Ultrasound A-mode measurement of skin thickness, in *Handbook of Non-Invasive Methods and the Skin* (Serup, J. and Jemec, G. B. E., eds.), CRC Press, Boca Raton, FL, pp. 289–292.

Treatment of Murine Transplanted Subcutaneous Tumors Using Systemic Drug Administration

Stéphane Orlowski and Lluís M. Mir

1. Introduction

In vitro data have shown an increased cytotoxic drug uptake into electropermeabilized cells in suspension, leading to a marked cytotoxicity increase (1). Preclinical experiments were required to demonstrate the in vivo applicability of these observations. Obviously, the most convenient laboratory animal model to test new antitumor treatments is the mouse. Indeed, there exist many tumors of different histological types which can be transplanted in mice, either in immunocompetent mice in the case of syngeneic tumors or in immunodepressed mice in the case of allogeneic or xenogeneic tumors. From a practical point of view, mice have the advantage to be rather cheap and to allow a large number of experiments. Moreover, murine tumors are generally easy to transplant, grow rapidly, and can be conveniently followed for their evolution, at least in the case of subcutaneous tumors. Finally, murine subcutaneous tumors are well adapted to test the antitumor effects of electrochemotherapy since they allow the use of a rather simple material to conveniently apply transcutaneous permeabilizing electric pulses.

As a matter of fact, the use of transplanted subcutaneous tumors in mice allowed the development of electrochemotherapy protocols using external electrodes (2,3), later tested on humans. It was also an excellent tool to study the basic mechanisms of this treatment such as the cell permeabilization in tissues and the role of the host immune response (4,5).

The cytotoxic drug that we chose to associate with the tumor cell electropermeabilization is bleomycin, in agreement with the specific properties of the cellular pharmacology of this drug (1,6,7). Indeed, bleomycin is a

nonpermeant molecule that cannot diffuse through the cell membrane, and it is incorporated into cells via an endocytosis-related mechanism which largely limits the access of bleomycin to DNA, its intracellular target. Cell permeabilization thus provokes a dramatic increase of the bleomycin access to the cytosol allowing the drug to reach its targets. Therefore, cell electropermeabilization leads to a huge increase of bleomycin efficacy: up to 650,000 times increased cytotoxicity *in vitro*, on cultured cells (1), and about 10,000 times increased antitumor effect *in vivo*, on murine tumors (2). An optimized incorporation of the drug into the electropermeabilized tumor cells requires an homogeneous distribution of bleomycin in the tumor interstitial fluids before the electric pulse delivery. In order to achieve such an homogeneous distribution, the bleomycin administration was performed by the systemic route. In our hands, both intramuscular and intravenous administrations led to similar results, provided the bleomycin dose and the time between bleomycin injection and electric pulse delivery were adapted for each case.

2. Materials

1. Mice and Tumor Obtention: Mice currently used are either the immunocompetent C57Bl/6 mice (R. Janvier, Orléans, France), or the immunodepressed “nude” *nu/nu* mice with Swiss background produced at the Institut Gustave-Roussy. Immunocompetent mice are maintained in animal housing facilities under conventional conditions, and immunodeficient mice are kept in sterile cages with filtering covers. They are both fed with usual laboratory diet and water given *ad libitum*. Only mice at least 6- to 8-week-old are used in the experiments. C57Bl/6 mice are left unmanipulated for at least one week after their arrival to the animal housing facilities.

The C57Bl/6 mice can be subcutaneously transplanted with different syngeneic tumors, such as:

- LPB sarcoma, a methylcholanthrene-induced fibrosarcoma. LPB tumors are obtained by the inoculation of $2-5 \times 10^5$ cultured cells into the flanks (*see Note 1*), which give tumor nodules of about 7 mm in 7–9 d.
- B16 melanoma, serially passaged *in vivo* on C57Bl/6 mice. B16 tumors are obtained by the inoculation into the flanks of 10^6 cells trypsinized from a passaged tumor, which give tumor nodules of about 7 mm in 7–8 d.
- Lewis carcinoma, an epidermoid lung tumor spontaneously developed and serially passaged in C57Bl/6 mice. Lewis tumors are obtained by the inoculation into the flanks of 10^6 cells mechanically dissociated from a passaged tumor, which give tumor nodules of about 7 mm in 6–7 d.

Nude mice can be inoculated with xenogeneic tumor cells such as the KB carcinoma, which is an oral epidermoid tumor of human origin. KB tumors are obtained by the inoculation into mice flanks of $2 \cdot 10^6$ cultured cells, which give tumor nodules of about 7 mm in 7–9 d.

2. Bleomycin: Bleomycin (Laboratoire Roger Bellon, Neuilly-sur-Seine, France) is dissolved in sterile 0.9% sodium chloride just before the infusion.
3. Generator: Square-waved electric pulses of adjustable voltage, length and frequency are produced by a PS15 electropulser (Jouan, Nantes, France), initially designed for *in vitro* electric pulse delivery. The electrical parameters of the delivered pulses are recorded and controlled with a digital oscilloscope (VC-6025, Hitachi, Tokyo, Japan).
4. Electrodes: The most convenient external electrodes consist of two parallel flat stainless steel rectangles, with rounded inferior edges to improve skin contact at the level of the cutaneous or subcutaneous tumor nodule to be treated (**Fig. 1**). They are held by an insulating template which sets the electrode gap (usually 6–8 mm), and allows safe electrical connection to the generator PS15. Typical dimensions of the electrode edge that will be applied on the skin are 1 cm width and 0.5 mm thickness. The electrical contact with the skin is ensured by a film of electrocardiography paste spread on the electrode edges.

3. Methods

3.1. Mice Preparation

1. Treat the same day all mice included in a given experiment, in order to have the same physiological conditions for every animal, in particular a similar immunological status regarding to time-dependent host reactions against the transplanted tumors. Thus, since tumor growth is always variable from mouse to mouse, select among all the inoculated mice the mice bearing well delimited tumor nodules of similar sizes, typically 6–9 mm diameter. Then randomly distribute these mice between different experimental groups if necessary.
2. Shave or gently remove the C57Bl/6 mice hairs from the area around the tumor nodules, avoiding skin scrapes.
3. Using a caliper, measure two perpendicular surface diameters, and, if possible, the thickness of every tumor nodule to be treated.

3.2. Bleomycin Administration

1. Intramuscular injection: inject a dose of 50 µg bleomycin dissolved in 100 µL saline into the thigh muscle, and wait for 30 min before the electric pulse delivery.
2. Intravenous injection: inject a dose of 10 µg bleomycin dissolved in 100 µL saline into the retroorbital sinus, and wait for 3 min before the electric pulse delivery.

3.3. Electric Pulse Delivery

1. Adjust the electric pulse parameters at 1300 V/cm of electric field intensity (that is the ratio of the delivered voltage to the distance between the electrodes), 100 µs length and 1 Hz repetition frequency. This electric field intensity was shown to be the minimal value allowing to optimally permeabilize the whole tumor volume comprised between two electrodes placed on the skin that covers the tumor nodule to be treated (2,4).

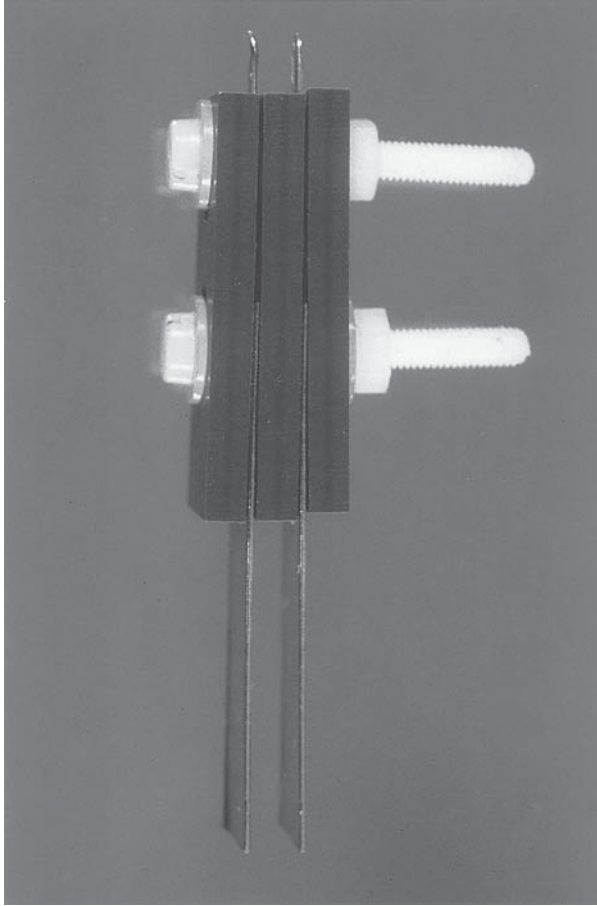


Fig. 1. Model of plate electrodes used for the application of transcutaneous electric pulses. To achieve the best fit between electrodes and the subcutaneous tumors to be treated: (i) appropriate distances between the two parallel plates can be achieved by inserting a variable number of nonconductive plastic spacers; (ii) geometry of the parallel metallic plates (length of the plate in contact with the skin, corners more or less rounded) can be chosen according to the size and geometry of the tumor.

2. Spread a thin film of electrocardiography paste on the inferior edge of the electrodes.
3. Locate by palpation the nodule to be treated and place the two electrodes at both sides of this nodule, which should have a size inferior to the gap between the electrodes (*see Note 2*).
4. Hold firmly the mouse in one hand, and apply a run of 8 electric pulses to the nodule, avoiding to change the electrode position during the run in spite of the muscular contraction presented by the mice at each pulse (*see Note 3*).

3.4. Tumor Follow-up

1. In the C57Bl/6 mice, evaluate the presence of a peritumoral edema within the first day after the electrochemotherapy session. This edema is a sign which indicates that treatment will be efficient, and therefore is an indicator of satisfactory treatment. This edema reveals in fact an intense local inflammatory reaction participating in the antitumor effect of electrochemotherapy.
2. Two to three times a week, measure with a caliper two perpendicular surface diameters, and, if possible, the thickness of the treated tumor nodules (*see Note 4*).
3. Score as complete regression every treated tumor which becomes unpalpable.
4. Score as cures the complete regressions which last more than 60 d after the treatment.

4. Notes

1. Inoculate preferentially the tumorigenic cells on the left flanks of the mice. Otherwise, the treatment of tumors located on the right flank could cause lesions to the liver located just below the tumor site, and lead to mouse death (at least in the case of intramuscular bleomycin injection).
2. In the case of a nonspherical, oblong tumor nodule, place the electrodes at both sides of the longest diameter of the nodule and adapt the electrode position to optimize the contact with the skin covering the nodule. If necessary, repeat the electric pulse delivery two times after repositioning the electrodes along the nodule.
3. Just after the electric pulse delivery to the tumor nodule on the mice flanks, it is regularly observed a transient paralysis of the hind legs of the treated mouse, which lasts less than 1 minute and which is always totally reversible.
4. Some days after the electrochemotherapy, it is often observed small scabs on the skin just at the level of electrode application. They always heal a few days after.

References

1. Poddevin, B., Orłowski, S., Bełehradek, J. Jr., and Mir, L. M. (1991) Very high cytotoxicity of bleomycin introduced into the cytosol of cells in culture. *Biochem. Pharmacol.* **42S**, 67–75.
2. Mir, L. M., Orłowski, S., Bełehradek, J. Jr., and Paoletti, C. (1991) Electrochemotherapy: Potentiation of antitumor effect of bleomycin by local electric pulses. *Eur. J. Cancer* **27**, 68–72.
3. Mir, L. M., Roth, C., Orłowski, S., Quintin-Colonna, F., Fradelizi, D., Bełehradek, J. Jr., and Kourilsky, P. (1995) Systemic antitumor effects of electrochemotherapy combined with histoincompatible cells secreting interleukin-2. *J. Immunother.* **17**, 30–38.
4. Bełehradek, J. Jr., Orłowski, S., Ramirez, L. H., Pron, G., Poddevin, B., and Mir, L. M. (1994) Electroporation of cells in tissues assessed by the qualitative and quantitative electroloading of bleomycin. *Biochim. Biophys. Acta* **1190**, 155–163.

5. Mir, L. M., Orlowski, S., Poddevin, B., and Belehradec, J. Jr. (1992) Electrochemotherapy tumor treatment is improved by interleukin-2 stimulation of the host's defenses. *Eur. Cytokine Netw.* **3**, 331–334.
6. Pron, G., Belehradec, J. Jr., Orlowski, S., and Mir, L. M. (1994) Involvement of membrane bleomycin-binding sites in bleomycin cytotoxicity. *Biochem. Pharmacol.* **48**, 301–310.
7. Mir, L. M., Tounekti, O., and Orlowski, S. (1996) Bleomycin: Revival of an old drug. *Gen. Pharmacol.* **27**, 745–748.

Electrochemotherapy of Murine Melanoma Using Intratumor Drug Administration

Richard Heller, Richard Gilbert, and Mark J. Jaroszeski

1. Introduction

Administering a chemotherapeutic agent in combination with electric fields (electrochemotherapy; ECT) has been shown to be an effective localized treatment for solid tumors (*1*). The drug used most often in this combination treatment has been bleomycin. ECT has been used successfully in both animal studies and clinical trials (*1–3*). The treatment was initially performed by exposing tumor cells to electrical fields following intravenous injection of the chemotherapeutic agent. Although ECT using intravenous bleomycin was successful, the procedure was limited by the existence of a narrow but optimal time window for effective treatment as well as the fact that a systemic drug dose was being administered for a localized therapy. In addition, the use of intravenous administration also precludes the treatment of patients with poor circulation.

The evolution of this successful drug delivery model included examining an alternate means of administering the drug before electric pulses. Direct injection of the drug into the tumor (intratumor) was tested in a mouse melanoma model. The intratumor procedure allowed each tumor to be treated individually which removed the need to treat all tumors within a specific time frame. It also further localized the therapy and removed possible systemic adverse effects. The results in both animal and clinical studies showed that ECT using intratumor delivery was as effective or more effective than ECT with intravenous bleomycin (*3–7*). This chapter describes a protocol that was developed to use ECT with intratumor bleomycin for treating melanoma in a mouse model.

2. Materials

1. Cell Line: B16 murine melanoma cell line (CRL 6322; American Culture Collection, Rockville, MD) was used to induce tumors.
2. Growth Medium: McCoy's 5A medium (Mediatech, Washington, DC) supplement; (v/v) 10% fetal bovine serum (PAA Laboratories, Newport Beach, CA) 90 $\mu\text{g}/\text{mL}$ of gentamicin sulfate (Gibco, Grand Island, NY). Non enzymatic cell dissociation solution (CDS; Sigma, St. Louis, MO), should be used instead of trypsin for harvesting cells. Cells should be grown at 37°C in a humidified atmosphere.
3. Animals: Female C57Bl/6 mice (Harlan Sprague Dawley, Inc., Indianapolis, IN).
4. Anesthesia: Sodium pentobarbital (Henry Schein, Port Washington, NY).
5. Chemotherapeutic Agent: Bleomycin (Blenoxane; Bristol-Meyer Squibb, Princeton, NJ).
6. Diluent: Sterile injectable saline (Abbott Laboratories, Chicago, IL).
7. Pulse Generator: BTX T820 (Genetronics, Inc., San Diego, CA).
8. Electrodes: Two stainless steel squares constructed of 316 stainless steel in a parallel plane configuration 10 mm on each side and mounted on a vernier caliper. The calipers allowed the distance between the electrodes to be adjusted depending on the size of the tumor (*see Note 1*). Electrocardiography paste is used to assure sufficient contact between electrode surface and skin (Spectra 360 Electrode gel, Parker Laboratories, Inc., Orange, NJ).
9. Digital Storage Oscilloscope: PM 3394A (Fluke Corporation, Palatine, IL).
10. Current Probe: 80i-110S (Fluke Corporation).

3. Methods

3.1 Tumor Induction

1. Induce tumors in 7- to 8-wk-old female C57Bl/6 mice.
2. Harvest B16 murine melanoma cells from culture using cell dissociation solution. Wash cells three times in Ca and Mg free phosphate buffered saline (PBS) by centrifugation (200g). Assess cell viability using the trypan blue exclusion dye method.
3. Induce tumors by injecting 10^6 B16 melanoma cells contained in 50 μl volume of Ca and Mg free PBS. Cells should be injected subcutaneously into the left flank using a 30-gauge needle. Injected cells should be greater than 90% viable.
4. Allow time for tumors were to develop. Generally, 7–10 d will generate tumors of approximately 6–8 mm from edge to edge. Tumors of this size are easily measured and followed.

3.2. ECT

1. Determine the tumor volume for each mouse. Randomly place animals in an experimental group or one of three control groups (*see Note 2*). Label each animal to allow for efficient follow-up (*see Note 3*).

2. Prepare bleomycin before initiating ECT protocol. Dissolve bleomycin in sterile injectable saline at a concentration of 5 U/mL. One unit of bleomycin is equal to 0.555 mg.
3. Inject the proper dose of bleomycin into an appropriately labeled animal using a 30-gauge, 3/8 in. length needle (*see Note 4*). Allow 10 min for the drug to disseminate within the tumor before delivering electric pulses (**4**).
4. Anesthetize animals approximately 2–3 minutes following drug injection. Animals are anesthetized with sodium pentobarbital (40 mg/kg). Animal should be anesthetized before proceeding to **step 5**.
5. Place conductive gel on each of the two flat plate electrodes. Place electrodes on both sides of the protruding tumor.
6. Apply electric pulses to tumor (*see Note 5*).
7. Follow animals after treatment by recording tumor dimensions and computing tumor volumes at periodic intervals. Every 3–5 d is sufficient (*see Note 6*).
8. Take biopsies to histologically confirm ECT results. Biopsy specimens should be fixed in 10% neutral buffered formalin. Standard imbedding and sectioning should be used for these samples. Hematoxylin and eosin staining is useful for visualization of the tissue.

4. Notes

1. There are several different types, sizes and configurations of electrodes that can be used to perform ECT protocols. A description and potential uses of some of these electrodes has been previously published (**8**). The specific electrode used will vary depending on the application being performed. Some applications may require different electrode shape, material or arrangement.
2. Tumor measurements can be taken quite efficiently using a digital vernier caliper. Tumor volume is obtained by first measuring the longest diameter (a) and the next longest diameter perpendicular to a (b). The volume is calculated by using the formula $ab^2\pi/6$. Animals should be placed into control and experimental groups such that the mean tumor volume for each group is not significantly different. A typical ECT experiment would require a minimum of 4 groups. Three control groups should be included and they are: D–E–, will receive no drug and no electric pulses and will serve as the no treatment control; D–E+, will receive no drug but will receive electric pulses and will serve as the electroporation control; D+E–, will receive drug but no electric pulses and will serve as the drug control. The experimental group D+E+, will receive drug and electric pulses. There may be several groups that receive the both drug and electric pulses if different drug doses or electroporation conditions are being examined.
3. A clear and unambiguous labeling system should be used. This is important in maintaining an accurate follow up of the animals following treatment. Mice can be labeled by punching holes in their ears. They can be distinguished by 0, 1, or 2 holes in either the right, left, or both ears.

4. Bleomycin injections can be made using a 30-gauge needle of 0.5 in. length. The injection should be made to assure that the entire tumor is perfused with the drug. This may be accomplished with a single-point injection, however, it may require manipulating the needle to inject at different angles or possibly multiple sticks depending on the size of the tumor. The bleomycin can be injected at predetermined dose irrespective of the tumor size, that is, 0.25 units per mouse (4,7) or it can be injected at a dose dependent on tumor size, that is, 5 U/mL and inject a volume equivalent to 25% of the tumor volume. Animals in control groups that are not receiving bleomycin should receive an equivalent injection of saline.
5. Electric pulses are applied through electrodes placed around the tumor. The plates are placed in such a way that they press against opposite sides of the tumor. The pulsing conditions may vary depending on the experimental protocol and site of the tumor. However, the application of 4–8 square wave pulses with a nominal electric field strength of 1250–1500 V/cm and a pulse width of 100 μ s (4,5).
6. Tumors should be measured at regular intervals following treatment. Measurements are performed as described for pretreatment tumor volume determinations (Note 2). The posttreatment tumor volume is compared to the treatment day volume. A complete response is defined as no palpable or measurable tumor detected for at least 10 days following treatment and partial response is defined as greater than 50% decrease in tumor volume for at least 10 days following treatment. Progressive disease is defined as continued growth. Animals are followed for 100 days or until the tumor volume grows to four times the treatment day volume. If a complete response is maintained for 100 days then the animal is considered cured.

References

1. Jaroszeski, M. J., Gilbert, R. and Heller, R. (1997) Electrochemotherapy: An emerging drug delivery method for the treatment of cancer. *Adv. Drug Deliv. Rev.* **26**, 185–197.
2. Mir, L. M., Glass, L. F., Serša, G., Teissie, J., Domenge, C., Miklavčič, D., Jaroszeski, M. J., Orlowski, S., Reintgen, D. S., Rudolf, Z., Belehradek, M., Gilbert, R., Rols, M-P., Belehradek, J. Jr., Bachaud, J. M., DeConti, R. C., Štabuc, B., Čemažar, M., Coninx, P., and Heller, R. (1998) Effective treatment of cutaneous and subcutaneous malignant tumours by electrochemotherapy. *Br. J. Cancer* **77**, 2336–2342.
3. Heller, R., Jaroszeski, M. J., Reintgen, D., Puleo, C., DeConti, R., Gilbert, R., and Glass, L. F. (1998) Treatment of cutaneous and subcutaneous tumors with electrochemotherapy using intralesional bleomycin. *Cancer* **83**, 148–157.
4. Heller, R., Jaroszeski, M. J., Perrott, R., Messina, J., and Gilbert, R. (1997) Effective treatment of B16 melanoma by direct delivery of bleomycin using electrochemotherapy. *Melanoma Res.* **7**, 10–18.
5. Jaroszeski, M. J., Gilbert, R., Perrott, R., and Heller, R. (1996) Enhanced effects of multiple treatment electrochemotherapy. *Melanoma Res.* **6**, 427–433.

6. Jaroszeski, M. J., Gilbert, R., and Heller, R. (1997) Successful treatment of hepatomas with electrochemotherapy in a rat model. *Biochem. Biophys. Acta* **1334**, 15–18.
7. Hyacinthe, M., Jaroszeski, M. J., Dang, V. V., Coppola, D., Karl, R. C., Gilbert, R. A., and Heller, R. (1999) Electrically enhanced drug delivery for the treatment of soft tissue sarcoma. *Cancer* **85**, 409–417.
8. Gilbert, R., Jaroszeski, M. J., and Heller, R. (1997) Novel electrode designs for electrochemotherapy. *Biochem. Biophys. Acta* **1334**, 9–14.

Treatment of a Tumor Model with ECT Using 4+4 Electrode Configuration

Maja Čemažar

1. Introduction

In order to be effective, electrochemotherapy must meet the following two requirements. First, the chemotherapeutic drug must be present around tumor cells, and second, each cell in the tumor must be exposed to an electric field that is above the threshold value for this particular tumor type.

In earlier research studies on electrochemotherapy, the electrodes were placed at the opposed margins of the tumor and a string of 8 electric pulses was thus delivered only in one direction (1–5). Very often, these tumors, after a substantial period of complete response, regrew at the margins of the tumor that were not in contact with the electrodes (Fig. 1). In these areas, the tumor cells were probably sub-optimally permeabilized; thus, some clonogenic cells remained and later regrew into a tumor. Based on this observation, we were considering how to improve the outcome of electrochemotherapy. We presumed that, if during the application of electric pulses the electrode orientation was changed, more cells in the tumor would be exposed to electric field intensity above the threshold value. Therefore, we decided to split the string of 8 electric pulses into two halves and deliver the first string of electric pulses in one direction then turn the electrodes 90° and deliver the second set of 4 electric pulses (4+4 configuration) (6,7).

Figure 2 shows our results of electrochemotherapy with standard 8 pulses delivered in one direction which we compared to the 4+4 configuration. In this experiment, due to very good antitumor effectiveness of electrochemotherapy, the end point was local tumor control. The tumor control doses 50 (TCD₅₀; the dose of bleomycin which is expected to control 50% of the tumors) for

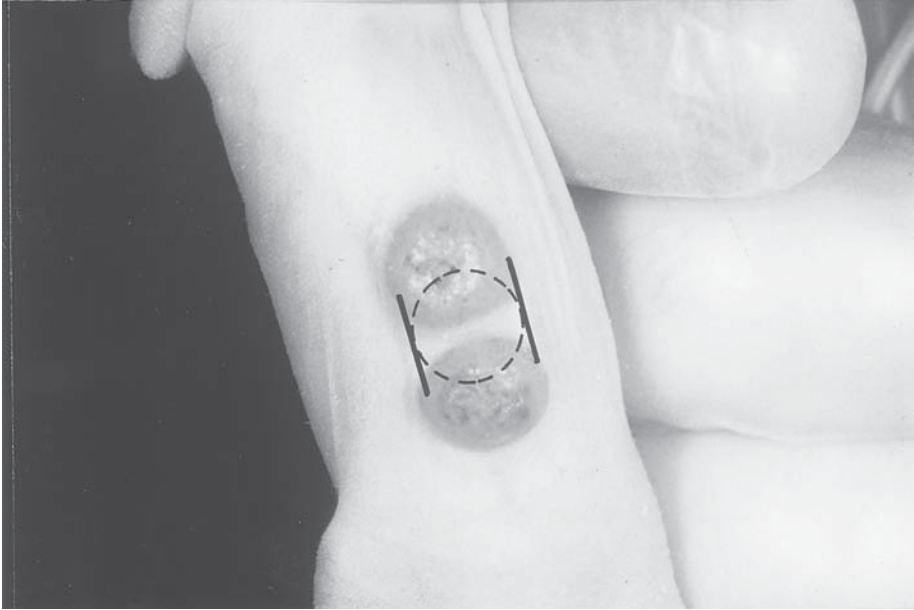


Fig. 1. Macroscopic appearance of the tumor 3 wk after electrochemotherapy with 8 electric pulses delivered in one direction. The position of the primary tumor and electrodes at the time of the treatment is indicated. According to location of the tumors it is evident that these tumors regrew from the area where there was no contact with the electrodes.

electrochemotherapy with 8 pulses and with the 4+4 configuration were 346 μg bleomycin (95% confidence interval: 200–600 μg) and 77 μg bleomycin (95% confidence interval: 33–182 μg), respectively. The shift in tumor control probability curve to lower doses of bleomycin by using the 4+4 configuration was statistically significant when compared to the electrochemotherapy treated tumors using a string of 8 electric pulses delivered in one direction. We also proposed two possible explanations for the observed increase in antitumor effectiveness of electrochemotherapy using the 4+4 configuration (7). First possible explanation is based on the electric field distribution in the tumor. Using numerical model we have shown that when electric pulses are applied in one direction, the electric field is strongly inhomogeneous in the tumor, decreasing toward the center of the tumors and further to the tumor edges in the middle plane. Therefore, the cells in these areas may be exposed to an electric field of insufficient intensity to induce permeabilization. The second explanation is based on observation of single cell in an external electric field. Since permeabilization of plasma membrane is a threshold phenomenon and occurs

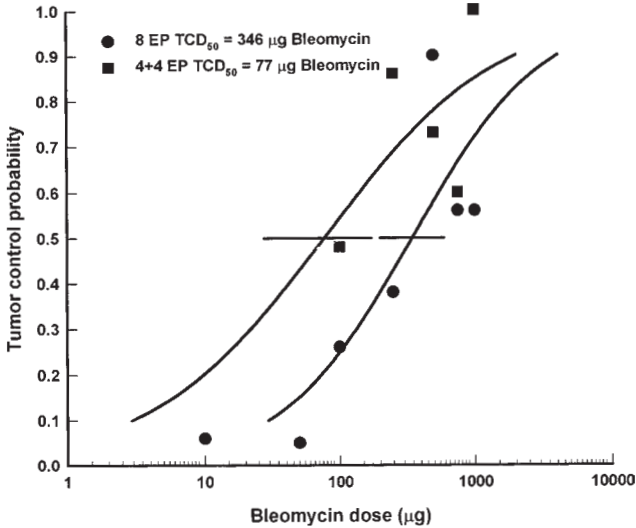


Fig. 2. Dose-response curve for EAT tumors treated by electrochemotherapy with 8 electric pulses (EP) delivered in one direction or with 4+4 configuration. Mice bearing subcutaneous tumors were treated with bleomycin and 3 min later tumors were exposed to electric pulses (1040 V, 1 Hz, 100 μ s, electrode distance, 8 mm). The TCD_{50} value is bleomycin dose that on the average would be expected to achieve control of the half of the electrochemotherapy treated tumors.

first on the poles facing the electrodes, the area, where increase in plasma membrane permeability is possible, depends on cell orientation in the electric field and cell shape deviation from the spherical. Therefore, by applying electric pulses in 4+4 configuration more cells in the tumor are exposed to electric field above threshold value, which consequently leads to increased antitumor effectiveness of electrochemotherapy using 4+4 configuration (7).

In this chapter, the protocol that we used for electrochemotherapy with bleomycin on CBA mice with EAT tumors is described; however, other drugs, mice and tumors can be used instead of the above-mentioned ones.

2. Materials

1. Mice: CBA mice may be maintained in a conventional colony with natural day/night cycle and constant room temperature (22°C). Mice are fed with food and water ad libitum. Mice used in this study were female, 10- to 12-wk-old, weighing approximately 24 g and without signs of infections.
2. Tumor model: Ehrlich Lettre Ascites Carcinoma (EAT; American Type Culture Collection, Rockville, MD) is a mouse tumor syngeneic to CBA mice. It may be maintained intraperitoneally as an ascites by serial transplantation every 7 d in carrier (donor) mouse. Tumor cells for the induction of subcutaneous solid

tumors are prepared from the tumor grown intraperitoneally as an ascites in the donor mouse.

3. Bleomycin: Bleomycin as a lyophilised powder may be purchased from the MACK, Germany. A 2 mg/mL stock solution is prepared in a sterile 0.9% NaCl solution.
4. Electrodes: Electrodes are composed of two parallel plates 8 mm apart. The plate is stainless steel strip with rounded tips of a length of 35 mm and width of 7 mm.
5. Generator of electric pulses: The generator used in this study is commercially available Jouan GHT 1287 (Jouan, France). It generates square-waved direct current electric pulses. The parameters, which should be set by the user for the application of electric pulses, are as follows: the length of the pulse, voltage and frequency.

3. Methods

3.1. Tumor Induction

1. Harvest tumor cells by washing the peritoneal cavity with 5 mL of sterile 0.9% NaCl solution.
2. Count the cells by means of hemocytometer. Determine viability of the cells with Trypan dye exclusion technique.
3. Prepare cells at a concentration of 3×10^7 cells/mL of 0.9% NaCl solution.
4. Inject 0.1 mL (3×10^6 cells) in the right flank of the mice to establish solid subcutaneous tumors (*see Note 1*).
5. Perform the treatment after 7–10 d, when the tumors are approximately 6–7 mm in diameter. Randomly divide mice bearing tumors into experimental groups and treat. The day of the treatment is denoted as d 0.

3.2. Bleomycin Injection

1. Dilute bleomycin with sterile 0.9% NaCl solution into appropriate dose (10, 50, 100, 250, 500, 750, and 1000 μg of bleomycin/mouse) (*see Note 2*).
2. Inject appropriate dose of bleomycin in a volume of 0.5 mL.
3. Heat mice for approximately 1 min before the injection in order to dilate the vein by using an infrared lamp.
4. Inject bleomycin as a bolus into the lateral tail vein of the preheated mice (*see Note 3*).

3.3. Application of Electric Pulses

1. Place electrodes at the opposed margins of the tumor. Ensure the contact between the electrodes and skin by use of conductive gel (*see Note 4*).
2. Apply eight electric pulses (amplitude 1040 V, length 100 μs , frequency 1 Hz) to the tumors.
3. Deliver electric pulses either in one direction or divided into two halves and deliver in two orientations (4+4 configuration). Rotate the electrodes 90° after

the first set of pulses and before the second. The interval between the two sets of four electric pulses is 1 s (see **Note 5**).

3.4. Assessment of response

1. Measure three mutually orthogonal tumor diameters with vernier caliper on each consecutive day. Calculate tumor volumes from these diameters (e_1, e_2, e_3) by the formula for an ellipsoid: $V = e_1 \times e_2 \times e_3 \times \pi / 6$ (see **Note 6**).
2. Score the response to treatment as complete response when the tumor is no longer palpable. Consider mice cured when tumors are in complete response 100 days after the therapy. Calculate tumor control probability using Logit analysis. Tumor control dose 50 (TCD₅₀) is the bleomycin dose in electrochemotherapy that, on average, would be expected to achieve tumor control in half of the treated animals (**8**).

4. Notes

1. EAT cells for the initiation of solid subcutaneous tumors can be also prepared from the in vitro cell culture. EAT cells are grown in NCTC 135 (Sigma, St. Louis, MO) supplemented with 15% fetal calf serum. The cells are maintained in a humidified atmosphere with 5% CO₂ at 37°C.
2. The bleomycin solution is not stable, therefore it should be freshly prepared for the daily injections.
3. Bleomycin can be injected also into the retroorbital sinus of the mouse. In this case the injection volume should be reduced to approximately 0.2 mL.
4. Conductive gel can be applied directly on each margin of the tumor or alternatively on the electrodes. The electrodes with a fixed distance in-between are connected with a plastic isolator. The electrodes should be placed on the each side of the tumor in a way that all tumor mass is encompassed between them.
5. We have chosen 1 second for the interval between the two sets of the electric pulses application because, in this case, the application is easy to perform. However, changing the electrode orientation without this interval or with a prolonged interval may be used. The interval between the applications of both sets of electric pulses should not be too long, since, in the meantime, the resealing of the plasma membranes of tumor cells could occur.
6. Since the subcutaneous tumors are usually nonspherical, the measurements of three longest orthogonal diameters and calculation of tumor volume by a formula for an ellipsoid represent a good estimation of tumor size (cell number). Alternatively, tumor size can be also present by mean diameter or cross-sectional area of the tumor because estimation of tumor growth delay is not affected by these different ways of presentation of measurements.

References

1. Mir, L. M., Orlowski, S., Belehradek, J. Jr., Teissié, J., Rols, M. P., Serša, G., Miklavčič, D., Gilbert, R., and Heller, R. (1995) Biomedical application of

- electric pulses with special emphasis on antitumor electrochemotherapy. *Bioelectrochem. Bioenerg.* **38**, 203–207.
2. Mir, L. M., Orlowski, S., Belehradec, J. Jr., and Paoletti, C. (1991) Electrochemotherapy potentiation of antitumour effect of bleomycin by local electric pulses. *Eur. J. Cancer* **27**, 68–72.
 3. Belehradec, J. Jr., Orlowski, S., Poddevin, B., Paoletti, C., and Mir, L. M. (1991) Electrochemotherapy of spontaneous tumors in mice. *Eur. J. Cancer* **27**, 73–76.
 4. Serša, G., Čemažar, M., Miklavčič, D., and Mir, L. M. (1994) Electrochemotherapy: Variable anti-tumor effect on different tumor models. *Bioelectrochem. Bioenerg.* **35**, 23–27.
 5. Heller, R., Jaroszeski, M., Leo-Messina, J., Perrot, R., Van Voorhis, N., Reintgen, D., and Gilbert, R. (1995) Treatment of B16 mouse melanoma with the combination of electropermeabilization and chemotherapy. *Bioelectrochem. Bioenerg.* **36**, 83–87.
 6. Čemažar, M., Miklavčič, D., Vodovnik, L., Jarm, T., Rudolf, Z., Štabuc, B., Čufer, T., and Serša, G. (1995) Improved therapeutic effect of electrochemotherapy with cisplatin by intratumoral drug administration and changing of electrode orientation for electropermeabilization of EAT tumor model in mice. *Radiol. Oncol.* **29**, 121–127.
 7. Serša, G., Čemažar, M., Šemrov, D., and Miklavčič, D. (1996) Changing electrode orientation improves the efficacy of electrochemotherapy of solid tumors in mice. *Bioelectrochem. Bioenerg.* **39**, 61–66.
 8. Suit, H. D., Sedlacek, R., and Thames, H. D. Jr. (1987) Radiation dose-response assays of tumor control. *Rodent Tumor Models in Experimental Cancer Therapy* (Kallman, R. F., ed.), Pergamon Press, New York, pp. 114–121.

Treatment of Multiple Spontaneous Breast Tumors in Mice Using Electrochemotherapy

Stéphane Orlowski and Lluís M. Mir

1. Introduction

Electrochemotherapy has been developed on the basis of *in vitro* data showing the huge increase of bleomycin cytotoxicity observed after cell electropermeabilization. Electrochemotherapy has been proven to be highly efficient as a local antitumor treatment on transplanted tumors (1). Indeed, electrochemotherapy resulted in high rates of tumor responses and even cures in preclinical trials on different experimental murine tumors (2). Treatment efficacy results from the local application of adequate electric pulses able to permeabilize the tumor cells located in the tissue volume crossed by the electric field, which allows the bleomycin present in tumor interstitial fluids to enter these cells and to kill them (3). Since the electric pulse delivery is designed to only reversibly permeabilize the tumor cells, electrochemotherapy is almost devoid of any side effects, and it can be safely proposed as a new antitumor treatment to be used in human clinics. Actually, a phase I–II clinical trial of electrochemotherapy has already given very satisfactory results on cutaneous tumors (4).

The physiological relations between host and tumor are very different for experimental transplanted tumors and for spontaneously developing tumors. From a practical point of view, murine models are particularly convenient for preclinical trials because mice are inexpensive, allowing a large number of experiments. Therefore, spontaneous tumors in mice provide interesting models for preclinical studies of new antitumor treatments, because these tumors are much closer to the real clinical situations than the transplanted tumors. Moreover, such experimental spontaneous tumors must be treated

individually when they appear, whatever their size or exact location. Therefore this is a much more complex carcinologic situation and a more stringent test for electrochemotherapy, as compared to the “simple” situation of repeated treatments of a series of calibrated experimental transplanted tumors. Taking into account such a “clinical-like” situation, we treated these spontaneous tumors several times, weekly, until the obtention of complete regressions (5). Since the murine model chosen develops multiple tumors, individual tumor follow-up has to be done, but the most relevant evaluation of electrochemotherapy efficiency is given by animal survival.

2. Materials

1. Mice and tumor appearance: C3H/Bi are C3H mice naturally infected by the Bittner murine mammary tumor virus (6). Multiparous female mice spontaneously develop mammary tumors at 5–11 mo of age. In most of the animals, additional mammary tumor appearance occurs at different sites on the thoracic or abdominal wall, at various times after the development of the first tumor(s). Untreated mice die within 1–2 mo after the detection of their initial tumor(s).

Mice were maintained in animal housing facilities under conventional conditions, fed with usual laboratory diet and water given ad libitum.

2. Bleomycin: Bleomycin (Laboratoire Roger Bellon, Neuilly-sur-Seine, France) is dissolved in sterile 0.9% sodium chloride just before the intravenous infusion.
3. Generator: Square-waved electric pulses of adjustable voltage, length and frequency are produced by a PS15 electropulser (Jouan, Nantes, France), initially designed for in vitro electric pulse delivery. The electrical parameters of the delivered pulses are recorded and controlled with a digital oscilloscope (VC-6025, Hitachi, Tokyo, Japan).
4. Electrodes: The most convenient external electrodes consist of two parallel flat stainless steel rectangles, with rounded inferior edges to improve skin contact at the level of the subcutaneous tumor nodule to be treated (these are shown in Chapter 12, Fig. 1). They are held by an insulating template which sets the electrode gap (usually 6 to 8 mm), and allows safe electrical connection to the generator PS15. Typical dimensions of the electrode edge that will be applied on the skin are 1 cm width and 0.5 mm thickness. The electrical contact with the skin is ensured by a film of electrocardiography paste spread on the electrode edges.

3. Methods

3.1. Mice Selection

1. Maintain in observation a colony of adult multiparous female C3H/Bi mice, in order to detect as soon as possible the appearance of a tumor in a mouse, and include it as soon as possible in the treatment protocol. Since the tumor growth rate is fast, it is recommended to inspect the mice very regularly to avoid becoming too large tumors, or initially having multiple tumors on the same mouse, which makes it difficult to administer an efficient treatment.

2. Shave or gently remove hair from the area around the tumor nodules, avoiding skin scrapes.
3. Measure with a caliper two perpendicular surface diameters, and, if possible, the thickness of every tumor nodule to be treated.

3.2. Bleomycin Administration

1. Intramuscular injection: inject a dose of 50 μg bleomycin dissolved in 100 μL saline into the tight muscle, and wait for 30 minutes before the electric pulse delivery.
2. Intravenous injection: inject a dose of 10 μg bleomycin dissolved in 100 μL saline into the retroorbital sinus, and wait for 3 min before the electric pulse delivery.

3.3. Electric Pulse Delivery

1. Adjust the electric pulse parameters to 1300 V/cm of electric field intensity (that is the ratio of the delivered voltage to the distance between the electrodes), 100 μs of length and 1 Hz of repetition frequency. This electric field intensity was shown to be the minimal value allowing to optimally permeabilize the whole tumor volume comprised between two electrodes placed on the skin covering the tumor nodule to be treated (1,3).
2. Spread a thin film of electrocardiography paste on the inferior edge of the electrodes.
3. In the case of “small tumors,” that is tumor nodules having at least one diameter smaller than the gap between the two electrodes, place the electrodes at both sides of the protruding nodule to be treated.
4. In the case of “large tumors,” that is tumor nodules having both diameters larger than the gap between the two electrodes, reposition the electrodes along all the nodule surface as many times as necessary and repeat the electric pulse delivery at each place, in order to correctly permeabilize the whole tumor volume (*see Note 1*).
5. Hold firmly the mouse in one hand, apply a run of 8 pulses to each tumor site, avoiding to change the electrode position during the run in spite of the muscular contraction presented by the mice at each electric pulse (*see Note 2*).

3.4. Mice Follow-up

1. Two to three times a week, measure with a caliper two perpendicular surface diameters, and, if possible, the thickness of the treated tumor nodules (*see Note 3*).
2. For each given tumor nodule, repeat weekly the electrochemotherapy session until obtention of a complete regression for this nodule (*see Note 4*). In some cases, an arrest of the nodule growth without volume decrease can be observed, which indicates tumor necrosis without resorption. In such a situation, stop the treatment if no change in nodule size is noted during three weeks.
3. Score as complete regression every tumor which becomes unpalpable.

4. Score as local cures the complete regressions which last more than 60 days after the treatment (actual cures in the case of absence of other tumor).
5. Regularly inspect the treated mice to detect as early as possible the appearance of additional mammary tumors. Treat each new tumor nodule in the same manner as the first tumor(s) of the mouse (*see Note 5*).
6. Evaluate the treatment efficiency based on mice survival time after the first electrochemotherapy session, as compared with survival time after the detection of the first tumor of similar mice not receiving electrochemotherapy.

4. Notes

1. An excess of electrocardiography paste at the skin surface can result in risks of short-circuit between the two electrodes when they are successively placed at adjacent positions. Therefore, in case of multiple electric pulse delivery to the same mouse, wipe the skin between each electrode application to remove the presence of residual paste.
2. Just after the electric pulse delivery to the tumor nodule on the mice flanks, it is regularly observed a transient paralysis of the hind legs of the treated mouse, which lasts less than one minute and which is always totally reversible.
3. Some days after electrochemotherapy, small scabs are often observed on the skin just at the level of electrode application. They always heal a few days after.
4. Sometimes, a nodule which was repeatedly treated does not disappear and the skin scab tends to increase. This can lead to the formation of a fistula to the underlying necrotic material constituting the upper part of the tumor nodule (which can be still growing at its basal part). In this case, gently press the tumor site to extrude this necrotic material. This will allow a more convenient and more efficient electric pulse application on the residual tumor mass.
5. When a mouse bears several growing tumor nodules, which requires many independent electrochemotherapy sessions, the treatment of this mouse becomes difficult due to possible confluence of the nodules. The case of a mouse presenting too large of a tumor mass with uncontrolled growth after several treatment sessions is an indication for stopping the treatment and, in case of a bad health status, for euthanasia of the animal.

References

1. Mir, L. M., Orlowski, S., Belehradek, J. Jr., and Paoletti, C. (1991) Electrochemotherapy: Potentiation of antitumor effect of bleomycin by local electric pulses. *Eur. J. Cancer* **27**, 68–72.
2. Serša, G., Čemažar, M., Miklavčič, D., and Mir, L. M. (1994) Electrochemotherapy: Variable anti-tumor effect on different tumor models. *Bioelectrochem. Bioenerg.* **35**, 23–27.
3. Belehradek, J. Jr, Orlowski, S., Ramirez, L. H., Pron, G., Poddevin, B., and Mir, L. M. (1994) Electroporabilization of cells in tissues assessed by the qualitative and quantitative electroloading of bleomycin. *Biochim. Biophys. Acta* **1190**, 155–163.

4. Belehradec, M., Domenge, C., Luboinski, B., Orlovski, S., Belehradec, J. Jr., and Mir, L. M. (1993) Electrochemotherapy, a new antitumor treatment: first clinical phase I-II trial. *Cancer* **72**, 3694–3700.
5. Belehradec, J. Jr., Orlovski, S., Poddevin, B., Paoletti, C., and Mir, L. M. (1991) Electrochemotherapy of spontaneous mammary tumours in mice. *Eur. J. Cancer* **27**, 73–76.
6. Staats, J. (1986) Standardized nomenclature for inbred strains of mice: Eighth listing. *Cancer Res.* **45**, 945–977.

Electroporation of Muscle Tissue In Vivo

Julie Gehl and Lluís M. Mir

1. Introduction

Electroporation (also termed electropermeabilization) of muscle tissue has been studied in several contexts. It has been shown that electroporation plays an important role in muscle damage as a result of electrical injury (*1,2*) and that electroporation of cardiac muscle occurs during defibrillation or cardioversion (*3,4*). As electroporation has been shown to greatly enhance the cytotoxic effect of certain chemotherapeutic agents, and as clinical Phase I–II studies (*5–8*) have shown that the combination of electroporation and chemotherapy (electrochemotherapy) is highly efficient against various localized cancers, the question of normal tissue sensitivity to electroporation needs to be investigated. Finally, efficient *in vivo* gene transfection to muscle tissue by electroporation has recently been reported (*9,10*), warranting increased knowledge on *in vivo* electroporation of muscle tissue.

This chapter describes a quantitative method to study electroporation of skeletal muscle tissue in the *in vivo* setting. Results from using the method are reported in **refs. 11 and 12**.

2. Materials

1. Animals: We have used C57black mice (Bomholtgaard, Denmark), but other animal models could be used.
2. Anesthesia: Fentanyl 0.315 mg/mL with fluanisone 10 mg/mL (Hypnorm, Janssen-Cilag, UK) and midazolam 5 mg/mL (Dormicum, Hoffmann–La Roche, Switzerland) (*see Note 1*).
3. Electroporator: BTX T820 square wave electroporator (BTX, San Diego, CA) (*see Note 2*).

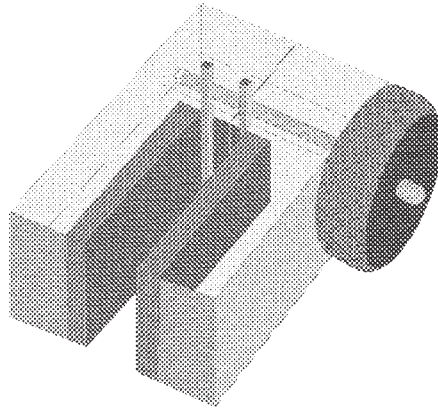


Fig. 1. Plate electrodes. Metal electrodes mounted on insulating material, with a screw that makes it possible to separate the two parts of the electrode for positioning. When the screw is tightened, the two plates of the electrode are held in parallel position. The distance between the plates is 4 mm, and the plates are 10 mm wide. The electric field distribution for these electrodes is reported in **ref. 11**.

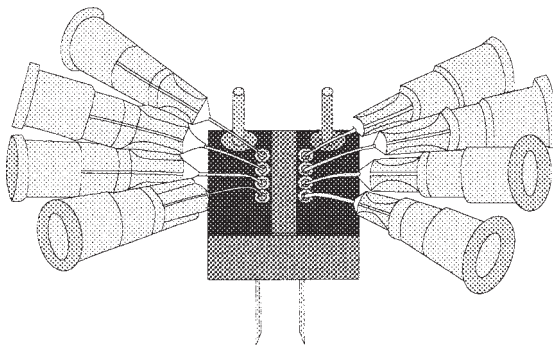


Fig. 2. Needle electrodes. On a piece of circuit board, where the middle is etched away, 4 metal sockets are mounted on holes on each side. These sockets fit 25 G (0.5 mm) hypodermic needles for single use, which can be replaced easily. The needles are bent after being placed in the sockets, which is sufficient to keep them in place. The spacing between the needles in the array is 2 mm, and the two arrays are placed 4 mm apart, one array being connected to the positive and the other to the negative pole. The electric field distribution for these electrodes is reported in **ref. 11**.

4. Electrodes: **Figs. 1** and **2** show plate and needle electrodes, constructed at our institution. The question of electrodes is further discussed in **Note 3**.
5. Electrode paste (Siemens-Elema AB, Sweden).
6. [⁵¹Cr]EDTA with a specific activity of 3.7 MBq/mL (Amersham, UK).

7. Ink: Black drawing ink (Pelikan, Hannover, Germany).
8. Gamma counter: Cobra 5002 (Packard Instrument Company, Meriden, CT).
9. Scale: AT261 scale and Balance Link (Mettler Toledo, Greifensee, Switzerland).

3. Methods

3.1. Anesthesia

It is important to use anesthesia when applying electric pulses to muscle tissue in vivo. We use Hypnorm (fentanyl/fluanisone) and Dormicum (midazolam) (*see Note 1*).

1. Mix the reagents, Hypnorm and Dormicum, separately on a 1 : 1 ratio with sterile water. Use only sterile water: if solvents other than water are used, for example, physiologic saline, crystals will form in the final mixture.
2. Mix the resulting solutions, again on a 1 : 1 basis. The final solution can be stored at room temperature for 1 or 2 days. Do not refrigerate or crystals will form.
3. Give mice 0.005–0.010 mL/g body weight of the final solution by intraperitoneal injection. Note that male mice are generally more sensitive to the anesthetic agent than female mice.
4. Anesthesia with this drug combination generally lasts 3–4 h, with maximal effect in the first hour. The onset of full anesthetic effect is around 10 min after intraperitoneal injection.

3.2. Delivering Pulses to the Muscle

3.2.1. Needle Electrodes

1. Make an incision over the gluteal muscle with surgical scissors.
2. Holding the electrode-device, dip the tips of the mounted needles in ink.
3. Insert the needles into the muscle, so that the arrays are parallel to the direction of the fibers (making the direction of the electrical field perpendicular to the long axis of the fibers (*see Note 4*)).
4. Administer the pulses and withdraw the needles. If you are working with small molecules such as [⁵¹Cr]EDTA, most dyes, isotopes and drugs, the following electric parameters would work well: 8 square wave pulses of 100 μ s duration at a frequency of 1 Hz and 1.2 kV/cm (ratio of applied voltage to distance between electrodes (*see Note 5*)). When working with larger molecules, for example, DNA, a longer pulse duration may be needed and consequently the applied voltage should be lowered in order not to cause tissue damage. When comparing pulsed with unpulsed samples, the needles can be inserted on both legs but pulses delivered on one side only.

3.2.2. Plate Electrodes

1. Shave the fur over the muscle in question, for example, the triceps brachii or the tibialis cranialis.
2. Apply electrode paste in a thin layer on the shaved skin.

3. Place the plate electrodes around the extremity (e.g., the leg).
4. Make sure that the extremity fits between the electrodes so that there is good contact with both electrodes.
5. Administer pulses (*see Subheading 3.2.1., step 4*).
6. When comparing pulsed with unpulsed samples, the plates can be placed on the contralateral side without administering pulses.

3.3. Excising Samples

3.3.1. Needle Electrodes

1. After sacrificing the animal, look for the ink marks on the muscle. Hold the animal so that the muscle is in more or less the same position as when you delivered the electric pulses.
2. Cut on the line of the ink marks with a pair of small surgical scissors.
3. Take out the sample and transfer to a plastic tube.

3.3.2. Plate Electrodes

1. After sacrificing the animal, remove the skin over the exposed area.
2. With a pair of small surgical scissors the muscle can be excised in toto.
3. Take out the sample and transfer to a plastic tube.

3.4. Determining Uptake as a Result of Electroporation

The following protocol uses [⁵¹Cr]EDTA to assess the effect of electroporation, but other isotopes, drugs, dyes, or DNA can be used according to the project planned.

1. Administer [⁵¹Cr]EDTA 50 μL iv to the anesthetized animals.
2. After 1.5 minutes (*see Note 6*), deliver electric pulses (as described in **Subheading 3.2.**).
3. Wait for exactly 60 minutes (*see Note 7*), then sacrifice the animals and excise samples as described (*see Subheading 3.3.*).
4. Put the samples in consecutively numbered tubes (e.g., tubes that fit into the gamma-counter), that have been weighed. If possible, use a scale with link to a computer so that data can be imported directly into a spread sheet.
5. Weigh the numbered tubes again, and calculate the net weight of the sample.
6. Measure the radioactivity of the samples in a gamma-counter.
7. Calculate the radioactivity of the sample expressed as cpm/g (counts per minute per gram of tissue), and make appropriate correction for the decay of the isotope. Determine the net uptake by subtracting the value of the sample not exposed to pulses from the value of the exposed sample.
8. Count a known amount of [⁵¹Cr]EDTA in the gamma-counter in order to obtain a relation between number of molecules of [⁵¹Cr]EDTA and the cpm measured in the particular counter that you are using.
9. Translate the net cpm per gram value obtained from the samples to net internalized nanomoles of [⁵¹Cr]EDTA per gram tissue.

4. Notes

1. Anesthesia: As fentanyl is a synthetic morphine analogue, permission to use this drug may be required. When using the fentanyl/fluanisone/dormicum anesthesia, it is possible to supplement the anesthesia by 0.02–0.05 ml iv at the time of experiment. With the type of anesthesia used, it is not necessary to take particular measures to warm up the animal during the anesthesia. We initially tried anesthetizing with pentobarbital, but found the anesthetic and analgesic effect insufficient. Another possibility which works is using xylazine (Bayer, Germany) combined with ketamine (Parke-Davis, Morris Plains, NJ); however this anesthesia is shorter lasting than fentanyl/fluanisone/dormicum.
2. When examining in vivo effects of electroporation it is important to use a square wave pulse generator in order to be able to control pulse length adequately.
3. It is not very difficult to construct simple electrodes. As the pulses generally used for electroporation are short, it is possible to disregard electrolysis as a problem. Thus, any type of insulating material combined with metal electrodes will do. It is however important that the electrodes are completely parallel in order to ensure even electrical field distribution. **Figures 1** and **2** shows plate and needle electrodes constructed at our institution. Of note, the needle electrode array has the advantage, that it is easy and inexpensive to change the needles frequently as ordinary single use hypodermic 0.5 mm needles are utilized.
4. As the cell diameter influences the threshold for electroporation, awareness of the position of the long axis of the muscle cell in relation to the direction of the electrical field is important.
5. A pulse number lower than 8 will result in lower uptake whereas increasing the pulse number will give rise to some, but not much, increase in uptake. The applied voltage is very important for obtaining optimal results, the 1.2 kV/cm setting should be fine for most purposes, but optimization could be important.
6. For [⁵¹Cr]EDTA the optimal time to deliver electric pulses is 1.5 min after administering the drug. However, larger molecules should be given a little more time to distribute into the extracellular space, for example, 3 min.
7. Based on preliminary studies indicating that most extracellular [⁵¹Cr]-EDTA is eliminated 60 minutes after administration of the compound, this time was chosen for excision of samples. However, it would be possible to choose another time frame, for example, 45 min or 90 min.

Acknowledgments

Bjarne Ølgaard, Per Theilman, and Henning Andersen at the Department of Radiophysics, Herlev Hospital, Denmark, constructed the needle and plate electrodes for administration of electric pulses.

References

1. Lee, R. C. and Kolodney, M. S. (1987) Electrical injury mechanisms: electrical breakdown of cell membranes. *Plast. Reconstr. Surg.* **80**, 672–679.

2. Lee, R. C., River, L. P., Pan, F. S., Ji, L., and Wollmann, R. L. (1992) Surfactant-induced sealing of electroporabilized skeletal muscle membranes in vivo. *Proc. Natl. Acad. Sci. USA* **89**, 4524–4528.
3. Tung, L., Tovar, O., Neunlist, M., Jain, S. K., and O'Neill, R. J. (1994) Effects of strong electrical shock on cardiac muscle tissue. *Ann. N. Y. Acad. Sci.* **720**, 160–175.
4. Tovar, O. and Tung, L. (1992) Electroporation and recovery of cardiac cell membrane with rectangular voltage pulses. *Am. J. Physiol.* **263**, H1128–36.
5. Belehradek, M., Domenge, C., Luboinski, B., Orłowski, S., Belehradek, J. Jr., and Mir, L. M. (1993) Electrochemotherapy, a new antitumor treatment. First clinical phase I-II trial. *Cancer* **72**, 3694–3700.
6. Heller, R., Jaroszeski, M. J., Reintgen, D. S., Puleo, C. A., DeConti, R. C., Gilbert, R. A., and Glass, L. F. (1998) Treatment of cutaneous and subcutaneous tumors with electrochemotherapy using intralesional bleomycin. *Cancer* **83**, 148–157.
7. Mir, L. M., Glass, L. F., Serša, G., Teissié, J., Domenge, C., Miklavčič, D., Jaroszeski, M., Orłowski, S., Reintgen, D. S., Rudolf, Z., Belehradek, M., Gilbert, R., Rols, M. P., Belehradek, J. Jr., Bachaud, J. M., DeConti, R., Štabuc, B., Čemažar, M., Coninx, P., and Heller, R. (1998) Effective treatment of cutaneous and subcutaneous malignant tumors by electrochemotherapy. *Br. J. Cancer* **77**, 2336–2342.
8. Panje, W. R., Hier, M. P., Garman, G. R., Harrell, E., Goldman, A., and Bloch, I. (1998) Electroporation therapy of head and neck cancer. *Ann. Otol. Rhinol. Laryngol.* **107**, 779–785.
9. Aihara, H. and Miyazaki, J. I. (1998) Gene transfer into muscle by electroporation in vivo. *Nat. Biotechnol.* **16**, 867–870.
10. Mir, L. M., Bureau, M. F., Gehl, J., Rangara, R., Rouy, D., Caillaud, J.-M., Delaere, P., Branellec, D., Schwartz, B., and Scherman, D. (1999) High efficiency gene transfer into skeletal muscle mediated by electric pulses. *Proc. Natl. Acad. Sci. USA* **96**, 4262–4267.
11. Gehl, J., Sørensen, T. H., Nielsen, K., Raskmark, P., Nielsen, S. L., Skovsgaard, T., and Mir, L. M. (1999) In vivo electroporation of skeletal muscle: Threshold, efficacy and relation to electric field distribution. *Biochim. Biophys. Acta* **1428**, 233–240.
12. Gehl, J. and Mir, L. M. (1999) Determination of optimal parameters for in vivo gene transfer by electroporation, using a rapid in vivo test for cell permeabilization. *Biochem. Biophys. Res. Commun.* **261**, 377–380.

Treatment of Human Pancreatic Tumors Xenografted in Nude Mice by Chemotherapy Combined with Pulsed Electric Fields

Sukhendu B. Dev, Gunter A. Hofmann, and Gurvinder S. Nanda

1. Introduction

Cancer of the pancreas is currently the fifth leading cause of cancer related deaths with a five year survival of less than 1% In the United States (1). It is one of the most difficult cancers to treat, since it is hard to detect in the early stages. The patients remain asymptomatic until late in the course of the disease. An excellent review of pancreatic carcinoma has appeared (2). Despite the progress made in our understanding of the biology of this cancer (3), the final outcome for this disease has remained extremely poor. Conventional chemotherapeutic agents have not been very effective for human pancreatic adenocarcinoma (4). Use of intratumoral chemotherapy in combination with monoclonal antibodies have been reported to produce better response rate and also reduced toxicity (5,6). Smith and colleagues (7) have recently shown that an injectable gel with a sustained release profile can inhibit tumor growth in vivo in human pancreatic cancer xenografts. This was demonstrated in nude mice with BxPC-3 xenografts using fluorouracil, cisplatin, and doxorubicin with a consequent size reduction of the tumors between 72% and 79%, compared to the controls at day 28 after the first treatment. Although these figures are impressive, by any standard, no cure was reported.

By contrast, a novel cancer treatment that uses a single intratumoral injection of bleomycin followed by pulsing of the tumor from a square wave generator has produced a large percentage of cures and also a substantial number of partial regressions in many different forms of cancers (8–13). The technique has also been applied in phase I/II clinical trials (14–16). The basis for this treatment is simply an extension of the well-established laboratory technique

of electroporation, which uses brief electrical pulses to create transient pores in the cell membrane and thus allowing agents to have intracellular access. The most important aspect for the *in vivo* applications of this technique is the design and fabrication of the new type of electrodes and the switching scheme between different sets of electrodes, which has made substantial impact on the treatment outcome (**16**). This new method of drug delivery is generally referred to as electroporation therapy (EPT) or electrochemotherapy (ECT).

2. Materials

1. Six-week-old BALB/c nu/nu mice from both sexes are used for this study. All animal experiments should be carried out after the approval of the IACUC and accordance with NIH rules and regulations. The mice should be housed under standard animal house conditions, which require the room temperature of 21–22°C with a 12-h light/dark cycle. Animals should be acclimatized for at least a week before implantation of the tumors.
2. Pan-4-JCK cell line: Human adenocarcinoma of the pancreas was provided by Professor T. Kubota of Keio University, Japan, to AntiCancer, Inc., San Diego, where it underwent several passages. The cells were injected on the flank of nude mouse. The resulting tumor was maintained by serial xenografts as stock tumor.
3. Bleomycin (Mead Johnson, New Jersey cat no: NDC-0015-3010-20).
4. Carboplatin (Sigma, cat no: C-2538).
5. Mitomycin C (Sigma, cat no: M-0503).
6. AErrane[®] (Isoflurane, Ohmeda Caribe Inc., NJ).
7. MedPulser[™] (Genetronics, Inc.).
8. Sterile 6-needle array (1.0 cm) electrodes (Genetronics, Inc.).
9. Clear-Rite (Richard Allan Scientific, MI)

3. Methods

3.1. Implantation of Tumors on the Flank of the Nude Mice

1. Euthanize the mouse with stock Pan-4-JCK tumor using carbon dioxide vapors.
2. Harvest the tumor tissue.
3. Wash the tumor tissue in RPMI-1640 medium.
4. Remove and discard the grossly necrotic and suspected necrotic tissue.
5. Cut the tumor tissue using sterile dissecting scissors into small pieces of about 2 mm³.
6. Anesthetize the experimental mouse with isoflurane.
7. Make a small incision pocket in the right flank of the nude mouse.
8. Implant two pieces of the tumor into the subcutaneous sac.
9. Suture or staple the incision.
10. Measure the tumor size using calipers and calculate the tumor volume using the formula $(\pi/6) \times a \times b \times c$, where, *a*, *b*, and *c* are dimensions of the length, width, and depth of the tumor in mm.
11. Allow the tumor to grow to a volume of 80 ± 20 mm³.

3.2. Pretreatment

1. Randomize the mice in four different groups, D–E–, D–E+, D+E– and D+E+ (D = Drug, E = Electric field, and +/- denotes presence or absence, respectively).
2. Label the mice in each group with a distinctive ear tag for identification.
3. Measure the tumor size and weight before treatment.
4. Photograph representative animals in all groups for record.

3.3. Electroporation Therapy

1. Anesthetize the mouse for electroporation therapy by exposing them to isoflurane vapors (*see Note 1*).
2. Inject intratumorally the drug dissolved in 0.15 mL saline by fanning, a process of slow injection of the drug at the base of the tumor with the needle tip rotating in different directions to achieve uniform drug distribution in the tumor. During the injection, an increase in the tumor volume due to the fluid penetration is observed.
3. Wait for 5–10 min before pulse application (*see Note 2*).
4. Insert the needle array in the in the skin surrounding the tumor so as to cover the entire tumor including a margin of 1.0 mm. (A typical electric field distribution plot generated by a 1.0-cm needle array is given in **ref. 9**.)
5. Connect the needle array to the MedPulser™, a specially designed square wave pulse generator. The instrument automatically sets the pulse parameters to six 100 μ s pulses of 1130 V at 4 Hz.
6. Activate the foot switch to automatically deliver pulses through the six-needle array. The electrical pulses are applied through two successive needles and the corresponding opposite pairs, such pairs having the opposite polarity. The pulse is then switched to the next adjacent pairs—a 60° displacement from the first pair of needles. This process is repeated so as to cover the whole tumor that also includes change of polarity (*see Note 3*).

3.4. Posttreatment Monitoring of Animals and Tumor Growth Measurements

1. Monitor all the mice in both the control and the pulse-treated groups every day for mortality and sign of any other disease.
2. Edema is observed in the mice treated with the drug and pulse.
3. Measure the tumor dimensions using a caliper and the weight of the mice twice a week for 2 wk followed by once a week for up to 90 d (*see Note 4*).
4. Calculate the tumor volume as described earlier to determine the tumor growth regression/progression (*see Note 5*).
5. Take representative photographs for record.
6. The tumor response is then scored based on the definitions given below:
Complete response (CR): Complete disappearance of all known disease.
Cure: Complete response for 8 wk and complete absence of tumor cells in histology of sample from tumor treatment site.

Partial response (PR): Estimated decreases in tumor size of 50% or more.

No response (NR) or No Change (NC): No significant change. These include stable disease (SD); estimated decrease of less than 50% and lesions with estimated increase of less than 25%.

Progressive disease (PD): Appearance of any new lesions not previously identified or estimated increase of 25% or more in existent lesions.

3.5. Histology of Samples From Treatment Site

Histology of the samples from the treatment site of representative mice from all the control and the treatment groups should be carried out to confirm visual observations. The typical procedure is as follows:

1. Euthanize the mouse using carbon dioxide vapors.
2. The tissue from treatment site is cut into small pieces of about 0.5 cm diameter and fixed in 10% formalin for 24 h.
3. The tissue is then processed for dehydration, first in 95% alcohol for 3 h, followed by 100% alcohol for 3 h. Alcohol is changed every hour in both the cases.
4. The tissue is then immersed in Clear-Rite for 3 h followed by immersion in liquid paraffin for 2 h.
5. The dehydrated tissue is then embedded in paraffin for sectioning into 5 μm sections that were spread on microslides for subsequent staining.
6. The slide is kept in a 60°C oven overnight and then stained with hematoxylin and eosin.

3.6. Representative Results

Using the protocol described herein, electroporation therapy treatments of human pancreatic tumor Pan-4-JCK grown subcutaneously in nude mice was carried out. Three anticancer drugs namely, bleomycin (0.5 U), carboplatin (8 mg/kg), and mitomycin C (3 mg/kg) were used. In all the control groups including drug only treatments (D–E–, D–E+, and D+E–), the tumor volumes increased with the days after treatment and showed progressive disease (PD). However, in the treated group (D+E+) the number of CR with bleomycin, mitomycin, and carboplatin on day 89 after treatment were 75%, 22%, and 12.5%, respectively, while the others showed progressive disease. Histological examination of tissue samples (**Fig. 1**) removed from the tumor site showed total absence of tumor cells with only normal skin structures and fibrosis. This is in contrast to the control groups, which show the presence of tumor cells.

4. Notes

1. In EPT experiments, care must be taken that the animal is not over anesthetized, which can lead to death.
2. The drug should also be injected very slowly at the base of the tumor. This is seen as gradual swelling of the tumor. It has also been found that ‘fanning’ of the

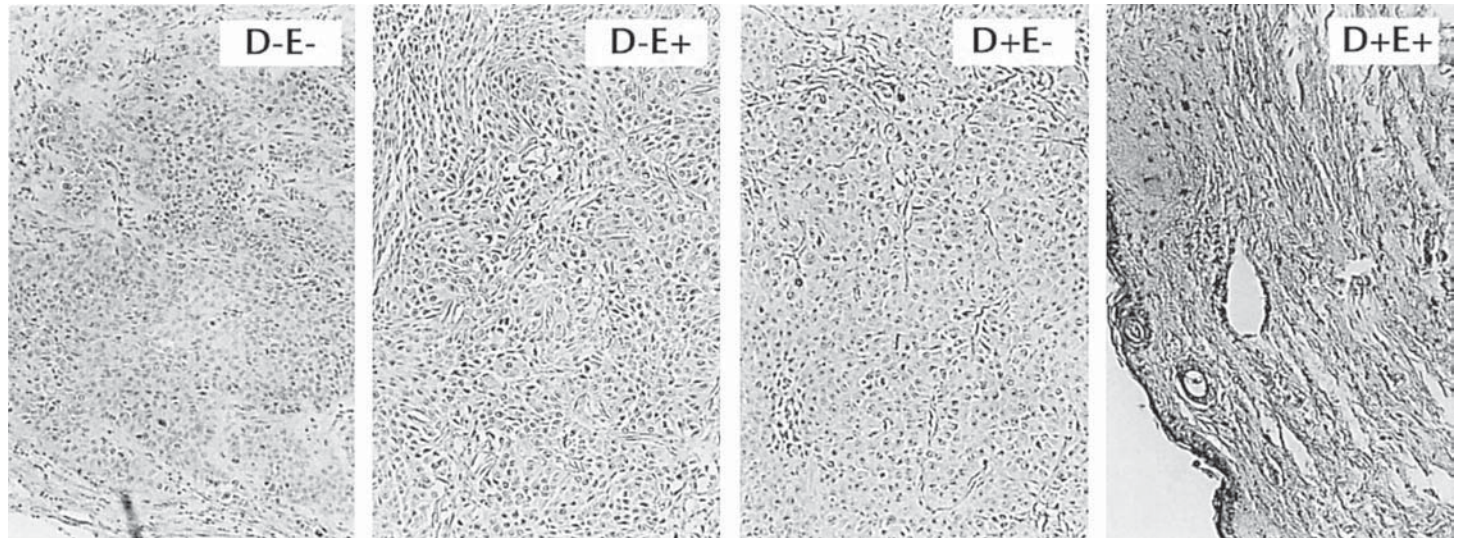


Fig. 1. Histological examination of tissue samples.

needle, together with increased volume of the diluent (0.15 ml saline) gives substantially better outcome for the treated tumors. Combination of all this may help in proper distribution of the drug throughout the tumor volume.

3. During the actual experiment, when the tumor is pulsed, one should be careful that the action of twitching by the animal after each pulse does not dislodge the needle array. Also, the needle array should not be pushed hard and instead held gently in order to avoid hitting and damaging underlying organs. Ideally, one should measure the dimensions along all three perpendicular directions and use an appropriate needle array.
4. Severe edema is generally noticed in all the animals treated with bleomycin and electrical pulses. However, with other drugs, only mild edema appears. Normally, this edema disappears within a week or so. Measurements of tumor volume taken during this period will not reflect the 'true' volume of the tumor.
5. In case of reappearance of the tumor after initial regression, it is strongly recommended that the tumor be retreated with the same parameters as before, but with a needle array of a suitable size that surrounds the tumor along the margin. Finally, the number of mice to be chosen should be enough to be statistically significant.

References

1. Keller, J. W. and Peacock, J. L. (1993) In *Clinical Oncology* (Rubin, P., ed.), W. B. Saunders, Philadelphia, p. 597.
2. Warshaw, A. L. and Castillo, C. F-D. (1992) Pancreatic carcinoma. *N. Engl. J. Med.* **326**, 455–465.
3. Poston, G. J. (1991) Biology of pancreatic cancer. *Gut* **32**, 800–812.
4. Wils, J. A. (1991) Chemotherapy in pancreatic cancer: a rational pursuit. *Anticancer Drugs* **2**, 3–10.
5. Otsuji, E., Yamaguchi, T., Yamaoka, N., Kitamura, K., Yamaguchi, N., and Takahashi, T. (1993) Intratumoral administration of neocarzinostatin conjugated to monoclonal antibody A7 in a model of pancreatic cancer. *J. Surg. Oncol.* **53**, 215–219.
6. Otsuji, E., Yamaguchi, T., Tsuruta, H., Yata, Y., Nishi, H., Okamoto, K., Taniguchi, K., Kato, M., Kotani, T., Kitamura, K., and Takahashi, T. (1995) The effect of intravenous and intra-tumoral chemotherapy using a monoclonal antibody-drug conjugate in a xenograft model of pancreatic cancer. *Eur. J. Surg. Oncol.* **21**, 61–65.
7. Smith, J. P., Stock, E., Orenberg, E. K., Yu, N. Y., Kanekal, S., and Brown, D. M. (1995) Intratumoral chemotherapy with a sustained release drug delivery system inhibits growth of human pancreatic xenografts. *Anticancer Drugs* **6**, 717–726.
8. Dev, S. B. and Hofmann, G. A. (1994) Electrochemotherapy: A novel method of cancer treatment. *Cancer Treat. Rev.* **20**, 105–115.
9. Hofmann, G. A., Dev, S. B., and Nanda, G. S. (1996) Electrochemotherapy: Transition from laboratory to the clinic. *IEEE Eng. Med. Biol.* **15**, 124–132.

10. Jaroszeski M. J., Gilbert, R. A., and Heller, R. (1997) In vivo antitumor effects of electrochemotherapy in a hepatoma model. *Biochim. Biophys. Acta* **1334**, 15–18.
11. Dev, S. B., Nanda, G. S., An, Z., Wang, X., Hoffman, R. M., and Hofmann, G. A. (1997) An effective electroporation therapy of human pancreatic tumors implanted in nude mice. *Drug Deliv.* **4**, 293–299.
12. Nanda, G. S., Sun, F. X., Hofmann, G. A., Hoffman, R. M., and Dev, S. B. (1998) Electroporation therapy of human larynx tumors HEP-2 implanted in nude mice. *Anticancer Res.* **18**, 999–1004.
13. Nanda, G. S., Sun F. X., Hofmann G. A. Hoffman R. M. and Dev, S. B. (1998) Electroporation enhances therapeutic efficacy of anticancer drugs: Treatment of human pancreatic tumor in animal model. *Anticancer Res.* **18**, 1361–1366.
14. Mir, L. M., Belehradek, M., Domenge, C., Orłowski, S., Poddevin, B., Belehradek, J. J., Schwaab, G., Luboinski, B., and Paoletti, C. (1991) Electrochemotherapy, a novel antitumor treatment: First clinical trial. *C. R. Acad. Sci. III* **313**, 613–618.
15. Heller, R., Jaroszeski, M. J., Glass, L. F., Messina, J. L., and Rapaport, D. P. (1996) Phase I/II trial for the treatment of cutaneous and subcutaneous tumors using electrochemotherapy. *Cancer* **77**, 964–966.
16. Hofmann, G. A., Dev, S. B., Dimmer, S., and Nanda, G. S. (1998) Electroporation therapy of head and neck cancer. *IEEE Trans. Tech. Biomed. Eng.* **46**, 752–759.

Distribution of Bleomycin in a Rat Model

Per Engström, Leif G. Salford, and Bertil R. R. Persson

1. Introduction

Bleomycin has, in the years of developing electrochemotherapy (ECT), proven to be an extremely potent drug for this cancer treatment modality and is also the most frequently applied chemical agent. It is of importance to investigate the pharmacokinetics of bleomycin under normal conditions and particularly in combination with ECT.

There is limited information available concerning the pharmacokinetics of bleomycin in mice and rats when used under normal conditions, that is, in healthy animals not affected by tumors or tumor treatments. After intramuscular and intravenous administration to humans and dogs, bleomycin has shown to be absorbed rapidly in the body and essentially 100% bioavailable. Elimination of bleomycin after intramuscular administration is equivalent to that observed after intravenous administration. Studies of mice and rabbits have shown corresponding results of rapid and extensive body distribution. Tissues tending to accumulate the highest concentrations are skin and spleen but also kidneys, lungs, and heart receive relatively high levels of bleomycin. No significant amount of bleomycin has been found in brain or cerebrospinal fluid of mice (*1*).

Bleomycin binds to several metals such as Cu I, Cu II, Fe (II), Fe (III), and Co (II) and can form chelates with several radionuclides such as ^{99m}Tc , ^{57}Co , ^{62}Zn , and ^{111}In , which is an iron analog (*2*). By labeling bleomycin with a radioactive compound (e.g., ^{111}In), the drug absorption and clearance can be traced *in vivo* with a gamma detector.

In this way, the kinetics and distribution patterns of pharmaceuticals such as bleomycin administered to animals or humans can continuously be followed

and recorded in the system. The labeling stability of [^{111}In]bleomycin *in vivo* can be verified by comparing the kinetics of [^{111}In]bleomycin to $^{111}\text{InCl}_3$ in normal rats. Unstable [^{111}In]bleomycin labeling results in a rapid release of ionic In^{3+} into the circulation. The $^{111}\text{In}^{3+}$ then rapidly binds to plasma transferrin in the blood and forms a very stable [^{111}In]transferrin complex as is observed after an $^{111}\text{InCl}_3$ injection. However, [^{111}In]bleomycin prepared under particularly low pH will form a complex ([^{111}In]bleomycin complex) which has a rapid whole body clearance, is stable *in vivo* and does not bind to plasma transferrin in the blood (3–5). A comparison of gamma camera images of $^{111}\text{InCl}_3$ and [^{111}In]bleomycin complex ([^{111}In]BLMC) distribution patterns can be regarded as a quality assurance of the labeling stability.

This chapter details a protocol for using [^{111}In]BLMC for imaging drug uptake resulting from ECT. The protocol describes the experimental procedure in imaging the effect of ECT on subcutaneously implanted gliomas in rats.

2. Materials

1. Indium-111 (^{111}In) (Mallinckrodt BV, Netherlands), a radioactive indium isotope, can be used to label bleomycin. ^{111}In is a radioisotope very suitable for diagnostic purposes because of its advantageous gamma energies and decay characteristics. ^{111}In has a half-life of 2.81 d and emits low-energy electrons and photons of 171 and 245 keV.
2. A scintillation gamma camera together with a graphical software is used to view and evaluate the ^{111}In -BLMC distribution in the animals.
3. An electropermeabilization unit (BTX 600; BTX Inc., San Diego, CA 92109) is used to generate high-voltage pulses with possibilities to alter voltage and duration of the electric pulses.
4. Electric pulses were in this study delivered through two stainless steel plate electrodes of $1.5 \times 2.5 \text{ cm}^2$ each mounted on a vernier caliper to set the correct distance between the electrodes.
5. Male and female rats of the Fischer-344 strain were used with or without subcutaneous N32 glioma tumors, implanted on the thigh of the hind leg. Glioma tumors were produced by injecting 100 000 N32 cells (6) just under the skin of the thigh. Solid tumors develop and grow to a size of about 10-mm diameter in 4 wk.

3. Methods

3.1. [^{111}In]BLMC Labeling Procedure

1. [^{111}In]BLMC labeling requires to be carried out in an acid environment maintained at pH 1.5–2.0 by using a 0.2 M HCl buffer solution.
2. ^{111}In is preferably delivered as an $^{111}\text{InCl}_3$ solution and requires a high radiochemical (i.e., the radionuclide exists only in one specific chemical form), radionuclear (i.e., no other radionuclides present in the batch) and chemical (no chemical impurities) purity.

3. Evaporate the required amount of $^{111}\text{InCl}_3$ to dryness, either by applying a gentle flow of nitrogen gas (N_2) or by heating the $^{111}\text{InCl}_3$ to approximately 90°C .
4. Dissolve the $^{111}\text{InCl}_3$ residue in a small volume of 0.2 M HCl.
5. Dissolve the required amount of solid bleomycin (Lundbeck, Sweden) in 0.9% physiologic NaCl solution with a volume three times the HCl volume. Calculate approximately 27 MBq $^{111}\text{InCl}_3$ per mg bleomycin.
6. Put the $^{111}\text{InCl}_3$ and the bleomycin solution together and mix thoroughly for 1 h.
7. A quality control of the labeling efficiency is preferentially performed before dilution to injection concentration, using thin layer chromatography (TLC) on silica gel (4).
8. Put a droplet (approx. 1.5 μL) of the radiolabeling on the TLC plate.
9. Develop the TLC plate, with the labeling applied, in equal parts of methanol and 10% aqueous ammonium acetate.
10. Labeled bleomycin migrates along the plate whereas the free (unlabeled) indium remains at the application point.
11. For quality control of the labeling, measure the R_f value of the labeled compound(s). The R_f value for [^{111}In]BLMC is 0.65 and ≈ 0 for $^{111}\text{InCl}_3$.
12. Cut the TLC plate in two and measure the activity of the [^{111}In]BLMC vs the unlabeled indium with an activity meter or with a gamma spectrometry detector. Pay attention to possible additional labeling groups, since this may indicate a suboptimal labeling result.
13. Dilute the labeled [^{111}In]BLMC to 1 mg/mL bleomycin with 0.9% NaCl. An injection volume of 0.3 mL will consist of 9 MBq ^{111}In labeled to 0.3 mg bleomycin, that is, 1 mg/kg b.w. in a 300-g rat.

3.2. Dynamic Study of Activity Distribution of [^{111}In]-Bleomycin Complex

Uptake and clearance of radiolabeled drugs in tissue and in specific organs of normal Fischer-344 rats can be studied and compared with a gamma camera. In the following experimental results, ^{111}In were coupled to bleomycin but other radiopharmaceuticals can excellently be used to investigate the biokinetic behavior of a certain drug (*see Note 1*). Here, 9 MBq of [^{111}In]BLMC is injected intravenously as bolus injection during acquisition of the gamma camera images.

1. Anesthetize the animal and put it on its back, on the gamma camera, fixed to a plate with plastic underneath to avoid contamination of the collimator.
2. Inject the [^{111}In]BLMC in the femoral vein of the rat.
3. To be able to capture the initial drug propagation in the body, set the image acquisition rate to one image per second and start immediately before injection.
4. Continuously increase the image acquisition intervals to follow the more slowly physiological functions such as kidney and bladder uptake and finally, whole-body clearance.

3.3. Electrochemotherapy Treatment and Study of Bleomycin Uptake and Retention in N32 Tumors

1. [^{111}In]BLMC (0.3 mg bleomycin per 9 MBq ^{111}In in 0.3 mL) corresponding to 1 mg bleomycin per kg body weight is assigned to each animal and is given intravenously as a bolus injection.
2. To make a correct comparison of the drug distribution in pulsed vs non-pulsed animals, one group (D + E+), receives [^{111}In]BLMC (D) followed by electropermeabilization (E), while the control group (D + E-), receives [^{111}In]BLMC only.
3. The fur over the tumor is shaven and the tumor is fixed in position between the electrodes.
4. Use electrocardial paste to ensure electrical contact between skin and electrodes. Electropermeabilization is performed on the fourth minute after [^{111}In]BLMC administration.
5. In order to deliver pulses of the same electric field strength for all tumors, being of different volumes, the electric potential is adjusted corresponding to the distance between the electrodes.
6. Altogether 16 pulses with a field strength of 1200 V/cm and a time constant of 1.0 ms are then delivered at approximately one pulse per second. Follow **steps 3 and 4 of Subheading 3.2.** to gather images. Owing to the half-life of ^{111}In of 2.8 d, it is possible to follow the whole-body distribution of [^{111}In]BLMC for several days (see **Note 2**).

3.4. Experimental Results

3.4.1. Dynamic Study of ^{111}In -Bleomycin in Normal Rats

Using the treatment and labeling protocols above, body distribution and elimination of [^{111}In]BLMC in normal rats indicates a stable [^{111}In]BLMC labeling in vivo. The [^{111}In]BLMC shows a rapid whole body removal with 80% of the drug eliminated within 2.5 h almost entirely by renal excretion. Consequently, no binding of ^{111}In to plasma-transferrin occurs.

Figure 1 shows the amount of [^{111}In]BLMC in the heart, kidneys, and bladder of a normal rat as percent of total injected activity versus time. There is a distinct peak in kidney activity corresponding to a maximum [^{111}In]BLMC concentration 130 s after injection. After 28 min, 35% of the total amount of injected [^{111}In]BLMC is located in the bladder.

Figure 2 shows the time scale of the drug uptake and clearance in the thigh muscle after intravenous administration of [^{111}In]BLMC. The [^{111}In]BLMC activity concentration is recorded over a region covering the thigh of the rat. A peak is reached approximately 3 min after injection and after 1.6 h the [^{111}In]BLMC concentration is reduced to half the peak value.

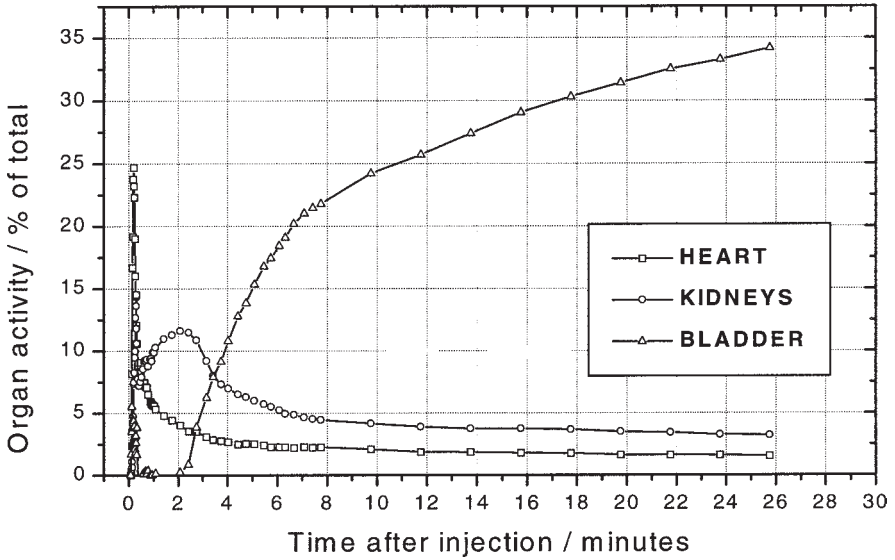


Fig. 1. Initial kinetics of [¹¹¹In]BLMC in heart (□), bladder (○) and kidney (Δ) of a normal rat after i.v. administration.

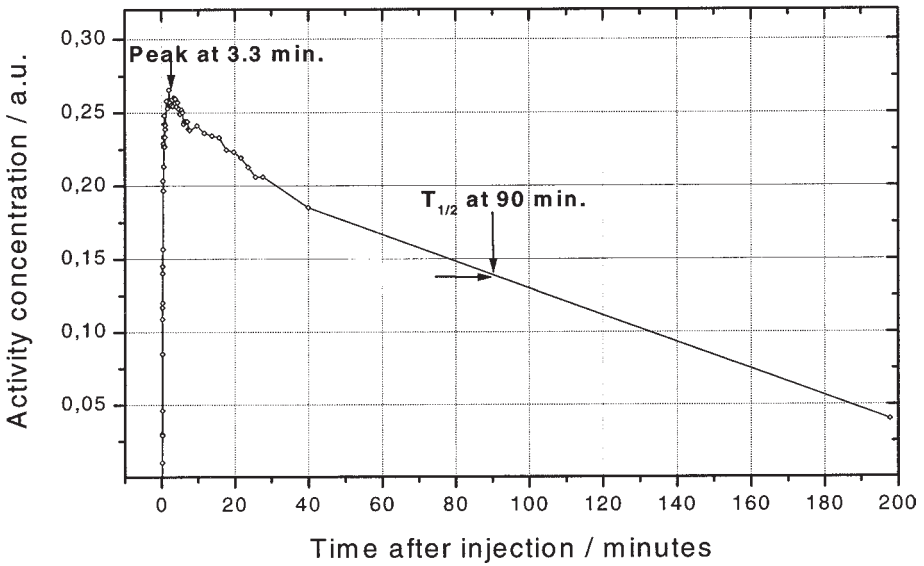


Fig. 2. [¹¹¹In]BLMC uptake and clearance of muscle tissue recorded over the thigh during the first 200 minutes after injection.

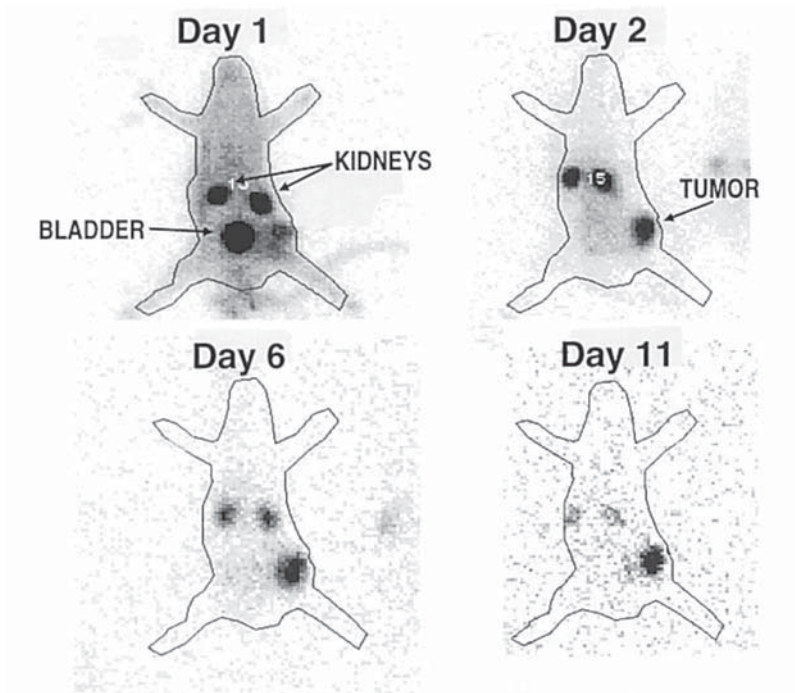


Fig. 3. Gamma camera images of a rat with an N32 tumor on the right thigh treated with $[^{111}\text{In}]\text{BLMC}$ and electropermeabilization.

3.4.2. Dynamic Study of $[^{111}\text{In}]\text{BLMC}$ in N32 Glioma-Bearing Rats After ECT

Figure 3 shows the $[^{111}\text{In}]\text{BLMC}$ distribution recorded at successive occasions in a rat with a N32 tumor on the flank treated with ECT after intravenous administration. As the drug is eliminated from the blood and normal tissues, the treated tumor area becomes more expressed in the images due to the very high drug retention in the electropermeabilized area.

In **Fig. 4**, the elimination of $[^{111}\text{In}]\text{BLMC}$ is displayed as a function of time for electropermeabilized tumors, D + E+ (upper curve, $n = 3$), and untreated tumors, D + E- ($n = 3$). All animals treated and nontreated, shows rapid initial drug elimination due to clearance from blood and normal, nonelectropermeabilized tissue. The drug concentration in the D + E+ group leveled after approximately 48 h where it maintained constant drug retention for up to 10 d. For the normal tissue and untreated tumors, the drug concentration continued to decrease 5 d after injection. At this time the radioactivity in these tissues was close to the detection limit of the imaging system.

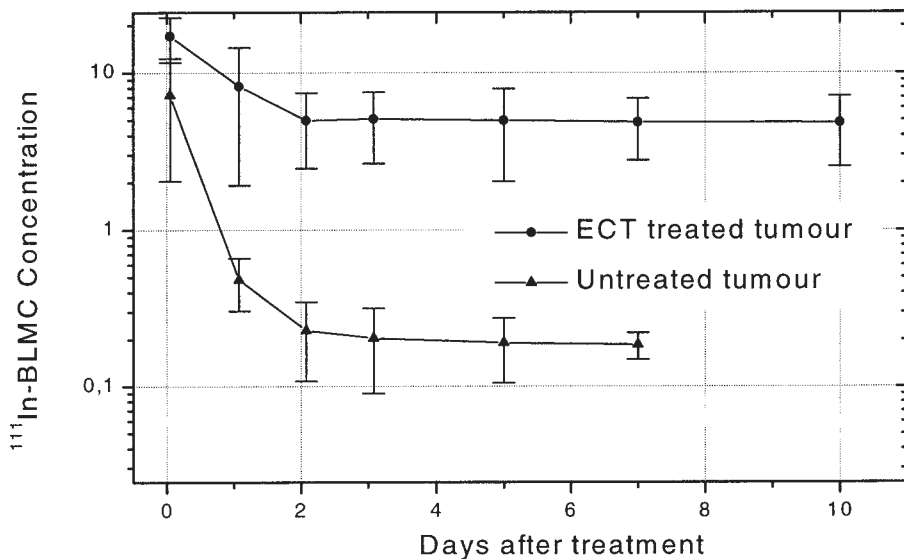


Fig. 4. Tumor uptake of [^{111}In]BLMC in rats treated with (●) and without (▲) ECT.

The results reported here shows that [^{111}In]BLMC is rapidly absorbed in the body after injection and also rapidly cleared from the system. The whole body clearance of [^{111}In]BLMC is known to have a faster elimination rate than [^{57}Co]bleomycin (7). In these studies of ECT treatment of N32 tumors, it was found that the retention of [^{111}In]BLMC was very stable in electropermeabilized areas.

The uptake process seems to be almost instant and [^{111}In]BLMC is completely retained in the treated tumor volume over several days. As observed from **Fig. 3**, the radioactivity concentration from [^{111}In]BLMC after 6 d are just above the noise level and after 11 d only the electropermeabilized tumor shows a distinct [^{111}In]BLMC retention.

The control groups, given [^{111}In]BLMC only, showed a slight but notable increase of [^{111}In]BLMC in the tumors. [^{111}In]BLMC have in earlier studies shown to have affinity for various tumors and has been used as a tumor imaging agent for gliomas in mice and rats (4,5).

4. Notes

1. In this study, relatively low ^{111}In concentrations was used and for tracing the bleomycin pathways only. Other radiolabeled agents such as ^{193}Pt or ^{195}Pt -labeled cisplatin might also be interesting complexes to use in ECT in this aspect since cisplatin is the anticancer drug besides bleomycin that has shown to gain a substantial increase in cytotoxicity after electropermeabilization (9).

2. From the gamma camera images of the N32 bearing rats, an accumulation of ^{111}In can also be noticed in the kidneys. ^{111}In might selectively be localized within the cytoplasmic fraction of the proximal tubule cells. ^{111}In binds to the sulfhydryl groups of δ -aminolevulinic acid dehydratase, an enzyme present in rat kidney (8). Possibly, [^{111}In]BLMC also binds to an enzyme in the kidney, causing an accumulation of [^{111}In]BLMC in the kidney.

References

1. Crooke, S. T. (1983) *Pharmacokinetics of Anticancer Agents in Humans* (Ames, M. M., Powis, G., and Kocach, J. S., eds.), Elsevier Science, Amsterdam, pp. 279–290.
2. Thakur, M. L. (1973) The preparation of indium-111 labelled bleomycin for tumor localisation. *Int. J. Appl. Radiat. Isot.* **24**, 357–359.
3. Hou, D. Y., and Yosh, M. (1992) Distribution of 111In-bleomycin complex in small cell lung cancer cells by autoradiography. *J. Surg. Oncol.* **49**, 93–97.
4. Hou, D. Y., Hoch, H., Johnston, G. S., Tsou, K. C., Farkas, R. J., and Miller, E. E. (1983) Stability of 111In-bleomycin in vivo: properties compared with 57Co-bleomycin. *Eur. J. Nucl. Med.* **8**, 535–540.
5. Hou, D. Y., Hoch, H., Johnston, G. S., Tsou, K. C., Jones, A. E., Miller, E. E., and Larson, S. M. (1984) A new tumor imaging agent—111In-bleomycin complex: Comparison with 67-Ga-citrate and 57-Co-bleomycin in tumor-bearing animals. *J. Surg. Oncol.* **27**, 189–195.
6. Siesjö, P., Visse, E., Lindvall, M., Salford, L. G., and Sjögren, H.-O. (1993) Immunization with mutagen-treated (tum-) cells causes rejection of nonimmunogenic rat glioma isografts. *Cancer Immunol. Immunother.* **37**, 67–74.
7. Hou, D. Y., Hoch, H., Johnston, G. S., Tsou, K. C., Jones, A. E., Farkas, R. J., Miller, E. E., and Larson, S. M. (1985) A new 111-In-bleomycin complex for combined radiotherapy and chemotherapy. *J. Surg. Oncol.* **29**, 91–98.
8. Woods, J. S. and Fowler, B. A. (1982) Selective inhibition of delta-aminolevulinic acid dehydratase by indium chloride in rat kidney: Biochemical and ultrastructural studies. *Exp. Mol. Pathol.* **36**, 306–315.
9. Serša, G., Čemažar, M., and Miklavčič, D. (1995) Antitumor effectiveness of electrochemotherapy with cis-diamminedichloroplatinum(II) in mice. *Cancer Res.* **55**, 3450–3455.

Treatment of Rat Bladder Cancer With Electrochemotherapy In Vivo

Yoko Kubota, Teruhiro Nakada, and Isoji Sasagawa

1. Introduction

It has been reported that the application of strong electric fields across a cell results in the formation and expansion of temporary membrane pores. Electrochemotherapy is a method which enhances the effectiveness of chemotherapeutic agents by administering the drugs in combination with short intense electric pulses (**1**). Cell electroporability allows nonpermeant or weakly permeant drugs to enter the cells. Electrochemotherapy is effective because electric pulses permeate any type of tumor cell membrane in vitro and in vivo. We have shown that electroporabilization induces a twofold increase in the concentration of Bleomycin, in bladder cancer cells in vitro and in normal bladder tissue of rats in vivo (**2**). Here we introduce our method to assess the effectiveness of this therapy for rat's bladder cancer.

2. Materials

1. Carcinogen: 0.05% *N*-butyl-*N*-(4-hydroxybutyl)nitrosamine (BBN; Tokyo Kasei Co., Ltd., Tokyo, Japan) solution in drinking water (*see Note 1*).
2. Animals: 5-wk-old male Wistar rats (*see Note 2*).
3. Bleomycin (Nihonkayaku Co., Tokyo, Japan) solution: A 10 U/mL solution in saline. This solution can be stored at -20°C for several months (*see Note 3*).
4. Electropulsation apparatus: a high power pulse generator (BTX820; BTX, San Diego, CA) is used, connected to twoplanar parallel electrodes made of gilded stainless steel mounted on insulated tweezers with one or two plastic screws (Unique Medial Imada Inc. Sendai, Japan) (**Figs. 1 and 2**; *see Note 4*) and an oscilloscope (AD-5141; A&D, Tokyo) to monitor the shape of the pulses.
5. Pentobarbital: Pentobarbital sodium injection 50 mg/mL (Abbott Laboratories, Chicago, IL).

From: *Methods in Molecular Medicine, Vol. 37: Electrically Mediated Delivery of Molecules to Cells*
Edited by: M. J. Jaroszeski, R. Heller, and R. Gilbert © Humana Press, Inc., Totowa, NJ

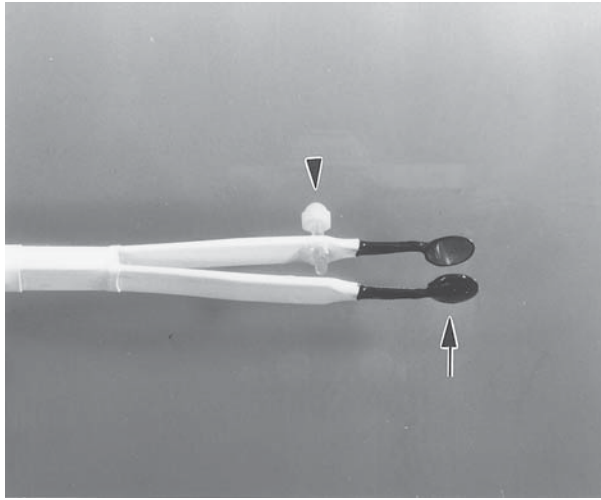


Fig. 1. Guided stainless steel electrodes mounted on tweezers. The distance between the two electrodes (arrow) can be fixed by a plastic screw (arrowhead).

6. 10% buffered formalin: 16.5 g $\text{Na}_2\text{HPO}_4 \cdot 12\text{H}_2\text{O}$ and 4.5 g $\text{NaH}_2\text{PO}_4 \cdot 2\text{H}_2\text{O}$ in 900 mL distilled water plus 100 mL formalin (pH 7).

3. Methods

3.1. Preparation of Rats With Bladder Cancer

Maintain rats under standard laboratory conditions and give drinking water supplemented with carcinogen (0.05% BBN in drinking water). The optimal maintenance duration for rats with BBN is generally 20–30 wk followed by 5–10 wk maintenance without BBN.

3.2. Electrochemotherapy

1. Make a lower abdominal midline incision. After peritoneal cavity has been entered, expose the urinary bladder, under intraperitoneal pentobarbital anesthesia (40 mg/kg). Then, dissect the urinary bladder and bladder neck sufficiently from seminal vesicles and skirts of peritoneum.
2. Inject a dose of 5 mg/kg of BLM (10 U/mL solution) through the caudal vein. After checking the back flow of the blood, infuse the solution rapidly.
3. Pause exactly 5 minutes before proceeding. One critical aspect of this procedure, which should be followed explicitly, is the time from the injection of BLM to the start the electric pulses. We have obtained lower efficiency using other time-windows. We suppose that in rats the highest concentration of BLM in the blood and urinary bladder tissue is acquired at this period. Optimal time-windows can be determined empirically for other species.

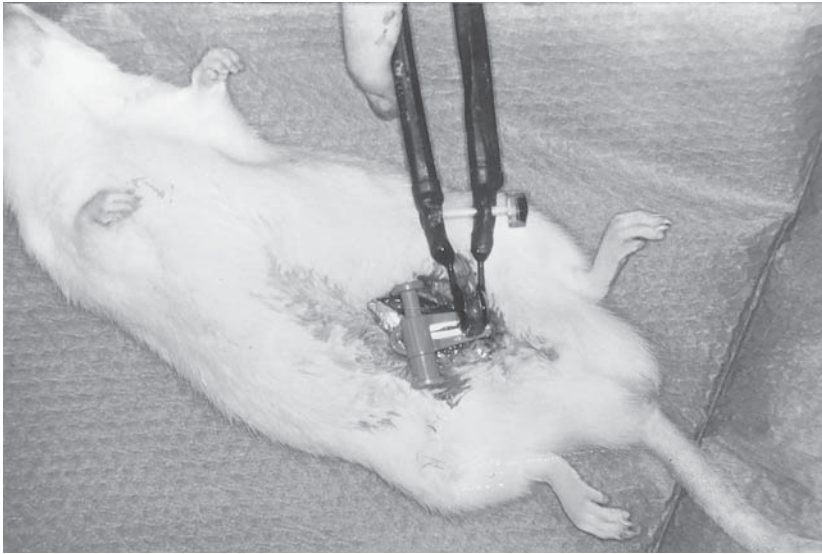


Fig. 2. Urinary bladder is held with the electrodes. The space between the electrodes is fixed to 2 mm.

4. Hold the urinary bladder between two electrodes during the pause in **step 3**. Measure the distance between the electrodes (*see Note 5*), and set the electric field according to the distance between the electrodes. The condition of 1000–1250 V/cm, 100 μ s pulse, 1 Hz, and 8 pulses” is recommended.
5. Apply the electric pulses.
6. Close the wound in one layer.

3.3. Evaluation of the Effects of Electrochemotherapy

Assess the effect of the therapy by histological findings and tumor weights.

Extract the bladder 10–14 d after the treatment (*see Note 6*). Under intraperitoneal pentobarbital anesthesia (40 mg/kg), make a lower abdominal mid-line incision. Open peritoneal cavity. Usually the urinary bladder is adherent to the seminal vesicles and surrounding fat tissue. Free the bladder and bladder neck by blunt dissection. Push out the urine from the bladder. By puncturing from bladder neck with 27-gauge needle, insert 0.5–0.7 mL of 10% buffered formalin into the bladder (*see Note 7*). Ligate the bladder neck with 3-0 silk to prevent the back flow of formalin from punctured pore on the bladder neck. Amputate the bladder at just distal point of the bladder neck ligation. Fix the excised bladder in 10% buffered formalin for 4–5 d. Cut the bladder sagittally or frontally and weight. Make histological specimens stained with hematoxylin–eosin.

4. Notes

1. Storage conditions: BBN is stable for 2–3 mo in a refrigerator; 0.05% BBN solution in drinking water can be stably stored several days in a refrigerator.
2. BBN induces bladder cancer in rats and mice but not in hamsters or guinea pigs (3,4). Although both rats and mice can be used, rats are recommended because the urinary bladders of mice are too small for the precise application of electrodes. Because the administration of 0.05% BBN for 8 wk was reported to induce bladder tumors in 100% of ACI rats, 85.7% in Wister rats, 50% in BDIX rats, and 0% in Lewis rats (3), use ACI or Wistar rats. Bladder cancer can be induced earlier in male rats than in female.
3. Bleomycin was, originally, reported to be an effective drug for the treatment of bladder cancer (5). But in our experiment which assessed the sensitivity of BBN-induced rats bladder tumor to BLM, at the dose of 5 mg/kg via intravenous injection, tiny foci of necrosis and cytolysis were seen in only about 10% of the bladders, and we observed a low efficacy for a single application of BLM at this dose (6). By using electroporation, the LD₅₀ of external BLM was seen to be about 1000 times lower than the value for cells without electroporation (7). In the case of cisplatin (8) and adriamycin (unpublished, our data), the most popular chemotherapeutic agents for urinary bladder cancer, by contrast, the difference in survival curves between the electroporated and nonelectroporated cells was reported to represent only a threefold dose-enhancing effect. Thus, we postulated that the best use of electroporation is made by using this technique in conjunction with treatment with BLM. However, the usefulness of only small number of cytotoxic agents have been assessed for bladder cancer electrochemotherapy, so there is still room for further experiments.
4. The role of the screws attached to the tweezers is to fix the space between the two electrodes to every possible distance we need. Because the surface of the urinary bladder is wet, paste is not needed for the electrodes to ensure good electrical contact. Since electric resistance increases as the surfaces of the electrodes become dirty, clean the electrodes after each use and soak in saline. The high-power pulse generator must be connected to an oscilloscope to monitor the actual shape of pulses. As for the electric pulses, square shape which proves the constant voltage during all the pulse duration is extremely important. If deformation is found, the pulse must be neglected.
5. If the urinary bladder tumor is small and creates difficulty in keeping an exact distance between two electrodes, an injection 0.5–0.7 mL of RPMI 1640 (Sigma Chemical Co., St. Louis, MO) into the bladder lumen increases the thickness of the bladder. After the injection with a 27-gauge needle from the bladder neck, the bladder is clamped with insulated blood vessel clamp (Applied Medical Resources Co., CA) (Fig. 3), otherwise injected solution will leak from the punctured region.
6. From about 10 d after chemotherapy, severe histological changes begin to be seen (unpublished, our data). And, from our clinical experience, we deduce that



Fig. 3. Bladder neck is clamped with an insulated blood vessel clamp (arrowhead).

regrowth of cancer cells starts from 21–28 d after chemotherapy. Thus we extract the bladders at 10- to 14-d period.

7. With this procedure, the urinary bladder can be fixed in a dilated state, which makes macroscopic observation of the tumor easy.

References

1. Mir, L. M., Glass, F. L., Serša, G., Teissié, J., Domenge, C., Miklavčič, D., Jaroszeski, M. J., Orłowski, S., Reintgen, D. S., Rudolf, Z., Belehradec, M., Gilbert, R., Štabuc B., Belehradec, J., Jr., Bachaud, J. M., DeConti, R., Rols, M.-P., Coninx, P., Čemažar, M., and Heller, R. (1998) Effective treatment of cutaneous and subcutaneous malignant tumors by electrochemotherapy. *Br. J. Cancer* **77**, 2336–2342.
2. Kubota, Y., Nakada, T., Yanai, H., Kakizaki, H., Sasagawa, I., and Watanabe, M. (1996) Electropermeabilization in bladder cancer chemotherapy. *Cancer Chemother. Pharmacol.* **39**, 67–70.
3. Ito, N., Arai, M., Sugihara, S., Hirao, K., Makiura, S., Matayoshi, K., and Denda, A. (1975) Experimental urinary bladder tumors induced by *N*-butyl-*N*-(4-hydroxybutyl)nitrosamine. *Gann Monogr.* **17**, 367–381.
4. Hirose, M., Fukushima, S., Hananouchi, M., Shirai, T., Ogiso, T., Takahashi, M., and Ito, N. (1976) Different susceptibility of the urinary bladder epithelium of animal species to three nitroso compounds. *Gann* **37**, 175–189.
5. Bracken, R. B., Johnson, D. E., Rodriguez, L., Samuels, M. L., and Ayala, A. (1977) Treatment of multiple superficial tumors of bladder with intravesical bleomycin. *Urology* **9**, 161–163.

6. Kubota, Y., Nakada, T., Yanai, H., Itoh, K., Sasagawa, I., and Kawai, K. (1998) Histological evaluation of the effects of electropermeabilization after administration of bleomycin on bladder cancer in rat. *Eur. Urol.* **34**, 372–376.
7. Poddevin, B., Orłowski, S., Bełhradec, J. Jr., and Mir, L. M. (1991) Very high cytotoxicity of bleomycin introduced into the cytosol of cells in culture. *Biochem. Pharmacol.* **42 (Suppl.)**, 67–75.
8. Milvik, J. E., Pettersen, E. O., Gordon, P. B., and Siglen, P. O. (1986) Increase in *cis*-dichlorodiammineplatinum (II) cytotoxicity upon reversible electropermeabilization of the plasma membrane in cultured human NHIK 3025 cells. *Eur. J. Cancer Clin. Oncol.* **22**, 1523–1530.

Electrochemotherapy for the Treatment of Soft Tissue Sarcoma in a Rat Model

Richard Gilbert, Mark J. Jaroszeski, and Richard Heller

1. Introduction

Each year approximately 6000 new cases of soft tissue sarcoma are diagnosed in the United States (1). The disease affects the extremities in 60% of the reported cases with the lower extremity the most likely tumor site (2,3). Management of soft tissue sarcomas is challenging but over the last 20 yr treatment has evolved from radical procedures such as amputation or compartmental resection to limb-sparing approaches (4,5). However, current limb sparing procedures are not applicable to all adult soft tissue sarcomas of the extremity. Limb sparing techniques are not employed when tumors are located close to joints, bone, or neurovascular bundles (6).

Electrochemotherapy, ECT, has been shown in human trials to be an effective anticancer treatment (7,8). Successful application of this treatment modality to sarcoma has been achieved in vivo in nude rats bearing human sarcomas (9,10). Thus, there is strong evidence that ECT may be an additional approach that can be used alone or combined with other limb sparing techniques. The future challenge is to determine if ECT can be used for the effective local control of tumors situated near joints, bone, or neurovascular bundles. This chapter describes protocols that were developed for the treatment of sarcoma in a rat model.

2. Materials

1. Cell line: Human A204 rhabdomyosarcoma cells (HTB 82; American Type Culture Collection, Rockville, MD).
2. Growth medium: McCoy's 5A medium (Mediatech, Washington, DC), supplement; 10% (v/v) fetal bovine serum (PAA Laboratories, Newport Beach, CA),

From: *Methods in Molecular Medicine, Vol. 37: Electrically Mediated Delivery of Molecules to Cells*
Edited by: M. J. Jaroszeski, R. Heller, and R. Gilbert © Humana Press, Inc., Totowa, NJ

90 µg/ml gentamicin sulphate (Gibco, Grand Island, NY). Nonenzymatic cell dissociation solution (CDS; Sigma, St Louis, MO) should be used instead of trypsin for harvesting cells. Cells should be grown at 37°C in a humidified atmosphere.

3. Animals: Male athymic rats (Harlan Sprague Dawley, Inc, Indianapolis, IN).
4. Anesthesia: Isoflurane (Mallinckrodt Veterinary, Inc., Mundelein, IL).
5. Drug: Bleomycin (Blenoxane; Bristol-Meyer Squibb, Princeton, NJ).
6. Pulse Generator: BTX T820 (Genetronics, Inc., San Diego, CA).
7. Electrode: Six needles equally spaced on the circumference of a 1 cm circle (Genetronics, Inc.) (*see Note 1*).
8. Mechanical Switch: for distributing pulses to needles (Genetronics Inc.).
9. Digital Storage Oscilloscope: PM 3394A (Fluke Corporation, Palatine, IL).
10. Current Probe: 80i-110S (Fluke Corporation).

3. Methods

Soft tissue sarcomas vary in size and can be larger than 10 cm³. Therefore, methods for electrochemotherapy in animal models bearing human sarcomas must include several possible experimental situations. This section presents protocols to deal with small (6–8 mm) and large tumors as well as single and multiple ECT treatment applications. In all cases a single ECT treatment is defined as the injection of a chemotherapeutic drug followed by the administration of electric pulses to the entire tumor.

3.1. Tumor Induction

1. Order male athymic rats so that they are 3–4 wk old at the time of tumor induction.
2. Harvest cells from culture using cells dissociation solution and wash three times in Ca and Mg free phosphate buffered saline (PBS) by centrifugation (200g).
3. Anesthetize all animals prior to tumor induction (this must also be done prior to tumor treatment and post treatment monitoring). Place the nude rats into an induction chamber that is charged with a mixture of 5% isoflurane in oxygen for several minutes. Rats should then be fitted with a standard rodent mask and kept under anesthesia using 3% isoflurane until the procedure is complete.
4. Induce tumors by injecting 8×10^6 cells contained in 70 µL of Ca and Mg free PBS. Cells should be injected into the biceps femoris muscle using a 25-gauge needle.
5. Allow time for tumors to grow to desired size. Generally, a growth time of 7–10 d will produce tumors that are 6–8 mm in diameter (small tumors). A 35-d growth time will yield tumors that are 18–20 mm in diameter (large tumors). Tumors will be well-defined, firm, and palpable.
6. Randomly place animals in an experimental group or one of three groups in a control group set and label each animal (*see Note 2*). Proceed to **Subheading 3.2.** if smaller tumors are being treated or **Subheading 3.3.** if larger tumors are being treated.

3.2. Single ECT Treatment of Small Tumors

1. Prepare Bleomycin prior to conducting ECT protocols. Bleomycin should be dissolved in normal saline for injection to a concentration of 5 U/mL. One unit of bleomycin is equal to 0.555 mg.
2. Anesthetize animals, one at a time, then record the dimensions of each tumor and compute the tumor mass volume (*see Note 3*).
3. Inject the proper drug dose into an appropriately labeled animal. A dose equal to 25% of the tumor volume is recommended for bleomycin (*see Note 4*). Allow 10 minutes for the drug to disseminate within the tumor before proceeding to **step 4**.
4. Insert the six-needle array electrode around the perimeter of each tumor.
5. Apply the electric pulse sequence to tumor (*see Note 5*).
6. Follow animals after treatment by anesthetizing, recording tumor dimensions, and computing tumor volumes at periodic intervals. Once or twice per week is sufficient (*see Note 6*).
7. Take biopsies to histologically confirm ECT experimental effects. Specimens should be fixed in 10% neutral buffered formalin and submitted for standard imbedding/sectioning. Hematoxylin and eosin staining is useful for visualization of the tissue.

3.3. Single ECT Treatment of Large Tumors

1. Dissolve bleomycin in normal saline for injection to a concentration of 5 U/mL.
2. Anesthetize animals, one at a time, then record the dimensions of each tumor and compute the tumor mass volume (*see Note 3*).
3. Approximate the number of one cm diameter circular areas that are present on the surface of the tumor. Each one cm diameter circle will be the insertion area of the one cm diameter six-needle electrode array. Thus it is important to carefully plan insertion points of the electrode so that electrical treatment is administered to the entire tumor mass. Failure to electrically treat the entire mass will result in incomplete tumor regression.
4. Inject a volume of bleomycin equal to 25% of the tumor volume (*see Note 4*).
5. Systematically treat each circular segment by repeatedly inserting the electrode into and applying pulses to each tumor section (*see Note 7*).
6. Follow **steps 6 and 7 in Subheading 3.2.** for following animals after treatment.

3.4. Multiple ECT Treatment

1. Follow **steps 1 to 5 of Subheading 3.2.** or **steps 1 to 5 in Subheading 3.3.** depending on whether small or large tumors, respectively, are being treated.
2. Repeat appropriate small or large tumor single treatment protocol on any palpable tumor that reappears in the original treatment site after the first ECT treatment (*see Note 8*).

4. Notes

1. There are a variety of possible electrodes that can be used in ECT applications. A discussion of some of these electrodes types has been published (*11*). Individual researchers may have specific preferences as to electrode material, shape, and arrangement.
2. The experimental design for ECT experiments should include experimental animal groups and three types of control groups. The experimental group, D^+E^+ , should receive drug injection followed by electric pulses. There may be multiple groups of this type, for example, if different electrical treatment parameters or drug doses are under investigation. The first type of control group, D^-E^- , should not receive drug nor electric pulses. The second type of control group, D^-E^+ , should be electrically pulsed with no drug injection. A normal saline injection can be used as a sham drug injection. The final type of control group, D^+E^- , should be injected with drug but not followed by electrical treatment.
3. Tumor volume is calculated from the product of the maximum lengths of three mutually orthogonal common referenced measurements of the nodule multiplied by π divided by six.
4. A clear unambiguous animal labeling system must be used. A combination of punching holes in ears and body "magic marker" labeling is strongly recommended. Bleomycin injections can be carried out using a 0.5 in. 30-gauge needle. Control animals that are not to receive bleomycin, the (D^-E^-) and (D^-E^+) control groups, should be given an intratumor injection of saline that is also equal to 25% of the tumor volume.
5. The applicator has six needles arranged on the circumference of a 1 cm diameter circle such that each needle is 60° apart. Individual researchers may have specific preferences with respect to the pulse parameters and pulsing sequence. However, a square wave pulse with an amplitude that corresponds to a nominal electric field strength of 1300 V/cm and a pulse width of 100 μ s will work (*9,10*). For animals that are in either control group that should not receive pulses, D^-E^- or D^+E^- , insert the electrodes for an equivalent amount of time but do not deliver any pulses.
6. Posttreatment tumor volumes are compared to the treatment day tumor volumes. Complete response is defined as no palpable tumor. Animals can be considered cured if a complete response is maintained for 100 d.
7. The electrodes may have to be inserted deeper in the center of tumors, relative to the edges, in order to treat the entire tumor volume.
8. Three is the recommended maximum number of replicates used to date. A 1-wk interval between treatments has been the minimum time. Animals can be considered cured if a complete response is maintained for 100 d.

References

1. Wingo, P. A., Tong, T., and Bolden, S. (1995) *Cancer Stat.* **45**, 12.
2. Levine, E. A., Trippon, M., and Das Gupta, T. K. (1993) Preoperative multimodality treatment for soft-tissue sarcomas. *Cancer* **71**, 3685–3689.

3. Yang, J. C., Glatstein, E. J., Rosenberg, S. A., and Antman, K. H. (1993) Sarcomas of soft tissue. *Principles and Practices of Oncology*, 5th ed. (Devita, V. T. Jr., Hellman, S., Rosenberg, S. A. eds.), J. B. Lippincott, Philadelphia, pp. 1437–1488.
4. Willard, W. C., Collin, C., Casper, E. S., Hajdee, S. I., and Brennan, M. F. (1992) The changing role of amputation for soft tissue sarcomas of the extremity in adults. *Surg. Gynecol. Obstet.* **75**, 389–400.
5. Brennan, M. F. (1990) Management of extremity soft tissue sarcoma. *Eur. J. Surg. Oncol.* **16**, 520–531.
6. Pollock, R. E., Kranell, L. H., Menck, H. R., and Winchester, D. P. (1996) The national cancer data base report on soft tissue sarcoma. *Cancer* **78**, 2247–2257.
7. Mir, L. M., Belehradec, M., Domenge, C., Orłowski, S., Poddevin, J. Jr., and Schwab, G. (1991) Electrochemotherapy, a novel antitumor treatment: First clinical trial. *C. R. Acad. Sci.* **313**, 613–618.
8. Heller, R., Jaroszeski, M. J., Glass, L. F., Messina, J. L., Rapaport, D. P., DeConti, R. C., Fenske, N. A., Gilbert, R. A., Mir, L. M., and Reintgen, D. S. (1996) Phase I/II trial for the treatment of cutaneous and subcutaneous tumors using electrochemotherapy. *Cancer* **77**, 964–971.
9. Hyacinthe, M., Jaroszeski, M. J., Dang, V. V., Copolla, D., Karl, R. C., Gilbert, R. A., and Heller, R. (1999) Electrically enhanced drug delivery for the treatment of soft tissue sarcoma. *Cancer* **85**, 409–417.
10. Pendas, S., Jaroszeski, M. J., Gilbert, R., Hyacinthe, M., Dang, V., Hickey, J., Pottinger, C., Illingworth, P., and Heller, R. (1998) Direct delivery of chemotherapeutic agents for the treatment of hepatomas and sarcomas in rat models. *Radiol. Oncol.* **32**, 53–64.
11. Gilbert, R., Jaroszeski, M., and Heller, R. (1997) Novel electrode designs for electrochemotherapy. *Biochim. Biophys. Acta* **1334**, 9–14.

Treatment of Spontaneous Soft Tissue Sarcomas in Cat

Stéphane Orlowski and Lluís M. Mir

1. Introduction

Preclinical experiments performed on mice clearly showed that electrochemotherapy can efficiently treat subcutaneous tumors of different histological types (1–4). However, the possibility of relevant clinical applications for electrochemotherapy requires the demonstration of its efficacy as a treatment of tumors larger than those encountered in mice. This necessitates the use of tumors growing in animals that are larger than mice. Since models for such tumors are rare and expensive, a convenient possibility is to test electrochemotherapy on spontaneous tumors that veterinarians have to treat in clinical presentations. Among them, cat soft-tissue sarcomas constitute a set of closely related tumors (fibrosarcoma of grade I or of grade II, and malignant fibrohistiocytoma) which are well suited for electrochemotherapy trials. Indeed, they are subcutaneous tumors, which always escape the conventional surgical treatment after a more or less long time, but which have only a local development for a long period of the disease evolution. Thus this carcinologic situation provides the possibility of testing the local efficiency of electrochemotherapy on animals having a good health status and bearing tumors for which no further conventional therapy can be proposed (5).

Due to the size of the tumors to be treated, it was necessary to use needle-electrodes in order to deliver the permeabilizing electric pulses intratumorally and to reach the deepest parts of the tumors. We also used external electrodes placed on the skin when there were additional tumor nodules of small size, and when the normal tissues surrounding the main tumor masses were infiltrated by tumor tissue without palpable thickness. Moreover, due to the fact that the

trial was performed under true clinical conditions, which means that it was necessary to propose an optimized treatment to the cat owners who accepted to enter the trial, electrochemotherapy was associated with an additional treatment based on an immunotherapy previously tested in preclinical experiments on mice (6,7).

The excellent results in term of tolerance to the treatment, absence of side effects and animal survival increase obtained during the first trial (5) are encouraging for further applications of our electrochemotherapy protocol in this veterinarian carcinologic situation, as well as for the extension of this treatment to other types of cutaneous or subcutaneous tumors presented by cats or dogs in the veterinarian practice.

2. Materials

2.1. Animal Recruitment

1. The cats who enter the trial should preferably bear tumors locally relapsing after multiple surgical excisions, and for which one supplementary surgical excision cannot be proposed again. Electrochemotherapy application is not limited by the fact that the cats previously received additional treatments, like teleradiotherapy with cobalt or curietherapy with iridium wires.
2. The progressive disease should be proven by histological examination.
3. Protocols for veterinarian clinical trials should be approved by an ethics committee for animal experimentation.

2.2. Drugs

1. The anesthetics typically used is a mixture of tiletamine and zolazepam (Zoletil®, Laboratoire Reading, Carros, France).
2. Bleomycin (Laboratoire Roger Bellon, Neuilly-sur-Seine, France) is dissolved in sterile 0.9% sodium chloride just before the intravenous infusion.

2.3. Electric Pulse Generators and Electrodes

2.3.1. Electrical Apparatus for External Electrodes

1. *Generator:* Square-waved electric pulses of adjustable voltage, length and frequency are produced by a PS15 electropulser (Jouan, Nantes, France), initially designed for in vitro electric pulse delivery. The electrical parameters of the delivered pulses are recorded and controlled with a storage oscilloscope (VC-6025, Hitachi, Tokyo, Japan).
2. *Electrodes:* The most convenient external electrodes consist in two parallel flat stainless steel rectangles, with rounded angles at the level of skin contact (see **Fig. 1** in Chapter 12). They are held by an insulating template which sets the electrode gap (usually 6–8 mm), and allows safe electrical connection to the generator PS15. Typical dimensions of the electrode edge that will be applied on the

skin are 2 cm width and 0.5 mm thickness (*see Note 1*). The electrical contact with the skin is ensured by a film of electrocardiography paste spread on the electrode edge.

2.3.2. Electrical Apparatus for Intratumoral Electrodes

1. *Generator*: Square-waved electric pulses of adjustable voltage, length and frequency are produced by a MK0 generator (CELTEM, Antony, France), specifically designed for electric pulse delivery to multiple electrodes by the means of an integrated switch which allows the successive distribution of the applied voltage to every pair of closest electrodes.
2. *Electrodes*: The electrodes are constituted by a set of seven parallel and equidistant needles, held by an insulating template which sets the electrode gap and allows safe electrical connection to the generator MK0. The seven electrodes are arranged according to a centered hexagonal array, with a distance of 6 mm between every pair of closest electrodes (*see Fig. 1* in Chapter 24). The pulsing sequence driven by the generator consists in the succession of the twelve closest pairs of electrodes, first involving the central needle with each of the six peripheral needles, and second the six pairs of peripheral neighboring needles. The exact sequence is of no importance, provided all the closest pairs of electrodes are fed by the generator, without two consecutive recruitments of the same electrode.

2.4. Interleukin-2 Secreting Cells

We used the xenogeneic CHO(IL-2) cells, which are Chinese hamster ovary cells in vitro transfected with the human interleukin-2 (IL-2) gene, and in vitro secreting 3500 units of IL-2 per ml, 72 hours and 80,000 initially seeded cells (8) (*see Note 2*). Cells were routinely cultured in usual culture medium without selective pressure to maintain transgene expression.

3. Methods

3.1. Animal Preparation

1. *Anesthesia*: Put an intravenous catheter in the saphene vein, and anesthetize the cat by the injection of 15 mg/kg of Zoletil. During the electric pulse delivery session, supplementary bolus of anesthetics can be given to prolong the anesthesia duration if necessary.
2. *Inspection and palpation of the tumor masses*: Shave the skin at the level of the tumor masses and around them. The evaluation of treatment efficacy requires careful measurements of the dimensions (at least the areas) of these masses, which should be reported on a drawing or on a photograph. It is also recommended to determine the thickness and the consistency of the masses, which could be modified by the treatment. In case of the presence of some liquid content (blood or necrosis) in the masses, drain it as much as possible in order to avoid perturbations of the electric field distribution during the electric pulse delivery.

3. *Bleomycin administration:* Infuse bleomycin intravenously via the catheter, in a bolus of about 30 seconds, at a dose of 0.5 mg/kg. This dose is equivalent to that used when electrochemotherapy is applied to tumor treatment in rats, rabbits and humans (9–11). Then wait for 4 min before beginning the electric pulse delivery, in order to let bleomycin to reach a sufficient concentration in the intratumoral interstitial fluids. According to preliminary experiments, the bleomycin concentration remains at a therapeutic level in the interstitial fluids for about 30 minutes after the bolus injection.

3.2. Electric Pulse Delivery Using External Electrodes

1. Use the external electrodes to treat only the thin tumors (<1 cm), for which the transcutaneously delivered electric pulses can efficiently permeabilize all the tumor volume.
2. Adjust the electric pulse parameters at 1300 V/cm of electric field intensity (that is the ratio of the delivered voltage to the distance between the electrodes), 100 μ s of length and 1 Hz of repetition frequency. This electric field intensity is chosen according to preclinical data and ex vivo experiments performed on mice, which have shown that this is the minimal value allowing to optimally permeabilize the whole tumor volume between two electrodes placed on the skin above the tumor nodule to be treated (1,12).
3. Put the electrodes on each tumor site and apply runs of 8 pulses (see Note 3). To treat a small protruding nodule with a size inferior to the gap between the electrodes, place the two electrodes at both sides of this nodule. To treat larger nodules, place successively the electrodes at adjacent positions over the tumor nodule in order to completely cover the tumor area (see Note 4).
4. Use the external electrodes to cover the periphery of the large tumor masses treated by the needle-electrodes in order to treat possible tumor infiltrations, not yet palpable but responsible for tumor recurrences after the treatment of the palpable masses.

3.3. Electric Pulse Delivery Using Intratumoral Needle-Electrodes

1. Use the needle-electrodes to treat the thick tumors, for which the intratumorally delivered electric pulses can efficiently permeabilize all the tumor volume.
2. Adjust the electric pulse parameters at 100 μ s of length and at 800 V/cm of electric field intensity, that is at a delivered voltage of 480 V for the 6 mm of distance between the closest electrodes. This electric field intensity is chosen according to ex vivo experiments performed on mice showing that this value is above the threshold for permeabilization of the tumor cells present in a tumor volume comprised between two parallel flat electrodes placed at its contact (12). Adjust at 6 Hz the generator pulse frequency, that results in 0.5 Hz of repetition frequency for a given pair of electrodes since there are 12 closest equidistant pairs of electrodes in the array formed by the seven electrodes.
3. Insert the array of seven needle-electrodes into each tumor site and apply runs of 8 pulses, each run thus lasting 16 seconds. To treat the whole of a large tumor

mass, reposition the electrode array at adjacent sites as many times as necessary (*see Note 5*).

3.4. IL-2 Based Immunotherapy

1. Prepare 30×10^6 CHO(IL-2) cells by trypsinization, centrifugation and resuspension in 2–3 ml of culture medium without fetal calf serum.
2. Inject 30×10^6 CHO(IL-2) cells into the tumor and its close vicinity by several successive injections of about 300–500 μ L. Perform this procedure the day after electrochemotherapy.
3. Repeat weekly the CHO(IL-2) cell injection for 6 wk. It is important to prepare the cells immediately prior to injection to preserve viability.

3.5. Animal Follow-up

1. If possible, keep the treated animal for one day in the clinics, for observation (*see Note 6*).
2. Each month, evaluate the tumor evolution by measuring the tumor size (take photographs if possible).
3. In the case of an arrest of tumor progression without apparent tumor regression, perform a biopsy for an histological control of the treated masses, about 2–3 mo after the first electrochemotherapy session, since massive tumor necrosis and peripheral fibrosis without tissue resorption can occur.
4. In the case of tumor relapse, repeat the electrochemotherapy provided the cat health status is still good (*see Note 7*).
5. Evaluate the treatment efficiency by the survival time after the first electrochemotherapy session, which must of course be compared to the survival time of animals in similar clinical situations but just followed without any treatment. As an example, a recent trial reported a very satisfying increase of lifespan of the cats treated by electrochemotherapy, with a median survival time of 5 mo (12 animals, maximum survival 18 mo), in comparison with the control untreated cats, having a median survival time of 3 wk (11 animals, maximum survival 1.5 mo) (5).

4. Notes

1. We also used external electrodes of 1 cm or 4 cm width. The 1 cm electrodes (initially designed for mouse tumor treatment) covered too small of an area above the subcutaneous tumors, and the 4 cm electrodes were too wide to allow regular electrical contact with the skin.
2. In the absence of IL-2 secreting cell availability, it is of course possible to treat the tumors by electrochemotherapy alone without the additional immunotherapy. In such a case, marked local antitumor effects are nevertheless expected.
3. At each electric pulse delivery, an instantaneous muscular contraction is observed. Its amplitude depends on the exact location of the electrodes on the body, in particular on the distance to the nervous centers. In no case these

contractions represent a limitation to the treatment, but they require firm holding of the cat during the electric pulse delivery.

4. Add a small amount of electrocardiograph paste on the electrodes at each time they are placed on the skin, but take care to avoid an excess of the conducting paste that could make a paste bridge between the two electrodes and provoke a short-circuit. Similarly, to avoid such risk of a short-circuit between the two electrodes when they are successively placed at adjacent positions, wipe the skin from time to time to remove the presence of residual paste on the skin.
5. Even in the case of multiple applications of the needle-electrode array into tumor masses, we never observed bleeding hampering the treatment. This could be due to a kind of microscopic cauterization of the tissues in contact with the electrodes.
6. During a few days after the electrochemotherapy session, a peritumoral oedema around all the treated areas is always observed. This oedema is related to the intense local inflammatory reaction that is an active part of the final efficacy of the treatment. This reaction is also stimulated by the locally administered IL-2. In the case of treatment by needle-electrodes, a local hyperthermia restricted to the treated volume is sometimes observed, without systemic fever.
7. A bad health status of the treated cat is the indication of a general metastatic spreading, typical of a very advanced stage of the disease, and this contraindicates further electrochemotherapy session.

References

1. Mir, L. M., Orlowski, S., Belehradec, J. Jr., and Paoletti, C. (1991) Electrochemotherapy: potentiation of antitumour effect of bleomycin by local electric pulses. *Eur. J. Cancer* **27**, 68–72.
2. Belehradec, J. Jr., Orlowski, S., Poddevin, B., Paoletti, C., and Mir, L. M. (1991) Electrochemotherapy of spontaneous mammary tumours in mice. *Eur. J. Cancer* **27**, 73–76.
3. Serša, G., Čemažar, M., Miklavčič, D., and Mir, L. M. (1994) Electrochemotherapy: variable anti-tumor effect on different tumor models. *Bioelectrochem. Bioenerg.* **35**, 23–27.
4. Heller, R., Jaroszeski, M., Leo-Messina, J., Perrit, R., Van Voorhis, N., Reintgen, D., and Gilbert, R. (1995) Treatment of B16 mouse melanoma with the combination of electropermeabilization and chemotherapy. *Bioelectrochem. Bioenerg.* **36**, 83–87.
5. Mir, L. M., Devauchelle, P., Quintin-Colonna, F., Delisle, F., Doliger, S., Fradelizi, D., Belehradec, J. Jr., and Orlowski, S. (1997) First clinical trial of cat soft-tissue sarcomas treatment by electrochemotherapy. *Br. J. Cancer* **76**, 1617–1622.
6. Mir, L. M., Orlowski, S., Poddevin, B., and Belehradec, J. Jr. (1992) Electrochemotherapy tumor treatment is improved by interleukin-2 stimulation of the host's defenses. *Eur. Cytokine Netw.* **3**, 331–334.

7. Mir, L. M., Roth, C., Orłowski, S., Quintin-Colonna, F., Fradelizi, D., Belehradec, J. Jr., and Kourilsky, P. (1995) Systemic antitumor effects of electrochemotherapy combined with histoincompatible cells secreting interleukin-2. *J. Immunother.* **17**, 30–38.
8. Ferrara, P., Pecceu, P., Marchese, E., Vita, N., Roskam, W., and Lupker, J. (1987) Characterization of recombinant glycosylated human interleukin-2 produced by a recombinant plasmid transformed CHO cell line. *FEBS Lett.* **226**, 47–52.
9. Salford, L. G., Persson, B. R. R., Brun, A., Ceberg, C. P., Kongstad, P. C., and Mir, L. M. (1993) A new brain tumour therapy combining bleomycin with in vivo electropermeabilization. *Biochem. Biophys. Res. Commun.* **194**, 938–943.
10. Belehradec, M., Domenge, C., Luboinski, B., Orłowski, S., Belehradec, J. Jr., and Mir, L. M. (1993) Electrochemotherapy, a new antitumor treatment: first clinical phase I-II trial. *Cancer* **72**, 3694–3700.
11. Ramirez, L. H., Orłowski, S., An, D. J., Bindoula, G., Dzodic, R., Ardouin, P., Bognel, C., Belehradec, J. Jr., Munck, J. N., and Mir, L. M. (1998) Electrochemotherapy on liver tumours in rabbits. *Br. J. Cancer* **77**, 2104–2111.
12. Belehradec, J. Jr., Orłowski, S., Ramirez, L. H., Pron, G., Poddevin, B., and Mir, L. M. (1994) Electropermeabilization of cells in tissues assessed by the qualitative and quantitative electroloading of bleomycin. *Biochim. Biophys. Acta* **1190**, 155–163.

Treatment of Rat Glioma With Electrochemotherapy

Leif G. Salford, Per Engström, and Bertil R. R. Persson

1. Introduction

The first attempt to apply electrochemotherapy (ECT) to the brain was reported in 1993 by Salford et al. 1993 (**1**). They managed to significantly prolong the survival of RG2 glioma bearing Fischer-344 rats by 200% by iv administration of bleomycin followed by intracranial electrochemotherapy with exponential decaying pulses. In collaboration with the department of tumor immunology, Lund University, an ethyl-nitroso-urea induced rat glioma cell line (N32) is developed that produces glioma of malignant astrocytoma type with only half the growth rate of the RG2 cells (**2**). The N32 tumor implanted in rats was treated with intracranial electrochemotherapy and enhanced uptake of [¹¹¹In]bleomycin from intracranial ECT was also demonstrated with a scintillation camera (**3**). ¹¹¹In-labeled bleomycin has been used to investigate the uptake and retention after ECT treatment of subcutaneous N32 tumors (**4**).

Although ECT is in its first stages of development, it is clear that electropermeabilization therapy can be used in conjunction with chemotherapy to deliver drugs to target areas. ECT with bleomycin is currently in Phase II clinical trials for head and neck carcinoma and is promising as an effective therapy for localized solid tumors (**5**). ECT has shown to be a very efficient treatment for various solid tumors but has markedly diminished effects for treating metastatic tumor growth. Electrochemotherapy is primarily a local treatment where the tumor volume exposed to high-voltage pulses responds. However, there are results that demonstrate a systemic immunologic response, provoked from the electrochemotherapy as well (**6**).

Experimental evidence suggests that combining ECT with immunotherapy may resolve the problem of metastatic disease. The immune system can be

stimulated with such agents as interferon or cytokines. These chemicals are normally present in the body in small amounts, but are used in immunotherapy in larger amounts. This approach would allow a systemic response to be generated from local electrochemotherapy treatment. Current efforts are focused in this direction. Mir et al. (6) have shown, that murine tumors treated on the flank with ECT using bleomycin, followed by injection of low-dosage of IL-2 over a few days, or injection of histoincompatible IL-2 secreting cells, can have a systemic effect that can greatly enhance cure rate in treated animals. This chapter reports our efforts in applying ECT with bleomycin for treatment of tumors in the brain using a glioma rat model.

2. Materials

1. Tumor cells: Rat glioma (RG2), originally emanating from an ethylnitrosourea-induced rat tumor was used. The cell line grows very well in infinite cell and produces malignant astrocytoma-like tumors when inoculated in the brain of Fischer 344 rats (7). When at least 1000 RG2 cells are inoculated, well-delineated tumors develop in 100% of our animals within 3 weeks. Untreated tumors have by then reached a diameter of 3–6 mm at this time.
2. Animal model: Fischer 344 rats of both sexes, weighing 150–250 g, bred at our laboratory in Lund, Sweden. The animals were housed with free access to water and food (Pellets, SAN-bolagen, Malmö, Sweden).
3. Electric pulse generator: A BTX 600 (Genetronics Inc., San Diego, CA) that delivers exponentially decaying pulses.
4. R5 nutrient solution (5%): 25 mL fetal calf serum, 4 mL HEPES (140 g / 500 mL, pH 7) (Sigma, St. Louis, MO); 50 mL of 10X RPMI-1640, 15 mL of 200 mM L-glutamine, 5 mL of 100 mM sodium-pyruvate, 0.5 mL of 50 mg/ml gentamycin (Gibco BRL/Life Technologies), 13.75 mL of 8% NaHCO₃, 5 mL of 1 M NaOH.

3. Method

3.1. Tumor Induction and ECT Treatment

1. Maintain cells in continuous serial passage in nutrient medium (RPMI 1640, Labdesign, Stockholm, Sweden) with addition of 5.5% fetal calf serum. Add gentamicin (50 µg/mL) to avoid infection.
2. Harvest RG2 cells immediately before inoculation into rat brains by washing twice in a Trypsin buffer (Trypsin 0.04%, EDTA 1%) for 1 min, followed by 5 min incubation at 38°C (see **Note 1**). Count cells in a Bürker chamber and dilute to 1,000,000 cells per mL in R5 nutrient solution.
3. Anaesthetize rats with 5% chloral hydrate, 6 mL/kg body weight, given intraperitoneally (see **Note 2**).
4. Fix rats, one at a time, in a stereotaxic instrument. Make a sagittal skin incision in the midline over the anterior part of the brain. Identify the coronal suture and drill a borehole in the vertex of the skull for cell injection.

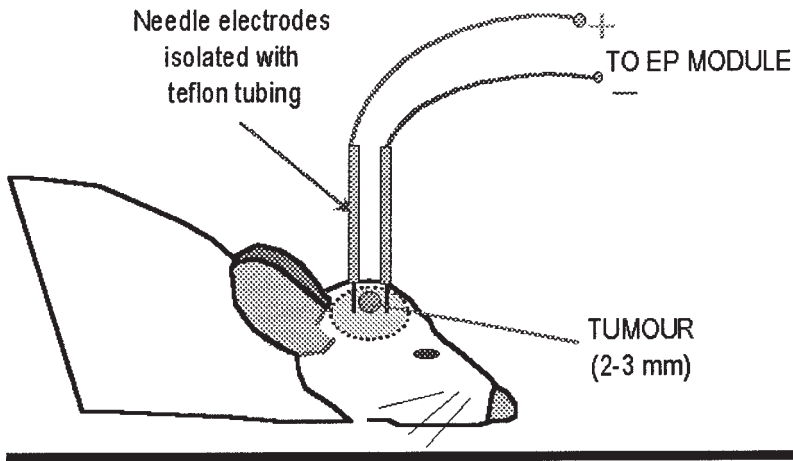


Fig. 1. The arrangement for electroporation therapy of brain tumors implanted in the right caudate nucleus of a rat.

5. Inject, by stereotaxic technique, 5000 RG2 cells in 5- μ L R5 nutrient solution using a Hamilton syringe into the head of the right caudate nucleus of the brain. To avoid extracranial tumor growth, clean the injection site with 70% ethanol after injection. Seal the borehole bone wax (*see Note 3*). The N32 cell line can also be used in Fisher rats. However, each rat should be injected with 15,000 N32 cells in the head of the right caudate nucleus. Inoculate groups of two to eight animals during each instance with cells harvested immediately before the procedure.
6. Match every animal that is scheduled to receive electrochemotherapy treatment to a control animal that was inoculated with identical tumor cells immediately before the treatment animal. Treat animals on the tenth day after inoculation when the tumors are approximately 2 mm in diameter. If the tumors are not treated, large lethal gliomas develop after 3 wk (5).
7. Prepare two acupuncture needles (0.3 mm in diameter) that have been insulated with Teflon tubing along their lengths except for 5 mm at the tip. These insulated needles will serve as electrodes when introduced through two predrilled holes in the skull, located 5 mm apart. One hole should be drilled 2.5 mm in front of and the other 2.5 mm behind the original bore hole used for cell inoculation 10 days earlier. Insert the needles stereotaxically to a depth of 4 mm to reach the level of the tumor (*see Note 4*). In sham experimental conditions, the electrodes are inserted to the same positions in the normal brain. Electrode positioning relative to the tumor is shown in **Fig. 1**.
8. Electroporabilization of the tumor is performed on the fourth and the seventh minute after an intravenous bolus injection of 0.3 mL bleomycin. Altogether

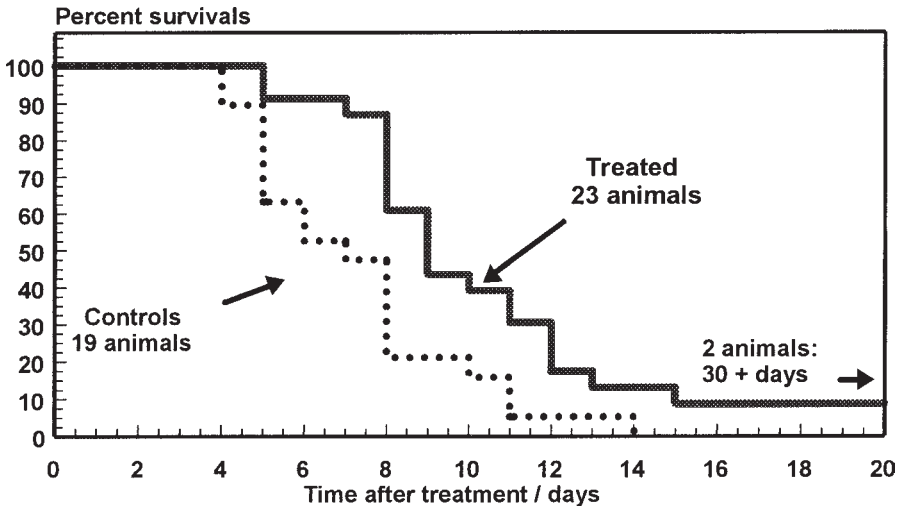


Fig. 2. Results of in vivo electrochemotherapy with bleomycin. The treatment was started 10–13 d after inoculation of 5000 RG2 tumor cells in the right caudate nucleus of rat brains. Two of the animals lived longer than 30 d while all controls died within 14 d.

16 pulses (8 + 8) with a field strength of approximately 800 V/cm and a time constant of 1.0 ms should be administered at a frequency of 1 Hz (*see Note 5*). A memory oscilloscope (Fluke Philips PM97 50 MHz scopemeter) is useful for monitoring the characteristics of the given pulses. Control groups that receive not treatment as well as bleomycin injection with no subsequent electroporation should be included for comparison.

9. After treatment the wound was closed and the animals are kept in their cages for daily observation of the tumor growth. When the animal start to develop neurological signs of tumor growth, the animals are sacrificed by perfusion-fixation of the brains under anesthesia.

3.2. Experimental Results

Animals with inoculated brain tumors were treated with bleomycin followed by electroporation as described in the protocol above (*I*). Survival data are shown in **Fig. 2**. Animals that were treated with bleomycin and electric pulses had prolonged survival time compared to the controls. Some complete remissions were observed, yielding an altogether 18% survival. Controls animals that received bleomycin only did not show a difference in survival time compared to the non treated controls and did not result in any complete remissions. This indicates that the drug alone has no effect on RG2 tumors.

4. Notes

1. Be sure not to exceed a concentration of 0.05% trypsin when detaching cells because higher concentration may kill cells.
2. Make sure not to exceed a chloral hydrate dose of 6 ml 5% chloral hydrate per kg body weight, because rats may be euthanized by higher dose.
3. The injection site must be sealed to avoid extracranial tumor growth.
4. Make sure not to insert needles beyond 5 mm to avoid injuries in the brainstem.
5. Do not exceed a field strength of 900 V/cm because it may kill the animal.

References

1. Salford, L. G., Persson, R. B. R., Brun, A., Ceberg, C. P., Kongstad, P. C., and Mir, L. M. (1993) A new brain tumour therapy combining bleomycin with in vivo electropermeabilization. *Biochem. Biophys. Res. Commun.* **194**, 938–943.
2. Siesjö, P., Visse, P., Lindvall, M., Salford, L. G., and Sjögren, H.-O. (1993) Immunization with mutagen-treated (tum-) cells causes rejection of non-immunogenic rat glioma isografts. *Cancer Immunol. Immunother.* **37**, 67–74.
3. Engström, P. E., Persson, R. B. R., and Salford, L. G. (1997) Dynamic gamma camera studies of ¹¹¹In-bleomycin complex in normal and glioma (N32, RG2) bearing rats after in vivo electropermeabilization using exponential high-voltage pulses. *Proceedings of the Second World Congress on Biological Effects of Electrical and Magnetic fields, Bologna, Italy, 1997*.
4. Engström, P., Salford, L. G., and Persson, R. B. R. (1998) Dynamic gamma camera studies of ¹¹¹In-bleomycin complex in normal and glioma bearing rats after in vivo electropermeabilization using exponential high-voltage pulses. *Bioelectrochem. Bioenerg.* **46**, 241–248.
5. Mir, L. M., Glass, L. F., Serša, G., Teissié, J., Domenge, C., Miklavčič, D., Jaroszeski, M. J., Orłowski, S., Reintgen, D. S., Rudolf, Z., Belehradek, M., Gilbert, R., Rols, M. P., Belehradek, J., Bachaud, J. M., DeConti, R., Štabuc, B., Čemažar, M., Coninx, P., and Heller, R. (1998) Effective treatment of cutaneous and subcutaneous malignant tumours by electrochemotherapy. *Br. J. Cancer* **77**, 2236–2342.
6. Mir, L. M., Roth, C., Orłowski, S., Quintin-Colonna, F., Fradelizi, D., Belehradek, J., and Kourilsky, P. (1995) Systemic antitumor effects of electrochemotherapy combined with histoincompatible cells secreting interleukin-2. *J. Immunother.* **17**, 30–38.
7. Aas, A. T., Brun, A., Blennow, C., Stromblad, S., and Salford, L. G. (1995) The RG2 rat glioma model. *J. Neurooncol.* **23**, 175–183.

Treatment of Liver Malignancies with Electrochemotherapy in a Rat Model

Mark J. Jaroszeski, Richard Gilbert, and Richard Heller

1. Introduction

Electrochemotherapy (ECT) is a combination treatment which involves administering a chemotherapeutic agent followed by the delivery of electric pulses to cells or tissue. Electrical treatment results in increased drug uptake by the cells which provides an improved therapeutic benefit relative to using the drug alone. Increased drug uptake is due to a process that has been termed electroporabilization, or electroporation.

The process of electroporabilization effects cells at the membrane level and is the result of exposure to pulsed electric fields (1). This type of electrical treatment induces membranes to become more permeable by destabilizing the lipid bilayer structure. The permeabilized state is transient and typically lasts on the order of minutes (2). It is the result of dielectric membrane breakdown, which is a physical phenomenon.

Electroporabilization has become popular for introducing DNA, fluorescent molecules, and drugs *in vitro* because it allows exogenous molecules to more freely enter the cytosol. This popularity is largely due to the physical nature of electroporation which makes the technique universally applicable. More recently, electroporation and the chemotherapeutic agent bleomycin have been used together in ECT protocols for the treatment of tumors *in vivo* (3–16).

Electrochemotherapy has been performed in a number of animal models. Models for melanoma (3–5), lung carcinoma (6), mammary tumors (7), fibrosarcoma (5), sarcoma (4), Ehrlich-Lette Ascites carcinoma (5), hepatocellular carcinoma (8), and glioma (9) have been treated with ECT. Response rates have ranged from 70% to 85% which demonstrated the effectiveness of the combination treatment. Clinical trials were initiated based on early research

findings. Currently, there are ECT clinical trials for melanoma (**10–12**), basal cell carcinoma (**10,11,13**), and head and neck squamous cell carcinoma (**14–16**).

The majority of ECT animal studies have utilized subcutaneously induced tumors. All of the human clinical ECT trials have treated tumors at the level of the skin only. Methods and devices for performing ECT on skin cancers or subcutaneously induced tumors are becoming more refined. However, little has been done to assess the applicability of ECT for the treatment of tumors that involve internal organs. Therefore, a study was conducted in order to explore the applicability of ECT for the treatment of hepatomas in a rat model (**17**). The protocol described below was developed and used for treating this type of tumor.

2. Materials

1. Rats: Male or female Sprague Dawley rats (Harlan, Indianapolis, IN, USA) 200 g, or greater, should be utilized. Animals should be housed and fed under standard conditions.
2. Hepatoma Cell line: N1S1 rat hepatocellular carcinoma cells (CRI-1604; American Type Culture Collection, Rockville, MD, USA). Cells should be grown in Swimms S-77 medium (Sigma, St. Louis, MO, USA) modified to contain 4 mM L-glutamine, 0.01% Pluronic F68 (WPMO-568B, BASF Corp., Parsippany, NJ), 9% fetal bovine serum (v/v), and 90 µg/mL gentamicin sulfate. Cell Dissociation Solution (CDS; Sigma, St. Louis, MO, USA) should be used instead of trypsin for detaching cells.
3. Anesthesia: Isoflurane (Mallinckrodt Veterinary, Inc., Mundelein, IL, USA) and an appropriate vaporizer to administer the inhaled anesthetic are required.
4. Electroporator: A direct current pulse generator such as a BTX T820 (Genetronics, Inc. San Diego, CA).
5. Oscilloscope: A digital storage device to monitor administered electric pulses. A Philips PM3375 oscilloscope (Philips, Eindhoven, Netherlands) has been used for the protocol described in this chapter.
6. Electrode and Switch: A 1 cm diameter array of needle electrodes (Genetronics, Inc.) comprised of six needles arranged circumferentially as shown in **Fig. 1**. A mechanical switch (Genetronics, Inc.) should be used to direct the pulses from the pulse generator to opposing pairs of needles as indicated in **Fig. 2**.
7. Chemotherapeutic Agent: Bleomycin (Bristol-Meyers Squibb, Inc, Princeton, NJ) should be dissolved in sterile saline for injection to a concentration of 5 U/ml (*see Note 1*).

3. Methods

3.1. Anesthesia and Surgical Procedures

All procedures in this protocol require gaining access to the liver. Therefore, methods for anesthesia and surgery are very important. These procedures

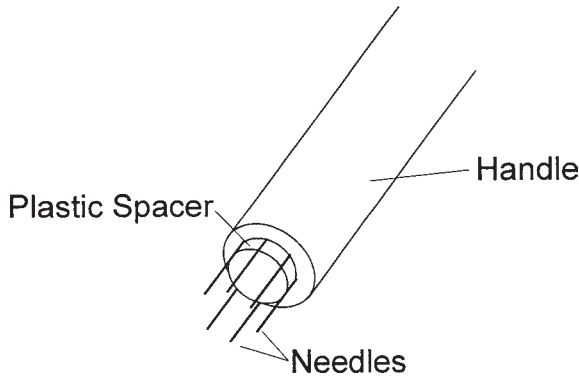


Fig. 1. Electrode used to deliver pulses to liver tumors in rats. Each needle had an independent electrical connection. Needles were equispaced at 60° intervals around a 1-cm diameter circle and held in place by a handle. A plastic spacer was inserted into the end of the device to limit the maximum penetration depth of the needles.

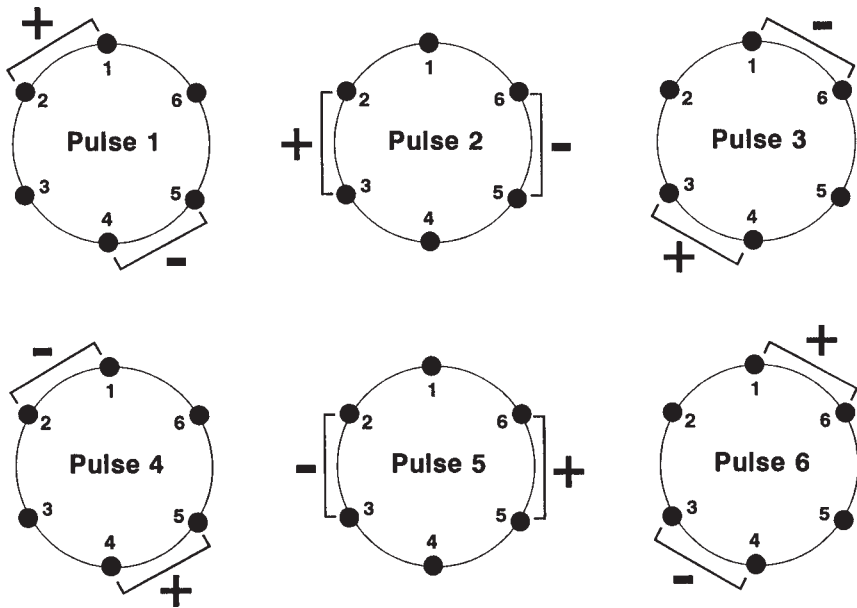


Fig. 2. Scheme used by mechanical switch to apply electric fields to the liver tissue by energizing opposing needle pairs during pulse delivery. Dark circles indicate the insertion point of needles into the liver tissue surrounding each tumor. Applying pulses in this manner rotated the field around the treatment site.

are described below and should be followed when tumors are induced, during electrochemotherapy treatment, and also during follow-up.

1. Induce anesthesia by placing a rat into a chamber charged with 3% isoflurane in oxygen until the animal is unconscious (*see Note 2*). This should require about 2 min.
2. Transfer the animal to surgical table and fit with a standard rodent mask supplied with 2.5–3% isoflurane.
3. Shave the abdomen of the animal and clean the abdomen with betadine solution.
4. Surgically expose the median liver lobe by making a 3-cm transverse incision approximately 0.5 cm caudal to the xiphoid process.
5. Apply pressure, gently by hand, to the chest in order to force the median liver lobe out of the incision for tumor induction, ECT treatment, or follow-up.
6. Perform necessary manipulations such as tumor induction, ECT treatment, or follow-up.
7. Close animal by inserting the liver back into the abdomen, suturing the abdominal muscles, and stapling the overlying skin.
8. Monitor the animal until fully awake. This should require 5–10 min.

3.2. Tumor Induction

1. Seed N1S1 cells into culture in swimms media. Introduce 10,000 viable cells per cm^2 of growth surface. Place cells into incubator at 37°C in a humidified atmosphere containing 5% CO_2 .
2. Allow cells to grow for 3–4 d which should result in nearly confluent cultures.
3. Harvest cells by aspirating media and then adding enough CDS to cover the growth surface. Allow cells to incubate in CDS for approximately 2 min at room temperature or until all cells detach.
4. Remove cells suspended in CDS and place into a centrifuge tube. Wash residual cells from the growth surface using Ca and Mg free phosphate-buffered saline (PBS); add these cells to the tube.
5. Wash cells three times by centrifugation in Ca and Mg free PBS at 200g. Resuspend cells in a small volume of PBS after the final wash.
6. Determine the concentration of cells in the suspension and assay for viability by enumerating a small quantity of suspension, using a hemacytometer, that has been mixed with trypan blue dye.
7. Adjust cell concentration in the suspension to 2×10^7 viable cells/ml by adding Ca and Mg free PBS. Alternatively, centrifuge cells again and removing an appropriate volume of Ca and Mg free PBS if the enumerated suspension has a fewer than 20×10^7 viable cells/mL.
8. Store cells on ice until they are utilized. Cell viability is typically maintained for 3–4 h after harvesting.
9. Surgically expose the right half of the median liver lobe in each animal using the procedures detailed in **Subheading 3.1**. Inject 50 μL of well-mixed N1S1 cell suspension (1×10^6 cells) into the lobe just beneath the capsule. Close each

animal and allow 7–10 d for tumor growth before attempting to treat animals with ECT (*see Note 3*).

3.3. Electrochemotherapy Treatment

1. Anesthetize animals, one at a time, and surgically expose the tumors for treatment as described in **Subheading 3.1**.
2. Measure three mutually orthogonal tumor dimensions using a Vernier caliper and record measurements. Compute tumor volume using the formula: $a \times b \times c \times \pi/6$ and keep a record of these data for each animal (*see Note 4*).
3. Inject 100 μL of 5 U/mL bleomycin solution (0.5 unit dose) directly into each tumor using a 30-gauge needle attached to a 1 cc tuberculine syringe. Inject in a manner that perfuses the entire tumor.
4. Insert the six-needle electrode array into the perimeter of the tumors 90 s after completing the bleomycin injection. Insertion depth can be limited by spacers that are supplied with the electrodes. It is important to insert the needles to a depth that is greater than the tumor depth. It is also critical to make sure that the entire tumor perimeter is encompassed by the electrode.
5. Administer a series of six 100 μs pulses to each tumor immediately after electrode insertion. A field strength of 1000 V/cm is recommended; however, this can also be an experimental variable. The series of pulses is generated by the T820 at 1-s intervals and an audible beep is generated for each pulse. It will be necessary to manually rotate the switch one position immediately after the audible sound is heard. A clockwise or anticlockwise direction can be used for rotation, but the same direction should be used for all six pulses in each series. This will ensure that the pulses are distributed in the proper manner as indicated in **Fig. 2**.
6. Close animals after the treatment has been completed as described in **Subheading 3.1**.

3.4. Posttreatment Monitoring

1. Open the abdomen of each animal using the procedure described in **Subheading 3.1**. The time points for following each animal are dependent on the experiment. One week intervals beginning immediately after treatment are reasonable for the first few weeks after ECT. After this time, longer periods between surgeries are advisable.
2. Measure dimensions of each tumor and compute tumor volumes as described in **step 2 of Subheading 3.3**.
3. Compare data from different animals/treatment groups in the experiment. Data can be expressed in several different manners. For example, mean tumor volumes at each follow-up time can be computed. These mean data at each time point can also be normalized to the mean tumor volumes at the time of treatment which indicates relative changes in tumor load. A system of rating treatment response can also be used. Animals that have increased tumor volumes relative to individual tumor sizes on the day of treatment are scored as progressive disease.

Table 1
Response of N1S1 Tumors 14 d After Treatment

Treatment Group	Number of Tumors Treated	Response			
		% Progressive Disease	% Stable Disease	% Partial Response	% Complete Response
D-E-	9	100	0	0	0
D-E+	9	100	0	0	0
D+E-	10	90	0	0	10
D+E+	13	15.4	0	15.4	69.2

D, drug (bleomycin) treatment; E, electrical treatment; +/-, presence and absence of drug or electrical treatment.

Animals that have tumor volumes that are 50% or greater than their respective volumes at the time of treatment are scored as no effect. Tumors that decrease by more than 50% by volume are scored as partial responses. Finally, animals with no visible or palpable tumor are scored as complete responses. These data are then tabulated by treatment group to indicate success or failure of the treatment. An example of this type of representation is shown in **Table 1**.

4. Humanely euthanize animals at the end of the study.

4. Notes

1. OTHER CHEMOTHERAPEUTIC AGENTS CAN BE SUBSTITUTED FOR BLEOMYCIN. The literature should be consulted for guidelines that will help identify an appropriate dose.
2. ISOFLURANE RESULTS IN VERY CONTROLLED ANESTHESIA WITH RAPID RECOVERY. Alternatively, a subcutaneous 3 mg/kg dose of atropine sulfate (WAB10125; The Butler Company, Columbus, OH) followed ten minutes later by a 45 mg/kg intraperitoneal dose of sodium pentobarbital (WAB10505, The Butler Company) can be used for anesthesia. The depth of anesthesia is much more difficult to control using pentobarbital due to variation from animal to animal. It may be necessary to deliver a small booster dose of pentobarbital in order to achieve sufficient anesthesia.
3. A 7-10-DAY GROWTH TIME RESULTS IN TUMORS THAT ARE APPROXIMATELY 100 MM³. Longer tumor growth times will result in larger tumors for treatment. The doubling time of these tumors is approximately 2.5 days.
4. KEEPING TRACK OF ANIMALS IS CRITICAL FOR FOLLOW-UP. A system of punching holes in the ears or striping tails with ink is an excellent means uniquely labeling each animal in the study.

Acknowledgment

This protocol described in this chapter was developed as part of a study supported by the University of South Florida Departments of Surgery and Chemical Engineering and by Genetronics, Inc., San Diego, CA.

References

1. Chang, D. C., Saunders, J. A., Chassy, B. M., and Sowers, A. E. (1992) *Guide to Electroporation and Electrofusion*. Academic Press, San Diego, CA.
2. Teissié, J. and Rols, M. P. (1992) Time course of electroporability, in *Charge and Field Effects in Biosystems*, Vol. 3 (Allen, M. J., Cleary, S. F., Sowers, A. E., and Shillady, D. D., eds.), Birkhauser, Boston, MA, pp. 285–301.
3. Heller, R., Jaroszeski, M., Leo-Messina, J., Perrott, R., Van Voorhis, N., Reintgen, D., and Gilbert, R. (1995) Treatment of B16 melanoma with the combinations of electroporation and chemotherapy. *Bioelectrochem. Bioenerg.* **36**, 83–87.
4. Mir, L. M., Orłowski, S., Belehradek, J. Jr., and Paoletti, C. (1991) Electrochemotherapy potentiation of antitumor effect of bleomycin by local electric pulses. *Eur. J. Cancer* **27**, 68–72.
5. Serša, G., Čemažar, M., and Miklavčič, D. (1995) Antitumor effectiveness of electrochemotherapy with cis-diamminedichloroplatinum (II) in mice. *Cancer Res.* **55**, 3450–3455.
6. Kanesada, H. (1990) Anticancer effect of high voltage pulses combined with concentration dependent anticancer drugs on lewis lung carcinoma, in vivo. *J. Jpn. Soc. Cancer Ther.* **25**, 2640–2648.
7. Belehradek, J. Jr., Orłowski, S., Poddevin, B., Paoletti, C., and Mir, L. M. (1991) Electrochemotherapy of spontaneous mammary tumors in mice. *Eur. J. Cancer* **27**, 73–76.
8. Okino, M., Tomie, H., Kanesada, H., Marumoto, M., Morita, N., Esato, K., and Suzuki, H. (1991) Induction of tumor specific selective toxicity in electrical impulse chemotherapy-analysis of dose response curve. *Oncologia* **24**, 71–79.
9. Salford, L. G., Persson, B. R. R., Brun, A., Ceberg, C. P., Kongstad, P. C. H., and Mir, L. M. (1993) An new brain tumour therapy combining bleomycin with in vivo electroporability. *Biochem. Biophys. Res. Commun.* **194**, 938–943.
10. Heller, R., Jaroszeski, M. J., Glass, L. F., Messina, J. L., Rapaport, D. P., DeConti, R. C., Fenske, N. A., Gilbert, R. A., Mir, L. M., and Reintgen, D. S. (1996) Phase I/II trial for the treatment of cutaneous and subcutaneous tumors using electrochemotherapy. *Cancer* **77**, 964–971.
11. Heller, R. (1995) Treatment of cutaneous nodules using electrochemotherapy. *J. Florida Med. Assoc.* **82**, 147–150.
12. Rudolf, Z., Štabuc, B., Čemažar, M., Miklavčič, D., Vodovnik, L., and Serša, G. (1995) Electrochemotherapy with bleomycin: The first clinical experience in malignant melanoma patients. *Radiol. Oncol.* **29**, 229–235.
13. Glass, L. F., Fenske, N. A., Jaroszeski, M. J., Perrott, R., Harvey, D. T., Reintgen, D. S., and Heller, R. (1996) Bleomycin-mediated electrochemotherapy of basal cell carcinoma. *J. Am. Acad. Dermatol.* **34**, 82–86.
14. Mir, L. M., Belehradek, M., Domenge, C., Orłowski, S., Poddevin, J. Jr., Schwab, G., Luboinnski, B., and Paoletti, C. (1991) Electrochemotherapy, a novel antitumor treatment: First clinical trial. *C. R. Acad. Sci.* **313**, 613–618.

15. Belehradec, M., Domenge, C., Luboinnski, B., Orłowski, S., Belehradec, J., and Mir, L. M. (1993) Electrochemotherapy, a new anticancer treatment. *Cancer* **72**, 3694–3700.
16. Domenge, C., Orłowski, S., Luboinnski, B., DeBaere, T., Schwaab, G., Belehradec, J. Jr., and Mir, L. M. (1996) Antitumor electrochemotherapy. *Cancer* **77**, 956–963.
17. Jaroszeski, M. J., Gilbert, R. A., and Heller, R. (1997) In vivo antitumor effects of electrochemotherapy in a hepatoma model. *Biochem. Biophys. Acta* **1334**, 15–18.

Treatment of Liver Tumors in Rabbit

Stéphane Orlowski and Lluís M. Mir

1. Introduction

Electrochemotherapy has been proven to be efficient for the treatment of subcutaneous tumors of different histological types in mice, rats and cats (1–3). Electrochemotherapy is essentially a local treatment. Indeed, it is based on the potentiation of the cytotoxicity of a low-permeant drug, typically bleomycin, by tumor cell permeabilization using brief and intense electric pulses. In the tissues exposed to such electric pulses, the so-called cell electropermeabilization is obtained only in the volume crossed by an electric field of intensity higher than a threshold value (4). The existence of this threshold for tissue permeabilization implies that the potentiation of the cytotoxic drug by the applied electric pulses is limited to the space roughly comprised between the electrodes. In the case of rather small and prominent cutaneous or subcutaneous tumors, it is easy to place two external electrodes on each side of the tumor nodule to be treated and to transcutaneously deliver the permeabilizing electric pulses. For thick and for deep subcutaneous tumors as well as for tumors located in internal organs, this electrode configuration is not appropriate because the electric pulses have to be delivered directly to the tumor tissues. Externally placed electrodes simply do not supply electric fields that extend deep enough for these situations. Intratumoral electric pulse delivery can, however, be achieved using needle-electrodes that are inserted into the tumor volume. We have designed an applicator constituted by multiple parallel and equidistant needles in order to avoid the delivery of very high-voltage electric pulses. A specifically manufactured generator ensures the multiplexed supplying of the electric current to each pair of closest needle electrodes. Thus, the entire tumor volume is divided in small units which are separately permeabilized by the different pairs of closest electrodes.

The clinical relevance of electrochemotherapy depends on the demonstration of the possibility to deliver permeabilizing electric pulses to any tumor location: this is particularly true for internal organs that are accessible only by a surgical approach. This is the reason why we chose to address the treatment of tumors transplanted into rabbit liver, since the rabbit is a common laboratory animal well adapted to experimental surgery. The treatment protocol that we established for liver (5) can obviously be transposed to the treatment of other types of internal tumors present in other parenchymatous tissues.

2. Materials

2.1. Rabbits and Tumor Cells

1. New-Zealand white rabbits (Elevage Scientifique des Dombes, Romans, France) are maintained in animal housing facilities under standard conditions, with a laboratory diet and water given ad libitum.
2. The VX2 carcinoma is a rabbit tumor of epithelial origin, initially explanted from papillomas of the domestic rabbits (Dr. G. Orth, Institut Pasteur, Paris, France). It is easily inoculatable in liver, and it is routinely maintained in vivo by serial passages in carrier animals.

2.2. Drugs

1. Rabbit sedation is obtained by acepromazine (Calmivet[®], Vétotoquinol, Luré, France) and general anesthesia by ketamine hydrochloride (Ketamine[®], Parke Davis, Courbevoie, France) and xilazine 2% (Rompun[®], Bayer, Puteaux, France).
2. Bleomycin (Laboratoire Roger Bellon, Neuilly-sur-Seine, France) is dissolved in sterile 0.9% sodium chloride just before the intravenous infusion.

2.3. Electric Pulse Generator and Electrodes

1. *Generator*: Square-waved electric pulses of adjustable voltage, length and frequency are produced by a MK0 generator (CELTEM, Antony, France), specifically designed for electric pulse delivery to multiple electrodes by the means of an integrated switch which allows the successive distribution of the applied voltage to every pair of closest electrodes.
2. *Electrodes*: The electrodes are constituted by a set of seven parallel and equidistant needles, held by an insulating template which sets the electrode gap and allows safe electrical connection to the generator MK0. The seven electrodes are arranged according to a centered hexagonal array, with a distance of 6 mm between every pair of closest electrodes (**Fig. 1**). The pulsing sequence driven by the generator consists in the succession of the twelve closest pairs of electrodes, first involving the central needle with each of the six peripheral needles, and second the six pairs of peripheral neighboring needles. The exact sequence is of no importance, provided all the closest pairs of electrodes are fed by the generator, without two consecutive recruitments of the same electrode.

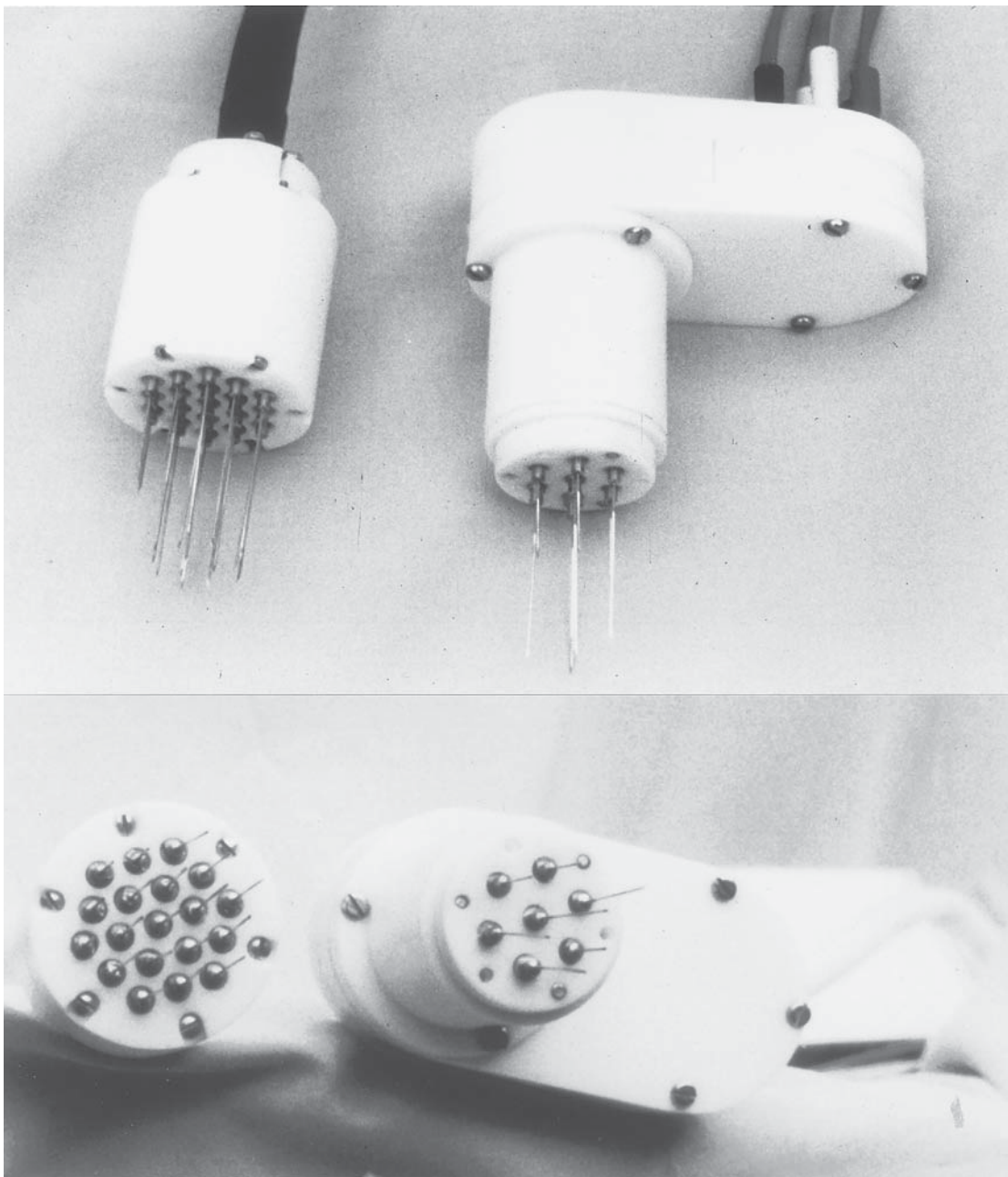


Fig. 1. Two examples of electrodes based on the principle reported in the text. **Right:** Template supporting seven parallel equidistant needles. **Left:** Template supporting nineteen parallel equidistant needles (the core of seven needles, as in the template shown above, surrounded by one more ring consisting of 12 parallel needles placed equidistantly to themselves and to the other needles in the inner array).

3. Methods and Treatment

3.1. Surgical Approach

1. Prepare the rabbit by a subcutaneous injection of 3.5 mg/kg of Calmivet to obtain sedation. Then put an intravenous catheter in the ear vein, and anesthetize the rabbit by the injection of 0.5 mL of a mixture of ketamine and xilazine. Boluses of 0.5 ml of the anesthetics are given a few minutes later, and then at the beginning of the surgery. Supplementary boluses of 0.5 mL can be given to prolong the anesthesia duration, if necessary, during the electric pulse delivery session.
2. Place the rabbit in dorsal decubitus on a surgical table, shave its abdominal wall, disinfect the skin, and put a sterile operative field.
3. Perform a median subxyphoid incision (about 10 cm long) to gain access to the left lobe of the liver.
4. Expose the liver out of the body, for tumor transplantation or treatment as indicated below. If necessary, irrigate the liver surface with sterile physiological saline during procedures.

3.2. Tumor Obtention

1. Follow the surgical approach to expose liver as stated in **Subheading 3.1**.
2. Harvest tumor tissue from a carrier rabbit, and cut sterily a small fragment (2–4 mm³) from a nonnecrosed part of the tumor excised.
3. Within 3 h, implant this tumor fragment under the hepatic capsula on the left lobe of the liver (*see Note 1*).
4. Wait for about 2 wk after the transplantation, in order to obtain a well limited tumor of 12–18 mm.

3.3. Electrochemotherapy

3.3.1. Surgery

1. Perform surgery to expose the liver tumor as in **Subheading 3.1**.
2. Visualize and palpate the tumor, and measure its diameter with a sterile caliper. Then place the liver back inside the body in order to avoid vascular constrictions during the time of bleomycine infusion.

3.3.2. Bleomycin Administration

1. Infuse bleomycin via the intravenous access in a bolus of about 30 seconds, at a dose of 1 mg/kg. This dose is equivalent to that used when electrochemotherapy is applied to tumor treatment in rats, cats, and humans (3,6,7).
2. Wait for 4 minutes before the beginning of the electric pulse delivery in order to let bleomycin to reach a sufficient concentration in the intratumoral interstitial fluids. Then, expose again the liver out of the body, and apply the electric pulses within a time window of about 10 min.

3.3.3. Electric Pulse Delivery

1. Adjust the electric pulse parameters at 100 μ s of length and at 850 V/cm of electric field intensity, that is at a delivered voltage of 510 V for the 6 mm of distance between the closest electrodes. This electric field intensity is chosen according to *ex vivo* experiments showing that this value is above the threshold for permeabilization of the tumor cells present in a tumor volume between two parallel flat electrodes (**4**). Adjust the generator pulse frequency at 8 Hz, that results in 0.67 Hz of repetition frequency for a given pair of electrodes since there are 12 closest equidistant pairs of electrodes in the array formed by the seven electrodes.
2. Insert the array of seven needle-electrodes into the tumor nodule and apply runs of 8 pulses, each run thus lasting 12 s. To suitably treat the whole tumor mass, reposition as many times as necessary the electrode array at adjacent sites into the visible tumor and into the apparently healthy tissue in the immediate vicinity of the tumor (*see* **Notes 2** and **3**). When the tumor is large enough as to be apparent from both sides of the liver lobe, insert the needle-electrodes into the two sides of the tumor.

3.4. Animal Follow-up

1. At the end of the treatment, suture the median incision by sewing the muscular and the cutaneous walls (*see* **Note 4**). Monitor the rabbit until it is conscious.
2. Keep the treated rabbits under observation, either for a fixed period in the case of histological evaluation of electrochemotherapy efficiency, or for an undefined time in the case of survival experiments.
3. If necropsies are part of the follow-up, in order to quantify the relative extension of the primary treated tumor and metastases appearance, weigh the rabbits at regular times and euthanize them when their general health status is too low.

4. Notes

1. VX2 tumors can also be obtained in the liver by the injection under the hepatic capsula of a suspension of the VX2 cells (10^7 cells in 100 μ L of medium) prepared by dissociation of a tumor excised from a carrier animal. This protocol for liver tumor obtention appears however less satisfactory than fragment transplantation because it generally produces multiple liver tumor nodules, due to cell spreading at the time of tumor cell inoculation.
2. The electric pulse delivery (even in the absence of bleomycin) induces a local modification of the treated tissue color, reversible in 15–20 min. This change is probably due to a transient vascular lock resulting in a blood flow arrest in the electropulsed tissue volume. Therefore, never apply electric pulses to the tumor site before the bleomycin intravenous injection.
3. In spite of a rather high number of needle insertions into the liver, we noticed an unexpected almost complete absence of bleeding, which is perhaps due to the electric pulse-induced vascular lock. However, take care to dry the liver lobe

surface in order to avoid electric short-circuit between the needle-electrodes when they are inserted into the liver.

4. It is possible to improve the antitumor effect of the treatment by associating it with an interleukin-2 (IL-2) based immunotherapy, according to previous pre-clinical trials performed on mice (8,9). Briefly, a few minutes after the end of the electric pulse delivery, inject 30×10^6 CHO(IL-2) cells, resuspended in 200–300 μ L of culture medium without serum, into the tumor and its close vicinity. These xenogeneic IL-2 secreting cells are Chinese hamster ovary cells in vitro transfected with the human IL-2 gene, and in vitro secreting 3500 units of IL-2 per ml, 72 hours and 80,000 initially seeded cells (10).

References

1. Mir, L. M., Orlowski, S., Belehradec, J. Jr, and Paoletti, C. (1991) Electrochemotherapy: potentiation of antitumour effect of bleomycin by local electric pulses. *Eur. J. Cancer* **27**, 68–72.
2. Okino, M., Tomie, H., Kanesada, H., Marumoto, M., Esato, K., and Suzuki, H. (1992) Optimal electric conditions in electrical impulse chemotherapy. *Jpn. J. Cancer Res.* **83**, 1095–1101.
3. Mir, L. M., Devauchelle, P., Quintin-Colonna, F., Delisle, F., Doliger, S., Fradelizi, D., Belehradec, J. Jr., and Orlowski, S. (1997) First clinical trial of cat soft-tissue sarcomas treatment by electrochemotherapy. *Br. J. Cancer* **76**, 1617–1622.
4. Belehradec, J. Jr., Orlowski, S., Ramirez, L. H., Pron, G., Poddevin, B., and Mir, L. M. (1994) Electroporomeabilization of cells in tissues assessed by the qualitative and quantitative electroloading of bleomycin. *Biochim. Biophys. Acta* **1190**, 155–163.
5. Ramirez, L. H., Orlowski, S., An, D. J., Bindoula, G., Dzodic, R., Ardouin, P., Bognel, C., Belehradec, J. Jr., Munck, J. N., and Mir, L. M. (1998) Electrochemotherapy on liver tumours in rabbits. *Br. J. Cancer* **77**, 2104–2111.
6. Salford, L. G., Persson, B. R. R., Brun, A., Ceberg, C. P., Kongstad, P. C., and Mir, L. M. (1993) A new brain tumour therapy combining bleomycin with in vivo electroporomeabilization. *Biochem. Biophys. Res. Commun.* **194**, 938–943.
7. Belehradec, M., Domenge, C., Luboinski, B., Orlowski, S., Belehradec, J. Jr., and Mir, L. M. (1993) Electrochemotherapy, a new antitumor treatment: first clinical phase I-II trial. *Cancer* **72**, 3694–3700.
8. Mir, L. M., Orlowski, S., Poddevin, B., and Belehradec, J. Jr. (1992) Electrochemotherapy tumor treatment is improved by interleukin-2 stimulation of the host's defenses. *Eur. Cytokine Netw.* **3**, 331–334.
9. Mir, L. M., Roth, C., Orlowski, S., Quintin-Colonna, F., Fradelizi, D., Belehradec, J. Jr., and Kourilsky, P. (1995) Systemic antitumor effects of electrochemotherapy combined with histoincompatible cells secreting interleukin-2. *J. Immunother.* **17**, 30–38.
10. Ferrara, P., Pecceu, P., Marchese, E., Vita, N., Roskam, W., and Lupker, J. (1987) Characterization of recombinant glycosylated human interleukin-2 produced by a recombinant plasmid transformed CHO cell line. *FEBS Lett.* **226**, 47–52.

Electrically Mediated Reporter Gene Transfer into Normal Rat Liver Tissue

Mark J. Jaroszeski, Richard Gilbert, Claude Nicolau,
and Richard Heller

1. Introduction

Gene therapy is a relatively new type of treatment compared to other modalities such as surgical intervention and drug therapy. Unfortunately, gene therapy is not yet a reality. However, this type of treatment continues to show promise due to the wealth of molecular information about human disease that has been accumulated in the past two decades. This information has a high potential for therapeutic benefit because the molecular basis for many diseases has been identified (1–3). It is clear that the introduction of DNA that codes for therapeutic translation products is a rational strategy for correcting diseased or dysfunctional cells. This type of therapy, gene therapy, is particularly promising for the treatment of cancer and metabolic diseases. It also has a high potential for vaccination against disease.

One difficulty that is faced in gene therapy is delivering DNA to the cells of interest. A number of strategies have been employed to delivery DNA in vivo. Viruses have been used most commonly for transfection (1). Several different physical methods have also been investigated for transferring genes. Three of these methods include the use of plasmid liposome complexes, cationic lipids, and direct injection (4). Another interesting physical method involves bombarding the cells with particles that have been coated with DNA (4).

Ideally, a gene transfer method would allow the introduction of DNA into the desired cells/tissue in an efficient manner with minimal side effects. None of the currently used methods is ideal (4). For example, the use of viruses has a safety concern relative to introducing exogenous DNA into the host genome,

subtherapeutic efficiency, potential immunological effects (**I**). In spite of these drawbacks, viral methods remain the most common method for gene transfer in the literature. This is probably due to the lack of other suitable methods. However, the number of published papers that utilize physical methods for gene delivery is increasing which indicates the need for alternative delivery mechanisms.

Electroporation as a means of delivering genes *in vivo* has become an area of greater research interest. The physical nature of electroporation makes it universally applicable. Although electroporetic gene transfer is a very young technology, some very encouraging results with reporter genes have been established (**5–10**). This chapter will detail a protocol for delivering a gene coding for luciferase to normal rat liver *in vivo*.

2. Materials

1. Rats: Sprague Dawley rats (Harlan, Indianapolis, IN, USA). Animals weighing 175–200 g are suitable. Standard housing and feeding are sufficient (*see Note 1*).
2. Anesthesia: Isoflurane (Mallinckrodt Veterinary, Inc., Mundelein, IL, USA) and an appropriate vaporizer to administer the inhaled anesthetic is required.
3. Electroporator: Direct current pulse generator that produces rectangular waves such as a BTX T820 (Genetronics, Inc., San Diego, CA).
4. Oscilloscope: Philips PM3375 oscilloscope (Philips, Eindhoven, Netherlands) is used as a digital storage device to monitor administered electric pulses.
5. Electrode and Switch: 1 cm diameter needle array electrode (Genetronics, Inc.) comprised of six needles arranged circumferentially as shown in Chapter 23, **Fig. 1**. A mechanical switch (Genetronics, Inc.) should be used to direct the pulses from the pulse generator to opposing pairs of needles as indicated in **Fig. 1**.
6. Plasmid DNA: pRc/CMV plasmid (Invitrogen, San Diego, CA) containing the luciferase coding sequence.
7. Plasmid preparation: Kits for plasmid preparation MegaPrep (Qiagen, Inc., Valencia, CA).
8. Luminometer: Turner Model TD20E (Turner Design, Sunnyvale, CA) or similar device.
9. Luciferase Detection: Luciferase expression was detected using a luciferase detection kit with CoA-luciferin as a substrate (Promega, Madison, WI). A commercial firefly luciferase (Sigma, St. Louis, MO) was used to quantitate results.

3. Methods

3.1. Reporter Gene Transfer into Liver

1. Induce anesthesia by placing a rat into a chamber charged with 3% isoflurane in oxygen until the animal is unconscious (*see Note 2*). This should require about 2 minutes.

<u>Pulse Number</u>	<u>Anodic Needles</u>	<u>Cathodic Needles</u>
1	1, 2	4, 5
2	2, 3	5, 6
3	3, 4	6, 1
4	4, 5	1, 2
5	5, 6	2, 3
6	6, 1	3, 4

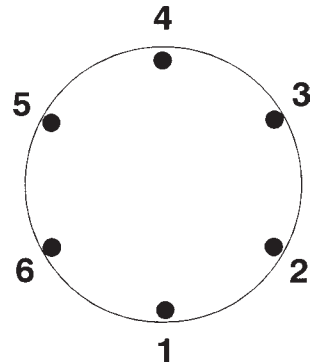


Fig. 1. Scheme used to apply electric fields to normal liver tissue using a six-needle array of electrodes. Dark circles indicate insertion points of needles into the normal liver tissue. Opposing needle pairs were energized during electrical treatment as indicated by the table. Applying pulses in this manner rotated the field around the treatment site.

- Transfer the animal to surgical table and fit with a standard rodent mask supplied with 2.5–3% isoflurane.
- Shave the abdomen of the animal and clean the abdominal area with betadine solution.
- Surgically expose the median liver lobe by making a 3 cm transverse incision approximately 0.5 cm caudal to the xiphoid process.
- Apply pressure, gently by hand, to the chest in order to force the median liver lobe out of the incision for treatment.
- Inject 100 μL of plasmid solution into a single location in the liver using a 30 gauge needle attached to a 1-cc syringe. The optimal concentration of plasmid is application dependent; however, between 10 and 500 μg of injected DNA has resulted in detectable expression (5).
- Insert the six-needle electrode (**Fig. 1**) array into the treatment site taking great care to encompass the injection site entirely within the volume delineated by the electrode. The electrode should be inserted 1.5 min after injecting the plasmid. This time allows for dissemination of the gene through the treatment site. Insert the electrode so that the needles extend through the full thickness of the liver. Maximum electrode depth can be limited by spacers that are supplied with the electrodes.
- Administer a series of six 100 μs pulses to each tumor immediately after electrode insertion. Field strengths of 1000–1500 V/cm are recommended. Successful gene delivery has been achieved in vivo using a broad range of field strengths, pulse widths, and replicate pulses. Thus, the parameters used for gene delivery may be experimental variables. The series of pulses is generated by the T820 at

1-s intervals and an audible beep is generated for each pulse. It will be necessary to manually rotate the switch one position immediately after the audible sound is heard. A clockwise or anticlockwise direction can be used for rotation; however, the same direction should be used for all six pulses in each series. This will ensure that the pulses are distributed in the proper manner as indicated in **Fig. 1**.

9. Mark the treatment site by applying very fine sutures at a predetermined location adjacent to the insertion point of the electrodes. This is very important step because it will be necessary to identify the exact treatment site for subsequent sampling (*see Note 3*).
10. Close animals by inserting the liver back into the abdomen, suturing the abdominal muscles, and stapling the overlying skin.
11. Uniquely identify each treated animal. A system of ear punches and tail striping is effective for labeling each rat.
12. Monitor the animal until fully awake. This should require 5–10 min.

3.3. Detection of Reporter Genes in Liver

1. Humanely euthanize rats, one at a time, by administering an 100 mg/kg intraperitoneal dose of sodium pentobarbital.
2. Surgically expose the livers of euthanized animals immediately after respiratory and cardiac functions have ceased.
3. Locate the treatment site. Perform a full thickness biopsy punch of the treatment area in the liver. An 11-mm biopsy punch will insure that the entire electrically treated area is removed.
4. Immediately weigh each piece of tissue, record the weight, and freeze the biopsies in liquid nitrogen and store.
5. Perform luciferase enzyme assay on frozen tissue as described in the instructions supplied by the manufacturer.
6. Express luminometer data in units of pg luciferase per mg of tissue in order to compare data from different treatment groups in the experiment. **Table 1** shows example data for investigating expression resulting from different plasmid doses. The number of experimental groups and the number of animals per group will vary depending on the experimental objective. However, the following control groups are recommend: no pulses and no electrical treatment, gene injection only, and electric pulses only.

4. Notes

1. Rats weighing 175–200 g or greater are recommended because their median liver lobe is thick enough to withstand surgical manipulation. Smaller rats have thinner lobes which are more difficult to manipulate without tearing.
2. This protocol has also been performed using a subcutaneous 3 mg/kg dose of atropine sulfate (WAB10125; The Butler Company, Columbus, OH) followed ten minutes later by a 45 mg/kg intraperitoneal dose of sodium pentobarbital (WAB10505, The Butler Company). However, variation in the depth of anesthe-

Table 1
Luciferase Expression Two Days After Plasmid Delivery by Electroporation in Rat Liver

Treatment Group	Number of Animals	Luciferase Plasmid Dose	Expression pg/mg Tissue
G-E-	3	—	< 100
G-E+	3	—	< 100
G+E-	3	500	< 100
G+E+	3	10	292
G+E+	3	25	9,100
G+E+	3	50	750
G+E+	3	100	525
G+E+	3	250	575
G+E+	3	500	725

G, gene (luciferase) injection; E, electrical treatment; +/-, presence and absence of gene or electrical treatment, respectively.

sia from animal to animal was a difficulty. Isoflurane is recommended because it results in very controlled anesthesia with rapid recovery.

3. Stop any bleeding that results from marking the treatment site with sutures before closing the animal.

Acknowledgment

This protocol described in this chapter was developed as part of a study supported by the University of South Florida Departments of Surgery and Chemical Engineering.

References

1. Feuerbach, F. J. and Crystal, R. G. (1996) Progress in human gene therapy. *Kidney International* **49**, 1791–1794.
2. Vile, R. C. (1996) Gene therapy for cancer: In the dock, blown off course or full speed ahead? *Cancer Metastasis Rev.* **15**, 283–286.
3. Dranoff, G. (1997) Gene therapy 1996. *Biochem. Biophys. Acta* **1332**, R21–R24.
4. Fouillard, L. (1996) Physical methods for gene transfer: An alternative to viruses. *Hematol. Cell Ther.* **38**, 214–216.
5. Heller, R., Jaroszeski, M., Atkin, A., Moradpour, D., Gilbert, R., Wands, J., and Nicolau, C. (1996) In vivo gene electroinjection and expression in rat liver. *FEBS Lett.* **389**, 225–228.
6. Nishi, T., Kimio, Y., Yanashiro, S., Takeshima, H., Sato, K., Hamada, K., Kitamura, I., Yoshimura, T., Saya, H., Kuratsu, J., and Ushio, Y. (1996)

- High-efficiency in vivo gene transfer using intraarterial plasmid DNA injection following in vivo electroporation. *Cancer Res.* **56**, 1050–1055.
7. Zhang, L., Lingna, L., Hofmann, G. A., and Hoffman, R. M. (1996) Depth-targeted efficient gene delivery and expression in the skin by pulsed electric fields: An approach to gene therapy of skin aging and other diseases. *Biochem. Biophys. Res. Commun.* **220**, 633–636.
 8. Muramatsu, T., Shibata, O., Ryoki, S., Ohmori, Y., and Okumura, J. (1997) Foreign gene expression in the mouse testis by localized in vivo gene transfer. *Biochem. Biophys. Res. Commun.* **233**, 45–49.
 9. Rols, M. P., Delteil, C., Golzio, M., Dumond, P., Cros, S., and Teissié, J. (1998) In vivo electrically mediated protein and gene transfer in murine melanoma. *Nat. Biotechnol.* **16**, 168–171.
 10. Titomirov, A. V., Sukharev, S., and Kistanova, E. (1991) In vivo electroporation and stable transformation of skin cells of newborn mice by plasmid DNA. *Biochem. Biophys. Acta* **1088**, 131–134.

Reporter/Functional Gene Transfer in Rat Brain

**Toru Nishi, Kimio Yoshizato, Tomoaki Goto,
Hideo Takeshima, Shigeo Yamashiro, Jun-ichi Kuratsu,
Hideyuki Saya, and Yuki-taka Ushio**

1. Introduction

Of the many methods and techniques for *in vivo* gene transfer, some have already been used in clinical trials. In most cases, genes are transferred into tissues using the infectivity of viral particles. However, viral systems have some known drawbacks (1,2). If an efficient and specific transfer method could be developed, naked plasmid DNA would be an ideal system for gene transfer. Plasmid-mediated methods would be economical and easy. Also, the transfer procedure could be easily repeated, as naked plasmid DNA has little antigenicity for the host (3,4).

Electroporation or electrical permeabilization of cell membranes was developed for highly efficient *in vitro* gene and/or drug transfer (5–7). This system provides markedly higher efficiency transfer than do other nonviral transfer systems including cationic liposomes. In cultured cells, electroporation is well established, and *in vivo* electroporation is receiving increased attention. The electrical permeabilization method has been used for *in vivo* drug transfer in the treatment of cancer and a clinical trial has been started (8,9). This method is called electrochemotherapy or electric impulse chemotherapy.

We have demonstrated the efficacy of *in vivo* electroporation for gene transfer using plasmid DNA (10,11). This method is called *electro-gene therapy*. As a marker gene, a mammalian expression plasmid carrying the bacterial *lacZ* gene was injected into the carotid artery of rats immediately after *in vivo* electroporation. In our rat brain tumor model, the carotid artery was the feeding artery. We obtained highly efficient and specific transfer. There was no

treatment-related toxic reactions nor was there increased *lacZ* activity in organs other than those located between the electrodes. Using an Epstein–Barr virus (EBV) episomal replicon vector, we were also able to demonstrate the long-lasting expression of the transferred functional gene. Our method makes possible the delivery of gene(s) of interest to desired tissues or organs and facilitates gene therapy in the treatment of malignant solid tumors and metabolic disorders.

2. Materials

2.1. Electrodes and Electroporator

1. Electrodes for in vivo electroporation: a pair of stainless steel, gold-coated electrodes, 0.5 cm long and 0.5 mm in diameter (Unique Medical Imada Co., Tokyo) (*see Note 1*).
2. Electroporation apparatus: the rectangular direct-current generator (BTX T820, BTX Inc., San Diego, CA) is used, connected to the BTX 500 optimizer (BTX Inc.) for determining the resistance between the electrodes which permitted the T820 voltage output to be adjusted for a specified current (*see Note 2*).

2.2. Plasmid DNA

1. Marker gene: the *lacZ* gene expression vector (pCH110, Pharmacia Biotech, Uppsala, Sweden). In the plasmid the *lacZ* gene is driven by the SV40 early promoter (*see Note 3*).
2. Marker gene for long term expression: the mammalian expression vector pCEP4 (Invitrogen, San Diego, CA). This vector system includes discrete DNA elements, the EB virus origin of replication and the EB virus nuclear antigen-1. Because together these elements confer an episomal replicon capacity to DNA circles in an array of human cell types, this vector not only offers an expeditious means for achieving amplification of transfected genes, but also bypasses *cis* effects on promoter function at the chromosomal integration sites. A cDNA encode for MCP-1 (**12,13**), a chemokine gene, was ligated into this vector and used in the experiment (*see Note 4*).
3. The plasmid DNA was purified using the QIAGEN plasmid purification kit (QIAGEN Inc., Valencia, CA).

2.3. Solutions and Reagents for X-gal Staining

1. Solution for perfusion of the rat body: PBS and 4% paraformaldehyde in PBS.
2. X-gal mix: 5 mM $K_3Fe(CN)_6$, 5 mM $K_4Fe(CN)_6 \cdot 3H_2O$, 1mM $MgCl_2$ in PBS. This solution can be safely stored for a few weeks at room temperature.
3. X-gal stock solution (5-bromo-4-chloro-3-indolyl- β -D-galactoside): 40 mg/mL in dimethylformamide; store in a foil-covered glass container at $-20^\circ C$.
4. Working solution for X-gal staining: add the X-gal stock solution to a X-gal mixer to achieve a final concentration of 1 mg/mL.

2.4. Solutions and Reagents for the Measurement of β -Galactosidase Activity

1. Solution for perfusion of the rat body: Ice-cold PBS.
2. Homogenizing buffer: Ice-cold 0.25 M Tris-HCl (pH 7.8).
3. Measurement of protein concentration: BCA Kit (Pierce, Rockford, IL).
4. Z buffer: 60 mM Na_2HPO_4 , 40 mM NaH_2PO_4 , 10 mM KCl, 1 mM MgCl_2 , 50 mM β -mercaptoethanol.
5. Substrate solution: Prewarmed 15 mM chlorophenol red- β -D-galactopyranoside in Z buffer.
6. Stop solution: 1 M Na_2CO_3 .
7. ELISA reader set at 570 nm.

3. Method

3.1. Establishment of the Brain Tumor Model

1. Inoculate 1×10^7 C6 glioma cells (American Type Culture Collection, Rockville, MD) stereotactically into the right striatum of each Wistar rat weighing 150–200 g.

3.2. Carotid Artery Cannulation, Electroporation, and Plasmid Injection

1. Anesthetize rats 10 d after inoculation by halothane inhalation.
2. Cannulate the right internal carotid artery through the external carotid artery using a microcatheter connected to a 2.5 mL syringe for plasmid injection. Coagulate the pterygopalatine artery, a major branch of the internal carotid artery, in order to concentrate delivery of the injected plasmid into the brain circulation (*see Fig. 1 and Note 5*).
3. Fix the head of each rat to a stereotaxic operating table. Cut and then retract the skin covering the head. Drill a burr hole in front of and behind the burr hole that had been drilled for cell inoculation. Insert the pair of gold coated stainless steel electrodes into the brain through the new burr holes, and measure the resistance between the electrodes using the optimizer. The average distance between the electrodes should be 0.5 cm.
4. Deliver a series of eight electrical pulses, the pulse length should range from 95 to 99 μs (**14–16**), using a standard square wave electroporator. Based on premeasured resistivity, the voltage should be adjusted to deliver 0.5 A of current between the electrodes. An average voltage should be 300 V/0.5 cm (*see Note 6*).
5. Inject 10 μg of pCH110 or 30 μg of pCEP-hMCP-1 in 0.5 ml PBS via the carotid catheter using a microinfusion pump for 5 minutes (*see Fig. 1 and Notes 7–9*). Begin this procedure immediately after pulsing. Then, evacuate the catheter and coagulate the external carotid artery with silk.

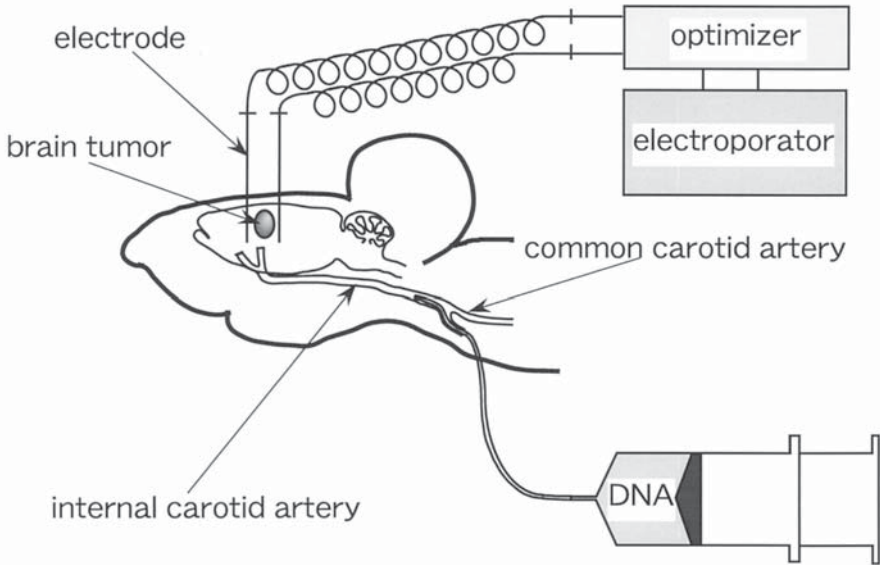


Fig. 1. Schema of the method for electro-gene therapy. For intraarterial injection, a microcatheter was cannulated into the right internal carotid artery through the external carotid artery. After cannulation, a pair of stainless steel electrodes was inserted into the brain, and the resistance between the electrodes was measured with an optimizer. A series of eight electrical pulses, the pulse length ranging from 95 to 99 μ s, was delivered with a square wave electroporator. Immediately after the electrical pulsing, expression plasmid in 0.5 ml PBS was injected via the carotid catheter. (Modified from Fig. 1 in **ref. 10**, with permission.)

3.3. X-gal Staining

1. Perfuse the bodies of the rats via the heart with 200 ml of PBS followed by 200 ml of 4% paraformaldehyde in PBS 3 days after application of the electrical pulses with or without plasmid injection (intraarterial or intravenous).
2. Remove the brain, heart, lung, liver, spleen, kidney, and testes were removed and fixed them in fixation buffer overnight. Cut the brains with a vibratome into 60- μ m-thick slices and soak in PBS. Soak the other tissues in sucrose buffer (10% sucrose in PBS) overnight, and gradually increase the concentration of sucrose to 30%. Freeze-embed the tissues in O.C.T. Compound (Miles Inc. IN), cut these other tissues into 10- μ m thick slices with a cryotome; stain the resulting sections with hematoxylin and eosin (H & E) to observe histological changes.
3. Stain sections of the brain, including the electrode tracts, with H & E for histological observations (*see Note 10*).
4. Detect expression of β -galactosidase using x-gal histochemical stain (17). The staining of tissues with X-gal turns cells that express β -galactosidase blue.

Therefore, only cells that accepted the injected plasmid and cells with endogenous β -galactosidase are stained by this method and can therefore be distinguished from other cells under a light microscope. Transfer brain slices into the working solution for X-gal staining and incubate at 37°C for 6 hours (*see Note 11*).

3.4. Immunohistochemistry of Human MCP-1 Protein in Rat Brain

1. Stain rat brain tumors by the indirect immunoperoxidase method 3 weeks, or another suitable time point, after electrogene transfer.
2. Cut cryostat sections to a thickness of 6 μm and air-dry them. To inhibit endogenous peroxidase activity, immerse the sections in 5 mM periodate solution for 10 min, wash with PBS, and then place in a 3 mM sodium borohydrate solution for 30 min (**18**). Then incubate the sections with optimally diluted monoclonal IgG anti-human MCP-1 (**19**). After washing with PBS, covered the sections for 60 minutes with peroxidase-conjugated species-specific goat anti-mouse Ig(Fab'2) diluted to 1:100 (Amersham, Arlington Heights, IL). Visualize peroxidase activity by incubating the sections for 10 minutes with 3,3'-diaminobenzidine (0.5 mg/ml Tris-HCl buffer, pH 7.6, containing 0.01% H_2O_2 ; Sigma Chemical Co., St. Louis, MO) (*see Note 12*).

3.5. Measurement of β -Galactosidase Activity

1. Perfuse each rat body with 200 ml of ice-cold PBS. Then remove the brain region that harbors the inoculated tumor and the contralateral brain. Immediately freeze these tissues. Also sample the heart, lung, liver, spleen, kidney, and testes. Mince about 100 mg of each tissue and immediately freeze in a 1.5 mL Eppendorf tube in dry ice and stored at -80°C until use.
2. Add 150 μL of ice-cold homogenization buffer to each sample tube. After triple freeze-thawing, centrifuge the samples for 30 min at 4°C (20,000g). Measure the protein concentration of the resulting 150 μL supernatant using a BCA Kit.
3. Conduct a β -galactosidase assay in the supernatant using a microtiter plate. Add 10 μL of the supernatant to 290 μL of Z buffer in a microtiter plate well and incubated at 37°C for 10 minutes. Then, add 30 μL of prewarmed substrate buffer to each well and incubate at 37°C for 60 minutes (**20**). Stop the reaction by adding 75 μL of the stop solution to each well and then quantitate the color reaction in an ELISA reader set at 570 nm. Express the β -galactosidase activity as O.D. (at 570 nm)/mg protein \times 10,000 (*see Notes 13 and 14*).

4. Notes

1. The selection of appropriate electrodes for electroporation is one of the most important preconditions for efficient gene transfer. Especially in *in vivo* electroporation, it is essential to select electrodes that are appropriate for the target tissues or organs.
2. A carefully chosen electroporator is also a key factor for successful electroporation. Improved results have been reported with electroporators that can deliver repeated, short, high-voltage, square electric pulses (**21**).

3. Excellent marker genes such as *luciferase* and *green fluorescent protein (GFP)* are also available. We currently use a luciferase expression plasmid for quantitation and a GFP expression plasmid for analyzing the distribution of the transferred gene within the tissue.
4. MCP-1 cDNA (12,13) is produced at low levels in normal tissues and at high level in some kinds of tumors, including brain tumors; it also plays a significant role in intratumoral monocyte infiltration (22,23). Since the reported antitumor effect of this chemokine was based on transfection experiments (24), we assume that this gene is a candidate transgene for genetherapy of brain tumors.
5. The injected DNA was distributed throughout the tumor tissue; the transfer efficiency was uneven within the tumor tissue. This efficient transfer could be achieved only by intravascular, especially intraarterial, delivery of the gene. The observation that the transgene was highly expressed in the border region between the tumor and the adjacent brain, where tumor neovascularization was abundant, seems to support this hypothesis.
6. The pores of the cell membrane created by electric pulses are reportedly asymmetric (25). A great number of smaller pores is created on the anode side and fewer but larger pores are observed on the cathode side. This suggests that a change in the polarity of the electrodes during application of the electric pulses may create larger pores on both sides of the cell surface, leading to better transfer efficiency. To create a homogeneous electric field in the target tissue, a new type of electrodes, needle-array electrodes, has been developed (26).
7. The timing of the plasmid DNA injection is one of the most important issues. Considering the very short duration of pore formation, DNA molecules should be present when the electric pulses are applied to cells or tissue. However, previous data indicated that the uptake by electroporated cells through the membrane pores is not affected, irrespective of whether the molecules were present during, or added after, the electroporating pulse (25,27). Hui (28) reported that the permeated state of cell membranes may last tens of minutes after the termination of the pulse field, this is in contrast to lipid bilayers that reseal immediately after the breakdown. Therefore, we injected DNA immediately after electroporation to supply higher concentrations of DNA to the electroporated region using a smaller amount of DNA. We will test other timings of plasmid DNA-injection in our system.
8. The temperature during in vitro electroporation is also a very important parameter. To limit DNA degradation or to increase the stability of the transiently permeable structure of the membrane, control of the temperature before and after electroporation is essential (29). However, in the case of in vivo electroporation, it is almost impossible to control the temperature of the target organ unless it is located on the surface.
9. Zheng and Chang (30) demonstrated that high-efficiency gene transfection can be obtained by directly electroporating cultured mammalian cells in their attached state using a pulsed radiofrequency electric field. Over 80% of the adherent COS-

M6 cells took up plasmid DNA and expressed the *lacZ* gene, whereas the transfection efficiency was less than 20% when the M6 cells were electroporated in suspension. They speculated that the high efficiency transfer into attached cells is due to their higher surface-to-volume ratio compared to trypsin-EDTA treated suspension cells and the intact submembrane cytoskeleton system.

10. In animals, bleomycin administration by electrochemotherapy using *in vivo* electroporation was successful for the treatment of both inoculated and spontaneous tumors (14,31). Salford et al. (14) applied this method in the treatment of brain tumors in an animal model system. No adverse effects were detected during the month following electroporation, which was performed with 8 to 12 exponential 400-V pulses with the time constant at 325 μ s. Likewise, in our model, we failed to observe side effects such as seizures or abnormal behavior during a 3-wk follow-up period. Histological examination also revealed no significant pathological changes even in the areas of electrode insertion.
11. The *lacZ* gene was not transferred well into normal brain cells except for cells in the vascular walls, even inside the field between the electrodes. This may be partly explained by differences in the vascular structure of normal brain and tumor tissue. Capillaries in tumor tissue may demonstrate cellular fenestrations, wide intercellular junctions, pinocytotic vesicles, and infolding of luminal surfaces (32). Due to these significant anatomical changes, molecules normally excluded by the blood-brain barrier may be able to penetrate the structure (32). To achieve efficient transfer into normal brain tissue, more drastic parameters may be required.
12. By using the EBV episomal replicon vector encoding human MCP-1 cDNA, transgene expression of MCP-1 cDNA in tumor cells was confirmed to last at least 3 wk. Furthermore, the expressed MCP-1 protein appeared to be functional since many monocytes were observed in the tumor tissue.
13. Although we observed very specific and efficient transfer of injected plasmid by X-gal staining, a potential major limitation of this method is the nonspecific delivery of injected plasmid outside the field between the two electrodes. Zhu et al. (33) reported injury to brain tissue by the insertion of the electrodes and the application of high voltage lasting only a fraction of a millisecond. However, our measurement of enzyme activities in major rat organs upon plasmid injection confirmed that no transferred gene was present outside the vicinity of the electrodes. Consistent with our data, Nabel et al. (34) observed no abnormal pathology upon histological examination after systemic (intravenous and intraarterial) injection of plasmids encoding several different genes into rabbits and pigs. This was the case even for plasmid-liposome complexes. They also reported that plasmid was not detected in testes or ovaries.
14. Further study is required to determine optimal gene transfer conditions such as the strength of the electric current in electroporation, the concentration of plasmid DNA for injection, the timing of the DNA injection, and the proper vector

system. In addition, to avoid tissue injury by the electric impulse, optimum electrical parameters for adequate gene transfer must be determined.

References

1. Kozarsky, K. F. and Wilson, J. M. (1993) Gene therapy: Adenovirus vectors. *Curr. Opin. Genet. Dev.* **3**, 499–503.
2. Suhr, S. T. and Gage, F. H. (1993) Gene therapy for neurologic disease. *Arch. Neurol.* **50**, 1252–1268.
3. Gilkeson, G. S., Pritchard, A. J., and Pisetsky, D. S. (1991) Specificity of anti-DNA antibodies induced in normal mice by immunization with bacterial DNA. *Clin. Immunol. Immunopathol.* **59**, 288–300.
4. Jiao, S., Williams, P., Berg, R. K., Hodgeman, B. A., Liu, L., Repetto, G., and Wolff, J. A. (1992) Direct gene transfer into nonhuman primate myofibers in vivo. *Hum. Gene Ther.* **3**, 21–33.
5. Matthews, K. E., Dev, S. B., Toneguzzo, F., and Keating, A. (1995) Electroporation for gene therapy. *Methods Mol. Biol.* **48**, 273–280.
6. Mir, L. M., Banoun, H., and Paoletti, C. (1988) Introduction of definite amounts of nonpermanent molecules into living cells after electroporation: Direct access to the cytosol. *Exp. Cell Res.* **175**, 15–25.
7. Poddevin, B., Orłowski, S., Belehradek, J. J., and Mir, L. M. (1991) Very high cytotoxicity of bleomycin introduced into the cytosol of cells in culture. *Biochem. Pharmacol.* **42**, 567–575.
8. Dev, S. B. and Hofmann, G. A. (1995) Clinical applications of electroporation, in *The Electrical Manipulation of Cells* (Lynch, P. T. and Davey, M. R., eds.), Chapman and Hall, New York, pp. 185–199.
9. Belehradek, M., Domenge, C., Luboinski, B., Orłowski, S., Belehradek, J. Jr., and Mir, L. M. (1993) Electrochemotherapy, a new antitumor treatment. First clinical phase I-II trial. *Cancer* **72**, 3694–3700.
10. Nishi, T., Yoshizato, K., Yamashiro, S., Takeshima, H., Sato, K., Hamada, K., Kitamura, I., Yoshimura, T., Saya, H., Kuratsu J., and Ushio, Y. (1996) High-efficiency in vivo gene transfer using intra-arterial plasmid DNA injection following in vivo electroporation. *Cancer Res.* **56**, 1050–1055.
11. Oshima, Y., Sakamoto, T., Yamanaka, I., Nishi, T., Ishibashi, T., and Inomata, H. (1998) Target gene transfer to corneal endothelium in vivo by electric pulse. *Gene Ther.* **5**, 1347–1354.
12. Yoshimura, T., Yuhki, N., and Moore, S. K. (1989) Human monocyte chemoattractant protein-1 (MCP-1). Full-length cDNA cloning, expression in mitogen-stimulated blood mononuclear leukocytes, and sequence similarity to mouse competence gene JE. *FEBS Lett.* **244**, 487–493.
13. Leonard, E. J. and Yoshimura, T. (1990.) Human monocyte chemoattractant protein-1 (MCP-1). *Immunol. Today* **11**, 97–101.
14. Salford, L. G., Persson, B. R. R., Brun, A., Ceberg, C. P., Kongstad, P. C., and Mir, L. M. (1993) A new brain tumour therapy combining bleomycin with in vivo electroporation. *Biochem. Biophys. Res. Commun.* **194**, 938–943.

15. Yamaguchi, O., Irisawa, C., Baba, K., Ogihara, M., Yokota, T., and Shiraiwa, Y. (1994) Potentiation of antitumor effect of bleomycin by local electric pulses in mouse bladder tumor. *Tohoku J. Exp. Med.* **172**, 291–293.
16. Belehradek, J. J., Orłowski, S., Poddevin, B., Paoletti, C., and Mir, L. M. (1991) Electrochemotherapy of spontaneous mammary tumours in mice. *Eur. J. Cancer* **27**, 73–76.
17. Bondi, A., Chieragatti, G., and Eusebi, V. (1982) The use of β -galactosidase as a tracer in immunocytochemistry. *Histochemistry* **76**, 153–158.
18. Isobe, S., Nakane, P., and Brown, W. R. (1977) Studies on translocation of immunoglobulin across intestinal epithelium. 1. Improvement in the peroxidase-labeled antibody method for application to study of human intestinal mucosa. *Acta Histochem. Cytochem.* **10**, 167–171.
19. Yoshimura, T., Takeya, M., Takahashi, K., Kuratsu, J., and Leonard, E. J. (1991) Production and characterization of mouse monoclonal antibodies against human monocyte chemoattractant protein-1. *J. Immunol.* **147**, 2229–2233.
20. Herbomel, P., Bourachot, B., and Yaniv, M. (1984) Two distinct enhancers with different cell specificities coexist in the regulatory region of polyoma. *Cell* **39**, 653–662.
21. Presse, F., Quillet, A., Mir, L., Marchiol-Fournigault, C., Feunteun, J., and Fradelizi, D. (1988) An improved electrotransfection method using square shaped electric impulses. *Biochem. Biophys. Res. Comm.* **151**, 982–990.
22. Takeshima, H., Kuratsu, J., Takeya, M., Yoshimura, T., and Ushio, Y. (1994) Expression and localization of messenger RNA and protein for monocyte chemoattractant protein-1 in human malignant glioma. *J. Neurosurg.* **80**, 1056–1062.
23. Sato, K., Kuratsu, J., Takeshima, H., Yoshimura, T., and Ushio, Y. (1995) Expression of monocyte chemoattractant protein-1 in meningioma. *J. Neurosurg.* **82**, 874–878.
24. Yamashiro, S., Takeya, M., Nishi, T., Kuratsu, J., Yoshimura, T., Ushio, Y., and Takahashi, K. (1994) Tumor-derived monocyte chemoattractant protein-1 induces intratumoral infiltration of monocyte-derived macrophage subpopulation in transplanted rat tumors. *Am. J. Pathol.* **55**, 854–867.
25. Tekle, E., Astumian, R. D., and Chock, P. B. (1994) Selective and asymmetric molecular transport across electroporated cell membranes. *Proc. Natl. Acad. Sci. USA* **91**, 11,512–11,516.
26. Heller, R., Jaroszeski, M., Atkin, A., Moradpour, D., Gilbert, R., Wands, J., and Nicolau, C. (1996) In vivo gene electroinjection and expression in rat liver. *FEBS Lett.* **389**, 225–228.
27. Sukharev, S. I., Klenchin, V. A., Serov, S. M., Chernommordik, L. V., and Chizmadzhev, Y. A. (1992) Electroporation and electrophoretic DNA transfer into cells: The effect of DNA interaction with electropores. *Biophys. J.* **63**, 1320–1327.
28. Hui, W. H. (1995) Effects of pulse length and strength on electroporation efficiency. *Methods Mol. Biol.* **48**, 29–40.
29. Rols, M. P., Delteil, C., Serin, G., and Teissié, J. (1993) Temperature effects on electroporation of mammalian cells. *Nucleic Acids Res.* **22**, 540.

30. Zheng, Q. and Chang, D. C. (1991) High-efficiency gene transfection by in situ electroporation of cultured cells. *Biochim. Biophys. Acta* **1088**, 104–110.
31. Zimmermann, U. (1982) Electric field-mediated fusion and related electrical phenomena. *Biochim. Biophys. Acta* **694**, 227–277.
32. Pollay, M. (1985) Blood-brain barrier; cerebral edema. *Neurosurgery* (Wilkins, R. H. and Rengachary, S. S., ed.), McGraw-Hill, New York, pp. 322–342.
33. Zhu, N., Liggitt, D., Liu, Y., and Debs, R. (1993) Systemic gene expression after intravenous DNA delivery into adult mice. *Science* **261**, 209–211.
34. Nabel, E. G., Gordon, D., Yang, Z. Y., Xu, L., San, H., Plautz, G. E., Wu, B. Y., Gao, X., Huang, L., and Nabel, G. J. (1992) Gene transfer in vivo with DNA-liposome complexes: Lack of autoimmunity and gonadal localization. *Hum. Gene Ther.* **3**, 649–656.

In Vivo Gene Electroporation in the Mouse Testis

Tatsuo Muramatsu

1. Introduction

Until today, gene transfer to germ cells has been attempted by a variety of methods including microinjection, embryonic stem cell-mediated transfection, virus mediated transfection, lipofection (1), microparticle bombardment (2), and sperm mediated transformation (3). In vivo gene electroporation (EP) now is a viable option for gene transfer purposes as demonstrated by strong short-term gene expression and long-term expression after gene transfer (4,5 and unpublished). In vivo gene EP is simple and convenient. Adequate development and differentiation of transfected cells can be maintained in the in vivo environment. Furthermore, it can be applied, in principle, to any types of cells and tissues so long as the target is accessible. The advantages of in vivo EP over other nonviral methods such as lipofection and microparticle bombardment are: possible tissue damage is less; there is no limitation of DNA to be transfected at a time; and DNA can be transferable to cells deep inside the target tissue.

In this chapter, brief protocols for examples of in vivo gene EP in the mouse testis are described. Although gene expression is deemed most probably transient, in vivo EP would serve as a convenient and efficient means of gene transfer to spermatogenic cells in the testis of living mice. Methods for detecting luciferase (Luc), chloramphenicol acetyltransferase (CAT), and β -galactosidase (β -Gal) expression are presented along with EP methodology.

2. Materials

2.1. Animals

Depending on objectives, any age mice could be used, except for those at 1 wk. In such young mice, there may be slight difficulty in completing the

following procedures because the size of testes is small. Therefore, older mice are recommended as experimental animals. In the following description, male mice of ICR strain at 8–10 wk of age are used. The width of each testis ranges from 6 to 8 mm with an average of 7 mm. Assuming that the resistance value is the same for mouse testes, voltages for in vivo EP should be adjusted accordingly. The way in which voltages are optimized is described in **Subheading 3.2**.

2.2. Plasmid DNA

Examples of reporter DNAs are listed in **Table 1**. The choice of reporter DNA is based on sensitivity, simplicity, and rapidity of assays and on the availability of instruments for assays. For some reporter assays such as luciferase, expensive instruments are required. They are also listed in **Table 1**. Apart from these, commercially available reporter genes encoding *Renilla* luciferase (Promega, Madison, WI), human placental alkaline phosphatase (Clontech Laboratories, Palo Alto, CA), or *Aequorea victoria* green fluorescent protein (Clontech Laboratories, Palo Alto, CA) can also be used. The expression of the luciferase and alkaline phosphatase can be measured with a luminometer, while the expression of the latter can be easily detected by green fluorescence (**10**).

The type of DNA transferred is usually circular plasmids. For measurement of gene expression shortly, that is, within several days after in vivo gene EP, circular plasmid DNAs are suitable. If longer gene expression, that is, at 1 mo or longer after in vivo gene EP, is preferred, linearized plasmid DNAs are better than circular ones as the chance of integration into spermatogenic cells may increase. Together with the linearized reporter plasmids, co-transfection with virus integrase genes may further increase gene expression (**11**). Alternatively, episomally self-replicating plasmids can be used for attaining prolonged gene expression (**12**). Indeed in the mouse testis, inclusion of the self-replicating sequences derived from the Epstein-Barr virus significantly prolonged the duration of gene expression (**6**).

2.3. Solutions and Reagents

1. TE buffer: 10 mM Tris. HCl, 25 μ M EDTA. Adjust pH to 7.5 with 5 M NaOH. Filter-sterilize through a 0.22- μ m membrane, and store at 4°C or room temperature.
2. Plasmid DNA: CsCl-purified plasmid DNA (or Qiagen-purified DNA, Qiagen, Chatsworth, CA) is resuspended in sterile TE buffer to give final concentrations at 1–3 μ g/ μ L. Expression plasmids of CAT, Luc and β -Gal are used as examples in this chapter.
3. Transfection solution: Dissolve 10–100 μ g (or more where necessary) plasmid DNA in 50 μ L of 137 mM NaCl and 2.5 mM CaCl₂ for one testis (*see Note 1*).

Table 1
Examples of Reporter Plasmids and Assay Instruments
for In Vivo Gene Electroporation in the Mouse Testis

Plasmid	Comments	Source/Ref.
<i>Chloramphenicol acetyltransferase (CAT)</i>		
pCAT control	CAT assay with thin layer or in solution; no special instrument required; the SV40 promoter confers universal expression, but the expression intensity may not be strong enough.	Commercially available ^a
pSVEP9CAT	CAT assay; for prolonged expression due to the presence of the Epstein-Barr virus self-replication sequences; the SV40 promoter confers universal expression.	6
pmp1CAT	CAT assay; the mouse protamin-1 promoter confers spermatid-specific reporter expression, but the intensity may be weak.	7
<i>Firefly luciferase</i>		
pGL control	Luciferase assay; a luminometer, photon counter or imaging system required; the SV40 promoter confers universal expression; convenient for normalization of transfection efficiency.	Commercially available
pmiwLuc	Luciferase assay; a hybrid miw promoter of the RSV-LTR and chicken β -actin promoter confers strong and universal gene expression.	8
<i>Bacterial β-galactosidase</i>		
pmiwZ	X-gal staining or fluorescent analysis; for staining, no special instrument required; the miw promoter confers strong and universal gene expression.	7, 9

^aPromega, Madison, WI.

4. Buffer A: 15 mM Tris, 60 mM KCl, 15 mM NaCl, 12 mM EDTA, 1 mM dithiothreitol, 0.15 mM spermine, and 0.4 mM phenylmethylsulfonyl fluoride. Adjust the pH to 8.0 with 5 M NaOH. Store at 4°C.
5. PBS: 137 mM NaCl, 2.7 mM KCl, 10.1 mM Na₂HPO₄ and 1.8 mM KH₂PO₄. Adjust the pH to 7.4 with 5M HCl. Autoclave, and store at room temperature.

6. Fixation solution: 4% formaldehyde and 0.2% glutaraldehyde solution in PBS. Store at 4°C.
7. XG buffer: 2 mM MgCl₂, 5 mM K₄Fe(CN)₆ · 3H₂O and K₃Fe(CN)₆ in PBS. Store at 4°C.
8. X-gal reaction mixture: 0.1% 5-bromo-4-chloro-3-indolyl-β-D-galactopyranoside (X-gal), 5% *N,N*-dimethylformamide, and 0.1% Triton-X in the XG buffer. Adjust pH to 7.6, and store at 4°C.

2.4. Instruments

1. Electro-square porator: T820 in combination with an optimizer 500 (BTX, San Diego, CA) or CUY-1 (Tokiwa Science, Tsukushino, Japan).
2. Use tweezer type electrodes (CUY641, Tokiwa Science, Tsukushino, Japan) having one circular gold-plated steel of 10 mm in diameter on each end of forcep with separate electrical connection to the above electro-square porator.
3. Luminometer: AutoLumat LB953 (EG & Berthold, Germany).

3. Methods

3.1. Operation and DNA Injection

The following simple operation of testis exposure is recommended when strong gene expression is desired.

1. Anesthetize animals with sodium pentobarbital by intraperitoneal injection at dose of 30 mg/kg body weight.
2. Incise the skin 1 cm long about 2 cm cranial to the testis, and expose one testis at a time as shown in **Fig. 1A**.
3. Inject designated doses of plasmid DNA dissolved in the transfection solution into the exposed testis with a 1 ml syringe and a 27G needle (**Fig. 1B**).

3.2. Voltage Optimization for In Vivo Electroporation

1. Immediately after the injection, apply square electric pulses five times with an electro-square porator T820 in combination with an optimizer 500 (BTX, San Diego, USA) at 25 V with the pulse width of 99 ms/pulse. Where necessary, voltages and pulse widths were varied (*see Note 3*). If possible, exchange the cathode and anode during the pulse application as it is empirically known that the exchange substantially enhances the intensity of gene expression.
2. After the EP treatment, stitch the skin with No. 3 silk suture. Surgical adhesive may be used instead of suturing. Descend the testis to the original position.
3. Maintain the mice for the planned period of time. Detection of gene expression is best achieved at 1–2 d after the EP treatment. However, by employing linearized DNA and other refinements, gene expression in the testis of living mice can be sustained as long as 2 mo after in vivo gene EP, though gradually decreasing (*unpublished*).

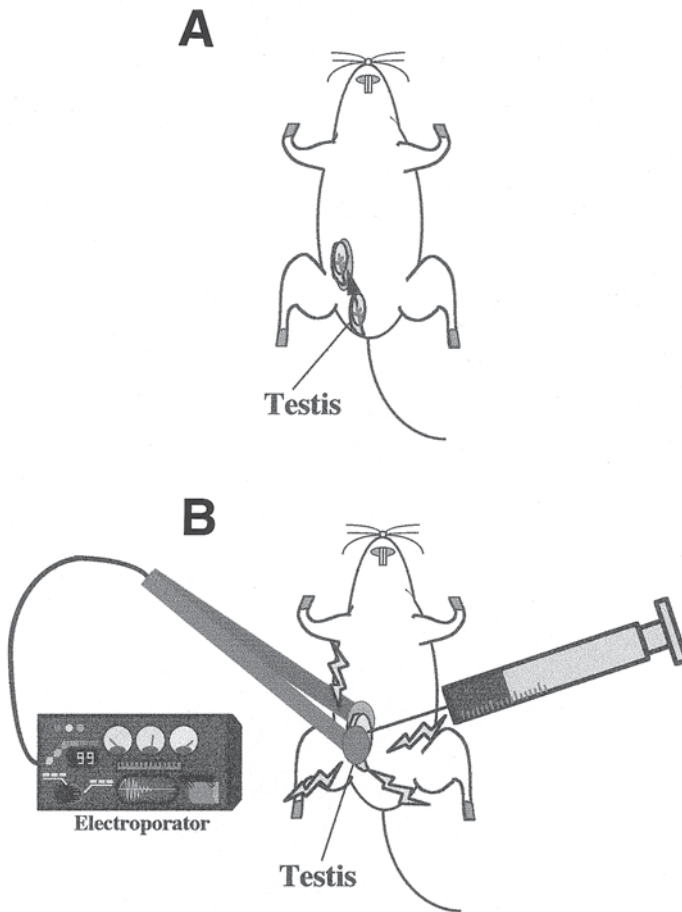


Fig. 1. Diagrammatic presentation of in vivo gene electroporation. **(A)** Testis on one side is exposed by simple operation, and plasmid DNA is injected. **(B)** Electric square pulses are applied with a tweezer type electrode as soon as possible.

3.3. Assays

3.3.1. Tissue Sampling

1. Sacrifice the mice by decapitation at the planned time point after in vivo gene EP.
2. Excise the testis samples quickly.
3. Wash with PBS twice, blot with paper towels, and weigh.

3.3.2. CAT Assay

1. Homogenize the whole testis sample with three volumes of ice-cold buffer A for CAT and luciferase assays. For the measurement of CAT but not luciferase

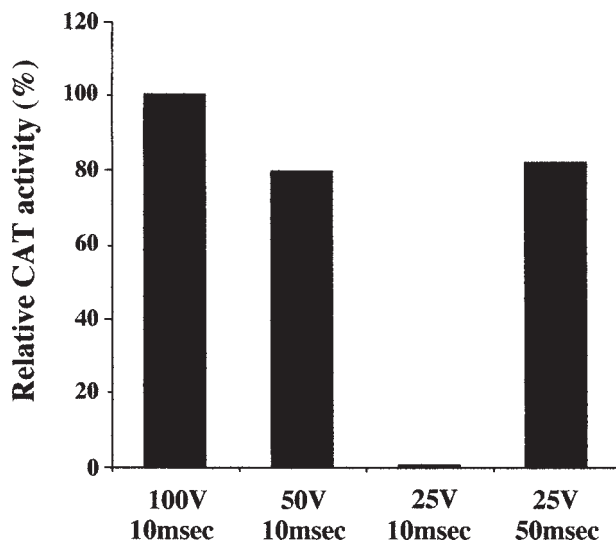


Fig. 2. Effects of varying voltage and time constant on CAT activity expressed as percentage of the mean value for the 100V/10 ms group. CAT activity was determined at 48 hours after transfection (7).

activities, heat the homogenate at 70°C for 60 min to increase the sensitivity as suggested previously (13).

2. Centrifuge the homogenate at 6000g for 10 min, and use the supernatant for measurements of protein content and CAT activity using standard methods (14).
3. Express results as % conversion of chloramphenicol to its acetylated forms on a basis of 100 µg protein. Alternatively, CAT activity can be expressed as relative values per whole testis by taking a control value as 100 or 1 depending on experimental conditions. An example of varying voltage and pulse loading period on CAT activity is given in Fig. 2.

3.3.3. Luciferase Assay

1. Use the supernatant of the unheated homogenate. For determining the activity of firefly luciferase, mix 20 µL tissue extract with 100 µL luciferin solution. Avoid the increase in sample volume as it may inhibit the overall counting efficiency.
2. Take 1 min or longer for photon counting with a luminometer. Bioluminescence should be constant over at least 3 min.
3. Express luciferase activity as counts/min per 100 µg protein or per whole testis. When the comparison of transcriptional intensity of various promoters is intended, take the ratio of CAT driven by various promoters to luciferase driven by the SV40 promoters. This kind of normalization procedure is required as the transfection efficiency varies within and between the treatment groups.



Fig. 3. Expression of the bacterial β -galactosidase gene observed at a typical blue color by X-gal staining. Photograph shows the gene expression detected at 48 hours after transfecting *pmiWZ* in the mouse testis by *in vivo* gene electroporation (7).

3.3.4. Histochemical Staining with X-gal

1. Fix the excised testes with 4% formaldehyde and 0.2% glutaraldehyde solution in PBS at room temperature overnight for detection of β -gal activity.
2. Rinse with PBS twice, and soak in the X-gal reaction mixture for not more than 1 h. This staining time should be kept strictly to minimize endogenous greenish-blue color development in the whole testis samples. Specific blue color due to bacterial β -galactosidase is easily distinguished. A typical example of an X-gal stained whole testis is shown in **Fig. 3 (7)**.
3. For light microscopic examination, embed the stained testis in paraffin for sectioning and counterstaining with hematoxylin.

4. Notes

1. DNA is better dissolved in buffered salt solutions rather than in buffered solutions of nonionic substances such as mannitol or sucrose. However, there is little systematic studies conducted on the optimal ionic strength of DNA solution for *in vivo* gene EP. An increase in the calcium chloride concentration from 2.5 mM to 5 mM did not significantly affect the intensity of gene expression. Similarly, the use of liposome-treated DNA resulted in diminished gene expression in the

mouse skin. The total volume to be injected in each testis ranges from several to 50 μL . Beyond this, the testis may not be able to hold the entire volume, and leak may occur. For small testes, the volume should be reduced accordingly.

2. A micromanipulator may be used to inject DNA solution in individual seminiferous tubules of the exposed testis. This procedure requires a special apparatus and injection skill. According to my experience, however, simple and direct injection into the testis using a syringe may also confer similarly strong foreign gene expression covering a relatively wide area in spermatogenic cells. The same in vivo gene EP procedure in the chicken and quail testes cannot give good and widespread gene expression, and the gene expression is limited to the area only along the injection needle. The difference may be ascribable to density or compactness of seminiferous tubules between different animal species.
3. When electric square pulses are applied to a field, heat will be generated. The quantity of heat is given by the following equation (15) as:

$$Q (J) = V^2 \times T / (4.2R)$$

where Q , R , and T stand for the heat (joule/treatment period, seconds), resistance (ohm) and loading period (or time constant) (seconds), respectively. Based upon our experience, the gene transfection efficiency (or intensity of foreign gene expression) is roughly proportional to the amount of heat generated unless the tissues or cells are irreversibly damaged too much. Accordingly, EP conditions such as 1000 V/cm for 100 μs are equivalent to those of 25 V/cm for 160 ms (i.e., 160 ms with 1 pulse, or 80 ms with 2 pulses, etc.).

In practice, for a given testis or other tissues, recommended pulse numbers and width are 4–8 pulses, and 99 ms per pulse, respectively. The reason for using such long pulse widths in the present in vivo gene EP method is that the longer the loading period, the longer the opening of cell surface. Consequently, the amount of DNA transferable from the extracellular to intracellular spaces would probably be greater by employing a longer pulse width. Under the above conditions of pulse numbers and widths, optimal voltage usually varies from 20 to 80 V/cm from one tissue to another. Beyond these voltages, irreversible tissue damage may occur. If long-term gene expression is desired in the mouse testis, recommended voltage is 35–45 V/cm (*unpublished*).

4. To demonstrate testis-specific gene expression, normalize CAT activities, for example, between tissue samples for transfection efficiency based on the expression of the firefly luciferase originating from the cotransfected pGL control driven by the SV40 promoter or pmiwLuc driven by the RSV-LTR and the chicken β -actin promoter, both of which are deemed to confer universal gene expression.

References

1. Northrop, J. P., Ringlod, G. M., and Danielsen, M. (1987) Lipofection: A highly efficient, lipid-mediated DNA-transfection procedure. *Proc. Natl. Acad. Sci. U.S.A.* **84**, 7413–7417.
2. Williams, R. S., Johnston, S. A., Reidy, M., de Vit, M. J., McElligott, S. G., and

- Sanford, J. C. (1991) Introduction of foreign genes into tissues of living mice by DNA-coated microprojectiles. *Proc. Natl. Acad. Sci. U.S.A.* **88**, 2726–2730.
3. Lauria, A. and Gandolfi, F. (1993) Recent advances in sperm cell mediated gene transfer. *Mol. Reprod. Dev.* **36**, 255–257.
 4. Nishi, T., Yoshizato, K., Yamashiro, S., Takeshima, H., Sato, K., Hamada, K., Kitamura, I., Yoshimura, T., Saya, H., Kuratsu, J., and Ushio, Y. (1996) High-efficiency in vivo gene transfer using intraarterial plasmid DNA injection following in vivo electroporation. *Cancer Res.* **56**, 1050–1055.
 5. Muramatsu, T., Nakamura, A., and Park, H.-M. (1998) In vivo electroporation: A powerful and convenient means of nonviral gene transfer to tissues of living animals. *Int. J. Mol. Med.* **1**, 55–62.
 6. Muramatsu, T., Shibata, O., and Okumura, J. (1997) Effect of self-replication DNA sequences of Epstein-Barr virus on the expression of a foreign gene transfected in vivo to the mouse testis. *Anim. Sci. Technol. Jpn.* **68**, 650–653.
 7. Muramatsu, T., Shibata, O., and Okumura, J. (1997) Foreign gene expression in the mouse testis by localized in vivo gene transfer. *Biochem. Biophys. Res. Commun.* **233**, 45–49.
 8. Nakamura, A., Okumura, J., and Muramatsu, T. (1998) Quantitative analysis of transcriptional activity of viral and hybrid promoters in bovine preimplantation embryos. *Mol. Reprod. Dev.* **49**, 368–373.
 9. Muramatsu, T., Mizutani, Y., Ohmori, Y., and Okumura J. (1996) In vivo electroporation: a convenient method for gene transfer to testicular cells in mice. *Anim. Sci. Technol. Jpn.* **67**, 975–982.
 10. Okabe, M., Ikawa, M., Kominami, K., Nakanishi, T., and Nishimune, Y. (1997) ‘Green mice’ as a source of ubiquitous green cells. *FEBS Lett.* **407**, 313–319.
 11. Shoji-Tanaka, A., Mizuochi, T., and Komuro, K. (1994) Gene transfer using purified retroviral integrase. *Biochem. Biophys. Res. Commun.* **203**, 1756–1764.
 12. Hauer, C. A., Getty, R. R., and Tykocinski, M. L. (1989) Epstein-Barr virus episome-based promoter function in human myeloid cells. *Nucleic Acids Res.* **17**, 1989–2003.
 13. Pothier, F., Ouellet, M., Julien, J.-P., and Guerin, S. L. (1992) An improved CAT assay for promoter analysis in either transgenic mice or tissue culture cells. *DNA Cell Biol.* **11**, 83–90.
 14. Sanders, M. M. and McKnight, G. S. (1988) Positive and negative regulatory elements control the steroid-responsive ovalbumin promoter. *Biochemistry* **27**, 6550–6557.
 15. Hofmann, G. A. (1995) Instrumentation. *Methods Mol. Biol.* **47**, 27–45.

Ex Vivo Stromal Cell Electroporation of Factor IX cDNA for Treatment of Hemophilia B

Armand Keating, Edward Nolan, Robin Filshie,
and Sukhendu B. Dev

1. Introduction

Hemophilia B is an X-linked genetic disorder that typically results from chronic circulating deficiency of blood coagulation factor IX (FIX) (1). While the occurrence of hemophilia B is significantly less frequent than hemophilia A (factor VIII, deficiency) it has received special attention as a model for gene therapy. This is because hemophilia B is one of the least complicated genetic diseases from the point of view of demonstrating the proof of principle of a gene therapy protocol. Specifically, hemophilia B is a single gene recessive disorder and a wide range of tissues can be targeted for FIX gene delivery and strict regulation of FIX expression is not required. In addition, the 2.8 kb FIX cDNA is much smaller than the 9 kb FVIII cDNA, and FIX expression in transfected mammalian cells has been less problematic than FVIII expression (2). Since clinical severity of bleeding episodes closely corresponds to a patient's FIX activity, achieving even partial restoration of normal FIX levels in the bloodstream can alleviate internal bleeding. Individuals with FIX levels less than 1% of normal experience severe symptomatic episodes but providing roughly 5% of normal levels (i.e., 250 ng/mL plasma) can significantly reduce the frequency and severity of bleeding episodes and reduce long term complications (3). Treatment of hemophilia B primarily relies on intravenous injections of FIX protein purified from pooled human plasma, or very recently, on newly developed recombinant FIX. Treatment is applied typically only when bleeding episodes have occurred or are expected, for example, in case of a trauma or surgery. Although the risk of viral transmission of HIV and hepatitis

viruses has been largely eliminated the absolute safety of any product derived from blood cannot be guaranteed. Furthermore, supplies of factor concentrates are limited and costs (especially if prophylactic treatment is being considered) are high. Thus, the application of gene therapy to hemophilia, whereby long-term correction of factor IX deficiency might be achieved, would be extremely useful.

Currently, clinical trials involving many different applications of gene therapy are underway throughout the world, with the majority based in the United States. The subject of gene therapy for hemophilia has gained enough attention that an international conference devoted solely to this subject was held in 1997. This conference, the International Symposium on Gene Therapy for Hemophilia, (ISGT, September 4–6, 1997, Vitadata Corporation) covered a broad spectrum of topics, including current vectors, target tissues, gene delivery methods, and mechanisms of immune recognition and antigen processing. Although conceptually, the idea of gene therapy and its clinical application appears simple, especially for single gene recessive disorders, practical experience indicates that a great deal of effort is needed to reduce it to general practice (4,5). A brief overview of the current strategies and complications of FIX gene replacement therapy are discussed below.

Since the goal of hemophilia gene therapy is to achieve adequate in vivo steady state levels of the missing factor, animal models have been critically important. For this purpose, nude and normal mice as well as the hemophilia dog model has been useful for testing FIX gene therapy protocols and vectors (6). Recently, a FIX knockout mouse model (7) has become available that should be very useful for FIX gene replacement studies. Most delivery systems for gene therapy, including hemophilia gene therapy, are currently based on viral vectors. Recombinant retroviral (RV) and adenoviral vectors (AV) have been used to transfer FIX cDNA into target tissues that include liver (8,9), muscle (10) skin fibroblasts (11), and keratinocytes (12,13), and each of these tissues has demonstrated expression and secretion of the FIX protein. A group in China has used skin fibroblasts from human hemophilia B patients for RV-mediated FIX gene transfection and expression in culture (11). This group has expanded their research to include the only reported human clinical trial of FIX gene delivery (14). In this study, retroviruses were used to introduce human FIX cDNA into autologous primary skin fibroblasts ex vivo. The engineered cells were then pooled, embedded in collagen and injected subcutaneously back into the patient. In one patient, the FIX level increased from 71 ng/ml to 220 ng/ml and in the second patient the concentration rose from 130 to 250 ng/ml. These levels were maintained over 5 months at the time the paper was published.

While effective at gene delivery, each viral vector has its unique limitations and complications. RV vectors, for example, require cell division for integra-

tion (15) and long term expression of the integrated transgene is subject to down regulation (16) due to methylation and/or chromatin reorganization. Growing evidence indicates that the target of this suppressive activity is the retroviral LTR promoter sequence (17). For this reason, endogenous cell specific promoters/enhancers have been used to improve duration of expression of the FIX gene in RV transduced tissues such as epidermal keratinocytes (18) or in transgenic animals (13). Likewise, in vivo exposure to AV vectors elicits host immune responses to viral proteins (19) that result in loss of transgene activity. More recently the development of adeno-associated virus (AAV) vectors has lessened certain complications of viral-based gene therapy. AAV vectors contain no viral genes, and can integrate into nondividing cells. FIX expressing AAV vectors have been used to transduce liver (20,21) and muscle (22) resulting in therapeutic levels of expression. While promising, AAV has limited DNA carrying capacity and still often induces immune responses from contaminating AV material. In general, viral vectors still carry the risk of unwanted viral contamination, oncogenic induction resulting from integration, high cost, and complex production methods.

In light of problems with viral gene therapy, both practical and potential, there recently has been a marked shift toward nonviral gene transfer methods, primarily with liposomes or naked DNA. For a review of nonviral gene transfer methods, the readers are referred to Schofield and Caskey (23) and the 1998 Keystone Symposia on Synthetic Non-Viral Gene Delivery Systems (24). Such efforts at novel modalities of gene delivery or modifications of existing technology have sustained the impetus to continue research in this exciting field.

One of the new developments in the area of nonviral gene therapy is the application of pulsed electric fields, more commonly known as electroporation (25,26). The application of electroporation to gene therapy may potentially obviate many of the problems associated with viral-assisted delivery. Electroporation provides the ability to efficiently deliver naked DNA directly to cells in vitro or in vivo (27), thereby eliminating the problems of viral induced immune responses. Delivery of naked DNA is repeatable and simpler, as well as more cost effective. However, the limitations of plasmid based systems for uses in gene therapy, regardless of the mode of delivery, are well known. In brief, plasmid vectors offer only transiently high levels of gene expression, since integration into the cell's genome is infrequent. Thus, while plasmid-based approaches are less likely to potentiate deleterious effects due to vector integration, they also provide only transiently high expression. To maximize nonviral gene delivery efficiency, we are actively investigating new methodology to improve ex vivo transfection using electroporation to a point where it rivals efficiencies obtained with viruses. Our long-term objectives are to address the problems of vector longevity and expression within transfected

cells. For these studies, we are interested in targeting the stromal cell population within bone marrow as discussed below.

Ex vivo electroporation of human bone marrow stromal cells with the human FIX cDNA is currently being tested by our group in a phase I IND at the Toronto Hospital (28). Bone marrow stromal cells possess several attributes that may qualify them as useful vehicles for ex vivo gene therapy (29–31). For example, these cells are readily obtainable through the widely used procedure of bone marrow aspiration, can be expanded and transfected in vitro, and then returned to the recipient by infusion (32,33). Evidence is accumulating that the genetically modified stromal cells can engraft into the marrow and deliver transgene products to the circulation. In addition to serving as cellular vectors for transgenes, the stromal cells themselves should have beneficial therapeutic influences in bone and blood homeostasis. This is because the bone marrow stromal microenvironment is composed of a heterogeneous population of cells that play a critical role in hematopoietic and osteogenic regulation and differentiation. Thus, ex vivo expansion and reinfusion of stromal cells to a patient potentially may prove beneficial. In vivo, bone marrow stromal cells are a quiescent, noncycling, population with low cell turnover that makes them especially attractive as long-lived suppliers of transgene product. For examples, in canine studies (34), reinfused retroviral transduced stromal cells produced human growth hormone or human FIX transgene products in plasma for several weeks. For these reasons, increased attention has been placed on using stromal cells as gene delivery vehicles for treatment of diseases such as hemophilia A (35) and B (28) and other deficiencies of plasma protein (34). The experimental approaches we have developed are described below.

2. Materials

1. Bone marrow aspirates were obtained from consenting donors at The Toronto Hospital according to institutional review board-approved protocols.
2. Long-term culture media (LTCM): McCoy's 5A (Life Technologies, ON, Canada) supplemented with 16.5% fetal bovine serum (FBS), 1% glutamine, 1% sodium pyruvate, 1% sodium carbonate, 1% vitamins, 0.8% essential and 0.4% non-essential amino acids (all from Life Technologies). The cultures can be further supplemented with 20 U/ml interleukin-1 and 0.5 ng/ml basic fibroblast growth factor (bFGF) (both from R&D Systems, Minneapolis, MN) (*see Note 1*).
3. Trypsin buffer: 0.05% trypsin, 0.53 mM EDTA in Hank's balanced salt solution (HBSS) Life Technologies.
4. Qiagen Maxi-Kit plasmid purification kit. (Qiagen, Inc. Santa Clarita, CA).
5. T820 (Electro Square Porator) and cuvettes with a 0.4 cm gap (BTX, A Division of Genetronics, Inc. San Diego, CA). This instrument generates a square wave (the voltage is constant over the duration of the pulse length) and our experience

is that this type of electrical field is superior to exponential waves for the introduction of DNA into mammalian cells.

6. Electroporation media: McCoy's 5A media with 2% FBS (36).

2.1. Plasmid Vectors

The plasmid pEGFP-C1 (Clontech, Palo Alto, CA) was used as a reporter vector. This vector encodes the enhanced green fluorescent protein (GFP) which is reported to have 35 times greater fluorescence than the wild-type protein. The CMV promoter transcribes the GFP gene.

3. Methods

3.1. Stromal Cell Culture

1. Centrifuge bone marrow material at 180g for 10 min.
2. Add 2 volumes of 7% NH₄Cl (prewarmed to 37°C) to cell pellet to lyse red cells and incubate at 37°C for 10 min.
3. Centrifuge at 180g for 10 min and wash in PBS or medium.
4. Resuspend cells in culture medium at a concentration of 2–3 × 10⁶/mL.
5. Add the resuspended cells to culture flasks (approximately 30 mL in a 150 cm² flask) and culture in a 5% humidified CO₂ environment (*see Note 2*).
6. After 5 days discard half of the medium and replace with fresh medium.
7. Maintain cultures until the adherent layer approaches confluency (usually after about 2–3 weeks for the first passage).
8. Wash with either PBS or medium (without FBS).
9. Add Trypsin-EDTA (sufficient to just cover cells) and incubate for 5–10 minutes at 37°C.
10. Add serum-containing medium (to neutralize action of trypsin-EDTA).
11. Centrifuge at 180g for 10 min and wash × 1.
12. Resuspend in culture medium and replat cultures. After first passage IL-1 and basic-FGF are added to the culture medium to improve growth rate.
13. Repeat the procedure until cultures have been passaged four times before proceeding to electroporation (*see Note 3*).

3.2. Preparation of Plasmid DNA

1. Plasmid DNA (for example, pEGFP-C1) should be transfected into a suitable strain of *E. coli* (such as JM-109 strain or other similar strain) and individual colonies are selected and streaked onto fresh selective plates and grown overnight. A well-separated individual colony is picked and inoculated into a 250-mL liquid culture and grown overnight or until saturation.
2. Purify the plasmid using the Qiagen endotoxin free purification procedures. Typically 0.5–1.0 mg of plasmid is obtained.
3. Resuspend the plasmid in sterile water or TE buffer to a concentration of 2–4 mg/mL and do not freeze, but maintain at 4°C for up to 2 mo.

4. If linearized vectors are used, digest the plasmid with the appropriate restriction enzyme according to the supplier's recommendations. After digestion, phenol extract the DNA and precipitate in ethanol. Resuspend the pelleted DNA to an appropriate concentration (2–4 mg/mL). However, we recommend using supercoiled plasmid (*see Note 4*).

3.3. Electroporation Protocol

1. Detach the stromal cell layers from their flasks by trypsin, resuspend in 5 mL of LTCM and wash twice.
2. Resuspend the stromal cells to a concentration of $2\text{--}6 \times 10^6/\text{ml}$ of electroporation media.
3. Add the DNA (50–100 $\mu\text{g}/\text{mL}$) to the cell suspension and place on ice for 5 min (**36**).
4. Mix the DNA/cell suspension and aliquot 0.8 mL into a 0.4-cm cuvette.
5. Immediately place the cuvette into the electroporation chamber and pulse. Use one pulse from the T820 or other square wave generator of 150–200 V at 50–70 ms duration (*see Note 5*). The critical parameter is the electric field strength, measured in V/cm. For this example the field strength is 375–500 V/cm.
6. Immediately remove the cuvette and place in a 37°C waterbath for 5 min (*see Note 6*).
7. Remove the cells from the cuvette with a sterile pasture pipette and plate into an appropriate culture dish and add LTCM. Wash the walls of the cuvette with fresh LTMC media and add to the plate.
8. Incubate the transfected cells overnight under the same growth conditions.

3.4. Transfection Efficiency

Using GFP as a reporter gene, an estimate of the proportion of cells expressing GFP can be obtained by inverted fluorescence microscopy of cultures without disruption. Alternatively, cells can be detached with trypsin-EDTA and accurate quantitation performed by flow cytometry. GFP is excited by a standard 488-nm argon laser and emits in a range similar to FITC. It is helpful to have a control (non-transfected) sample for this analysis. Expression of GFP is apparent within 24 hours following electroporation (*see Note 7*). This approach consistently yields transfection efficiency in the surviving cells of greater than 50–60% as measured by GFP expression. In vitro transgene expression studies using a CMV driven human growth hormone (GH) expression plasmid have produced appreciable levels of GH. Transfection into human primary stromal cells under the above-described conditions has resulted in GH production of $8 \pm 2 \mu\text{g GH}/10^6 \text{ cells}/24 \text{ h}$. Similar studies with the human FIX cDNA are underway.

4. Notes

1. Some variations in constituents of medium are acceptable. The original long-term culture medium contained 12.5% horse serum and 12.5% FBS. Stromal cells

can also be cultured in lower concentrations of FBS-containing medium (without horse serum) and without added IL-1 or bFGF, but cultures may expand more slowly under these conditions.

2. Haematopoietic cells are maintained for several weeks under these culture conditions, but are a negligible component of the cultures after the third passage.
3. When passaging cultures, the number of flasks are typically doubled at each passage; however, the rate of growth of the individual cultures may vary (most probably a donor-dependent factor). We have found that stromal cells from different donors can have significantly different growth rates.
4. Plasmid DNA of high purity is necessary to obtain high levels of transfected cells and high levels of cell survival. The use of supercoiled DNA increases the efficiency of transfection (37) but the use of a linearized plasmid may lead to higher levels of integration. Whether the free ends of a linear DNA molecule induce higher rates of integration is not clear, but integration usually involves preexisting DNA termini.
5. The use of a square wave generator (T820) improves the yield of transfected cells compared to an exponential wave generator. This is theoretically due to the added electrophoretic capability of the square wave over the exponential wave, and to the ability to use longer pulses of lower voltage.
6. The presence of serum (1–2%) in the electroporation media increases cell survival (38). Raising the temperature rapidly after pulsing improves expression and cell survival probably is promoting the rapid closing of the pores, trapping the DNA inside.
7. Using an inverted fluorescent microscope (Zeiss, Germany) we have noticed that the appearance of GFP positive expression in the stromal cells can be seen as early as 4 hours after electroporation. This may be interpreted to mean that the plasmid enters the nucleus very rapidly, and may indicate that electroporation is also effective at permeabilizing the nuclear envelope. We also observe that the percentage of GFP positive cells is essentially constant by 24 hours after electroporation.

References

1. Walker, I. D. and Greer, I. A. (1997) Inherited bleeding disorders in pregnancy. *Hemophilia and Other Inherited Bleeding Disorders* (Rizza, C. and Lowe, G., eds.), W. B. Saunders, London, p. 391.
2. Pittman, D. D., Tomkinson, K. N., and Kaufman, R. J. (1994) Post-translational requirements for functional factor V and factor VIII secretion in mammalian cells. *J. Biol Chem.* **269**, 17,329–17,337.
3. Monahan, P. E., Samulski, R. J., Tazelaar, J., Xiao, X., Nichols, T. C., Bellinger, D. A., Read, M. S., and Walsh, C. E. (1998) Direct intramuscular injection with recombinant AAV vector results in sustained expression in a dog model. *Gene Ther.* **5**, 40–49.
4. Verma, I. M. and Somia, N. (1997) Gene therapy: Promises, problems, and prospects. *Nature* **389**, 239–242.

5. Rigby, P. (1995) *Gene Therapy: Simple in Theory but Difficult in Practice*. Mill Hill Essays, National Institute of Medical Research, U.K.
6. Kay, M. A., Landen, C. N., Rothenberg, S. R., Taylor, L. A., Leland, F., Wiehle, S., Fang, B., Bellinger, D., Finegold, M., and Thompson, A. R. (1994) In vivo hepatic gene therapy: Complete albeit transient correction of factor IX deficiency in hemophilia B dogs. *Proc. Natl. Acad. Sci. USA* **91**, 2353–2357.
7. Wang, L., Zoppe, M., Hackeng, T. M., Griffin, J. H., Lee, K.-F., and Verma, I. M. (1997) A factor IX-deficient mouse model for hemophilia B gene therapy. *Proc. Natl. Acad. Sci. USA* **94**, 11,563–11,566.
8. Armentano, D., Thompson, A. R., Darlington, G., and Woo, S. L. (1990) Expression of human factor IX in rabbit hepatocytes by retrovirus-mediated gene transfer: Potential for gene therapy of hemophilia B. *Proc. Natl. Acad. Sci. USA* **87**, 6141–6145.
9. Kay, M. A., Rothenberg, S., Landen, C. N., Bellinger, D. A., Leland, F., Toman, C., Finegold, M., Thompson, A. R., Read, M. S., and Brinkhous, K. M. (1993) In vivo gene therapy of hemophilia B: Sustained partial correction in factor IX-deficient dogs. *Science* **262**, 117–119.
10. Dai, Y., Schwartz, E. M., Gu, D., Zhang, W.-W., Sarvetnick, N., and Verma, I. M. (1995) Cellular and humoral responses to adenoviral vectors containing the factor IX gene: Tolarization of factor IX and vector antigens for long-term expression. *Proc. Natl. Acad. Sci. USA* **92**, 1402–1405.
11. Dai, Y. F., Qiu, X. F., Xue, J. L., and Liu, Z. D. (1992) High efficient transfer and expression of human clotting factor IX cDNA in cultured human primary skin fibroblasts from hemophilia B patient by retroviral vectors. *Sci. China B* **35**, 183–193.
12. Gerrard, A. J., Hudson, D. L., Brownlee, G. G., and Watt, F. M. (1993) Towards gene therapy for hemophilia B using primary human keratinocytes. *Nat. Genet.* **3**, 180–183.
13. Alexander, M. Y., Bidichandani, S. I., Cousins, F. M., Robinson, C. J., Duffie, E., and Akhurst, R. J. (1995) Circulating human factor IX produced in keratin-promoter transgenic mice: A feasibility study for gene therapy of hemophilia B. *Hum. Mol. Genet.* **4**, 993–999.
14. Lu, D. R., Zhou, J. M., Zheng, B., Qiu, X. F., Xue, J. L., Wang, J. M., Meng, P. L., Han, F. L., Ming, B. H., and Wang, X. P. (1993) Stage I clinical of gene therapy for hemophilia B. *Sci China B* **36**, 1342–1351.
15. Miller, D. G., Adam, M. A., and Miller, A. D. (1990) Gene transfer by retrovirus vectors occurs only in cells that are actively replicating at the time of infection. *Mol. Cell Biol.* **10**, 4239–4242.
16. Hoeben, R. C., Migchielsen, A. A., van der Jagt, R. C., van Ormondt, H., and van der Eb, A. J. (1991) Inactivation of the Moloney murine leukemia virus long terminal repeat in murine fibroblast cell lines is associated with methylation and dependent on its chromosomal position. *J. Virol.* **65**, 904–912.
17. Deng, H., Qun, L., and Khavari, P. A. (1997) Sustainable cutaneous gene delivery. *Nat. Biotech.* **15**, 1388–1391.

18. Page, S. M. and Brownlee, G. G. (1997) An ex vivo keratinocyte model for gene therapy of hemophilia B. *J. Invest. Dermatol.* **109**, 139–145.
19. Dai, Y., Schwartz, E. M., Gu, D., Zhang, W.-W., Sarvetnick, N., and Verma, I. M. (1995) Cellular and humoral responses to adenoviral vectors containing the factor IX gene: Tolarization of factor IX and vector antigens for long-term expression. *Proc. Natl. Acad. Sci. USA* **92**, 1402–1405.
20. Snyder, R. O., Miao, C. H., Patijin, G. A., Spratt, S. K., Danos, O., Nagy, D., Gown, A. M., Winther, B., Meuse, L., Cohen, L. K., Thompson, A. R., and Kay, M. A. (1997) Persistent and therapeutic concentrations of human factor IX in mice after hepatic gene transfer of recombinant AAV vectors. *Nat. Genet.* **16**, 270–276.
21. Koeberl, D. D., Alexander, I. E., Halbert, C. L., Russell, D. W., and Miller, A. D. (1997). Persistent expression of human clotting factor IX from mouse liver after intravenous injection of adeno-associated virus vectors. *Proc. Natl. Acad. Sci. USA* **94**, 1426–1431.
22. Herzog, R. W., Hagstrom, J. N., Kung, S.-H., Tai, S. J., Wilson, J. M., Fisher, K. J., and High, K. A. (1997) Stable gene transfer and expression of human blood coagulation factor IX after intramuscular injection of recombinant adeno-associated virus. *Proc. Natl. Acad. Sci. USA* **94**, 5804–5809.
23. Schofield, J. P. and Caskey, C. T. (1995) Non-viral approaches to gene therapy. *Br. Med. Bull.* **51**, 56–71.
24. *The Keystone symposia on molecular and cellular biology. Jan. 19–25, 1998.*
25. Chu, G., Hayakawa, H., and Berg, P. (1987) Electroporation for the efficient transfection of mammalian cells with DNA. *Nucleic Acids Res.* **15**, 1311–1324.
26. Keating, A. and Toneguzzo, F., (1990) Gene transfer by electroporation: a model for gene therapy. *Prog. Clin. Biol. Res.* **333**, 491–498.
27. Muramatsu, T., Nakamura, A., and Park, H.-M. (1997) In vivo electroporation: A powerful and convenient means of nonviral gene transfer to tissue of living animals (review). *Int. J. Mol. Med.* **1**, 55–62.
28. Keating, A., Berkahn, L., and Filshie, R. (1998) A phase I study of the transplantation of genetically marked autologous bone marrow stromal cells. *Hum. Gene Ther.* **9**, 591–600.
29. Keating, A., Just-Mitchell, K., Toor, P., Klein, M., and Sodek, J. (1986) Passaged human marrow stromal cells: A unique cell population. *Exp. Hematol.* **14**, 426.
30. Nolte, J. A., Hanley, M. B., and Kohn, D. B. (1994) Sustained human hematopoiesis in immunodeficient mice by cotransplantation of marrow stroma expressing human interleukin-3: Analysis of gene transduction of long-lived progenitors. *Blood* **83**, 3041–3061.
31. Keating, A. and Leslie, K. (1993) Gene therapy and bone marrow transplantation. *Clinical Bone Marrow Transplantation* (Atkinson, K., ed.), Cambridge University Press, Cambridge, U.K., pp. 715–724.
32. Wu, D. D. and Keating, A. (1991) Engraftment of donor-derived bone marrow stromal cells. *Exp. Hematol.* **19**, 485.
33. Lazarus, H. M., Haynesworth, S. E., Gerson, S. E., Rosenthal, N. S., and Caplan,

- A. I. (1995) Ex vivo expansion and subsequent infusion of human bone marrow-derived stromal progenitor cells (mesenchymal progenitor cells): Implications for therapeutic use. *Bone Marrow Transplant.* **16**, 557–564.
34. Hurwitz, D. R., Kirchgesser, M., Merrill, W., Galanopoulos, T., McGrath, C. A., Emami, S., Hansen, M., Cherington, V., Appel, J. M., Bizinkauskas, C. B., Brackmann, H. H., Levine, P. H., and Greenberger, J. S. (1997) Systemic delivery of growth hormone or human factor IX in dogs by reintroduced genetically modified autologous bone marrow stromal cells. *Hum. Gene Ther.* **8**, 137–156.
35. Chuah, M. K. L., Brems, H., Vanslebrouck, V., Collen, D., and Vandendriessche, T. (1998) Bone marrow stromal cells as targets for the gene therapy of hemophilia A. *Hum. Gene Ther.* **9**, 353–365.
36. Rols, M. P., Delteil, C., Serin, G., and Teissié, J. (1994) Temperature effects of electrotransfection of mammalian cells. *Nucleic Acids Res.* **22**:540.
37. Xie, T. D. and Tsong, T. Y. (1993) Study of mechanisms of electric-field-induced DNA transfection. Effects of DNA topology on surface binding, cell uptake, expression, and integration into host chromosomes of DNA in the mammalian cell. *Biophys. J.* **65**, 1684–1689.
38. Bahnson, A. B. and Boggs, S. S. (1990) Addition of serum to electroporated cells enhances survival and transfection efficiency. *Biochem. Biophys. Res. Commun.* **171**, 752–757.

In Ovo Gene Electroporation into Early Chicken Embryos

Tatsuo Muramatsu

1. Introduction

In chicken embryos, viral vectors have been successfully used to transfer foreign genes in somatic cells. By using retroviral vectors, for example, genes involved in myocyte growth and differentiation in chicken embryos have been characterized (1–3). The reason for the use of viral vectors is its high efficiency of gene transfection, particularly when stable gene expression is desired. However, if only transient gene expression is considered, several nonviral methods may be useful at present. In ovo lipofection gave spatial expression of a reporter gene in embryonic tissues of chickens (4–6). In addition, two other nonviral methods may be applicable to chicken embryos in ovo. One is microparticle bombardment which has been widely used to transfect genes to tissues of a variety of animal species in vivo (7–9), and the other is electroporation (EP) by which foreign genes are transferred into cells through nanometer pores made on the cell membrane by applying electric pulses (10). The latter method is found to be more efficient than other nonviral methods (11), and has been tested in various animal tissues such as the rat brain, the mouse testis, and the chicken embryo (12–14).

In this chapter, brief protocols of in ovo gene EP in chicken embryos are described. Protocols for detecting two common reporter genes, *lacZ* and luciferase, in ovo are also described.

2. Materials

2.1. Animals

Keep fertilized eggs of chickens obtained commercially from a local hatchery in an incubator at 38.5°C usually for 48 h, and use the incubated embryos at stages 11 to 12 of development (**15**). The reason for using 48-h incubated embryos is that after injecting DNA solution into the embryonic body, the viability of 48-h incubated embryos is found to be higher than that of 24-h incubated ones (**16**) (*see Note 1*). At later stages, bleeding may occur while injecting with DNA solution.

2.2. Plasmid DNAs

For short-term gene expression, that is, within several days after in ovo gene EP, use circular plasmid DNAs. In this chapter, two plasmids, that is, pmiwZ containing the bacterial *lacZ* gene driven by RSV-LTR and the chicken β -actin promoter (VE052, Human Science Research Resources Bank, Osaka, Japan) (*see Note 2*), and pGL control, containing the firefly luciferase gene, obtained commercially (Promega, Madison, WI) were transferred as examples.

If longer gene expression is preferred, use linearized DNA as the chance of integration may increase. Cotransfection with the integrase gene derived from the Rous sarcoma virus (**17,18**) may also help enhanced gene expression. Indeed, at 5 d after EP in ovo, higher frequency of bacterial β -galactosidase gene expression was observed in Japanese quail embryos when an integrase gene was cotransferred (*unpublished*). Unlike the case in mouse testes, however, there seems little effect of using the Epstein–Barr virus self-replicating DNA sequence on prolonging and strengthening gene expression (*see Note 3*). Instead, a translation stimulating expression plasmid, pAdVantage vector (Promega, Madison, WI) may provide another means of enhanced and sustained gene expression.

2.3. Solutions and Reagents

1. TE buffer: 10 mM Tris.HCl, 25 μ M EDTA. Adjust pH to 7.5 with 5 M NaOH. Filter-sterilize through a 0.22- μ m membrane, and store at 4°C or room temperature.
2. Plasmid DNA: CsCl-purified plasmid DNA (or Qiagen-purified DNA, Qiagen, Chatsworth, CA) is resuspended in sterile TE buffer to give final concentrations at 1–3 μ g/ μ L.
3. Transfection solution: Dissolve 10–50 μ g (or more where necessary) plasmid DNA in 50 μ L of 137 mM NaCl and 2.5 mM CaCl₂. For one embryo, 1–5 μ L of the transfection solution is used.
4. PBS: 137 mM NaCl, 2.7 mM KCl, 10.1 mM Na₂HPO₄ and 1.8 mM KH₂PO₄. Adjust the pH to 7.4 with 5 M HCl. Autoclave, and store at room temperature.

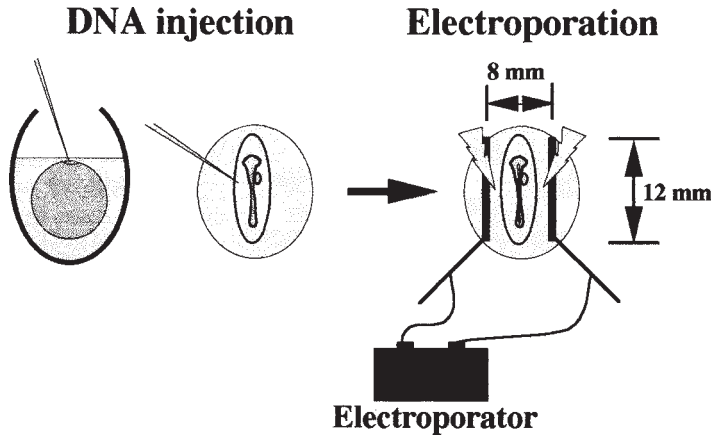


Fig. 1. Diagrammatic presentation of in ovo gene electroporation.

5. Fixation solution: 4% formaldehyde and 0.2% glutaraldehyde solution in PBS. Store at 4°C.
6. XG buffer: 2 mM MgCl₂, 5 mM K₄Fe(CN)₆ · 3H₂O and K₃Fe(CN)₆ in PBS. Store at 4°C.
7. X-gal reaction mixture: 0.1% 5-bromo-4-chloro-3-indolyl-β-D-galactopyranoside (X-gal), 5% *N,N*-dimethylformamide and 0.1% Triton-X in the XG buffer. Adjust the pH to 7.6, and store at 4°C.
8. Luciferin solution: Use commercially available substrate solution, Picca Gene (Nippon Gene, Tokyo, Japan).

2.4. Instruments

1. Electro-square porator: T820 in combination with an optimizer 500 (BTX, San Diego, CA) or CUY-1 (Tokiwa Science, Tsukushino, Japan).
2. Use L-shaped electrodes made from gold-plated wire of 1 mm in diameter, having efficient application length of 12 mm (CUY610, Tokiwa Science, Tsukushino, Japan) with separate electrical connection to the above electro-square porator (*see Fig. 1*).
3. Photon imaging system : Argus-50/2D (Hamamatsu Photonics, Hamamatsu, Japan).

3. Methods

3.1. DNA Injection

A simple diagrammatic presentation of the in ovo gene EP is given in **Fig. 1**.

1. Place fertilized eggs in an upright position with the blunt edge at the top.
2. Sterilize the blunt edge with 70% (v/v) ethanol.
3. Make a hole of approximately 10 mm in diameter on the blunt edge of egg shell.

Table 1
Effects of Voltages and Pulse Width on the Viability
and the Transfection Efficiency of a LacZ Reporter Gene
in Chicken Embryos After In Ovo Electroporation

Voltage (V)	Pulse width (ms)	Surviving embryos (%)	Gene transfection efficiency (%)
10	50	55.6 ^c (20/36) ^a	10.0 ^c (2/20) ^b
25	50	56.0 ^c (28/50)	50.0 ^c (14/28)
25	99	10.4 ^c (8/77)	37.5 ^c (3/8)

From **ref. 11**, with permission.

^aNumber of surviving/number of total.

^bNumber of lacZ positive/number of surviving.

^cSignificantly different at $p < .01$.

4. Remove carefully shell membrane and allantocholeonic membranes located underneath to expose embryos (*see also Note 4*).
5. By using a micromanipulator, inject DNA (lacZ plasmid, luciferase plasmid, or other genes) which is held in a fine-drawn glass pipette into embryonic body or a circumference area at 1–5 μL . A manipulator that allows only a vertical movement will do. When DNA transfer to a particular embryonic tissue is desired, the injection procedure should be performed under macromicroscopes. Do not inject excessive volume of DNA solution above 5 μL . By doing so, viability of embryos may decrease severely.

3.2. Voltage Optimization for In Ovo EP

1. Immediately after the injection, apply square electric pulses three times with an electro-square porator T820 in combination with an optimizer 500 (BTX, San Diego, USA) at 25 V (31 V/cm) with the pulse width of 50 ms/pulse. The voltage may have to be optimized according to the stage and size of embryos or limited gene transfer site of interest. Generally speaking, chicken embryos are susceptible to heat damage caused by electric pulse application. Therefore, use a milder condition than those for various tissues in adult animals. The results of varying voltages and pulse widths on viability and gene transfection efficiency are presented in **Table 1 (II)**. The viability of embryos was not affected by raising voltages from 10 to 25 V (i.e., 12.5 to 31 V/cm). However, by elevating pulse widths from 50 to 99 ms, the viability was significantly decreased. The gene transfection efficiency was the highest at 25 V in combination with 50 ms, followed by 25 V with 99 msec and 10 V with 50 ms in the decreasing order.
2. If possible, exchange the cathode and anode during the pulse application as it is empirically known that the exchange substantially enhances the intensity of gene expression.
3. After the EP treatment, place a small amount of egg white onto the treated embryo. This procedure is optional.

4. Seal the hole on the shell with a mending tape or vinyl wrap.
5. Incubate at 38.5°C for the subsequent 24 h or longer, without rocking or possibly with rocking at 30° angle. If good sealing is attained, rocking the eggs is recommended.

3.3. Assays

3.3.1. Histochemical Staining for β -Galactosidase (*lacZ*) with X-Gal

1. Remove the embryos from egg yolk with scissors, and carefully transfer them to a Petri dish.
2. Wash with PBS twice, and remove PBS with an aspirator.
3. Fix the excised embryos with 4% formaldehyde and 0.2% glutaraldehyde solution in PBS at room temperature for 3 h or longer.
4. Rinse with PBS twice, and soak in the X-gal reaction mixture for not more than 1 h. This staining time period should be kept strictly to minimize endogenous greenish-blue color development in the whole embryo samples. To eliminate ambiguity, untreated control embryos should be stained at the same time along with the treated embryos to monitor endogenous color development. Specific blue color due to bacterial β -galactosidase is easily distinguished. A typical example of an X-gal stained whole embryo is shown in **Fig. 2A (11)**.
5. Where necessary, embed the stained embryos in paraffin for sectioning and counter-staining with hematoxylin for light microscopic examination. The endogenous blue color can no longer be observed under microscopic observation whereas the blue staining due to the bacterial *lacZ* gene expression can be easily identified.

3.3.2. Bioluminescence Imaging Analysis for Detecting Luciferase

1. Take out eggs from an incubator, and set them in an upright position with the blunt edge top. For bioluminescence imaging analysis, it is not necessary to remove embryos and extraembryonic membranes from egg yolk.
2. Enlarge the visual area around the embryo by taking off pieces of egg shell fragments with pincers.
3. Place eggs in the box of imaging analysis apparatus.
4. Inject 100 μ L of luciferin solution into embryonic body with a 27-G needle, and pour another 100 μ L of luciferin solution over the embryonic body and surrounding membrane areas.
5. Place the egg to the camera lens as close as possible, that is, approximately 5–10 cm. By doing so, the sensitivity of photon imaging increases substantially. Take several min or longer for photon imaging with the Argus 50/2D system. For penetration of luciferin into embryonic cells, slight delay, that is, for several min, of bioluminescence emission may occur. Unlike the photon counting with cell extract, photon signal will be observed even at 30 min after injecting with the luciferin solution into the embryos. An example of photon imaging is shown in **Fig. 2B (14)**.

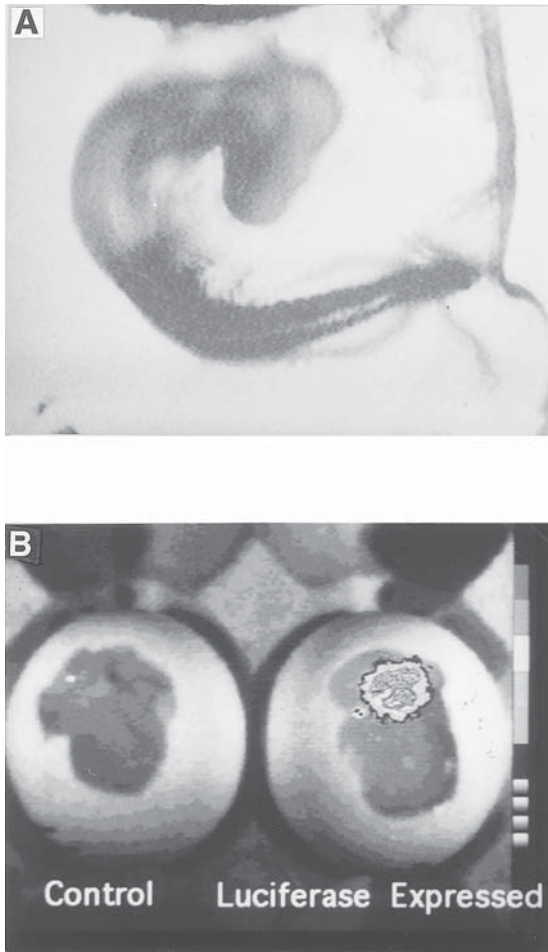


Fig. 2. (A) Typical example of an X-gal stained chicken embryo to which the bacterial lacZ gene driven by RSV-LTR and chicken β -actin promoter was transfected by in ovo electroporation (11). Detection of the lacZ gene expression by X-gal staining was conducted at 48 h after gene transfection. (B) Bioluminescence detected in ovo by the single-photon imaging system in the chicken embryonic body and extraembryonic tissues to which the firefly luciferase was transfected by in ovo electroporation. Relative intensity of the bioluminescence is indicated by a vertical bar (14).

4. Notes

1. If the injection of DNA solution can be done carefully not to cause bleeding, embryos at stages later than 11 to 12 of development (15) could be suitably used. One may prefer more developed and larger embryos, especially when spatial gene expression is desired in a particular tissue at any given developmental stage.

2. For requesting this gene, a special form is needed. Information can be obtained through the home page as: <http://www.nih.go.jp/yoken/genebank/index.html>.
3. In the mouse testis, inclusion of the self-replicating sequences derived from the Epstein-Barr virus significantly prolonged the duration of gene expression (19), whereas the same sequences did neither enhance nor prolong expression of foreign genes transferred in ovo in chicken embryos (unpublished). The self-replication sequences may have to be derived from DNA of infectious viruses to avian species.
4. If hatching is aimed, do not remove shell membrane. With the membrane, DNA injection is still possible, though the accurate injection site cannot be known. For EP with shell membrane, voltage optimization is needed as the resistance changes.

References

1. Mikawa, T., Cohen-Gould, L., and Fischman, D. A. (1992) Clonal analysis of cardiac morphogenesis in the chicken embryo using a replication-defective retrovirus: I. Formation of the ventricular myocardium. *Dev. Dyn.* **193**, 11–23.
2. Mima, T., Ueno, H., Fischman, D. A., Williams, L. T., and Mikawa, T. (1995) Fibroblast growth factor receptor is required for in vivo cardiac myocyte proliferation at early embryonic stages of heart development. *Proc. Natl. Acad. Sci. U.S.A.* **92**, 467–471.
3. Itoh, N., Mima, T., and Mikawa, T. (1996) Loss of fibroblast growth factor receptors is necessary for terminal differentiation of embryonic limb muscle. *Development* **122**, 291–300.
4. Brazolot, C. L., Petite, J. N., Etches, R. J., and Gibbins, A. M. V. (1991) Efficient transfection of chicken cells by lipofection, and introduction of transfected blastodermal cells into the embryo. *Mol. Reprod. Dev.* **30**, 304–312.
5. Demeneix, B. A., Abdel-Taweb, H., Benoist, C., Seugnet, I., and Behr, J. P. (1994) Temporal and spatial expression of lipospermine-compacted genes transferred into chick embryos in vivo. *Biotechniques* **16**, 496–501.
6. Rosenblum, C. and Chen, H. Y. (1995) In ovo transfection of chicken embryos using cationic liposomes. *Transgenic Res.* **4**, 192–198.
7. Yang, N. S., Burkholder, J., Roberts, B., Martinell, B., and McCabe, D. (1990) in vivo and in vitro gene transfer to mammalian somatic cells by particle bombardment. *Proc. Natl. Acad. Sci. U.S.A.* **87**, 9568–9572.
8. Williams, R. S., Johnston, S. A., Reidy, M., de Vit, M. J., McElligott, S. G., and Sanford, J. C. (1991) Introduction of foreign genes into tissues of living mice by DNA-coated microprojectiles. *Proc. Natl. Acad. Sci. U.S.A.* **88**, 2726–2730.
9. Klein, T. M., Arentzen, R., Lewis, P., and Fitzpatrick-McElligott, S. (1992) Transformation of microbes, plants and animals by particle bombardment. *Biotechnology* **10**, 286–291.
10. Tur-Kaspa, R., Teicher, L., Levine, B. J., Skoultchi, A. L., and Shafritz, D. A. (1986) Use of electroporation to introduce biologically active foreign genes into primary rat hepatocytes. *Mol. Cell. Biol.* **6**, 716–718.

11. Muramatsu, T., Mizutani, Y., Ohmori, Y., and Okumura, J. (1997) Comparison of three nonviral transfection methods for foreign gene expression in early chicken embryos in ovo. *Biochem. Biophys. Res. Commun.* **230**, 376–380.
12. Nishi, T., Yoshizato, K., Yamashiro, S., Takeshima, H., Sato, K., Hamada, K., Kitamura, I., Yoshimura, T., Saya, H., Kuratsu, J., and Ushio, Y. (1996) High-efficiency in vivo gene transfer using intraarterial plasmid DNA injection following in vivo electroporation. *Cancer Res.* **56**, 1050–1055.
13. Muramatsu, T., Shibata, O., and Okumura, J. (1996) In vivo electroporation: A convenient method for gene transfer to testicular cells in mice. *Anim. Sci. Technol. Jpn.* **67**, 975–982.
14. Muramatsu, T., Mizutani, Y., and Okumura, J. (1996) Live detection of firefly luciferase gene expression by bioluminescence in incubating chicken embryos. *Anim. Sci. Technol. Jpn.* **67**, 906–909.
15. Hamburger, V. and Hamilton, H. L. (1951) A series of normal stages in the development of the chick embryo. *J. Morphol.* **88**, 49–92.
16. Muramatsu, T., Mizutani, Y., and Okumura, J. (1996) Effects of incubation time and injection sites on gene transfection efficiency in chicken embryos by in ovo lipofection. *Anim. Sci. Technol. Jpn.* **67**, 882–885.
17. Katz, R. A., Merkel, G., Kulkosky, J., Leis, J., and Skalka, A. M. (1990) The avian retroviral IN protein is both necessary and sufficient for integrative recombination in vitro. *Cell* **63**, 87–95.
18. Katz, R. A. and Skalka, A. M. (1994) The retroviral enzymes. *Annu. Rev. Biochem.* **63**, 133–173.
19. Muramatsu, T., Shibata, O., and Okumura, J. (1997) Effect of self-replication DNA sequences of Epstein-Barr virus on the expression of a foreign gene transfected in vivo to the mouse testis. *Anim. Sci. Technol. Jpn.* **68**, 650–653.

Electrical Impedance Spectroscopy for Rapid and Noninvasive Analysis of Skin Electroporation

Uwe Pliquett and Mark R. Prausnitz

1. Introduction

Transient disruption of skin's barrier properties using high-voltage pulses involves complex changes in skin microstructure believed to be due to electroporation. Electroporation of cell membranes is a well known phenomenon which has found extensive use as a method of DNA transfection in biological laboratories (1–3). More recently, it has been shown that the multilamellar lipid bilayer membranes found in skin can also be electroporated (4–7). The dramatic and reversible increases in skin permeability caused by electroporation indicate that drugs might be delivered transdermally at significantly enhanced rates. Especially for macromolecules, such as protein- and gene-based drugs, electroporation-mediated transdermal drug delivery could be an important pharmaceutical approach.

Overcoming the skin barrier is especially challenging because skin's outermost layer—the stratum corneum—has remarkably low permeability to most compounds. Its structure consists of a mosaic of keratinocytes imbedded in an intercellular lipid matrix (8,9). The keratinocytes are cell remnants filled with crosslinked keratin. The intercellular lipids are organized in bilayer structures. It is these bilayers which make stratum corneum so impermeable and which are believed to be disrupted during electroporation. While stratum corneum occupies the outermost 10–20 μm of skin, the viable epidermis fills the next 50–100 μm below that and finally the dermis makes up skin's deepest layer, which is typically 1–2 mm thick. These deeper layers do not contribute a significant transport barrier for most drugs. Thus, disruption of stratum corneum by electroporation can dramatically influence overall skin permeability.

The intriguing biophysical phenomena and potential drug delivery applications of skin electroporation have prompted study using a variety of different approaches. Most studies have emphasized measuring changes in molecular flux across the skin, which can transiently increase by as much as four orders of magnitude (7). Others have used microscopy and other spectroscopic and biophysical tools (5,10–13) to characterize changes in skin properties, both in vitro and in vivo. In this chapter, we describe an especially useful technique: electrical impedance spectroscopy.

Measuring skin electrical properties to assess the effects of electroporation is an especially sensitive and rapid method. Electroporation is believed to create nanometer-scale pores within stratum corneum (4). Because an “electropore” filled with saline has a conductivity orders of magnitude greater than the bulk stratum corneum, even a small number of pores will make a big change in skin’s electrical resistance. Impedance spectroscopy has previously been applied in other studies of transdermal delivery, including the use of chemical enhancers (14–18) and low-voltage electric fields for iontophoresis (19,20). Using conventional equipment which probe the impedance spectrum by making a series of measurements sequentially over a range of frequencies, the time required for one scan is sufficiently short to assess changes which occur on the minutes time scale or slower. Many of the changes in skin electrical properties associated with electroporation, however, occur on the microsecond to millisecond time scale (21,22). Therefore, impedance spectroscopy analysis of skin electroporation requires faster methods, as described in this chapter.

1.1. Skin Impedance

Any material can be characterized by its passive electrical properties, which describe the relationship between the voltage across the material and the current through it (23–25). The passive electrical property most commonly used to describe a material is resistance, expressed in Ohm’s law as $U = IR$, where U is voltage, I is current, and R is resistance. However, Ohm’s law only applies for materials whose electrical properties are both time invariant and linear (i.e., R is independent of the electric field) during the measurement.

The resistance to flow of an alternating current is called the impedance. As frequency increases, the resistance becomes complex if the material has the ability to store energy, for instance by charging up a capacitive element. A capacitor can be formed if a high resistive medium such as a biological membrane is contacted by electrolytes which have a low resistance (e.g., a lipid bilayer bathed in saline). Because inductive elements are generally not found in biological matter, they are not considered here.

The greatest resistance of the skin resides in the stratum corneum (26,27). Although the stratum corneum is in series with the viable epidermis and dermis,

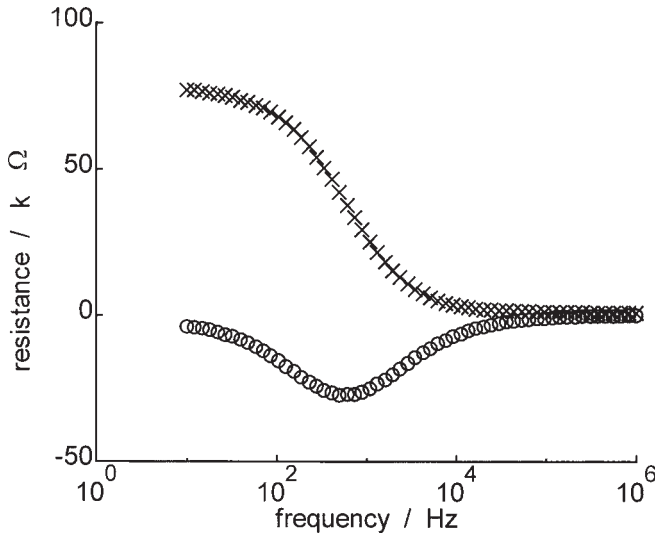


Fig. 1. Impedance spectrum of human stratum corneum in vitro ($A_{\text{skin}} = 0.67 \text{ cm}^2$) for a frequency range between 10 Hz and 1 MHz. Both the real (\times) and the imaginary (\circ) parts of the impedance are represented.

the stratum corneum resistance is typically three orders of magnitude greater than the deeper tissues. Thus, measurements of skin resistance primarily reflect the resistance of stratum corneum. This large stratum corneum resistance is due to the multilamellar structure of the long chain sphingolipids between the corneocytes (28,29). Paths for direct current across the skin include routes through the appendages (i.e., hair follicles and sweat ducts) as well as routes through the bulk of stratum corneum involving tortuous intercellular paths and possibly transcellular paths too. At higher frequency (i.e., $>10 \text{ Hz}$) the modulus of the stratum corneum resistance drops because of its capacitive behavior (23–25). At very high frequencies (e.g., $>100 \text{ kHz}$), the impedance approaches zero and the membranes appear as a short circuit.

A typical frequency spectrum of human stratum corneum is given in **Fig. 1**. It shows the real part of the impedance which is associated with resistive pathways across the skin (e.g., hair follicles, sweat ducts, and defects in the bulk multilamellar system possibly created by desmosomes) and the imaginary part of the impedance which is associated with capacitive pathways (e.g., membrane structures). A large real part of the impedance is found at 10 Hz (near to DC, i.e., 0 Hz). Here only the appendages and small additional DC-pathways within the bulk stratum corneum contribute to the resistance. With increasing frequency (f) the real part of the impedance decreases and the imaginary part becomes more and more important. Since the resistance of a capacitor

(membrane structures) is $X_C = 1/2 \pi f C$ (where C is capacitance), the imaginary part of the impedance disappears at very high frequencies and only a small real part remains. When the frequency is so high, current is only being moved back and forth between membrane surfaces and thus neither the DC pathways across skin nor the capacitive charging pathways of the membranes have time to play a role. The current is only limited by the real resistance of the electrolyte contained between the multilamellar membranes especially within the corneocytes.

One approach to analyzing impedance spectra involves fitting the spectrum to the Cole–Cole equation (23), which accounts for distributed characteristic times. However, the parameters of the Cole–Cole equation lack a clear assignment to structural features of the skin and therefore is of less use for mechanistic interpretation.

Using a better approach, passive electrical properties are presented in terms of an equivalent circuit, consisting of real electrical elements like resistors and capacitors. A very simple equivalent electrical circuit which could describe the electrical behavior shown in **Fig. 1** would contain a resistor for the DC path and a capacitor in parallel for the membrane capacitance. This however could not account for the resistance seen at high frequencies. Another resistor in series with the capacitor can appropriately model the direct pathway crossing membrane structures and electrolyte reservoirs like hydrated corneocytes. In **Fig. 2**, this three-element equivalent electrical circuit is shown together with its locus diagram. The locus diagram, which plots the imaginary versus the real part of the impedance, is a standard representation of electrical properties of cells and tissues.

The locus diagram of the three-element equivalent circuit is an ideal half circle (**Fig. 2**). However, the diagram for real skin has a different shape, because stratum corneum is not as homogeneous as the equivalent circuit models. The three-element circuit models a material with just one characteristic frequency, but experimental data from skin show at least two characteristic frequencies: ~ 50 kHz, which is believed to be associated with pathways directly across the stratum corneum (pathway 2B in **Fig. 3A**) and ~ 1 kHz which is thought to be due to tortuous pathways (pathway 2A in **Fig. 3A**). Therefore the locus diagram of skin is better approximated by a five-element circuit (**Fig. 3B**) with two characteristic frequencies, which appears as the sum of two half circles on a locus diagram (**Fig. 2B**) (21). However, the analysis is more complex and therefore for simplicity all analysis in the methods described below will be based on using the three-element circuit.

In previous studies of skin electrical properties (30,31), most investigators have focused on the low frequency behavior or just DC resistance of the skin, since these properties are associated with the transport pathways for most drugs. If the skin is electroporated and thereby new pathways are created across

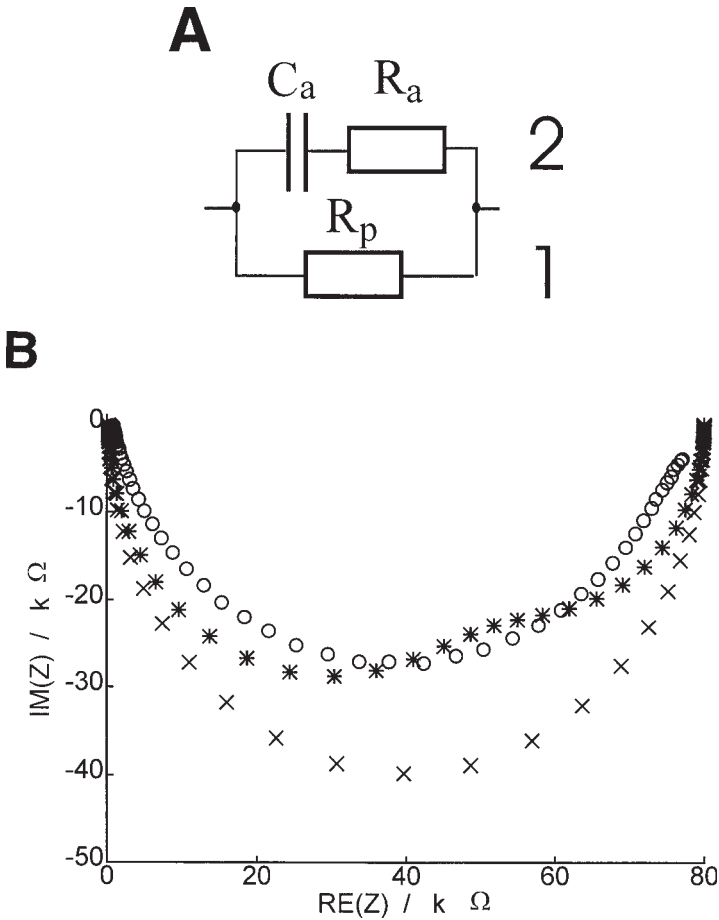


Fig. 2. (A) Simple equivalent electrical circuit of the stratum corneum. R_p represents the resistance of the dc-path (path 1) across the stratum corneum (e.g., via appendages), R_a represents the electrolyte between membrane structures (e.g., inside the keratinocytes), and C_a is the capacitor modeling the intercellular bilayer membranes (path 2). (B) A locus diagram for impedances measured over a frequency range of 10 Hz to 1 MHz for: (x) the ideal circuit shown in (A), (*) the ideal 5-element circuit shown in Fig. 3B, and (o) experimental measurements on human stratum corneum. The 5-element circuit provides a better model of measured stratum corneum electrical properties.

the skin, these pathways shunt the existing DC pathways which can drop skin's DC resistance by orders of magnitude (21). This resistance drop is due to increased ionic transport and may be correlated with increased skin permeability to drugs (32). If skin's electrical properties are also monitored at high

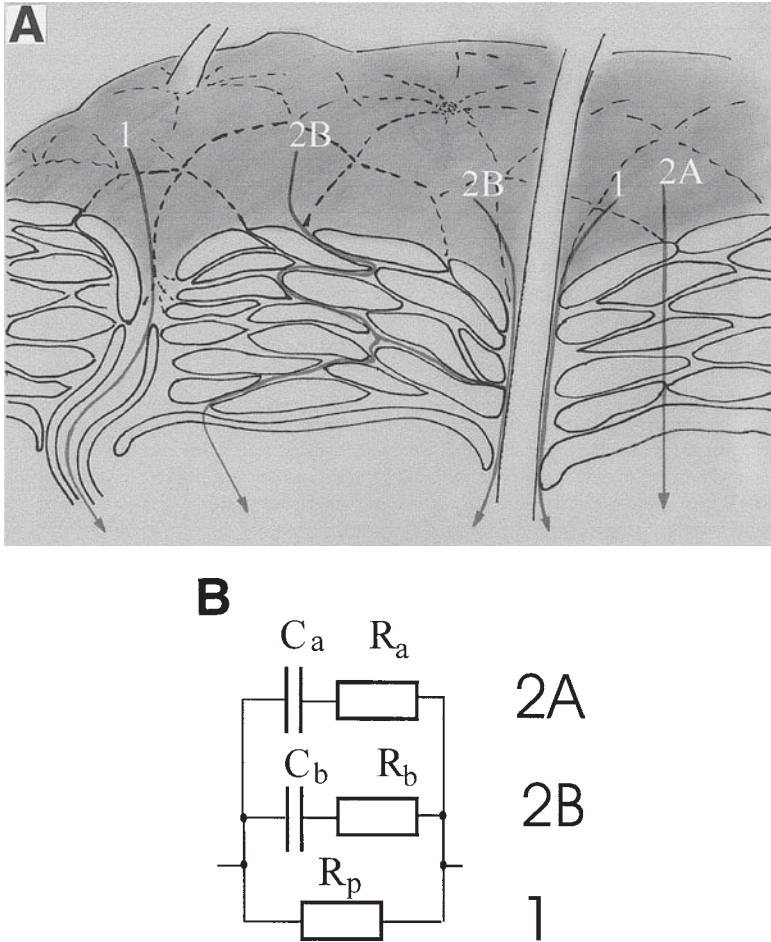


Fig. 3. (A) Schematic of pathways across the stratum corneum and (B) the equivalent circuit which describes these pathways. Pathway 1 represents the DC-path mainly through appendages (R_p). Pathway 2A represents the direct route through keratinocytes and intercellular lipid structures (R_a , C_a). Pathway 2B represents the tortuous route through water-rich layers between the intercellular lipid sheets (R_b , C_b). The tortuous route can also involve the crossing of lipid layers and the walls of appendages.

frequency, changes in impedance suggest other changes in skin structure not related to permeability (capacitive properties).

1.2. Impedance Measurements in Frequency and Time Domain

Impedance measurements can be made in the frequency or time domain. Frequency domain-based measurements are more accurate but slower, while

time domain-based measurements sacrifice some accuracy for speed of the measurements. In the frequency domain the real and the imaginary parts of the impedance are determined sequentially over a range of different frequencies (24,33). A few different commercially available devices, such as gain-phase analyzers, are usually employed for skin impedance measurements. Typically, tens of frequencies between approximately 5 Hz and 10 MHz are scanned, which requires tens of seconds to minutes. For this reason, frequency domain measurements are far too slow for following the fast changes in passive electrical properties of electroporated skin.

Time domain measurements provide a much faster method in which a broad band signal, such as a rectangular wave, is applied to the skin and its deformation is then measured (Fig. 4) (33). If the skin did not have energy-storing (i.e., capacitive) structures like membranes, the response signal would have the same shape as the excitation (i.e., both rectangular waves). However, the skin does have membrane structures which act as capacitors. Because charging these membranes is a time-consuming event, the voltage across the skin is deformed (Fig. 4B,C). If the applied rectangular wave and the measured deformed signal are both measured over time, collected with a digital oscilloscope, and fed to a computer which can perform a fourier transform, then these time-domain signals can be converted to the frequency domain using standard engineering calculations (34,35). With the algorithms described in this chapter, the resistance and capacitance values for the elements of a simple equivalent circuit (Fig. 2) can be directly calculated from the deformed time-domain signal (Fig. 4).

1.3. Changes in Skin Resistance During a High-Voltage Pulse

Skin impedance is defined only for materials with linear electrical properties (i.e., the resistance does not depend on the applied voltage) (36). Because skin resistance is known to drop during high-voltage exposures, it is impossible to directly measure skin resistance during a high-voltage pulse. However the “apparent” resistance (quotient of voltage and current, $R' = U/I$) can serve as a useful parameter to describe the effects of skin electroporation. In a semirigorous way, the “apparent” resistance during a pulse can be used, for example, to follow the onset and evolution of electroporation. For more sophisticated studies, calculating the dynamic resistance, $R_{dy} = \Delta U/\Delta I$, is the better approach (21), which is beyond the scope of this chapter.

2. Materials

2.1. Skin Preparation

Three types of skin preparation can be used; all work well for skin impedance measurements. However, concurrent flux or microscopy experiments may determine the best preparation to use. Full thickness skin is the easiest, since

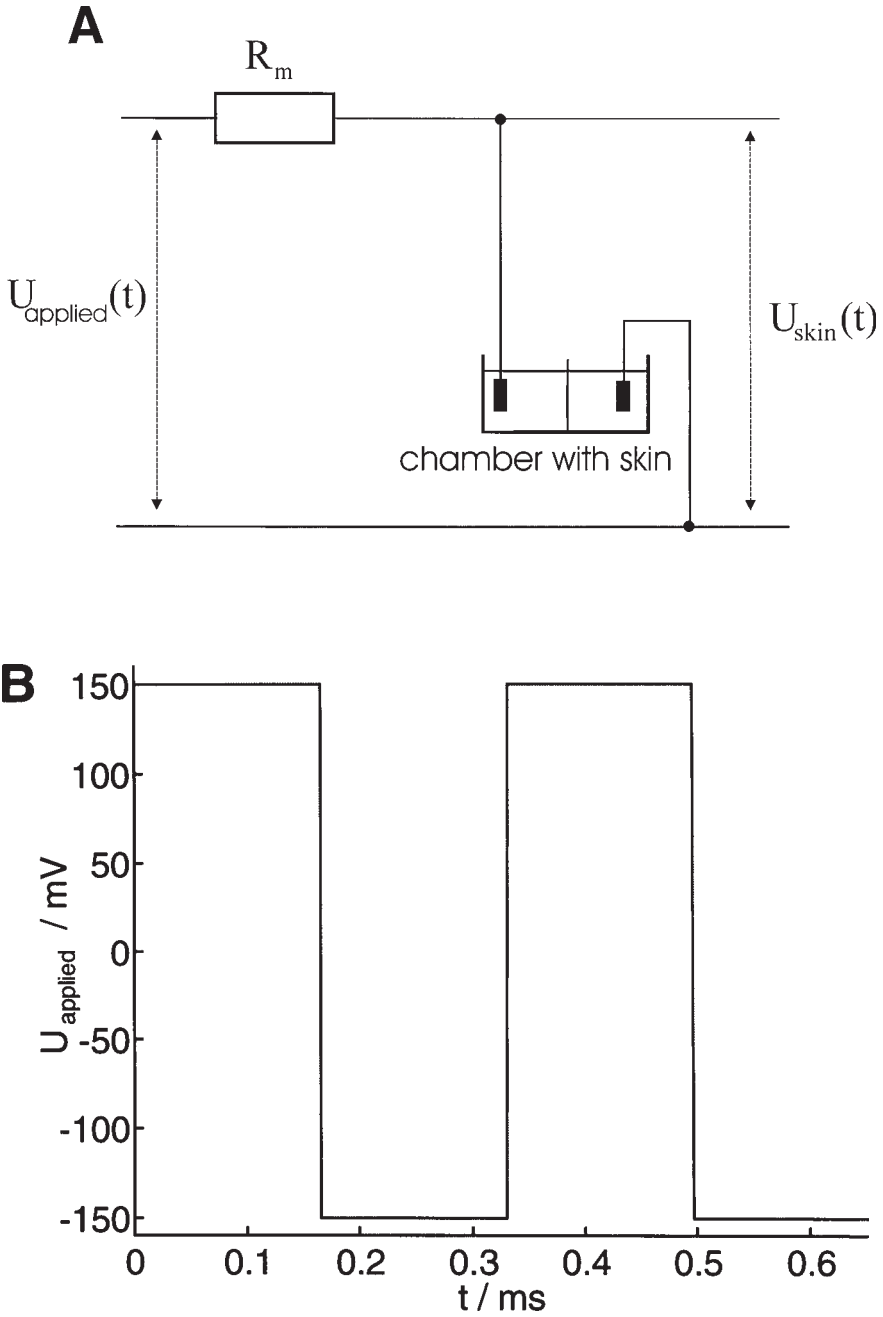


Fig. 4. Apparatus and representative signals for measuring skin electrical properties in the time domain. (A) The apparatus includes a measuring resistor (R_m) in series with a chamber containing skin. (B) A rectangular wave [$U_{\text{applied}}(t)$] is applied

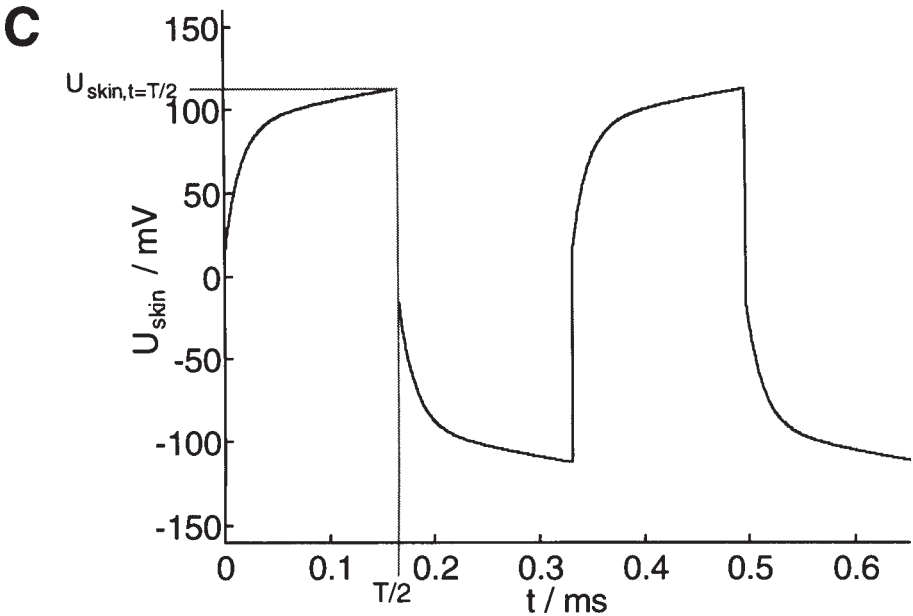


Fig. 4 (*continued*) and (C) the transdermal voltage [$U_{\text{skin}}(t)$] can be measured. These time domain measurements can be analyzed to yield values for the electrical circuit elements shown in **Fig. 3**.

little preparation is required, but the presence of the dermis may be problematic for microscopy and flux studies. Heat-separated epidermis is commonly used for flux studies, since it removes the complication of molecule binding within the dermis. Isolated stratum corneum can also be used and is especially useful for microscopy studies, where the presence of epidermis may impede clear viewing of the stratum corneum, but this tissue is quite fragile. Viable skin may be needed for some studies, but is not required for impedance measurements. Human skin is often obtained from cadavers or surgical procedures. Animal skin, such as hairless mouse or pig skin, is obtained from laboratory animal suppliers or slaughter houses. Skin stored at -70 , -20 , or 4°C can usually be kept for months, weeks, or days, respectively (37,38).

2.1.1. Full-Thickness Skin

1. Scrape fat from the bottom of the dermis using a scalpel handle or other blunt object.

2.1.2. Heat-Stripped Epidermis

See **ref. (37)**.

1. Scrape fat from the bottom of the dermis using a scalpel handle or other blunt object.
2. Soak skin for 2 min in a 60°C water bath using gentle stirring.
3. Place skin dermis-side down onto an absorbent piece of paper so that it does not roll up or slide around.
4. Using a rounded spatula or similar object, scrape off the epidermis from the dermis. This is best done by starting at one edge of the skin and vigorously scraping until the epidermis begins to separate. Then, more gently work across the skin surface, slowly scraping with small, firm strokes.
5. Place the isolated epidermis onto the surface of a room-temperature water bath and allow it to spread out. Because stratum corneum is hydrophobic and viable epidermis is hydrophilic, it will naturally spread itself with the stratum corneum side up.
6. Dip a piece of heavy waxy paper, such as some commercially available benchtop liner, into the water bath and underneath the spread epidermis. Slowly raise the paper to the surface and remove the epidermis, which should be spread across the paper's waxy surface. The use of paper keeps the epidermis from balling up and the waxy coating keeps the epidermis from sticking to the paper.
7. Cut epidermis (while still on the waxy paper) into pieces of appropriate size for use in subsequent experiments. This can be done simply with scissors, but using a hammer and punch may be easier.
8. Epidermis can be used right away or stored in the refrigerator in a moist (e.g., 95% humidity) environment.

2.1.3. Isolated Stratum Corneum

See **ref. (39)**.

1. Place heat-stripped epidermis on the waxy side of a piece of heavy waxed paper with the stratum corneum side down.
2. Soak the skin in a 2% trypsin solution at room temperature over night.
3. With forceps peel away residual pieces of tissue and then rinse away the rest of the digested tissue using deionized water squirted from a wash bottle. Gently hold the stratum corneum to the waxy paper so it does not get washed away too. Note that the pigment associated with the skin washes away with the viable epidermis. The remaining stratum corneum is very thin (10–20 μm), fragile, and transparent.

2.2. Measurement Chamber

Commercial glass chambers (Permegear, Riegelsville, PA) consist of two horizontal compartments (donor and receiver) (**Fig. 5**), filled with well-stirred saline. Each can hold two electrodes for pulse application and electrical

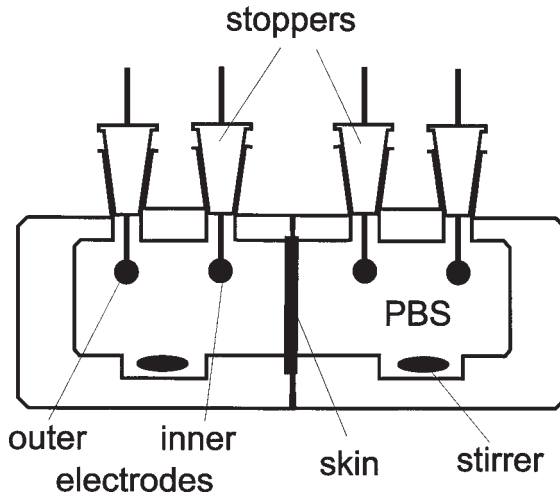


Fig. 5. Side-by-side permeation apparatus for clamping and bathing the skin specimen during electrical measurements. Four electrodes are held in place using Teflon stoppers as holders. The outer electrodes are used to apply electrical stimuli, while the inner electrodes are used only to make measurements. The skin is bathed on both sides by well-stirred saline. A water jacket surrounding the apparatus provides temperature control.

measurements. For the purpose of continuous sampling the receiver compartment can have flow-through capabilities. A water jacket allows temperature control.

2.3. Electrodes

Four electrodes should be used: a pair of inner electrodes and a pair of outer electrodes (Fig. 5). The inner electrodes should be made of Ag/AgCl (e.g., In Vivo Metric, Healdsburg, CA) and are used only as sensing electrodes (i.e., almost no current passes through them). The outer electrodes for pulse application or current electrode in a four electrode impedance measurement interface are preferably made from silver, carbon or stainless steel. They should be physically stable and as large as possible. If the transport of fluorescent molecules is monitored at the same time, silver electrodes or protected electrodes (gel or flow) should be used to help prevent loss of fluorescence due to electrochemical by-products (40).

2.4. Saline

Physiological phosphate buffered saline, pH 7.4, is preferred, since the skin impedance is slightly affected by pH-changes.

2.5. Electrical Devices

2.5.1. Digital Oscilloscope

A digital oscilloscope (DSO) (e.g., HP 45601, Hewlett Packard) is needed for capturing the waveforms. The choice is not critical, since a large variety of DSOs are on the market. It should have at least two channels with a minimum bandwidth of 100 MHz. For transferring the data to a computer either a RS232 or IEEE-488 (HPIB) interface is necessary. An RS232 port is standard equipment on a computer but it is slow. By contrast, IEEE-488-interfaces are much faster, but must be purchased as separate plug-in cards.

2.5.2. Function Generator

To apply the signals for time domain based impedance measurements a square wave generator (e.g., HP 8116A, Hewlett Packard, Palo Alto, CA) is needed. The rise time of the signals should be less than 100 ns and the output voltage range between 0.01 and 1 V (minimum). The minimum upper frequency limit should be 10 MHz and the output impedance 50 Ω . The requirements for the generator are met by most commercial devices.

2.5.3. Computer

An IBM-compatible computer is preferred, since there is a wide range of software for transferring data from external devices to PCs. The capabilities of the computer depend on the requirements of the user. If more sophisticated programs (e.g., Matlab 5, The MathWorks, Natick, MA), are used for data analysis a Pentium based computer is needed. For fast data transfer from the DSO to the computer a IEEE-488-interface should be added (i.e. HP82341D, Hewlett Packard, Palo Alto, CA). Software for capturing curves from the oscilloscope into a PC-compatible computer can be obtained from a number of different suppliers (e.g., Hewlett Packard) or can be relatively easily written by someone with a programming background.

3. Methods

3.1. Chamber Setup

Impedance measurements are usually performed in a standard permeation apparatus which holds the skin between two chambers filled with saline (**Fig. 5**) (7). The apparatus is temperature-controlled, the saline is well stirred, and electrodes are provided on either side of the skin to make the electrical measurements. A side-by-side (i.e., horizontally oriented) permeation apparatus is preferable, because it provides easy access for electrodes.

1. Attach tubing to the water jacket inlets and outlets on the permeation apparatus and to a temperature-controlled water bath. Start water flowing through the tubing. It is better to hook up the tubing and remove air bubbles from the system before mounting the skin, because the movement associated with attaching tubing to the apparatus can damage the skin. Usually a temperature of 37°C (body temperature) or 32°C (estimate of skin surface temperature) is used. In some experiments, temperature control is not used for convenience. Although there can be highly localized heating within the skin during an electroporation pulse, the overall temperature rise within the saline due to Joule heating is minimal (<1°C) (41).
2. Mount the skin onto the surface of one of the permeation chambers. This is easy if full thickness skin is used, but can be difficult if epidermis or stratum corneum is used. The skin sample should be resting on a small piece of waxy paper (*see Subheading 2.1.*). Slip one arm of a pair of forceps between the skin and the paper and grab the paper with the forceps. Then place the skin and paper, with the paper side down, onto the permeation chamber surface. Apply gentle pressure with a gloved finger to the skin resting on the permeation chamber on the side opposite that of the forceps. Finally, pull the waxy paper out from under the skin, leaving the skin resting on the permeation chamber. The stratum corneum side of epidermis should be facing up.
3. Place the two chambers (one of which has skin mounted onto it) which make up the permeation apparatus into a clamp holder. Be sure to have opened the clamp so that there is a gap of a few millimeters or more between the chambers. Once the two chambers are in place and aligned, press them together and firmly hold the chambers next to each other while tightening the clamp holder. The clamp should be tight, but be careful not to damage the permeation apparatus.
4. Add saline to each chamber of the permeation apparatus. Fill each chamber equally, so that no pressure gradient is created across the skin, which can stretch it and thereby cause a drop in resistance.
5. Add stir bars and place the apparatus onto a magnetic stirrer. Allow to sit for about an hour to allow the skin to fully hydrate before performing experiments.
6. Insert electrodes into the ports of the permeation apparatus. Four electrodes should be used: a pair of inner electrodes and a pair of outer electrodes (**Fig. 5**). The inner electrodes are used only as sensing electrodes (i.e., almost no current passes through them). The outer electrodes are used for application of high-voltage pulses for electroporation, as well as lower voltage rectangular waves for impedance measurements utilizing a four electrode interface. These electrodes need to be capable of passing high current densities. All electrodes need to be reproducibly positioned within the apparatus. This can be facilitated by mounting the electrodes on teflon stoppers which fit into the permeation apparatus ports.
7. Make preliminary resistance measurements with a standard ohmmeter to be sure the skin barrier is intact, or, preferably, with a device in which the measurement

voltage can be controlled ($\ll 1$ V, since larger voltages lower skin resistance) and electrode polarization can be avoided by making the measurement with a low frequency (e.g., 10 Hz) alternating current signal. Skin resistivity should be at least $50 \text{ k}\Omega \text{ cm}^2$; a lower resistance suggests that the skin is “leaky” and should not be used.

3.2. Prepulse and Postpulse Skin Impedance Measurement

Skin impedance measurements can be made using just a few pieces of commercially available equipment: a function generator, a digital oscilloscope with computer connection for transferring data, a resistor ($R_m \approx 10 \text{ k}\Omega$) and a computer (21).

1. Connect the output of the function generator (i.e., from the inner wire of the coaxial cable) to channel 1 of the oscilloscope and to one of the inner electrodes of the permeation apparatus via the $10 \text{ k}\Omega$ resistor (**Fig. 6**). Channel 2 of the oscilloscope connects to the point between the resistor and the permeation apparatus. It is unimportant how the skin is oriented within the chamber. The outer shield of the coaxial cable from the function generator, the ground clips from both channels of the oscilloscope and the other inner electrode in the permeation chamber should all be connected to ground. In all cases the resistance of the ground connections should be as small as possible. In this way, channel 1 measures the voltage applied by the signal generator (U_{applied}) and channel 2 measures the voltage across the skin (U_{skin}). Actually, channel 2 measures the voltage across the skin and across the saline between the electrodes and the skin. For pre- and post-pulse analysis, the voltage across the saline can be neglected. However, as described below, this must be accounted for when making measurements during a pulse when skin resistance is much lower.

Note that this measurement circuit should not be connected during application of a high-voltage pulse, because the high voltage can damage it. It should only be connected before and after the pulse. To obtain measurements within milliseconds after a pulse, an automated high-voltage relay should be used to switch from the pulse application circuit to the measurement circuit. Switching by hand can be performed if time resolution is less important.

2. Set the function generator according to the following guidelines:
 - *Signal shape*: Although the only requirement for the signal is it have a high bandwidth (i.e., a broad range of frequency components), use of a rectangular wave is recommended for easy data processing. Since the range of characteristic times of the skin are $100 \mu\text{s}$ or longer, the rise and fall time of the signal must each be $100 \mu\text{s}$ or shorter, which is not a problem, since virtually all modern function generators are faster than that. For easier data processing a symmetric wave form is preferable (i.e., the positive and negative portions of the signal are mirror images, such as the curve in **Fig. 4B**).

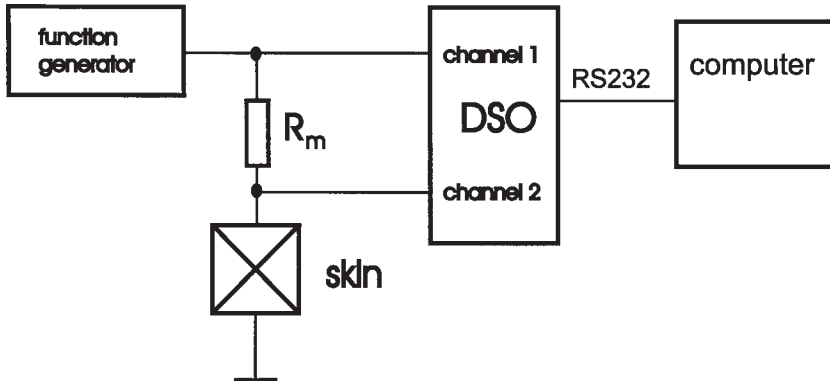


Fig. 6. A function generator provides a voltage across a measuring resistor (R_m is usually 10 k Ω) and the skin chamber. For an applied voltage step the voltage across the skin will be deformed (e.g., as shown in Fig. 4C or Fig. 7) due to charging of capacitive structures in the skin.

- *Amplitude:* The amplitude of the rectangular wave should be between 100 and 500 mV with no offset (i.e., no dc-component). Lower voltages give noisy signals, but higher voltages can alter skin resistance. For low frequency measurements, a few hundred millivolts can lower skin resistance, while larger voltages are required for measurements at higher frequencies.
- *Frequency:* Choice of frequency depends on three parameters. First, even reversible electrodes (e.g., Ag/AgCl) show electrode polarization, which becomes important at frequencies below about 50 Hz. Thus, higher frequencies should be used. Second, time resolution of measurements is limited by the frequency selected: higher frequencies are again preferred, since faster measurements can be made. And third, information about all pathways across skin (Fig. 3) can only be obtained with measurements whose frequency is close to or less than skin's characteristic frequencies (i.e., 1 and 50 kHz for unelectroporated skin; see Introduction). Thus, measurements at 300 Hz are a good compromise which is fast enough to avoid electrode polarization, fast enough to provide time resolution on the order of 10 ms and slow enough to give information about the full impedance spectrum which is relevant to transdermal pathways. For measurements made during the first milliseconds after an electroporation pulse, a higher frequency (e.g., 6 kHz) may be useful, since it can better follow the rapid kinetics of initial skin recovery and still provide the complete relevant spectrum, since skin's characteristic frequencies are higher after electroporation.
- If the HP 8116A function generator is used, choose the following representative settings:

mode	normal
control (CTRL)	nothing selected
frequency (FRQ)	1.25 kHz
voltage (AMP)	200 mV
duty cycle (DTY)	50 % (automatically, when square wave selected)
offset (OFS)	0 V
square wave	selected
AUTO,LIMIT,COML,DISABLE	off (LED not lighted)

- In general, choose the oscilloscope settings according to the following guidelines:
 - trigger*: After electroporation of skin, the signal to channel 2 (U_{skin}) can become very small. For this reason, the signal to channel 1 (U_{applied}) from the function generator should be used as the trigger. For example, for an applied signal of $U_{\text{applied}} = 200$ mV, the trigger should be set at the rising edge of channel 1 at about 50 mV.
 - display*: The vertical scale of the oscilloscope should be chosen so that at least two-thirds of the screen is covered by the signals. For example, for an applied signal of $U_{\text{applied}} = 200$ mV, the attenuation of both channels should be 50 mV/division. Note that because the signal from channel 2 can become small after electroporation, the attenuation should be chosen before pulses are applied. The horizontal display should be such that the trigger is placed at the first division line on the screen (i.e., 10% of the way across the screen). The horizontal scale should be selected based on the frequency of the applied rectangular wave. Since only one half (e.g., the positive half) of a wave is needed for analysis, the full screen should be a little larger than one half wave period. For example, for a frequency of 1.25 kHz (period of 0.889 ms), a horizontal attenuation of 50 μs / division is a suitable setting. These settings are important because they maximize the resolution of the data collected.
 - data storage and transfer*: If very fast time resolution is not important, data can be averaged by the oscilloscope (e.g., 8 or 32 times) for a better signal-to-noise ratio. Because the transfer of data from the oscilloscope to the computer is the slowest step in data capture, the number of points transferred to the computer should be minimized. Usually 100 data points per measurement are sufficient. An example of a curve transferred from an oscilloscope and stored in a computer is given in **Fig. 7**.
 - If the HP 54601 digital oscilloscope is used, chose the following settings. Channels 1 and 2 should be selected and the other channels should be off. Set both channels to 50 mV/division. Chose the trigger mode “auto” and the trigger at the rising edge of channel 1. If a horizontal delay before the trigger of 50 ms is chosen, a picture like **Fig. 7** should appear at the screen.
- As a final step, it is important to validate some measurements made on known circuits to be sure that the apparatus has been set up correctly. Build a circuit like the one shown in **Fig. 2A** using resistors and capacitors with values representa-

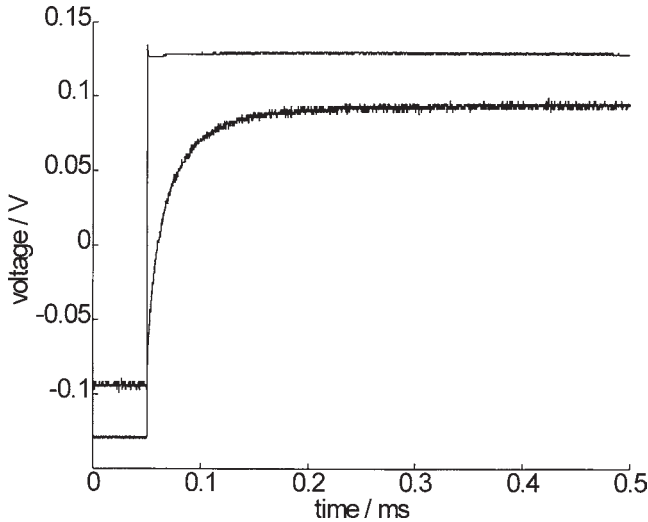


Fig. 7. Typical signal captured by the oscilloscope following electroporation of skin using the apparatus shown in **Fig. 6**. The step curve was recorded in channel 1 (U_{applied}) and the deformed curve in channel 2 (U_{skin}). The trigger appears at 0.05 ms. No averaging was used. The skin specimen was previously pulsed with $U_{\text{skin}} \approx 55$ V and $\tau = 1.1$ ms.

tive of skin (i.e., $R_p = 100$ k Ω , $R_a = 100$ Ω , $C_a = 10$ nF) (21). Collect the impedance spectra of the circuit and analyze the data as described in **Subheading 3.4**. The analysis should yield the correct circuit element resistance and capacitance values.

3.3. Apparent Skin Resistance Measurement During the Pulse

The actual resistance or impedance cannot be measured during a pulse, but the “apparent” resistance (see above) can provide a rough idea of the kinetics of changes in ionic pathways of skin during a high voltage pulse (21,42). Using this approach, three important parameters can be determined: (i) a characteristic voltage at which the skin resistance drops, which can be interpreted as the threshold voltage for creation of new ionic pathways, (ii) the extent and kinetics of changes in skin resistance caused by a high-voltage pulse, and (iii) the dependence of skin resistance on changes on the pulse rise time and peak voltage.

A high-voltage pulse and the simultaneous measurement of apparent resistance can be accomplished using a setup such as that shown in **Fig. 8**. A pulse is applied across the outer electrodes of the permeation apparatus in series with a low-resistance, high-power current sampling resistor (e.g., 5 Ω /50W). The voltage across the inner electrodes and across the series resistor are measured

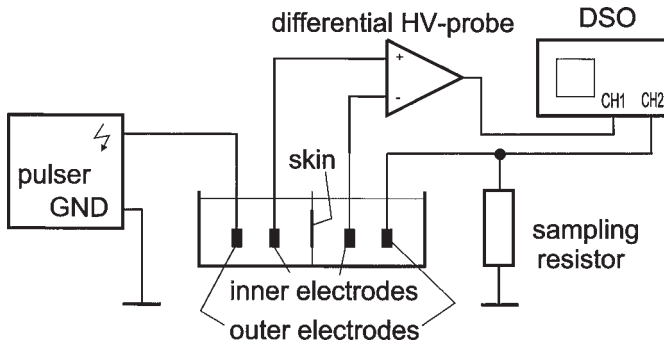


Fig. 8. Set-up for measuring the apparent resistance during a high voltage pulse. The pulser applies the voltage to the outer electrodes. A sampling resistor in series is used for current measurement (U_{sampling}), recorded at the second channel (CH2) of the digital oscilloscope (DSO). To measure the voltage across the inner electrodes (U_{inner}), a high voltage differential amplifier is used and U_{inner} recorded at channel 1 (CH1).

using a digital oscilloscope. The transdermal voltage and apparent skin resistance can then be calculated.

1. Apply a high voltage pulse across the outer pair of electrodes in the permeation apparatus. An exponential-decay or square-wave voltage pulse can be given using commercially-available equipment (e.g., BioRad, Richmond, CA; Genetronics, San Diego, CA; CytoPulse, Columbia, MD). For some applications, a pulse with a different wave form or a pulse of controlled current (rather than voltage) may be useful. However, commercially available equipment which delivers sufficient power may not be available for alternative wave forms or current pulses. The Notes section (*see Note 2*) below provides advice on how an experienced electrical engineer could build such a pulser.
2. Measure the voltage across the inner electrodes of the permeation apparatus (U_{inner}) using channel 1 of the oscilloscope. This should be done with a high-voltage differential probe (e.g., P5205, Tektronix, Wilsonville, OR). In the absence of a such a probe, two conventional 10 X probes can be plugged into channels 1 and 2 (of a four-channel oscilloscope) and the inner-electrode voltage determined using the oscilloscope's mathematical function feature which displays the difference between the two inputs (A-B). However, this is less accurate and may cause problems because it uses up two oscilloscope channels. This measurement needs to be collected in single-shot mode (i.e., no averaging).
3. Measure the voltage across the current sampling resistor (U_{sampling}), which can be done with a conventional probe (i.e., 10 X). This measurement needs to be collected in single-shot mode simultaneously with the inner electrode measurement.
4. Calculate the current during the pulse (I). Using Ohm's law, this is simply the quotient of the measured voltage across the current sampling resistor (U_{sampling}) and its resistance (R_{sampling}).

$$I = \frac{U_{\text{sampling}}}{R_{\text{sampling}}} \tag{1}$$

5. Calculate the transdermal voltage during the pulse (U_{skin}). The voltage across the skin during the pulse can be much less than that applied across the outer electrodes and therefore should be determined

$$U_{\text{skin}} = U_{\text{inner}} - IR_{\text{saline}} \tag{2}$$

6. R_{saline} is the resistance of the saline between the inner electrodes, which can be independently measured in a chamber without skin. Calculate the apparent skin resistance during the pulse (R'_{skin}).

$$R'_{\text{skin}} = \frac{U_{\text{skin}}}{I} \tag{3}$$

3.4. Skin Impedance Data Analysis

The impedance data collected before and after an electroporation pulse (*see Subheading 3.2.*) can be analyzed to yield the resistance and capacitance values for the elements of the equivalent electrical circuit of the skin. The analysis presented below is the easiest case, based on the three-element circuit shown in **Fig. 2A** and the apparatus shown in **Fig. 6**. Although the three-element circuit does not provide as complete a model as more complex equivalent circuits, it is adequate in many situations. A different, although similar, analysis would be needed if any other equivalent circuit or apparatus is used (*see Note 1*).

1. The analysis can be performed using data collected over the time scale of a half period of the applied rectangular wave (e.g., only the positive portion of a complete wave, from $U_{\text{skin}}(t = 0)$ to $U_{\text{skin}}(t = T/2)$, where T is the period). According to the model proposed in **Fig. 2A**, the voltage across the skin (U_{skin}) in response to a rectangular wave applied to the apparatus (U_{applied}) can be described as exponential

$$U_{\text{skin}}(t) = A_0 - A_1 e^{t/\tau} \tag{4}$$

where A_1 and τ are the fitted parameters of the exponential function associated with the pathway involving a capacitive element (pathway 2 in **Fig. 2A**), and A_0 is the fitted parameter associated with the DC-pathways across skin (pathway 1 in **Fig. 2A**). Use standard curve-fitting algorithms [e.g., downhill simplex or least squares (43)] to determine the values of the three unknowns in the equation. Calculate the three elements of the electrical equivalent circuit (**Fig. 2A**) as follows.

2. Calculate the resistance of the parallel resistor (R_p) directly from

$$R_p = \frac{R_m A_0}{(U_{\text{applied}} - A_0)} \tag{5}$$

where R_m is the resistance of the measuring resistor in **Fig. 6**. To make further calculations simpler, R_{mp} is introduced as the equivalent resistance of the parallel combination of R_m and R_p .

$$R_{mp} = \frac{R_m R_p}{R_m + R_p} \quad (6)$$

It may be interesting to note that A_0 and R_{mp} model a voltage source with an open circuit voltage of A_0 and an internal resistance of R_{mp} .

3. Calculate the rest of the elements (R_a , C_a) using the following equations.

$$R_a = \frac{2A_0}{A_1 + A_1 e^{-T/2\tau}} R_{mp} - R_{mp} \quad (7)$$

$$C_a = \frac{\tau}{R_a + R_{mp}} \quad (8)$$

Calculation of electrical properties as described above, or by any other method, assumes that the measurement method does not alter the measurement and that the measurement does not change within the time scale over which it is made. This will be the case as long as the voltage is kept sufficiently low (e.g., less than a few hundred millivolts applied at, for example, 1 kHz to human skin) and the skin properties do not change more quickly than the period of the measurement signal (e.g., 1 ms for 1 kHz).

3.4.1. Sample Results from Pre and Postpulse Resistance

Using the method described in **Subheading 3.4.** and the apparatus shown in **Fig. 6**, skin impedance was measured before and after an electroporation pulse, as shown in **Fig. 9**. Initially, skin resistance was high. After the pulse, skin resistance was lower and then showed significant recovery within seconds. To apply the high-voltage pulse without damaging the impedance apparatus, a high-voltage relay switched between the pulser and the measuring circuit. An end-of-pulse signal was generated by the pulser when the voltage fell to less than about 3 V, which triggered the relay to switch the impedance measuring circuit back on within 6 ms.

3.4.2. Sample Results from Apparent Resistance During the Pulse

As an example measurement of the passive electrical properties of skin during a high-voltage pulse, the transdermal voltage was measured during a current pulse (**Fig. 10**). Initially, there is a steep increase in voltage with increasing current, which is due to the high resistance of unelectroporated stratum corneum. At a transdermal voltage around 70 V, a dramatic change (kink) in the slope occurs (**Fig. 10B**), which corresponds to an order of magnitude drop in apparent skin resistance. In other experiments (data not shown), the kink in voltage occurred between 30 and 75 V, depending on the skin specimen and the temperature (4–37°C). This measurement was made using the protocol described in **Subheading 3.3.** and with a pulser described in **Note 2**.

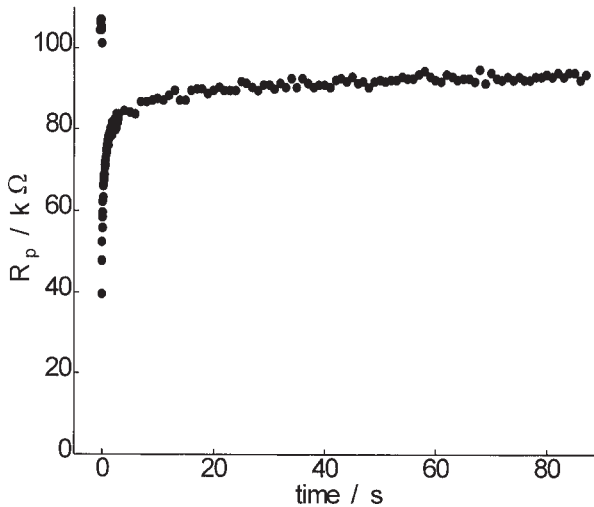


Fig. 9. Pre- and post-pulse impedance of human skin in vitro ($A = 0.69 \text{ cm}^2$). An exponential-decay pulse ($\tau = 1.1 \text{ ms}$) was applied at $t = 0$ with an amplitude of 500V across the outer electrodes, which yielded a voltage across the skin of about 65 V. Since the DC-resistance (R_p) is the most sensitive parameter it is the only one shown here.

4. Notes

1. VARIATIONS ON THE IMPEDANCE MEASUREMENT APPARATUS. The measurement circuit described in **Subheading 3.2.** uses a two electrode system (the outer electrodes are not used during measurement, but are employed only for the high-voltage electroporation pulses) to apply a voltage across the whole apparatus (chamber + R_{sampling}) and measure the voltage across just the chamber, which is approximately equal to U_{skin} . Three variations on this approach are summarized below.
 - a. To eliminate electrode polarization, which can be a problem for low frequencies used to access the behavior of skin close to DC, a four-electrode system may be needed (**Note 1.1, Fig. 11**).
 - b. For simplified data processing, a voltage can be applied across the skin and the current measured directly (**Note 1.2, Fig. 12**).
 - c. If very fast time resolution is needed, a less accurate, but more rapid method of data capture is described (**Note 1.3, Fig. 13**).

For each of these variations, a different, but similar, set of data analysis equations is needed.

- 1.1. FOUR ELECTRODE INTERFACE. A four-electrode system can be useful if the skin's characteristic frequencies are low (i.e., the characteristic relaxation times are long), because the electrodes in a two-electrode system will become polarized during a long period of stationary voltage (**44**), which introduces error.

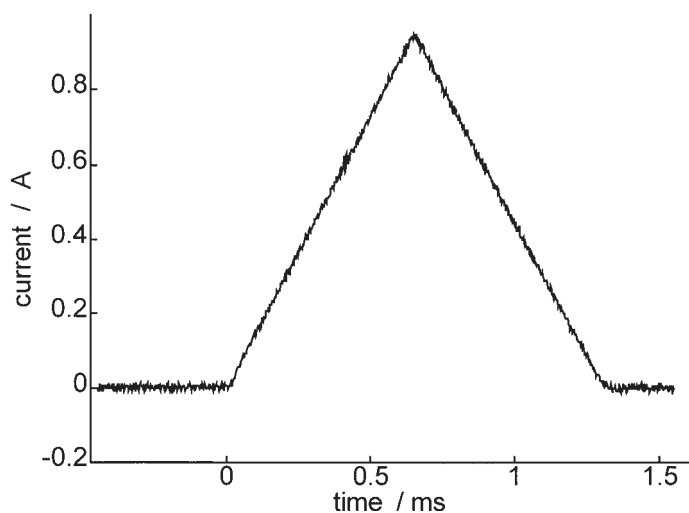
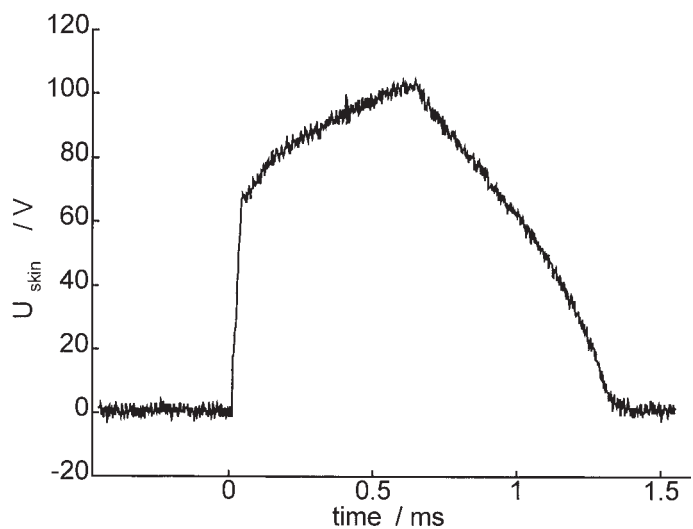
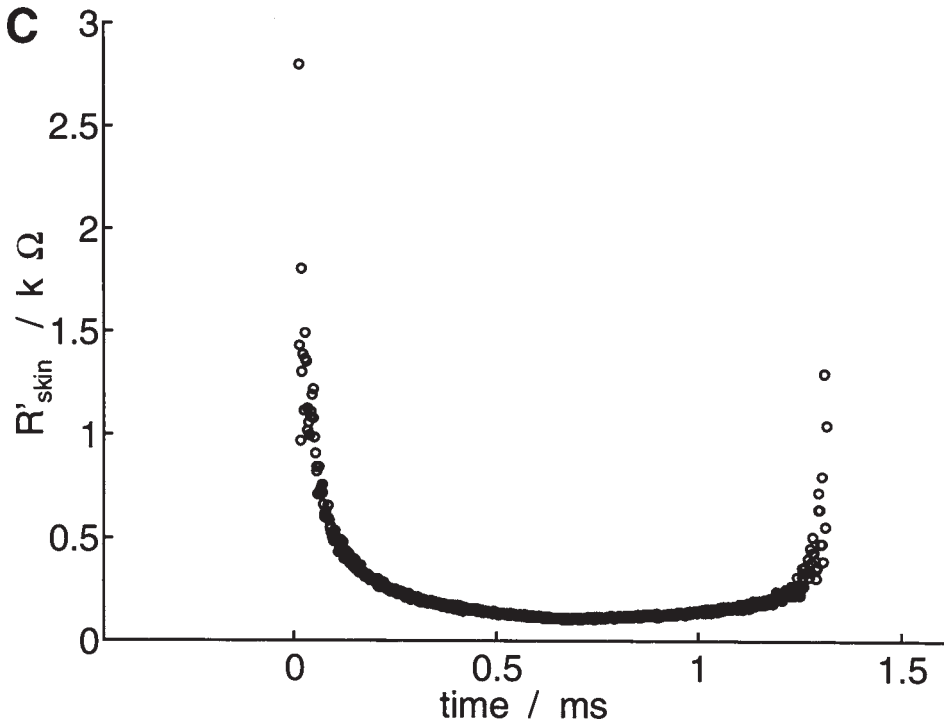
A**B**

Fig. 10. Applied current ramp (A), measured transdermal voltage (B), and calculated “apparent” skin resistance (C) during a high-voltage pulse. Using a custom-designed high-power function generator described in **Note 2**, a triangle-shaped current pulse was applied to human skin (rising and falling ramp of $2 \times 10^3 \text{ A s}^{-1}$; temperature of 25°C). The transdermal voltage and apparent skin resistance are shown to exhibit non-linear behavior at $\sim 70 \text{ V}$, believed to be due to skin electroporation (data from **ref. 42**).



In this approach, a current is applied through the outer electrodes and the transdermal voltage is measured across the inner electrodes. A simple circuit which could be used for this measurement is shown in **Fig. 11**. This circuit needs to be well shielded, since the high input impedance of the instrumentation amplifier (IA) makes it especially susceptible to noise from 50 or 60 Hz lines.

- 1.2. **SIMPLE DATA PROCESSING.** Another simple approach for measuring skin impedance applies a voltage to the skin and measures the current through it (**Fig. 12**). The advantage of this design is the easy interpretation of the output signal. The skin resistance is simply equal to the transdermal voltage divided by the current. Compared to the design in **Fig. 6**, the bandwidth of the (-1)-amplifier needs to be much higher, which increases the noise of the system.
- 1.3. **MEASUREMENTS WITH GREATER TIME RESOLUTION.** Measurements with very fast time resolution are limited by transfer of data from the oscilloscope to the computer or, if that step is eliminated, by the limited memory available for storage by the oscilloscope. An alternative approach involves capture of only a few time points per waveform, which, if selected correctly, can be used to approximate the shape of the full curve (**Fig. 13**). A fast 12-bit analog-to-digital converter can be used to collect, for example, six individual measurements during each period of the applied rectangular wave. The data are

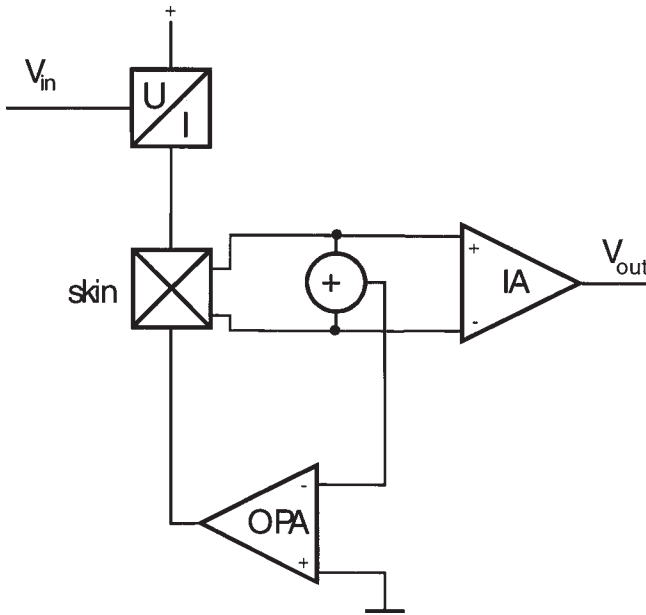


Fig. 11. Sample circuit for a four-electrode measurement system, which avoids problems of electrode polarization. A symmetric signal (e.g., rectangular wave) is fed into the voltage-controlled current source (U/I), which converts it into a current which flows through the outer electrodes of the skin chamber. The instrumentation amplifier (IA) measures the voltage drop across the skin measured with the inner electrodes. Since the measuring current is small ($< 10\text{mA}$), the voltage drop within the saline can be neglected. To avoid artifacts by a dc offset, the voltage drop across the skin is summarized (+) (integration time at each input $> 10\text{T}$) and used for a feedback loop (OPA). If the applied rectangular wave is symmetric, the output after summarizing is 0, which is used as balanced loop condition. Therefore the signal across the skin is maintained with a zero offset.

stored in a microcontroller and transferred to a computer afterward. The six sampling times should be chosen so that there are two from the initial rapidly changing part of the response curve (needed to establish one of the two time constants associated with skin), three from the slow changing part (needed for the other time constant and the dc properties) and one from the negative half-wave of the signal (used for offset correction). As an example, the frequency of the applied rectangular wave can be set to 3.8 kHz and the samples taken at 1.2, 4, 40, 80, and 120 μs during the first half of the applied rectangular wave and at $T/2$ plus 120 μs (i.e., at 383 μs) during the second half. In this way, the time resolution of the impedance measurement can be equal to that of the period of the applied wave (e.g., 0.26 ms for 3.8 kHz).

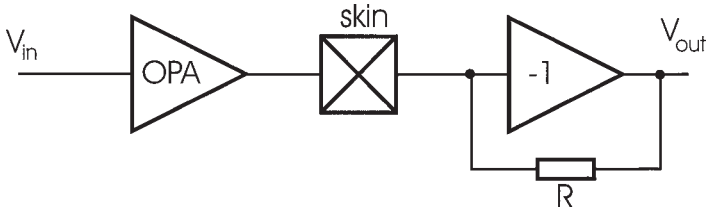


Fig. 12. Alternative design for an apparatus to measure skin impedance with simpler data processing. The applied signal is a voltage while the current through the skin is measured using the transimpedance ($R, -1$), which is a circuit that converts the measured current into a voltage output.

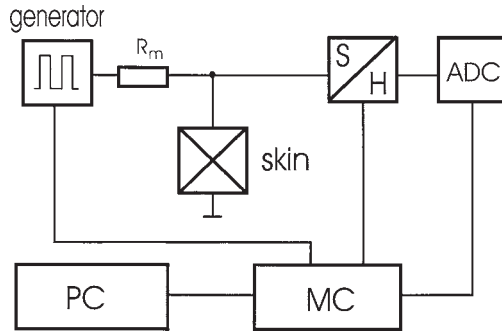


Fig. 13. Schematic of apparatus for very fast acquisition of skin impedance measurements, which is accomplished by minimizing data transfer by only saving measurements made at a few selected time points. The generator supplies a rectangular wave which is deformed by the skin (as in the system shown in **Fig. 6**). A microcontroller (MC) controls the sampling (sample & hold, S/H) of the signal. The digitized sample (using an analog-to-digital converter, ADC) is stored in the microcontroller and after the experiment transferred to a computer (PC).

The data processing involves first calculating the offset compensation using the mean value of the two $120 \mu\text{s}$ samples collected during the positive and negative half-waves. This offset compensation is especially important just after a high-voltage pulse, because the pulse leaves a charge on the skin for several milliseconds, which, if not compensated for, would introduce a significant measurement artifact. The five points from the positive half-wave are used for the data-fit which yields the constants in **Eq. 4**. An additional boundary condition for the data fit stipulating the existence of only positive coefficients is needed to eliminate meaningless results (e.g., negative time constants or resistors). Once the constants in **Eq. 4** have been determined, the analysis using the subsequent equations can be performed as described in **Subheading 3.4**.

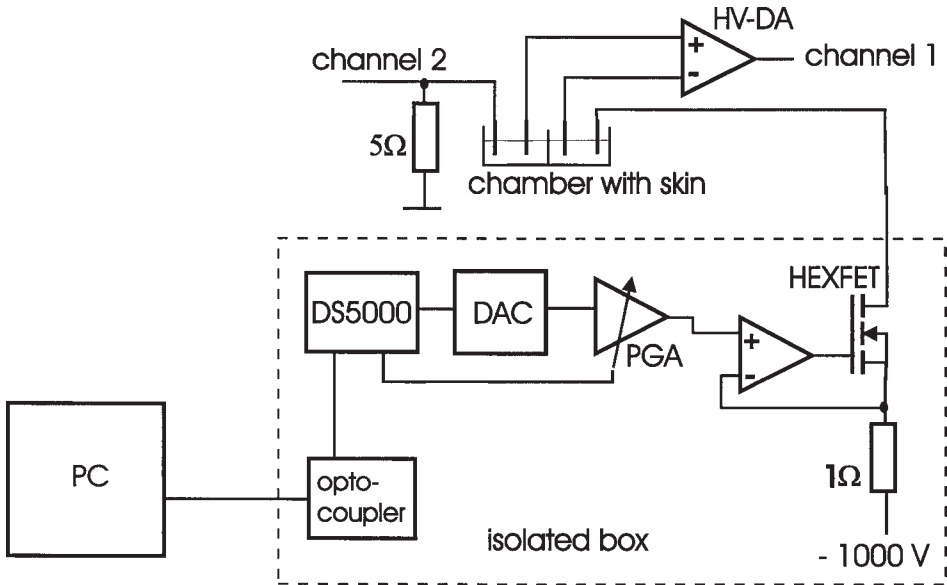


Fig. 14. Setup for the application of high-voltage signals of arbitrary wave form to skin. See text for explanation.

2. DESIGN OF APPARATUS FOR ALTERNATE WAVE FORMS OR CURRENT PULSES. Commercial equipment is available for applying exponential-decay and square wave voltage pulses (see above). However, we are not aware of equipment which can apply the large voltages needed for skin electroporation having other waveforms and or applying current pulses. Following is a guide to building such a pulser. Because of the dangers associated with this high-voltage apparatus, its construction and use are recommended only for experienced electrical engineers.

A suitable approach is to feed the output of an arbitrary function generator into a voltage-controlled current source which is able to deliver large currents (e.g., 4A) and voltage sweeps (e.g., 1000V) (42). As shown in Fig. 14, an optically insulated microcontroller (DS5000, Dallas Semiconductor) can be used together with a fast 8-bit digital-to-analog converter (DAC) to generate the control voltage for a current source made with a high-voltage HEXFET transistor. Since the pulses are short (i.e., milliseconds), the cooling of the transistor is not critical and the application of large currents should not damage the apparatus.

More specifically, an 8-bit microcontroller (DS5000) writes a word corresponding to the actual output current into the DAC (8-bit type, e.g., AD558). This signal is amplified using a programmable gain amplifier (PGA, e.g., AD603) to always use the full range of the DAC. The output is fed to a voltage-controllable current source consisting of a HEXFET (high-voltage, e.g., IRFPG50,

IRFBG30 or BUK4561000B), operational amplifier (many types are possible, e.g., TL081, AD844), and current sampling resistor (5Ω). To keep the system stable, the time constant of the current source should be set to $4\ \mu\text{s}$. This keeps the circuit from oscillating if large steps (i.e., 1 A) are applied. The arbitrary function generator is controlled by a personal computer (PC) via an optical coupler. The entire circuit is placed in an electrically-isolated box, which is important because it works entirely with respect to $-1000\ \text{V}$. The $-1000\ \text{V}$ and the power supply for the circuit are generated using a transverter circuit (standard circuit for switching power supply). A capacitor of $200\ \mu\text{F}$ (e.g., cascade of flash-light capacitors) buffer the high voltage.

The voltage across the inner electrodes is measured using a high-voltage differential amplifier (HV-DA). Either a homemade or commercial amplifier (e.g., P5202, Tektronix) can be used and connected to the first channel of a digital oscilloscope (e.g., TDS 540B, Tektronix). Using the second channel of the same oscilloscope, the current through the skin is obtained from the voltage drop measured across the current sampling resistor (5Ω).

Since it is critical to make the circuit electrically stable, the wiring should be as short as possible. To minimize wiring, the thermostated skin permeation chamber can be mounted directly on top of the waterproof electrical device.

For safety reasons, the entire apparatus should be electrically insulated and controlled only via an opto-coupled RS232-interface. Note that all of the arbitrary function generator circuitry works with respect to $-1000\ \text{V}$, which poses a significant safety hazard. A good ground connection is also important for safety. The core of the arbitrary function generator must be carefully isolated and made waterproof in case saline leaks out of the measuring chamber.

Using a device of this design, the minimum rise time of a current step of 1A was measured to be $4\ \mu\text{s}$. Shorter rise times are possible, but it made the system unstable due to wiring and electrode behavior. With this setup it is possible to apply functions such as current ramps having different rise times and current-controlled rectangular stimuli. The use of current pulses eliminates uncertainties associated with voltage drops at electrode interfaces within the measurement apparatus. It is however also possible to apply any kind of waveform by sending a stored byte array from the memory of the microcontroller to the DAC. For bipolar pulses, an electronic switch can be used, but a switching time of at least $6\ \mu\text{s}$ was required to prevent the system from becoming unstable for tens of microseconds.

References

1. Bouwstra, J.-A., Gooris, G. S., Weerheim, A., Kempenaar, J., and Ponc, M. (1995) Characterization of stratum corneum structure in reconstructed epidermis by X-ray diffraction. *J. Lipid Res.* **36**, 496–504.
2. Weaver, J. C. and Chizmadzhev, Y. A. (1996) Electroporation, in *CRC Handbook of Biological Effects of Electromagnetic Fields* (Polk, C. and Postow, E., eds.), CRC Press, Boca Raton, FL, pp. 247–274.

3. Chang, D. C., Chassy, B. M., Saunders, J. A., and Sowers, A. E. (1992) *Guide to Electroporation and Electrofusion*, Academic Press, New York.
4. Chizmadzhev, Y. A., Zarnitsin, V. G., Weaver, J. C., and Potts, R. O. (1995) Mechanism of electroinduced ionic species transport through a multilamellar lipid system. *Biophys. J.* **68**, 749–765.
5. Pliquett, U., Zewert, T. E., Chen, T., Langer, R., and Weaver, J. C. (1996) Imaging of fluorescent molecule and small ion transport through human stratum corneum during high-voltage pulsing: Localized transport regions are involved. *Biophys. Chem.* **58**, 185–204.
6. Vanbever, R., Lecouturier, N. and Preat, V. (1994) Transdermal delivery of metoprolol by electroporation. *Pharmacol. Res.* **11**, 1657–1662.
7. Prausnitz, M. R., Bose, V. G., Langer, R., and Weaver, J. C. (1993) Electroporation of mammalian skin: A mechanism to enhance transdermal drug delivery. *Proc. Natl. Acad. Sci. USA*, **90**, 10,504–10,508.
8. Moghimi, H. R., Williams, A. C., and Barry, B. W. (1996) A lamellar matrix model for stratum corneum intercellular lipids. I. Characterisation and comparison with stratum corneum intercellular structure. *Int. J. Pharmacol.* **131**, 103–115.
9. Champion, R. H., Burton, J. L., and Ebling, F. J. G. (1992) *Textbook of Dermatology*, Blackwell Scientific, London.
10. Vanbever, R., Fouchard, D., Jodoul, A., de Morre, N., Preat, V., and Marty, J.-P. (1998) In vivo noninvasive evaluation of hairless rat skin after high-voltage pulse exposure. *Skin Pharmacol.* **11**, 23–34.
11. Jadoul, A., Regnier, V., Duocet, J., and Preat, V. (1997) X-ray-scattering analysis of the stratum corneum treated by high voltage pulses. *Pharmacol. Res.* **14**, 1275–1277.
12. Jadoul, A., Tanajo, H., Preat, V., Spies, F., and Bodde, H. E. (1998) Electroperturbation of human stratum corneum fine structure by high voltage pulses : A freeze fracture electron microscopy and differential thermal analysis. *J. Invest. Dermatol. Symp. Proc.* **3**, 153–158.
13. Prausnitz, M. R., Gimm, J. A., Guy, R. H., Langer, R., Weaver, J. C., and Cullander, C. (1996) Imaging regions of transport across human stratum corneum during high voltage and low voltage exposures. *J. Pharm. Sci.* **85**, 1363–1370.
14. Nicander, I., Ollmar, S., Rozell, B. L., Eek, A., and Emtestam, L. (1995) Electrical impedance measured to five skin depths in mild irritant dermatitis induced by sodium lauryl sulphate. *Br. J. Dermatol.* **132**, 718–724.
15. Kontturi, K., Murtomaki, L., Hirvonen, J., Paronen, P., and Urtti, A. (1993) Electrochemical characterization of human skin by impedance spectroscopy: The effect of penetration enhancers. *Pharmacol. Res.* **10**, 381–385.
16. Emtestam, L. and Ollmar, S. (1993) Electrical impedance index in human skin: Measurements after occlusion, in 5 anatomical regions and in mild irritant contact dermatitis. *Contact Dermatitis* **28**, 104–108.
17. Nicander, I., Ollmar, S., Eek, A., Lundh Rozell, B., and Emtestam, L. (1996) Correlation of impedance response patterns to histological findings in irritant skin reactions induced by various surfactants. *Br. J. Dermatol.* **134**, 221–228.

18. Ollmar, S., Eek, A., Sundstrom, F., and Emtestam, L. (1995) Electrical impedance for estimation of irritation in oral mucosa and skin. *Med. Prog. Technol.* **21**, 29–37.
19. Kalia, Y. N., Nonato, L. B., and Guy, R. H. (1996) The effect of iontophoresis on skin barrier integrity: Non-invasive evaluation by impedance spectroscopy and transepidermal water loss. *Pharmacol. Res.* **13**, 957–960.
20. Craane van Hinsberg, W. H. M., Verhoef, J. C., Junginger, H. E., and Bodde, H. E. (1997) Electroperturbation of the human skin barrier in vitro (I): The influence of current density on the thermal behaviour of skin impedance. *Eur. J. Pharm. Biopharm.* **43**, 43–50.
21. Pliquett, U., Langer, R., and Weaver, J. C. (1995) Changes in the passive electrical properties of human stratum corneum due to electroporation. *Biochim. Biophys. Acta* **1239**, 111–121.
22. Prausnitz, M. R., Lee, C. S., Liu, C. H., Pang, J. C., Singh, T. P., Langer, R., and Weaver, J. C. (1996) Transdermal transport efficiency during skin electroporation and iontophoresis. *J. Controlled Release* **38**, 205–217.
23. Foster, K. R. and Schwan, H. P. (1989) Dielectric properties of tissues and biological materials: A critical review. *CRC Crit. Rev. Biomed. Eng.* **17**, 25–104.
24. McDonald, J. R. (1992) Impedance Spectroscopy. *Ann. Biomed. Eng.* **20**, 289–305.
25. Burnette, R. R. and DeNuzzio, J. D. (1997) Impedance spectroscopy: Applications to human skin, in *Mechanisms of Transdermal Drug Delivery* (Potts, R. O. and Guy, R. H., eds.), Marcel Dekker, New York, pp. 215–230.
26. Potts, R. O., Francoeur, M. L., and Guy, R. H. (1992) Routes of ionic permeability through mammalian skin. *Solid State Ionics* **53–56**, 165–169.
27. Bodde, H. E., Kruithof, M. A. M., Brussee, J., and Koerten, H. K. (1989) Visualisation of normal and enhanced HgCl_2 transport through human skin in vitro. *Int. J. Pharm.* **53**, 13–24.
28. Elias, P. M. (1988) Structure and function of the stratum corneum permeability barrier. *Drug Dev. Res.* **13**, 97–105.
29. Elias, P. M. and Menon, G. K. (1991) Structural and lipid biochemical correlates of the epidermal permeability barrier. *J. Adv. Lipid Res.* **24**, 1–26.
30. Craane van Hinsberg, W. H. M., Bax, L., Flinterman, N. H., Verhoef, J. C., Junginger, H. E., and Bodde, H. E. (1994) Iontophoresis of a model peptide across human skin in vitro: effects of iontophoresis protocol, pH, and ionic strength on peptide flux and skin impedance. *Pharmacol. Res.* **11**, 1296–1300.
31. Gersing, E., Hofmann, B., and Osypka, M. (1996) Influence of changing peripheral geometry on electrical impedance tomography measurements. *Med. Biol. Eng. Comput.* **34**, 359–361.
32. Pliquett, U. and Weaver, J. C. (1996) Electroporation of human skin: Simultaneous measurement of changes in the transport of two fluorescent molecules and in the passive electrical properties. *Bioelectrochem. Bioenerg.* **39**, 1–12.
33. Schwan, H. P. (1963) Determination of biological impedances. *Phys. Tech. Biol. Res.* **6**, 323–407.

34. Stanley, W. D. (1982) *Electronic Communications Systems*. Reston Publishing, Reston, VA.
35. Jong, M. T. (1982) *Methods of Discrete Signal and System Analysis*. McGraw-Hill, New York.
36. Horowitz, J. C. and Hill, F. R. (1980) *The Art of Electronics*. Cambridge University Press, Cambridge, UK.
37. Gummer, C. L. (1989) The in vitro evaluation of transdermal delivery, in *Transdermal Drug Delivery: Development Issues and Research Initiatives* (Hadgraft, J. and Guy, R. H., eds.), Marcel Dekker, New York, pp. 177–186.
38. Kasting, G. G. and Bowman, L. A. (1990) Electrical analysis of fresh excised human skin: A comparison with frozen skin. *Pharmacol. Res.* **7**, 1141–1146.
39. Tanojo, H., Roemele, P. E. H., Van Veen, G. H., Stieltjes, H., Junginger, H. E., and Bodde, H. E. (1997) New design of a flow-through permeation cell for studying in vitro permeation studies across biological membranes. *Controlled Release* **45**, 41–47.
40. Pliquett, U. and Gusbeth, C., Calcein as model for hydrophilic drugs, manuscript under review.
41. Martin, G. T., Pliquett, U., and Weaver, J. C., Temperature rising during tissue electroporation: Theoretical modeling, manuscript under review.
42. Pliquett, U. and Weaver, J. C., Passive electrical properties of human stratum corneum during application of electric fields, in *Electricity and Magnetism in Medicine and Biology* (Bersani, F., ed.), in press.
43. Press, W. H., Flannery, B. P., Teukolsky, S. A., and Vetterling, W. T. (1992) *Numerical Recipes in Pascal*. Cambridge University Press, Cambridge, UK.
44. Atkins, P. W. (1995) *Physical Chemistry*. Oxford University Press, Oxford, UK.

An In Vitro System for Measuring the Transdermal Voltage and Molecular Flux Across the Skin in Real Time

Tani Chen, Robert Langer, and James C. Weaver

1. Introduction

In many in vitro transdermal drug delivery experiments, the skin is placed within a permeation chamber, and measurements are taken every hour or so. However, during skin electroporation, significant molecular transport can occur within the first few minutes (*1*).

To take transdermal flux measurements more frequently, on the order of tens of seconds instead of hours, some degree of automation is required. In addition, the pulsing electrodes should be protected so that contamination of the donor and receptor compartments by electrochemical by-products does not occur. The pulser and the other electrical equipment require safety protection, in case of a short circuit. Finally, to facilitate comparisons with the literature (*2–5*), the high-voltage pulser should deliver high-voltage pulses every 5 s, with measurements of the transdermal voltage being recorded on a per-pulse basis. Such measurements are necessary since the voltage drop across the skin can vary significantly during the course of an experiment (*1,6*).

Building such a system with these capabilities is a significant task. The equipment and procedures described in this chapter allow pulsing to be applied continuously to the skin. The current and voltage across the skin are recorded on a per-pulse basis (with 1 pulse every 5 seconds), and the contents of the receptor compartment are continuously pumped through a spectrofluorimeter for real-time flux measurements, allowing this system to have a molecular transport time resolution of ~14 s. Sample data from this system can be seen in

ref. 1. This chapter describes, in detail, how to develop and use a system with these capabilities.

2. Materials

2.1. Solutions

The day before the experiment, prepare solutions 1 to 5 (solution 5, PBS, is needed to prepare solution 1). On the day of the experiment, prepare solutions 5 (again) and 6, since these solutions can not be stored and have to be used immediately.

1. Acrylamide monomer solution: 7.5 g of 19:1 acrylamide:bis(*N,N'*-methylene-bisacrylamide) powder (Bio-Rad, Hercules, CA) in 50 mL PBS (solution 5, below). Prepare and mix together in a fume hood (the monomer is carcinogenic). Let the solution stand for >12 h before using, to allow the monomer to fully dissolve. This solution can be prepared well in advance of the experiment; it will not polymerize without addition of the catalyst.
2. Stock mounting solution: 10 mg Nile Red (Molecular Probes) in 20 mL acetone (7). Wrap in aluminum foil to protect from light. This solution can be stored indefinitely if protected from light.
3. Final mounting solution: 7.5 mL glycerol in 2.5 mL deionized water. Mix thoroughly. Add 250 μL of the stock mounting solution (solution 2). Wrap in aluminum foil to protect from light. This solution can also be stored indefinitely if protected from light.
4. Acrylamide initiator solution: 0.3 g $(\text{NH}_4)_2\text{S}_2\text{O}_8$ in 3 mL H_2O . This solution can be stored for only a week.
5. Phosphate buffered saline (PBS): 0.4 g (1.1 mM) KH_2PO_4 , 0.4 g (2.7 mM) KCl, 2.3 g (8.1 mM) Na_2HPO_4 , 16.0 g (138 mM) NaCl (total of 150 mM) in 2.0 L deionized H_2O (see **Note 1**). Stir under vacuum for >30 min to remove dissolved gases from solution (see **Note 2**). Adjust to pH 7.4 with HCl and NaOH. This solution should be degassed immediately before use.
6. Donor solution: A typical donor solution consists of 1 mM of a fluorescent tracer in PBS. Examples of fluorescent tracers include lucifer yellow (457 Da) (**1,2**), calcein (623 Da) (**2,4,8**), and sulforhodamine (607 Da) (**4**) (all from Molecular Probes, Eugene OR). Wrap the solution immediately in aluminum foil to protect it from light (see **Note 2**). Gently shake on a Nutator for >30 min to ensure complete dissolution. This solution should be made immediately before use, right after preparing the PBS solution (solution 5).

2.2. Permeation Chamber with Four-Electrode System

The permeation chambers are custom-designed, side-by-side glass diffusion chambers (see **Note 3**) (Crown Bio Scientific, Somerville, NJ), with an outer water jacket (to maintain the temperature at 37°C) and an inner compartment (**Fig. 1**) (**9**). Ports extend from the inner compartment, through the water jacket,

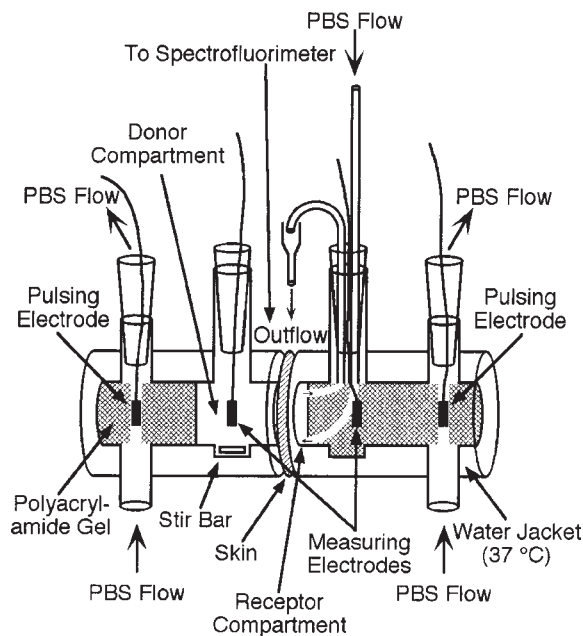


Fig. 1. Skin permeation chamber with flow-through sampling system. The two outer electrodes are used for pulsing, and the two inner electrodes are used to measure the voltage drop across the skin. PBS is pumped around the pulsing electrodes to remove any chemical by-products generated during pulsing. PBS is also pumped through the receptor compartment to a spectrofluorimeter for real-time detection.

to the outside, allowing direct access to the inner compartment. Each chamber half has one large port (for the measuring electrodes and the flow-through sampling system), with two smaller additional ports on the far ends (for placement of the electrodes and the flow-protection system around the electrodes). The volume of the inner compartment is ~ 3.1 mL, and the area of the circular opening is 0.64 cm² (0.9 cm diameter).

There are four electrodes in this system (**Figs. 1** and **2**). The two outer electrodes are used to apply pulses (see **Note 4**), and the two inner electrodes are used to measure the transdermal voltage. Due to limitations of space within the donor and receptor compartments, the electrodes are constructed to allow both electrical access and liquid flow to the chamber. Thus, there are three types of electrodes in this system: the donor measuring electrode, the receptor measuring electrode, and the pulsing electrodes (the same design is used in both the donor and the receptor compartments).

The electrodes are made from silver wire (see **Notes 5** and **6**), and the connectors are made from 200 μ L pipet tips (see **Note 7**), with assorted amounts

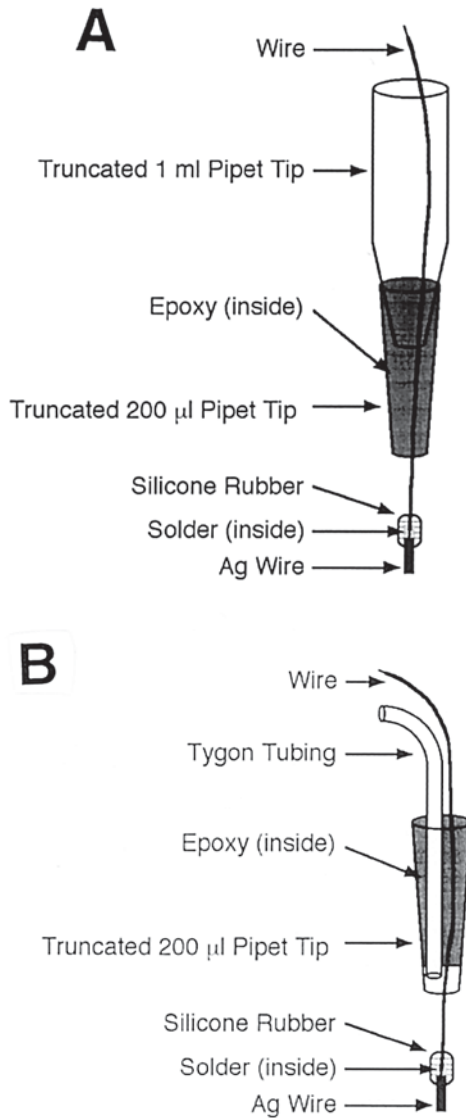
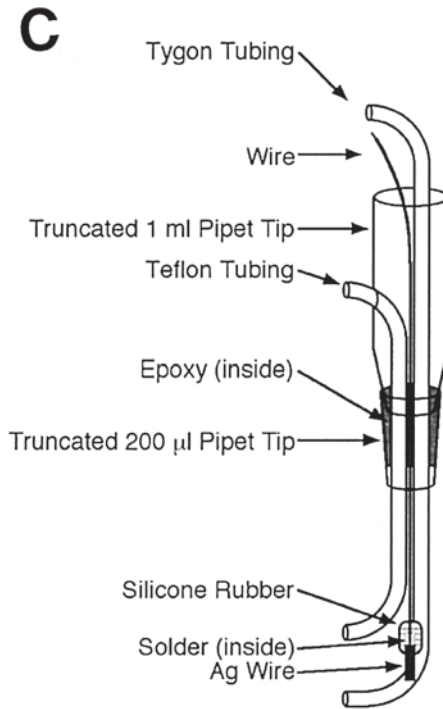


Fig. 2. Pulsing and measuring electrode construction. **(A)** Donor side measurement electrode. Only the silver wire electrode is exposed to the donor solution; the solder is encased in nonconducting silicone rubber. **(B)** Pulsing electrodes. This electrode is similar to the previous one, except a tube permits the flow of PBS around the electrode, allowing the removal of chemical by-products. **(C)** (*facing page*) Receptor side measurement electrode. Two tubes allow the flow of PBS into and out of the receptor compartment.



of tubing, all held in place by epoxy (Devcon, Wood Dale, IL). The fabrication of each of these electrodes is described below, in order of increasing complexity.

While the electrodes are generally reusable between experiments if sufficiently cleaned with fine-grain sandpaper, they should be periodically examined. Worn-out or broken electrodes should be discarded. The pulsing electrodes can typically survive about a month of intense use before wearing out; the measurement electrodes can last somewhat longer.

2.2.1. Donor Measurement Electrode Fabrication

The main requirement for this electrode is that it should not be able to move once it is snugly placed within the chamber (**Fig. 2A**).

1. Cut off a piece of pure silver wire, ~ 0.040 in. diameter, ~ 0.5 cm long.
2. Solder the end of the silver wire to a piece of copper bell wire, as shown in **Fig. 2A**.
3. Once the solder hardens, cover the solder (but not the silver wire) with nonconducting silicone rubber (General Electric, Waterford, NY). Use as little silicone rubber as possible, but make sure that the solder is completely covered. Wait for the silicone rubber to harden (~ 1 d).

4. Cut the end off a 200 μL pipet tip. The hole at the end of the pipet should be just large enough to accommodate the wire.
5. Insert the wire with the silver electrode up through the end of the pipet tip. The silver electrode should be placed so that when the pipet tip is placed snugly into the large port of the permeation chamber, the silver electrode is positioned in the middle of the chamber.
6. If the 200 μL pipet tip is smaller than the large port, it could get stuck inside. Thus, a “handle” is needed, so that there is a way to remove the pipet tip from the chamber (**Fig. 2A**). Cut the end off a 1-mL pipet tip so that the copper bell wire will just fit through the opening. Slide the electrode wire through this pipet tip.
7. Fill the 200- μL pipet with epoxy. Immediately insert the 1-mL pipet tip into the epoxy at the top of the 200- μL pipet tip. Hold everything in place until the epoxy cures, and verify that the silver wire does not move while the epoxy is curing.

2.2.2. Pulsing (Outer) Electrode Fabrication

Each pulsing electrode is designed to allow electrical pulses to be applied, as well as allowing a stream of PBS to flow around the electrode and out to a waste beaker (**Fig. 2B**). A separate port in the permeation chamber supplies fresh PBS to the pulsing electrode (see **Fig. 1**).

1. Cut off a piece of pure silver wire, ~ 0.040 in. diameter, ~ 0.5 cm long.
2. Solder the end of the silver wire to a piece of copper bell wire, as shown in **Fig. 2B**. Keep the solder to a minimum, since the entire electrode, when completed, must still fit within the small port of the permeation chamber.
3. Once the solder hardens, cover the solder (but not the silver wire) with nonconducting silicone rubber. Use as little silicone rubber as possible, but make sure that the solder is completely covered. This will ensure that the electrical pulses are delivered by only the silver, not the solder. Wait for the silicone rubber to harden (~ 1 d).
4. Cut the end off a 200- μL pipet tip. The hole at the end of the pipet should be slightly larger than the bell wire, so that there is room for PBS to flow around the wire.
5. Insert the wire with the silver electrode up through the end of the pipet tip, as shown in **Fig. 2B**. The silver electrode should be placed so that when the pipet tip is placed snugly into the small port of the permeation chamber, the silver electrode is positioned in the middle of the chamber.
6. Cut off a piece of Tygon tubing, $1/32$ in. ID, ~ 3 in. long. Insert it into the wider end of the pipet as far as possible, wedging the bell wire into place.
7. Fill the wider end of the pipet with epoxy, to fix both the tubing and the wire in place. The epoxy should completely seal off the end of the pipet. Make sure that the epoxy does not flow far enough into the pipet tip so that it covers the opening of the tubing, and verify that the wire and the tubing do not move while the epoxy is curing.

2.2.3. Receptor Measurement Electrode Fabrication

The receptor measurement electrode must allow PBS to flow into and out of the receptor compartment, as well as detecting pulses (**Fig. 2C**).

1. Cut off a piece of pure silver wire, ~0.040 in. diameter, ~0.5 cm long.
2. Solder the end of the silver wire to a piece of copper bell wire, as shown in **Fig. 2C**.
3. Once the solder hardens, cover the solder (but not the silver wire) with nonconducting silicone rubber. Use as little silicone rubber as possible, but make sure that the solder is completely covered. Wait for the silicone rubber to harden (~1 d).
4. Cut off a piece of Tygon tubing, 1/32 inch ID, ~9 inches long. This will be used for the inflow into the receptor compartment. Cut off a piece of Teflon tubing, 1/16 in. ID, ~5 in. long. This will be used for outflow (*see Note 8*).
5. Cut the end off a 200- μ L pipet tip. The hole at the end of the pipet should be large enough to accommodate the wire and the two tubes. Cut the end off a 1-mL pipet tip so that the wire and the two tubes will fit through that hole as well.
6. A hole needs to be drilled into the side of the 1-mL pipet for the Teflon outflow tubing. This hole must be placed high enough so that the tubing clears the side of the port, and large enough to accommodate the Teflon tubing. Insert the 200- μ L pipet tip and the 1-mL pipet tip into the large port of the permeation chamber. Mark the level where the 1-mL pipet tip just clears the side of the port. Take the pipet tips out, and drill a hole in the side of the 1-mL pipet tip, just above this level.
7. Insert the Teflon outflow tubing through the 200- μ L pipet tip, through the opening of the 1-mL pipet tip, and out through the hole on the side of the 1-mL pipet tip. Insert the Tygon inflow tubing and the wire through the 200- μ L pipet tip and the 1-mL pipet tip (*see Fig. 2C*). The wire should be placed so that when the 200- μ L pipet tip is placed snugly into the large port of the permeation chamber, the silver electrode is positioned in the middle of the chamber. The two tubes should extend about 2 in. from the bottom of the 200- μ L pipet tip.
8. Fill the 200- μ L pipet with epoxy, to immobilize the wire and the two tubes in place. Insert the 1-mL pipet tip into the epoxy at the top of the 200- μ L pipet tip (keeping the tubes and wires properly positioned inside) and hold everything in place until the epoxy cures. Verify that the wires and the tubing do not move while the epoxy is curing.
9. Completely insert the electrode through the large port of the receptor compartment, such that the two tubes come out through the side (*see Fig. 1*). The silver wire electrode should be positioned in the middle of the compartment. Mark both tubes where they emerge from the chamber. Take the electrode out of the compartment and cut both tubes on those marks. The tubes should now be the proper size for the receptor compartment.

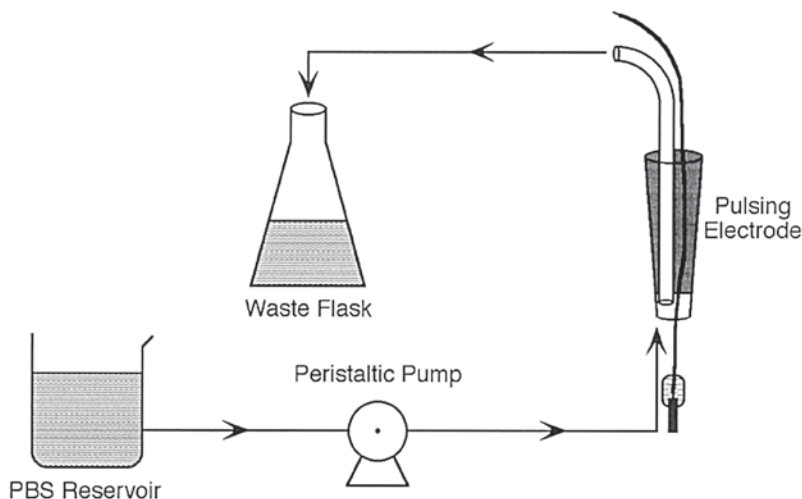


Fig. 3. Flow around the flow-protected pulsing electrodes. There are two pulsing electrodes, so this arrangement is used twice. PBS is pumped into the permeation chamber, and up through the pulsing electrode to a waste flask.

2.3. Electrode Flow-Protection System

Three different streams of PBS flow through this system. Each of the two pulsing electrodes is continuously washed in a stream of PBS, pumped from a peristaltic pump. A third stream of PBS flows through the receptor compartment to the spectrofluorimeter; this stream requires three peristaltic pumps to properly maintain flow (see **Fig. 4**).

For each of the pulsing electrodes, PBS is pumped from a reservoir into each compartment through the side ports, up around the electrode (channeled by the polyacrylamide gel), and up through the tubing connected to the pulsing electrodes. From there, the PBS flows to a waste flask (**Fig. 3**).

Since the purpose of the flow-protection system is to wash any chemical by-products out of the system, the pumps in this system do not need to be very precise. A good flowrate is roughly 6 mL/min per electrode. Tygon tubing should be used to connect the reservoir, the pumps, and the permeation chamber together. The fittings needed to connect the tubing to the pump and the chamber will vary, depending on the type of equipment available. If a connector to the chamber is not available, a good one can be made by epoxying a piece of Tygon tubing to a pipet tip (see **Note 7**). (This is similar to the fabrication of the pulsing electrode, except without the additional wiring.)

2.4. Flow-Through Sampling System

In the receptor compartment, PBS is pumped from a reservoir, through the long Tygon tube of the receptor measurement electrode, into the receptor compartment (**Fig. 4**). It then flows back up through the short Teflon tube of the electrode into a collection tube on the side of the electrode. From there, the PBS is pumped to a cuvet inside the spectrofluorimeter, and then out to a waste flask.

2.4.1. Fabrication of the Receptor Venting System

In a sealed receptor compartment with such a small volume (~400 μL), the minute pressure differences introduced by the peristaltic action of the pump can build up within the chamber. The receptor compartment design should allow these pressure differences to be eliminated.

Figure 4 shows a small collection tube (made from a centrifuge tube) near the outflow of the receptor compartment. Liquid from the receptor compartment drips down into the collection tube, which is then pumped to the spectrofluorimeter. Pressure differences from the receptor compartment are eliminated by venting the system at this location. The collection tube is not permanently fixed to the receptor measurement electrode, to allow for easier disassembly and cleaning.

1. Cut the lid off of a 2-mL centrifuge tube.
2. Cut off a piece of Tygon tubing, 1/32 in. ID, ~3 in. long.
3. Drill a hole in the bottom of the centrifuge tube. The piece of Tygon tubing should just fit inside this hole.
4. Drill a second hole near the midpoint of the centrifuge tube. This hole should be just large enough to accommodate the Teflon tube from the receptor measurement electrode.
5. Attach the piece of Tygon tubing to the hole with epoxy. This tube should be flush with the bottom of the centrifuge tube and should not protrude into it (**Fig. 4**).

2.4.2. Cuvet Fabrication

The cuvet in the spectrofluorimeter has to accommodate both the inflow and outflow of liquid from the permeation chamber. The volume of the liquid within the cuvet should be the smallest amount needed to obtain an accurate fluorescence measurement. The apparatus described here can be assembled and disassembled as needed.

The spectrofluorimeter cuvet is a 1 mL polystyrene semi-micro cuvet with two holes drilled into the side (**Fig. 4**). Liquid enters through the upper hole

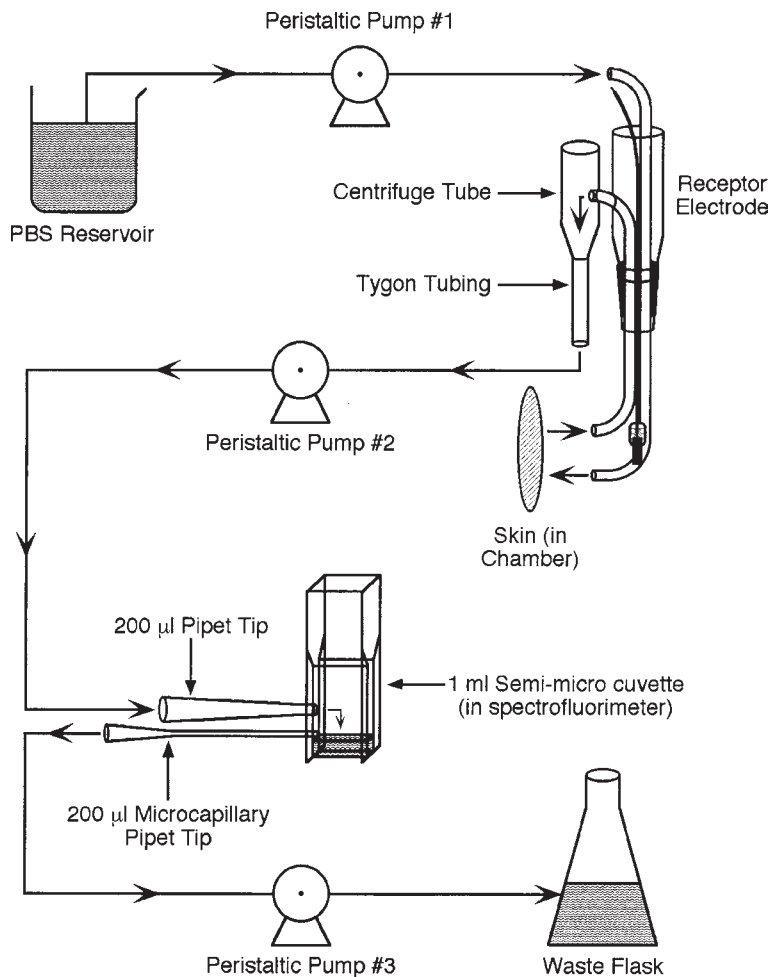


Fig. 4. Liquid circuit for flow-through measurements of the receptor compartment. PBS is pumped from a reservoir into the receptor measurement electrode, and down into the permeation chamber. PBS then exits the receptor compartment into a collection (centrifuge) tube. From there, it is pumped into a cuvet in the spectrofluorimeter for real-time detection. Finally, PBS from the cuvet is pumped to a waste flask. The arrangement of pumps and tubing allow this system to maintain a constant throughput.

and exits through the lower hole. Since the outflow rate of the cuvet is set higher than the inflow rate, the level of liquid within the cuvet stays at a constant height, immediately below the level of the outlet. The desired height of liquid depends on the minimum volume of liquid in the cuvet that yields a sufficiently accurate signal in the spectrofluorimeter.

However, even with this scheme, there is a cyclical rise and fall in the height of liquid within the cuvet, due to the differences between the inflow rate and the outflow rate. Since liquid leaves the cuvet faster than it enters, the level of liquid within the cuvet will drop. However, the liquid in the cuvet cannot be drawn out unless the outlet is completely submerged. Once the outlet is exposed, it begins to draw in air instead of liquid. When this occurs, the level of liquid in the cuvet will rise, since liquid is still entering the cuvet. This level will rise until the outlet is submerged again, causing the cycle to repeat.

The cyclic rise and fall of the height of liquid within the cuvet systematically varies from the bottom to the top of the outlet. This cycling pattern can be detected on relatively sensitive spectrofluorimeters. To minimize this effect, the outlet size must be kept as small as possible (*see Note 9*). Using a 200- μL microcapillary pipet tip (the inner diameter of the tip opening is approximately 500 μm) keeps the level reasonably constant (*see Note 10*).

Mixing within the cuvet is accomplished by the dripping of liquid into the cuvet. The height of the inlet should be high enough to allow the falling liquid to form droplets. The volume of the cuvet is small enough that the splashing of the drops into the liquid will cause adequate mixing to occur.

Before making the cuvet, the minimum volume of liquid that the spectrofluorimeter needs for an accurate signal has to first be determined. Most spectrofluorimeters pass a vertical beam of light through the cuvet. The beam of light is probably centered inside the cuvet, so that the liquid above and below this beam do not contribute to the fluorescence measurement.

1. Make up a solution of an easily obtainable highly fluorescent molecule.
2. Add 1 mL of this test solution to a 1-mL semi-micro cuvet and place the cuvet in the spectrofluorimeter.
3. Pipet small amounts of liquid out of the cuvet until the readings on the spectrofluorimeter begin to respond.
4. Attach a clamp to the top of the cuvet. This clamp will keep the cuvet from sliding down fully into its holder; thus, the cuvet will sit higher in the incident beam of light.
5. Adjust the position of this clamp downward on the cuvet (forcing the cuvet to rise higher and higher in the incident beam of light) until the readings on the spectrofluorimeter begin to respond.
6. Repeat **Steps 3 to 5** until no more adjustments can be made. This is the minimum amount of liquid needed for an accurate signal in the spectrofluorimeter. Lightly mark these levels on the side of the cuvet.
7. Obtain two 200- μL microcapillary pipet tips. The openings of these pipet tips are approximately 500- μm in diameter, smaller than the openings on the standard 200- μL pipet tips.

8. Two holes now should be drilled into the side of the cuvet to allow for inflow and outflow. These holes should allow the two microcapillary pipet tips to just fit through. These holes should be drilled on the same side of the cuvet, on a side that will not interfere with either the excitation beam or the fluorescence emission from the cuvet. The first hole (for outflow) should be drilled just above the first mark, and the second hole (for inflow) should be drilled approximately 0.25 in. above that.
9. The two microcapillary pipet tips should be attached to Tygon tubing with epoxy, for attachment to the peristaltic pumps. However, they should not be attached to the cuvet. This allows the entire system to be removed from the spectrofluorimeter for cleaning between experiments.

2.4.3. Pump Balancing

There are three pumps that are used in the flow-through sampling system. It is vital that these pumps be properly “balanced,” to avoid any accumulations or leakage within the flow-through system. The three pumps should all have flowrates of ~ 0.03 mL/s, and should provide consistent flowrates over very long times. However, these flowrates will probably not be identical. These differences cannot be avoided (*see Note 11*), and in fact can be used advantageously to maintain the flow-through system at steady state.

The pumps (*see Fig. 4*) should be set up such that the fastest pump is Peristaltic Pump 3, followed by Peristaltic Pump 2, with Peristaltic Pump 1 being the slowest. The differences in flowrates will cause air to be drawn into the flow-through system in two places: the collection tube and the spectrofluorimeter cuvet. This is necessary to keep the throughput of the system constant. Determining which pump is the fastest requires very careful measurements of the flowrates of each of the three pumps (up to three significant digits).

2.4.4. Flow-Through System Characteristics

At this point, all of the components should now be in place, correctly connected by tubing. The lengths of the tubing used to connect all of the components in the flow-through system probably will vary. While most of the tubing lengths are relatively unimportant, the length of the tubing between the chamber and the spectrofluorimeter should be minimized.

Although there is mixing within the tubing, the pump, and in the cuvet, the chamber/tubing/pump/cuvet system can be modeled as having two components: a plug flow region, where no mixing occurs, and a continuous stirred tank reactor region, where instant perfect mixing occurs (*10*).

Several parameters are needed for this model: the cuvet volume (V_{cuv}), the liquid bulk flow rate (Q), the reaction time (t_{react}), and the residence time (τ_{cuv}).

The reaction time, t_{react} , is the time it takes for a molecule leaving the receptor compartment to reach the spectrofluorimeter (the plug flow region). The residence time, τ_{cuv} , of the cuvet is the average time it takes for a molecule entering the cuvet to leave (the continuous stirred tank reactor region) (10). For an ideal continuous stirred tank reactor, the residence time distribution of this system can be predicted as an exponentially decaying function. The time constant for this decay gives τ_{cuv} , or the time resolution of the system. If this system is properly set up, its performance should be reasonably close to ideal.

To measure t_{react} and τ_{cuv} , a technique known as a “pulse-chase” experiment is used, where a drop of tracer (the “pulse”) is added to the system, and then flushed through it (the “chase”). The drop should be as small and as narrow as possible (ideally, it should be a δ function).

1. Make up a tracer solution of an easily obtainable highly fluorescent molecule.
2. Partially assemble the flow-through system, from the receptor measurement electrode onwards.
3. Pump water through the system until the spectrofluorimeter reads a constant background.
4. Add an aliquot of tracer to the receptor measurement electrode. (By selectively turning on and off the pumps, this drop can be made reasonably small.)
5. Turn on the pumps and measure the time it takes for the spectrofluorimeter to first detect the spike of tracer. This is the reaction time (t_{react}).
6. Pump water through the system until the spectrofluorimeter reads a constant background again.
7. Add another pulse of the tracer to the receptor measurement electrode.
8. Record the fluorescence on the spectrofluorimeter. If the system is behaving close to an ideal system, after a short delay (t_{react}), the fluorescence in the cuvet should quickly peak, then decay exponentially afterward.
9. Save the data from the spectrofluorimeter and import it into a graphing program.
10. Fit the decay of fluorescence to an exponential curve. The time constant for the exponential decay of the curve is τ_{cuv} . This is also the time resolution of the system.
11. Assemble the rest of the flow-through system. This includes the polyacrylamide gel within the permeation chamber (described in **Subheading 2.8**).
12. Measure the average flowrate through the entire system (Q). This should be done in the waste stream. Ignore the air getting pumped through the system.
13. The working cuvet volume can be calculated by multiplying the residence time (τ_{cuv}) by the flow rate (Q) (10):

$$V_{\text{cuv}} = \tau_{\text{cuv}} Q$$

2.5. Electrical Circuit

The electrical circuit (shown in **Fig. 5**) has to perform two functions. First, it must deliver high-voltage pulses to the permeation chamber once every 5 s.

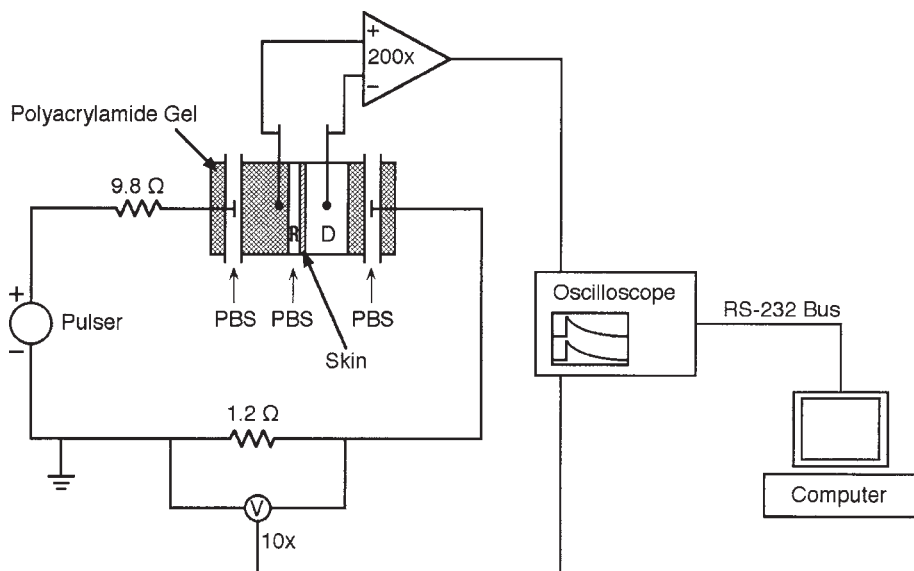


Fig. 5. Electrical circuit used during pulsing. The $9.8\ \Omega$ resistor is a safety device in the event of a short circuit. The transdermal voltage is measured by a $200\times$ differential voltage probe, and the current is measured by a $10\times$ voltage probe across a $1.2\ \Omega$ resistor placed in series with the chamber. Both voltage probes are connected to an oscilloscope, which downloads the data into a computer for later analysis. R indicates the receptor compartment and D indicates the donor compartment. The two outer PBS streams and the polyacrylamide gel around the pulsing electrodes are used to prevent chemical contamination of the donor and receptor compartments by the electrodes. The inner PBS stream flows from the receptor compartment to a spectrofluorimeter for detection.

Second, it has to measure and record the transdermal voltage and the current across the skin in real time. Since pulses are being applied to the skin every 5 s, there is very little time to manually record data or make adjustments between pulses. Thus, all of these operations have to be completely automated.

All of the components, including the wires and the clip leads, should be able to withstand high voltages and positioned with safety in mind. The electrical circuitry should be set up in a protected area away from the permeation chamber (e.g., on a different bench), so that any fluid leaks or spills do not reach the electrical components.

In a commonly used protocol (2–5), the pulser delivers a high-voltage exponential pulse to the permeation chamber once every 5 s. The current and the voltage during the pulse are detected by two high-voltage probes connected to

a digital oscilloscope. The data is then downloaded from the oscilloscope into a computer for later processing. The system stores all of the data and is ready to download the next pulse in less than 5 s.

2.5.1. Modifying the High-Voltage Pulser

There are presumably no commercially available devices that can produce 1000 V exponentially decaying voltage pulses into a load of $\sim 500 \Omega$, at the rate of 1 pulse every 5 s. Instead, a commercial pulser has to be internally modified to be able to deliver pulses at that rate (*U. Pliquett, personal communication*).

The procedure for modifying the internal workings of a high-voltage pulser will depend mainly on the type of pulser being modified. Modifying high-voltage equipment is very dangerous. Any modifications to the pulser should only be undertaken by a qualified electrical engineer, thoroughly familiar with high-voltage electronics (*see Note 12*).

Briefly, the pulser needs to be modified so that it immediately begins recharging its capacitors after discharging each pulse (some pulsers require a button to be pressed to reset the pulser between pulses). A flip-flop timing circuit can be used to cause the pulser to discharge itself at a fixed frequency (here, 1 pulse every 5 s). This timing circuit should be located near the pulse activation button, so as to avoid the high-voltage areas of the pulser (*E. A. Gift, personal communication*).

Knowledge of the timing of the firing circuit is crucial to determining the transdermal fluxes. The pulsing spacing (t_{int}) is defined as the amount of time between successive pulses. This should be determined to within ± 0.001 s (± 1 s in 3 h); thus, pulses can not be delivered manually. The pulsing spacing can be measured by setting the pulser up to pulse a permeation chamber filled with PBS, and using the computer (described below) to count the number of pulses delivered in a 3-h period.

2.5.2. The Pulsing Circuit

The chamber is connected to the circuit so that the receptor pulsing electrode is positive and the donor electrode is negative (**Fig. 5**). This provides a favorable driving force for a negatively charged molecule. However, for a positively charged species, the positive and negative terminals to the chamber should be interchanged.

The 9.8Ω resistor is a safety device used to protect the system in the event of a short circuit. It should be a 50-W noninductive power resistor.

The $1.2\text{-}\Omega$ resistor in series with the skin is used to measure the current across the skin during pulsing. It should also be a 50-W noninductive power resistor. A 10x voltage probe from the digital oscilloscope should be connected

across the 1.2- Ω resistor. Once the voltage drop across the resistor is known, the current can be determined by applying Ohm's law.

The donor and receptor compartments each contain a measuring electrode. Connected across these electrodes is a 200x differential high-voltage probe (B9017RT Active Differential Probe, Yokogawa Corp., Newnan, GA) (*see Note 13*). Between the two measurement electrodes are the skin and PBS, where the resistivity of PBS is constant for a given temperature. The differential probe is also connected to the oscilloscope.

2.5.3. Real-Time Data Acquisition and Storage

The digital oscilloscope records data simultaneously from two channels, and uploads the acquired data to a computer for subsequent analysis. The computer downloads that data from the oscilloscope and stores it on disk. All of these operations must be completed in less than 5 s, before the next pulse arrives.

One digital oscilloscope that has worked well is a Hewlett Packard 54601 with an 54641A RS-232 Interface Module (Hewlett Packard, Palo Alto, CA), which can be connected with an RS-232 cable to the serial port of a 486 DX computer.

The program the computer is running will be machine-specific, depending on which serial port the oscilloscope is connected to, and the programming languages of the computer and the oscilloscope. In general, though, the computer program should be in a low-level programming language, and the computer itself should be reasonably fast. The oscilloscope should transfer data in the most compact format available (i.e., as unformatted ASCII characters instead of formatted arrays of numbers).

The computer program needs to direct the oscilloscope to transfer data once a pulse has been triggered, and it should store that raw data on the hard drive (or on a ramdisk if enough memory is available). No mathematical processing needs to be done during the experiment. The computer has to be able to complete the transfer and save the data in under 5 s (*see Note 14*).

A transfer rate of 9600 baud between the oscilloscope and the computer allows roughly 1 kb of raw data to be transferred in 5 s, which corresponds to a time resolution of approximately 10 μ s for each pulse waveform. Before starting, verify that there is adequate space on the hard drive, since one experiment can consume nearly 1 MB of space.

2.5.4. Resistance of PBS

The skin, PBS, and some polyacrylamide gel are located between the two measurement electrodes. The resistivities of the PBS and the polyacrylamide gel are constant, but should be measured.

1. Make up a solution of PBS (solution 5).
2. Prepare the permeation chamber, with the four electrodes and the polyacrylamide gel (described in **Subheading 2.8.**).
3. Fill the chamber with PBS.
4. Connect the pulser, the voltage probes, and the oscilloscopes to the chamber (*see Fig. 5*). Heat the chamber to 37°C using a water bath (the resistivity of PBS is a function of temperature).
5. Manually apply pulses to the chamber, starting from 0 V and increasing in units of 100 V, up to 1000 V. Apply 5 to 10 pulses per setting. For each pulse, record the voltage drops appearing across the inner electrodes (U_{curr}) and the 1.2- Ω resistor (R_{curr}).
6. To find the current (I), apply Ohm's law to the 1.2- Ω resistor:

$$I = U_{\text{curr}} / R_{\text{curr}} = U_{\text{curr}} / 1.2 \Omega$$

7. Plot the voltage drop across the measurement electrodes (U_{meas}) versus the current (I). The slope of the line is the resistance of the PBS and the polyacrylamide gel (lumped together in one variable, R_{pbs}) between the two measurement electrodes:

$$R_{\text{pbs}} = U_{\text{meas}} / I$$

2.6. Impedance Measurement Circuit

The resistance of the skin should be checked to make sure the skin is in good condition. However, an ohmmeter or other DC source should not be used to measure the resistance of the skin, since it may cause iontophoresis to occur in the skin during the measurement (*see Note 15*).

A bipolar sinusoidal AC voltage source does not deliver a net current to the skin, and should be used instead of a DC source. However, using an AC voltage source gives the impedance, not the resistance, of the skin. At low frequencies (<1 kHz), the skin's impedance approximates its resistance, but at higher frequencies, the capacitance of the skin can introduce errors. Thus, besides low RMS voltages (<0.1 V), low frequencies (10 Hz or 100 Hz) should be used.

Although commercial test equipment is available (e.g., Model 5R715 LCR Meter, Stanford Research Systems, Sunnyvale, CA), a skin impedance tester can also be set up using an AC sinewave generator. This circuit is shown in **Fig. 6**. The AC source should be able to produce a 10 Hz, 50 mV (RMS) bipolar sine wave. For a good piece of skin, the maximum RMS current this system will produce is $\sim 1 \mu\text{A}$.

In this circuit, the impedance of the skin can be determined by measuring the RMS voltage across the 1.0 Ω resistor. From this value, Ohm's law gives the current (which should be $<1 \mu\text{A}$). The voltage drop across the skin, divided by the current, gives the skin's impedance.

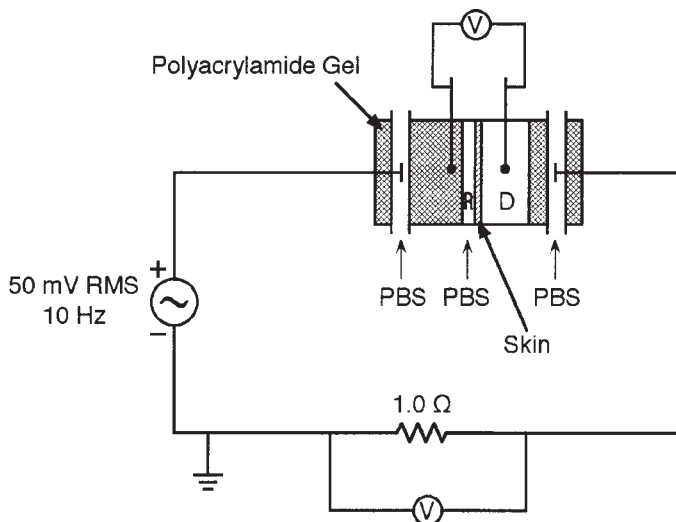


Fig. 6. Impedance measurement of the skin. The AC source produces a 50 mV RMS, 10 Hz bipolar sine wave. The current across the skin is determined by measuring the RMS voltage across the 1.0 Ω resistor placed in series with the skin. The voltage across the skin is measured with the voltmeter placed across the permeation chamber. The impedance of the skin is then found by Ohm's law.

2.7. Preparation of Human Skin

This technique for removing the epidermis (with the overlying stratum corneum) from the dermis by heating the skin to 60°C is commonly called heat-stripping (11).

1. Cadaver skin should be stored at -80°C for up to 6 months before use (11). Cadaver skin should be fresh-frozen within 24 h after surgery or after death. It should be as hairless as possible; good areas are the abdomen, thighs, or back. The skin should not be dermatomed or frozen with any preservative media.
2. To thaw the skin to room temperature, take the skin from the freezer and place it on an undisturbed counter for approximately 2 to 3 hours (longer if the piece is large). Wait until the skin has been completely thawed.
3. Heat a bath of deionized water to 60°C. It is crucial that the temperature be as close to 60°C as possible (see Note 16). The water bath should be sufficiently large that the addition of the skin will not significantly change the temperature of the water bath.
4. Immediately place the skin (removing any packaging) into the 60°C water bath for 2 min.
5. Remove the skin and place it on a sheet of wax paper.

6. Using a blunt metal object (such as a rounded spatula), gently scrape away the epidermis from the stratum corneum. Hold the dermis firmly in place with a pair of tweezers while gently scraping away the epidermis. The epidermis can be folded up and moved aside during this process, but it should not be stretched or touched with anything sharp or metal. Try to keep the hair follicles with the epidermis.
7. Once the epidermis has been removed from the dermis, place the epidermis in a tray of clean, deionized water (do not use the 60°C water bath).
8. The epidermis is now probably folded up. Gently open the epidermis until it is floating as a flat sheet on top of the water. Metal objects of any kind should not be used. At this point, the stratum corneum (which is hydrophobic) is on top, and the epidermis (which is hydrophilic) is on the underside.
9. Take a sheet of wax paper, place it underwater, under the epidermis, and gently lift up the wax paper out of the water so the epidermis attaches to it and remains flat (*see Note 17*). Place the wax paper on a cutting board.
10. Using a 0.75 in. diameter hole punch (Small Parts, Miami Lakes, FL) and a hammer, cut the skin and wax paper into 0.75 in. disks (*see Note 18*). Keep the punches as close together as possible. Avoid any regions that are discolored or torn. Place the discs into a weigh boat.
11. The skin should be stored at 4°C, 95% humidity before use. Fill the bottom of a sealed glass chamber (such as a desiccation chamber) with a saturated solution of K_2SO_4 in water, which will maintain the chamber at 95% humidity. There should be a level within this chamber, away from the water, where the weigh boat will remain dry. Place the weigh boat containing the skin into this chamber. Under these conditions, the skin can last for up to 10 d before use (*II*).

2.8. Permeation Chamber Preparation

2.8.1. Preparation of Mold

The polyacrylamide gel around each pulsing electrode directs PBS in and out of the chamber, without contacting the donor or receptor solutions (these are the hollowed-out regions that run around each of the two pulsing electrodes in **Fig. 1**). On the receptor side, the polyacrylamide also keeps the volume of the receptor compartment at a minimum (on the right half of **Fig. 1**). Embedded in this side are the tubes entering and leaving the receptor chamber, and the measurement electrode.

Acrylamide in solution takes approximately 10 min to polymerize into polyacrylamide gel. In this time, the acrylamide solution has to be poured into the chamber. To create the channels that run through the polyacrylamide gel, plastic tubes are inserted into the chamber, which are then removed once the acrylamide has polymerized. Preparing the mold within the permeation chambers can be done the day before the experiment.

1. Find two flexible plastic tubes, approximately 9 inches long, that will fit through the two small ports on each chamber half.
2. Slide the plastic tubes protrudes these ports (use tweezers as needed), so that roughly 1–2 in. of the tube protrudes out on either side. These tubes are the mold for the electrode flow-protection channel.
3. Place Parafilm around each opening tightly. Use two layers of Parafilm. This should create a watertight seal around the openings, so the acrylamide solution can not leak out.
4. Insert the receptor measuring electrode into the receptor compartment. Make sure the two tubes that lead to the receptor compartment are angled toward the opening. Place Parafilm tightly around this electrode as well.
5. Owing to the elasticity of the tubing, however, the two tubes of the electrode are probably stuck next to each other instead of on opposite sides of the chamber as shown in **Fig. 1**. Using a thin stainless steel wire, attach the outlet tubing to the top of the chamber. This wire will be removed after the polyacrylamide gel has been added.
6. Seal the back ends of each tube with Parafilm. The air trapped within each tube will prevent acrylamide solution from entering the tube.
7. Position each of the two chambers sideways, so that the large opening (where the skin will be located) is on top. The chambers should be braced in some fashion (i.e., propping them up on pencils or test tubes) so that they can not tip or move when filled with liquid.

2.8.2. Adding the Polyacrylamide Gel

Acrylamide monomer in solution (solution 1) will polymerize into a gel in approximately 10 min upon addition of a catalyst (*N,N,N',N'*-tetramethylethylenediamine) (Bio-Rad) and a free radical initiator (solution 4). Most of the gel is still liquid (PBS, in this case), surrounded by crosslinked polymer. Thus, the conductivity and the electrical properties of the polyacrylamide gel are essentially the same as PBS.

Synthesizing the polyacrylamide gel should be performed just before the experiment (the chambers should already be prepared), since polyacrylamide gel dehydrates after a few hours.

1. Thoroughly mix together 10 mL of acrylamide solution (solution 1), 87.5 μ L of the initiator (solution 4), and 6 μ L of *N,N,N',N'*-tetramethylethylenediamine.
2. On the donor side, immediately pour in the acrylamide solution so that it reaches the level of the large port (embedding the plastic tube for the flow-protection system). This should leave a donor volume of \sim 2.1 mL.
3. On the receptor side, immediately pour in the acrylamide solution, completely filling the chamber. The top of the solution should be perfectly flush with the top of the chamber, and there should not be a meniscus above the chamber. The acrylamide solution will completely cover the plastic tubing of the flow protec-

- tion system, and the silver measurement electrode. Make sure that the liquid does not enter the two tubes that form the receptor compartment. The solution will shrink slightly as it gels; this shrinkage is what forms the receptor compartment. Thus, to get a consistent, reproducible volume for the receptor compartment, the solution should always be poured so that it is flush with the top of the chamber.
4. Do not disturb the chambers while the gel is polymerizing, as disturbances will cause the gel to take longer to harden, and the gel will set poorly as a result. It will take approximately 10 min for the gel to harden. Any leftover acrylamide solution can be used to monitor the gelation process.
 5. After the gel forms, carefully remove the Parafilm around the each of the plastic tubes. Remove the plastic tubes through one of the small ports. Do not remove the receptor measurement electrode or the surrounding Parafilm.
 6. Carefully remove the stainless steel wire holding the outlet tube of the receptor compartment in place, which should now be held in place by the polyacrylamide gel.
 7. Using a syringe, force air through the inlet and outlet tubes of the receptor chamber to ensure that they are not blocked by stray bits of polyacrylamide gel.
 8. Connect the collection tube (*see Subheading 2.4.1.*) to the outlet tube on the side of the receptor electrode, as shown in **Fig. 4**. Hold it in place with Parafilm.
 9. Before using, fill the permeation chambers with PBS to keep the polyacrylamide gel from drying out.

3. Methods

3.1. Preparing the Equipment

On the day of the experiment, the following should have already been prepared and assembled: solutions 1 to 4, the permeation chamber and the electrodes (**Subheadings 2.2.** and **2.7.1.**), the electrode flow-protection system (**Subheading 2.3.**), the flow-through system in the spectrofluorimeter (**Subheading 2.4.**), the electrical circuit (**Subheading 2.5.**), the skin (**Subheading 2.6.**), and the impedance meter (**Subheading 2.7.**). Immediately before the experiment, solutions 5 and 6, and the polyacrylamide gel in the chamber (**Subheading 2.7.2.**) need to be prepared. Once the gel in the chamber is ready, place the chamber on a magnetic stirring plate and connect it to a 37°C water bath.

All of the tubes in the flow-through and the electrode flow-protection system should be flushed through with PBS. Use a piece of Parafilm instead of skin in the permeation chamber. There should be a steady stream of air bubbles entering the flow-through system at the collection tube and the spectrofluorimeter cuvet. The flushing should continue until the spectrofluorimeter gives stable readings for the fluorescence. This can take up to an hour in some cases, especially if the lines were not sufficiently cleaned and flushed the last time the equipment was used.

3.2. Loading Skin into the Chamber

The condition of the skin is checked by measuring its electrical impedance and monitoring the passive flux of the donor solution. The impedance of “good skin” should be $>20 \text{ k}\Omega \text{ cm}^2$ at 100 Hz (*I,14*). The passive flux of the donor solution across the skin should be negligible (below the detection limit of the spectrofluorimeter). Low impedances or large passive fluxes indicate that the skin’s integrity has been compromised in some way. This could be due to a hole in the skin, shearing of the skin during the loading process, or the poor quality of skin’s preservation post-mortem.

The impedance is measured across the two measurement electrodes in the permeation chamber. However, besides the skin, this measurement also includes PBS and the polyacrylamide gel. The other impedances can be neglected, though, since the impedance of the skin is much larger than PBS (*2*) (*M. R. Prausnitz, personal communication*).

1. Float a piece of skin (*see Subheading 2.7.*) in a dish of PBS for ~1 min.
2. Gently remove the wax paper backing. Do not use tweezers. The skin should float on the surface, with the stratum corneum side facing upwards.
3. Fill the receptor compartment completely with PBS. There should not be any air bubbles present.
4. Position the skin in the chamber so that the stratum corneum faces the donor compartment and the epidermis faces the receptor compartment. Clamp the chamber shut. Verify that the receptor compartment is still completely filled with PBS.
5. Fill the donor with PBS.
6. Connect the impedance meter (*see Subheading 2.6.*) to the measurement electrodes. Good skin has an impedance $>20 \text{ k}\Omega \text{ cm}^2$ at 100 Hz (*I*) (*T. R. Gowrishankar, personal communication*). Poor skin should be discarded.
7. Disconnect the impedance meter.
8. Remove the PBS from the donor compartment and add donor solution (Solution 6). Add a 1.5 mm “flea”-type magnetic stir bar to the donor compartment.
9. Connect the chamber to the pulsing circuit as shown in **Fig. 5**, verifying that all four electrodes are properly connected.
10. Turn on the stirring plate and the water bath.

3.3. Passive Control

After the skin has been loaded in the chamber, the flow-through system should be activated. The skin should be left for at least an hour to fully hydrate the skin and check for leaks (i. e., holes or tears in the skin). Leaks can be detected by observing large or increasing readings in the background fluorescence observed on the spectrofluorimeter. If the skin begins to leak, it should be discarded.

3.4. Pulsing Conditions

High-voltage pulses can be applied to the skin at the rate of 1 pulse approximately every 5 s. Both the time constant and the applied voltage should be set on the pulser as needed before pulsing is started. The transdermal voltage is a nonlinear function of the applied voltage (**1,6**) (see **Note 19**). Thus, given a desired transdermal voltage, a guess of the applied voltage should be made at this time.

1. Set the pulser to deliver the appropriate types of pulses.
2. Gradually start the pumps for the electrode flow-protection system. Make sure that the polyacrylamide gel in the chamber does not crack or break when this is turned on. If the gel breaks, new gel will have to be made, which will cause the experiment to be aborted.
3. Turn on the oscilloscope and the computer (see **Note 21**). They should be set to start recording once the first pulse is applied.
4. Start the spectrofluorimeter for a time-based scan. The spectrofluorimeter should record fluorescence for the time of pulsing (typically 1 h), plus some additional time at the beginning to measure the background fluorescence, and some time at the end to measure recovery. The time interval between successive measurements should be as short as possible (e.g., 0.5 s). Record about a minute of passive flux (control) to establish the baseline.
5. Start the pulser. The oscilloscope and the computer should start recording pulses immediately with the first pulse. Note the exact time when pulsing starts, on the clock and on the spectrofluorimeter (t_{start}). These times will be needed later to synchronize the pulsing data and the fluorescence data.
6. Since the spectrofluorimeter, the pulser, and the oscilloscope/computer are all automated, during the experiment, no additional effort is needed during pulsing. However, the equipment should be watched at all times in case something goes wrong during the experiment.

3.5. Ending the Experiment

After pulsing, the recovery of the skin can be measured by recording the fluorescence once the pulser has been turned off. Afterward, the skin should be removed from the permeation chamber and mounted on a microscope slide for analysis. Voltage and current data from the computer and data from the spectrofluorimeter should be saved on disk for later analysis. The standard curve should also be measured.

1. After pulsing, turn off the pulser, but leave the rest of the equipment running. Wait until the fluorescence reaches steady state to stop recording on the spectrofluorimeter.
2. Turn off all of the pumps.

3. Empty the donor compartment. Flush it out three times with PBS.
4. Open the permeation chamber and carefully remove the skin. Place it carefully on a microscope slide. Gently spread the skin out so it lies flat, and lightly blot it dry with a paper towel. Do not rub the skin.
5. Add a drop of mounting solution (solution 3).
6. Gently put a coverslip on top. This will cause the mounting solution to spread out and cover the skin. Seal in place with nail polish. Bring the slide to a fluorescence microscope for immediate analysis and photography (**Subheading 3.7**).
7. Save the data from the computer and from the spectrofluorimeter. These should be copied to a workstation for later analysis (*see Subheading 3.8*).

3.6. Measuring the Standard Curve

The standard curve should be measured under exactly same conditions that the experiment was performed under, including the same flowrates, tubing, and the same measurement cuvet. Placing the calibration solutions in separate cuvetts and measuring their fluorescence will not work, since the volume of liquid within the cuvet needs to be exactly the same for each sample. Thus, each calibrating solution needs to be separately pumped through the spectrofluorimeter.

Since the calibration curve is continually being pumped through the spectrofluorimeter, 10 mL will be needed for each concentration, to allow the fluorescence in the system to reach steady state.

1. Prepare a standard curve, starting at the donor concentration. Make up 10 mL of solution for each concentration.
2. Set up the spectrofluorimeter for a time-based scan.
3. Run each sample through the spectrofluorimeter, obtained from the outlet tube of the permeation chamber (*see Note 20*). Start from the most dilute sample and increase to the most concentrated. Record the times that each solution passes through the spectrofluorimeter.
4. Save the calibration curve onto disk for later analysis.

3.7. Fluorescence Microscopy

Immediately after the skin has been mounted, it should be brought over to a fluorescence microscope for analysis. Many fluorescence microscopes (e.g., Olympus BH-2, Olympus, Woodbury, NY) also allow illumination of the sample under white light, which allows the identification of the sweat ducts and hair follicles in the skin. Regions where fluorescence occurs can thus be compared to the location of sweat ducts and hair follicles within the skin.

Note that fluorescence microscopy does not directly indicate the regions involved in molecular transport. The fluorescence observed under the microscope could be coming from either the surface of the skin (*12*) or from inside

the skin (13). Some authors have established a correlation between the regions of fluorescence on the surface of the skin and the regions where molecular transport occurs (13).

3.8. Analysis of the Flux and Voltage Data

All of the fluorescence, voltage, current, and calibration data needs to be downloaded into a computer for analysis. Due to the amount of data one experiment can generate, a workstation, rather than a PC, is recommended (e.g., Sun Sparc 10, Sun Microsystems, Palo Alto, CA)

The first step in the analysis is to convert all of the voltage and current data into the transdermal voltage. The next step is to calibrate and deconvolve the fluorescence data into molecular flux. The final step is to correlate the two sets of measurements, to determine the amount of molecular flux that occurs during each pulse.

3.8.1. Transdermal Voltage

The voltage drop across the skin can be determined by applying Ohm's law to the current and the voltage. The resistance of the intervening PBS (R_{pbs}) should already be known (**Subheading 2.5.4.**).

1. Since the data from the oscilloscope have probably been transferred in a compacted format, the first step is to uncompress the data and convert it into voltage and current data.
2. Ohm's law is used to convert the voltage drop (U_{curr}) across the 1.2 Ω resistor (R_{curr}) into the current (I):

$$I = U_{\text{curr}} / R_{\text{curr}} = U_{\text{curr}} / 1.2 \Omega$$

3. The current across the skin (I) and the voltage drop across the measurement electrodes (U_{meas}) for each pulse should now be known. To calculate the transdermal voltage (U_{skin}), use:

$$U_{\text{skin}} = U_{\text{meas}} - IR_{\text{pbs}}$$

3.8.2. Deconvolution of the Fluorescence Data

The fluorescence measured in the spectrofluorimeter is really the sum of two components: the molecular flux out of the skin, and the mixing that occurs in the tubing and the cuvet (*see Subheading 2.4.4.*). With a model of the mixing that occurs in this system, the molecular flux across the skin can be determined.

1. Using the standard curve (**Subheading 3.6.**), convert all of the fluorescence data into concentrations. These are molecular concentrations within the cuvet, not transdermal fluxes.

- The molecular flux across the skin is determined by the following equation (14).

$$J_{\text{skin}} = V_{\text{cuv}} \frac{C_2 - C_1}{A \Delta t} + \frac{Q}{A} \frac{C_1 + C_2}{2}$$

In this equation, J_{skin} is the molecular flux across the skin, V_{cuv} is the volume of the cuvet (**Subheading 2.4.4.**), A is the exposed area of the skin, C_1 and C_2 are two successive measurements on the spectrofluorimeter (expressed as concentrations), Δt is the length of time between the measurements of C_1 and C_2 , and Q is the average flow rate through the cuvet (**Subheading 2.4.4.**). C is assumed to be linear and J_{skin} is assumed to be constant, both over the time interval Δt , which should be kept small (~ 0.5 s). This equation has to be applied to every pair of measurements made on the spectrofluorimeter. Note that due to mixing within the cuvet, the time resolution for these measurements is not more accurate than τ_{cuv} .

3.8.3. Correlation of Fluxes and Voltages

At this point, there are two arrays of data, representing the transdermal voltages appearing during each pulse, and the molecular fluxes across the skin (at a time resolution of τ_{cuv}). These data need to be correlated in time with each other.

- Define the first pulse to occur at a time 0. Then the n th pulse occurs at time $t = (n - 1) t_{\text{int}}$.
- To correlate the time on the spectrofluorimeter with the time of each pulse, the time on the spectrofluorimeter (t_{fluor}) needs to be corrected for the elapsed time before pulsing was started (t_{start}) and the plug flow time (t_{react}).

$$t = t_{\text{fluor}} - t_{\text{start}} - t_{\text{react}}$$

- Now that the two measurements have been synchronized in time (t), the molecular flux during each pulse can be determined. Note, however, that the time resolution is still τ_{cuv} . If pulses were applied more rapidly than that ($t_{\text{int}} < \tau_{\text{cuv}}$), then the flux measurements will still be confounded by subsequent pulses.

4. Notes

- Although the volume of the receptor compartment is very small (~ 400 μL), a typical experiment can consume a surprisingly large volume of PBS, since both the flow-through fluorescence measurement system and the electrode flow-protection systems are continuously pumping PBS through the chamber. One experiment will usually consume 1.5–2 L of PBS.
- Both light and O_2 can cause the bleaching of fluorescent molecules, but this can be reduced by removing the dissolved gases from solution, and protecting the solution from light whenever possible.
- Side-by-side permeation chambers (where the skin is mounted vertically), are preferable to vertical permeation chambers (where the skin is mounted horizontally) for two reasons. First, any bubbles produced by the electrodes can easily be removed from the system, before they reach the skin. In a vertical chamber, the bubbles would float upward toward the skin. Second, mounting the skin vertically eliminates gravity

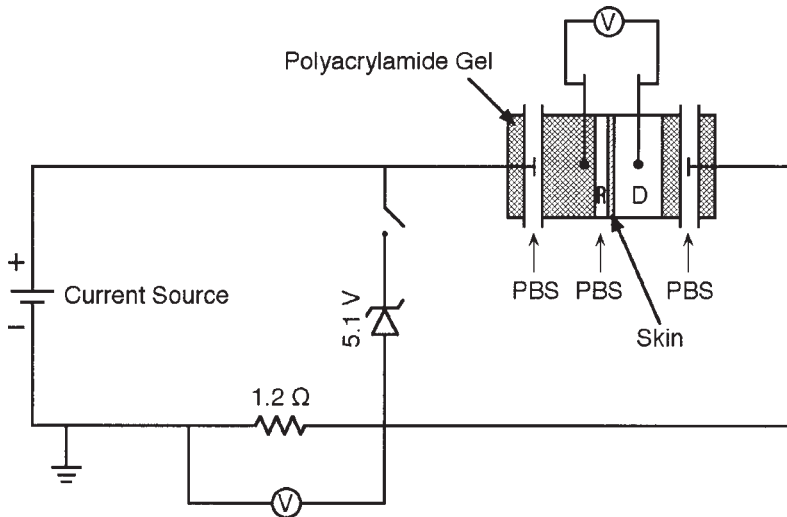


Fig. 7. Constant current iontophoresis circuit. The switch next to the Zener diode is initially closed, before the current source is activated. After the current source has been activated, the switch is then opened. This arrangement prevents any electrical transients from reaching the skin. Measuring the voltage drop across the 1.2Ω resistor placed in series with the skin gives the current across the skin.

as a possible driving force, which is important for mechanistic studies. Here, gravity includes effects such as the weight of liquid pushing down on the skin.

4. This system can also be iontophoresis or sonophoresis. For example, for iontophoresis, instead of attaching a pulser to the outer electrodes, attach the iontophoretic device instead. The circuit diagram for iontophoresis is shown in **Fig. 7** (cf. **Fig. 5**). The 5.1-V Zener diode is used to prevent electrical transients from occurring across the skin (which could inadvertently cause electroporation to occur) when the constant current source is activated. The switch should be closed before turning on the constant current source, then opened afterward.
5. The electrodes in this system are pure silver, rather than the Ag/AgCl electrodes which are more commonly used. With Ag/AgCl electrodes, after only a few pulses, enough of the AgCl is removed so that the silver becomes directly exposed to the solution. Thus, using Ag/AgCl electrodes to avoid polarization effects does not work very effectively.
6. There are probably some polarization effects caused by the silver wire electrodes during pulsing. However, this polarization can generally be ignored, since the voltage drop forming across the skin (and intervening PBS) is directly measured by the pair of measuring electrodes, and is not calculated or inferred from the applied voltage (I).
7. Pipet tips are used for much of the construction of this system. Due to their tapered shape, the pipet tips can tightly fit and seal virtually any opening. They are

hollow and can allow the flow of liquids, and they are inexpensive and readily available in the laboratory.

8. In general, Tygon tubing is more flexible than Teflon tubing and is easier to manipulate. Thus, most of the tubing in this system is made from Tygon tubing. However, Tygon tubing is not strong enough to support the venting system; thus, Teflon tubing is used instead.
9. A problem with using very small tubing is that it can frequently become blocked by stray bits of dirt and debris, especially from the skin. The amount of dirt and debris can be minimized by continuously flushing the system with PBS (even during passive controls, and between experiments), and by very thorough washing of the entire system before shutting it down. To clear a blocked tube, the system should be backflushed to remove the clog.
10. A diameter of only 500 μm for the outlet may not seem particularly worrisome, but that size is still significant compared to the working volume of the cuvet, which is only $\sim 200 \mu\text{L}$. With an outlet this small, the cyclic changes in the height of the liquid in the cuvet are not significant compared to the shot noise of the spectrofluorimeter.
11. The differences in the flow rates of the various pumps may be on the order of $0.3 \mu\text{L/s}$ ($\pm 1\%$ of the flow rate) or less. While minuscule, over time, these differences can still quickly build up in a system as small as this one.
12. Note that opening up and modifying the high-voltage pulser will probably void all existing warranties. This work should be done in close consultation with the pulser manufacturer, and should only be done by an electrical engineer thoroughly trained in high-voltage electronics.
13. Using a grounded high-voltage probe in the receptor compartment instead of a differential probe is not recommended, since it introduces other voltages into the measurement, such as the polarization voltage of the pulsing electrodes.
14. The 5-s spacing between pulses allows very little time for the correction of problems, so care must be taken in setting up this system. Examples of problems that can occur include loose serial plugs, line noise due to faulty or excessively long cables, errors in the proper recording of an NL (“New Line” command, ASCII string #0A) or an EOT (“End of Transmission” command, ASCII string #04), improper triggering of the oscilloscope by line noise in either voltage probe, and failure of the oscilloscope and the computer to properly synchronize headers and data streams.
15. Some commercial ohmmeters can apply voltages of up to $\sim 5 \text{ V}$ during ordinary resistance measurements. In a good piece of skin, this can generate current densities of up to $\sim 0.5 \text{ mA/cm}^2$. A current density of 0.5 mA/cm^2 is also the maximum current density that can be applied to the skin in humans during iontophoresis. Thus, such ohmmeters should never be used to measure the resistance of the skin.
16. The temperature “window” at which the skin can be heat-stripped is very small. If the temperature is too low ($< 57^\circ\text{C}$), the epidermis will not easily separate from the dermis. If the temperature is too high ($> 62^\circ\text{C}$), the lipids in the stratum corneum will start to reorder, which permanently reduces the electrical resistance of the stratum corneum (15).

17. Several brands of wax paper will curl when soaked in water, which makes it very difficult to slide the paper under the floating epidermis. One type of wax paper that works well and does not curl is the 4 in. \times 4 in. weighing paper that can be obtained from VWR (West Chester, PA).
18. Even with a new, sharp hole punch, it can be very difficult to cut completely through both the skin and the wax paper. The hole punch should be hit very hard, several times, to ensure a clean cut through both the skin and the wax paper.
19. Only a small fraction of the voltage applied to the system appears across the skin during high-voltage pulsing (**6,16**). Voltage drops also occur across the power resistors, the electrodes, the PBS, and the polyacrylamide gel. During pulsing, the skin's resistance can drop from $\sim 50 \text{ k}\Omega \text{ cm}$ to $\sim 100 \Omega \text{ cm}$ (**1,2,4,6**), while the resistances of the other components remains constant. Thus, up to 90% of the applied voltage does not appear across the skin.
20. With only 10 mL of solution per concentration, steady state for each concentration in this system will only last for a few minutes. It is simpler to let the spectrofluorimeter run continuously, than to start and stop the spectrofluorimeter between each concentration and risk missing the steady-state regime.
21. Make sure that all screen savers, energy savers, and any other software drivers that can cause process interrupts in the computer have been completely turned off. The computer should not be doing anything during the experiment besides downloading data. Any timing glitches between the computer and the oscilloscope could cause either the computer or the oscilloscope to crash.

Note Added in Proof

A more advanced version of this system has recently been described in: Chen, T. (1999) The Pathways and Mechanisms of Skin Electroporation. Sc. D. Thesis, Massachusetts Institute of Technology, Cambridge, MA, USA. Additional modifications include a real-time, inter-pulse skin impedance measurement system with high time resolution (100 ms), thus allowing the monitoring of skin recovery between successive pulses; a donor flow-through recycle system, which allows for rapid changes of the donor solution, even during pulsing, for mechanistic studies; the ability to measure random or irregularly spaced pulses or trains of pulses (thus negating the importance of accurately measuring t_{int} in **Subheading 2.5.1.**); and an improved liquid flow system to correct the pressure imbalance between the donor and receptor compartments (due to differences in their liquid heights). Furthermore, this reference also has complete listings for the computer programs used to record and analyze the data.

References

1. Chen, T., Segall, E. M., Langer, R., and Weaver, J. C. (1998) Skin electroporation: rapid measurements of the transdermal voltage and the flux of four fluorescent molecules show a transition to large fluxes near 50 V. *J. Pharm. Sci.* **87**, 1368–1374.

2. Prausnitz, M. R., Bose, V. G., Langer, R., and Weaver, J. C. (1993) Electroporation of mammalian skin: a mechanism to enhance transdermal drug delivery. *Proc. Natl. Acad. Sci. USA* **90**, 10,504–10,508.
3. Prausnitz, M. R., Edelman, E. R., Gimm, J. A., Langer R., and Weaver, J. C. (1995) Transdermal delivery of heparin by skin electroporation. *Biotechnology* **13**, 1205–1209.
4. Pliquett, U. and Weaver, J. C. (1996) Electroporation of human skin: simultaneous measurement of changes in the transport of two fluorescent molecules and in the passive electrical properties. *Bioelectrochem. Bioenerg.* **39**, 1–12.
5. Prausnitz, M. R., Lee, C. S., Liu, C. H., Pang, J. C., Singh, T.-P., Langer, R., and Weaver, J. C. (1996) Transdermal transport efficiency during skin electroporation and iontophoresis. *J. Controlled Release* **38**, 205–217.
6. Pliquett, U., Langer, R., and Weaver, J. C. (1995) Changes in the passive electrical properties of human stratum corneum due to electroporation. *Biochim. Biophys. Acta* **1239**, 111–121.
7. Prausnitz M. R., Gimm, J. A., Guy, R. H., Langer, R., Weaver, J. C., and Cullander, C. (1996) Imaging of transport pathways across human stratum corneum during high-voltage and low-voltage electrical exposures. *J. Pharm. Sci.* **85**, 1363–1370.
8. Vanbever, R., Pliquett, U. F., Pr at, V., and Weaver, J. C. (1999) Comparison of the effects of short, high-voltage and long, medium-voltage pulses on skin electrical and transport properties. *J. Controlled Release* **60**, 35–47.
9. Friend, D. R. (1996) In vitro skin permeation techniques. *J. Controlled Release* **18**, 235–248.
10. Fogler, H. S. (1992) *Elements of Chemical Reaction Engineering*. Prentice Hall, Englewood Cliffs, NJ.
11. Gummer, C. L. (1989) The in vitro evaluation of transdermal delivery. *Transdermal Drug Delivery: Developmental Issues and Research Initiatives* (Hadgraft, J. and Guy, R. H., eds.), Marcel Dekker, New York, pp. 176–186.
12. Chen, T., Langer, R., and Weaver, J. C. (1999) Charged microbeads are not transported across the human stratum corneum by short high-voltage pulses. *Bioelectrochem. Bioenerg.* **48**, 181–192.
13. Pliquett, U., Zewart, T. E., Chen, T., Langer, R., and Weaver, J. C. (1996) Imaging of fluorescent molecule and small ion transport through human stratum corneum during high voltage pulsing: localized transport regions are involved. *Biophys. Chem.* **58**, 185–204.
14. Pliquett, U., Prausnitz, M. R., Chizmadzhev, Y. A., and Weaver J. C. (1995) Measurement of rapid release kinetics for drug delivery. *Pharm. Res.* **12**, 549–555 [Errata in (1995) *Pharm. Res.* **12**, 1244].
15. Craane-Van Hisberg, W. H. M., Verhoef, J. C., Junginger, H. E., and Bodd , H. E. (1994) Thermoelectric analysis of the human skin barrier. *Thermochimica Acta.* **248**, 303–318.
16. Weaver, J. C., Vaughan, T. E., and Chizmadzhev, Y. A. (1999) Theory of electrical creation of aqueous pathways across skin transport barriers. *Adv. Drug Deliv. Rev.* **35**, 21–39.

Using Surface Electrodes to Monitor the Electric-Pulse-Induced Permeabilization of Porcine Skin

Stephen A. Gallo, Patricia G. Johnson, and Sek Wen Hui

1. Introduction

The stratum corneum, the outermost layer of the skin, acts as a barrier between the skin and the outside world, preventing evaporation of water from underlying tissues while impeding the diffusion of foreign molecules into the body (1,2). Densely packed layers of flattened, dead, keratinized cells (2,3) are incorporated into a lipid lamellae matrix consisting primarily of ceramides, cholesterol, and fatty acids (2,4), forming an impermeable, hydrophobic partition. The stratum corneum represents the main obstacle to efficient transdermal drug delivery (1,2). If the stratum corneum is disrupted, the barrier to molecular transport is greatly reduced.

Disruption of the stratum corneum can be achieved by electroporation. Electroporation is a technique first applied to create pervious cell membranes for cell loading and transfection (5,6). This method employs short (microseconds to milliseconds) pulses of sufficiently high voltage to permeabilize cell membranes. Molecules may pass through permeabilized membranes which reseal shortly after the pulses. The thin layer of highly resistive stratum corneum over less resistive dermis and underlying tissue is electrically analogous to the highly resistive plasma membrane over conductive cytoplasm on the cellular scale. If an electric field is imposed across the skin, most of the potential drop is developed across the resistive stratum corneum, where a breakdown is likely to occur when the imposed electric field rises beyond a certain critical strength (7).

Electroporation of the stratum corneum is different from iontophoresis, which is the movement of ions across the skin driven by a low electric field,

primarily through hair follicles and sweat glands. Electroporation, on the other hand, can be described as the creation of aqueous pores in lipid bilayers by an electric pulse. Ions are suggested to move through the gaps or pores of the keratinocyte layer of the stratum corneum (8).

The feasibility of transporting molecules through the stratum corneum has been explored by several groups, using heat-stripped stratum corneum or skin mounted in a side- by-side flow-through chamber. Molecular transport studies of a variety of species, electrical characterizations, and theoretical models have been achieved using data from this type of system (8–11). Full-thickness pig skin studies with surface electrodes have also been conducted, examining both electric properties and dye penetration (12,13) (see Note 1). This method is applied to simulate human, in vivo, transdermal drug delivery by electroporation. These studies on high voltage pulsing, together with the rich data on the mechanism and models for iontophoresis (14), provide the foundation for further studies of electroporation of the stratum corneum as a means to enhance transdermal molecular transport. In this chapter, a protocol for the electrical characterization of porcine skin after high-voltage pulsing is described.

2. Materials

2.1. Porcine Skin

Full thickness porcine skin is used as a model for in vivo human skin drug delivery (see Note 1). Belly skin from domestic pigs can usually be obtained from a local butcher or from a research laboratory, and can be kept on ice for several days before degradation occurs (see Notes 2 and 3).

2.2. Electrodes

Disposable Ag–AgCl electrodes (diameter = 18 mm, 2235-5, 3M Red Dot, St. Paul, MN) are used in conjunction with Sigma Gel[®] Saline electrode gel (Parker Laboratories, Orange, NJ) to ensure a good electrical connection (see Note 4).

2.3. Pulse Apparatus and Resistance Measuring Circuit

The following is a list of components used in the electrical setup for these procedures:

- a Dynascan Model 3300 pulse generator (Chicago, IL)
- a recording digital oscilloscope (Fluke 99 Scopemeter Series II, Holland)
- a pulse generator, such as a Model 345, Velonex (Santa Clara, CA)
- an electrical isolation switch
- a ceramic load resistor (5–20 k Ω)

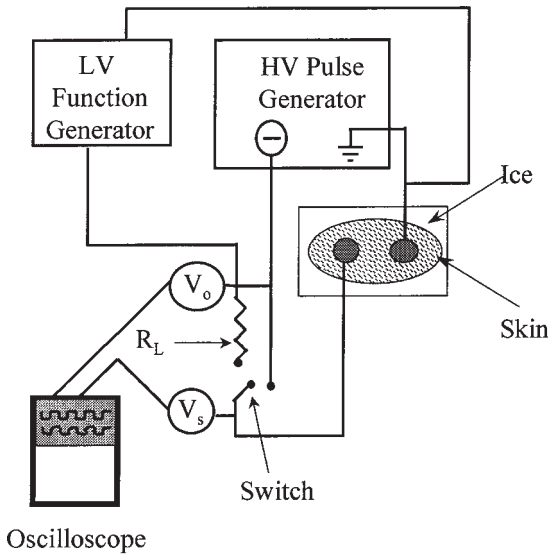


Fig. 1. Schematic diagram of electrical set-up. The low voltage function generator was used to measure the pre/post pulse resistance from oscilloscope measurements of V_o and V_s . The high voltage pulse generator was used to apply the permeating pulses and to measure the resistance during the pulse.

Pre and postpulse skin resistance can be measured using continuous low voltage (100–300 mV, 250–1000 Hz) bipolar square waveforms from a function generator (Dynascan Model 3300 pulse generator) (*see Note 5*). A load resistor (R_L) should be placed in series with the skin, so that the voltage drop across the whole circuit (V_o) and just across the skin (V_s) can be measured by a recording digital oscilloscope (Fluke 99 Scopemeter Series II, Holland) (*see Fig. 1*).

Electroporation is carried out using short, high voltage pulses (10–500 V, 0.5–10 ms, 0–100 Hz) from a pulse generator such as a Model 345, Velonex (Santa Clara, CA). Resistances can be measured during the pulse with the same voltage divider as with the low voltage generator, but a recording oscilloscope is needed. An electrical switch is connected to the circuit to isolate the low-voltage and high-voltage components (*see Note 6*) (**Fig. 1**).

3. Methods

3.1. Skin Preparation

1. Store fresh samples on ice in a watertight bag and use within 48 hours (*see Note 2*).
2. Wash a full-thickness 10×20 cm section and shave with electric clippers.

3. Place skin dermal side down, on Saran Wrap™, on a flat aluminum stage connected to aluminum cold fingers which dip into an ice reservoir. The skin is maintained at a temperature of 10°C in this fashion (see **Note 3**).
4. Skin should be gently but thoroughly dried to prevent surface current.
5. Place both electrodes on a previously unused region of the sample before resistance measurements or pulsing begin. Samples with initial resistance smaller than 5 kΩ should not be used because of the inconsistent results these samples can give (see **Note 7**).

3.2. Electrode Placement

1. Add conductive gel to the electrode surface to ensure good contact with the skin.
2. Attach electrodes to the skin with adhesive tape.
3. Place electrodes at a constant distance apart from each other (e.g., 5–10 cm).

3.3. Single Pulse Experiments

1. Apply a square wave signal to skin and record values for V_O and V_S from oscilloscope (see **Notes 5** and **8**).
2. Approximate skin resistance (in kilohms) from the formula $R_S = (V_S \times R_L) / (V_O - V_S)$, where R_S = skin resistance and R_L = load resistor, when the capacitive load of the stratum corneum is small compared to the resistive load (see **Fig. 1**). Match loads to the initial value of the skin to minimize error in resistance measurement.
3. Apply a single pulse to the skin. Measure the resistance during the pulse (R_s) using the pulse itself, which should be captured, and stored in the oscilloscope. The value of R_s/R_o during the pulse represents the transient resistance drop. Define a drop in skin resistance as transient if the resistance after the pulse (R_p) recovers to 90% or more of the prepulse resistance R_o within seconds.
4. Vary pulse width and voltage and record the resistance changes. The transient resistance drop (R_s/R_o) can be plotted against the parameter of interest (voltage, time, VT).
5. The transient resistance drop can be plotted against VT , which is calculated as the initial voltage across the skin multiplied by the exposure time of the skin to the pulse (**7,20**). This quantity can be considered as an electrical exposure dosage. In the single-pulse experiment, the exposure time is the pulse width. In our results, the normalized resistance decreased rapidly with increasing VT , and leveled out at a critical VT value of about 0.4 V-s (see **Fig. 2**).

3.4. Multiple Pulse Experiments

1. Calculate the skin's resistance according to **Subheading 3.3.2**.
2. Measure the resistance (R_o) before the pulse with the bipolar square wave.
3. Apply a train of pulses to the skin with a fixed voltage (V), pulse length (τ), frequency (f), and electrode contact time (t) (see **Note 9**).

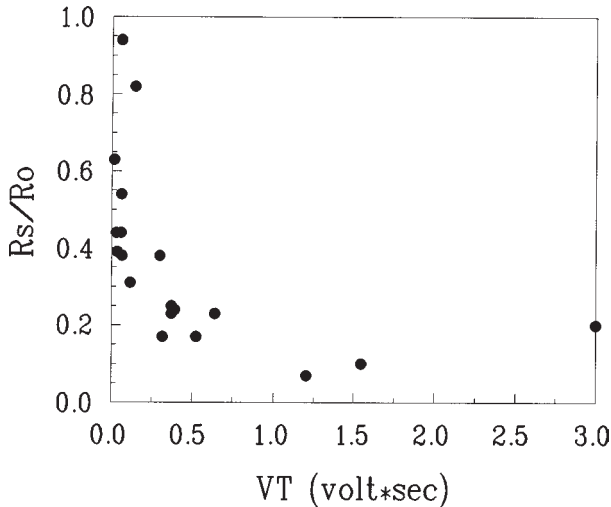


Fig. 2. Normalized skin resistance versus VT (voltage x exposure time). A single pulse was applied, and the resistance measured during the pulse was normalized by the pre-pulse value (*12*) (courtesy of Biophysical Journal).

4. Measure the postpulse resistance R_p with the square wave after the pulse train application. Monitor the recovery process every 10 min for 30 min. Define the resistance drop (R_p/R_o) as “long term” if only partial recovery of the initial resistance occurs after 30 minutes.
5. The influence of the independent parameters voltage, pulse length, frequency, and contact time on long-term permeabilization can be investigated separately.
6. The long term resistance drop (R_p/R_o) can also be plotted against VT (*see Note 10*). In these experiments, we have the formula $\tau ft = T$, where T represents the cumulative exposure time during which the skin experiences a pulsed electric field. In our results, a rapid decrease and then leveling of normalized resistance is observed (*see Fig. 3, ●*). However, superimposed on these data were points that did not follow the trend. Those data from pulse trains of voltages lower than 160 V do not show any apparent VT dependency, and most resistances remain more than 70% of the initial (*see Fig. 3, ■*).

4. Notes

1. Pig skin is a good model of human skin with respect to the size, structure, and composition of the stratum corneum (*2,15*). Full-thickness samples can be used to simulate human in vivo delivery, avoiding heat stripping and trypsinization procedures for excising the stratum corneum. The total resistance of the epidermal, dermal, and fatty layers has been measured to be less than 20% of that of the stratum corneum, the site at which most of the voltage drop occurs (*12*).

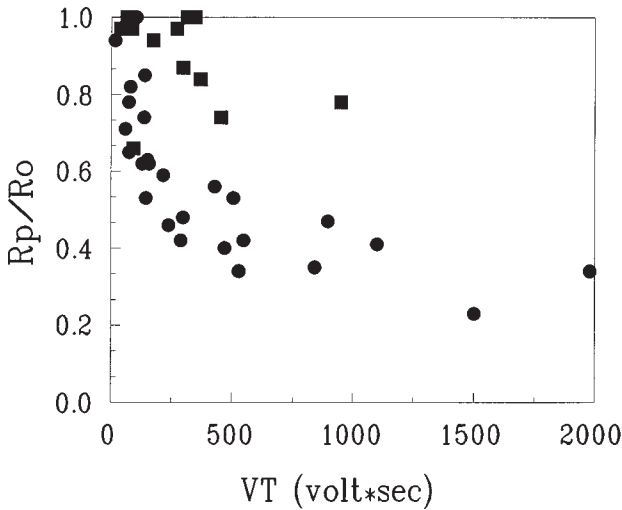


Fig. 3. Normalized post-pulse skin resistance versus VT for all voltages. The circles represent applied voltages above 160 volts while the squares represent less than 160 volts (*12*) (courtesy of Biophysical Journal).

2. Stratum corneum ultrastructure is altered with water content (*17,18*). Skin resistance also varies with its hydration state, higher water content translating into lower resistance (*19*). Sample preparation and storage protocols will have an effect on the variability of results. Samples should be stored in a closed environment, possibly with a water reservoir, and should be allowed to equilibrate before using. Samples should be allowed to equilibrate for about an hour after removal from storage.
3. It has been shown that temperature affects the electrical properties of the skin, specifically the resistance which goes down with increasing temperature (*14*). Time for temperature equilibration should be allotted before experimenting. In our system, the skin temperature is about 10°C and stays relatively constant for the duration of the study. Cooling the skin avoids degradation, and methylene blue transport studies at room temperature show no significant difference from those at 10°C (*13*).
4. Ag-AgCl gel electrodes are used in human iontophoretic delivery to reduce the generation of hydroxonium and hydroxy ions which have been implicated in skin irritation and burning (*16*). Reusable electrodes are also available (diameter = 8 mm, #E256A, In Vivo Metric, Healdsburg, CA).
5. A square wave signal should be used for resistance measurements, enabling the observation of the charging and discharging of the skin capacitor. Depending on the circuit charging time, frequencies of 250–1000 Hz should be used so that

the voltage is allowed to saturate or plateau, enabling accurate resistance measurements.

6. A negatively polarized square pulse of voltages 10–500 V and lengths of 0.5 ms to 10 ms is needed. The pulse length should be greater than the charging time of the circuit, 0.5–2 ms. The generator may be triggered manually, for single pulses, and internally, for multiple pulses, at frequencies of 1–100 Hz, although the duty cycle should not exceed 10% due to the risk of overloading the generator and excessive damage to the skin. A high power generator, in this case with an input impedance of 200 Ω can produce square, high voltage pulses even with low loads. It is necessary for use with electroporated tissues which lose the bulk of their resistance during the pulse. A small ceramic resistor is placed in parallel with the circuit to maintain a relatively constant load to the pulse generator.
7. The resistance of skin samples can vary cyclically with the time of the year, fall to winter being times of high resistance and spring and summer being times of low resistance. This may be due to a variety of reasons; stratum corneum thickness variation, sunburn, seasonal parasites, etc. Resistances seldom peak above 5 k Ω during the warmer seasons and because these samples give highly scattered data, they are not used. If the pigs used come from farms, seasonal variations may come into play more often than those maintained in a research laboratory because of sterile, controllable conditions in which the animals are likely to be kept.
8. Both electrodes are placed on the skin surface in an attempt to simulate pulsing conditions in human in vivo delivery. Different areas of the skin have different resistances, due to inhomogeneity of stratum corneum thickness and density of skin appendages (hair follicles, sweat ducts, etc.). Because resistances vary regionally, only normalized results are applicable to these kinds of studies.
9. Although some discoloration occurs, usually the Ag–AgCl electrodes (3M Red Dot) can withstand exposure to high-voltage pulse trains for minutes to hours. Electrode failure is observed at voltages above 300 V by a large increase in the measured skin resistance. After this, the electrodes should be disposed of and replenished with another pair.
10. Although electrical data can characterize the skin's electrical properties, further information must be collected on the specific molecule of interest. For instance, the size of electropores necessary for ion transport are likely to be much smaller than those allowing drug transport. Consequently, higher voltages or more pulses may be necessary to create a pathway. Thus the critical electrical dosage (VT) may be much larger than those for ion transport and will depend on size and charge of the molecule. Even so, the relationships with electrical dosage are similar for molecular and ion transport (13).

References

1. Bronaugh, R. L. and Maibach, H. I. (1989) *Percutaneous Absorption, Mechanisms—Methodology—Drug Delivery*. Marcel Dekker, New York.

2. Hadgraft, J. and Guy, R. H. (1989) *Transdermal Drug Delivery, Developmental Issues and Research Initiatives*. Marcel Dekker, New York.
3. Madison, K. C., Swartzendruber, D. C., Wertz, P. W., and Downing, D. T. (1987) Presence of intact intercellular lipid lamella in the upper layers of the stratum corneum. *J. Invest. Dermatol.* **88**, 714–718.
4. Schurer, N. J. and Elias, P. M. (1992) The biochemistry and function of stratum corneum lipids. *Adv. Lipid Res.* **24**, 27–56.
5. Chang, D. C., Chassy, B. M., Saunders, J. A., and Sowers, A. E. (1992) *Handbook of Electroporation and Electrofusion*. Academic Press, New York.
6. Liang, H., Purucker, W. J., Stenger, D. A., Kubinieć, R. T., and Hui, S. W. (1988) Uptake of fluorescence-labeled dextrans by 10T1/2 fibroblasts following permeation by rectangular and exponential-decay electric field pulses. *Biotechniques* **6**, 550–558.
7. Yamamoto, T. (1977) Electrical properties of the epidermal stratum corneum. *Med. Biol. Eng.* **14**, 151–158.
8. Chizmadzhev, Y., Zarnytsin, V., Weaver, J. C., and Potts, R. O. (1995) Mechanism of electroinduced ionic species transport through a multilamellar lipid system. *Biophys. J.* **68**, 749–765.
9. Prausnitz, M., Bose, V., Langer, R., and Weaver, J. C. (1993) Electroporation of mammalian skin: A mechanism to enhance transdermal drug delivery. *Proc. Natl. Acad. Sci. USA* **90**, 10,504–10,508.
10. Vanbever, R. and Preat, V. (1995) Factors affecting transdermal delivery of metoprolol by electroporation. *Bioelectrochem. Bioenerg.* **38**, 223–228.
11. Pliquett, U., Langer, R., and Weaver, J. C. (1995) Changes in the passive electrical properties of human stratum corneum due to electroporation. *Biochim. Biophys. Acta* **1239**, 111–121.
12. Gallo S. A., Oseroff A. R., Johnson P. G., Hui S. W. (1997) Characterization of electric-pulse-induced permeabilization of porcine skin using surface electrodes. *Biophys. J.* **72**, 2805–2811.
13. Johnson P. G., Gallo S. A., Hui S. W., Oseroff, A. R. (1998) A pulsed electric field enhances cutaneous delivery of methylene blue in excised full-thickness porcine skin. *J. Invest. Dermatol.* **111**, 457–463.
14. Oh, S. Y., Leung, L., Bommannan, D., Guy, R. H., and Potts, R. O. (1993) Effect of current, ionic strength and temperature on the electrical properties of skin. *J. Controlled Release* **27**, 115–125.
15. Ferry, L., Argentieri, G., and Lochner, D. (1995). The comparative histology of porcine and guinea pig skin with respect to iontophoretic drug delivery. *Pharm. Acta Helv.* **70**, 43–56.
16. Ledger, P. W. (1991) Skin biological issues in electrically enhanced transdermal delivery. *Adv. Drug Deliv. Rev.* **9**, 289–307.
17. Bouwstra, J. A., Gooris, G. S., van der Spek, J. A., and Bras, W. (1991) Structural investigations of human stratum corneum by small-angle X-ray scattering. *J. Invest. Dermatol.* **97**, 1005–1012.

18. Van Hal, D. A., Jeremiase, E., Junginger, H. E., Spies, F., and Bouwstra, J. A. (1996) Structure of fully hydrated human stratum corneum: A freeze-fracture electron microscopy study. *Soc. Invest. Dermatol.* **106**, 89–95.
19. Alonso, A., Meirelles, N. C., Yushmanov, V. E., and Tabak, M. (1996) Water increases the fluidity of intercellular membranes of stratum corneum: Correlation with water permeability, elastic, and electrical resistance properties. *J. Invest. Dermatol.* **106**, 1058–1063.
20. Kubinieć, R. T., Liang, H., and Hui, S. W. (1990) Effects of pulse length and pulse strength on transfection by electroporation. *Biotechniques* **8**, 1–3.

Transdermal Delivery Using Surface Electrodes in Porcine Skin

Patricia G. Johnson, Stephen A. Gallo, and Sek Wen Hui

1. Introduction

The main barrier to cutaneous or transcutaneous drug and gene delivery is the impermeability of the stratum corneum (SC), the outermost layer of the skin (1). If the integrity of the SC is disrupted, the barrier to molecular transit may be greatly reduced. Cutaneous absorption can be increased by removal of the SC by tape-stripping or dermabrasion, by vehicle (solvent-carrier) optimization, or by the use of penetration enhancers like DMSO (dimethylsulfoxide), oleic acid, and alcohols (2,3). An electric field can also be used to enhance delivery. Disruption of the SC can be achieved by electroporation, which is the creation of penetration sites by an electric pulse. Ions and molecules move through induced gaps of the SC by diffusion and electromotive or electroosmotic transport (4–6). Electroporation differs from iontophoresis, in which there is an increased migration of ions or charged molecules through the skin when an electrical potential gradient is applied. The primary transdermal route for iontophoresis seems to be appendageal or intercellular through preexisting pathways (5,7), or as a result of low-voltage (<5 V) induced permeabilization of appendageal bilayers (8). A third form of electroenhanced drug delivery, electrochemotherapy (9), refers to localized delivery of electric pulses across a tumor following systemic or intratumor drug administration, and usually does not involve cutaneous or transcutaneous delivery.

The bulk of studies describing electric field-enhanced transport of molecules across skin have used heat-stripped SC or epidermis mounted between flow-through chambers (10–13), and measures the amount of material traversing the skin sample. Some animal in vivo work has been reported using murine mod-

els to study the electroporative delivery of drugs (**14**), microspheres (**15**), and DNA (**16**). However, mouse skin is often not an ideal model for human skin in transport studies, because of the differences in anatomical features, and especially the thickness of the stratum corneum (**17,18**).

A convenient model for transport studies is porcine skin. Its structure and characteristics closely approximate those of human skin (**17,19,20**), and pig skin is easy to obtain. In vivo conditions are well-simulated by full-thickness skin with two electrodes attached to the skin surface. In this way, it is possible to monitor delivery to the skin, measuring both the amount in the sample and the penetration depth. This system should more closely model any projected in vivo use.

2. Materials

2.1. Skin

1. Belly skin from domestic pigs can usually be obtained from a local butcher, or from a research laboratory (*see Note 1*).
2. Remove skin as soon as possible after the animal is euthanized.
3. Using a surgical scalpel, make an incision and remove the skin down to the dermis/adipose tissue junction.
4. Rinse the skin, pat dry, and store in an airtight plastic bag held on ice in a cold room.
5. Fresh skin samples should be used within 3 d.
6. Alternatively, skin samples may be stored in an airtight plastic bag and frozen (-80°C) for up to several months (*see Note 2*).

2.2. Electroporation Equipment

1. Low-Voltage Continuous Wave Generator: An electronic function generator is used to provide continuous low voltage waves (e.g., 300 mV, 1000 Hz bipolar square waves) so that the pre- and postpulse skin resistance can be measured without pulse-induced damage to the sample. Function generators are available from a number of sources, including Stanford Research Systems (Sunnyvale, CA) and Electronix Express (Avenel, NJ).
2. Electroporation Pulse Generator: Suppliers of pulse generators that have been used for electroporation experiments include Velonex (**21**) in Santa Clara, CA, BioRad in Hercules, CA (**14**), and BTX (**7**), from Genetronics, San Diego, CA (*see Note 3*).
3. Electrodes: Electrodes may be fabricated in-house, or purchased. Silver–silver chloride (Ag–AgCl) electrodes are a good choice for in vivo work because the silver and silver chloride are virtually insoluble in water, so very few silver ions are generated, and toxicity is very low. Ag–AgCl electrodes (diameter = 8 mm, E256A) and adhesive electrode washers (E410) may be purchased from In Vivo Metric, Healdsburg, CA. Because these electrodes have a 2-mm-deep cavity, an

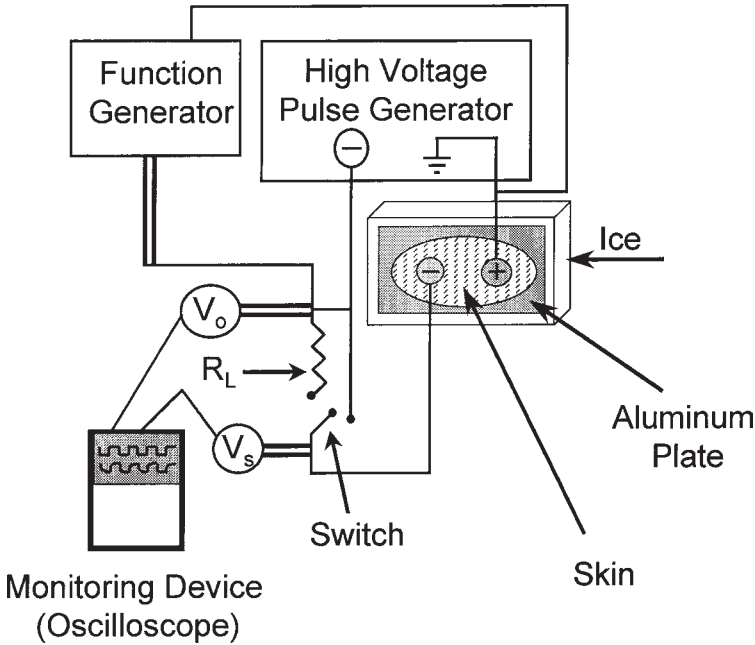


Fig. 1. Diagram of components assembled for delivering pulses to an excised skin sample. Note that connections drawn as double lines must be grounded.

electrode gel (e.g., Signa Gel[®] Saline electrode gel, Parker Laboratories, Orange, NJ) should be used to ensure a good electrical connection (*see Subheading 3.2.*).

4. Monitoring Device: A recording digital oscilloscope, such as a Fluke Scopemeter (Holland), is used to monitor the voltage, pulse width, and pulse frequency. The electric exposure dose in V-s (21,22) is calculated as

$$VT = V \times f \times \tau \times t \tag{1}$$

where V = applied voltage, $T = f \times \tau \times t$ = field application time, f = frequency (hertz), τ = pulse width (milliseconds), and t = treatment duration (seconds).

5. Resistor: A load resistor (R_L) is placed in series with the skin for the purpose of current measurement, and the voltage drop across the whole circuit (V_0) or just across the skin (V_S) is measured. The R_L should be chosen to approximate the resistance of the skin. For example, $R_L = 4.7, 22,$ or $56 \text{ k}\Omega$ are often used. Skin resistance (in kilohms) is approximated from the formula

$$R_S = R_L \left(\frac{V_S}{V_0 - V_S} \right) \tag{2}$$

where R_S = skin resistance, R_L = load resistor, V_0 = the voltage drop across the whole circuit, and V_S = the voltage drop across just the skin (*see Fig. 1*).

2.3. Selection of Transport Material

The choice of material to be delivered to or through the skin is dictated in large part by the experimental design. Several properties of the material will have an effect on the success of cutaneous or transcutaneous delivery. These properties include its lipophilicity, charge, and molecular size. For purposes of monitoring transport, a colored material can be easily detected in a skin section with light microscopy, and its absorbance in biopsy samples can be measured spectroscopically (*see Subheading 3.5.*). Fluorescent material can often be seen with a fluorescence microscope, and fluorescence spectroscopy can be used to quantitate the material in a sample. Methylene blue is used as an example in this chapter. Fluorescent molecules can also be used; protocol modification for using these types of molecules are mentioned throughout.

2.4. Transport Assay Materials

1. Frozen biopsy materials: A disposable biopsy punch (5 mm diameter), such as is available from Fray Products, Amherst, NY, is used to isolate a sample of known diameter. Tissue-Tek[®] Cryomolds (15 mm × 15 mm × 5 mm) and Tissue-Tek[®] O.C.T Compound (Miles Inc., Elkhart, IN) or Cryo-Gel[™] (Instrumedics, Inc., Hackensack, NJ) are used to prepare frozen specimens for cryosectioning.
2. Imaging: A light (phase) microscope, preferably with fluorescence capabilities, is necessary for observing histologic sections. A CCD camera is useful for recording the microscope images for further processing, using an image processing program.
3. Solubilizer: The punch biopsy samples are solubilized with Solvable[™] tissue and gel solubilizer (0.5 M solution) from Packard Instrument Co., Meriden, CT.
4. Spectroscopy: An absorption spectrometer will be used for quantitating the amount of colored material in a biopsy sample, and/or a fluorescence spectrometer will be necessary for measuring transport of a fluorescent material (*see Note 4*).

3. Method

3.1. Skin Preparation

1. Cut a conveniently sized full-thickness skin sample (e.g., 10 × 20 cm).
2. Remove the hair using standard animal clippers prior to electroporation experiments.
3. Gently wash the skin with an antibacterial soap and thoroughly pat dry. Care should be taken not to disrupt the stratum corneum layer.
4. Place the skin, dermal side down, on plastic wrap on ice (*see Note 5*).
5. Keep the sample covered with plastic wrap to prevent the skin from drying out when the skin is not being actively treated (*see Note 6*).

3.2. Electrode Loading and Placement

1. For skin resistance measurements, fill both electrode cavities with an electrode gel, or with a small piece of cotton soaked in a buffer (e.g., PBS).

2. For delivery of a drug or other material, fill the passive electrode cavity with an electrode gel, or with a small piece of cotton soaked in a buffer (e.g., PBS). Soak a small piece of cotton with a known amount of a solution of the material to be delivered (*see Note 7*), and place in the cavity of the active electrode (*see Note 8*).
3. Attach electrodes to the skin using adhesive washers (In Vivo Metric, Healdsburg, CA). Alternatively, electrodes may be placed on the skin and lightly weighted to ensure good contact, or secured with surgical tape.
4. Place electrodes a constant distance apart (e.g., 5–10 cm).

3.3. Determining Skin Resistance

With the switch connecting the function generator (**Fig. 1**), apply low voltage square waves. Record the voltage drop across the whole circuit (V_O) and across just the skin (V_S). Calculate the skin resistance R_S using **Eq. 2**. Generally a skin sample should not be used if the resistance $R_S < 5 \text{ k}\Omega$ (*see Note 9*).

3.4. Pulse Application for Transdermal Delivery

Deliver electric pulses using a pulse generator that delivers multiple unipolar square pulses at a constant frequency and with a fixed pulse width. We found that optimum results for transport of methylene blue were obtained with 1 ms pulses of 240 V, delivered at a frequency of 40 Hz for 30 minutes (**21**).

3.5. Quantitation of Material in Dissolved-Sample Supernatant

1. After treatment, rinse the skin to remove superficial material.
2. Cut full-thickness 5-mm punch biopsy samples.
3. Dissolve each biopsy sample overnight in 1 ml Solvable™ at 37°C.
4. Centrifuge the solutions.
5. Record the absorbance spectra of the supernatant fractions.
6. Plot the optical density at λ_{max} as a function of whatever parameter is under investigation (e.g., V , τ , f , t , or VT). *See Fig. 2* for an example.
7. To quantitate the amount of material in each sample, a calibration curve should be generated for known amounts of the dye dissolved in Solvable™ and incubated at 37°C overnight. This is because Solvable™, which is very basic, will often shift the absorbance maximum. The amount of material transported per unit area of the stratum corneum (as determined from the punch biopsy diameter) can be calculated.
8. If fluorescent molecule transport is under investigation, perform a similar assay using a fluorescence spectrometer. Follow the protocol outlined above (**steps 1–4**), then determine the correct excitation and emission maxima for the material dissolved in Solvable™ and incubated at 37°C overnight. Collect fluorescence spectra of the supernatant fractions (analogous to **step 5**), plot the fluorescence intensity at λ_{max} as a function of whatever parameter is under investigation

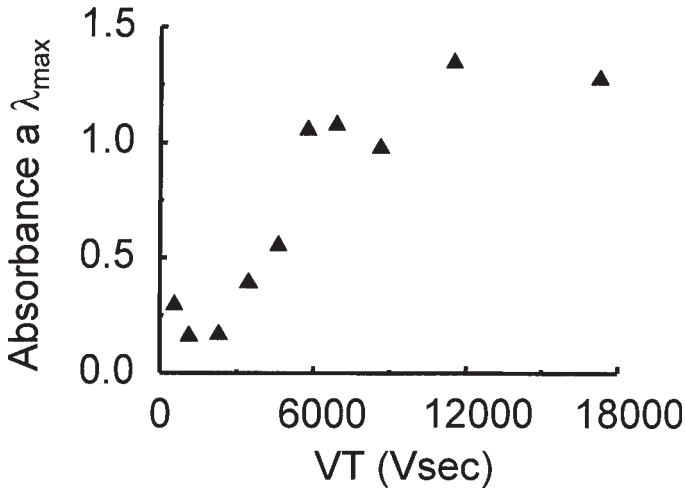


Fig. 2. Illustrative results of the effect of the electroporating dose VT (in volt-seconds) on the amount of methylene blue delivered to punch biopsy samples of pig skin. The data was generated by following the procedure in **Subheading 3.5., steps 1–7.**

(analogous to **step 6**), and generate a fluorescence emission calibration curve for known amounts of the dye dissolved in Solvable™ and incubated at 37°C overnight (analogous to **step 7**).

3.6. Microscopy

1. Embed full-thickness biopsies in Tissue-Tek O.C.T. compound or Cryo-Gel in Cryomolds.
2. Freeze in isopentane (*n*-methylbutane) cooled by liquid nitrogen.
3. Cut cryostat sections (10 μm) perpendicular to the skin surface.
4. Collect images with an ordinary camera mounted on the microscope or with a CCD camera.
5. Using image processing software, quantitate the dye by measuring the transmittance at the appropriate wavelength for each pixel along a line normal to the skin surface.
6. Convert pixel number to depth in micrometers by calibration with a section of known dimensions.
7. Plot the adsorbance (transmittance⁻¹) intensity vs penetration depth (*see Fig. 3*).
8. Fluorescence Microscopy: Perform the assay as above, but using a fluorescence microscope. Excite the fluorescence of the material with light of an appropriate wavelength, and detect using an appropriate long-pass filter.

4. Notes

1. We have found seasonal variations in the quality of pig skin. Skin obtained during late spring and summer is usually of lower quality, as indicated by a dramatic

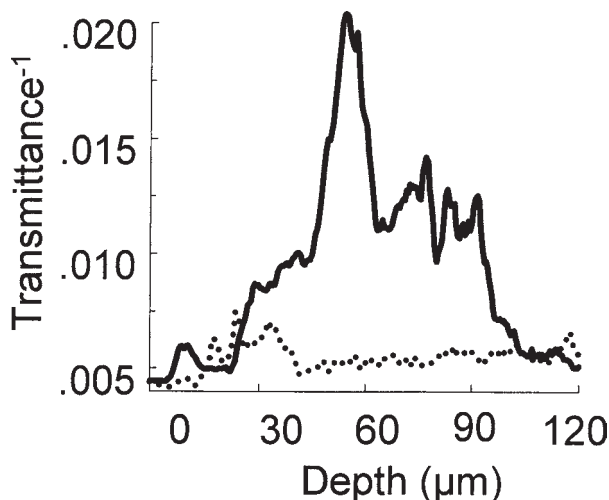


Fig. 3. Relative amounts of dye appearing at various depths in porcine skin following passive diffusion (•••) and pulse application (—). The data was generated by following the procedure in **Subheading 3.6., steps 1–7.**

drop in electrical resistance (to $<5 \text{ k}\Omega$). This is probably due, at least in part, to SC damage induced by sun, parasites, and other factors. It is more acute in skin harvested from domestic pigs raised under normal livestock conditions, and is somewhat less in animals spending a period of time indoors under laboratory animal housing conditions.

2. When there is a surplus of pig skin, and/or shortages are anticipated, it is recommended that some skin be frozen and preserved for future use. It is convenient to remove the hair (using animal clippers) and wash the skin before freezing. Pat the sample dry and measure the electrical resistance. Cover the sample with plastic wrap, place in an airtight container, and store at -80°C for up to 6 mo.
3. Pulse generators typically produce square and/or exponential pulses, although other pulse shapes are available. We prefer to use square pulses for electroporation. The pulse generator selected should have the capability to produce pulses of different widths (e.g., microseconds to seconds) and to deliver pulses at different frequencies, including single pulses. Also, the instrument should be able to deliver high-voltage pulses, up to at least 300 V.
4. Radiolabeled material can also be quantitated, using scintillation counting of dissolved biopsy samples, or autoradiography of cryosections.
5. An aluminum stand can easily be constructed which will sit in an ice bucket. This provides a flat surface on which the skin rests, and ensures even cooling. The stand should be covered with a sheet of plastic wrap so that no electrical conductance to the aluminum is possible.
6. The hydration level of a skin sample will affect its electrical resistance. Therefore it is important to limit hydration changes over the course of an experiment.

The skin should be covered with plastic wrap whenever possible to prevent extensive drying.

7. For the experiments described above, we used 200 μl of methylene blue (obtained from Fisher Scientific, Fairlawn, NJ) diluted to 1% in ddH₂O (w/v).
8. When delivering a charged molecule, the active electrode will be the electrode with the same charge as the molecule. That is, a positively charged molecule is placed beneath the anode, and will travel in the direction of the current flow. Negatively charged material is placed beneath the cathode, and moves in the direction of the electron flow. A neutral molecule is usually placed beneath the anode, since electroosmosis will tend to carry aqueous material (23).
9. We have found that when the electrical resistance of the skin is low ($<5\text{ k}\Omega$), inconsistent results are obtained. This is probably due to damage to the stratum corneum, as discussed in **Note 1** above.

References

1. Scheuplein, R. J. and Bronaugh, R. L. (1983) Percutaneous absorption. *Biochemistry and Physiology of the Skin* (Goldsmith, L. A., ed.), Oxford University Press, New York, pp. 1255–1295.
2. Berti, J. J. and Lipsky, J. J. (1995) Transcutaneous drug delivery: A practical review. *Mayo Clin. Proc.* **70**, 581–586.
3. Singh, S. and Singh, J. (1993) Transdermal drug delivery by passive diffusion and iontophoresis: A review. *Med. Res. Rev.* **13**, 569–621.
4. Edwards, D. A., Prausnitz, M. R., Langer, R., and Weaver, J. C. (1995) Analysis of enhanced transdermal transport by skin electroporation. *J. Controlled Release* **34**, 211–221.
5. Edwards, D. A. and Langer, R. (1994) A linear theory of transdermal transport phenomena. *J. Pharm. Sci.* **83**, 1315–1334.
6. Chizmadzhev, Y. A., Zarnitsin, V. G., Weaver, J. C., and Potts, R. O. (1995) Mechanism of electroinduced ionic species transport through a multilamellar lipid system. *Biophys. J.* **68**, 749–765.
7. Lee, R. D., White, H. S., and Scott, E. R. (1996) Visualization of iontophoretic transport paths in cultured and animal skin models. *J. Pharm. Sci.* **85**, 1186–1190.
8. Chizmadzhev, Y. A., Indendom, A. V., Kuzmin, P. I., Galichenko, S. V., Weaver, J. C., and Potts, R. O. (1998) Electrical properties of skin at moderate voltages: Contribution of appendageal macropores. *Biophys. J.* **74**, 843–856.
9. Mir, L. M., Orłowski, S., Belehradek, J., Teissié, J., Rols, M. P., Serša, G., Miklavčič, D., Gilbert, R., and Heller, R. (1995) Biomedical applications of electric pulses with special emphasis on antitumor electrochemotherapy. *Bioelectrochem. Bioenerg.* **38**, 203–207.
10. Bommannan, D. B., Tamada, J., Leung, L., and Potts, R. O. (1994) Effect of electroporation on transdermal iontophoretic delivery of luteinizing hormone releasing hormone (LHRH) in vitro. *Pharmacol. Res.* **11**, 1809–1814.
11. Pliquett, U. F., Zewert, T. E., Chen, T., Langer, R., and Weaver, J. C. (1996) Imaging of fluorescent molecule and small ion transport through human stratum

- corneum during high voltage pulsing—localized transport regions are involved. *Biophys. Chem.* **58**, 185–204.
12. Prausnitz, M. R., Edelman, E. R., Gimm, J. A., Langer, R., and Weaver, J. C. (1995) Transdermal delivery of heparin by skin electroporation. *Biotechnology* **13**, 1205–1209.
 13. Vanbever, R. and Pr eat, V. (1995) Factors affecting transdermal delivery of metoprolol by electroporation. *Bioelectrochem. Bioenerg.* **38**, 223–228.
 14. Prausnitz, M. R., Bose, V. G., Langer, R., and Weaver, J. C. (1993) Electroporation of mammalian skin: A mechanism to enhance transdermal drug delivery. *Proc. Natl. Acad. Sci. USA* **90**, 10,504–10,508.
 15. Hofmann, G. A., Rustrum, W. V., and Suder, K. S. (1995) Electro-incorporation of microcarriers as a method for the transdermal delivery of large molecules. *Bioelectrochem. Bioenerg.* **38**, 209–222.
 16. Titomirov, A. V., Sukharev, S., and Kistanova, E. (1991) In vivo electroporation and stable transformation of skin cells of newborn mice by plasmid DNA. *Biochim. Biophys. Acta* **1088**, 131–134.
 17. Bronaugh, R. L., Stewart, R. F., and Congdon, E. R. (1982) Methods for in vitro percutaneous absorption studies. II. Animal models for human skin. *Toxicol. Appl. Pharmacol.* **62**, 481–488.
 18. Panchagnula, R., Stemmer, K., and Ritschel, W. A. (1997) Animal models for transdermal drug delivery. *Methods Find. Exp. Clin. Pharmacol.* **19**, 335–341.
 19. Steinstrasser, I. and Merkle, H. P. (1995) Dermal metabolism of topically applied drugs: Pathways and models reconsidered. *Pharm. Acta Helv.* **70**, 3–24.
 20. Ferry, L. L., Argentieri, G., and Lochner, D. H. (1995) The comparative histology of porcine and guinea pig skin with respect to iontophoretic drug delivery. *Pharm. Acta Helv.* **70**, 43–56.
 21. Johnson, P. G., Gallo, S. A., Hui, S. W., and Oseroff, A. R. (1998) A pulsed electric field enhances cutaneous delivery of methylene blue in full-thickness porcine skin. *J. Invest. Dermatol.* **111**, 457–463.
 22. Liang, H., Purucker, W. J., Stenger, D. A., Kubiniec, R. T., and Hui, S. W. (1988) Uptake of fluorescence-labeled dextrans by 10T1/2 fibroblasts following permeation by rectangular and exponential-decay electric field pulses. *Biotechniques* **6**, 550–558.
 23. Riviere, J. E. and Heit, M. C. (1997) Electrically-assisted transdermal drug delivery. *Pharm. Res.* **14**, 687–697.

Transdermal Drug Delivery by Skin Electroporation in the Rat

Rita Vanbever and Véronique Pr at

1. Introduction

Drug delivery across skin offers advantages over conventional modes of administration. It avoids gastrointestinal degradation and the hepatic first-pass effect, has potential for controlled and sustained delivery, is user-friendly and therefore improves patient compliance (1–2). However, because the skin’s outer layer, the stratum corneum, is an extremely effective barrier, transdermal transport of most drugs is very slow, exhibits lag times of hours and steady-state rates that are often subtherapeutic. Chemical and physical approaches to increasing transdermal transport have been explored. Recently, the intermittent application of short (e.g., milliseconds), high-voltage (e.g., 100 V across skin) pulses has been shown to increase transport across skin by several orders of magnitude on a time scale of minutes, probably by a mechanism involving electroporation (3–6).

Electroporation (or electropermeabilization) involves the creation of transient aqueous pathways across lipid bilayer membranes by applying a short, high-voltage pulse (7–9). The electrical conductance, permeability and molecular transport across the membrane rapidly increase by orders of magnitude. This phenomenon occurs in the lipid bilayer membranes of nonliving systems, such as liposomes or red blood cell ghosts, as well as the plasma membranes of living cells, either isolated or part of a tissue. Most recently, electroporation of the multilamellar, intercellular lipid bilayers of stratum corneum has also been demonstrated (3–6).

Electroporation of skin can increase transport across and/or into skin for compounds presenting different size (e.g., metoprolol, 267 Da; heparin,

~12 kDa), solubility (e.g., water-soluble as oligonucleotide, oil-soluble as domperidone) as well as electrical charge (e.g., highly charged as calcein, neutral as mannitol) (4). Within a few minutes of high-voltage pulsing, transdermal transport can increase by up to four orders of magnitude, mainly due to electrophoretic movement and diffusion through newly created aqueous pathways (10–12). Control on molecular flux is achieved by controlling the electrical parameters of the pulses (e.g., pulse voltage, duration, number, and spacing) and the physicochemical parameters of the drug and solution (e.g., drug concentration) (3,13,14).

The features of transdermal transport due to electrical pulses suggest new opportunities for transdermal drug delivery. Using high-voltage pulses, transdermal delivery might be applicable to a broader range of drugs, that is, to drugs presenting variable physicochemical properties, and might offer an alternative to the injectable route. Skin electroporation might also open new perspectives for topical delivery, where the ability of electrical pulses to permeabilize the cell membrane of the cutaneous or subcutaneous tissue could be useful for chemotherapy, gene therapy and DNA vaccination (15–19). In addition, biophysical investigation of the stratum corneum *in vitro*, noninvasive investigation of the skin *in vivo* in hairless rats as well as clinical experience with electrochemotherapy suggest that electroporation is a safe procedure that could be used in humans for drug delivery (15,16,20–24).

Most work on transport across skin due to high-voltage pulses has been performed *in vitro*, however, the few studies carried out *in vivo* have shown similar features of transport. Results yielded *in vivo* and relevant to this chapter on transdermal drug delivery by skin electroporation in the rat are developed in more details below.

Transdermal fluxes of calcein, a moderate-sized, highly polar fluorescent molecule which does not normally cross skin in detectable quantities, were measured following application of low-duty cycle electric-field pulses *in vivo* in hairless rats (3,25). Calcein plasma concentrations under pulsed conditions were at least two orders of magnitude higher than the controls (no electric field pulses), where transport was below the detection limit.

A subsequent more comprehensive study with fentanyl demonstrated, in addition to the enhanced transport, the fast onset of therapeutic action and the control achieved on the dose delivered transdermally using high-voltage pulses (11). Fentanyl is currently administered by injections, passive transport across skin, or via the oral mucosa. Transdermal fentanyl delivery has been developed for the management of moderate to severe chronic pain. After placement of a fentanyl transdermal system, serum concentrations increase during the first 14 hours and then reach a plateau (26). Pain treatment can however require rapid and pulsed administration of drugs. Fentanyl delivered across skin by

high-voltage pulsing in vivo in hairless rats exhibited an onset time of action reduced to a few minutes. High-voltage pulsing was applied for 5 min. Immediately after pulsing, fentanyl plasma levels already reached the third of the maximal plasma concentrations attained approximately 45 min after the electroporation (**Fig. 1A**). Elevated plasma concentrations were associated with strong pharmacological effects: deep analgesia was achieved and lasted for one hour. Without application of pulses, no antinociception effects were measured (**Fig. 1B**). Supraspinal side effects of fentanyl, that is, total blockade of the pinna and cornea reflexes and strong increases in skeletal muscle tone, were also observed immediately after the electroporation. When comparing electroporation to a subcutaneous injection, the onset time to achieve pharmacological response was as fast. When comparing electroporation to iontophoresis at identical duration, the onset time to achieve pharmacological response was faster and the response stronger and longer following high-voltage pulsing. This study with fentanyl also demonstrated the control on transport obtained by controlling the electrical parameters of the pulses, where electrical protocols transporting more electrical charges through skin induced stronger and longer antinociception effects of fentanyl.

Flurbiprofen, a potent nonsteroid antiinflammatory drug, has been used as a model drug to compare transdermal transport due to high-voltage pulses and iontophoresis in vivo in hairless rats (27). Flurbiprofen transport across skin was greater and more rapid following electroporation than following iontophoresis of same amount of transported charges. Plasma concentrations and the area under the curve were almost twice as high, and the peak in plasma concentrations reached earlier following electroporation, that is, immediately at the end of high-voltage pulsing vs 15 min after stopping iontophoretic current.

This protocol chapter gives materials and methods used for in vivo transdermal drug delivery by skin electroporation. The thorough protocol followed with fentanyl in the rat has been chosen as model protocol and is presented in detail (11). The methods are valid for other conventional drugs or macromolecules provided that the formulation of the donor solution and the electrical pulses are optimized for the specific use. Additional notes are given in a separate section and provide explanations, criticism and optional variants for the protocol.

2. Materials

1. Animals: 2-mo-old hairless male rats (200–300 g, Iops mutant from Iffa Credo, France) housed in standard cages at room temperature on a 12-h light and 12-h dark cycle, with access to standard laboratory food (A04, UAR-France) and water ad libitum (*see* **Notes 1** and **2**).

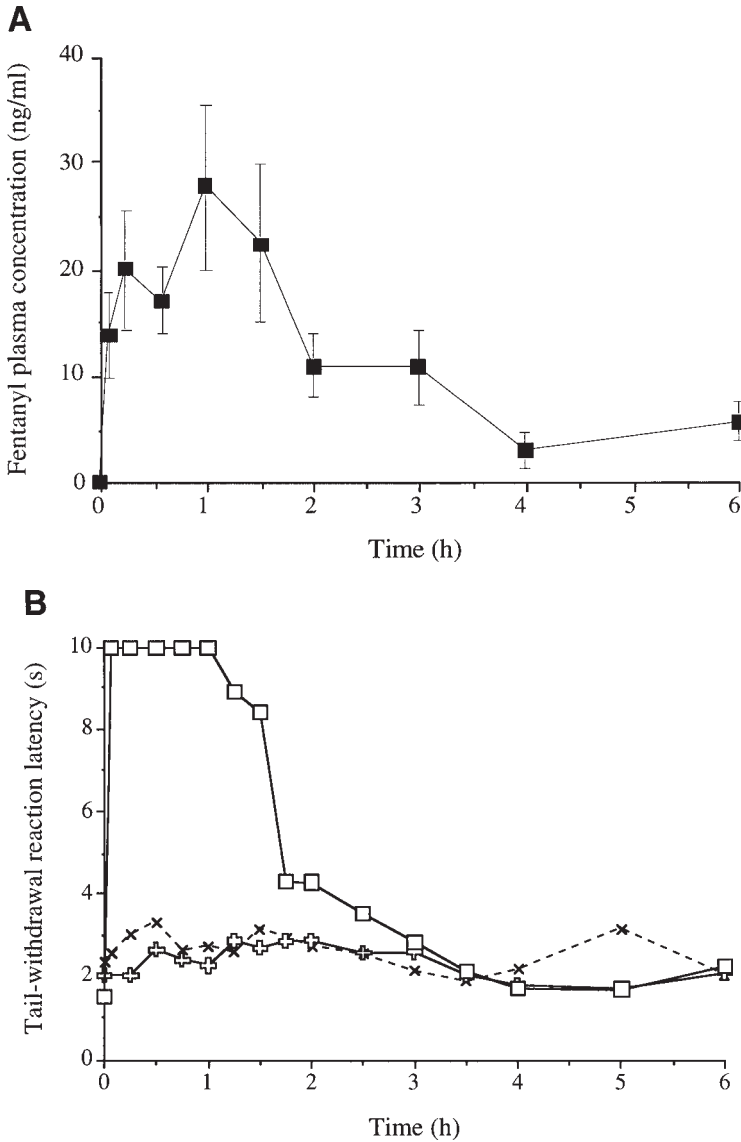


Fig. 1. Transdermal delivery of fentanyl using skin electroporation in the hairless rat. **(A)** Fentanyl plasma concentrations and **(B)** tail-withdrawal reaction latency as a function of time after transdermal delivery of fentanyl using 15 exponential pulses of 250 V (voltage applied across the electrodes) and 200 ms, applied from time 0 to 5 min (□). Foams at the cathode and anode were soaked with a solution of fentanyl (400 $\mu\text{g/ml}$ in citrate buffer 0.01 M at pH 5). The controls, no pulsing, no fentanyl present (×), and no pulsing, fentanyl present (⊕), are shown in (B). (From **ref. 11**, with permission.)

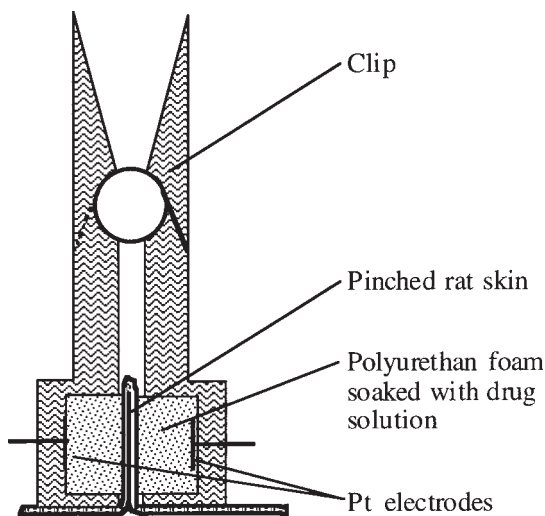


Fig. 2. Drawing of the custom-built clip used for transdermal administration of drugs by skin electroporation in vivo.

2. Electroporation device: an instrument capable of delivering exponential-decay capacitive discharge pulses (e.g., Easyject Plus from Equibio Ltd., Kent, England) is preferable (*see Note 5*). The pulse time constant is defined as the length of time between the beginning of the pulse (maximum voltage) and the time when the voltage reaches 37% of its initial value. During a pulse, electrical behavior is measured with an oscilloscope (model 54602B, Hewlett-Packard; *see Sub-heading 3.1.*).
3. Electrodes: high-voltage pulses are applied across a fold of abdominal skin using a custom-built clip (**Fig. 2**). The clip, made of polycarbonate (Makrolon, Obra, Liège, Belgium), is composed of two compartments each containing a polyurethane hydrophilic foam of 1 cm thickness and $1 \times 3 \text{ cm}^2$ surface. A platinum electrode of $0.5 \times 2 \text{ cm}^2$ (99.99% purity, Aldrich Chemie, Belgium) is stuck on the inner surface of each compartment, at the outer surface of each foam, and connected to the electroporation apparatus (*see Note 4*).
4. Drug: fentanyl citrate is purchased from Janssen Pharmaceutica (Beerse, Belgium). For delivery by skin electroporation, an acidic solution of fentanyl at $400 \mu\text{g/mL}$ in a citrate buffer 0.01 M at pH 5 is freshly prepared (*see Note 6*). Salts for buffer preparation are analytical grade (Union Chimique Belge, Drogenbos, Belgium). Fentanyl plasma levels are measured by radioimmunoassay (RIA; Janssen Biotech, Beerse, Belgium; *see Note 8*). The limit of detection and accuracy of the assay is 0.1 ng/mL and 6%, respectively.

3. Methods

Transdermal delivery of fentanyl by skin electroporation in vivo in the rat is assessed by measuring fentanyl plasma levels and pharmacological response in two separate sets of experiments (*II*). Common parts of the protocols are presented first. Then, specific pharmacokinetic and pharmacological measurements as well as relevant informations on the experiments are described.

3.1. Drug Delivery

1. Before delivering the drug, take a blood sample or test rat behavior to get the baseline for the pharmacokinetic or pharmacological study, respectively (*see Subheadings 3.2. and 3.3.*).
2. Anesthetize the rat by ether breathing for the pharmacokinetic study (*see Note 3*), or keep it motionless in a restraining cage for the pharmacodynamic study (custom-built cage, with a hole at the abdominal site for placement of the clip).
3. Abundantly soak both foams of the clip (**Fig. 2**) with the fentanyl solution (400 $\mu\text{g}/\text{mL}$) or with the drug free buffer (control group; *see Subheading 3.4.*).
4. Pinch the abdominal skin of the rat and hold the skin fold with the clip (**Fig. 2**). Only use the abdominal skin and not the back skin, which is thicker.
5. Connect the electrodes of the clip to the electroporation device.
6. Apply high-voltage pulses to the skinfold (*see Note 5*). Measure voltages applied across the electrodes ($U_{\text{electrodes}}$) with an oscilloscope. Calculate corresponding peak currents using Ohm's law by measuring the voltage across a sampling resistor (5 Ω) in series with the clip. Once $U_{\text{electrodes}}$, the current and electrical resistance of the solutions between the electrodes and skin known, calculate corresponding transdermal voltages (U_{skin}) and skin resistances using Ohm's law (**28**). During a pulse, skin resistance can drop up to a few tens of ohms. As a result, significant voltage drops occur within solutions soaking the foams making U_{skin} up to an order of magnitude smaller than $U_{\text{electrodes}}$. For example, pulses applied at 250 V and 200 ms yielded 45 V across the skin, 150 Ω skin resistance and 0.1 A/cm^2 peak current density (*II*).
7. After application of pulses, let the rat wake up or set it free from the restraining cage.
8. Take blood samples from the rat for the pharmacokinetic study or assess pharmacological response using behavioral tests (*see Subheadings 3.2., 3.3., and 3.4.*).

3.2. Pharmacokinetic Study

1. Take plasma samples by tail incision and transfer on anticoagulant (ethylenediaminetetraacetate; Sigma Chemical Co., St. Louis, MO) before (baseline) and immediately (within 1 min) after the electroporation, and then after at 15 min, 35 min, 1 h, 1.5 h, 2 h, 3 h, 4 h, and 6 h after the beginning of the electroporation treatment (*see Subheading 3.1.; Fig. 1A; and Note 7*).
2. Store samples at -20°C until analysis.

3. Determine fentanyl plasma concentrations by RIA without extraction and express as average values (*see Note 8*).
4. Because in vivo pharmacokinetic data are variable, use at least six rats per condition. Measure the area under the curve (AUC) by the trapezoidal rule for each individual rat and then average. In the same manner, average peaks in fentanyl plasma concentrations (C_{\max}) and times for peak plasma concentrations (t_{\max}).

3.3. Pharmacodynamic Study

In another set of experiments, test the rats for pharmacological response, that is, analgesic effect and supraspinal side effects on pinna and cornea reflexes and on skeletal muscle tone, before (baseline), and at different times after the delivery of fentanyl by electroporation, that is, immediately after, and then every 15 min until 6 h after pulsing (*see Subheading 3.1.*). Blockade of the cornea and pinna reflexes are characteristic effects of opioid analgesics at the level of the tenth and fifth cranial nerves, whereas rigidity probably originates in the striatum and substantia nigra. Supraspinal effects require approximately twofold higher doses of fentanyl than antinociception (**31–33**). Make measurements blindfold for each test.

3.3.1 Analgesia Assay

Measure nociceptive response using the tail-withdrawal reaction (TWR) method (**Fig. 1B**) (**31–33**).

1. Place the rat in a cylindrical rat holder with its tail hanging freely outside the cage.
2. Immerse the distal 5 cm of the tail in a warm water bath at $55 \pm 0.5^\circ\text{C}$.
3. Measure the time for tail withdrawal to the nearest 0.1 s. To minimize tissue damage at repeated testing, use a cutoff time of 10 s. Adopt a criteria of mild and deep analgesia such as TWR latency >5.0 s and ≥ 10.0 s, respectively. These can be chosen as a TWR latency >5.0 s and thus also ≥ 10.0 s never occurs in untreated control rats (**31–33**).
4. Remove the rat from the cylindrical holder.

3.3.2. Supraspinal Effects

Score the blockade of the cornea and pinna reflexes and the muscular tone, as follows.

1. Take the rat in hands or keep it motionless on the table by hand (**31–33**).
2. Gently touch the inner ear with a blunt metal rod (diameter 1.5 mm). The pinna reflex consists of a characteristic head twitch induced by the gentle mechanical stimulation. Score the response of the animal from 0 (normal reflex) to 3 (absence of any motor response). Scores 1 and 2 indicate that the reflex is slightly or markedly attenuated, respectively.

3. Gently touch the cornea with the metal rod. The cornea reflex consists in quickly closing the eyes. Score from 0 (normal reflex) to 3 (absence of any motor response).
4. Determine muscular tone by hand and visually. The scores given for overall skeletal muscle tone range from 0 (normal tone) to 3 (lead pipe rigidity); scores 1 and 2 represent weakly and moderately increased tone, respectively.
5. In untreated control animals, a score >1 never occurs for the pinna and cornea reflexes and for muscle tone. Use a score of 3 as criterion of significant blockade of the pinna and cornea reflexes and of significant induction of muscle rigidity (31–33).

3.3.3. Data Analysis

Express TWR latencies, pinna and cornea scores, and muscle tones as median (minimum–maximum) values. Use at least four rats per condition. Because pharmacological responses are less variable than plasma concentrations, a smaller number of rats can be used.

For further analysis, convert TWR latencies to percentage of maximal possible effect (%MPE) according to the formula:

$$\%MPE = \frac{\text{post-drug latency} - \text{pre-drug latency}}{\text{cut-off time (10 s)} - \text{pre-drug latency}}$$

and calculate the area under the effect curve using the trapezoidal rule (11,31–33).

3.4. Commentary

Select one or several skin electroporation protocols to deliver fentanyl across skin (*see Note 5*). Use for comparison and as positive control of pharmacological response a subcutaneous injection of fentanyl. Eventually, compare also to iontophoresis (*see Note 5*). In the pharmacological study, use three additional groups of rats as controls: Group 1: maintain the rat in the restraining cage with the clip clamping a skinfold and the foams being soaked with the citrate buffer; Group 2 as Group 1, except apply high-voltage pulses to measure a possible analgesic effect due to pulsing alone; Group 3 as Group 1, except soak the foams with the drug solution to evaluate possible fentanyl effects due to passive diffusion (11).

4. Notes

1. OTHER DRUGS. When delivering another compound than fentanyl, conditions to optimize include the drug concentration and the ionic strength of the buffer of solution put on skin, the electrical parameters of the high-voltage pulses and the exposed skin surface area (*see Note 5*). Because the dose delivered depends on drug concentration and skin surface area which are kept constant among rats, it

is important to use rats of similar weight (i.e., similar age) in order to avoid too large variability in dose delivered per kilogram. Measurement of pharmacological response is useful as it yields further information on transport as well as allows correlation with pharmacokinetic data; pharmacodynamic tests proper to the drug delivered should be selected.

2. **ANIMAL MODEL.** In vivo studies on transdermal drug delivery using skin electroporation were performed in animal models (3,5,11). The choice of a model is critical (34,35). Pig skin most closely approaches human skin, except that porcine skin lacks eccrine sweat glands as do the various species of hairless rodents. Although skin toxicology of combined electroporation to iontophoresis was evaluated in pigs (12), this animal has not been used for studies of transdermal transport by skin electroporation in vivo. Pigs are difficult to handle for pharmacokinetic and pharmacodynamic studies, as well as more expensive.

Hairless rodents are commonly used for both in vitro and in vivo transdermal drug delivery experiments (34,35). They have a much thinner stratum corneum than man, although they exhibit similar residual hair follicle density. Consequently, skin absorption rates can be substantially greater than in man, although for iontophoretic transport rates level out. Since the blood content of mice for pharmacokinetic studies is very small, hairless rats were chosen for our study with fentanyl (11).

When transdermal transport is not localized at the hair follicles but rather occurs through the bulk of the stratum corneum (e.g., transdermal transport due to ultrasound), the use of hairy rodents (e.g., rats, guinea pigs), shaved before cutaneous treatment, is reasonable (36).

3. **ANESTHESIA.** Because high-voltage pulsing causes sensation in the rats (e.g., vocalization and spontaneous movements), as well as induces muscle twitches, brief anesthesia is induced by ether breathing for the time of pulsing in the pharmacokinetic study. The rat is placed in a cylindrical rat holder with a gauze moistened with ether placed at its muzzle. After a few minutes of ether breathing, the rat is anesthetized. It is then removed from the holder and put on its back for electroporation of its abdominal skin. A face-mask of ether is put back and forth near its muzzle to keep it anesthetized. Overdose can be avoided by checking the rat breathing.

Instead of using a cylindrical rat holder to start the anesthesia, the rat can be placed in an anesthesia chamber with atmosphere loaded with ether. However, as ether has chemical enhancer properties, one might question its effect on skin and therefore the influence of this procedure on transdermal transport.

Optional methods to anesthetize rodents can be selected based on different purposes (37). Halothane is another inhalational anesthetic, possible alternative to ether; intramuscular or intraperitoneal injection of combined ketamine/xylazine (90/10 mg/kg), subcutaneous injection of combined droperidol/fentanyl (4/0.08 mg/kg), or intraperitoneal injection of pentobarbital (40 mg/kg) are also commonly used.

4. **ELECTRODES DESIGN.** The design of the electrodes is critical for both drug delivery and tolerance issues. The electric field should be efficient to enhance stratum corneum permeability and to drive the drug to the blood vessels. However, if the electric field penetrates below the skin, pain, sensation, muscle contraction, and/or tissue damage can be induced (5,30).

Our setup involves a custom-built clip enclosing parallel-plate electrodes and clamping a skin fold (Fig. 2). The electrodes are introduced at the outer surfaces of the clip instead of being in direct contact with skin. This allows a homogenous distribution of the electric field to the skin surface, as well as avoids burning the skin by direct contact. Inert electrodes, such as the platinum electrodes, induce electrolysis of water with acidification at the anode and alkalization at the cathode. A buffer is therefore required in order to avoid any pH shift of the solution. The use of a buffer not sufficiently concentrated to maintain the pH but regularly replenished is another possibility which can be advantageous by reducing concentration of competing ions and therefore promoting drug transport (13,38). Traditional active electrodes (e.g., Ag/AgCl) are not ideal. The electrochemical reaction is not fast enough and silver cations produced at the anode do not remain on the electrode but precipitate in solution as well as AgCl plating the cathode can detach during pulsing. However, electrodes made of homogeneously mixed Ag/AgCl (*In vivo* Metrics, Healdsburg, CA) have been shown to work properly in skin electroporation experiments (3,25).

The parallel-plate electrodes configuration has been used in most animals studies as well as in humans for electrochemotherapy (3,11,15–18,24,25,27). However, this design causes side effects (e.g., sensation) by exposing underlying tissues to the high-voltage electric field (5,29,30); also it is not the most convenient method for application in humans in case of transdermal drug delivery. A different electrode configuration which is more suited to an implementation in a patch, has been mentioned (39). It consists of an array of interweaving electrode fingers called “meander electrodes.” This configuration was theoretically expected to provide equipotential lines parallel to the electrode and to concentrate the electric field in the upper layers of the skin. However, no supportive experimental data were provided in this study. A microfabricated electrode array, another plane and closely spaced electrodes system, is presently under development at the Massachusetts Institute of Technology (J. C. Weaver, personal communication, 1997).

5. **ELECTRICAL CONDITIONS.** Experiments on transdermal transport using skin electroporation *in vitro* generally use exponential-decay electric field pulses of 100 V to 1500 V applied voltage, 30–100 V transdermal voltages and 1 ms to hundreds of ms pulse duration (3–6,10–14,19–25,27,38). Increasing transported charges by increasing pulse voltage, duration and/or number all increases drug transport. In this range of electrical conditions, two main pulse protocols can be differentiated: the intermittent application (1 pulse per 5 s) of short (~1 ms) high-voltage (1000 V across the electrodes, ~100 V across skin) pulses and a few (5 to 20) applications of long (≥ 100 ms) smaller voltage (>100 V across the electrodes,

>30 V across skin) pulses. For the same total transported charge, more rapid and greater transdermal transport was achieved using long pulses of medium voltage (40).

In contrast to skin electroporation experiments, electrochemotherapy (i.e., the electropermeabilization of tumor tissue shortly after an intravenous injection of bleomycin) studies have only used square-wave electrical pulses (15,16). When comparing square-wave to exponential-decay pulses at same total transported charge in vitro, exponential pulses induced in some cases greater transport across skin than square-wave pulses (41). However, due to different electrical configurations, square-wave devices provide less variability in pulse time constant with skin sample.

Selection of electrical parameters for electroporation experiments in vivo is based on the guideline provided by in vitro experiments. In the case of the study with fentanyl, the two following protocols have particularly demonstrated excellent efficiency for transport: 15 exponential pulses of 250 V $U_{\text{electrodes}}$ and 200 ms pulse time constant, and 15 exponential pulses of 100 V $U_{\text{electrodes}}$ and 500 ms pulse time constant, both applied at an approximate pulse rate of 1 pulse per 15 s (11). Using noninvasive bioengineering methods, these protocols were also shown to be well tolerated (24). In exploratory experiments in our setup in vivo, the maximal tolerated voltage ranged around 300 V (applied voltage) when using pulses ≥ 100 ms. Above this value, skin presented an intense erythema.

Comparison of skin electroporation with iontophoresis in vivo has been made at identical duration of current application (see the study with fentanyl) and in a second more rigorous comparison, at identical duration of current application and identical total transported charge (see the study with flurbiprofen) (11,27). Both studies concluded that skin electroporation transported more efficiently molecules across skin than iontophoresis, whereas the techniques were shown equally well tolerated (24).

6. FORMULATION OF DRUG SOLUTION. During a pulse, the electric field is believed to play the dual role of causing pore formation and providing a local driving force for ionic and molecular transport through the pores (3,4,6–9,13). When administering a drug by skin electroporation, the drug should therefore be charged whenever possible, in order to benefit from electrophoresis. An appropriate pH where the drug is under ionized condition can be chosen by considering the pK_a of the drug.

In the case of fentanyl ($pK_a = 8.9$), a pH of 5 is chosen so that fentanyl carried one positive charge. Another advantage is that the aqueous solubility of fentanyl in the ionized form is higher, allowing increased concentration of drug exposed to skin. A citrate buffer is chosen as fentanyl is sold as a citrate salt.

The solution of fentanyl is placed in contact with skin using foams impregnated with solution. Another possibility is to directly fill the compartments with solution (without the foams) once the clip clamping skin, through a hole made on top of the compartments.

7. BLOOD SAMPLING. Blood samples can be withdrawn from the rat by tail sectioning, retroorbital bleeding using a capillary, or by jugular or femoral vein

cannulation. Catheterization is the best technique (e.g., collection of blood having the most representative concentrations of analytes vs the systemic circulation), but it requires a surgical operation and therefore some training (42).

Times for sampling need to be chosen based on the pharmacokinetic profile expected. Transport across skin due to electroporation has been shown to occur within minutes of pulsing (10–12). A first blood sample should therefore be withdrawn as soon as the electroporation finished or even during the electroporation, if practical (e.g., when using catheterization). High-voltage pulsing has been shown to load the skin and/or underlying tissues with the drug, plasma concentrations can therefore still increase after pulsing stops. In order to obtain the entire pharmacokinetic profile (peak in plasma concentrations and return to zero), collection of blood should be based on this effect as well as the elimination half-life of the drug (Fig. 1A).

8. DRUG ANALYSIS. The analytical method for drug analysis must be selected based on the physicochemical properties of the drug, its dosage and expected plasma levels. The method must be sensitive, robust, and accurate. High-performance liquid chromatography (HPLC) methods with ultraviolet (UV) or fluorimetric detection can be used if UV absorption or fluorescence of the drug and/or plasma levels are sufficiently high. An advantage of HPLC lies in its ability to quantify metabolites. Radioimmunoassay (RIA) techniques are more sensitive. A cross-reaction of the antibody with metabolites should be avoided. New sensitive analytical methods such as LC/MS (HPLC coupled with mass spectrometry) or capillary electrophoresis (CE) have been developed. They require, however, more expensive equipment and expertise (43).

References

1. Hadgraft, J. and Guy, R. H. (1989) *Transdermal Drug Delivery: Development Issues and Research Initiatives*. Marcel Dekker, New York.
2. Smith, E. W. and Maibach, H.I. (1995) *Percutaneous Penetration Enhancers*. CRC Press, Boca Raton, FL.
3. Prausnitz, M. R., Bose, V. G., Langer, R., and Weaver, J. C. (1993) Electroporation of mammalian skin: A mechanism to enhance transdermal drug delivery. *Proc. Natl. Acad. Sci. USA* **90**, 10,504–10,508.
4. Prausnitz, M. R. (1999) A practical assessment of transdermal drug delivery by skin electroporation. *Adv. Drug Deliv. Rev.* **35**, 61–76.
5. Vanbever, R. and Pr eat, V. (1999) In vivo efficacy and safety of skin electroporation. *Adv. Drug Deliv. Rev.* **35**, 77–88.
6. Pliquett, U. (1999) Mechanistic studies of molecular transdermal transport due to skin electroporation. *Adv. Drug Deliv. Rev.* **35**, 41–60.
7. Neumann, E., Sowers, A. E., and Jordan, C. A. (1989) *Electroporation and Electrofusion in Cell Biology*. Plenum, New York.
8. Chang, D. C., Chassy, B. M., Saunders, J. A., and Sowers, A. E. (1992) *Guide to Electroporation and Electrofusion*. Academic Press, New York.

9. Weaver, J. C. (1993) Electroporation: A general phenomenon for manipulating cells and tissues. *J. Cell. Biochem.* **51**, 426–435.
10. Pliquett, U. F. and Weaver, J. C. (1996) Electroporation of human skin: Simultaneous measurement of changes in the transport of two fluorescent molecules and in the passive electrical properties. *Bioelectrochem. Bioenerg.* **39**, 1–12.
11. Vanbever, R., Langers, G., Montmayeur, S., and Pr at, V. (1998) Transdermal delivery of fentanyl: Rapid onset of analgesia using skin electroporation. *J. Controlled Release* **50**, 225–235.
12. Riviere, J. E., Monteiro-Riviere, N. A., Rogers, R. A., Bommannan, D., Tamada, J. A., and Potts, R. O. (1995) Pulsatile transdermal delivery of LHRH using electroporation: Drug delivery and skin toxicology. *J. Controlled Release* **36**, 229–233.
13. Vanbever, R., Lecouturier, N., and Pr at, V. (1994) Transdermal delivery of metoprolol by electroporation. *Pharm. Res.* **11**, 1657–1662.
14. Vanbever, R., Le Bouleng , E., and Pr at, V. (1996) Transdermal delivery of fentanyl by electroporation I. Influence of electrical factors. *Pharm. Res.* **13**, 559–565.
15. Mir, L., Orłowski, S., Belehradek, J. J., and Paoletti, C. (1991) Electrochemotherapy: Potentiation of antitumor effect of bleomycin by electric pulses. *Eur. J. Cancer* **27**, 68–72.
16. Heller, R., Jaroszeski, R., Glass, L. F., Messina, J., Rappaport, D., De Conti, R., Fenske, N., Gilbert, B., Mir, L., and Reintgen, D. (1996) Phase I/II trial for the treatment of cutaneous and subcutaneous tumor using electrochemotherapy. *Cancer* **77**, 964–971.
17. Titomirov, A., Sukharev, S., and Kistanova, E. (1991) In vivo electroporation and stable transformation of skin cells of newborn mice by plasmid DNA. *Biochim. Biophys. Acta* **1088**, 131–134.
18. Zhang, L., Li, L. N., An, Z. L., Hoffman, R. M., and Hofmann, G. A. (1997) In vivo transdermal delivery of large molecules by pressure-mediated electroincorporation and electroporation: A novel method for drug and gene delivery. *Bioelectrochem. Bioenerg.* **42**, 283–292.
19. Regnier, V. and Pr at V. (1999) Localisation of a FITC-labelled phosphorothioate oligodeoxynucleotide in the skin after topical delivery by iontophoresis or electroporation. *Pharm. Res.* **15**, 1596–1602.
20. Pliquett, U. F., Langer, R., and Weaver, J. C. (1995) Changes in the passive electrical properties of human stratum corneum due to electroporation. *Biochim Biophys. Acta* **1239**, 111–121.
21. Jadoul, A., Regnier, V., Doucet, J., Durand, D., and Pr at, V. (1997) X-ray scattering analysis of the stratum corneum treated by high voltage pulses. *Pharm. Res.* **14**, 1275–1277.
22. Jadoul, A., Tanajo, H., Pr at, V., Spies, F., and Bodd , H. (1998) Electroperturbation of human stratum corneum fine structure by high voltage pulses: A freeze fracture electron microscopy and differential thermal analysis study. *J. Invest. Dermatol. Symp. Proc.* **3**, 153–158.

23. Jadoul, A., Bouwstra, J., Pr eat, V. (1999) Effects of iontophoresis and electroporation on the stratum corneum: Review of biophysical studies. *Adv. Drug Deliv. Rev.* **35**, 89–105.
24. Vanbever, R., Fouchard, D., Jadoul, A., De Morre, N., Pr eat, V., and Marty, J.-P. (1998) In vivo non-invasive evaluation of hairless rat skin after high-voltage pulse exposure. *Skin Pharmacol. Appl. Skin Physiol.* **11**, 23–34.
25. Prausnitz, M. R., Seddick, D. S., Kon, A. A., Bose, V. G., Frankenburg, S., Klaus, S. N., Langer, R., and Weaver, J. C. (1993) Methods for in vivo tissue electroporation using surface electrodes. *Drug Delivery* **1**, 125–131.
26. Varvel, J. R., Shafer, S. L., Hwang, S. S., Coen, P. A., and Stanski, D. R. (1989) Absorption characteristics of transdermally administered fentanyl. *Anesthesiology* **70**, 928–934.
27. Perez de la Cruz, M., Eeckhoudt, S., Verbeeck, R., and Pr eat, V. (1997) Transdermal delivery of flurbiprofen in the rat by iontophoresis and electroporation. *Pharm. Res.* **11 (S14)**, 309.
28. Prausnitz, M. R., Pliquett, U., and Vanbever, R. (1999) Mechanistic studies of skin electroporation using biophysical methods. *Electrically-Mediated Delivery of Molecules to Cells—Electrochemotherapy, Electrogenotherapy, and Transdermal Delivery by Electroporation* (Jaroszeski, M. J., Gilbert, R., and Heller, R., eds.), pp. 213–245.
29. Ledger, P. W. (1992) Skin biological issues in electrically enhanced transdermal delivery. *Adv. Drug Del. Rev.* **9**, 289–307.
30. Prausnitz, M. R. (1996) The effects of electric current applied to the skin: a review for transdermal drug delivery. *Adv. Drug Deliv. Rev.* **18**, 395–425.
31. Meert, T. F., Noorduyn, H., Van Craenendonck, H., Vermote, P., Boersma, F. P., and Janssen, P. A. J. (1989) Effects of adrenaline, an α_2 -adrenoceptor agonist, the volume of injection, and the global pain state of the animal on the activity of epidural fentanyl. *Acta Anaesthesiol. Belg.* **40**, 247–261.
32. Meert, T. F. and De Kock, M. (1994) Potentiation of the analgesic properties of fentanyl-like opioids with α_2 -adrenoceptor agonist in rats. *Anesthesiology* **81**, 677–688.
33. Buerkle, H. and Yaksh, T. L. (1996) Continuous intrathecal administration of short-lasting μ opioids remifentanyl and alfentanil in the rat. *Anesthesiology* **84**, 926–935.
34. Kempainen, B. W. and Reifenrath, W. G. (1990) *Methods for Skin Absorption*. CRC Press, Boca Raton, FL.
35. Shah, V. P., Flynn, G. L., Guy, R. H., Maibach, H. I., Schaefer, H., Skelly, J. P., Wester, R. C., and Yacobi, A. (1991) In vivo percutaneous penetration/absorption. *Pharm. Res.* **8**, 1071–1075.
36. Levy, D., Kost, J., Meshulam, Y., and Langer, R. (1989) Effect of ultrasound on transdermal drug delivery to rats and guinea pigs. *J. Clin. Invest.* **83**, 2074–2078.
37. Flecknell, P. A. (1987) *Laboratory Animal Anaesthesia*. Academic Press, New York.

38. Vanbever, R., De Morre, N., and Pr at, V. (1996) Transdermal delivery of fentanyl by electroporation. II. Mechanisms involved in drug transport. *Pharm. Res.* **13**, 1359–1365.
39. Hofmann, G. A., Rustrum, W. V., and Suder, K. S. (1995) Electro-incorporation of microcarriers as a method for the transdermal delivery of large molecules. *Bioelectrochem. Bioenerg.* **38**, 209–222.
40. Vanbever, R., Pliquett, U., Pr at, V. and Weaver, J. C. (1999) Effects of short and long high-voltage pulses on skin electrical and transport properties. *J. Controlled Release* **69**, 35–47.
41. Pr at V. and Vanbever, R. (1995) Transdermal drug delivery by electroporation, in *Prediction of Percutaneous Penetration* (Brain, K. R. James V. J., and Walters, K. A., eds.), Cardiff, 4b: pp. 26–29.
42. Waynforth H. B. and Flecknell P. A. (1992) Experimental and surgical technique in the rat. Academic Press, New York.
43. Harris, D. C. (1995) *Quantitative Chemical Analysis*. W. H. Freeman, New York.

In Vivo Skin-Targeted Gene Delivery by Pulsed Electric Fields

Lei Zhang

1. Introduction

The skin is an especially attractive target for gene therapy. In particular, the ability to target genes to the epidermis of the skin could be used to correct skin-specific disorders as well as for the production of proteins secreted into the skin and the circulatory system to correct certain systemic diseases (1–3). For example, genes expressing cytokines, interferons, or other biologically active molecules could be used to treat skin tumors or other lesions. In addition, keratinocytes and fibroblasts in the skin may secrete protein factors to treat systemic conditions such as hemophilia (4). In other words, this technology for skin-targeted gene therapy would be useful not only for treating local indications, but also for treating systemic diseases by exploiting the secretory capability of the epidermal keratinocytes (5). It is reasonable to believe that skin-targeted gene delivery has great potential and is biologically sound as is indicated by the substantial *in vitro* and *ex vivo* data (6,7). However, despite the clear potential in using skin as a target for gene therapy, the major technical problem of an *in vivo* method of gene delivery remains mostly unresolved. Since the stratum corneum (SC) acts as a significant physical barrier against molecular transfer into the skin, the technical problem of how to deliver molecules as large as genes through this layer still persists. This chapter describes an *in vivo* method using pulsed electric fields to deliver naked reporter genes into the skin as “proof of principle.”

1.1. Epidermis as a Target Tissue for Gene Therapy

There are several potential advantages to targeting the epidermis of the skin for gene therapy (8–11). First, the epidermis is an accessible tissue, which sim-

plifies approaches for the introduction of a transgene. In addition, the accessibility of the epidermis also facilitates monitoring of the site of gene introduction, which may be removed easily in the event of any adverse occurrence. Keratinocytes, the predominant cell type in the epidermis, and hence the cellular target for gene transfer, form the skin barrier making them amenable to in vivo manipulation. Second, there may be advantages to differentially target transgene expression to the epidermal compartments. The epidermis is a stratified squamous epithelium consisting of a basal proliferating compartment and a suprabasal, differentiating compartment (12). The transcriptional promoters of a number of genes expressed in the epidermis have been characterized (7,13–16). Third, keratinocytes function as synthetic and secretory cells (17). Keratinocytes have been shown to synthesize and secrete in vivo the products of transfected genes. Circulating transgene-derived proteins such as growth hormone (GH) (16), apolipoprotein E (ApoE) (18), and factor IX (FIX) (5,7,13) have been detected in athymic mice bearing grafts of keratinocytes. This demonstrates that transgene products expressed in the epidermis can penetrate the basement membrane zone and reach the systemic circulation. Fourth, it has recently been demonstrated that a systemic disease phenotype can be corrected by virtue of expressing the deficient gene product in the epidermis. Fakharzadeh et al. (19) have demonstrated correction of the coagulation defect in hemophilia A through targeting FVIII expression to the epidermis in transgenic mice. The results of these studies provide proof of principle that the epidermis can serve as a suitable target for gene replacement therapy for a systemic disorder.

1.2. Background of Skin Electroporation

Despite the suitability of the epidermis as a target tissue for gene therapy, there are significant barriers to accomplishing gene delivery in a safe, easy, efficient, and economical manner. In particular, the lipid-rich SC (15–30 μm), which is composed of dead keratinocytes consisting mainly of multiple, parallel bilayer membranes, represents a formidable physical barrier to epidermal gene transfer. Methods for increasing the transdermal flux include chemical enhancers (20), ultrasound (21), iontophoresis (22,23), electroporation (EP) (24), and electroincorporation (EI) (25,26). Iontophoresis, the application of low transdermal voltage (0.1–5 V) and constant current ($\leq 0.5 \text{ mA/cm}^2$) over a long period of time could deliver charged molecules $< 5000 \text{ Da}$ through skin hair follicles and sweat ducts.

As a noninvasive approach, in vivo EP could penetrate the SC to control gene expression to a certain extent in a tissue- or cell-specific manner. EP is a well-established physical technique to introduce DNA or chemical reagents

into cells in culture and tissues of living animals by pulsed electric fields that create transient pores in cell membranes (27–32). The similar method of EI can also be utilized in this process while genes are formulated into liposomes or particles. EI can be defined as the mass transport of particles through the SC by means of pulsed electric fields. It requires a two-step process to take place for large molecules to be transported into the skin; first, the formation of new pathways in the SC by EP and electrical pore creation (**Fig. 1**); and second, a driving force to move the molecules or particles through the new pathways (25). The nature of the driving force is not fully understood at this time; dielectrophoresis (particle size >100 nm) and pressure are possible candidates. However, this novel and simple in vivo topical gene delivery method has the potential for reversing age damage and genetic disease of the skin (33).

2. Materials

1. Animal model: hairless mice, strain SKH1 (female), 8–10 wk of age (20–25 g), are obtained from Charles River Laboratories (Wilmington, MA) and are maintained in accordance with state and federal guidelines (*see Note 4*).
2. Plasmid: plasmid (pM-MuLV-SV-*lacZ*) (6.8 kb) under the transcription control of the SV40 early promoter is used. The *lacZ* gene encodes the β -galactosidase enzyme as a marker for monitoring transfection efficiency (*see Note 4*).
3. Instrumentation: an exponential pulse generator (ECM 600 Electro Cell Manipulator[®], BTX, San Diego, CA) delivers pulses at a given voltage and pulse length (by selecting a resistor and capacitor setting). A Hewlett-Packard 54600A digital oscilloscope monitors the actual voltage and current through the caliper electrodes and the mouse skinfold during the pulse. The BTX Optimizor[®] measures the resistance before and after the pulse (*see Notes 1, 2, 4, and 8*).
4. Electrodes: a caliper-type electrode (1 cm² each electrode) (**Fig. 2**) holds the skinfold of a hairless mouse (*see Notes 3, 4, and 8*).
5. Microtome: a microtome is used for slicing fixed skin cross sections of 5–10 μ m thickness.
6. Light microscope: a light microscope with a camera is used for observing and photographing β -gal staining in the skin cross sections.

2.1. Solutions and Reagents for DNA Purification

1. Cell lysis solution: 0.2 M NaOH, 1% SDS.
2. Cell resuspension solution: 50 mM Tris-HCl (pH 7.5), 10 mM EDTA, 100 μ g/mL Rnase A.
3. Column wash solution (concentrations after addition of 95% ethanol): 80 mM potassium acetate, 8.3 mM Tris-HCl (pH 7.5), 40 μ M EDTA. Add 170 mL of 95% ethanol for its final concentration of 55%.
4. Neutralization solution: 1.32 M potassium acetate (pH 4.8).
5. TE buffer: 10 mM Tris-HCl (pH 7.5), 1 mM EDTA.

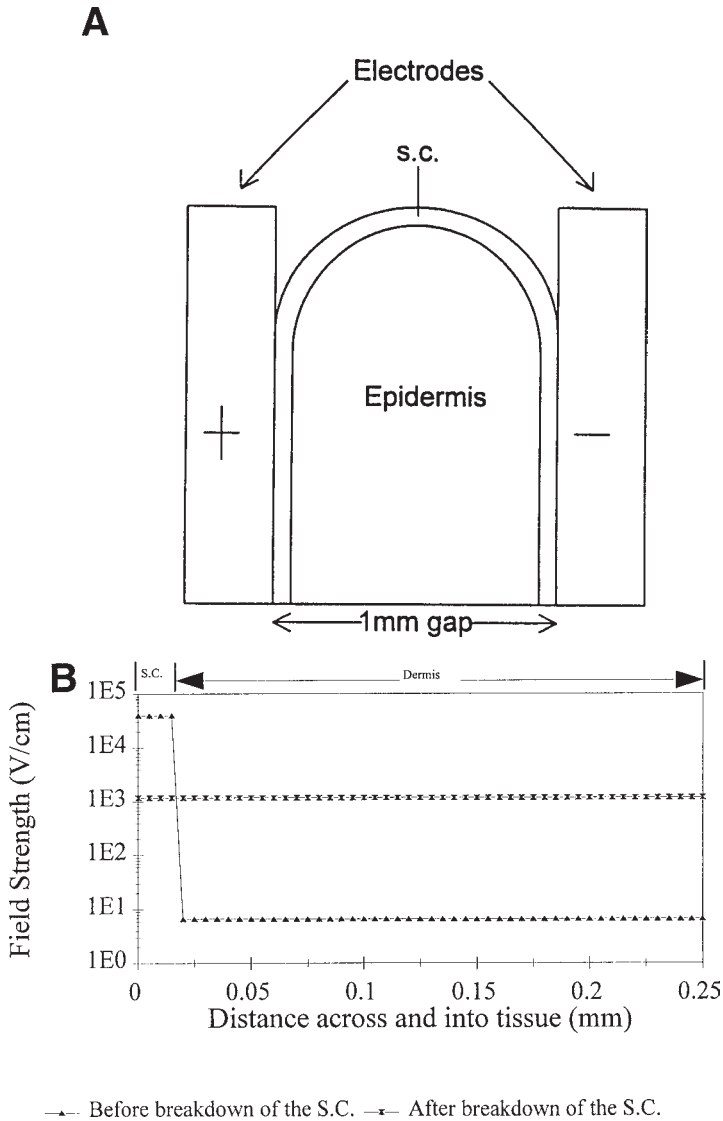


Fig. 1. (A) Model for electric field plot of a skin-fold between caliper electrodes. (B) The caliper electrodes have been simulated through the EMP software before and after breakdown of the SC.

2.2. Solutions and Reagents for X-Gal Staining

1. Stock solutions of 50 mM potassium ferricyanide [$K_3Fe(CN)_6$] and 50 mM potassium ferrocyanide [$K_4Fe(CN)_6$]: Prepare in distilled water and store foil-wrapped glassware in the dark at 4°C where they will be stable for at least 3 mo.

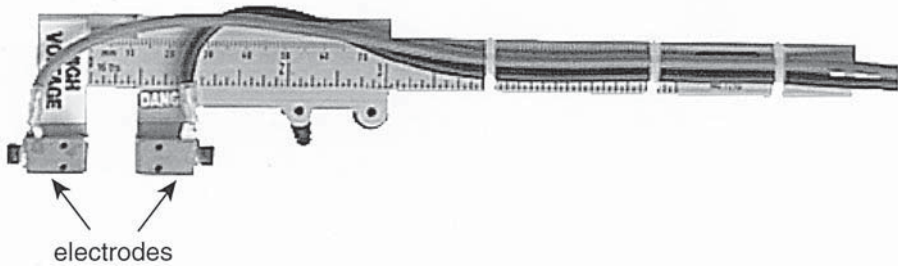


Fig. 2. Caliper electrode P/N 384 (Genetronics, Inc.) for in vivo transdermal drug or gene delivery. It consists of two brass electrodes that grasp the skinfold to be electroporated. The size of each electrode is 1 cm \times 1 cm. The caliper scale allows accurate measurement of the distance between the electrodes.

2. X-Gal stock: Dissolve in *N,N*-dimethylformamide at 20 mg/mL and store in a glass container (not polycarbonate or polystyrene) in the dark at -20°C .
3. 4% (w/v) paraformaldehyde (Sigma, St. Louis, MO): is purchased as 10% formalin solution.
4. Glutaraldehyde (Fischer) is purchased as a 25% solution.
5. To prepare the working fixative (2% paraformaldehyde/0.2% glutaraldehyde), combine 50 ml of 4% paraformaldehyde with 49.2 mL of 0.1 M sodium phosphate pH 7.3 and 0.8 mL 25% glutaraldehyde. This can be stored at 4°C for up to 1 wk.
6. X-Gal stain: 100 mM sodium phosphate pH 7.3 (80 mM Na_2HPO_4 , 20 mM NaH_2PO_4), 2 mM MgCl_2 , 5 mM $\text{K}_3\text{Fe}(\text{CN})_6$, 5 mM $\text{K}_4\text{Fe}(\text{CN})_6$, and 1 mg/mL X-Gal. Filter through a $0.45\ \mu\text{M}$ disposable filtration unit before use.
7. Phosphate buffer saline (PBS): 150 mM NaCl, 15 mM sodium phosphate, and pH 7.3.
8. Modified Eagle's medium (MEM, Sigma): 1 g glucose/L, 0.29 g/l L-glutamine, and 0.85 g/l sodium bicarbonate. Sterile-filtered. Store at $2-8^{\circ}\text{C}$.

3. Methods

The plasmid is transformed to HB 101 *Escherichia coli*. competent cells (Promega, Madison, WI). The purification of plasmid *lacZ* DNA is achieved by using the Promega Wizard[®] Megaprep DNA purification system.

3.1. DNA Extraction

1. Pellet 500–1000 mL of cells by centrifugation at 1500g for 20 min at $22-25^{\circ}\text{C}$. Resuspend the cell pellet in 30 mL of cell resuspension solution.
2. Add 30 mL of cell lysis solution and mix gently, but thoroughly, by stirring or inverting. Do not vortex. Cell lysis is complete when the solution becomes clear and viscous (up to 20 min.)
3. Add 60 mL of neutralization solution and immediately mix by inverting the centrifuge bottle 10–20 times and incubate the lysate at room temperature for 10 min.

4. Centrifuge at 14,000g for 15 min at 22–25°C.
5. Transfer the cleared supernatant by filter into a clean 200 mL graduated cylinder. Measure the supernatant volume and transfer to a centrifuge bottle.
6. Add 0.5 mL of room temperature isopropanol and mix by inversion.
7. Centrifuge at 14,000g for 15 min at 22–25°C.
8. Discard the supernatant and resuspend the DNA pellet in 4 mL of TE buffer.

3.2. DNA Purification

1. Add 20 mL of Wizard® Megapreps DNA purification resin to the DNA solution from **Subheading 3.1., step 8**. Swirl to mix.
2. Transfer the resin/DNA mix into the megacolumn. Apply a vacuum to pull the resin/DNA mix into the megacolumn.
3. Add 25 mL of column wash solution to the Megacolumn and apply a vacuum to draw the solution through the megacolumn.
4. Repeat **step 3**.
5. To rinse the resin, add 10 mL of 80% ethanol to the megacolumn and apply a vacuum to draw the ethanol through the megacolumn. Allow the vacuum to draw for an additional 1 min.
6. Dry the resin to completion by drawing a vacuum for an additional 5 min. Remove megacolumn from the vacuum source. Place the megacolumn in the reservoir (50 mL screw cap tube) provided.
7. Add 3 mL of TE buffer to the megacolumn and wait 1 min. Elute the DNA by centrifuging the megacolumn/reservoir at 1300g for 5 min.
8. A white pellet of resin fines may be present in the final eluate. It is important to separate the fines from the DNA by attaching the syringe barrel with 0.2 µm filter. Pipette the eluate into the syringe barrel.
9. Carefully insert the plunger into the syringe barrel and gently push the liquid into the 15 mL plastic tube.
10. Transfer eluate to a 1.5 mL centrifuge tube and centrifuge at 14,000g for 1 min. Immediately transfer the supernatant to a new microcentrifuge tube and store at 4°C or –20°C.

3.3. In Vivo Topical Delivery of Naked lacZ DNA by EP

1. Set BTX 600 pulse-generator at 120 V and 10 ms (R1–13 Ω and 775 µF).
2. Weigh the mouse on the scale and anesthetize it by inhalation of isoflurane (2–3% and flow rate at 2L/min) from a vaporizer.
3. Clean the dorsal skin surface of hairless mouse with 70% isopropyl alcohol.
4. Connect the caliper electrode to the output of the pulse generator.
5. Apply 40 µg lacZ DNA in 15–20 µL Tris-EDTA buffer and spread it slowly in the area that the caliper electrode will be applied (*see Note 4*).
6. Lift the skinfold with DNA gently with two forceps. Place the caliper electrode onto the skinfold and clamp it until it is tight. Write down the thickness of the skinfold measured by the caliper.

7. Turn on the generator and push the PULSE button to deliver single pulse. For multipulses, push the RESET button before delivering the next pulse. Read and record actual voltage and pulse length from the screen of BTX 600 (see **Notes 4** and **8**).
8. Turn off the pulse-generator. Hold the caliper for an additional period of time (2–10 min) to measure the postpulse effect or release it immediately from the skinfold. Mark the area that was treated by positive and negative electrodes with a surgical marker.
9. To measure the skin resistance during the pulsing, connect an oscilloscope to the pulse-generator. Save the imaging of the voltage and current trace. Then, calculate the resistance during the breakdown of the SC. To measure the recovery of the skin resistance after pulsing, connect the Optimizor[®] to the pulse-generator and caliper electrodes before doing **step 5**. After **step 8**, record the skin resistance by pushing the RESISTIVITY button on the Optimizor[®] at given time points (see **Notes 1** and **2**).
10. Bring the mouse back to the cage.
11. For the control group (DNA, no pulse), repeat the above steps, except **steps 1, 4, 7, 8, and 9**.

3.4. X-Gal-Based Histochemical Assay

The substrate, 5-bromo-4-chloro-3-indolyl- β -D-galactoside (X-Gal) is hydrolyzed by β -galactosidases to generate galactose and soluble indoxyl molecules that in turn are converted into insoluble indigo. The deep blue color generated by the hydrolysis of X-Gal by β -Gal facilitates cellular localization of the β -Gal activity (see **Notes 5** and **6**).

1. At a given time point of postapplication of *lacZ* gene (i.e., 48 h), excise the skin samples from marked areas (see **Note 7**).
2. Put the skin samples immediately into a modified Eagle's medium (MEM) for 5 min at 4°C.
3. Fix the skin tissue in a prepared fixative solution for 30 min at 4°C.
4. Rinse the tissues with PBS three times and incubate them in the X-Gal staining solution at 37°C for 18 h.
5. Section paraffin-embedded tissue (5- μ m thick slices) by standard histological procedures.
6. Counterstain with 0.1% nuclear fast red and photograph under light microscopy.
7. An example result of *lacZ* gene expression 3 d after in vivo application is shown in **Fig. 3A–D**. A cell that expresses the *lacZ* gene undergoes blue staining of its cytoplasm when exposed to X-Gal.
 - a. Efficient gene transfer and expression were found in the dermis by pulsing and pressure treatment for 1 min (**Fig. 3B**). In the case of control (pressure only by caliper electrode), gene expression appeared only around hair follicles in the very upper layers of the skin where there is light blue staining (**Fig. 3A**).

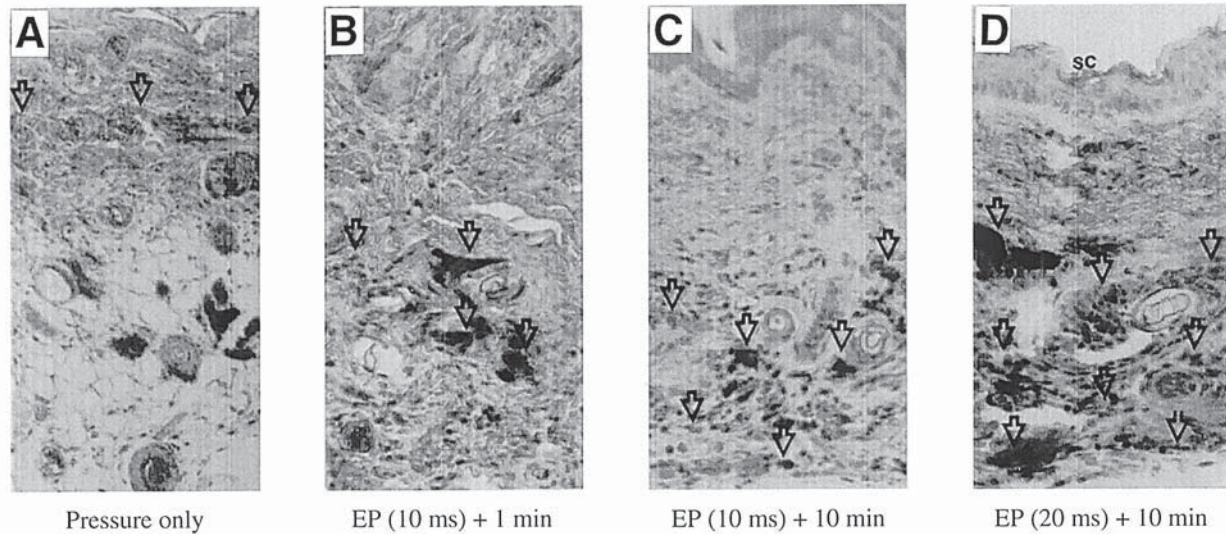


Fig. 3. Depth-targeted delivery of naked *lacZ* DNA to hairless mice by pulsed electric fields and extended pressure. Stain indicates gene activity in the dermal tissue cells after staining with the X-gal substrate. All samples except panel (A) were treated by electrical pulses (120 V, 3 pulses). The pulse length and duration of the pressure were variable. (A) Control with caliper on the skin for 10 min without pulses. (B) Pulse length 10 ms and pressure for 1 min during the pulses. (C) Pulse length 10 ms and pressure for 10 min after pulsing. (D) Pulse length 20 ms and pressure for 10 min after pulsing. Note the depth-targeted efficient gene delivery and expression in the skin (B–D). Note that the maximum depth of *lacZ* gene expression was much greater with extended pressure for 10 min after pulsing (panels C and D) compared to 1 min during the pulses (panel B). The number of transfected cells was more significant with 20 ms pulse length compared to 10 ms. In the control (panel A), only light staining was found around hair follicles and only in the very upper layers of the skin. Light microscopy. Original magnification: $\times 125$ (a), $\times 250$ (B–D). Pressure-only: gene expression was found only in hair follicles.

- b. This indicates that the electrical pulse creates new pathways to permit passage of DNA through the epidermis.
- c. Pressure maintained after the pulses, increases the depth as well as the efficiency of gene expression in the dermis (**Fig. 3C, D**).
- d. It appears that applying a longer pulse length or duration of the post-pulse pressure increases the depth and the efficiency of the *lacZ* gene expression (**Fig. 4**).
- e. No β -gal activity was found in the control groups such as no *lacZ*, pulse; no pulse, *lacZ*; no *lacZ* or pulse.
- f. There was no evidence of tissue injury in the pulsed skin as shown by visual observation and per histological studies.

4. Notes

1. The electrical property of the SC is an important parameter to measure for this study. The skin is not an electrically homogeneous material due to the fact that the SC has a much higher resistance than the underlying tissues. For *lacZ* gene delivery, the skin resistance was measured before and after pulsing by a BTX Optimizer[®] (upper resistance limit is 2.14 k Ω). The in vivo resistance measurements have demonstrated that the high resistance of the SC decreased dramatically during pulsing. The initial steady state of electrical resistance of the skin was >2 k Ω . After the breakdown of the SC by applying the first pulse, the resistance of the skin decreased to 0.76 k Ω ; it decreased to 0.4 k Ω after the second pulse and to as low as 0.28 k Ω after the third (**Fig. 5**). It shows a slow recovery profile after pulses. During the application of the pulse, the voltage $V(t)$ and current $I(t)$ curve were monitored by a digital oscilloscope (**Fig. 6**). The resistance of the skin was calculated as 200 Ω (at $t = 2 \mu\text{s}$) during the first pulse (**Fig. 6A**), and was 130 Ω (at $t = 2 \mu\text{s}$) during the third pulse (**Fig. 6B**). These results indicate that EP forms electrically conducting “pores” in the SC.
2. Results of skin resistance measurements have shown a strong time-dependence of recovery of skin resistance on the number of the pulses as well as on the size and modality of the large molecules or particles. There is about 50% recovery after application of *lacZ* DNA and pulses for 13 min; in the case of gold particles (1.5–3.0 μm) delivery, 100% recovery appears for the same time period under the same treatment of pulses (data not shown). In our series of experiments, the *lacZ* DNA and liposomes (< 5 μm) result in a slower recovery profile than gold particles and latex particles (< 4 μm) (data not shown). Considering the rearrangement of lipid bilayers in the SC after electrical pore formation, it is possible that the interaction between *lacZ* DNA or liposome and the lipid membrane of the skin prolongs the resealing time of the pores. In addition, successive pulses or a longer pulse length appears to increase the pore size or the number of pores in the SC; however, it may cause the skin damage (irreversible pore formation) if the voltage across the SC is too high (>130 V) and the pulse length is too long (longer than hundreds of milliseconds) (**34**).

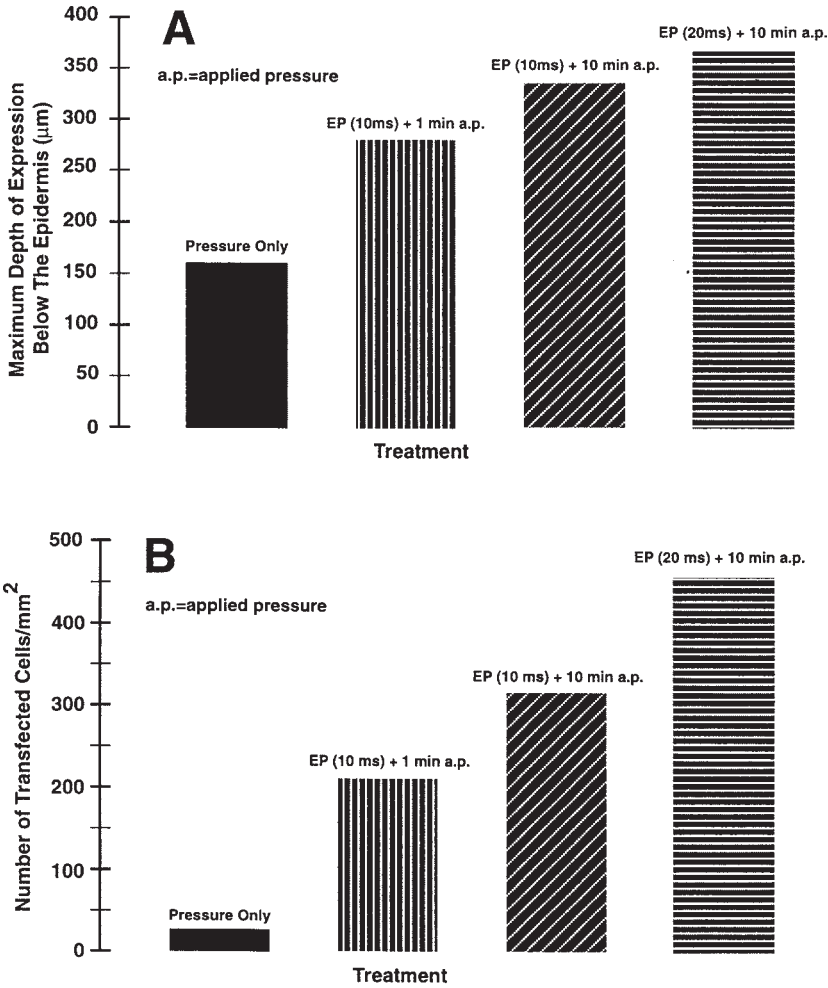


Fig. 4. Maximum depth and amount of *lacZ* gene expression in the skin as the function of pulse length and/or duration of the pressure. Conditions indicated in the graph are 120 V and three pulses for each case. **(A)** The maximum depth of gene expression below the epidermis was determined. Pressure-only: gene expression was found only in the hair follicles. **(B)** The number of transfected cells in the dermis per square millimeter was counted.

3. Using the same method and similar electrical parameters, we have demonstrated gene expression from GFP plasmid DNA as the second marker gene in hairless mice. Positive results were obtained with surface electrodes and caliper electrodes (data not shown).
4. It is desirable to increase the efficacy of topical gene delivery.

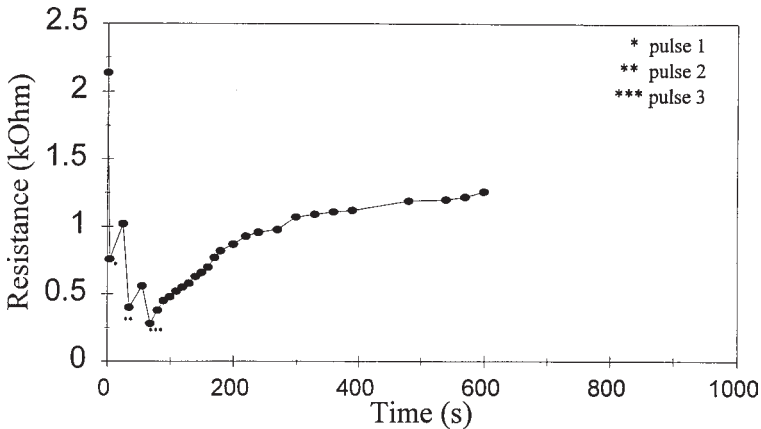


Fig. 5. Recovery profile of the resistance after pulsing *lacZ* genes on hairless mice in vivo. Total of three pulses was applied at 120 V and 10 ms.

- a. FORMULATION. It is possible to encapsulate DNA into liposome or biodegradable particles prior to topical application with pulsed electric fields. Our feasibility studies demonstrate that pulsed electric fields can be applied to different formulations of deliverable molecules (Fig. 7).
- b. VISCOSITY. To prevent leakage of DNA solution (see Subheading 3.3., steps 5 and 6), one can increase the solution's viscosity by adding a suitable chemical agent that becomes relative gelatinous.
- c. TEMPERATURE. Cool the skin tissue locally to 4°C before pulsing so that the electrically induced pore may stay open longer than at room temperature.
- d. CONFORMATION AND CONCENTRATION OF DNA. These are also important factors to be considered.
- e. CHEMICAL ENHANCER. Since the high resistance of the SC is favorable for skin electroporation (electrical field strength mostly located within the SC), it is preferable not to use a chemical enhancer (e.g., ethanol) prior to EP treatment.
- f. TIME DEPENDENCE. It is reasonable to explore the time window of gene expression to find the maximum expression (generally, 1–3 d). It depends on the DNA constructs and property of the tissue.
- g. ANIMAL SPECIES. The level and depth of gene expression depends on the animal species being used due to the variable thickness of skin layers.
- h. COMBINATION OF METHODS. A synergistic effect of DNA delivery may be obtained by taking the advantage of combining EP and iontophoresis (IPH). After creating new pathways in the SC by EP, the electrophoretic driving force provided by IPH pushes more DNA through the new pathways as well as the existing ones (hair follicles and sweat ducts).
- i. ELECTRODE. Different electrode configurations play a role in the effectiveness of gene delivery.

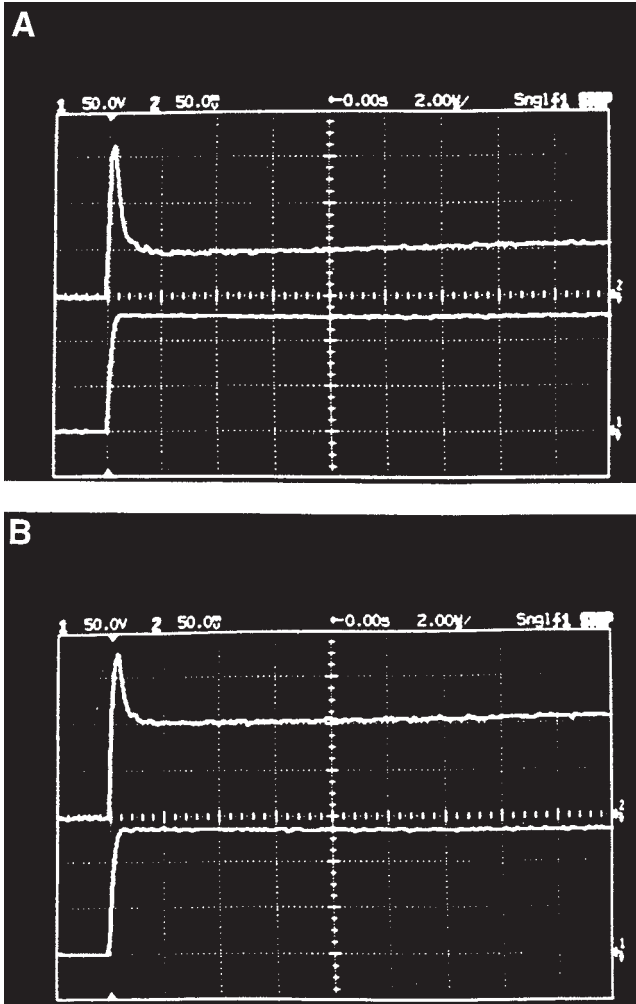


Fig. 6. Time track of the $V(t)$ and $I(t)$ curve during the pulsing monitored by a digital oscilloscope. In both panels A and B, the upper curve is $I(t)$ and the lower curve is $V(t)$. (A) Breakdown of the SC during the first pulse (120 V, 10 ms). (B) Breakdown of the SC during the third pulse (same as the first one). The resistance of the SC was decreased ($I(t)$ was increased compared with the first pulse) by electrical pore formation.

- j. PULSING PARAMETERS. One should try to find an optimum voltage (transdermal threshold is 60–100 V), pulse length (microseconds to milliseconds), and the number of pulses. It is useful to apply multipulses at certain frequencies for certain applications.

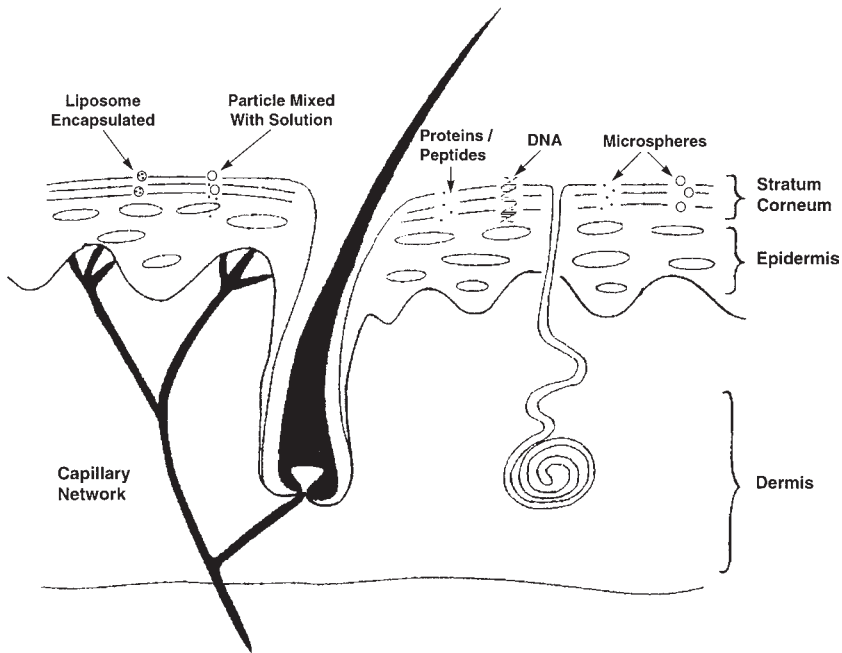


Fig. 7. Topical or transdermal delivery of different formulations of molecules by pulsed electric fields.

5. It is necessary to run the negative control sample (untreated skin) for X-Gal assay.
6. For a quick and qualitative study of the delivery method, one can run in situ tissue X-gal. It is simpler than the histochemical method. Repeat **steps 1–3** in **Subheading 3.4**. Rinse the tissues with PBS three times and incubate in X-Gal staining solution at room temperature for at least 2 h.
7. It is necessary to measure a transient and a long-term (if any) gene expression. For instance, at d 1, 2, 3, 7, 14, 21, or longer.
8. Skin damage and sensation caused by electrical parameters were reviewed and discussed (35). This is a very important issue to be addressed. Sensation is related to the design of the electrodes and the parameters of the pulse (voltage and pulse length). Muscle twitching occurs during the pulse. One should be careful not to use voltages or pulse lengths that result in any skin damage; i.e., a burn effect, etc.

References

1. Hoeben, R. C., Fallaux, F. J., Van Tilburg, N. H., Cramer, S. J., VanOrmond, H., Briet, E., and Van Der Eb, A. J. (1993) Toward gene therapy for hemophilia A: Long-term persistence of factor VIII-secreting fibroblasts after transplantation into immunodeficient mice. *Hum. Gene Ther.* **4**, 179–186.

2. Lu, B., Federoff, H. J., Wang, Y., Goldsmith, L. A., and Scott, G. (1997) Topical application of viral vectors for epidermal gene transfer. *J. Invest. Dermatol.* **108**, 803–808.
3. Medalie, D. A., Eming, S. A., Tompkins, R. G., Yarmush, M. L., Krueger, G. G., and Morgan, J. R. (1996) Evaluation of human skin reconstituted from composite grafts of cultured keratinocytes and human acellular dermis transplanted to athymic mice. *J. Invest. Dermatol.* **107**, 121–127.
4. Brinkhous, K. M. (1992) Gene transfer in the hemophilias: Retrospect and prospect. *Thromb. Res.* **67**, 329–338.
5. Gerrard, A. J., Hudson, D. L., Brownlee, G. G., and Watt, F. M. (1993) Towards gene therapy for haemophilia B using primary human keratinocytes. *Nat. Genet.* **3**, 180–183.
6. Fenjves, E. S., Schwartz, P. M., Blaese, R. M., and Taichman, L. B. (1997) Keratinocyte gene therapy for adenosine deaminase deficiency: A model approach for inherited metabolic disorders. *Hum. Gene Therapy* **8**, 911–917.
7. Page, S. M. and Brownlee, G. G. (1997) Differentiation-specific enhancer activity in transduced keratinocytes: A model for epidermal gene therapy. *J. Invest. Dermatol.* **109**, 139–145.
8. Greenhalgh, D. A., Rothnagel, J. A., and Roop, D. R. (1994) Epidermis: An attractive target tissue for gene therapy. *J. Invest. Dermatol.* **103**, 63S–69S.
9. Krueger, G. G., Morgan, J. R., Jorgensen, C. M., Schmidt, L., Li, H. L., Kwan, M. K., Boyce, S. T., Wiley, H. S., Kaplan, J., and Petersen, M. J. (1994) Genetically modified skin to treat disease: Potential and limitations. *J. Invest. Dermatol.* **103**, 76S–84S.
10. Meng, X., Sawamura, D., Tamai, K., Hanada, K., Ishida, H., and Hashimoto, I. (1998) Keratinocyte gene therapy for systemic diseases. *J. Clin. Invest.* **101**, 1462–1467.
11. Vogel, J. C. (1993) Keratinocyte gene therapy. *Arch Dermatol.* **129**, 1478–1483.
12. Choate, K. A. and Khavari, P. A. (1997) Direct cutaneous gene delivery in a human genetic skin disease. *Hum. Gene Ther.* **8**, 1659–1665.
13. Alexander, M. Y., Bidichandani, S. I., Cousins, F. M., Robinson, C. J. M., Duffle, E., and Akhurst, R. J. (1995) Circulating human factor IX produced in keratin-promoter transgenic mice: a feasibility study for gene therapy of haemophilia B. *Hum. Mol. Gen.* **4**, 993–999.
14. Carroll, J. M., Alberts, K. M., Garlick, J. A., Harrington, R., and Taichman, L. B. (1993) Tissue- and stratum-specific expression of the human involucrin promoter in transgenic mice. *Proc. Natl. Acad. Sci. USA* **90**, 10,270–10,274.
15. Carroll, J. M. and Taichman, L. B. (1992) Characterization of the human involucrin promoter using a transient β -galactosidase assay. *J. Cell Sci.* **103**, 925–930.
16. Wang, X., Zinkel, S., Polonsky, K., and Fuchs, E. (1997) Transgenic studies with a keratin promoter-driven growth hormone transgene: Prospects for gene therapy. *Proc. Natl. Acad. Sci. USA* **94**, 219–226.

17. Boyce, S. T. (1994) Epidermis as a secretory tissue. *J. Invest. Dermatol.* **102**, 8–10.
18. Fenjves, E. S., Smith, J., Zaradic, S., and Taichman, L. B. (1994) Systemic delivery of secreted protein by grafts of epidermal keratinocytes: Prospects for keratinocyte gene therapy. *Hum. Gene Ther.* **5**, 1241–1248.
19. Fakharzadeh, S. S., Sarkar, R., and Kazazian, H. H. Jr. (1997) Correction of factor VIII deficiency in a mouse model of hemophilia A through targeting factor VIII transgene expression to skin. *Proc. Am. Soc. Hematol.* **39**, 569a.
20. J. Hadgraft and Guy, R. H. (1989) *Drugs and the Pharmaceutical Sciences*. Marcel Dekker, New York.
21. Kost, J., Levy, D., and Langer, R. (1989) Ultrasound as a transdermal enhancer. *Percutaneous Absorption: Mechanisms—Methodology—Drug Delivery*, 2nd ed. (Bronaugh, R. L. and Maibach, H. I., eds.), pp. 595–601.
22. Banga, A. K. and Chien, Y. W. (1988) Iontophoretic delivery of drugs: fundamentals, developments and biomedical applications. *J. Controlled Release* **7**, 1–24.
23. Chien, Y. W. and Banga, A. K. (1989) Iontophoretic (transdermal) delivery of drugs: Overview of historical development. *J. Pharm. Sci.* **78**, 353–354.
24. Prausnitz, M. R., Bose, V. G., Langer, R., and Weaver, J. C. (1993) Electroporation of mammalian skin: A mechanism to enhance transdermal drug delivery. *Proc. Natl. Acad. Sci. USA* **90**, 10,504–10,508.
25. Hofmann, G. A., Rustrum, W. V., and Suder, K. S. (1995) Electro-incorporation of microcarriers as a method for the transdermal delivery of large molecules. *Bioelectrochem. Bioenerg.* **38**, 209–222.
26. Hofmann, G. A., Zhang, L., Bremer, U., and Spencer, T. (1996) Investigation of electroincorporation phenomena. [Abstract]. *Proc. 13th Int. Symp. Bioelectrochem. Bioenerg. January 7–12, Israel*, pp. 132.
27. Muramatsu, T., Nakamura, A., and Park, H-M. (1997) In vivo electroporation: A powerful and convenient means of nonviral gene transfer to tissues of living animals. [Review]. *Int. J. Mol. Med.* **1**, 55–62.
28. Neumann E., Sowers A. E., and Jordan C. A. (1989) *Electroporation and Electrofusion in Cell Biology*. Plenum, New York.
29. Nickoloff, J. A. (1995) *Electroporation Protocols for Microorganisms; Animal Cell Electroporation and Electrofusion Protocols; Plant Cell Electroporation and Electrofusion Protocols*; Vols. 47, 48, and 55 in *Methods in Molecular Biology*, Humana Press, Totowa, NJ.
30. Weaver, J. C. (1993) Electroporation: A general phenomenon for manipulating cells and tissues. *J. Cell. Biochem.* **51**, 426–435.
31. Hofmann, G. A., Dev, S. B., and Nanda, G. S. (1996) Electrochemotherapy: Transition from laboratory to the clinic. *IEEE Eng. Med. Biol.* **Nov./Dec.**, 124–132.
32. Prausnitz, M. R., Bose, V. G., Langer, R., and Weaver, J. C. (1993) Electroporation of mammalian skin: A mechanism to enhance transdermal drug delivery. *Proc. Natl. Acad. Sci. USA* **90**, 10,504–10,508.
33. Zhang, L., Li, L., Hofmann, G. A., and Hoffman R. M. (1996) Depth-targeted efficient gene delivery and expression in the skin by pulsed electric fields: An

- approach to gene therapy of skin aging and other diseases. *Biochem. Biophys. Res. Commun.* **220**, 633–636.
34. Pliquett, U., Langer, R., and Weaver, J. C. (1995) Changes in the passive electrical properties of human stratum corneum due to electroporation. *Biochim. Biophys. Acta* **1239**, 111–121.
 35. Prausnitz, M. R. (1996) The effects of electric current applied to skin: A review for transdermal drug delivery. *Adv. Drug Deliv. Rev.* **18**, 395–425.